



HAL
open science

Understanding the behaviour of (macro)chain transfer agents for RAFT controlled dispersion polymerisation in supercritical CO₂

Ana Patricia Alves Costa Pacheco

► **To cite this version:**

Ana Patricia Alves Costa Pacheco. Understanding the behaviour of (macro)chain transfer agents for RAFT controlled dispersion polymerisation in supercritical CO₂. *Polymers*. Université de Lyon; University of Nottingham, 2021. English. NNT : 2021LYSE1249 . tel-03847741

HAL Id: tel-03847741

<https://theses.hal.science/tel-03847741>

Submitted on 10 Nov 2022

HAL is a multi-disciplinary open access archive for the deposit and dissemination of scientific research documents, whether they are published or not. The documents may come from teaching and research institutions in France or abroad, or from public or private research centers.

L'archive ouverte pluridisciplinaire **HAL**, est destinée au dépôt et à la diffusion de documents scientifiques de niveau recherche, publiés ou non, émanant des établissements d'enseignement et de recherche français ou étrangers, des laboratoires publics ou privés.



The University of
Nottingham

N°d'ordre NNT :
2021LYSE1249

THESE de DOCTORAT DE L'UNIVERSITE DE LYON

opérée au sein de

l'Université Claude Bernard Lyon 1

en cotutelle avec l'Université de Nottingham

Ecole Doctorale N° ED 206

Spécialité de doctorat : Chimie des polymères ; fluide supercritique

Discipline : Chimie

Soutenue publiquement le 12/11/2021, par :

Ana Patricia Alves Costa Pacheco

Analyse du comportement de (macro)agents de transfert de chaîne lors de la polymérisation en dispersion de type RAFT dans le CO₂ supercritique

Devant le jury composé de :

Nom, prénom grade/qualité établissement/entreprise

Perrier, Sébastien Professeur des Universités University of Warwick **Rapporteur**

Rieger, Jutta Directrice de Recherche CNRS Université Pierre et Marie Curie Paris 6

Rapporteuse

Beyou, Emmanuel Professeur des Universités l'Université Claude Bernard Lyon 1

President

Newton, Graham Professeur des Universités the University of Nottingham **Examineur**

Lansalot, Muriel Directrice de Recherche CNRS l'Université Claude Bernard Lyon 1

Directrice de thèse

Howdle, Steven M Professeur des Universités the University of Nottingham **Directeur de thèse**

D'Agosto, Franck Directeur de Recherche CNRS l'Université Claude Bernard Lyon 1 **Co-directeur de thèse et invité**

i. Declaration

I declare that except where specific reference has been made to other sources, the work presented in this thesis is the original work of the author. It has not been submitted, in whole, or in part, for any other degree or professional qualification.

Ana Patricia Alves Costa Pacheco

Date:.....23/08/21..... Signed:..........

ii. COVID impact statement

I detail here some of the impacts that have disrupted research activities in the third and fourth year of my doctoral studies as consequence of the COVID-19 pandemic. This was particularly detrimental to my research as I am part of a cotutelle program.

As a result of the lockdown imposed during the COVID-19 crisis, access to the research laboratories facilities and equipment has not been possible. Such restrictions were in place from March 2020 until the end of June 2020 in the University of Nottingham, and the laboratory was only back into operation in July 2020. This has been critically disruptive to my PhD studies as my research is primarily lab based and concerns the synthesis, study of reaction kinetics and characterisation of polymeric materials.

After re-opening of the University facilities at University of Nottingham, the time available to me in the lab has been reduced in comparison to pre-COVID times because of a reduction in the maximum capacity, which was significantly lower than the number of people requiring access to the lab. Therefore, the amount of lab work I was able to complete from July 2020 until the end of my scholarship (October 2020) was drastically reduced. Working hours were also reduced, limiting the possibility of monitoring long kinetic studies.

In particular, the access to key facilities for analysis was reduced or interrupted. For example, the access to the NMR facility was limited to about a tenth of the normal number of analysis per day. In addition, the Nanoscale and microscale research centre (nmRC) at Nottingham remained closed until late August 2020 and access hours were limited compared to pre-COVID times. Without access to the facility, it was not possible to perform some characterisation of produced materials.

Although I got an unfunded extension for my research in the lab, I was not able to accomplish all the experiments and analysis I wished I would complete until the end of January 2021. The missing experiments were added to the future work for each results Chapters (Chapter 3-5) and in Chapter 6.

iii. Acknowledgements

Firstly, I would like to thank my supervisors, Prof. Steve Howdle in Nottingham and Dr. Muriel Lansalot and Dr. Franck D'Agosto in Lyon, for giving me the opportunity to work in this project. Their support and guidance was fundamental during the course of this PhD and I could not ask for a better team of experts to assist me. I would also like to thank the European Doctoral Programme in Sustainable Industrial Chemistry (SINCHEM) for the funding.

I would like to thank everyone in B10 (and B10-A) that I shared my time in Nottingham with and were always there to help me and make this journey fun with lots of tea breaks, baked goods and cross words. There are too many people to name all (you know who you are). In particular, I cannot imagine my journey through the PhD in Nottingham without the support of the other CO₂ “enthusiasts” in the lab, in especial Alice, Ryan, Eduards, Kris and Kartini. Special thanks also to Fabricio, who helped me a lot in the final months in the lab and who is keeping up the Brazilian presence in B10. In special, I would like to give many thanks to the greatest postdoc ever Dr. Vincenzo Taresco for believing in my work, supporting me and always pushing me forward.

I would like to acknowledge Dr. Arnaldo Filho and Prof. Jonathan Hirst for their collaboration in the computational chemistry part of this work. I would also like to thanks Nikki Weston and Beth Steers for the training and advice at the Nanoscale and Microscale Research Centre (NMRC). Additionally, I am indebted to Mark Guyler, Rich Wilson and all the workshops team for their constant technical support with the equipment used throughout this work. It would be impossible to complete this project without their cheerful support. I am also grateful to Sue for always providing us with infinite tea, empathy and smiles at the tearoom.

I would also like to thanks the team in Lyon for their warm reception and for their patience with me while I tried to find myself around the lab and understand/speak French. In special, I would like to thanks Rémi, Florian, Pierre-Yves and Olivier. In addition, I would like to thanks Sofie and Harald from Kaneka Ltd. for giving me advice in my project, even though my visit to Kaneka had to be cancelled due to the pandemic.

I am also forever grateful to my SINCHEM colleagues with whom I shared the PhD experience and that became my new dysfunctional international family that was always there to support

me through good and bad days. Many thanks also to Valentina and Dara at Nottingham for their friendship and support throughout the PhD madness. I would like to extend my thanks to all my friends around the globe who were there for me during the past 4 years.

I also cannot thank enough my partner, Fred, who even from a distance supported me through this journey and pushed me to keep going when I felt like giving up. Finally, I would like to give thanks to my family, who have been a constant source of love and support, you are my inspiration and you keep me striving to be the best person I can be.

iv. Abbreviations

4VP	4-vinylpyridine
AA	Acrylic acid
AIBN	2,2 -Azobis(isobutyronitrile)
ASB	Anchor-soluble balance
ATRP	Atom transfer radical polymerisation
BA	Butyl acrylate
BSPA	3-(benzylsulfanylthiocarbonylsulfanyl)propionic acid
BzMA	Benzyl methacrylate
CDB	Cumyldithiobenzoate
CPAB	4-cyano-4-(phenylcarbonothioylthio) pentanoic acid
CPAD	4-cyano-4-[(dodecylsulfanylthiocarbonyl)sulfanyl]pentanoic acid
CPDB	2-cyanoprop-2-yl dithiobenzoate
CRP	Controlled radical polymerisation
CTA	Chain transfer agent
CTPPA	4-cyano-4-thiothiopropylsulfanylpentanoic acid
C_{tr}	Chain transfer constant
C_v	Coefficient of variance
\bar{D}	Dispersity
DCC	Dicyclohexylcarbodiimide
DCM	Dichloromethane
DDMAT	2-(dodecylthiocarbonothioylthio)-2-methylpropionic acid
DMA	Dynamic mechanical analysis
DMAEMA	2-(dimethylamino)ethyl methacrylate
DMAP	4-dimethylaminopyridine
DMF	Dimethylformamide
D_n	Mean particle diameter
$D_{n,th}$	Expected diameter
DP	Degree of polymerisation
EDX-TEM	Transmission electron microscope with energy dispersive X-ray analysis
EPDM	Ethylene propylene diene monomer
ε	Extinction coefficient
f	Initiator efficiency
FOA	1,1-dihydroperfluorooctyl acrylate
FT-IR	Fourier-transform infrared spectroscopy
HPLC	High performance liquid chromatography
HPMA	2-hydroxypropyl methacrylate
IBMA	Isobornyl methacrylate
IRT	Intermediate radical termination
ITP	Iodine-transfer polymerisation
J_{crit}	Critical chain length
k_d	Rate of decomposition
k_t	Termination rate
LAM	'Less activated' monomer
MA	Methyl acrylate
macro-CTA	Macromolecular CTA
MADIX	Macromolecular Design <i>via</i> Interchange of Xanthates
MALDI-TOF	Matrix assisted laser desorption ionisation time-of-flight mass spectrometry
MALS	Multiple angle light scattering
MAM	'More activated' monomer
MiB	Methyl isobutyrate
MMA	Methyl methacrylate
M_n	Number average molecular mass
$M_{n,tgt}$	Target Number Average Molecular Mass / molecular weight target
$M_{n,th}$	Theoretical Number Average Molecular Mass / theoretical molecular weight

MPPA	3-methoxycarbonyl-phenyl-methylsulfanyl-hiocarbonylsulfanyl)-propionic acid
M_w	Weight average molecular mass
NMP	Nitroxide mediated polymerisation
NMR	Nuclear magnetic resonance
NRV	Non-return valve
NVC	N-vinylcarbazole
NVP	N-vinylpyrrolidone
PAA	Poly(acrylic acid)
P_c	Critical pressure
PDFMA	Poly(dodecafluoroheptyl methacrylate)
PDMS	Polydimethylsiloxane
PDMS-MA	Methacrylate terminated polydimethylsiloxane
PDMS-OH	Monocarbinol terminated polydimethylsiloxane
PEEK	Polyether ether ketone
PEGMA	Poly(ethylene glycol methacrylate)
PETTC	4-cyano-4-(2-phenylethanesulfanylthiocarbonyl)sulfanylpentanoic acid
PFOA	Poly(1H,1H-perfluorooctyl acrylate)
PFOMA	Poly(1,1-dihydroperfluorooctyl methacrylate)
PFPE	Perfluoro polyether
PHEMA	Poly(2-hydroxyethyl methacrylate)
PISA	Polymerisation-induced self-assembly
PLMA	Poly(lauryl methacrylate)
PLP	Pulse laser polymerisation
PMMA	Poly(methyl methacrylate)
PNIPAM	N-isopropylacrylamide
PNVP	Poly(N-vinylpyrrolidone)
PRE	Persistent radical effect
PSt	Polystyrene
PTFE	Polytetrafluoroethylene
PVC	Poly(vinyl chloride)
PVDF	Poly(vinylidene fluoride)
RAFT	Reversible addition-fragmentation chain transfer
RDRP	Reversible-deactivation radical polymerisation
RI	Refractive index
ROP	Ring opening polymerisation
R_p	Rate of propagation
SANS	Small-angle neutron scattering
SAXS	Small-angle X-ray scattering
scCO ₂	Supercritical carbon dioxide
SCF	Supercritical fluid
SEC	Size exclusion chromatography
SEM	Scanning electron microscopy
SOP	Standard operation procedures
St	Styrene
T_c	Critical temperature
TEM	Transmission electron microscopy
TERP	Tellurium-mediated radical polymerisation
T_g	Glass transition temperature
THF	Tetrahydrofuran
v/v	Volume to volume
VAc	Vinyl acetate
VOC	Volatile organic solvent
VPI	Vinyl pivalate
wt %	Percentage by weight

v. Abstract

Our aim is to make a positive use of captured carbon dioxide (CO₂) as an alternative green solvent for polymer synthesis. Supercritical carbon dioxide (scCO₂) presents many advantages over other conventional solvents employed in polymer synthesis. It is non-flammable, has a very low toxicity and allows an easy recovery of the polymer. Dispersion polymerisation in scCO₂ is one established technique that provides dry polymer particles free of solvent contamination.

In this thesis, we focus on reversible addition-fragmentation chain transfer (RAFT) polymerisation in scCO₂ with both molecular chain transfer agents (CTAs) (DDMAT, CPAB, CTPPA) and polydimethylsiloxane (PDMS)-based macromolecular CTAs (macro-CTAs) soluble in scCO₂ (PDMS-DDMAT, PDMS-CPAB, PDMS-CTPPA), for the dispersion polymerisation of methyl methacrylate (MMA).

Although the use of PDMS-DDMAT macro-CTAs led to stable PMMA particles, successful RAFT control was not attained, and part of the macro-CTA remained unreacted. Therefore, RAFT dispersion polymerisation of MMA in scCO₂ was investigated using DDMAT and comparing to other molecular CTAs. Despite its low chain transfer constant (C_{tr}) towards MMA, DDMAT showed good control over PMMA molecular weight. A thorough investigation of the nucleation stage revealed an unexpected “*in situ* two-stage” mechanism that explains this result. Finally, a correlation between polymerisation control and the degree of solubility in scCO₂ of the CTAs was established, giving rise to a guideline to select the best molecular CTA for MMA RAFT dispersion polymerisation in scCO₂.

The use of PDMS-CPAB and PDMS-CTPPA, which present chain-ends of high C_{tr} towards MMA, allowed an overall improvement of MMA polymerisation and RAFT control in scCO₂ compared with PDMS-DDMAT. The good solubility of these macro-CTAs in scCO₂ and the good control observed led to the formation of PDMS-*b*-PMMA block copolymers, suggesting the establishment of a polymerisation-induced self-assembly (PISA) process. This is a step forward towards PISA polymerisation *via* RAFT in scCO₂ with fluorine-free macro-CTAs.

General Table of Contents

Chapter 1. Introduction and literature review.....	-1-
Chapter 2. Experimental equipment and characterisation techniques	-65-
Chapter 3. Polydimethylsiloxane-based macro-CTAs for block copolymer synthesis with PMMA in scCO₂.....	-97-
Chapter 4. Influence of structure and solubility of chain transfer agents on the RAFT control of dispersion polymerisation in scCO₂.....	-156-
Chapter 5. MMA polymerisation in scCO₂ with polydimethylsiloxane-based macro-CTAs of high chain transfer constant towards methacrylates	-249-
Chapter 6. Conclusions.....	-308-

Table of Contents

Chapter 1. Introduction and literature review	- 1 -
1.1. <i>Abstract</i>	- 1 -
1.2. <i>Polymer synthesis</i>	- 1 -
1.2.1. Homogeneous polymerisation	- 3 -
1.2.2. Heterogeneous polymerisation	- 4 -
1.2.2.1. Precipitation polymerisation	- 4 -
1.2.2.2. Emulsion polymerisation	- 4 -
1.2.2.3. Suspension polymerisation	- 6 -
1.2.2.4. Dispersion polymerisation	- 6 -
1.3. <i>Chain growth polymerisation mechanisms</i>	- 9 -
1.3.1. Conventional radical polymerisation	- 9 -
1.3.2. Controlled radical polymerisation	- 12 -
1.3.3. RAFT polymerisation	- 15 -
1.3.3.1 Chain transfer agent selection	- 19 -
1.4. <i>RAFT dispersion polymerisation</i>	- 23 -
1.4.1. Compartmentalisation	- 24 -
1.5. <i>Polymerisation-induced self-assembly</i>	- 27 -
1.6. <i>Supercritical carbon dioxide</i>	- 30 -
1.7. <i>Polymerisation in scCO₂</i>	- 32 -
1.7.1. General Considerations	- 32 -
1.7.2. Dispersion polymerisation in scCO ₂	- 35 -
1.7.2.1. Fluorinated stabilisers	- 38 -
1.7.2.2. Siloxane-based stabilisers	- 40 -
1.7.2.3. Hydrocarbon-based stabilisers	- 43 -
1.7.3. Kinetic and mechanistic considerations of dispersion polymerisation in scCO ₂	- 44 -
1.7.4. RAFT dispersion polymerisation in scCO ₂	- 50 -
1.7.5. Block copolymer synthesis in scCO ₂	- 54 -
1.7.6. Polymerisation-induced self-assembly in scCO ₂	- 57 -
1.8. <i>References</i>	- 58 -

Chapter 1. Introduction and literature review

1.1. Abstract

The aim of this chapter is to provide context and background to the underlying themes later presented in this thesis. My project has been focused on investigating in depth the reversible addition-fragmentation chain transfer (RAFT) mechanism in supercritical carbon dioxide (scCO₂) and applying silicone-based RAFT-terminated CO₂-soluble polymers for polymerisation-induced self-assembly (PISA) in scCO₂. This chapter gives a brief introduction to polymer chemistry, with focus on heterogeneous synthetic procedures and controlled polymerisation techniques. The concepts of PISA are presented and the advantages and disadvantages discussed. The use of scCO₂ as a green solvent for polymer synthesis is then discussed and an overview of the main advances in the field are reported. In this way, this chapter gives a broad overview of the key concepts touched in this work and present the state of the art of each topic. In addition, a more focussed and detailed discussion of immediately relevant topics is given at the start of each results chapter (Chapters 3-5).

1.2. Polymer synthesis

Polymers can be defined as molecules of very high molecular weight, usually in the range of thousands g mol⁻¹. Their structure comprises the repetition of low molecular weight units named monomer.^{1, 2} Depending on the way monomers are organized along the polymer chain, polymers can be classified into homopolymer, copolymer (random or alternating), block copolymer, graft or hyperbranched (co)polymer (Figure 1).

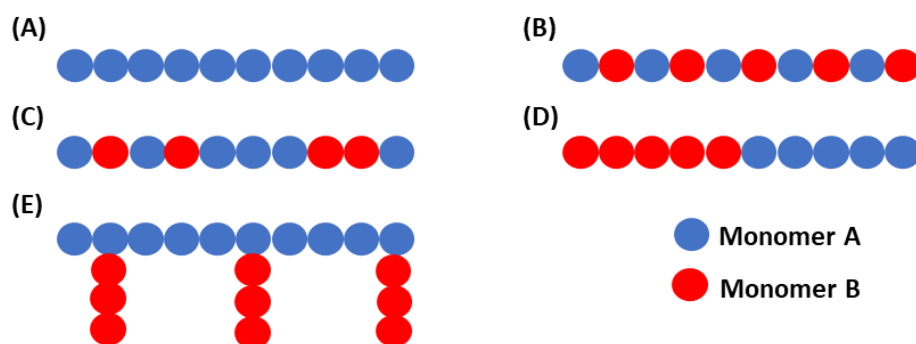


Figure 1 - Typical structures of polymers composed of one or two monomers: (A) homopolymer, (B) alternating copolymer, (C) random copolymer, (D) block copolymer and (E) graft copolymer.

The molecular weight of a polymer defines many of its properties. In contrast to other chemical compounds, synthetic polymers are characterised by a mixture of molecular weights, which is usually reported as a number-average molecular weight (M_n).^{1,2} M_n is simply the total weight of the sample divided by the number of macromolecules in the sample, as shown in Equation (1), where M_i is the molecular weight of a chain containing i monomer repeat units and n_i is the number of those chains. The average degree of polymerisation (DP) refers to the average number of monomer units in all chains and can be easily calculated through the ratio of the total number of monomeric units by the total number of macromolecules (Equation (2)). Other important metrics is the weight-average molecular weight (M_w), which is the weight fraction of molecules in a polymer sample. It is given by $M_i^2 n_i$ divided by the total weight of the sample (Equation (3)).

$$M_n = \frac{\sum M_i n_i}{\sum n_i} \quad (1) \quad DP = \frac{\sum i n_i}{\sum n_i} \quad (2)$$

$$M_w = \frac{\sum M_i^2 n_i}{\sum M_i n_i} \quad (3)$$

M_w is always greater than M_n . The ratio of the M_w to the M_n gives the dispersity (\mathcal{D}) of the polymer, Equation (4).¹ A \mathcal{D} of 1.00 would refer to a perfectly monodisperse system, where all chains would have the same length. In a polymer with high dispersity, the lower molecular weight fraction can act as a plasticiser, softening the material, while the high molecular weight tail can increase melt viscosity.¹

$$\mathcal{D} = \frac{M_w}{M_n} \quad (4)$$

Polymers are synthesised using two main mechanisms: step-growth or chain-growth polymerisation (Figure 2).¹ The former involves the reaction of functional groups A and B coming from two different molecules (monomer or oligomer). Examples of polymers synthesised by step-growth include polyurethanes, polyamides and polyesters.² Within step-growth mechanism, molecular weight increases very slowly with conversion, thus a high degree of polymerisation is achieved only at very high conversions.³ On chain-growth polymerisation, unsaturated vinyl monomer units add onto the active site of a growing polymer chain. Conventional radical polymerisation is the most widely used chain growth

polymerisation, according to this mechanism a high molecular weight chain is formed every second in average.¹

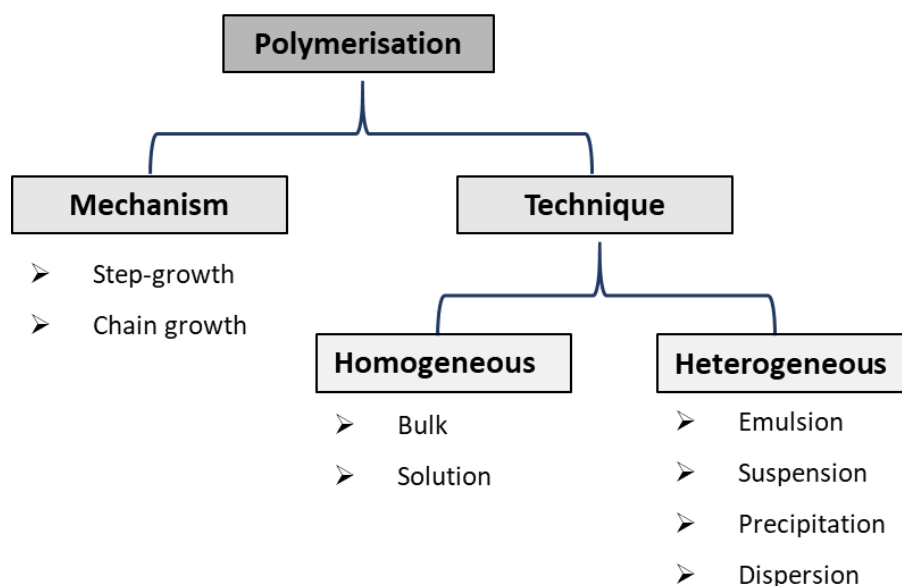


Figure 2 - Polymerisation mechanisms, divided in step-growth and chain growth, and polymerisation synthetic techniques, divided into homogeneous and heterogeneous systems.

In addition to the mechanism of polymerisation, there are several polymerisation processes, which are divided into homogeneous, *i.e.*, bulk and solution polymerisation, or heterogeneous systems, which include dispersion polymerisation.^{4, 5} Two main synthetic techniques were applied in this thesis, *i.e.*, dispersion and solution polymerisation. A brief introduction to the different types of polymer synthesis is presented next.

1.2.1. Homogeneous polymerisation

The simplest homogeneous system comprises only monomer and initiator, *i.e.*, bulk polymerisation. The absence of a solvent may be advantageous, as it does not require solvent removal at the end of the reaction. However, the absence of a solvent brings several drawbacks. Heat transfer is difficult without a solvent and, as the reaction progresses, viscosity increases, which makes it worse. In addition, auto-acceleration, known as the Trommsdorff effect, is more likely to happen in this system.⁶ As a result, bulk polymerisations usually have to be stopped at low conversion in order to make it less susceptible to thermal runaway. Furthermore, these issues may lead to lack of control in radical polymerisations.

The addition of a solvent makes solution polymerisation safer and easier to control than the bulk system. However, the solvent must be inert towards the polymerisation reaction. In addition, the solvent boiling point limits the maximum reaction temperature. Nevertheless, the biggest disadvantage of solution polymerisation is the difficulty of removing or treating the solvent at the end of the reaction. Therefore, this technique is usually applied when the solvent is part of the final product formulation, such as for coating applications.

1.2.2. Heterogeneous polymerisation

Any polymerisation system in which the formed polymer is insoluble in the reaction medium can be classified as a heterogeneous system.¹ The reaction thus occurs completely or partially within a second phase, *i.e.*, polymer-rich. There are four types of heterogeneous polymerisation: precipitation, emulsion, suspension and dispersion.

1.2.2.1. Precipitation polymerisation

In a precipitation polymerisation, the reaction starts as a normal solution polymerisation, *e.g.*, for a conventional radical polymerisation, there is a monomer, initiator and solvent. However, as the polymer chain grows it becomes insoluble and at a certain critical chain length (J_{crit}) it precipitates, into a polymer-rich phase. Precipitation thus produces a polymer phase that is easy to separate from the reaction mixture, although it typically lacks a controlled morphology and the product is agglomerated.⁷ Furthermore, the solid contents are usually low, increasing solvent waste and reducing productivity.

1.2.2.2. Emulsion polymerisation

A conventional radical polymerisation *via* emulsion involves the use of a surfactant, beside an initiator, a poorly soluble monomer and a solvent. Emulsion polymerisation is well established, with the majority of commercial polymer production by aqueous emulsion radical polymerisation.⁸

Due to its poor solubility, most of the monomer will be present as droplets dispersed by the surfactant, with few surfactant micelles also present. The initiator, on the other hand, is usually soluble in the continuous phase, *i.e.*, solvent.⁹ Thus, polymerisation initiates in the continuous phase and the forming solvophobic polymer chains rapidly diffuse into the micelles turning them into particles. The propagation and chain growth continue inside the

particles, where conditions resemble a bulk polymerisation. The reaction continues, with the monomer fed to the particles from the continuous phase, which, in turn, is replenished with monomer by diffusion from the droplets. The reaction continues until the monomer or initiator are exhausted, giving stable polymer particles dispersed in the continuous phase, *i.e.*, a latex (Figure 3). The final particle size typically ranges between 100 and 600 nm.⁹

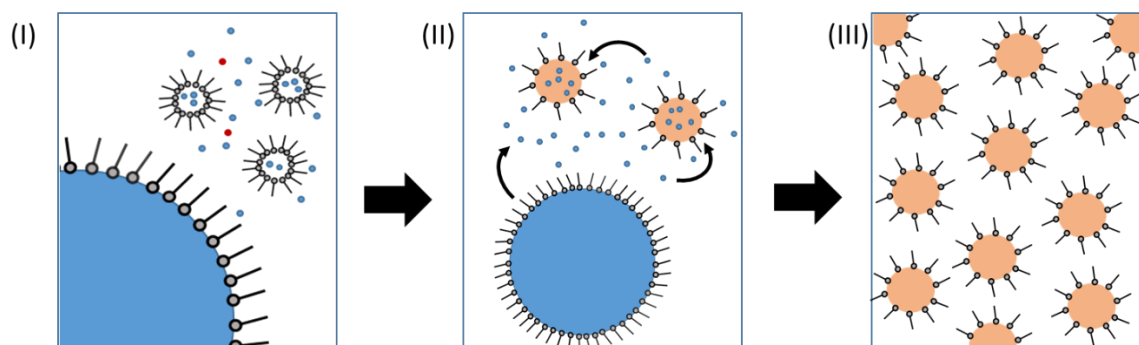


Figure 3 – Scheme showing emulsion polymerisation mechanism. At the reaction start (I), monomer (blue) is found in large monomer droplets in the continuous phase, stabilised by the surfactant (gray), and in small micelles (limited amount). The initiator (red) usually has high solubility in the continuous phase, and, therefore, polymerisation starts in the continuous phase. Later, (II) the monomer diffuses from the large droplets into micelles, establishing a slow feed of monomer, as polymer (orange) precipitates into the micelles and continues to grow. At the reaction end, (III) all the monomer is consumed and polymer particles are formed.

1.2.2.2.1. Miniemulsion polymerisation

It is important to distinguish emulsion from miniemulsion polymerisation, as they will be useful for our discussion in Chapter 4. A miniemulsion polymerisation is obtained when the reactants for an emulsion polymerisation are mixed *via* homogenisation techniques with high shear and/or cavitation, such as ultrasonication or microfluidisation, in order to form smaller monomer droplets (60-200 nm) than the ones formed in emulsion polymerisation (> 1 μm).^{5, 9, 10} A co-stabiliser is also required to limit Ostwald ripening (*e.g.* hexadecane). These small droplets are not thermodynamically stable, however they are considered kinetically stable for the time of the reaction. In a miniemulsion, the small monomer droplets act as the reaction *locus* and ideally, each droplet will result in a polymer particle, in a one-to-one copy (Figure 4).⁹

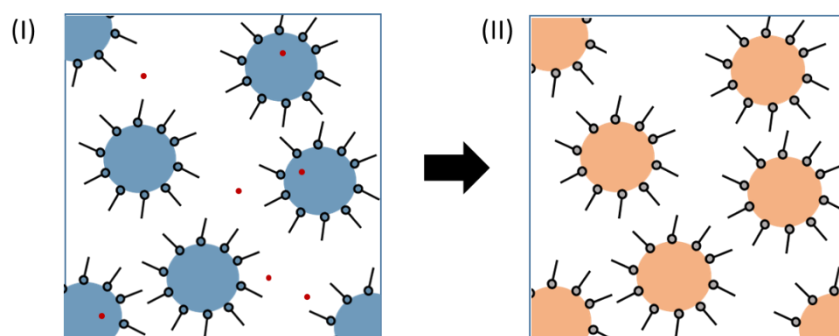


Figure 4 – Scheme showing a miniemulsion polymerisation. At the reaction start, (I) the monomer (blue) is present as many small droplets, stabilised by the surfactant and the co-stabiliser (gray), as a result of ultrasonication or microfluidisation. The initiator (red) can be either soluble in the continuous or monomer phase. The monomer droplets are the reaction locus and at the reaction end, (II) each droplet converts into a polymer particle.

Therefore, the miniemulsion polymerisation mechanism is fundamentally different from the emulsion mechanism, as it is not dependent on monomer feed from droplets. The initiator for this system can be either soluble in the continuous phase or in the monomer phase. The final particle sizes are similar to those obtained in emulsion, *i.e.*, 50-500 nm.¹¹

1.2.2.3. Suspension polymerisation

A suspension polymerisation, similarly to emulsion polymerisation, usually comprises a monomer, initiator, surfactant and a solvent, which is frequently water. The difference from the emulsion system is the solubility of the initiator. In this mechanism, the initiator must be insoluble in the solvent, and, therefore the polymerisation will occur in the monomer droplets.^{5, 9} As a result, the final particle will usually be a one-to-one copy of the monomer droplets, with particle diameters significantly larger than in emulsion or miniemulsion, *e.g.*, > 1 μm .⁹

1.2.2.4. Dispersion polymerisation

In this thesis, the main studied polymer synthesis process is dispersion polymerisation, which is very similar to precipitation polymerisation, but with the addition of a stabiliser, which prevents agglomeration and thus allows the synthesis of well-defined particles.⁵ Dispersion polymerisation can be divided into four steps (Figure 5):⁵ At the reaction start (I) all reactants are soluble in the reaction medium, but, as the molecular weight increases, J_{crit} is achieved and polymer precipitates from the solution (II). As polymer precipitates, stabiliser adsorbs

onto the new *nuclei*, preventing agglomeration (III) and leading to a colloidal dispersion. Once the stabiliser is exhausted, nucleation can no longer occur and the existing particles can only be enlarged by addition of the remaining monomer in solution (IV). This last process is the particle-growth step.¹² The final product is a latex, usually with narrow particle size distribution and particle diameter > 1 μ m.⁹ The stabiliser which is attached to the particle is the main disadvantage of this synthetic method.

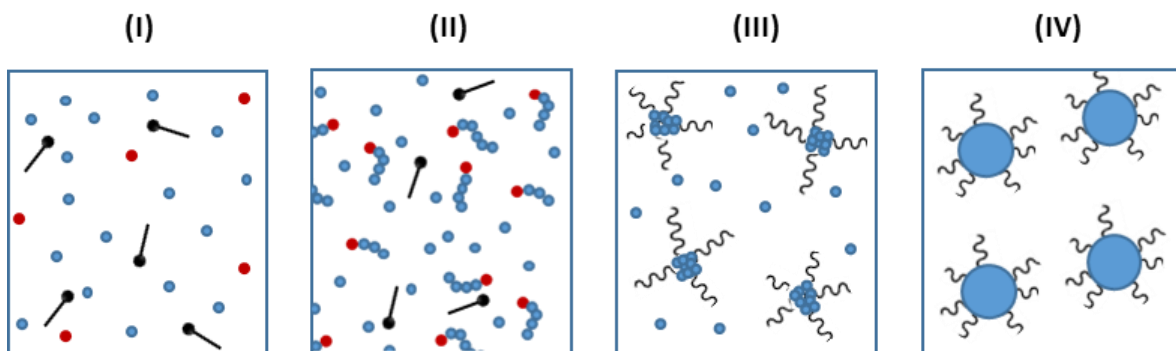


Figure 5 - Scheme showing the dispersion polymerisation mechanism. (I) The reaction begins with a homogeneous mixture of monomer (blue), initiator (red), and stabiliser (black) in the solvent; (II) Then polymeric chains start to grow until the J_{crit} is achieved. (III) As polymer chains precipitate, the stabiliser adsorbs onto the polymer creating nuclei and preventing agglomeration. (IV) Once the stabiliser is exhausted, further monomer and small chains diffuse into the nuclei and the particles grow until reaction is completed.

1.2.2.4.1. Stabilisation mechanism in dispersion polymerisation

Tseng *et al.* described qualitatively the particle formation and growth in dispersion polymerisation.¹³ According to their work, free radicals are generated and grow in the continuous phase until they attained a sufficiently high DP to precipitate, *i.e.*, J_{crit} , but once the nuclei are formed, polymerisation mainly takes place within the monomer swollen particles until all monomer is consumed.

Many groups investigated the stabilisation mechanism in dispersion polymerisation. There are usually two types of stabilisation considered: steric stabilisation and chemical anchoring of stabiliser *via* graft copolymers. Paine *et al.* developed a kinetic model for aggregation of precipitated oligomers or unstabilised particles in dispersion polymerisation.¹⁴ They investigated effects upon size, size distribution and chain molecular weight of the particles prepared in alcoholic media. It was assumed that the particle aggregation was controlled only by Brownian diffusion, and no steric stabilisation was considered. Therefore, stabilisation

would be a result of grafted copolymer stabiliser produced by the reaction of a polymer radical with a stabiliser molecule. It was assumed that when the particle surface was completely covered with the graft-stabiliser, the particles could no longer aggregate with each other.¹⁴ Thus, the radius of gyration of the stabilising chain in the solvent was used to calculate the amount of stabiliser necessary to cover the particle surface effectively.

Yasuda *et al.* demonstrated the importance of stirring rate for stabilisation in dispersed systems, by considering the particles aggregate with each other not only by the Brownian diffusion, but also by the shear stress of the fluid.¹⁵ Their model predictions of the particle concentration under various monomer concentrations and stirring speeds agreed well with the experimental data. They observed that at early stages the rate of particle aggregation is mainly caused by diffusion, because of the large number of small particles. Later, the shear stress of the fluid becomes dominant. The aggregation of particles increases with stirring speed, due to shear stress, while the radical absorption rate decreases, with polymerisation taking place mainly at the continuous phase at early reaction stages.¹⁵ Particle concentration then decreases until the required amount of graft stabiliser copolymer is attained, after which no aggregation occurs and the number of particles remains constant.

It was also found that monomer concentration could affect dispersion because of the solvency of the growing polymer chains delaying nucleation.¹⁵ The initiator concentration also impacts particle size, as a result of polymer molecular weight reduction, which impacts on the formation of graft copolymer stabiliser.¹⁴ By changing the reaction conditions, such as monomer and stabiliser concentration, the average particle size can be manipulated.

Wang *et al.* investigated the mechanisms of nucleation and stabilisation involved in the seeded dispersion polymerizations of n-butyl acrylate (BA) and styrene.¹⁶ They defined that nucleation can occur by a number of mechanisms including self-nucleation, aggregative nucleation, micellar nucleation (if micelles are present in the system) and coagulative nucleation (Figure 6). The stabiliser could act by forming micelles, adsorbing directly onto particles or forming a graft-stabiliser that then adsorbs to the particles with the insoluble block acting as an anchor. This study makes it evident that dispersion polymerisation is a complex process and many parameters will influence the formation of particles.

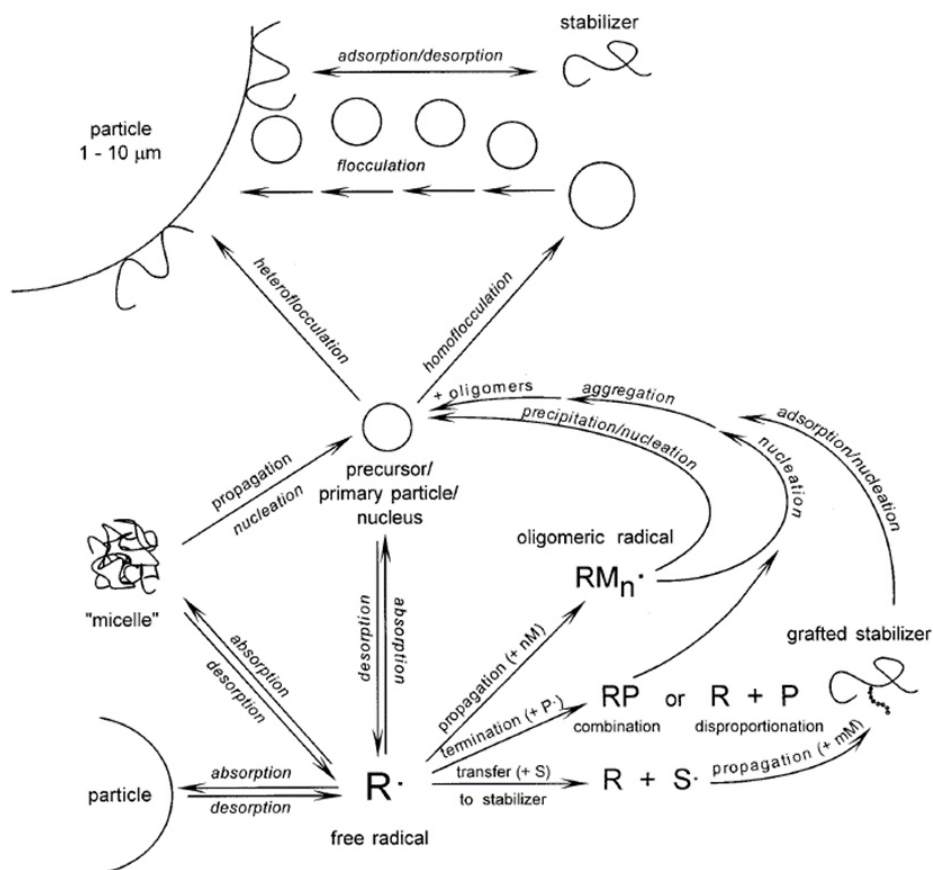


Figure 6 – Scheme of the complex mechanisms involved in particle formation via conventional radical dispersion polymerisations. Figure adapted from Wang et al.¹⁶

1.3. Chain growth polymerisation mechanisms

In this thesis, chain growth is the sole mechanism of polymerisation used, with two main processes: conventional and controlled radical polymerisation. The mechanisms operating in these polymerisations are detailed next.

1.3.1. Conventional radical polymerisation

Conventional radical polymerisation is suitable for several polymerisation conditions, including bulk, solution and dispersion. This type of reaction involves three fundamental steps: initiation, propagation and termination.¹⁷

In a conventional radical polymerisation, an initiator fragments into primary radical species that will react with the monomer, starting a chain reaction. Radical fragmentation can occur through several mechanisms (e.g. thermal, redox and light activated).¹⁸ However, thermal decomposition is the most widely adopted in both research and industry.¹⁹ In this thesis, 2,2-azobis(isobutyronitrile) (AIBN) was the thermal initiator of choice, due to its wide spread use.

The C-N linkage of AIBN undergoes thermolysis at relatively low temperatures, generating two isobutyronitrile radicals and a stable nitrogen molecule (Figure 7).

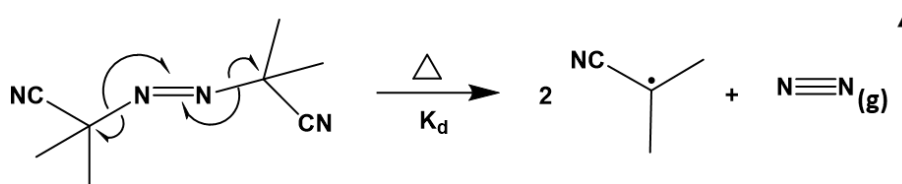


Figure 7 – Scheme showing the 2-azobis(isobutyronitrile) (AIBN) decomposition.

The polymerisation is initiated by addition of the primary radicals formed upon initiator decomposition to the monomer vinyl group. Propagation then occurs by the sequential addition of monomer to the generated radical end groups, transferring each time the active radical site to the end of the new chain (P^*). The active chain end allows the chain to grow by further addition of monomer, and the propagation stops only when the radical active site is destroyed through termination. Termination can occur by combination of two radicals or by proton abstraction from one propagating chain to another, *i.e.*, disproportionation (Figure 8).⁵

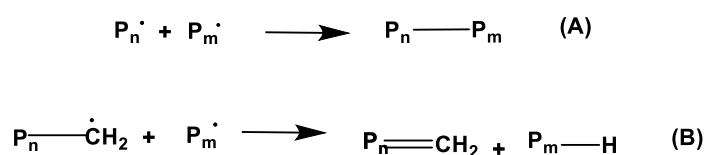


Figure 8 - Termination mechanisms for conventional radical polymerisation. (A) combination, where two radicals form a neutral chain. (B) Disproportionation, where a radical abstracts a hydrogen atom from another radical species forming two species with no active site.

Conventional radical polymerisation undergoes rapid termination. On average, a growing chain terminates within 5-10 seconds from initiation,²⁰ which means that chains are not simultaneously active throughout the reaction. The M_n of chains formed at the reaction start will be higher than at the end, since the availability of the monomer is reduced over time, this thus leads to a high \bar{D} .

It is important to mention that a propagating radical can also participate in abstraction reactions with the monomer, polymer, solvent, an impurity or a chain transfer agent, resulting in growth deactivation. This type of reaction is called chain transfer,¹⁷ which by definition is the reaction of a propagating radical with a non-radical substrate to produce a dead polymer

chain and a new radical capable of initiating a polymer chain.²¹ The occurrence of chain-transfer in conventional free-radical polymerisation was first discussed by Flory.²²

There are two main mechanisms of chain transfer: atom or group transfer and addition-fragmentation. In addition-fragmentation chain transfer, the rate constant for chain transfer (K_{tr}) is given by the rate constant for addition (K_{add}) and a partition coefficient (ϕ) of the adduct between product and reactants (Equation (5)).

$$K_{tr} = K_{add} \phi \quad (5)$$

The transfer constant (C_{tr}) is defined by dividing K_{tr} by the rate or propagation (K_p) (Equation (6)).¹⁹

$$C_{tr} = \frac{K_{tr}}{K_p} \quad (6)$$

The Mayo method is a known method to calculate the C_{tr} .²³ However, it does not require measuring K_{tr} and K_p , instead it can be calculated by measuring M_n in a series of reactions where the ratio between the monomer and the compound suspected of chain transfer (S) (e.g., an impurity) is changed.

The Mayo method is however restricted to systems where there is virtually no drift in the concentration ratio of monomer and S, thus it can only be applied at low monomer conversions (<5%) and if $C_{tr} < 1$. The Smith method has addressed this restrictions by plotting the change of monomer concentration and S in a log scale as function of monomer conversion.²⁴ In this method the slope of the plot gives the C_{tr} , but it does not correlate M_n to the obtained C_{tr} . More recently, Donald and Bon reported a new method to determining C_{tr} , especially when its value is thought to be greater than 1.²⁵ They used the analytical concentration ratio of S to monomer at reaction start and monomer conversion data, in combination with the cumulative molecular weight distributions as input.

The occurrence of chain transfer may however not be undesirable, as chain transfer agents can be used to control the polymers molecular weights and this was explored for controlled radical polymerisation, as will be discussed next.

1.3.2. Controlled radical polymerisation

Although free radical polymerization afford to produce a vast range of polymers of different nature, it does not allow precisely control of the molecular weight nor the chain end functionality, mainly because of termination reaction that are inherent to any free radical process. As the termination reaction can take place at any time throughout the polymerisation, the polymer chains will stop growing at different molecular weights and the final product will have a broad distribution of molecular weights.¹

The demand for well controlled polymeric materials with complex/well defined architectures, *e.g.*, for application in nanotechnology, drug delivery and other highly functional materials,²⁶⁻²⁸ led to the advent of reversible-deactivation radical polymerisation (RDRP), which was first introduced by Otsu *et al.* in 1982 and brought a revolution in the field of radical polymerisation.²⁹ With RDRP it was possible to obtain a low \bar{D} and target a given M_n . RDRP has been extensively investigated since then, with several reviews describing the state of the art.³⁰⁻³⁴ RDRP is based on radical polymerisation, enabling control over polymers molecular weight, molecular weight distribution and architecture while retaining the same versatility of conventional radical polymerisation. As a result, a vast range of monomers is accessible by RDRP, and a vast array of suitable reaction conditions can be used. An additional advantage of RDRP is the presence of dormant active sites at polymer chain ends, which can be reactivated enabling polymer extension. This allows the design of copolymers of diverse architectures, *e.g.*, block, stars, etc.^{18, 35}

It is important to define two terms frequently used in the literature when dealing with RDRP: livingness and control. Livingness refers to the number fraction of dormant chains that can be extended by further monomer addition, while control refers to the M_n linear increase with conversion and ideally with a low \bar{D} that decreases with conversion.^{9, 11} While control over molecular weight and molecular weight distribution can be determined by kinetic studies, livingness is difficult to assess. It can be investigated directly for low molecular weight polymer *via* matrix assisted laser desorption ionisation time-of-flight mass spectrometry (MALDI-TOF), or indirectly through chain extension of the polymer synthesised *via* RDRP.⁹

There has been plenty of discussion regarding the right terminology to be used for RDRP.^{36, 37} Although IUPAC does not recommend calling a polymerisation 'controlled' or 'living', these

are common terms broadly used in the relevant literature. A true living polymerisation refers to a polymerisation with zero termination events, which is not an achievable goal. In reality, thus, although ‘controlled’ polymerisations can successfully minimize termination, termination will unavoidably always occur as mentioned above.

RDRP is achieved by favouring propagation over termination events *via* a dynamic equilibrium between the propagating radicals, which are active species, and the dormant species (Figure 9).¹⁸ This is normally achieved by adding a controlling agent. The increased number of chains in RDRP compared to conventional radical polymerisation creates a decrease on the rate of termination per chain.³⁸

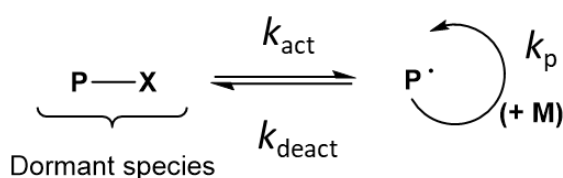


Figure 9 – Scheme of a generic RDRP, showing the equilibrium between an active propagating radical (P·) and dormant species (P-X), where X is a controlling agent, k_{act} is the rate of activation, k_{deact} the rate of deactivation, k_p , the rate of propagation and M the monomer.

The following are the typical features of a RDRP:^{39, 40}

- Linear evolution of molecular weight (M_n) with respect to conversion, as a result of all chains initiating only from the desired initiating species, which are kept at constant concentration throughout the reaction.
- Control over molecular weight, with M_n close to a given targeted molecular weight ($M_{n,\text{tgt}}$).
- Control over molecular weight distribution, with low \mathcal{D} values.
- Dispersity (\mathcal{D}) decreases with an increase in conversion. This is true in stems that have fast initiation and slow exchange of active species.

The main factor determining the \mathcal{D} of the system is the rate of exchange between active and dormant states of the polymer chain. The lifetime of P· is in the scale of 1 s, while the activation-deactivation cycles of RDRP is usually in the range 0.1-10 ms.^{38, 41} A higher number of activation-deactivation cycles ensure most of the chains will have very similar molecular

weights. Nevertheless, it has been previously demonstrated that the system may have high livingness, even if control over molecular weight distribution is poor.⁴²

In general, it is more difficult to obtain a successful RDRP when targeting high DPs, *e.g.*, 100 kg mol⁻¹, as result of the number of chain reduction, which increases the termination rate (k_t) per chain. This is because, the probability of termination or side reactions increases with the time a propagating chain remains active.¹⁸

Generally, RDRP is characterised by a linear semi-logarithmic kinetic plot of the monomer conversion ($\ln([M]_0/[M])$), versus time, where $[M]_0$ is the monomer concentration at the start of reaction and $[M]$ the monomer concentration at a given time. This is because of the constant concentration of the active propagating species, indicating first-order kinetics with respect to the monomer, *i.e.*, pseudo first-order kinetics. However, according to Goto and Fukuda, a linear $\ln [M]_0/[M]$ against time is not criterion for control/livingness.⁴³ There are cases where RDRP does not give such a plot, while “non-living polymerisation” can follow a pseudo-first order kinetics.^{9, 11} Therefore, it is more convenient to evaluate control/livingness by \bar{D} and the M_n linear evolution with conversion.

Two main mechanisms can be used in order to achieve RDRP: persistent radical effect (PRE)⁴⁴ or degenerative transfer. PRE is the mechanism used in two well-established RDRP techniques: nitroxide-mediated polymerisation (NMP) and atom transfer radical polymerisation (ATRP). Control in NMP is obtained through the dynamic equilibrium between an alkoxyamine and an actively propagating polymer chain. On the other hand, ATRP employs a redox active catalyst, usually a copper complex, to reversibly transfer an atom or group to the polymer growing chain, establishing a reversible termination equilibrium.³⁰ The PRE mechanism refers to an increase in the number of controlling agent compared to the number of propagating radicals as result of a small amount of coupling reactions at the reaction start, $t \ll 1s$. It shifts the equilibrium towards the dormant species and achieves a steady state of growing radicals through the activation-deactivation process.⁴⁵

On the other hand, the most used RDRP technique based on degenerative transfer mechanism is the reversible addition-fragmentation chain transfer (RAFT).^{33, 34, 46, 47} Although there are other reported techniques, such as iodine-transfer polymerisation (ITP)⁴⁸ and tellurium-mediated radical polymerisation (TERP),⁴⁹ RAFT is the most versatile and thus most

reported technique. RAFT is the main RDRP technique to be used in this thesis and it will be discussed in detail in the following section.

1.3.3. RAFT polymerisation

RAFT is a well-established, robust and versatile RDRP technique. When successfully implemented, it fulfils all requirements and presents all the characteristics of a RDRP, while offering the same versatility of conventional radical polymerisation. RAFT can be applied to a range of different monomer/initiator functionalities and can tolerate low levels of oxygen.^{33,}

³⁴ The reaction conditions for RAFT polymerisation are very similar to those of conventional radical polymerisation, with the addition of a chain transfer agent (CTA), which is typically a thiocarbonylthio species ($ZC(=S)S-R$).^{50, 51} RDRP using thiocarbonylthio CTA was first published in 1998 by Moad and co-workers.⁴⁴

The RAFT mechanism can be divided in five main steps (Figure 10):

(1) Initiation, in which the initiator generates primary radicals that react with monomers creating a propagating macromolecular radical.

(2) Pre-equilibrium, in which a growing polymer chain adds to the CTA to form a CTA intermediate (dormant species), which then fragments to give a radical reinitiating species (R^*) and a macromolecular CTA (macro-CTA).

(3) Re-initiation, in which the R^* adds to the monomer forming a new propagating polymer chain (P_m^*).

(4) Main equilibrium, which is established between the addition and fragmentation of propagating polymer chains (P_m^* and P_n^*) from a two arms adduct macro-CTA, *i.e.*, intermediate.

(5) Termination, which occurs by combination of radicals or by disproportionation to give a dead polymer.

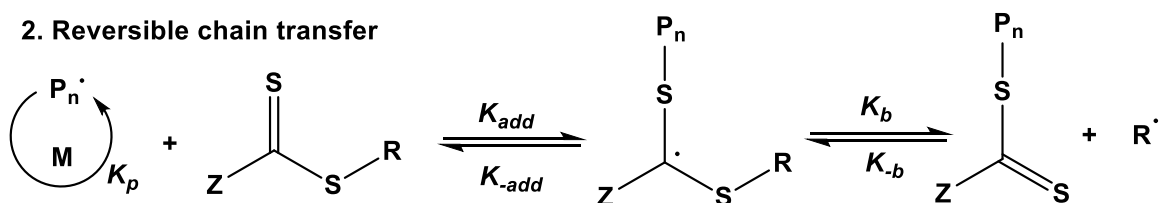
A key factor for the success of the RAFT process is a fast addition-fragmentation equilibrium, *i.e.*, higher number of activation-deactivation cycles compared to the rate of propagation (R_p), in a way that no more than one monomer unit is added to the propagating species per

activation cycle.¹⁸ This guarantees that all chains will always have a similar DP and therefore a low \mathcal{D} . However, as for other RDRP mechanisms, the higher the DP targeted, the harder it is to obtain good control. RAFT is usually successful when targeting M_n between 1-100 kg mol⁻¹.

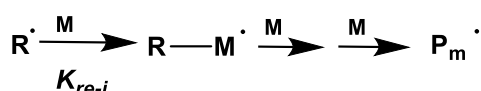
1. Initiation



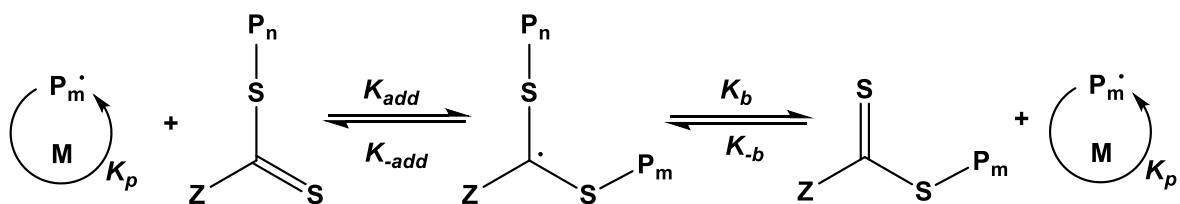
2. Reversible chain transfer



3. Reinitiation



4. Chain equilibration



5. Termination



Figure 10 - RAFT polymerisation mechanism. First, during initiation, the initiator (I) generates radicals through a thermal, redox or photochemical process, which react with the monomer (M) creating the propagating polymer radical (P_n^\cdot). At step 2, chain transfer of the growing polymer chain to the CTA forms a thiocarbonylthio terminated polymer and a reinitiating species (R^\cdot). At step 3, the R^\cdot group adds monomer units forming a new propagating polymer chain. At step 4, the equilibrium between propagating and dormant RAFT terminated polymer chain is established, where P_m is a second chain of length m . Step 5 shows irreversible termination occurring between 2 propagating chains.

It is important to notice the presence of an initiator in stage (1) of the RAFT mechanism (Figure 10). Systems operating according to the PRE, such as NMP and ATRP, are based on the

reversible deactivation of propagating radicals, where the dormant species also works as initiator and is constantly generating radicals.³² However, in RAFT the deactivation-activation equilibrium is dictated by chain transfer, therefore the number of radicals during the reaction remains constant and an external source of radical is required to start the reaction.³² As a result, the rate of polymerisation for RAFT is expected to be $\frac{1}{2}$ order with respect to the initiator concentration and independent of the CTA concentration.³² In addition, the number of radicals generated by the initiator will dictate the number of dead chains formed at the end of the reaction. If the initiator concentration is low enough, the number of chains is equal to the number of CTA molecules and the majority of chains will have the same M_n and the same structure ($P_n-S-C(=S)-Z$). Therefore, the initiator concentration must be high enough to give an acceptable rate of polymerisation, *i.e.*, reaction speed, but low enough for maintaining good livingness, *i.e.*, reducing the quantity of dead chains. A typical CTA : initiator ratio is between 5 to 10.¹⁸

As bimolecular termination in RAFT does not lead to loss of a living chain end, the number of chains with the CTA moiety remains the same throughout the reaction. The product of a RAFT polymerisation is thus a mixture of living chains with CTA chain ends, and dead chains (Figure 11). The dead chains can have an initiator-fragment end group or an R end group depending on the source of the radical that initiated the chain.

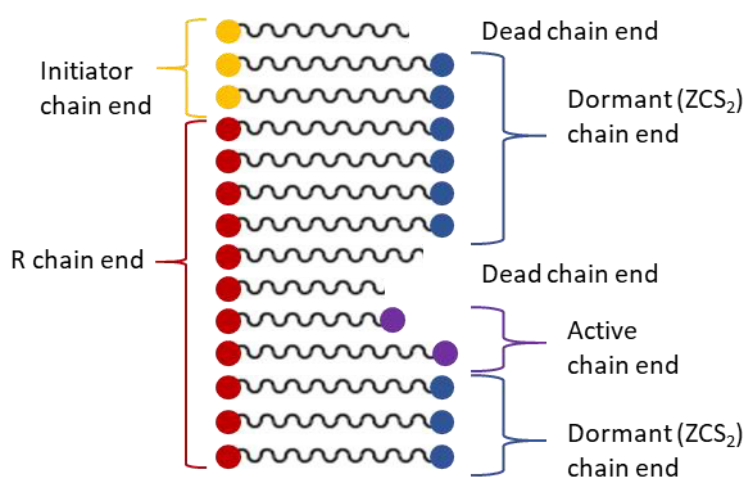


Figure 11 – Scheme showing the distribution of possible polymer chain ends in a RAFT polymerisation, with the active chain ends (purple), CTA's R chain ends (red), initiator-fragment chain end (yellow), dormant species with a CTA's Z group (blue) and dead polymer chain ends.

In an ideal RAFT process the relative number of chains with each end group can be predicted from the concentration of initiator, its decomposition rate and the number of CTA moieties.¹⁸

Thermal decomposition is the most used source of radicals for RAFT,⁴⁴ although there are reports of initiation *via* redox⁵² and UV irradiation.⁵³ In my work, AIBN is the chosen initiator for all reactions, which is usually a good choice for RAFT polymerisation of methacrylates, since the 2-cyano-2propyl radical is a good initiating group with respect to the propagating monomer.⁵⁴

Because of the controlled nature of RAFT polymerisation, the $M_{n,tgt}$ and the theoretical M_n ($M_{n,th}$) can be calculated. $M_{n,tgt}$ is given by the ratio of the initial monomer concentration ($[M]_0$) by the CTA concentration ($[CTA]_0$), plus the CTA molecular weight (M_{CTA}), since this will be attached to the polymer chain end (Equation (7)). The $M_{n,th}$ calculation must also take into consideration the reaction conversion (Equation (8)), where p is monomer conversion and M_M is the monomer molecular weight .

$$M_{n,tgt} = \left(\frac{[M]_0}{[CTA]_0} \right) + M_{CTA} \quad (7)$$

$$M_{n,th} = \left(\frac{[M]_0 p M_M}{[CTA]_0} \right) + M_{CTA} \quad (8)$$

If we consider that the polymer chain can be initiated by either the R^{*} fragment from the CTA or an initiator-fragment (Figure 101), the calculation becomes more complex. To account for the chains initiated by the initiator-fragment, we add an extra factor ($df([I]_0 - [I]_t)$), where d is the number of chains produced by termination, $d \approx 1.67$ for methyl methacrylate (MMA), f is the initiator efficiency and $[I]_0 - [I]_t$ is the concentration of initiator consumed until a time t (Equation (9)).³² Furthermore, the decomposition of the initiator can be determined by Equation (10), where k_d is the decomposition rate constant of the initiator in a particular solvent.

$$M_{n,th} = \left(\frac{[M]_0 p M_M}{[CTA]_0 + df([I]_0 - [I]_t)} \right) + M_{CTA} \quad (9)$$

$$[I]_0 - [I]_t = [I]_0 (1 - e^{-k_d t}) \quad (10)$$

Frequently the number of polymer chains derived from the initiator is negligible, in particular for high CTA: Initiator ratios, *e.g.*, 5-10. Thus, Equation (8) is more commonly used in the literature, and will be used in this thesis. It is however important to keep in mind that deviations can occur if the number of initiator derived chains becomes significant in the system.

1.3.3.1 Chain transfer agent selection

RAFT can control the polymerisation of a broad variety of monomers, covering most of the ones suitable for conventional radical polymerisation. Nevertheless, the choice of adequate CTA for a given monomer is fundamental to achieve good control over the polymerisation. The CTA is usually a thiocarbonylthio species ($ZC(=S)S-R$), with a Z group, which provides stabilisation, and an R group, also known as the leaving group, which should fragment and reinitiate a new growing chain. The different CTAs can be classified according to their Z group substituent into xanthates,^{55, 56} dithioesters,⁴⁴ dithiocarbamates^{57, 58} and trithiocarbonates⁵⁹ (Figure 12).

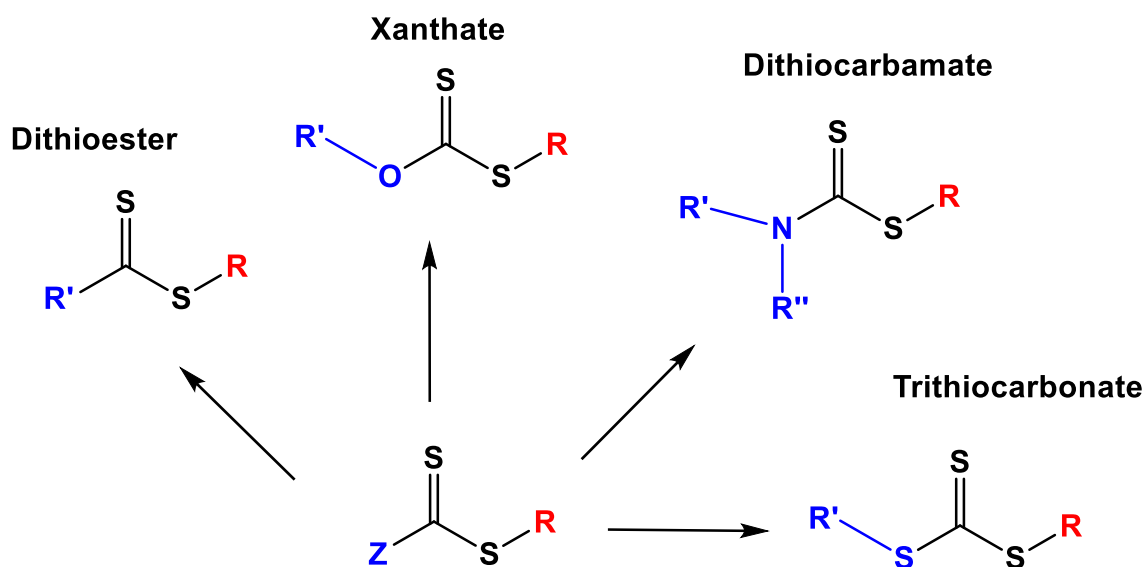


Figure 12 - Schematics showing the classes of CTA according to their Z groups (in blue) as derived from a generic thiocarbonylthio ($ZC(=S)S-R$).

When choosing the CTA for a given monomer, one must consider the balance between the chain transfer rate of the CTA and the propagation rate of the monomer. In an optimum RAFT polymerisation, the chain transfer rate must be higher than the propagation rate, thus the chain transfer constant (C_{tr}), which can range from below 10^{-2} to above 10^3 ,³² must have a value greater than unity. With that aim, it is important to ensure that the C=S bond is more reactive towards radical addition than the vinyl group of the monomer. Therefore, the CTA must have a high addition rate constant (k_{add}). The Z-group is mainly responsible for C=S activation (Figure 13) and the stabilisation of the intermediate radical,²⁰ but it should not stabilise the intermediate radical too strongly, otherwise the fragmentation step in the pre-equilibrium (Figure 10–(2)) will be unfavourable, which can cause inhibition.⁶⁰

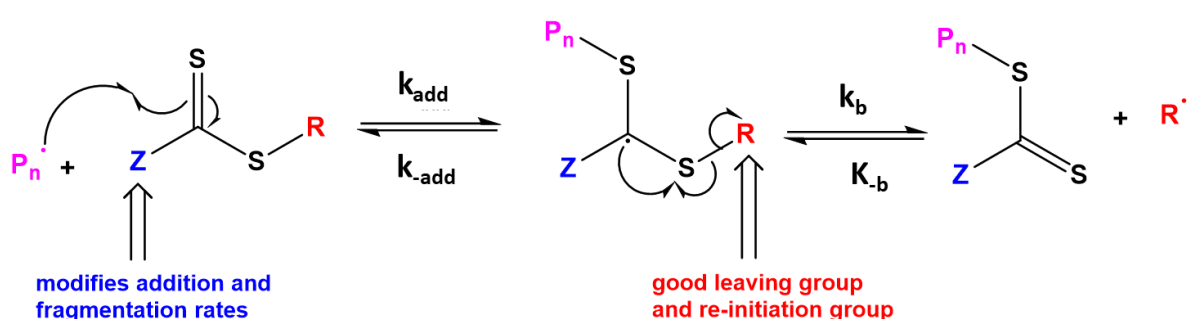


Figure 13 - Schematics showing the CTA structure and effect of R and Z groups on the addition rate (k_{add}) to the thiocarbonylthio group and on the fragmentation rate (k_b) of R from the intermediate radical, in order to form a R^\bullet re-initiation group. P_n^\bullet is a monomer derived radical of n units.

Vinyl monomers are usually divided into two main categories: 'more activated' monomers (MAMs), which have the double bond conjugated to an aromatic ring, a carbonyl group or a nitrile group, and 'less activated' monomers (LAMs), which have the double bond adjacent to saturated carbon, a heteroatom of a heteroaromatic ring, or an oxygen or nitrogen lone pair.³⁴ Examples of MAMs include (meth)acrylates, (meth)acrylamides and styrene (St). Because of the electronic stabilisation of their substituents, MAMs produce more stabilised radicals.³³ Therefore, MAMs require CTAs with a Z group that favours stabilisation to make addition to the C=S bond more favourable. A high addition rate is attained with trithiocarbonate and dithioester with an alkyl or aryl Z group, thus those are the preferred CTAs for MAMs polymerisation.^{18, 32}

Benaglia *et al.* studied the effects of electron withdrawing and electron donating Z groups into a series of dithiobenzoates for MMA polymerisation.⁶¹ They found that electron-withdrawing substituents enhance the rate of addition to the C=S, providing low \bar{D} from the start of the reaction, while the opposite behaviour was noticed when electron-donating substituents were added.

Radicals originating from LAMs, *e.g.*, vinyl acetate (VAc), *N*-vinylpyrrolidone (NVP), *N*-vinylcarbazole (NVC), are poorly stabilised and thus a more activated CTA would act as a radical sink, as a result of the higher stability of the intermediate radical, and inhibit polymerisation. When Z groups are attached *via* an oxygen or nitrogen atom, the free electron pair will result in the delocalisation of electron density throughout the C=S bond and thus lower its double bond activity, making it less susceptible to the addition of the radicals, *i.e.*, lower the k_{add} .⁵¹ Therefore, xanthates (Z= O-alkyl) and dithiocarbamates (Z= N-alkyl) are more adequate CTAs for LAMs that lead to more reactive radicals. The choice of R group is critical because most monomers in this class have a high k_p ($>10^3 \text{ M}^{-1}\text{s}^{-1}$).²⁰

The R group has a more complex role. As the Z- group, it has an influence over the C=S bond activation, particularly for trithiocarbonates, which have thiocarbonyl R- and Z- groups. The R group also determines the rate of fragmentation (k_b) of the CTA and is responsible for re-initiating propagation (Figure 13).^{60,62} Therefore, the R group must be a good homolytic group relative to the attacking radical P_n^\bullet and be capable of rapidly reinitiating propagation, in order to give a narrow molecular weight distribution. An R group ability to leave can be determined by steric factors, radical stability and polar factors. R groups that are sterically bulky or that enhance the thiocarbonylthio sulfur electrophilicity will increase its homolytic ability.^{60,62} The choice of R group is particularly important for methacrylate polymerisations, with tertiary cyanoalkyl and cumyl groups as the most effective.

It is important to emphasise that an R group may be effective for one monomer but bad for another. Several guidelines define the best choice of CTA, according to their R and Z groups, for the polymerisation of a given monomer (Figure 14).⁶⁰

For example, the R group CH_2Ph is a poor leaving group with respect to the MMA propagating radical, although it is a good leaving group for acrylates and St. As a result, a CTA such as benzyl dithiobenzoate can appear almost inert towards MMA polymerisation.⁶² The R groups

that mimic monomer radicals or initiator radicals are usually assumed to be effective.¹⁸ However, it might not be ideal if the penultimate unit effect is relevant, *e.g.*, for methacrylates, in which case the P_n^* unit will be the preferential fragmenting group. The penultimate unit effect is particularly relevant for tertiary fragmenting R groups.⁶²

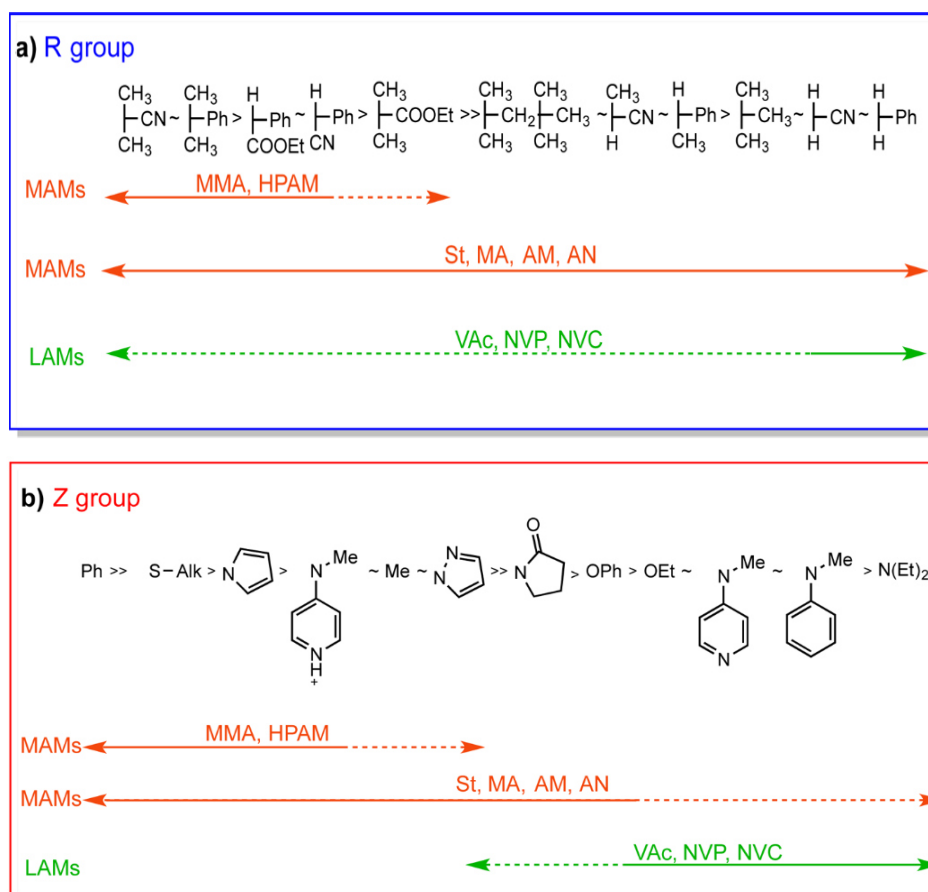


Figure 14 - Guidelines for selection of CTA for various monomers a) R group (Z-C(=S)S-R); Transfer coefficients C_{tr} and fragmentation rate decrease from left to right b) Z group (Z-C(=S)SR); Addition rates increase from left to right, and fragmentation rates decrease from left to right. A dashed line indicates partial control. Figure adapted from Keddie et al.⁶⁰

CTAs can also cause inhibition or retardation, which are normally seen in solution/bulk polymerisation. Inhibition is commonly attributed to the pre-equilibrium, but retardation is not well understood, although usually blamed on the intermediate radical.^{54, 63} There are mainly two hypotheses for retardation; (i) slow fragmentation and (ii) intermediate radical termination (IRT). The first one proposes that fragmentation of the RAFT intermediate, which is formed on addition of a propagating chain, is too slow and is responsible for retardation. The latter one proposes that intermediates are consumed in radical-radical termination with

themselves or with other radical species. The occurrence of IRT has been demonstrated but the mechanism remains unclear and its relevance for retardation phenomenon is uncertain.⁵⁴

Independently from the origin of these effects, inhibition and retardation must be considered when designing a RAFT reaction. For instance, aromatic dithioester offer the best control over polymerisation of MAMs monomers, and are the most popular CTA choices for methacrylates and methacrylamides.⁵⁴ However, they are susceptible to hydrolysis and known to give retardation. Therefore, the more stable and yet effective trithiocarbonates can be used instead for polymerisation of MAMs.

The choice of macro-CTA is also fundamental for block copolymer synthesis and as in most RDRPs, the order of the monomer addition is key for good control.^{62, 64} The propagating radical of the first block must be a better homolytic group than the second block. Therefore, MMA must be polymerised before acrylate or styrene. To polymerise styrene or acrylates prior to MMA, the monomer must be starve-fed into the reactor.⁶⁵ Furthermore, the block copolymerisation of MAMs and LAMs is particularly challenging, since CTAs that are effective for MAMs polymerisation are often not suitable for polymerisation of LAMs and *vice versa*. Switchable CTAs offer an option for the synthesis of such block copolymers, *e.g.*, PMMA-*b*-PVAc,⁶⁶ PMA-*b*-PNVC⁶⁶ and PSt-*b*-PVAc.⁶⁷

1.4. RAFT dispersion polymerisation

Dispersion polymerisation has been applied with various RDRP techniques, RAFT being the most documented.⁹ Nevertheless, the transposition of RAFT polymerisation from homogeneous systems into a dispersed system is not straightforward, due to various mechanistic aspects, such as compartmentalisation, which is explained in next subsection.^{9, 11}

Another main issue for RAFT polymerisation compared to conventional radical polymerisation is the nucleation stage. In a conventional dispersion polymerisation, J_{crit} of an individual chain is reached in less than one second, but in RAFT, the M_n increases linearly with conversion and J_{crit} is in general achieved later. The prolonged nucleation stage affects the rate of polymerisation and particle formation. The reaction will take place simultaneously at continuous and dispersed phases for longer, reducing the reaction rate and control over M_n and \mathcal{D} , while increasing particle size distribution. These challenges were present in the dispersion polymerisation of styrene in ethanol, for which Winnik and Song gave a solution

through a two-stage polymerisation.⁶⁸ This worked by delaying the addition of CTA until after the nucleation was complete. The topic of two-stage polymerisation is discussed in more detail in Chapter 4.

1.4.1. Compartmentalisation

Compartmentalisation is the confinement of reactants to a very small space. This occurs because in heterogeneous systems the polymerisation mainly takes place in the formed *nuclei*/particles. Compartmentalisation effect can be divided into two types: segregation and confined space effects (Figure 15).^{9, 69} The confined space effect refers to two species located in the same particle reacting at a higher rate in a small particle than in a large particle, while the confined space effect refers to the impossibility of two species to react when they are isolated in different particles.^{9, 69} In general, compartmentalisation improves livingness due to less termination, because of segregation effect, but control can be better or worse compared to a homogeneous system. For compartmentalisation effect to be significant, the particles must be sufficiently small or the concentration of reactants must be sufficiently low, so that the concentration of reactants per particle is low.

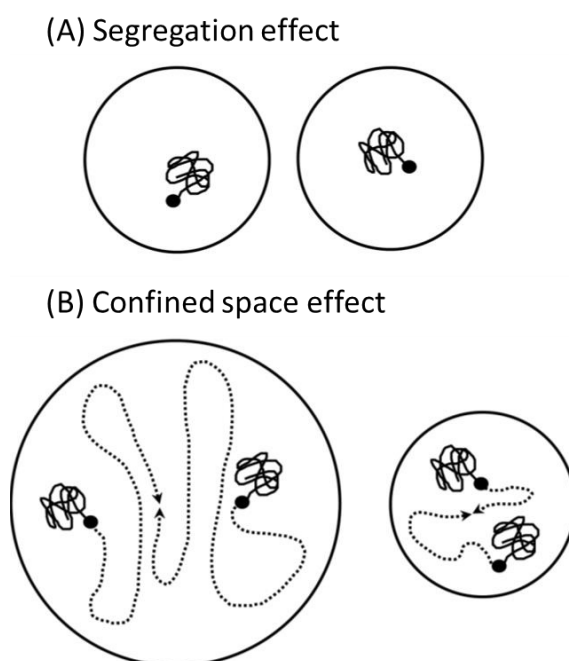


Figure 15 – Scheme showing the two types compartmentalisation effects: (A) the segregation effect and (B) the confined space effect. Figure adapted from Zetterlund et al.⁶⁹

Compartmentalisation in a conventional radical reaction can be better understood by the hypothetical case of each particle only having one radical (Figure 16A). Therefore, all the particles will be active and the polymer chain grows. However, if a second radical enters the particle, termination will occur and the particle is inactive. There is equal probability of a particle being active or inactive; as a result, the average number of radicals per particle is 0.5.⁹ Consequently, an increase in the number of particles will increase the number of active particles and give higher polymerisation rates. In addition, the lower the initiator concentration relative to particle number, the higher the molecular weight obtained, as the particle will be active for longer.

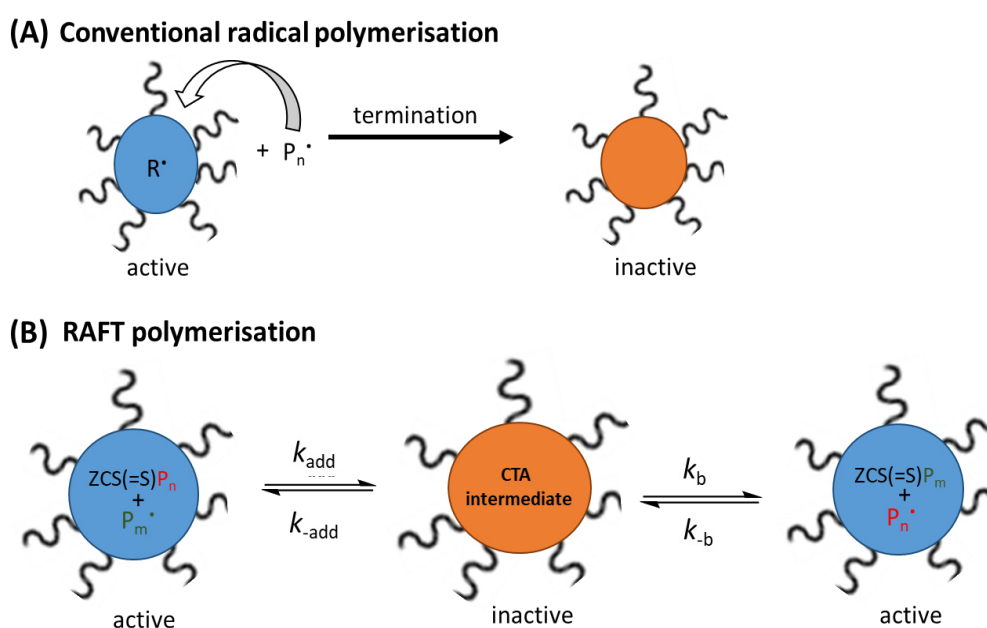


Figure 16 - Scheme showing the compartmentalisation in a dispersed system via (A) a conventional radical polymerisation and (B) a RAFT polymerisation. In (A), each particle that has one radical inside is an active particle, which means propagation happens within that particle. Once a radical (P_n^\bullet) enters the particle, it will cause termination and the particle will become inactive. (B) Each particle has one CTA. Once a propagating polymer chain P_m^\bullet adds to the active macro-CTA, it forms a CTA intermediate, which is inactive. After fragmentation, the active macro-CTA is restored and the radical fragment can diffuse to the continuous phase or propagate inside the particle, making it an active particle again.

In a RAFT polymerisation, this mechanism is slightly different. When a propagating radical adds into a macro-CTA or CTA, it forms a RAFT intermediate, which is a dormant species. Therefore, a particles containing only one radical will be inactive at times, due to the formation of dormant species (Figure 16B).⁹ This effect causes an increase in retardation

compared to homogeneous polymerisations, which is worse for CTAs with lower fragmentation rate coefficient. The IRT between a propagating radical and the CTA intermediate is considered instantaneous.⁹

In general, the compartmentalisation effect is only important if the particles are very small or the concentration of reactants is very small, hence it is more relevant for emulsion polymerisation than for dispersion polymerisation, and has a bigger impact for termination than for propagation.⁹ In addition, the confined effect generally does not affect RAFT, because the CTA concentration is too high for the reduction in particle size to affect its distribution.¹¹ Therefore, segregation is the dominant effect in RAFT dispersion polymerisation, with the influence of a number of factors, including RAFT-induced exit of species from the particles, chain-length dependent termination and monomer concentration variation.¹¹

The diffusion of species between the continuous phase and the particles is very important in RAFT polymerisation conducted in dispersed phase. It takes longer for a radical to grow to a high M_n polymer *via* RAFT than by conventional radical polymerisation, because of the activation-deactivation equilibrium. In this way, in a RAFT polymerisation in dispersed system, the entered radical may exit prior to reaching a M_n high enough to make it solvophobic, *i.e.*, the oligomer M_n is below J_{crit} .⁹

Prescott *et al.*⁷⁰ and Peklak and Buttle⁷¹ found that in dispersed RAFT polymerisation an additional retardation occurs as result of RAFT-induced exit. This occurs because CTA leaving groups below J_{crit} can diffuse out of the particle and re-initiate in the continuous phase, but once M_n is above J_{crit} , the CTA leaving group is confined to the particles. This effect of RAFT-induced exit is particularly strong for more solvent-philic and low molecular weight CTAs with high C_{tr} .⁹ In fact, no reaction disruption was observed for the emulsion RAFT polymerisation using xanthates.^{72, 73} This was attributed to the low C_{tr} of xanthates, which allowed the chains to grow to a higher M_n prior to adding to the CTA, resulting faster in oligomers above J_{crit} and avoiding the exit of the active oligomer.

Regarding termination, the rate of termination increases with decreasing particle size because the probability of an entering radical to add onto another radical instead of adding onto a CTA dormant species is increased in a smaller particle.⁹ As termination is diffusion controlled, k_t is chain-length dependent.⁹ As conversion increases, the dormant species

becomes longer and the radical chains too, resulting in terminations. Therefore, the RAFT system will deviate from the zero-one behaviour, *i.e.*, active-inactive behaviour, at high conversions.¹¹ Another simulation study reported that k_t increases in dispersed RAFT polymerisation as a result of chain-length dependent termination, and not just as a function of the particle volume.⁷⁴

In order to overcome some of the detrimental effects of dispersed systems, particularly regarding the nucleation stage and particle size distribution, most reported RAFT polymerisations in dispersion media using low molecular weight CTA make use of the two-stage polymerisation proposed by Winnik and Song.⁷⁵⁻⁷⁷ However, in the last decades, there was a lot of focus on the use of macro-CTAs for heterogeneous polymerisations.^{78, 79} This approach was coined polymerisation-induced self-assembly (PISA) and is discussed further in the following section.

1.5. Polymerisation-induced self-assembly

PISA is a surfactant-free polymerisation based on self-assembly of amphiphilic block copolymers formed *in situ*, which was first reported by Ferguson *et al.*⁸⁰ In this technique, a solvophilic macro-CTA is extended with a solvophobic monomer to form an amphiphilic block copolymer, which spontaneously self-assembles as the chains grow. PISA can be done *via* emulsion, which was mostly reported in water, or dispersion polymerisation, which was reported in different solvents, including water, toluene and methanol.^{11, 79, 81, 82} This section will give an overview on PISA, which will be discussed more in depth in Chapter 3.

PISA has been mostly reported *via* RAFT polymerisation.⁷⁸ However, because RAFT requires an initiator, homopolymers of the solvophobic monomer can form, leading to nucleation. Homopolymerisation can result from high concentration of initiator, low transfer efficiency of the macro-CTA and/or low macro-CTA concentration.⁸

PISA in aqueous dispersion has been extensively studied, although, it is restricted to a limited number of water-soluble monomers, and has been mostly based on *N*-isopropylacrylamide (PNIPAM) and 2-hydroxypropyl methacrylate (HPMA).⁷⁸ Polymerisation in non-aqueous media has been less reported, with most solvent systems based on *n*-alkanes or alcohols. A lot of attention was given to PISA with St or benzyl methacrylate (BzMA) as the core forming block in alcoholic media.⁸³⁻⁸⁵ Other monomers, such as MMA, were explored for PISA in non-

polar solvents, but they were restricted to the patent literature, and it is not possible to define if it is as well-controlled as PISA with BzMA.⁷⁹

In PISA, the solvent favours only one block of the block copolymer, and as a result, it self-assembles into discrete nanoparticles. Under optimal conditions, PISA, either *via* emulsion polymerisation or dispersion polymerisation, can yield different particle morphologies such as cylinders, spheres and vesicles.^{82, 86} In that system, the packing parameter (p) dictates what morphologies are obtained by self-assembly. p can be calculated by Equation (11), where v is the hydrophobic segment volume, a_0 is the contact area of the hydrophilic group and l_c is the length of the hydrophobic group.⁸⁷

$$p = \frac{v}{a_0 l_c} \quad (11)$$

When $p < 1/3$, spheres are formed. When $1/3 < p < 1/2$, cylinders. At $1/2 < p < 1$, vesicles are formed. And when $p = 1$, planar lamellae are formed (Figure 17).⁸⁷

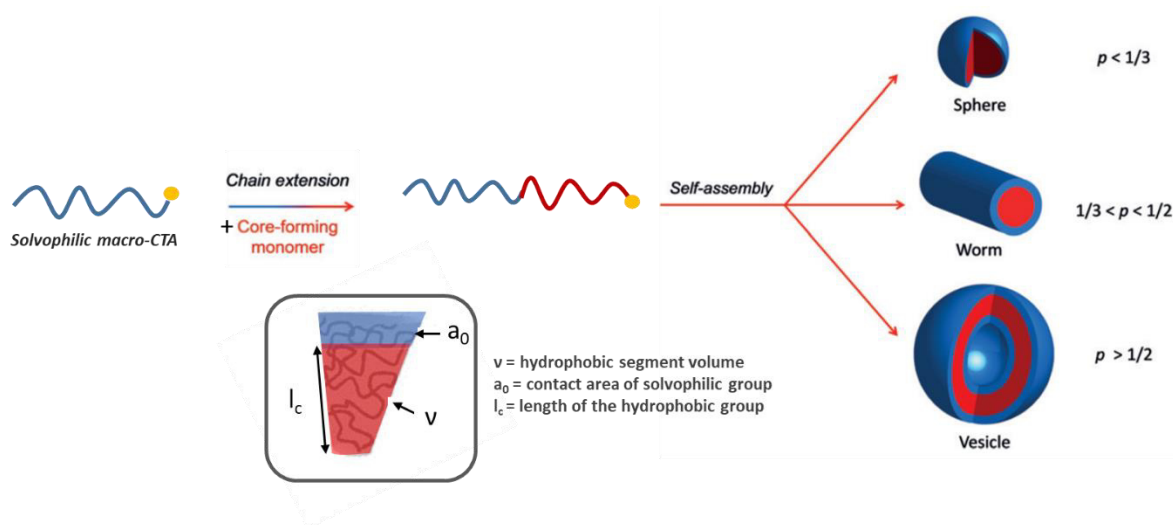


Figure 17 - Scheme of nano-assemblies of amphiphilic diblock copolymers in a selected solvent with relation to packing parameter (p). When $p < 1/3$, spheres are formed, when $1/3 < p < 1/2$, cylinders and when $p > 1/2$, vesicles are formed. A scheme of the micelle cut shows the hydrophobic segment volume (v), the contact area of the hydrophilic group (a_0) and the length of the hydrophobic group (l_c). Figure adapted from D'Agosto, Rieger and Lasalot.⁷⁸

Spherical micelles consist of a spherical core and a corona, and they are usually the first morphology formed. As the molecular weight of the solvophobic block increases, the core radius and the stretching of chains in the core increase.⁸⁷ As a result, entropy increases, and

eventually limits the growth of the sphere. To reduce total free energy of the system, the spherical micelles fuse with each other to form cylinders, reducing the stretching of the core. Cylindrical micelles, also called 'rods' or 'worms', are composed of a cylindrical core and a surrounding corona. This same process of releasing energy will cause the shape change from cylindrical micelles into lamellae or vesicles. Lamellae are flat or slightly curved bilayers, while vesicles are closed bilayers forming a hollow sphere.

The most common way to control morphology is to change the volume fraction of the solvophobic block by targeting different molecular weights. However, there has been some investigation into the influence of the hydrophilic segment over morphology transition.^{88, 89} Although these two examples focused in emulsion polymerisation, one must expect a similar effect in dispersion polymerisation by changing the molecular weight of the solvophilic segment.

PISA *via* dispersion in non-polar solvents has been less studied than in aqueous and alcoholic media. Charleux and co-workers reported the first PISA dispersion in iso-dodecane, polymerising methyl acrylate (MA) with a poly(2-ethylhexyl acrylate) (P2EHA) macro-CTA.⁹⁰ However, only spherical nanoparticles were obtained at high size dispersity. Later on, Fielding *et al.* reported a better control over morphology and molecular weight for the synthesis of poly(lauryl methacrylate-*b*-poly(benzyl methacrylate)) (PLMA-*b*-PBzMA) in n-heptane dispersion polymerisation.⁹¹

More recently Lopez-Oliva *et al.* studied PISA in n-heptane using polydimethylsiloxane (PDMS) as the stabilising block for BzMA dispersion polymerization.⁸¹ This study is presented in more details at Chapter 3, because of the potential use of PDMS as a solvophilic block in polymerisations in scCO₂.

1.6. Supercritical carbon dioxide

A supercritical fluid (SCF) is usually defined as the state of matter achieved for a substance above its critical temperature (T_c) and pressure (P_c) (Figure 18).⁹² However, SCFs can be better described by their density, and in this sense it would be better defined as a substance with temperature and pressure higher than their critical values, and which has a density close to or higher than its critical density.⁹³

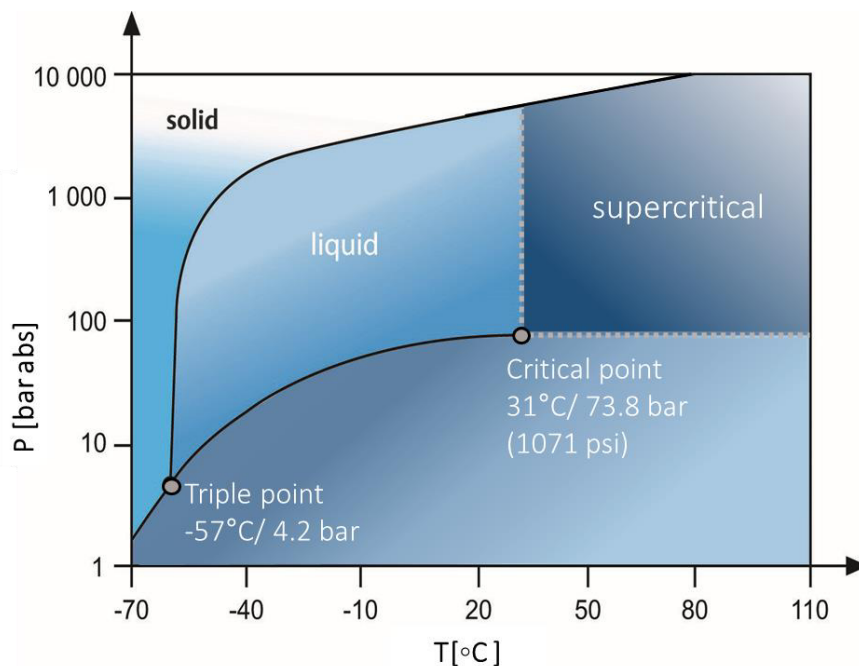


Figure 18 - Phase diagram of carbon dioxide showing the supercritical fluid region, which is above the critical point 31 °C and 73.8 bar. Figure adapted from Leitner et al.⁹⁹

Beyond the critical point, the liquid expands to form a single supercritical phase without undergoing a phase transition. SCFs have unique physicochemical properties, such as liquid-like density and gas-like diffusivity and viscosity, which results into a high mass transport capacity and a high diffusion coefficient.⁹⁴ Moreover, the solvation of SCFs can be easily tuned by altering their density, *i.e.*, varying temperature and pressure. This is possible, because density will alter the physical properties of the SCF, such as the coefficient of self-diffusion and the dielectric constant. In general, the probability of solute-solvent interactions increases with SCF density.⁹⁵

Supercritical carbon dioxide (scCO₂) is one of the most promising SCFs, since it has an easily attainable critical point of 31 °C and 73.8 bar, compared to other SCFs such as water (374 °C and 220.9 bar).⁹⁶ In addition, scCO₂ is nontoxic, non-flammable, and relatively inert.⁹⁶ Hence,

it emerged as a benign solvent for potential replacement of organic solvents.^{96,97} Additionally, CO₂ is inexpensive, highly abundant and can be easily recycled after used, avoiding greenhouse gas emissions.^{97,98} In fact, CO₂ can be sourced from waste streams, as it is a by-product of several industrial processes such as the combustion of fossil fuels and fermentation. Therefore, it is not surprising that scCO₂ has been investigated continuously in academia and industry since 1950. The most successful applications of scCO₂ are decaffeination from coffee beans, dry-cleaning and de-greasing.⁹⁹

scCO₂ has a low viscosity, almost one order of magnitude lower than typical solvents, *e.g.*, 10 times lower than water viscosity.⁹⁶ It also has high diffusivity, up to two orders of magnitude higher than for small molecules in typical solvents.⁹⁵ In addition, as CO₂ is a gas at ambient temperature and pressure, it can be easily removed from the reaction mixture by depressurisation. This avoids drying processes, which can be expensive and energy consuming, and it gives a final product free of solvent contamination while reducing waste generation.⁹⁷

However, there are disadvantages to the use of scCO₂, such as the requirement to use high-pressure equipment, which can be a concern for safety reasons. Another major disadvantage is the poor solvent power of scCO₂, in particular for large molecules. CO₂ has a zero permanent dipole moment and low dielectric constant ($\epsilon \approx 2$),⁹⁴ which is usually associated with low solvent power, in particular towards polar compounds.⁹⁶ However, it cannot be compared to other apolar solvents such as alkanes, because it possesses a large quadrupole moment. The small polarity resulting from this quadrupole reduces scCO₂ interactions with non-polar groups. It also makes it possible for scCO₂ to have various site-specific solvent-solute interactions, which determines its ability to dissolve certain solutes.⁹⁵

Polymerisation in scCO₂ gained lots of interest as an application of this SCF. There are several advantages of using scCO₂ for polymerisation and polymer processing. For instance, the absence of solvent contaminants in the final product makes scCO₂ a solvent suitable for several medical applications, such as biological tissue scaffolds and drug delivery.^{100,101} One of the greatest advantages, however, is the possibility to obtain dry polymer by simple depressurisation of the reactor at reaction completion.⁹⁷ In conventional polymerisation synthesis, removal of solvent after polymerisation brings a big energetic and cost burden.

Another important feature of scCO₂ is the plasticisation of polymers, which reduces glass transition temperature (T_g) and the degree of crystallinity.^{94, 97} This occurs because CO₂ is substantially soluble in most polymers, due to the high mobility of CO₂ molecules, which can then permeate the polymer phase and swell it, altering the morphology, physical and mechanical properties. The plasticisation of several polymers has been reported and reviewed, including polystyrene (PSt), polyurethanes, polycarbonates and polymethacrylates.¹⁰² The plasticisation, together with the high diffusivity and low viscosity, allows the removal of residual monomer and low molecular weight oligomers from the polymer, incorporation of additives, and formation of foams.^{95, 97} The unique properties of scCO₂ also offers opportunity to process advanced materials and to impregnate medical devices with drugs.⁹⁴

Goel and Beckman have studied the swelling of PMMA as a function of pressure *via* dielectric measurements and saw that plasticisation increases with pressure until it plateaus around 82 bar.¹⁰³ Since then, other groups studied extensively the swelling and sorption of CO₂ into PMMA films.¹⁰⁴⁻¹⁰⁶ Morbidelli and co-workers developed a system to measure simultaneously sorption and swelling of PMMA with CO₂, using a gravimetric apparatus to measure *in situ* the density of the fluid phase and by conventional visualisation technique for comparison.¹⁰⁴ They observed increasing swelling with pressure, up to 24.8% at 243 bar, which indicates how extensive is the swelling effect in scCO₂.¹⁰⁴

Furthermore, in heterogeneous polymerisations, plasticisation can facilitate diffusion of monomer and initiator into the polymer phase through the low viscosity and high diffusivity of scCO₂, overcoming problems of poor mass transfer and limiting the Trommsdorff effect.^{94, 97, 107} Increase of polymerisation rate in the highly plasticised polymer phase, as a result of enhanced diffusion of monomer, has also been reported.¹⁰⁸ Furthermore, scCO₂ also could offer a means to reduce polymer processing temperatures, due to the T_g drop, which can have applications for thermally sensitive materials.

1.7. Polymerisation in scCO₂

1.7.1. General Considerations

scCO₂ is inert towards radical reactions, therefore it is a suitable solvent for radical polymerisations.⁹⁶ However, only a few polymers can be synthesised *via* homogeneous

polymerisation, since most polymers are not soluble in scCO_2 . The most well-known soluble polymers are amorphous fluoropolymers and silicones.¹⁰⁹ In particular, amorphous fluoropolymers are poorly soluble in most common organic solvents, but are highly soluble in scCO_2 . Therefore, it offers a more environmental friendly solvent for amorphous fluoropolymers compared to chlorofluorocarbons (CFCs), which are restricted due to their negative environmental impacts.⁹⁷

DeSimone *et al.* investigated the solution polymerisation of fluoropolymers, such as 1,1-dihydroperfluorooctyl acrylate (FOA), and statistical copolymers of FOA with other hydrocarbon monomers.^{110, 111} Furthermore, DuPont Ltd. has commercialised the manufacturing of tetrafluoroethylene (Teflon) using scCO_2 as the solvent, although at present the synthesis is *via* precipitation polymerisation rather than solution polymerisation.⁹⁶

DeSimone *et al.* performed kinetic studies of the solution polymerisation of fluorinated monomers in scCO_2 with AIBN, and showed that the rate of decomposition (k_d) is 2.5 times lower in scCO_2 than in benzene.¹¹⁰ They also observed higher initiator efficiency (f) in scCO_2 , as a result of the lower viscosity of the SCF compared with conventional solvents, which decreases the solvent cage effect. The cage effect is the increased probability of recombination of a radical pair in solution compared to the gas phase (Figure 19). This occurs because a 'hole' in the solvent temporarily traps a pair of reactive molecules for a short period before they can separate through random motion.

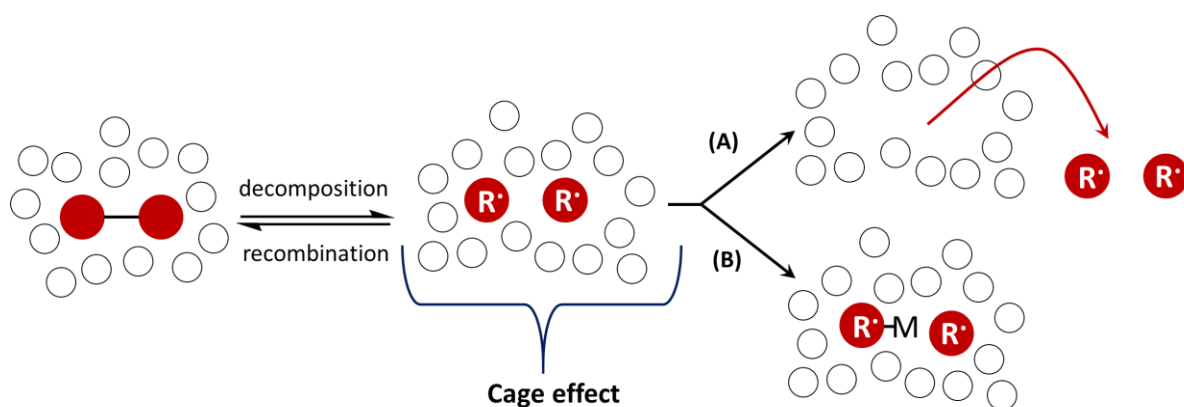


Figure 19 - Scheme showing the cage effect. An initiator can undergo decomposition into two radicals (red), which can then be trapped together by the solvent (white) into a hole, creating the cage effect. The radicals can recombine into the initiator molecule, escape the cage (A) or react within the cage (B) with for example a monomer molecule (M).

Czerwinski studied the efficiency of AIBN for MMA and NVP polymerisation in two different solvent systems, N-methyl-2-pyrrolidone (NMP) and methyl isobutyrate (MiB), and found that the viscosity increase of the solvent caused a stronger cage effect and consequently a decrease of f .¹¹² Therefore, in a solvent with lower viscosity, f is expected to increase.

Furthermore, Van Herk *et al.* identified that propagation rates (k_p) at the early stages, *i.e.*, when the reaction medium is still homogeneous, of St and MMA homopolymerisation in scCO₂ was close to the k_p of the bulk polymerisation of these monomers.¹¹³ These results further confirmed that scCO₂ does not interfere with the chain growth reaction and there is no chain transfer to solvent, which are important advantages.

The k_p of *n*-butyl acrylate and MMA in scCO₂ were further investigated by pulse laser polymerisation (PLP), however, propagation was found to be 40% lower than for the compared dilution in conventional solvents.¹¹⁴ This indicates a solvent effect, which was attributed to poor solvent quality for the polymer, which caused a reduction in the local monomer concentration near the radical chain ends and that reduced propagation. The increase in k_t was also demonstrated in scCO₂ compared to bulk polymerisation. This was attributed to the high diffusivity of scCO₂, since diffusion is beneficial for radical end groups to converge and termination to occur.¹¹⁵ However, the effects were dependent on the monomer being studied and cannot be generalised. For the case of MMA in 40% scCO₂, k_t increased mildly and was independent of monomer conversion, while for St, k_t was roughly one order of magnitude higher and not continuous throughout the reaction.¹¹⁵

Although there is still interest in the investigation of homogeneous polymerisation in scCO₂ of certain fluorinated monomers that require very extreme reaction conditions, *e.g.* poly(tetrafluoroethylene) (PTFE),^{116, 117} this does not apply to most polymers. Since the number of soluble polymers in scCO₂ is limited, research then focused on precipitation polymerisation, taking advantage of the high solubility of most monomers and low solubility of most polymers in scCO₂.⁹⁷

Precipitation polymerisation has the advantage of producing dry powder or solid product that can be easily recovered. Several polymers have been prepared *via* radical precipitation polymerisation, including polyethylene, poly(vinyl chloride) (PVC), PSt, poly(acrylic acid) (PAA) and PVAc.^{97, 102} Conventional radical precipitation polymerisation of acrylic acid in scCO₂

took advantage from a fast rate of reaction, allowing high molecular weight to be obtained.¹¹⁸ More recently, poly(2-hydroxyethyl methacrylate) (PHEMA)¹¹⁹ and poly(vinylidene fluoride) (PVDF)^{120, 121} were also prepared *via* precipitation polymerisation in scCO₂. The precipitation polymerisation of lactones in scCO₂ has also been investigated, due to the bioderived origin of the monomer and the biodegradable aliphatic polyesters produced.^{122, 123}

Although many monomers have been investigated for precipitation polymerisation and it is an interesting synthetic route for some materials, precipitation is not a suitable route for all polymers. For example, PAA precipitation *via* conventional radical polymerisation can achieve high conversion (> 90%) and high M_n , while MMA polymerisation only leads to low conversion (< 40%) and low M_n under the same synthetic route.¹¹⁸ Furthermore, precipitation usually leads to particle agglomerates with large size distributions or to non-descriptive morphologies.^{124, 125} Dispersion polymerisation in scCO₂ could resolve the existing issues with particle morphology, low yield and low molecular weight (Figure 20). However, the main challenge for dispersion polymerisations in scCO₂ is to find a highly CO₂-soluble and effective stabiliser. Dispersion polymerisation in scCO₂ is further discussed in the next section.

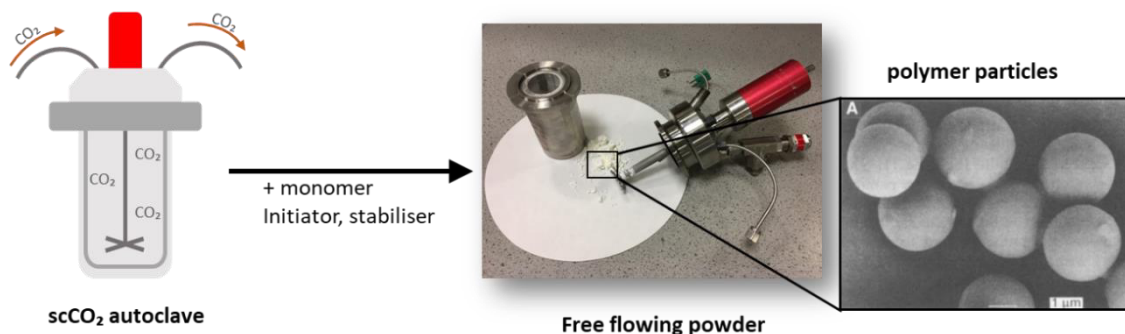


Figure 20 - Scheme showing a generic dispersion polymerisation in scCO₂, which gives a free-flowing powder, composed of well-defined polymer particles.

1.7.2. Dispersion polymerisation in scCO₂

As mentioned, a highly CO₂ soluble stabiliser is the key to a successful dispersion polymerisation. However, because of the poor solvent power of scCO₂, most polymers are poorly soluble in this SCF under mild conditions and are not suitable stabilisers. Because of their high solubility, fluorinated, silicone and polyester based polymers were first investigated as stabilisers.¹²⁶

It was noticeable that most of the polymers with reported good solubility in scCO₂ have electronegative groups, such as fluorine. Later, fluorination was found to enhance CO₂-philicity through specific interactions between the dipole of the C-F with the quadrupole of CO₂, which became the widely adopted theory.⁹⁶ In fact, Kazarian *et al.* investigated scCO₂ solute-solvent interactions *via* Fourier transform infrared (FT-IR) spectroscopy and demonstrated that the carbon of CO₂ acts as an electron acceptor, and therefore has specific Lewis acid-base interactions with polymers.¹²⁷

Some hydrocarbon-based polymers also present site-specific interactions, for instance PVAc present moderate solubility in scCO₂ as a result of Lewis acid-base interactions between its accessible carbonyl group and CO₂.¹²⁷ Silicones on the other hand have no electronegative groups or specific interaction. They are thought to dissolve because of their free rotation around Si-O, which results in a highly flexible backbone, low T_g and large free volume. Those characteristics reduce free energy of mixing, thus enhancing CO₂-solubility.¹⁰⁹

Beckman and co-workers proposed that in order to have good solubility in scCO₂ a polymer must have:¹²⁸

- (1) A flexible backbone;
- (2) A high free volume, hence a low T_g;
- (3) Groups that provide specific interactions with CO₂, such as a carbonyl group or a fluorine.

This guideline was then used as the strategy for the design of new low-cost sustainable stabilisers.

It is important to emphasise that scCO₂ is essentially a non-polar solvent and, therefore, steric stabilisers must be used, since charged colloids would provide no stabilisation. Steric stabilisers can be explained by entropic considerations. The stabiliser adsorbs or grafts at the polymer-solvent interface extending into the continuous phase. The approach of two colloids becomes thermodynamically unfavourable as the forced proximity of the stabiliser polymer chains restricts the number of conformations that a polymer chain can adopt (Figure 21A and 21B).¹²⁹ As a result, the stabiliser layer around the particles will repel each other and particles will not aggregate.¹²⁹ This repulsion must be greater than the long-range van der Waals attractions of the particles, in order to obtain a stable dispersion. Therefore, steric

stabilisation depends on the quantity of stabiliser, the molecular weight of the stabiliser and its conformation in the reaction mixture.

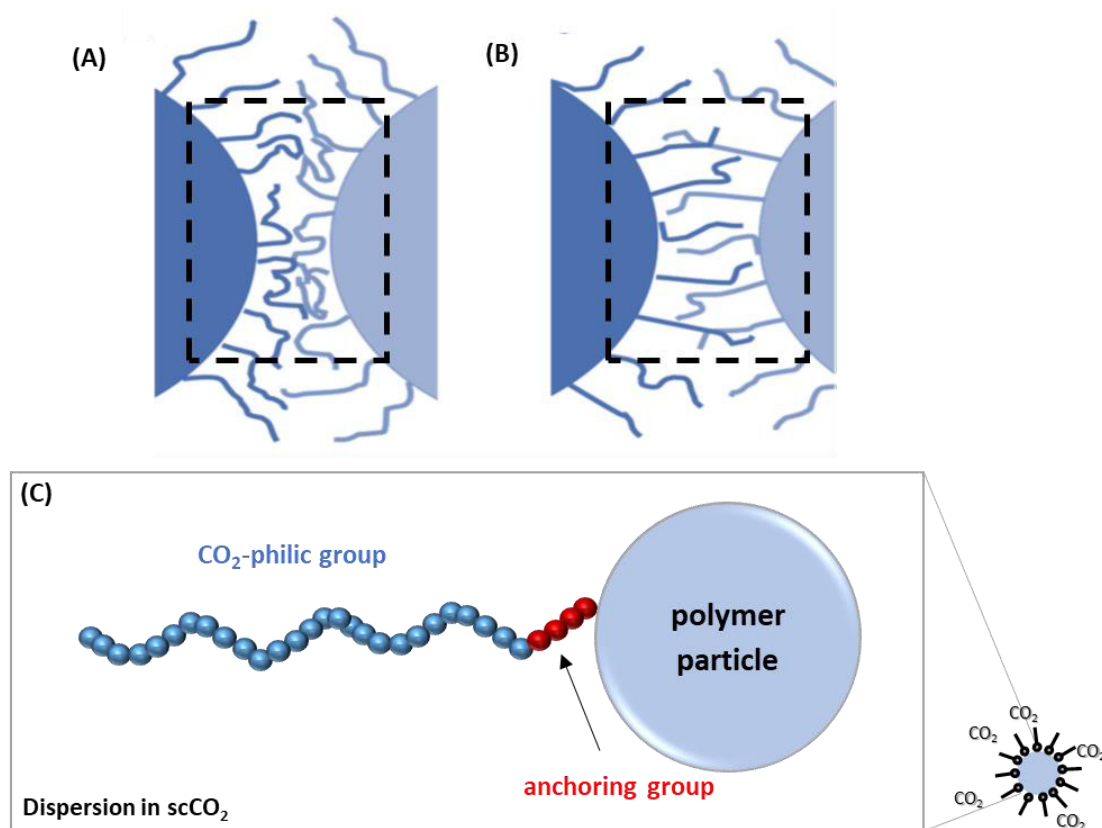


Figure 21 - Scheme of the two scenarios for steric stabilisation, in which stabiliser polymer chains are either compressed (A) or interwoven (B). The resulting decrease in entropy is thermodynamically unfavourable and particles repel each other. (C) Structure of a steric stabiliser containing a CO₂-philic group (blue) and an anchoring group (red). The CO₂-philic group extends into the scCO₂ phase, while the anchoring group attaches the stabiliser to the polymer particle.

Successful stabilisation also depends on the stabiliser being located at the polymer-solvent interface. Therefore, steric stabilisers are usually amphiphilic macromolecules and have an anchoring component that attaches to the growing particles.¹²⁴ Thus, besides being soluble in scCO₂, a successful steric stabiliser must anchor effectively to the growing polymer chains (Figure 21C).

The anchoring group can either be an insoluble portion of the stabiliser, which will prefer to phase segregate into the particles, or a reactive functional group, such as an initiator, monomer or CTA, which can graft to the growing polymer chains. Reactive functional anchoring groups will result in a chemically grafted stabiliser, which provides stronger

stabilisation and cannot be desorbed from the polymer, while the insoluble anchoring groups result in weaker physical adsorption that can be more easily broken. Nonetheless, the removal of the stabiliser after reaction can be advantageous for some applications, in particular for maintaining mechanical properties of the targeted polymer.

1.7.2.1. Fluorinated stabilisers

The first successful radical dispersion polymerisation in $scCO_2$ was reported by DeSimone and co-workers¹²⁴ They performed an MMA polymerisation at 65 °C and 207 bar, with AIBN as the initiator; and reported high conversions, > 90%, and $M_n > 300 \text{ kg mol}^{-1}$, when adding poly(1,1-dihydroperfluorooctyl acrylate) (PFOA) as stabiliser (Figure 22A-C). As comparison, the precipitation reaction had conversion < 40% and $M_n = 77 \text{ kg mol}^{-1}$.¹²⁴ In addition, they obtained well-defined spherical particles of 1-3 μm when using 2-4 wt% stabiliser, while for the precipitation reaction the product was an irregular thick film without any defined structure (Figure 22D).

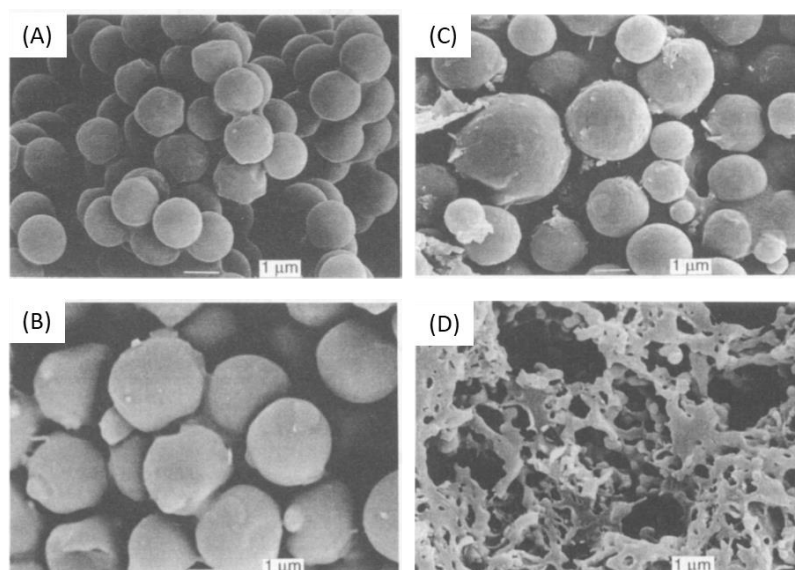


Figure 22 - SEM pictures of PMMA particles synthesised in $scCO_2$ with AIBN and using PFOA as the stabiliser, (A) 4 w/v %, (B) 2 w/v%, (C) 1 w/v% and (D) 0 w/v% (no stabiliser). Figure modified from DeSimone et al.¹²⁴

Further investigation identified that both PFOA and its methacrylate version, PFOMA (Figure 23), were good stabilisers for MMA polymerisation in $scCO_2$.¹⁰⁸ A load as little as 0.24 wt% of PFOA was sufficient to obtain a stable PMMA latex of particle size ranging from 1 to 3 μm .¹⁰⁸

Fluorinated stabilisers have since been used successfully in the synthesis of a variety of polymers, including PMMA, PSt, poly(N-vinylpyrrolidone) (PNVP) and PVAc.^{124, 126, 130, 131}

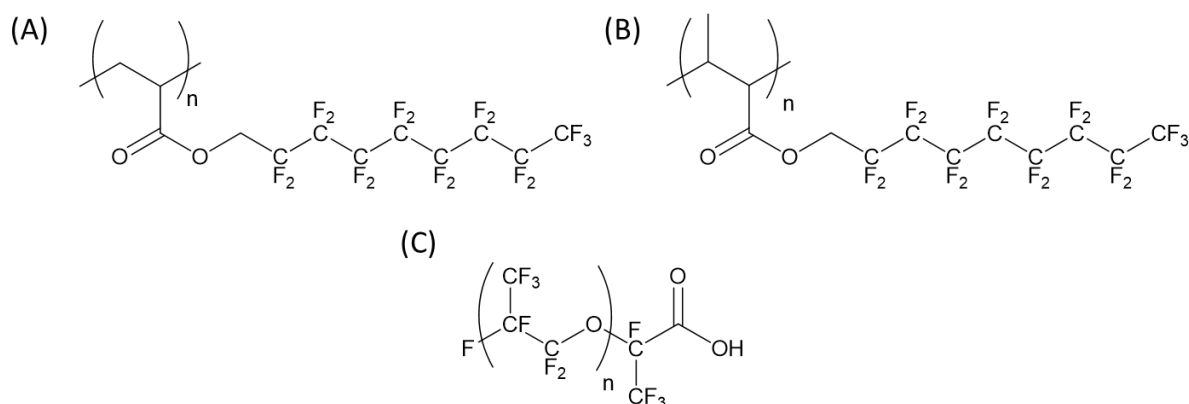


Figure 23 - Structure of common fluorinated stabilisers for dispersion polymerisation in scCO_2 . (A) Poly(1,1-dihydroperfluorooctyl acrylate) (PFOA), (B) Poly(1,1-dihydroperfluorooctyl methacrylate) (PFOMA) and (C) perfluoropolyether (PFPE), Krytox.

Christian *et al.* obtained successful dispersion polymerisation of MMA in scCO_2 using a commercially available carboxylic acid terminated perfluoropolyether (PFPE) of $M_n = 2.5 \text{ kg mol}^{-1}$ named Krytox (Figure 23-C).¹³² Meanwhile, the PFPE homopolymers without the carboxylic acid end group gave no stabilisation. Their results emphasise the importance of the anchor group. Since then, different anchor groups have been reported for PFPE based stabilisers.¹⁰⁷

Besides homopolymers, graft, block and random fluorinated copolymers have been investigated as stabilisers in scCO_2 dispersion polymerisation. For example, Lepilleur and Beckman used a stabiliser based on poly(MMA-*co*-hydroxyethyl methacrylate) backbone with grafted poly(perfluoropropylene oxide) (Figure 24) for dispersion polymerisation of MMA.¹³³ Larger particles were obtained when the size of the soluble block increased. When the anchoring group size increased, smaller particles were achieved. These results demonstrated that an adequate anchor-soluble balance (ASB) is required to achieve sufficient stabilisation. Another study compared random and block copolymers of PSt and PFOA, both stabilised the resulting polymer particles, although the random copolymer only achieved polymer of low molecular weight.¹³⁴

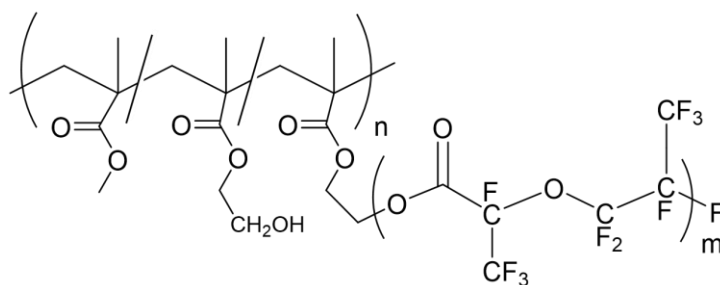


Figure 24 - Structure of a random copolymer stabiliser, based on poly(MMA-co-hydroxyethyl methacrylate) backbone with grafted poly(perfluoropropylene oxide) used by Lepilleur and Beckman.¹³³

Other graft copolymers, such as PVDF grafted copolymers were also used for stabilisation of PVDF dispersions in $scCO_2$.¹³⁵ Block copolymers have also been explored as stabilisers, usually with a block of the homopolymers which will be formed. This allows optimum grafting/anchoring. For example, PSt-*b*-PFOA was successfully used as stabiliser for the polymerisation of styrene, glycidyl methacrylate and 2-hydroxyethyl methacrylate in $scCO_2$.¹³⁶⁻¹³⁸

Although fluorinated polymers offer great stabilisation, the high price of fluorinated stabilisers reduces the viability of industrial applications for polymerisation in $scCO_2$. Furthermore, as many fluorinated stabilisers in use for $scCO_2$ dispersion polymerisation are toxic,⁹⁴ they would not be suitable for biomedical applications.

1.7.2.2. Siloxane-based stabilisers

In 1996, DeSimone and co-workers reported the first $scCO_2$ dispersion polymerisation using a silicone based stabiliser, *i.e.*, mono methacrylate terminated polydimethylsiloxane (PDMS-MA), for MMA polymerisation.¹³⁹ Good colloidal stabilisation with well-defined spherical particles (1.1-5.8 μm) were obtained when using PDMS-MA at concentrations above 2 wt% in relation to monomer.¹³⁹ The best yields and higher M_n of PMMA were obtained with 3.5-16 w/w% stabiliser in relation to the monomer.

Moreover, the authors observed that the PDMS homopolymers, *i.e.*, without the methacrylate end group, did not offer any stabilisation.¹³⁹ They attributed this result to the stability of PDMS to hydrogen abstraction by AIBN or by growing PMMA chains, which prevents formation of graft PDMS-*g*-PMMA and thus cannot stabilise the PMMA particles. Furthermore, Johnston and co-workers have shown that PDMS homopolymers, without any

end-group, are not active in the solvent-polymer interface for MMA polymerisation in scCO_2 , and as a result, physical stabilisation cannot take place.^{140, 141} Both findings showed that PDMS homopolymers are not good stabilisers and demonstrate the importance of the anchor group for stabilisation (Figure 25).

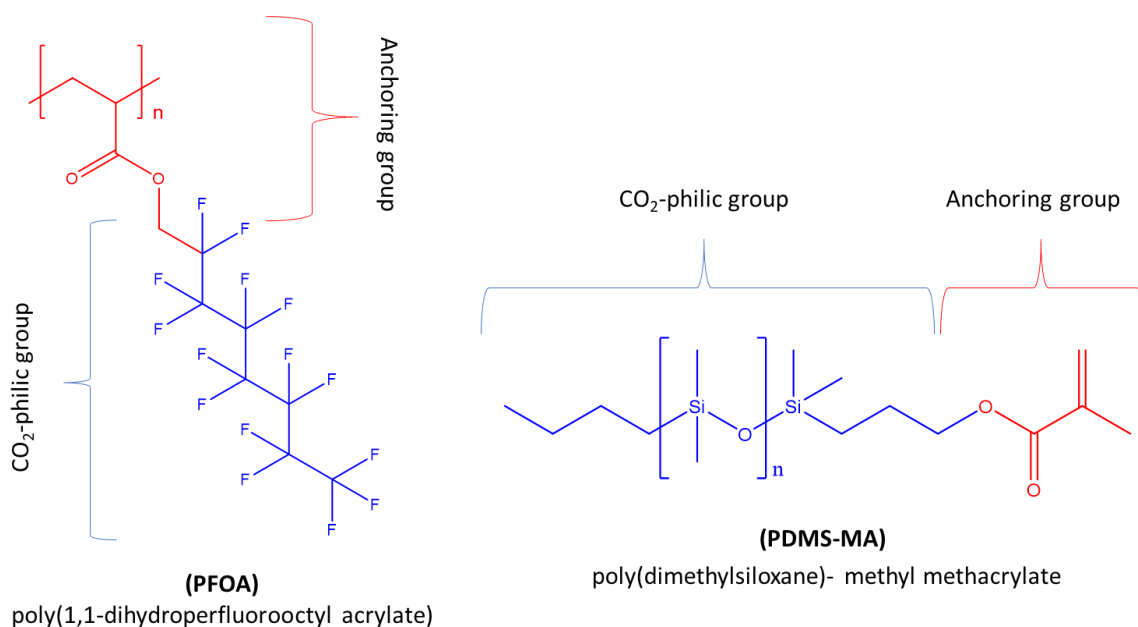


Figure 25 – Structures of poly(1,1-dihydroperfluorooctyl acrylate) (PFOA) and mono methacrylate terminated poly(dimethyl siloxane) (PDMS-MA), showing their CO₂-philic group and the anchoring group.

However, it was observed that only a low percentage, < 0.7 wt%, of the PDMS-MA stabiliser remained chemically grafted to PMMA.¹³⁹ Therefore, most of the stabiliser must be working *via* physical adsorption and not *via* chemical grafting. Thus, the methacrylic end-group of PDMS-MA appears to act as an anchoring group that physically adsorbs to the PMMA particle.

PDMS-MA has since been reported several times as a steric stabiliser for successful dispersion polymerisation in scCO_2 of MMA¹⁴²⁻¹⁴⁴ and St.¹³⁹ Although most reported polymerisations in scCO_2 focused on MMA and St, other monomers have also been investigated. Giles *et al.* investigated the polymerisation of isobornyl methacrylate (IBMA) and poly(ethylene glycol methacrylate) (PEGMA) in scCO_2 with PDMS-MA and with Krytox.¹⁴⁵ Better stabilisation was achieved with the latter, when compared to PDMS-MA at 5 wt%. Although both stabilisers could give high molecular weight and conversion, with discrete spherical particles, when the siloxane-based stabiliser was used the particles were more agglomerated.¹⁴⁵

Block copolymers based on polysiloxanes have also been used as stabilisers, for example PDMS-*b*-PSt was used for styrene polymerisation.¹⁴⁶ The authors demonstrated the importance of finding the ASB for the stabiliser by varying the length of both blocks that compose the stabiliser. When increasing the PSt block length, the resulting particles became larger and more monodisperse, while when increasing the PDMS length, particle size became more disperse. They attributed such loss in stability to the drop in PDMS solubility with M_n increase and the lower ASB.

In a similar way, Giles *et al.* explored the impact of PDMS length in PDMS-MA for stabilisation of MMA dispersion in $scCO_2$.^{147, 148} They found a $M_n = 2 \text{ kg mol}^{-1}$ to be more efficient at low stabiliser concentrations than 10 kg mol^{-1} PDMS, the former being able to stabilise the system at 0.2 wt% concentration. However, particles were twice as big when using the low M_n stabiliser compared to using 10 kg mol^{-1} PDMS. Furthermore, they identified a way to control the final diameter of PMMA particles by means of changing the stabiliser molecular weight and concentration.

Canelas *et al.* previously demonstrated that PSt particle size could be changed by varying the load of PSt-*b*-PFOA stabiliser. By varying the stabiliser concentration from 2.5 to 15% the particle diameter was changed from 1.15 to 0.31 μm .¹⁴⁶ Similar results were obtained for the polymerisation of MMA¹⁴⁹ and divinylbenzene¹⁵⁰ with PMMA-*b*-PFMA as stabiliser.

The study on particle size control was expanded by McAllister *et al.* By varying PDMS-MA stabiliser loading between 1 and 20 wt % for MMA polymerisation, the particle size could be tuned from 3.9 μm to 0.5 μm (Figure 26).¹⁵¹ The authors also explored the combination of monomer and stabiliser concentration to obtain even smaller particles, 0.3 μm . Finally, the implementation of a two-stage system allowed better control of the dispersion, by keeping the monomer concentration low during nucleation stage and injecting further monomer later. In this way, the range of PMMA particle diameter achieved with PDMS-MA was expanded to 5.3-0.3 μm .¹⁵¹

Silicone-based random copolymers have also been studied as stabilisers. For example poly(3-[tris(trimethylsilyloxy)silyl]propyl methacrylate-*co*-2-dimethylaminoethyl methacrylate) (P(SiMA-*co*-DMAEMA)) and poly(3-[tris(trimethylsilyloxy)silyl]propyl methacrylate-*co*-

diisopropylaminoethyl methacrylate) (P(SiMA-*co*-DPAEMA)), were investigated as stabilisers for PSt synthesis.¹⁴⁴

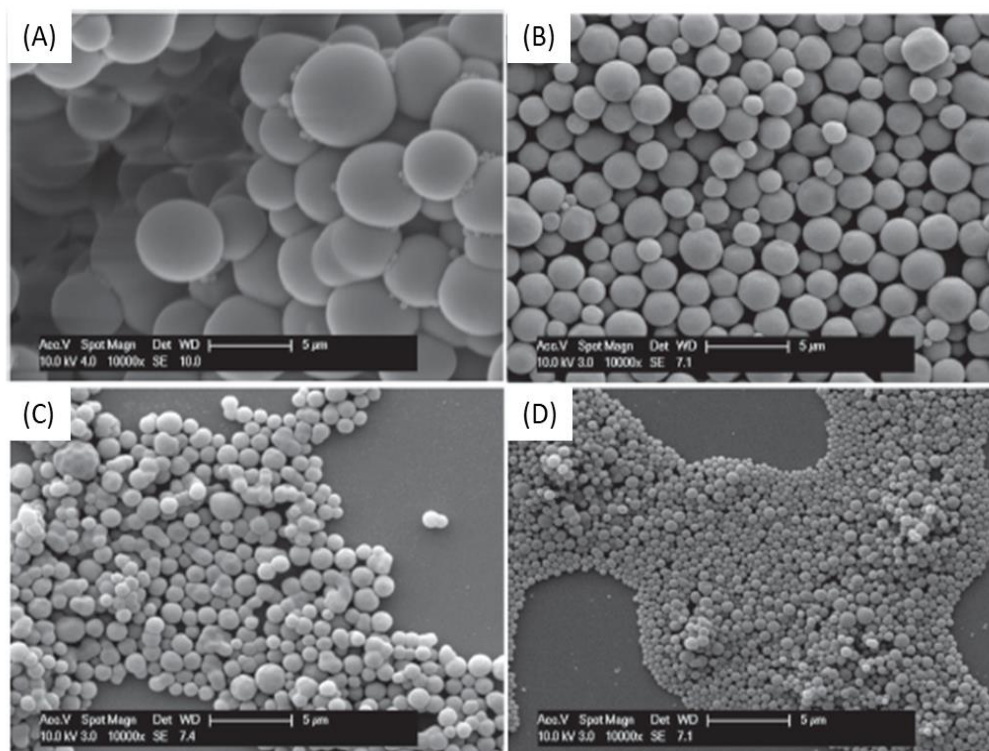


Figure 26 - SEM images showing PMMA particles synthesized by one pot conventional radical dispersion polymerisation in $scCO_2$ with different ratios of PDMS-MA stabiliser with respect to MMA: (A) 1 wt%, (B) 5 wt%, (C) 10 wt%, and (D) 20 wt%. Particles had diameters of 3.97, 1.82, 1.05, and 0.51 μm , respectively. Figure adapted from McAllister *et al.*¹⁵¹

1.7.2.3. Hydrocarbon-based stabilisers

Siloxane-based stabilisers are still not economically ideal for industrial applications. More recently, novel hydrocarbon stabilisers with moderate CO_2 solubility have been developed.¹⁵²⁻¹⁵⁶ Birkin *et al.* reported a series of PVAc-*b*-poly(vinyl pivalate) (PVAc-*b*-PVPI) for the polymerisation of NVP (Figure 27).¹⁵³ Different molecular weights of PVAc-*b*-PVPI at 50:50 volume fractions were tested. The stabiliser with the lowest molecular weight (Figure 27A) was not effective. However, increasing the M_n from 9.4 to 21.8 $kg\ mol^{-1}$ the particle size increased. This was attributed to the reduction of solubility as the stabiliser molecular weight increased. However, at the highest M_n tested (Figure 27F), stabilisation was no longer effective, probably because of the decreased solubility of the block copolymer.

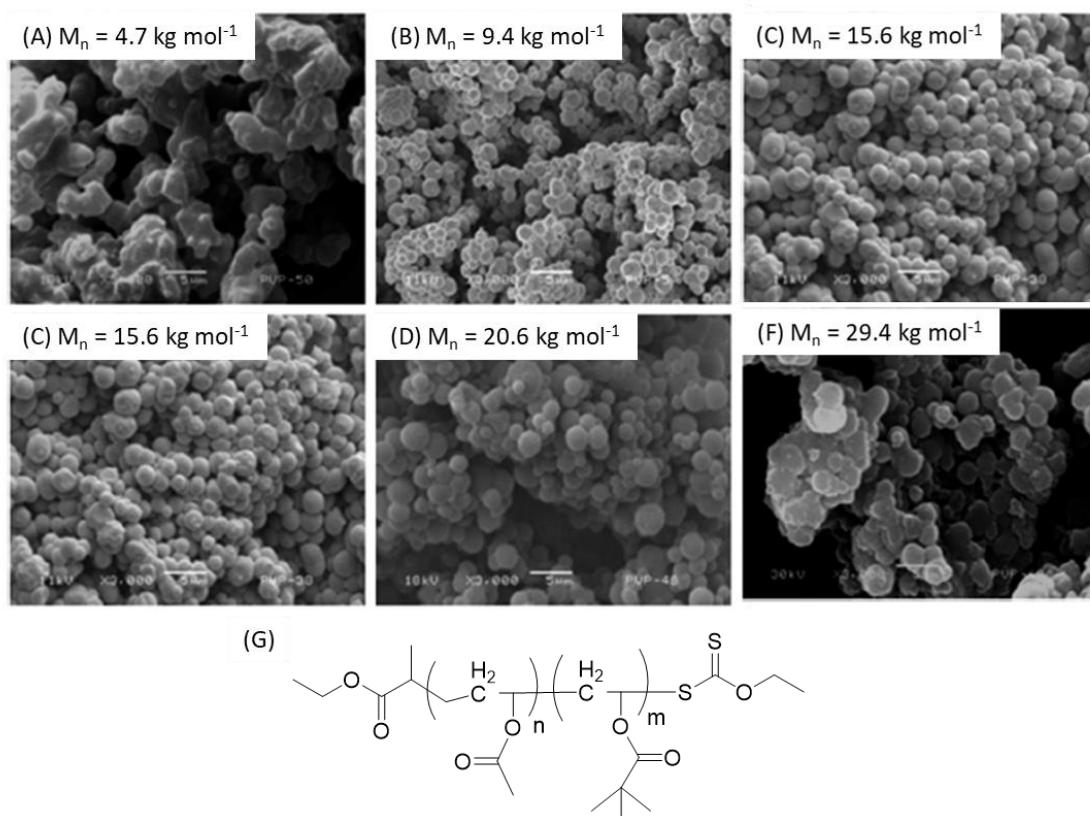


Figure 27 - Variation of poly(*N*-vinylpyrrolidone) particle morphology with different molecular weight PVAc-*b*-PVPi stabilisers of 50 : 50 ratio. (A) $M_n = 4.7$; (B) $M_n = 9.4$; (C) $M_n = 15.6$; (D) $M_n = 20.6$; (E) $M_n = 21.8$; and (F) $M_n = 29.4$, M_n given in kg mol^{-1} and (G) stabiliser structure. Figure adapted from Birkin *et al.*¹⁵³

Unfortunately, PVAc-*b*-PVPi was not suitable to a wide range of monomers. For example, MMA polymerisation with PVAc-*b*-PVPi produced ill-formed polymer particles.¹⁵⁷ This is probably an effect of the RAFT end-group of the PVAc-*b*-PVPi stabilisers, since the xanthate end-group provides good anchoring to PNVP but does not react with MMA.

The design of hydrocarbon-based stabilisers is complex and involves a fine balance between scCO_2 solubility and steric stabilisation. Therefore, although promising, only a limited number of successful hydrocarbon stabilisers for dispersion in scCO_2 have been reported so far, and those are still not applicable to an extensive library of monomers.^{152-156, 158}

1.7.3. Kinetic and mechanistic considerations of dispersion polymerisation in scCO_2

A lot of interest was directed towards understanding the kinetics and mechanism of dispersion polymerisation and stabilisation in scCO_2 . MMA has been used as model monomer for several studies.¹⁵⁹⁻¹⁶⁴

Dispersion polymerisation of MMA in scCO₂ at 65 °C with PDMS-MA 10 kg mol⁻¹ as the stabiliser has been study thoroughly by Johnston and co-workers.¹⁶⁵ Their predictions for final particle size and number of particles agreed with Paine's model.¹⁴ They concluded that primary particles precipitate at an early stage of polymerisation until stabilisation is achieved through a sufficient stabiliser coverage of the particles, after which the number of particles remains constant. Further growth of the particles takes place by controlled agglomeration, adsorption of polymer chains and polymerisation within the stable particles.

The same authors also monitored the reaction *via* turbidity analysis as measured by use of an optical cell through which the reaction mixture could be pumped.¹⁶⁶ They established a threshold for obtaining a stable dispersion with PDMS-MA 10 kg mol⁻¹, which was a minimum pressure of 206 bar and stabiliser concentration ≥ 2wt% relative to monomer. Below these conditions, precipitation occurred due to insufficient steric stabilisation. Pressures below 206 bar reduced solvency of the system and there was not enough graft-stabiliser available at stabiliser concentration below 2 wt%.

Furthermore, the authors predicted that the main *locus* of polymerisation was the dispersed phase, with no new particles formed through most of the polymerisation.¹⁶⁵ After nucleation, particle volume increased directly with conversion. The study suggested that radical termination in the continuous phase is too fast to allow polymer to adsorb to the particles before new particles are formed.

Two distinct agglomeration regimes were defined by turbidity analysis:¹⁶⁶ (i) nucleation agglomeration and (ii) controlled agglomeration. At first, nucleation creates an extremely high surface area. The nuclei then aggregate (i) and coalesce until the surface area is reduced sufficiently to allow stabilisation. The particle size then becomes stable, before controlled agglomeration (ii) starts. In this phase, the surface area becomes too large for the stabiliser to cover it, causing coagulation to occur. The number of particles thus decreases until the surface area can be stabilised.

Ballauf and Fehrmnacher further studied the early stage of MMA polymerisation by turbidimetry analysis in scCO₂ with newly designed equipment where reaction can be monitored *in situ*.^{167, 168} They confirmed that, in the first stage, < 300 s, polymerisation occurs in the continuous phase (Figure 28). Particles were only able to grow by precipitation of chains

onto their particles surface, and no polymerisation occurred inside the particles. After this first stage, when $t > 150$ s, the number of particles remained constant. The same authors also observed an induction of 10-50 s for the conventional radical polymerisation of MMA in $scCO_2$, even with the reactor already at reaction temperature and all impurities removed. Nevertheless, particle formation was observed as early as 75 s.¹⁶⁸ It is important to emphasise that the continuous phase was confirmed to be the *locus* of reaction only in the early stages of polymerisation.

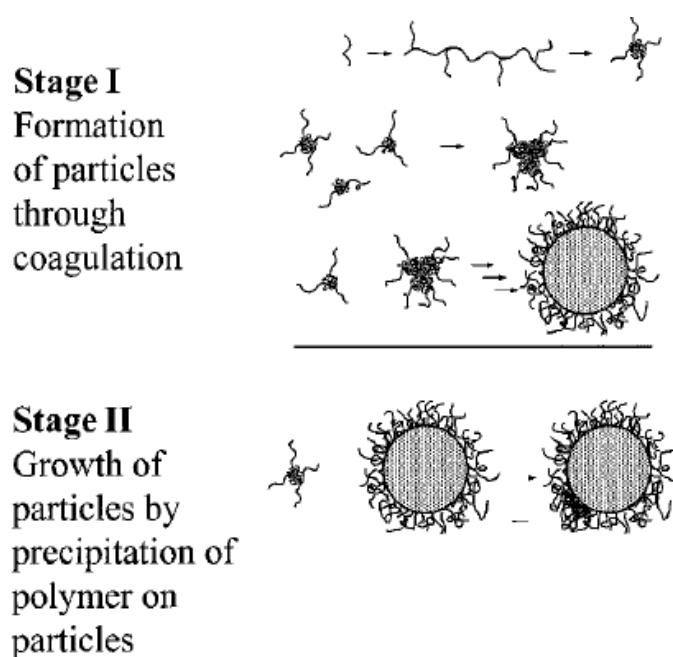


Figure 28 – Scheme of early stage of MMA dispersion polymerisation in $scCO_2$ as observed by turbidimetry analysis. In stage I, polymerisation occurs in the continuous phase and particles form through coagulation of polymer chains. In stage II, the number of particles remains constant and all newly formed polymer precipitates onto the particles, but no polymerisation occurs inside the particles. Figure adapted from Ballauf and Fehrmnacher.¹⁶⁷

The reaction *locus* in $scCO_2$ has been a topic of debate. The initiator is soluble in both the dispersed and continuous phase and so radicals can be generated in both. One hypothesis states that radical chain growth and termination is slower in the $scCO_2$ -rich phase than the transport into the particles. In that case, the dispersed phase is the main *locus* of reaction. Contrasting this, if a big fraction of polymer is made in the continuous phase, both *loci* must be considered, and two different molecular weight populations will coexist due to the distinctions in polymerisation rate in both phases. This last hypothesis was considered by

Saraf *et al.* for the precipitation polymerisation of vinylidene fluoride,¹²¹ and by Chatzidoukas *et al.*¹⁶⁹ for the dispersion polymerisation of MMA, assuming the growing radicals remained where they were originated. While, Chatzidoukas *et al.* presented a comprehensive mathematical model for the dispersion polymerisation of MMA in scCO₂, with a detailed kinetic mechanism predicting molecular weight evolution in both the continuous and dispersed phases (Figure 29).¹⁶⁹

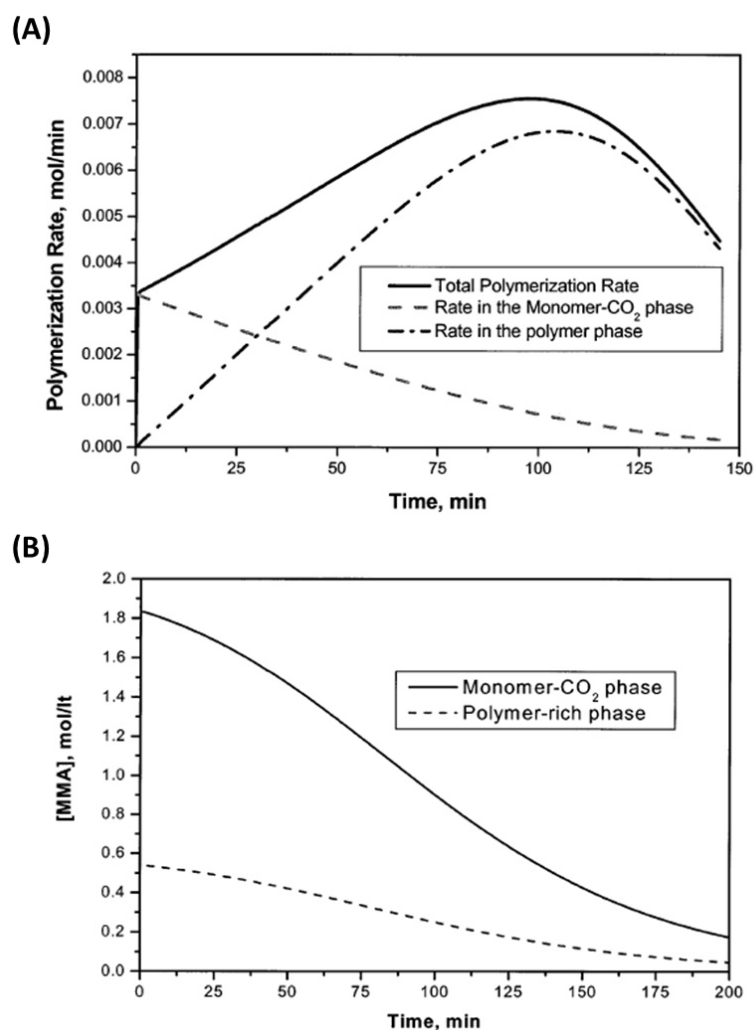


Figure 29 – Graphics showing the simulation results for MMA conventional radical dispersion polymerisation in scCO₂. In (A) the different rates of polymerisation in the polymer-rich phase and in the monomer-CO₂ phase are presented. The rate of polymerisation is higher in the monomer-CO₂ phase at the very beginning of the reaction, but after the polymer-rich phase becomes the main reaction locus. While in (B) the variation of monomer concentration in the monomer-CO₂ phase and in the polymer-rich phase is presented. Most of the monomer is in the monomer-CO₂ phase, which diffuses into the polymer-rich phase. The monomer concentration decreases in both phases with reaction time. Figure adapted from Chatzidoukas *et al.*¹⁶⁹

They observed in their simulations that the polymerisation rate in the continuous phase decreased with time, because the monomer becomes scarce, while it increased in the dispersed phase due to the increase of polymer volume and the gel effect. The gel effect is the increase in viscosity in the polymer phase, which limits the mobility of polymer chains, resulting in propagation and termination reactions becoming diffusion-controlled. Furthermore, the low solubility of high molecular weight polymer in scCO₂ restricts the polymerisation *locus* to within the particles.

Mueller *et al.* created a computer model to evaluate the polymerisation *locus* for the reaction in scCO₂.¹⁷⁰ With that aim, they created a radical segregation model (RS) and a radical partitioning model (RP). The RS model considered that interphase radical transport was much slower than the chain life. Therefore, the polymer should terminate in the phase where it initiated. On the other hand, the RP model assumed that the interphase radical transport is extremely fast, so that thermodynamic equilibrium conditions are achieved for the active species. The RP model considers the movement of radicals formed in the continuous phase into the particles, which was the dominant phenomenon, as well as the diffusion of small active oligomers from particles into the continuous phase.

The RS model strongly underestimated the rate of polymerisation because of the lower initiator efficiency within the particles, with hardly any radical being predicted to form within that phase.¹⁷⁰ As a result, the model presents bimodal molecular weight distributions, with the higher M_n peak representing a small quantity of polymer produced in the dispersed phase, while the majority of the polymer was formed in the continuous phase at a low M_n , pushing the total M_n below the experimental results (Figure 30A).¹⁷⁰ Furthermore, the predicted conversion versus time for this model was a linear increase, which is far from the sigmoidal trend previously observed experimentally. The assumption of complete radical segregation was thus considered unlikely for this reaction.

On the other hand, using the RP model, the rate of polymerisation and M_n evolution with conversion were overestimated, but within the experimental kinetic trend.¹⁷⁰ In this model the radicals that form in the continuous phase are rapidly transported into the particles, which thus becomes the main reaction *locus*. This gives higher polymerisation rates and higher M_n than the RS model. The M_n distribution is still a bimodal distribution, with a small

shoulder corresponding to the polymer formed in the continuous phase, which is negligible (Figure 30B).¹⁷⁰

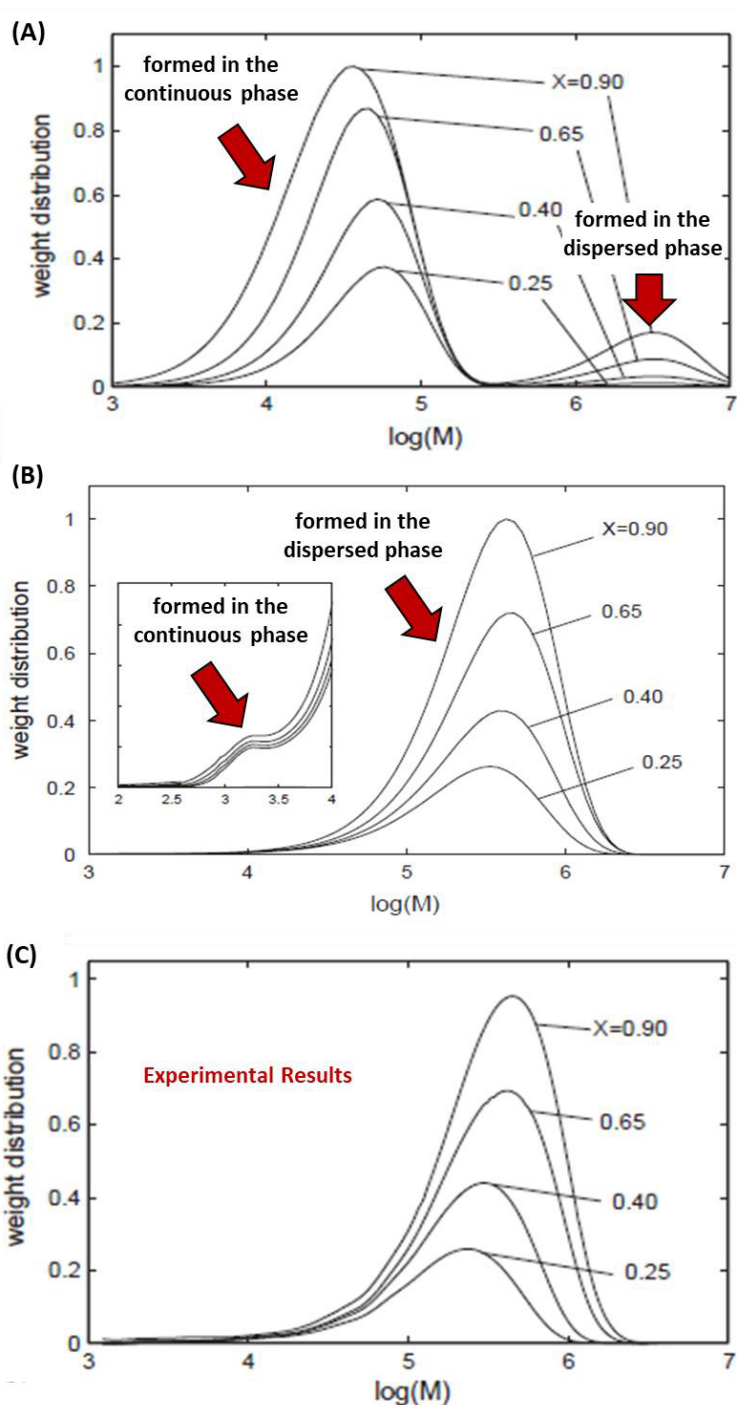


Figure 30 - Molecular weight distribution of PMMA at various conversions predicted by the RS model (A) and the RP model (B); and the experimental results of MMA conventional dispersion polymerisation in $scCO_2$ (C). Figure adapted from Mueller et al.¹⁷⁰

In general, the RP model described the dispersion polymerisation of MMA in $scCO_2$ better, aligning well with the experimental results (Figure 30C).¹⁷⁰ While the RS model is only

adequate for very small chains, as present at the start of the reaction. The authors further improved predictions by inclusion of a chain-length dependent partition coefficient and diffusion limitation by gel, cage and glass effects.¹⁷¹ With these additions, it was possible to predict the irreversible migration of radicals from the continuous phase into the dispersed phase after a certain chain length, *i.e.*, J_{crit} , and the simulations results were better aligned with the experimental results (Figure 30C). Both publications indicated that for the most of the reaction the particles are the main *locus* of the polymerisation.

1.7.4. RAFT dispersion polymerisation in scCO₂

Both Thurecht and Zetterlund have extensively reviewed the topic of RDRP in scCO₂.^{95, 172} The first RDRP reported in scCO₂ was an ATRP of FOMA followed by the block copolymerisation with MMA,¹⁷³ using the PFOMA synthesised in the reactor as a stabiliser generated *in situ*. Although ATRP¹⁷³⁻¹⁷⁷ and NMP¹⁷⁸⁻¹⁸³ in scCO₂ have been reported in literature, we will focus only on the RAFT controlled polymerisation in scCO₂.

Early investigations of RAFT solution polymerisation in scCO₂ was restricted to low monomer into polymer conversions.¹⁸⁴ For instance, Arita *et al.* reported the methyl acrylate RAFT polymerisation in scCO₂, however \bar{D} increased up to 1.44, with a maximum conversion of 50%.¹⁸⁴ Therefore, research interest shifted towards dispersion polymerisation, expecting to achieve higher conversions and well-defined particles in the same way as conventional radical dispersion polymerisation in scCO₂.

In 2007, Thurecht *et al.* presented the first successful RAFT dispersion polymerisation in scCO₂.¹⁴² They utilised α -cyanobenzyl dithionaphthylate (α -CBDN) as the CTA at 1:1 CTA:initiator ratio for the polymerisation of MMA, with AIBN as the initiator and 5 wt% PDMS-MA as the stabiliser. A series of experiments carried out at reaction times varying from 10 to 24 hours showed the increase of molecular weight with reaction time, reaching 99% conversion at 24 hours and producing a fine powder of well-defined spherical particles (Figure 31). Furthermore the reaction control over M_n was evident by the good agreement between the $M_n = 28.8 \text{ kg mol}^{-1}$ and $M_{n,th} = 34.3 \text{ kg mol}^{-1}$, while molecular weight distribution remained low, $\bar{D} = 1.19$.¹⁴² Livingness was confirmed by the increase of molecular weight with reaction time and by successful chain extension of PMMA with further addition of MMA. The authors

also synthesised the first block copolymer *via* RAFT dispersion in $scCO_2$ through injection of styrene into the reactor after the 24 h MMA polymerisation.

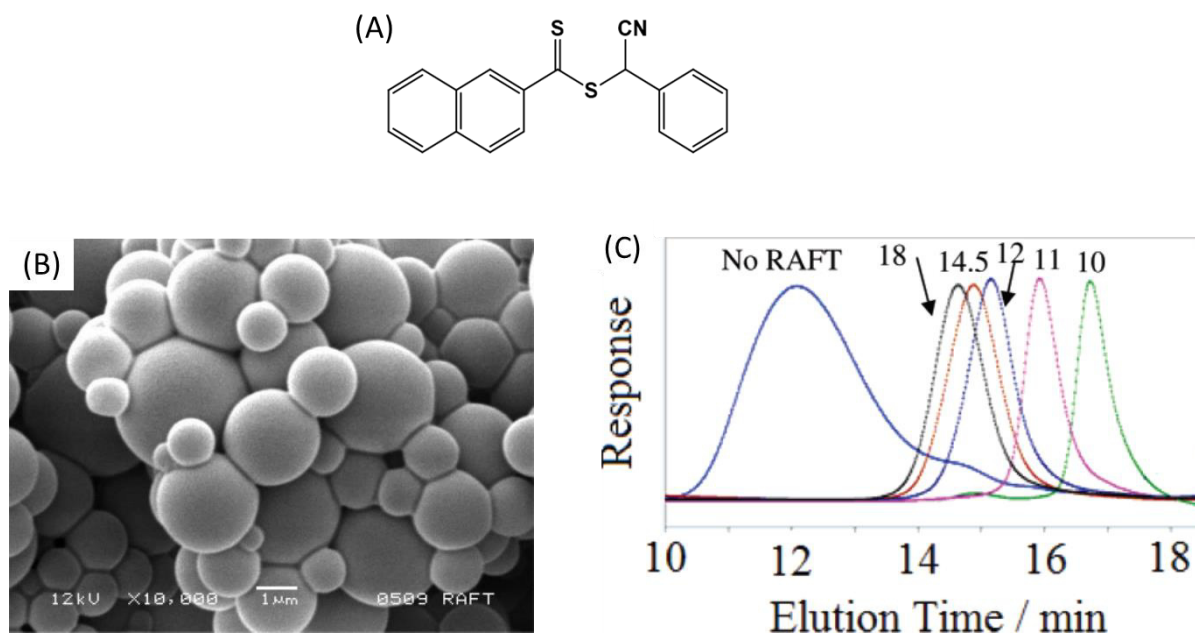


Figure 31 - First RAFT polymerisation in $scCO_2$; (A) CTA used, α -cyanobenzyl dithionaphthylate (α -CBDN); (B) SEM picture of PMMA particles formed; (C) SEC traces showing the increase in PMMA molecular weight as reaction time increases from 10 h to 18 h, compared to the conventional radical polymerisation (blue). Figure modified from Thurecht *et al.*¹⁴²

Later on, Gregory *et al.* expanded the range of CTAs suitable for MMA polymerisation in $scCO_2$.¹⁸⁵ α -CBDN and 3 other CTAs with naphthyl or phenyl Z-groups were successfully applied under the same reaction conditions (Figure 32). All reactions presented $\mathcal{D} \approx 1.20$ and M_n similar to the theoretical value. In addition, linear increase of M_n with conversion was confirmed for all CTAs tested. This may not be surprising, considering all CTAs have chemically equivalent dithiobenzoate reversible capping end-groups.

CTAs A and B (Figure 32) have less stable secondary R groups, and those should be less favourable for the polymerisation of MAMs such as MMA. Nevertheless, only a longer induction period was observed for those two CTAs, *i.e.*, above 10 h, but the control over M_n and \mathcal{D} was not affected.¹⁸⁵ In addition, all reactions reached high conversion > 90% and produced micrometric polymer particles, $d \approx 1.40 \mu m$. The particle size of a comparative reaction *via* conventional radical polymerisation was $4 \mu m$.¹⁸⁵ By targeting different molecular

weights, the impact of CTA on nucleation was evidenced. As the targeted DP decreased, *i.e.*, at higher CTA concentration, particle size decreased and the dispersity of particle sizes increased.¹⁸⁵ Therefore, a high CTA concentration had a negative impact on the homogeneity of particle sizes.

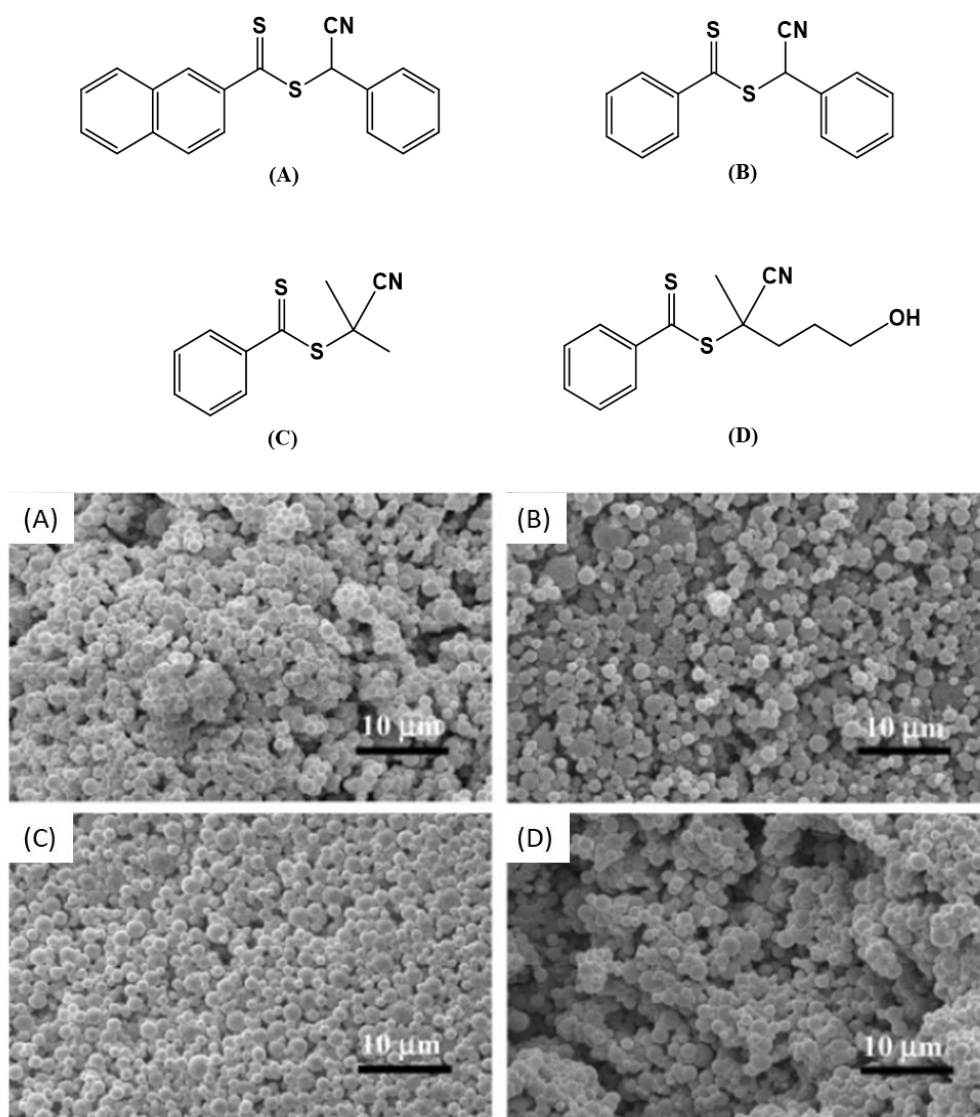


Figure 32 – CTAs investigated for RAFT polymerisation of MMA and SEM of particles obtained for each CTA, respectively. (A) α -cyanobenzyl dithionaphthalate, $d = 1.29\mu\text{m}$ $C_v = 31\%$. (B) α -cyanobenzyl dithiobenzoate, $d = 1.43\mu\text{m}$ $C_v = 44\%$. (C) 2-cyanoprop-2-yl dithiobenzoate, $d = 1.40\mu\text{m}$ $C_v = 43\%$. (D) 4-cyano-1-hydroxypent-4-yl dithiobenzoate, $d = 1.39\mu\text{m}$ $C_v = 30\%$. Figure modified from Gregory *et al.*¹⁸⁵

Interestingly, both studies^{142, 185} reported good control in a single step, with no need to follow Winnik and Song's two-stage polymerisation method.⁶⁸ The authors attributed this unusual result to the improved mobility of species in the supercritical fluid, due to its low viscosity and high diffusivity, which allows the degenerative chain transfer to occur without the common compartmentalisation effect problems found in conventional solvents.¹⁸⁵ A further hypothesis is the possibility of a faster nucleation in scCO₂ as a result of its known poor solvation of polymers, which should decrease J_{crit} .⁹⁵

Another interesting fact is the low CTA:initiator ratio used in scCO₂, both reports^{142, 185} used 1:1 CTA:AIBN, however usually a load of 5:1 is required. The initiator concentration is usually kept low to reduce the number of dead polymer chains formed during the polymerisation. However, DeSimone studied AIBN decomposition in scCO₂ to show that decomposition is 2.5 times slower in scCO₂ compared to in benzene, while the efficiency of the formed radicals is 1.5 times higher.¹¹⁰ Because of the slow decomposition, the AIBN load must be increased to allow the reaction to occur in a reasonable time in scCO₂.

In addition, the higher efficiency in scCO₂ can potentially increase initiator-initiator coupling, thus reducing the number of chains initiated by initiator fragments. Gregory *et al.* observed that the experimental plot of M_n vs conversion aligned better with $M_{n,th}$ calculated without considering the initiator concentration (Equation (8)), that when considering both initiator and CTA concentration (Equation (9)).¹⁸⁵ Therefore the number of chains initiated by initiator fragments must be negligible (Figure 33).

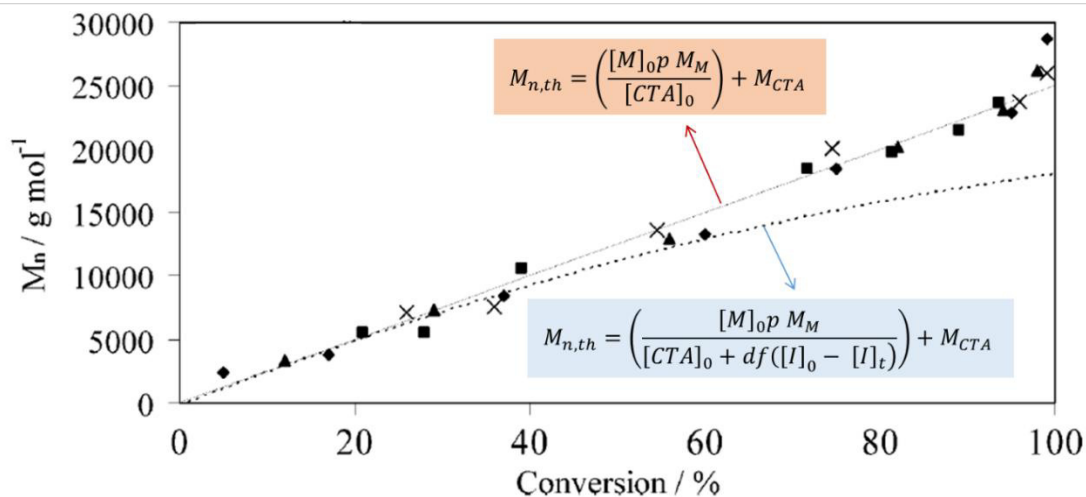
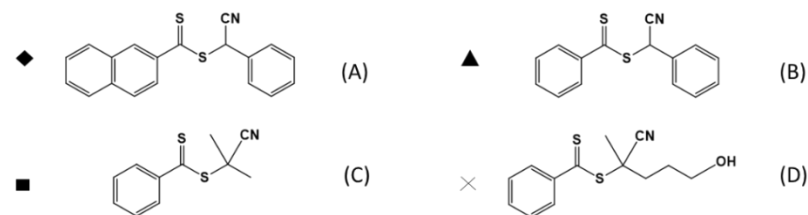


Figure 33 – Plot of PMMA molecular weight vs conversion for the dispersion polymerisation of MMA in $scCO_2$ with four different CTAs (A,B,C and D – Figure 32). Two theoretical molecular weight trend lines are presented, based on CTA concentration (solid line- red equation (8)) and based on CTA and AIBN concentrations (dashed line – blue equation (9)). The experimental results fit with the solid line $M_{n,th}$, indicating that the number of chains initiated by the initiator fragment are negligible. Figure modified from Gregory et al.¹⁸⁵

The topic of RAFT polymerisation in $scCO_2$ is further discussed in Chapter 4. While the use of RAFT polymerisation for synthesis of block copolymer in $scCO_2$ is discussed in the next section.

1.7.5. Block copolymer synthesis in $scCO_2$

To fully take advantage of the high diffusivity in $scCO_2$, studies on block copolymers synthesis *via* RAFT were performed. Block copolymers are applied in diverse advanced materials such as nanoporous membranes,¹⁸⁶ thermoplastic elastomers,¹⁸⁷ electronics¹⁸⁸ and catalyst supports.¹⁸⁹ They consist of two polymer chains composed of different repeat units attached at the centre, traditionally by means of a covalent bond. Synthesis of block copolymers can be achieved by many means, including ring opening polymerisation (ROP)¹⁹⁰, RDRP (*e.g.* RAFT), click chemistry¹⁹¹ and a combination of these methods (*e.g.* RAFT and ROP).¹⁹² Block copolymer synthesis *via* RAFT can be either formed *via* sequential RAFT polymerisation,³² or

by end-group modification of a pre-existing polymer with a CTA, which can then chain extend with a second monomer (Figure 34).⁵¹

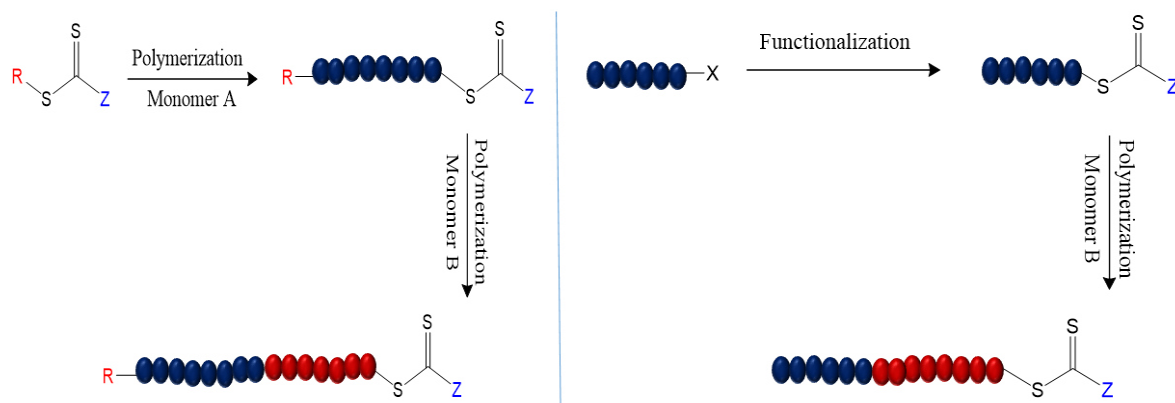


Figure 34 - Schematics of two paths for block copolymer synthesis via RAFT. a) Firstly a macro-CTA agent is formed from monomer M_A (blue), and then the chain is extended with monomer M_B (red). b) Firstly the end group of PM_A is functionalized with a RAFT group, then M_B is chain extended via RAFT polymerisation.

A key feature of block copolymers is the highly ordered nanostructures resulting from their self-assembly. When one block becomes immiscible with another, the covalent bond between them prevents complete phase separation, and instead, microphase separation can happen within nano or microparticles. The different polymer domains inside the particle create internal structures such as core-shell, spheres, rods and lamellae, all previously observed in solution.⁸⁷ Most common methodologies to obtain block copolymer nanostructures are time-consuming, require multiple steps and use large quantities of volatile organic solvents (VOCs).¹⁹³ Besides being a more environmental friendly solvent, the low viscosity and high diffusivity of $scCO_2$ ensure efficient plasticisation. This allows excellent access of the dormant CTA moiety to the incoming monomer, making block copolymerisation *via* dispersion in $scCO_2$ very efficient.^{194, 195}

Howdle and co-workers investigated microphase separation in one-pot block copolymerisation in $scCO_2$.^{193, 195-197} For all the reactions, PMMA was the first block, while a series of monomers were used for the second block, including BzMA, 2-dimethylaminoethyl methacrylate (DMAEMA), styrene and 4-vinylpyridine (4VP). The block copolymers presented

spherical, cylindrical and lamellar internal structures (Figure 35). In all cases, high conversions and good RAFT control was obtained.

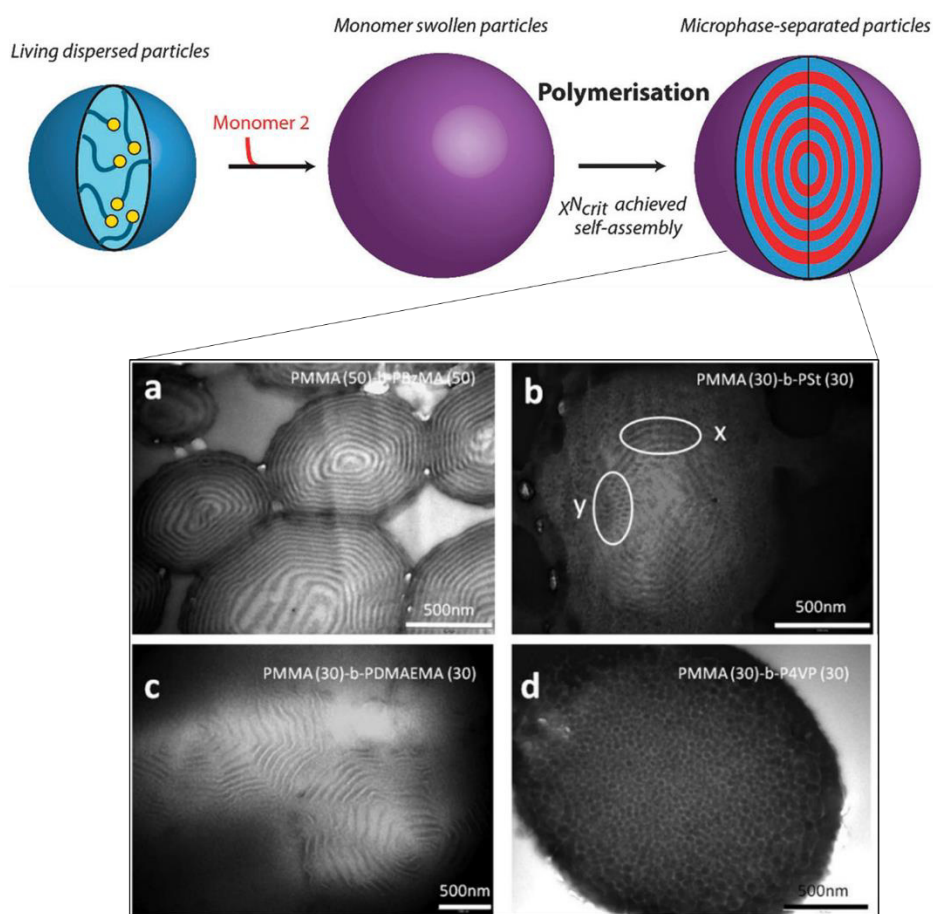


Figure 35 - Scheme of nanostructured polymer particles synthesis in $scCO_2$, showing two solvophobic blocks with polymer–polymer microphase separation taking place within the particles during polymerisation. Different nanostructures have been obtained by this method, (a) PMMA-*b*-PBzMA: lamellar; (b) PMMA-*b*-PSt: cylindrical (the regions labelled x and y demonstrate views perpendicular to and along the cylinder axis, respectively); (c) PMMA-*b*-PDMAEMA: lamellar; and (d) PMMA-*b*-P4VP: spherical. Figure adapted from Jennings et al.¹⁹⁶

However, the obtained internal morphologies did not follow the predictions according to the volume fractions of the blocks. Instead, the different CO_2 -philicity of each block changed the apparent volume fraction of the segments in $scCO_2$, which altered and induced morphological transitions not commonly seen in conventional solvents. In fact, when the block copolymers obtained in $scCO_2$ were cast in conventional solvents and annealed, the morphology returned to the predicted structures.¹⁹³ The internal morphology evolution has been further evaluated

by *in situ* SAXS, starting from a PMMA macro-CTA.¹⁹⁸ This confirmed the hypothesis of distinct morphology transitions in scCO₂, but also further confirmed the livingness of the macro-CTA.

1.7.6. Polymerisation-induced self-assembly in scCO₂

Another strategy for block copolymer synthesis in scCO₂ is *via* PISA. In fact, the first RDRP in scCO₂ can be classified as a PISA polymerisation based in ATRP.¹⁷³ For application of PISA in scCO₂, it is necessary to use a CO₂-philic macro-CTA. Therefore, fluorinated macro-CTAs, such as PFOMA¹⁹⁹ and poly(dodecafluoroheptyl methacrylate) (PDFMA) have been used.^{200, 201} Both those macro-CTAs were chain extended with MMA in scCO₂, with the fluorinated macro-CTA providing self-stabilisation of the block copolymers.

Many of the principles that govern self-assembly in aqueous and organic surfactant solutions are applicable in scCO₂, thus it was expected to see a morphology transition from spheres to vesicles with the change of the block volume fractions. However, in all three publications, there was no morphology transition in scCO₂, with only discrete spherical particles observed.

Particle morphology can be dictated by: (i) thermodynamics, with the morphology of lowest free energy obtained; or (ii) kinetics, with kinetic factors preventing the equilibrium morphology from forming. In general, the ability of scCO₂ to swell polymer particles and reduce T_g favours formation of thermodynamically controlled morphologies.

More recently, higher order morphologies, such as worms and vesicles were observed for the PISA of BzMA in scCO₂ *via* ATRP with a bromo-terminated PDMS.²⁰² In addition, the authors also observed the formation of microphase separation at certain volume fractions of the two blocks. This has been attributed to the PDMS being 'buried' inside the particles, as a result of the high plasticisation in scCO₂, instead of only remaining in the corona as normally is the case in conventional solvents.

As previously discussed, fluorinated polymers are expensive, and a lot of work has been done into finding new CO₂-philic polymers. Therefore, a thesis project at the Howdle group focused on PDMS macro-CTAs for RAFT dispersion polymerisation of MMA in scCO₂.²⁰³ This study showed promising results on the control over M_n and \mathcal{D} , while producing stable spherical particles with RAFT.²⁰³ This initial study presented an opportunity for further research and

development in the framework of this thesis. The topic of PISA dispersion in scCO₂ will be further discussed in Chapter 3.

1.8. References

1. D. Walton and P. Lorimer, *Polymers*, Oxford University Press, Oxford, 2000.
2. E. Saldívar-Guerra and E. Vivaldo-Lima, in *Handbook of Polymer Synthesis, Characterization, and Processing*, eds. E. Saldívar-Guerra and E. Vivaldo-Lima, John Wiley & Sons, New Jersey, United States of America, 2013, ch. Introduction to Polymers and Polymer Types, pp. 1-14.
3. L. E. Elizalde, G. de los Santos-Villarreal, J. L. Santiago-García and M. Aguilar-Vega, in *Handbook of Polymer Synthesis, Characterization, and Processing*, eds. E. Saldívar-Guerra and E. Vivaldo-Lima, John Wiley & Sons, Hoboken, New Jersey, 2013, ch. Step-Growth Polymerization pp. 41-63.
4. M. A. Villalobos and J. Debling, in *Handbook of Polymer Synthesis, Characterization, and Processing*, eds. E. Saldívar-Guerra and E. vivaldo-Lima, John Wiley & Sons, New Jersey, United States of America, 2013, ch. Bulk and Solution Processes, pp. 273-294.
5. J. Herrera-Ordóñez, E. Saldívar-Guerra and E. Vivaldo-Lima, in *Handbook of Polymer Synthesis, Characterization, and Processing*, eds. E. Saldívar-Guerra and E. Vivaldo-Lima, John Wiley & Sons, New Jersey, United States of America, 2013, ch. Dispersed-Phase Polymerization Processes, pp. 295-315.
6. E. Trommsdorff, H. Kohle and P. Lagally, *Macromol Chem Phys*, 1948, **1**, 169-198.
7. T. Liu, J. M. DeSimone and G. W. Roberts, *Polymer*, 2006, **47**, 4276-4281.
8. M. Lansalot, J. Rieger and F. D'Agosto, in *Macromolecular Self-Assembly*, eds. L. Billon and O. Borisov, John Wiley & Sons, New Jersey, United States of America, 2016, ch. 2, pp. 33-82.
9. P. B. Zetterlund, Y. Kagawa and M. Okubo, *Chemical reviews*, 2008, **108**, 3747-3794.
10. J. M. Asua, *Prog Polym Sci*, 2002, **27**, 1283-1346.
11. P. B. Zetterlund, S. C. Thickett, S. Perrier, E. Bourgeat-Lami and M. Lansalot, *Chemical reviews*, 2015, **115**, 9745-9800.
12. S. Shen, E. D. Sudol and M. S. El-Aasser, *J Polym Sci A Polym Chem*, 1994, **32**, 1087-1100.
13. C. M. Tseng, Y. Y. Lu, M. S. El-Aasser and J. W. Vanderhoff, *J Polym Sci A Polym Chem*, 1986, **24**, 2995-3007.
14. A. J. Paine, W. Luymes and J. McNulty, *Macromolecules*, 1990, **23**, 3104-3109.
15. M. Yasuda, H. Seki, H. Yokoyama, H. Ogino, K. Ishimi and H. Ishikawa, *Macromolecules*, 2001, **34**, 3261-3270.
16. D. Wang, V. L. Dimonie, E. D. Sudol and M. S. El-Aasser, *J Appl Polym Sci*, 2002, **84**, 2721-2732.
17. R. Guerrero-Santos, E. Saldívar-Guerra and J. Bonilla-Cruz, in *Handbook of Polymer Synthesis, Characterization, and Processing*, eds. E. Saldívar-Guerra and E. vivaldo-Lima, John Wiley & Sons, New Jersey, United States of America, 2013, ch. Free Radical Polymerization, pp. 65-83.
18. S. Perrier, *Macromolecules*, 2017, **50**, 7433-7447.
19. G. Moad, E. Rizzardo and S. H. Thang, *Polymer*, 2008, **49**, 1079-1131.
20. G. Moad, E. Rizzardo and S. H. Thang, *Acc Chem Res*, 2008, **41**, 1133-1142.
21. G. Moad and D. H. Solomon, *The Chemistry of Radical Polymerisation*, Elsevier, London, 2nd Edition edn., 1998.
22. P. J. Flory, *J Am Chem Soc*, 1937, 241-253.
23. F. R. Mayo, *J Am Chem Soc*, 1943, 2324-2329.
24. W. V. Smith, *J Am Chem Soc*, 1946, 2059-2064.
25. M. K. Donald and S. A. F. Bon, *Polym Chem-Uk*, 2020, **11**, 4281-4289.
26. G. K. Such, R. A. Evans and T. P. Davis, *Macromolecules* 2006, **39**, 1391-1396.
27. E. Baer, A. Hiltner and H. D. Keith, *Science*, 1987, **235**, 1015-1022.
28. C. J. Hawker and K. L. Wooley, *Science*, 2005, **309**, 1200-1205.

29. T. Otsu and M. Yoshida, *Macromol Rapid Commun*, 1982, **3**, 127-132.
30. W. A. Braunecker and K. Matyjaszewski, *Prog Polym Sci*, 2007, **32**, 93-146.
31. A. Favier and M. T. Charreyre, *Macromol Rapid Commun*, 2006, **27**, 653-692.
32. G. Moad, E. Rizzardo and S. H. Thang, *Aust J Chem*, 2005, **58**, 379-410.
33. G. Moad, E. Rizzardo and S. H. Thang, *Aust J Chem*, 2009, **62**, 1402-1472.
34. G. Moad, E. Rizzardo and S. H. Thang, *Aust J Chem*, 2012, **65**, 985-1076.
35. G. Riess, *Prog Polym Sci*, 2003, **28**, 1107-1170.
36. T. R. Darling, T. P. Davis, M. Fryd, A. A. Gridnev, D. M. Haddleton, S. D. Ittel, R. R. Matheson, G. Moad and E. Rizzardo, *J Polym Sci A Polym Chem*, 2000, **38**, 1706-1708.
37. S. Penczek, *J Polym Sci A Polym Chem*, 2002, **40**, 1665-1676.
38. P. B. Zetterlund, Y. Kagawa and R. K. O'Reilly, *M. Chem. Rev.*, 2008, **108**.
39. G. Moad and E. Rizzardo, *Macromolecules*, 1995, **28**, 8722-8728.
40. K. Matyjaszewski and T. P. Davis, *Handbook of Radical Polymerization*, John Wiley & Sons, Hoboken, 2002.
41. A. Goto, K. Sato, Y. Tsujii, T. Fukuda, G. Moad, E. Rizzardo and S. H. Thang, *Macromolecules*, 2001, **34**, 402-408.
42. M. F. Cunningham, D. C. T. Ng, S. G. Milton and B. Keoshkerian, *J Polym Sci A Polym Chem*, 2006, **44**, 232-242.
43. A. Goto and T. Fukuda, *Prog Polym Sci*, 2004, **29**, 329-385.
44. J. Chiefari, Y. K. B. Chong, F. Ercole, J. Krstina, J. Jeffery, T. P. T. Le, R. T. A. Mayadunne, G. F. Meijs, C. L. Moad, G. Moad, E. Rizzardo and S. H. Thang, *Macromolecules*, 1998, **31**, 5559-5562.
45. H. Fischer, *Chemical reviews*, 2001, **101**, 3581-3610.
46. G. Moad, E. Rizzardo and S. H. Thang, *Aust J Chem*, 2005, **58**, 379-410.
47. G. Moad, E. Rizzardo and S. H. Thang, *Aust J Chem*, 2006, **59**, 669-692.
48. C. Boyer, P. Lacroix-Desmazes, J.-J. Robin and B. Boutevin, *Macromolecules*, 2006, **39**, 4044-4053.
49. S. Yamago, *J Polym Sci A Polym Chem*, 2006, **44**, 1-12.
50. G. Moad, E. Rizzardo and S. H. Thang, *The Strem Chemiker*, 2011, **25**, 1-10.
51. C. Barner-Kowollik, in *Handbook of RAFT Polymerization*, John Wiley and Sons, New Jersey, United States of America, 2009, ch. Introduction.
52. G. Li, H. Zheng and R. Bai, *Macromol Rapid Commun*, 2009, **30**, 442-447.
53. Y. Z. You, C. Y. Hong, R. K. Bai, C.-Y. Pan and J. Wang, *Macromol Chem Phys*, 2002, **203**.
54. G. Moad, *Macromol Chem Phys*, 2014, **215**, 9-26.
55. R. Francis and A. Ajayaghosh, *Macromolecules*, 2000, **33**, 4699-4704.
56. M. H. Stenzel, L. Cummins, G. E. Roberts, T. P. Davis, P. Vana and C. Barner-Kowollik, *Macromol Chem Phys*, 2003, **204**, 1160-1168.
57. R. T. A. Mayadunne, E. Rizzardo, J. Chiefari, Y. K. Chong, G. Moad and S. H. Thang, *Macromolecules*, 1999, **32**, 6977-6980.
58. M. Destarac, D. Charmot, X. Franck and S. Z. Zard, *Macromol Rapid Commun*, 2000, **21**, 1035-1039.
59. R. T. A. Mayadunne, E. Rizzardo, J. Chiefari, J. Krstina, G. Moad, A. Postma and S. H. Thang, *Macromolecules*, 2000, **33**, 243-245.
60. D. J. Keddie, G. Moad, E. Rizzardo and S. H. Thang, *Macromolecules*, 2012, **45**, 5321-5342.
61. M. Benaglia, E. Rizzardo, A. Alberti and M. Guerra, *Macromolecules*, 2005, **38**, 3129-3140.
62. Y. K. Chong, J. Kristina, T. P. T. Le, G. Moad, A. Postma, E. Rizzardo and S. H. Thang, *Macromolecules*, 2003, **36**, 2256-2272.
63. C. Barner-Kowollik, M. Buback, B. Charleux, M. L. Coote, M. Drache, T. Fukuda, A. Goto, B. Klumperman, A. B. Lowe, J. B. McLeary, G. Moad, M. J. Monteiro, R. D. Sanderson, M. P. Tonge and P. J. Vana, *J Polym Sci A Polym Chem*, 2006, **44**, 5809.

64. Y. K. Chong, T. P. T. Le, G. Moad, E. Rizzardo and S. H. Thang, *Macromolecules*, 1999, **32**, 2071-2074.
65. G. Moad, J. Chiefari, Y. K. Chong, J. Krstina, R. T. A. Mayadunne, A. Postma, E. Rizzardo and S. H. Thang, *Polym Int*, 2000, **49**, 993-1001.
66. M. Benaglia, J. Chiefari, Y. K. Chong, G. Moad, E. Rizzardo and S. H. Thang, *J Am Chem Soc*, 2009, **131**, 6914-6915.
67. M. Benaglia, M. Chen, Y. K. Chong, G. Moad, E. Rizzardo and S. H. Thang, *Macromolecules*, 2009, **42**, 9384-9386.
68. J.-S. Song and M. A. Winnik, *Macromolecules*, 2006, **39**, 8318-8325.
69. P. B. Zetterlund, *Polym Chem-Uk*, 2011, **2**, 534-549.
70. S. W. Prescott, M. J. Ballard, E. Rizzardo and R. G. Gilbert, *Macromolecules*, 2005, **8**, .
71. A. D. Peklak and A. Butte, *J. Polym. Sci., Part A: Polym. Chem.* , 2006, **44**, 6114.
72. M. J. Monteiro, M. M. Adamy, B. J. Leeuwen, A. M. van Herk and M. Destarac, *Macromolecules*, 2005, **38**, 1538-1541.
73. M. J. Monteiro and J. de Barbeyrac, *Macromolecules*, 2001, **34**, 4416-4423.
74. S. W. Prescott, *Macromolecules*, 2003, **36**, 9608-9621.
75. P. J. Saikia, J. M. Lee, B. H. Lee and S. Choe, *J Polym Sci A Polym Chem*, 2007, **45**, 348-360.
76. P. J. Saikia, J. M. Lee, K. Lee and S. J. Choe, *J Polym Sci A Polym Chem*, 2008, **46**, 872-885.
77. S. E. Shim, H. Jung, H. Lee, B. J. and S. Choe, *Polymer*, 2003, **44**, 5563-5572.
78. F. D'Agosto, J. Rieger and M. Lansalot, *Angew Chem Int Ed*, 2020, **59**, 8368-8392.
79. M. J. Derry, L. A. Fielding and S. P. Armes, *Prog Polym Sci*, 2016, **52**, 1-18.
80. C. J. Ferguson, R. J. Hughes, B. T. T. Pham, B. S. Hawke, R. G. Gilbert, A. K. Serelis and C. H. Such, *Macromolecules*, 2002, **35**, 9243-9245.
81. A. P. Lopez-Oliva, N. J. Warren, A. Rajkumar, O. O. Mykhaylyk, M. J. Derry, K. E. B. Doncom, M. J. Rymaruk and S. P. Armes, *Macromolecules*, 2015, **48**, 3547-3555.
82. I. Chaduc, W. Zhang, J. Rieger, M. Lansalot, F. D'Agosto and B. Charleux, *Macromol Rapid Commun*, 2011, **32**, 1270-1276.
83. X. Zhang, J. Rieger and B. Charleux, *Polym Chem*, 2012, **3**, 1502-1509.
84. E. R. Jones, M. Semsarilar, A. Blanazs and S. P. Armes, *Macromolecules*, 2012, **45**, 5091-5098.
85. W. M. Wan, X. L. Sun and C. Y. Pan, *Macromolecules*, 2009, **42**, 4950 - 4952.
86. G. Delaittre, C. Dire, J. Rieger, J.-L. Putaux and B. Charleux, *Chem Commun*, 2009, **0**, 2887-2889.
87. Y. Mai and A. Eisenberg, *Chem Soc Rev*, 2012, **41**, 5969-5985.
88. J. Xu, X. Xiao, Y. Zhang, W. Zhang and P. J. Sun, *Polym Sci Part A Polym Chem*, 2013, **51**, 1147-1161.
89. J. Lesage de la Haye, X. Zhang, I. Chaduc, F. Brunel, M. Lansalot and F. D'Agosto, *Angew Chem Int*, 2016, **55**, 3739-3743.
90. L. Houillot, C. Bui, M. Save, B. Charleux, C. Farcet, C. Moire, J. A. Raust and I. Rodriguez, *Macromolecules*, 2007, **40**, 6500-6509.
91. L. A. Fielding, M. J. Derry, V. Ladmiral, J. Rosselgong, A. M. Rodrigues, L. P. D. Ratcliffe, S. Sugihara and S. P. Armes, *Chem Sci*, 2013, **4**, 2081.
92. A. Clifford, *Fundamentals of Supercritical Fluids*, Oxford Science Publications, 1999.
93. J. A. Darr and M. Poliakoff, *Chemical reviews*, 1999, **99**, 495-542.
94. C. Boyère, C. Jérôme and A. Debuigne, *Eur Polym J*, 2014, **61**, 45-63.
95. P. B. Zetterlund, F. Aldabbagh and M. Okubo, *J Polym Sci A Polym Chem*, 2009, **47**, 3711-3728.
96. E. J. Beckman, *J Supercrit Fluids*, 2004, **28**, 121-191.
97. J. L. Kendall, D. A. Canelas, J. L. Young and J. M. DeSimone, *Chemical reviews*, 1999, **99**, 543-563.
98. J. A. Behles and J. M. DeSimone, *Pure Appl Chem*, 2001, **73**, 1281-1285.
99. W. Leitner, *Nature*, 2000, **405**, 129-130.

100. R. A. Quirk, R. M. France, K. M. Shakesheff and S. M. Howdle, *Curr Opin Solid State Mater Sci*, 2004, **8**, 313-321.
101. B. Subramaniam, R. A. Rajewski and K. Snavely, *Journal of pharmaceutical sciences*, 1997, **86**, 885-890.
102. A. I. Cooper, *J Mater Chem*, 2000, **10**, 207-234.
103. S. K. Goel and E. J. Beckman, *Polymer*, 1993, **34**, 1410-1417.
104. A. Rajendran, B. Bonavoglia, N. Forrer, G. Storti, M. Mazzotti and M. Morbidelli, *Ind Eng Chem Res*, 2005, **44**, 2549-2560.
105. B. Bonavoglia, G. Storti, M. Morbidelli, A. Rajendran and M. Mazzotti, *J Polym Sci B Polym Phys*, 2006, **44**, 1531-1546.
106. U. Fehrenbacher, T. Jakob, T. Berger, W. Knoll and M. Ballauff, *Fluid Phase Equilib.*, 2002, **200**, 147-160.
107. H. M. Woods, C. Nouvel, P. Licence, D. J. Irvine and S. M. Howdle, *Macromolecules*, 2005, **38**, 3271-3282.
108. Y.-L. Hsiao, E. E. Maury, J. M. DeSimone, S. M. Mawson and K. P. Johnston, *Macromolecules*, 1995, **28**, 8159-8166.
109. C. F. Kirby and M. A. McHugh, *Chemical reviews*, 1998, **99**, 565-602.
110. Z. Guan, J. R. Combes, Y. Z. Menceloglu and J. M. DeSimone, *Macromolecules*, 1993, **26**, 2663-2669.
111. J. M. DeSimone, Z. Guan and C. S. Elsbernd, *Science*, 1992, **257**, 945-947.
112. W. K. Czerwinski, *Die Makromolekulare Chemie*, 1991, **192**, 1285-1296.
113. A. M. van Herk, B. G. Manders, D. A. Canelas, M. A. Quadir and J. M. DeSimone, *Macromolecules*, 1997, **30**, 4780-4782.
114. S. Beuermann, M. Buback, C. Schmaltz and F. D. Kuchta, *Macromol Chem Phys*, 1998, **199**, 1209-1216.
115. S. Beuermann and M. Buback, in *Polymer Reaction Engineering*, eds. M. F. Kemmere and T. Meyer, Wiley-VCH, Weinheim, Germany, 2005, ch. Kinetics of Free-Radical Polymerization in Homogeneous Phase of Supercritical Carbon Dioxide, pp. 55-80.
116. S. Beuermann and M. Imran-ul-Haq, *J Polym Sci A Polym Chem* 2007, **45**, 5626-5635.
117. E. Möller and S. Beuermann, *Macromol React Eng* 2011, **5**, 8-21.
118. T. J. Romack, E. E. Maury and J. M. DeSimone, *Macromolecules*, 1995, **28**, 912-915.
119. X.-H. Wang, L.-Q. Cao, L.-J. Zhang and J.-D. Wang, *Polym Adv Technol*, 2012, **23**, 529-533.
120. J. Liu, H. Tai and S. M. Howdle, *Polymer*, 2005, **46**, 1467-1472.
121. M. K. Saraf, S. Gerard, L. M. Wojcinski, P. A. Charpentier, J. M. DeSimone and G. W. Roberts, *Macromolecules*, 2002, **35**, 7976-7985.
122. D. Bratton, M. Brown and S. M. Howdle, *Macromolecules*, 2005, **38**, 1190-1195.
123. A. R. Goddard, S. Pérez-Nieto, T. M. Passos, B. Quilty, K. Carmichael, D. J. Irvine and S. M. Howdle, *Green Chem*, 2016, **18**, 4772-4786.
124. J. M. DeSimone, E. E. Maury, Y. Z. Menceloglu, J. B. McClain, T. J. Romack and J. R. Combes, *Science*, 1994, **265**, 356-359.
125. G. Hawkins, P. B. Zetterlund and F. Aldabbagh, *J Polym Sci A Polym Chem*, 2015, **53**, 2351-2356.
126. T. Carson, J. Jeermy and M. DeSimone, *Macromolecules*, 2000, **33**, 1917-1920.
127. S. G. Kazarian, M. F. Vincent, F. V. Bright, C. L. Liotta and C. A. Eckert, *J Am Chem Soc*, 1996, **118**, 1729-1736.
128. T. Sarbu, T. J. Styranecek and E. J. Beckman, *Ind Eng Chem Res*, 2000, **39**, 4678-4683.
129. D. W. J. Osmond and F. A. Waite, *Dispersion Polymerisation in Organic Media*, John Wiley And Sons, Bristol, 1975.
130. D. A. Canelas, D. E. Betts, J. M. DeSimone and M. Z. Yates, *Macromolecules*, 1998, **31**, 6794-6805.
131. H. Shiho and J. M. DeSimone, *J Polym Sci A Polym Chem*, 1999, **37**, 2429-2437.

132. P. Christian, S. M. Howdle and D. J. Irvine, *Macromolecules*, 2000, **33**, 237-239.
133. C. Lepilleur and E. J. Beckman, *Macromolecules*, 1997, **30**, 745-756.
134. K. K. Kapellen, C. D. Mistele and J. M. DeSimone, *Macromolecules*, 1996, **29**, 495-496.
135. H. Tai, W. Wang and S. M. Howdle, *Polymer*, 2005, **46**, 10626-10636.
136. D. A. Canelas, D. E. Betts and J. M. DeSimone, *Macromolecules*, 1996, **29**, 2818-2821.
137. H. Shiho and J. M. DeSimone, *Macromolecules*, 2001, **34**, 1198-1203.
138. H. Shiho and J. M. DeSimone, *J Polym Sci A Polym Chem*, 2000, **38**, 3783-3790.
139. K. A. Shaffer, T. A. Jones, D. A. Canelas and J. M. DeSimone, *Macromolecules*, 1996, **29**, 2704-2706.
140. J. C. Merdith and K. P. Johnston, *Macromolecules*, 1998, **31**, 5507-5517.
141. J. C. Merdith and K. P. Johnston, *Macromolecules*, 1998, **31**, 5518-5528.
142. K. J. Thurecht, A. M. Gregory, W. Wang and S. M. Howdle, *Macromolecules*, 2007, **40**, 2965-2967.
143. W. Wang, M. R. Giles, D. Bratton, D. J. Irvine, S. P. Armes, J. V. W. Weaver and S. M. Howdle, *Polymer*, 2003, **44**, 3803-3809.
144. H. Yuvaraj, H. S. Hwang, Y. S. Jung, J.-H. Kim, S.-S. Hong and K. T. Lim, *J Supercrit Fluids*, 2007, **42**, 351-358.
145. M. R. Giles, R. M. T. Griffiths, D. J. Irvine and S. M. Howdle, *Eur Polym J*, 2003, **39**, 1785-1790.
146. D. A. Canelas and J. M. DeSimone, *Macromolecules*, 1997, **30**, 5673-5682.
147. M. R. Giles, S. J. O'Connor, J. N. Hay, R. J. Winder and S. M. Howdle, *Macromolecules*, 2000, **33**, 1996-1999.
148. M. R. Giles, J. N. Hay, S. M. Howdle and R. J. Winder, *Polymer*, 2000, **41**, 6715-6721.
149. W. P. Hems, T.-M. Yong, J. L. M. van Nunen, A. I. Cooper, A. B. Holmes and D. A. Griffin, *J Mater Chem*, 1999, **9**, 1403-1407.
150. A. I. Cooper, W. P. Hems and A. B. Holmes, *Macromolecules*, 1999, **32**, 2156-2166.
151. T. D. McAllister, L. D. Farrand and S. M. Howdle, *Macromol Chem Phys*, 2016, **217**, 2294-2301.
152. N. A. Birkin, N. J. Arrowsmith, E. J. Park, A. P. Richez and S. M. Howdle, *Polym Chem*, 2011, **2**, 1293-1299.
153. N. A. Birkin, O. J. Wildig and S. M. Howdle, *Polym Chem*, 2013, **4**, 3791-3799.
154. E. J. Park, A. P. Richez, N. A. Birkin, H. Lee, N. Arrowsmith, K. J. Thurecht and S. M. Howdle, *Polymer*, 2011, **52**, 5403-5409.
155. H. Lee, J. W. Pack, W. Wang, K. J. Thurecht and S. M. Howdle, *Macromolecules*, 2010, **43**, 2276-2282.
156. H. Lee, E. Terry, M. Zong, N. Arrowsmith, S. Perrier, K. J. Thurecht and S. M. Howdle, *J Am Chem Soc*, 2008, **130**, 12242-12243.
157. N. A. Birkin, Doctor of Philosophy, University of Nottingham, 2012.
158. R. Parilti, A. Castañon, M. Lansalot, F. D'Agosto, C. Jérôme and S. M. Howdle, *Polym Chem*, 2019, **10**, 5760-5770.
159. J. M. DeSimone and J. S. Keiper, *Current Opinion in Solid State and Materials Science*, 2001, **5**, 333-341.
160. P. Christian, M. R. Giles, R. M. T. Griffiths, D. J. Irvine, R. C. Major and S. M. Howdle, *Macromolecules*, 2000, **33**, 9222-9227.
161. M. R. Giles and S. M. Howdle, *European Polymer Journal*, 2001, **37**, 1347-1351.
162. T. D. McAllister, L. D. Farrand and S. M. Howdle, *Macromolecular Chemistry and Physics*, 2016, **217**, 2294-2301.
163. P. F. Oliveira, R. A. F. Machado, D. Barth and E. D. Acosta, *Chemical Engineering and Processing: Process Intensification*, 2016, **103**, 46-52.
164. S. H. Han, K. K. Park and S. H. Lee, *Macromolecular Research*, 2009, **17**, 51-57.
165. M. L. O'Neill, M. Z. Yates, P. J. Johnston, S. C. D. and S. P. Wilkinson, *Macromolecules*, 1998, **31**, 2838-2847.

166. M. L. O'Neill, M. Z. Yates, K. P. Johnston, C. D. Smith and S. P. Wilkinson, *Macromolecules*, 1998, **31**, 2848-2856.
167. U. Fehrenbacher and M. Matthias Ballauff, *Macromolecules*, 2002, **35**, 3653-3661.
168. U. Fehrenbacher, O. Muth, T. Hirth and M. Ballauff, *Macromol Chem Phys*, 2000, **201**, 1532-1539.
169. C. Chatzidoukas, P. Pladis and C. Kiparissides, *Ind Eng Chem Res*, 2003, **42**, 743-751.
170. P. A. Mueller, G. Storti and M. Morbidelli, *Chem Eng Sci*, 2005, **60**, 377-397.
171. P. A. Mueller, G. Storti and M. Morbidelli, *Chem Eng Sci*, 2005, **60**, 1911-1925.
172. K. J. Thurecht and S. M. Howdle, *Aust J Chem*, 2009, **62**, 786-789.
173. J. Xia, T. Johnson, S. G. Gaynor, K. Matyjaszewski and J. M. DeSimone, *Macromolecules* 1999, **32**, 4802-4805.
174. H. Minami, Y. Kagawa, S. Kuwahara, J. Shigematsu, S. Fujii and M. Okubo, *Des Monomers Polym*, 2004, **7**, 553.
175. H. Minami, A. Tanaka, Y. Kagawa and M. Okubo, *J Polym Sci A Polym Chem*, 2012, **50**, 2578-2584.
176. B. Grignard, C. Calberg, C. Jérôme, W. Wang, S. Howdle and C. Detrembleur, *Chem Commun*, 2008, **44**, 5803-5805.
177. B. Grignard, C. Jérôme, C. Calberg, R. Jérôme, W. Wang, S. M. Howdle and C. Detrembleur, *Chem Commun*, 2008, **3**, 314-316.
178. R. McHale, F. Aldabbagh, P. B. Zetterlund, H. Minami and M. Okubo, *Macromolecules*, 2006, **39**, 6853-6860.
179. R. McHale, F. Aldabbagh, P. B. Zetterlund and M. Okubo, *Macromol Chem Phys*, 2007, **208**, 1813-1822.
180. F. Aldabbagh, P. B. Zetterlund and M. Okubo, *Macromolecules*, 2008, **41**, 2732-2734.
181. B. Grignard, T. Phan, D. Bertin, D. Gigmes, C. Jerome and C. Detrembleur, *Polym Chem*, 2010, **1**, 837-840.
182. P. O'Connor, P. B. Zetterlund and F. Aldabbagh, *Macromolecules*, 2010, **43**, 914-919.
183. P. O'Connor, P. B. Zetterlund and F. Aldabbagh, *J Polym Sci A Polym Chem*, 2011, **49**, 1719-1723.
184. T. Arita, S. Beuermann, M. Buback and P. Vana, *Macromol Mater Eng*, 2005, **290**, 283-293.
185. A. M. Gregory, K. J. Thurecht and S. M. Howdle, *Macromolecules*, 2008, **41**, 1215-1222.
186. E. A. Jackson and M. A. Hillmyer, *ACS nano*, 2010, **4**, 3548-3553.
187. Y. Luo, X. Wang, Y. Zhu, B.-G. Li and S. Zhu, *Macromolecules*, 2010, **43**, 7472-7481.
188. H. C. Kim, S. M. Park and W. D. Hinsberg, *Chemical reviews*, 2010, **110**, 146-177.
189. A. Lu and R. K. O'Reilly, *Curr Opin Biotechnol*, 2013, **24**, 639-645.
190. M. H. Huang, S. M. Li and M. Vert, *Polymer*, 2004, **45**, 8675-8681.
191. J. A. Opsteen and J. C. M. v. Hest, *Chem Commun*, 2005, **0**, 57-59.
192. K. J. Thurecht, A. M. Gregory, S. Villarroya, J. X. Zhoy, A. Heise and S. M. Howdle, *Chem Commun*, 2006, **0**, 4383-4385.
193. J. Jennings, M. Beija, A. P. Richez, S. D. Cooper, P. E. Mignot, K. J. Thurecht, K. S. Jack and S. M. Howdle, *J Am Chem Soc*, 2012, **134**, 4772-4781.
194. J. Jennings, S. P. Bassett, D. Hermida-Merino, G. Portale, W. Bras, L. Knight, J. J. Titman, T. Higuchi, H. Jinnai and S. M. Howdle, *Polym Chem*, 2016, **7**, 905-916.
195. J. Jennings, M. Beija, J. T. Kennon, H. Willcock, R. K. O'Reilly, S. Rimmer and S. M. Howdle, *Macromolecules*, 2013, **46**, 6843-6851.
196. J. Jennings, G. He, S. M. Howdle and P. B. Zetterlund, *Chem Soc Rev*, 2016, **45**, 5055-5084.
197. G. He, T. M. Bennett, M. Alauhdin, M. W. Fay, X. Liu, S. T. Schwab, C. G.-. Sun and S. M. Howdle, *Polym Chem*, 2018, **9**, 3808-3819.
198. M. Alauhdin, T. M. Bennett, G. He, S. P. Bassett, G. Portale, W. Bras, D. Hermida-Merino and S. M. Howdle, *Polym Chem*, 2019, **10**, 860-871.
199. M. Zong, K. J. Thurecht and S. M. Howdle, *Chem Commun*, 2008, **0**, 5942-5944.

200. A. Xu, Q. Lu, Z. Huo, J. Ma, B. Geng, U. Azhar, L. Zhang and S. Zhang, *Rsc Adv*, 2017, **7**, 51612-51620.
201. Z Y Huo, P D Xia, U Azhar, J C Ma, X M Zhang, X Y Zhou, S. X. Z. and and A. H. Xu, *IOP Conf Ser: Mater Sci Eng*, 2019, **479**.
202. A. Alzahrani, D. Zhou, R. P. Kuchel, P. B. Zetterlund and F. Aldabbagh, *Polym Chem-Uk*, 2019, **10**, 2658-2665.
203. M. Zong, Doctor of Philosophy University of Nottingham, 2010.

Contents

Chapter 2. Experimental equipment and characterisation techniques	65
2.1. <i>Abstract</i>	65
2.2. <i>Materials</i>	65
2.3. <i>High pressure equipment</i>	65
2.3.1. General high-pressure setup and considerations.....	65
2.3.2. Mk III clamp sealed autoclave.....	67
2.3.3. SOP for dispersion polymerisation in scCO ₂	70
2.3.3.1. Standard RAFT polymerisation procedure.....	71
2.3.3.2. Standard conventional radical polymerisation procedure.....	72
2.3.3.3. Standard polymerisation procedure with macro-CTA.....	72
2.3.4. Mk III clamp sealed autoclave with modified HPLC inlet.....	72
2.3.5. SOP for two-steps polymerisation.....	73
2.3.6. Fixed volume view cell.....	75
2.3.7. SOP for fixed volume view cell.....	78
2.3.7.1. Procedure for solubility studies in scCO ₂	80
2.3.7.2. Procedure for nucleation onset studies in scCO ₂	80
2.3.8. High pressure variable volume view cell.....	80
2.3.9. SOP for variable volume view cell.....	87
2.3.9.1. Procedure for cloud point study in variable volume view cell.....	88
2.3.10. High-pressure sampling autoclave.....	89
2.3.11. SOP for sampling autoclave.....	91
2.4. <i>Characterisation techniques</i>	92
2.4.1. Size exclusion chromatography.....	92
2.4.2. Nuclear magnetic resonance.....	94
2.4.3. Scanning electron microscopy.....	94
2.5. <i>References</i>	96

Chapter 2. Experimental equipment and characterisation techniques

2.1. Abstract

This chapter will describe the experimental equipment and characterisation techniques employed throughout this thesis. Dispersion polymerisation in scCO₂ is a specialised technique, which requires specific equipment with various safety and operational considerations. Therefore, the first half of this chapter is dedicated to the high-pressure equipment setup and standard operation procedures (SOPs). The second half of this chapter will focus on the main characterisation techniques used to analyse the materials synthesised in this thesis. In general, all products were analysed to determine conversion, molecular weight and dispersity. The products that were obtained as a powder from the polymerisations in scCO₂ were also analysed to determine particle morphology, size and particle size dispersity.

2.2. Materials

MMA was purchased from ProSciTech (99 %) and was filtered through aluminium oxide in order to remove the inhibitor (monomethyl ether hydroquinone) prior to polymerisation. 2,2'-azobis(isobutyronitrile) (AIBN) was purchased from Sigma Aldrich (98%) and purified by recrystallisation in methanol prior to use. All other chemicals were used as received. All CTAs were purchased from Sigma-Aldrich, with exception of two CTAs, the synthesis of these CTAs is reported in Chapter 3 and 4. Methacrylate terminated polydimethylsiloxane (PDMS-MA) 10 kg mol⁻¹ was purchased from ABCR GmbH & Co. Tetrahydrofuran (THF) (HPLC grade), deuterated chloroform (CDCl₃) and acetone (technical grade) were purchased from Fischer Scientific. Any other specific chemicals are presented in each results chapter.

2.3. High pressure equipment

2.3.1. General high-pressure setup and considerations

A typical high-pressure setup consists of a pressure supply system (CO₂ pump), high-pressure pipe connections, a high-pressure vessel and associated monitoring equipment for pressure and temperature. A schematic of the equipment is shown below (Figure 1).

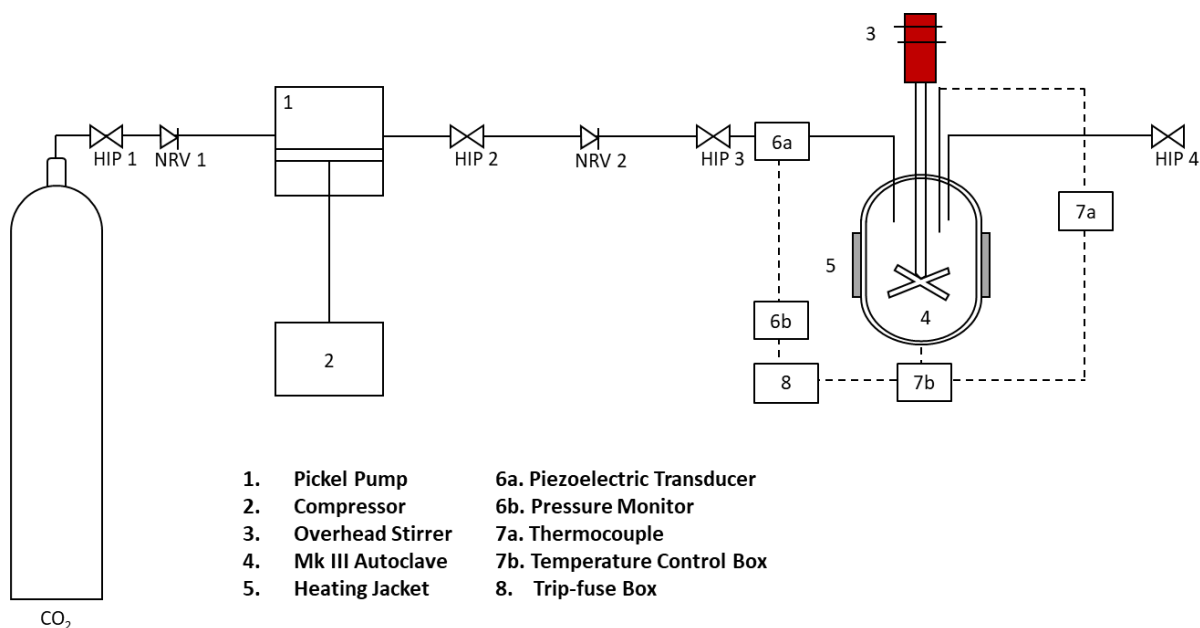


Figure 1 - Schematic diagram of high-pressure autoclave rig setup, depicting the autoclave, monitoring systems, trip box, heating jacket and stirrer; as well as the high-pressure line, which is supplied with pressurised CO₂ by the Pickel Pump which is connected to a compressor and a CO₂ cylinder. Apart from the trip-fuse box, the other safety features of the autoclave are not included here and will be presented in the next section.

In the system used throughout this thesis, a PM-101 SFE Pickel pump, supplied by New Ways of Analytics, was used to supply liquid CO₂ at 3-5 bar to the high-pressure vessel. The pump is fed with CO₂ from a high-pressure cylinder through a non-return valve (NRV) and a refrigerator unit within the pump is responsible for liquefaction of the gas. The liquid CO₂ then passes into a compressor, and is compressed by a high surface area piston (111:1 ratio), powered by an external air compressor. The difference in the piston areas allows the small initial pressure supplied by the air compressor, at 4.83 bar, to compress the fluid to the desired pressure. The pressurised CO₂ is fed into the CO₂ high-pressure main pipeline through NRVs. These valves prevent back-flow into the main line from the reactor vessels, which are operated at higher pressure. The CO₂ main line consists of HIP taps and Swagelok® tubing and fittings.

Stainless steel Swagelok 1/16" piping is used for the delivery of CO₂, while the autoclave head is equipped with 1/8" pipe from the same grade and vendor. HIP valves control the inlet of CO₂ from the main line and the outlet of the reaction vessel. These valves are securely

fastened to a magnet, which is attached to a steel plate on the base of the fume hood to minimise the wear and tear of the pipe work and thus reduce safety hazards.

The temperature was controlled by an in-house built digital heating controller, which supplies power either to a heating jacket, as in the case of the Mk III autoclave, or to cartridges fitted into the reactor vessel, as in the case of the view cells. A thermocouple inside the reaction vessel provides a feedback loop to allow autoregulation of the heater. The pressure of the system was measured by a piezoelectric transducer. This device uses a quartz crystal as the piezoelectric element, which under pressure experiences proportional displacement or strain. This displacement generates a short-lived electrical output, which is representative of the amount of pressure loading on the crystal. The voltage is read by an in-house built digital pressure box and translated into the systems internal pressure, allowing it to be effectively monitored. The positioning of the transducer is fundamental to ensure the internal pressure of the vessel is accurately measured. It is preferential to place it on the CO₂ inlet rather than on the outlet, in order to avoid blockages or the formation of a polymer coating which would lead to false readings. For the work described in this thesis, the pressure is recorded relative to atmospheric pressure, *i.e.*, 1 bar.

A trip-fuse box is incorporated into the setup as an additional safety feature. The mains power to the heating control box is connected through the trip, which receives a signal from the pressure box. This is to ensure that if the pressure exceeds a set maximum pressure, the power to the heating system is automatically disabled, allowing the vessel to cool down and consequently the pressure to decrease. The safe pressure limit for the equipment used in this work is 345 bar and the pressure trip was set to 310 bar.

2.3.2. Mk III clamp sealed autoclave

Most polymerisations in scCO₂ presented in this thesis were performed in an Mk III stainless steel 316 autoclave, for which the maximum operating working pressure is 345 bar. These vessels were designed and built in-house at the University of Nottingham and have previously been described in full elsewhere.¹⁻³ The reactor comprises of a head and base, which are held together by a clamp and sealed with an O-ring (Figure 2). The use of a metal-rubber seal rather than a direct metal-metal seal prevents damage to the stainless steel autoclave. Reactions

presented in this work used an ethylene propylene diene monomer (EPDM) O-ring, which limits the safe working temperature to between -50 and 150 °C.

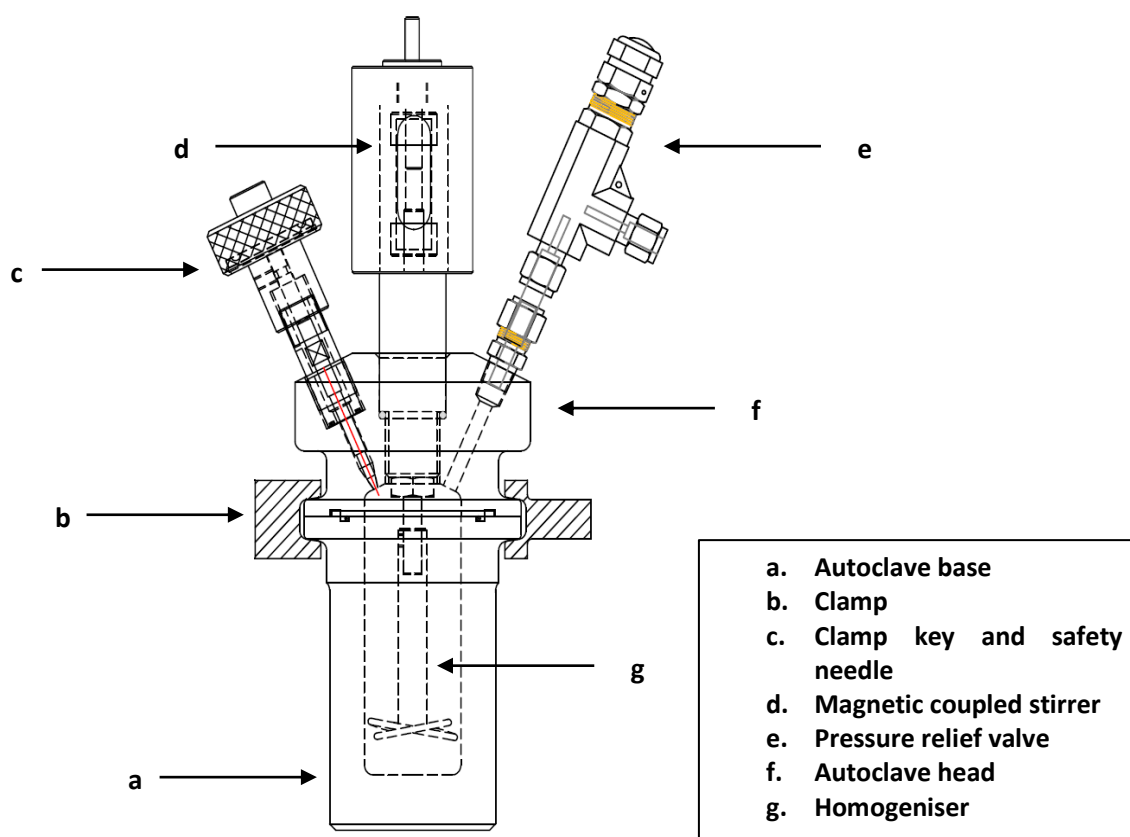


Figure 2 – Schematics of High-pressure Mk III autoclave, depicting all the components of the autoclave body, including the safety features, pressure release valve (e) and clamp key and safety needle (c).

The head has a magnetically coupled stirrer and contains five ports, in addition to a pressure release valve. Two ports are required for the CO₂ inlet pipe and outlet pipe, both are 1/8 " stainless steel Swagelok. A third is used for inserting a K-type thermocouple. The fourth aperture remains sealed with a metal plug, which can be removed if additional features need to be incorporated, such as an inlet for connection to a high performance liquid chromatography (HPLC) pump which would allow for the addition of liquids whilst the vessel is under pressure. A further opening in the head is a safety valve that must be sealed with a safety needle, which works as the final sealing point of the vessel. The safety needle also works as a key that is required to open the clamp. Each key is unique to each clamp, with a dented pattern on the pinwheel that only fits into a corresponding recess in the clamp's screw

(Figure 3). In this way, the safety key/valve must be loosened and removed, allowing the release of all residual pressure through the safety valve, before the clamp can be opened and the autoclave taken apart.

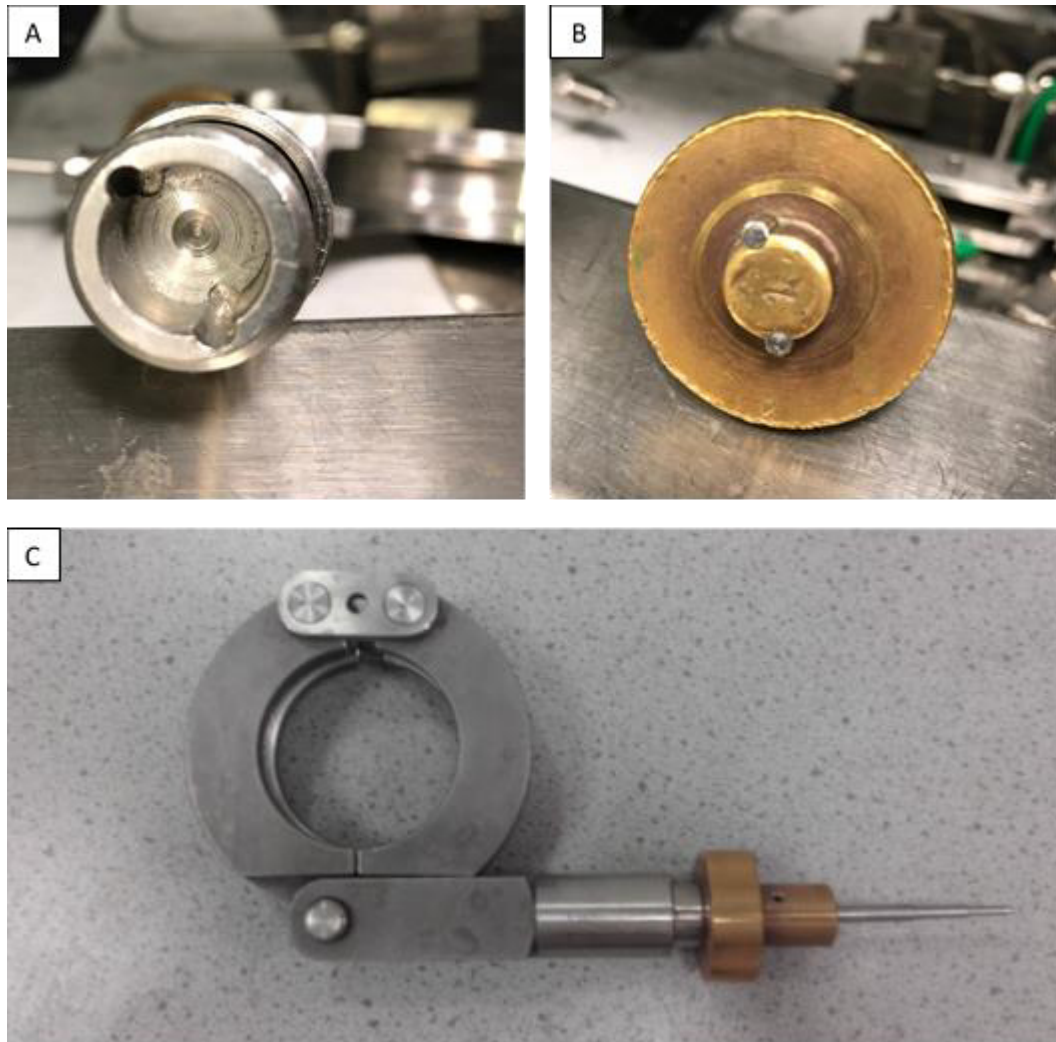


Figure 3 - Photographs of safety key mechanism. (A) Recess in clamp screw; (B) Unique dented pattern on key pinwheel matching clamp recess ; (C) Example of pinwheel and safety needle being employed as the key for the clamp.

The head was also equipped with a sprung pressure relief valve, as a last line of defence, to prevent the pressure of the autoclave exceeding the maximum working pressure of 345 bar. Since the valve is sprung, it should allow pressure to escape until it falls back below this threshold, at which point the valve should reseal.

The Mk III autoclave incorporates a magnetically coupled stirrer placed in the centre of the autoclave head, which is sealed with a small O-ring. The shaft of the stirrer extends down into

the main body of the autoclave, where a stirrer blade is attached allowing for the efficient mixing of the reaction contents. Stirring was achieved using an overhead stirrer, supplied from IKA Works GmbH - Germany, connected *via* rubber tubing to the magnetically coupled stirrer in the autoclave head. Stirring rates were kept at 300 rpm for all reactions, unless stated otherwise.

The autoclave body is the bulk volume of the reactor, and there are two exchangeable sizes, 20 and 60 mL. Heating is provided by a custom-made heating jacket, provided by Watlow, which fits around the exterior of the autoclave body, and is controlled by the heating box coupled to the internal thermocouple. The autoclave head is attached to the base using the stainless steel clamp and the EPDM O-ring, which sits in the recess in the base and fits tightly with the autoclave head recess. The clamp was hand tightened *via* a screw mechanism with the safety key. A torque system was incorporated into the pinwheel to prevent over-tightening of the clamp. In this way, once the clamp is tightened the key will turn around itself and will not tighten the clamp any further.

2.3.3. SOP for dispersion polymerisation in scCO₂

The standard operation procedure was followed rigorously to ensure safety. An outline for this procedure is given below.

1. To assemble the autoclave, an EPDM O-ring was placed in the autoclave body and the heating jacket was secured around the autoclave base. The head and base of the autoclave were coupled together using the clamp. Then, all Swagelok fittings were tightened, connecting the autoclave head to the CO₂ inlet and outlet pipes, making sure all HIP valves were closed. Finally, the safety valve in the autoclave head was closed with the safety key.
2. A pressure test was done by slowly filling the vessel with CO₂ to approximately 55 bar, checking all fitting for leaks with Swagelok Snoop[®] leak detector. Pressure was also monitored on the pressure box over a minimum of 2 hours. The temperature was also monitored over the leak test, making sure the thermocouple was well connected. If any leaks were detected, the vessel was vented through the outlet tap to ambient pressure prior to adjusting the fittings. This process was repeated until no leaks

occurred and the pressure did not drop. When happy with the leak test, the autoclave was vented and the safety key removed.

3. The autoclave was purged through the safety valve, while keeping the autoclave outlet closed, with a flow of CO₂, at around *circa* 2 bar for 30 minutes. This step removes residual oxygen from the system.
4. Whilst maintaining a small positive pressure of *circa* 2 bar to prevent the ingress of air, the autoclave was charged with required reactants *via* a glass syringe and needle through the keyhole.
5. The autoclave was sealed with the safety key and the overhead stirrer was connected and started at a stirring speed of 300 rpm.
6. The heating jacket was plugged in, making sure that the internal thermocouple was well connected. The pressure was increased to 55 bar then heating was set to 50 °C. After the autoclave reached that temperature, the pressure was slowly increased to *circa* 200 bar before setting the heating to 65 °C. If required, the pressure was carefully to the desired final pressure of 276 bar.
7. The pressure was monitored at the desired reaction conditions, making sure it was stable, and ensuring the tap connected to the CO₂ main line is closed.
8. After the desired reaction time, the heating box was set to 0 °C and the heating jacket was unplugged to prevent further heating. The autoclave was allowed to cool to room temperature, while monitoring the temperature by means of the internal thermocouple.
9. After allowing the autoclave to cool to ambient temperature, the heating jacket was removed and the CO₂ was vented slowly into the fume hood.
10. Once at ambient temperature and pressure, the key was removed and the Swagelok fittings were undone. Next, the clamp was loosen and removed, before finally opening the autoclave and collecting the product.
11. After the product collection, the autoclave was thoroughly cleaned with acetone.

2.3.3.1. Standard RAFT polymerisation procedure

A typical procedure, in which poly(methyl methacrylate) (PMMA) with a molecular weight of 60 kg mol⁻¹ was targeted, used the described high-pressure Mk III 20 mL autoclave. The autoclave was assembled, leak tested and degassed with CO₂ as described in the SOP. Methyl

methacrylate (MMA) (33 mmol, 3.3. mL), AIBN (0.08 mmol), polydimethylsiloxane (PDMS-MA) (5 wt % relative to MMA) and the respective chain transfer agent (CTA) (0.055 mmol, keeping a molar ratio of 1:2 AIBN/CTA), were placed in a vial and degassed by bubbling with argon whilst on ice for 30 minutes. The reactants were then added to the autoclave with a glass syringe and needle *via* the keyhole against a positive pressure of CO₂. The vessel was then sealed, heated and pressurised as stated in the SOP. After 24 hours, heating was turned off and the products were collected for analysis as dry free-flowing powders, unless stated otherwise.

2.3.3.2. Standard conventional radical polymerisation procedure

The same procedure as for the RAFT polymerisation was applied (See Section 2.3.3.1.), but in the absence of a CTA. In this way, the molar ratio of MMA to AIBN was 1200:1. Reaction conditions were kept the same, *i.e.*, 276 bar, 65 °C and 24 hours. All products were collected for analysis as dry free-flowing powders.

2.3.3.3. Standard polymerisation procedure with macro-CTA

A typical procedure used the described Mk III 20 mL autoclave and was identical to the RAFT dispersion polymerisation procedure (See Section 2.3.3.1.), but without addition of PDMS-MA, since the macro-CTA is expected to provide simultaneous control and stabilisation. Different macro-CTAs were used in this thesis and the full list is presented in Chapter 3 and Chapter 5. For a target of 60 kg mol⁻¹ PMMA, MMA (33 mmol) AIBN (0.028 mmol) and the respective macro-CTA (0.055 mmol) were used, with attention to maintaining a molar ratio of AIBN/macro-CTA ratio of 1:2. At the end of the reaction, all products were collected for analysis.

2.3.4. Mk III clamp sealed autoclave with modified HPLC inlet

A modified autoclave was also employed in this thesis to allow two-stage reactions to be carried out. As mentioned in Section 2.3.2., the head of the autoclave has five apertures: (1) the CO₂ inlet pipe, (2) the CO₂ outlet, (3) the thermocouple, (4) the safety keyhole and (5) remains sealed with a removable metal plug. This last aperture was used for incorporating an extra inlet pipe for the addition of reactants *via* a Jasco PU-980 HPLC pump (Figure 4). This allowed for addition of liquid reactants whilst the autoclave was under pressure. The HPLC pump was monitored *via* an internal pressure transducer that can cut the power to the pump

by an internal trip system in the event of over pressure. Again, an NRV was used to prevent back flow of CO₂ into the HPLC pump, since this kind of pump is not designed or able to pump vapour or vapour/liquid mixtures.

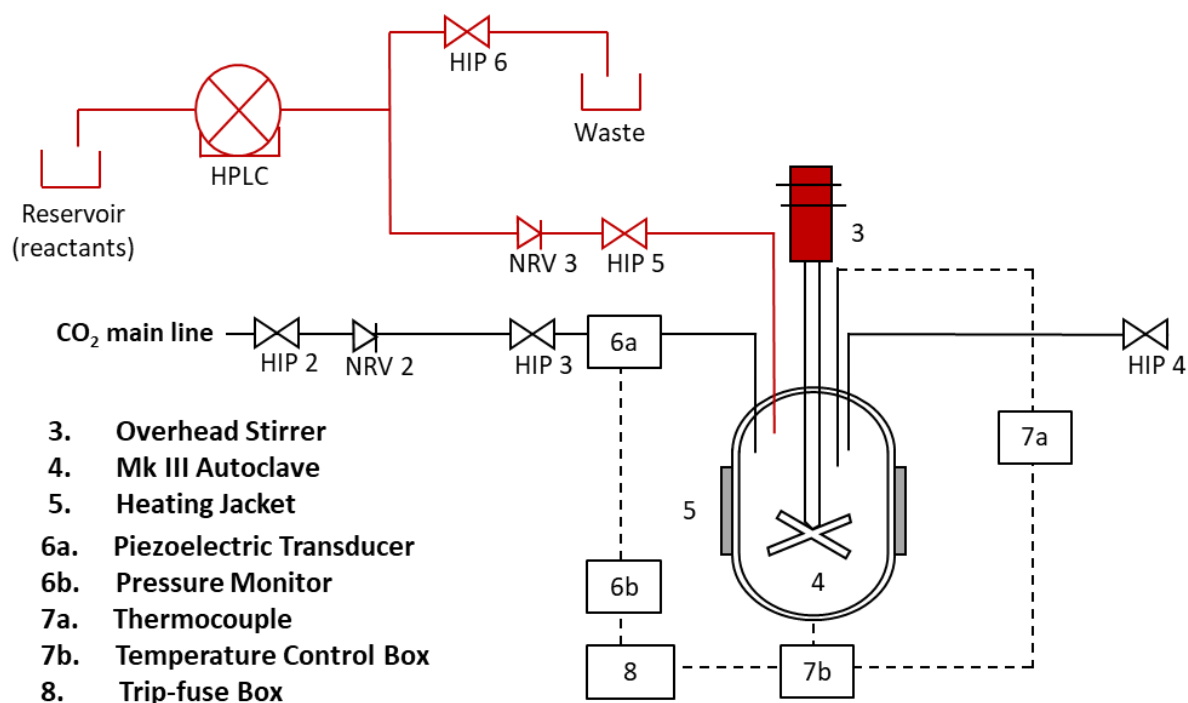


Figure 4 - Schematic diagram of high-pressure autoclave rig setup with addition of HPLC inlet. The additional pipework and equipment is highlighted in red. That comprise a HPLC pump, which is connected to a reactants reservoir and to a waste vial through a HIP valve; an additional HIP valve connection to the autoclave; a NRV to prevent return of CO₂ into the HPLC pump.

There are a few limitations associated with this system, only liquids can be injected *via* this inlet and the HPLC pump must be thoroughly cleaned and washed with the reactants to be added in order to avoid contamination. Furthermore, the pressure in the HPLC pump must be higher than the pressure inside the vessel, allowing the reactants to be successfully injected. It is important to note that the addition of reactants will cause the pressure inside the autoclave to rise and therefore the pressure must be constantly monitored in order to not exceed the maximum desired pressure or the working pressure. In the same way, fluctuations in temperature may occur, which will in turn affect the pressure of the vessel.

2.3.5. SOP for two-steps polymerisation

The SOP was followed rigorously to ensure safety during the injection of reactants *via* the HPLC inlet port. An outline for this procedure is given below.

1. The system was left at 65 °C and 200-276 bar for the desired time, following the SOP in section 2.3.3.
2. If necessary, depending on the amount of reagents to be added, the autoclave was depressurised slowly to 207 bar *via* the outlet pipe. This step is required to ensure the pressure does not increase with the addition of reactants above the trip pressure, which is the safety limit.
3. The HPLC pump was thoroughly cleaned by flushing with acetone, *circa* 10 mL, and then flushed with the reactant being injected, *e.g.*, monomer and CTA, until the HPLC pipeline was filled with this mixture. This was guaranteed by keeping track of the exiting volume, which was collected in a measuring cylinder.
4. The HPLC outlet line was then connected to the addition port on the autoclave *via* the 1/16" union and the desired pumping speed was set.
5. Pumping is initiated with the inlet tap (HIP 5 – Figure 4) closed until the pump pressure equals the pressure inside the autoclave. This step is important to ensure that no back flow occurs and that the reactants are successfully injected.
6. The level of reactants in the reservoir was noted and the autoclave HPLC inlet (HIP 5 – Figure 4) was opened for the desired injection time for addition of the required amount of reactants, taking into account the dead volume between the entry pipe and the autoclave head, *circa* 1 mL.
7. The autoclave and HPLC pump pressure was monitored throughout the injection.
8. Once the desired amount of reagents had been injected, the autoclave HPLC inlet (HIP 5 – Figure 4) was closed and the HPLC pump was stopped. The HPLC exit HIP valve (HIP 6 – Figure 4) was then opened slowly to release residual pressure in the pump.
9. The HPLC pipes were flushed with solvent, typically acetone, to prevent residual monomer solution polymerising in the pipes.
10. Post injection, the pressure inside the autoclave was monitored, as pressure increase lags may occur.
11. If necessary, more CO₂ was carefully added to restore the desired reaction pressure, usually 276 bar.
12. After the desired reaction time, the reactor was cooled down, the product was collected and the autoclave was cleaned following steps 8 -11 of section 2.3.3.

2.3.6. Fixed volume view cell

Although the Mk III autoclave is an efficient reaction vessel for the scCO₂ reactions, it does not allow for visual monitoring of what was happening *in situ*. In order to observe a reaction under supercritical conditions, a fixed volume view cell was employed. This cell is made of 316 stainless steel and is rated for use up to 345 bar. As with the Mk III autoclave, this vessel was designed and built in-house at the University of Nottingham. . A schematic of the equipment is shown below (Figure 5).

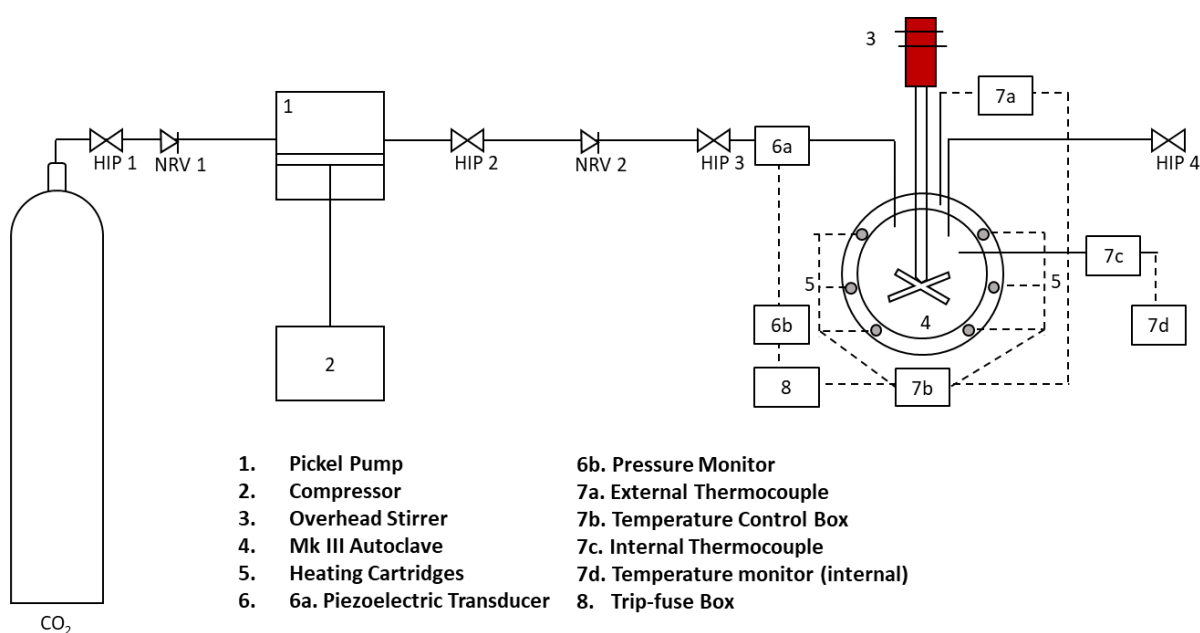


Figure 5 - Schematic diagram of high-pressure fixed volume view cell, depicting the view cell body, monitoring systems, including internal and external thermocouples, trip box, heating cartridges, stirrer and the high-pressure line Apart from the trip-fuse box, the other safety features are not included here, but are presented in Figure 6.

The fixed volume view cell shares several features with the Mk III autoclave, including an overhead magnetically coupled stirrer, a safety key/valve and the clamp system. It can be divided into three parts, two heads with sapphire windows, *i.e.*, back and front, and a cylindrical horizontal body (Figure 6).

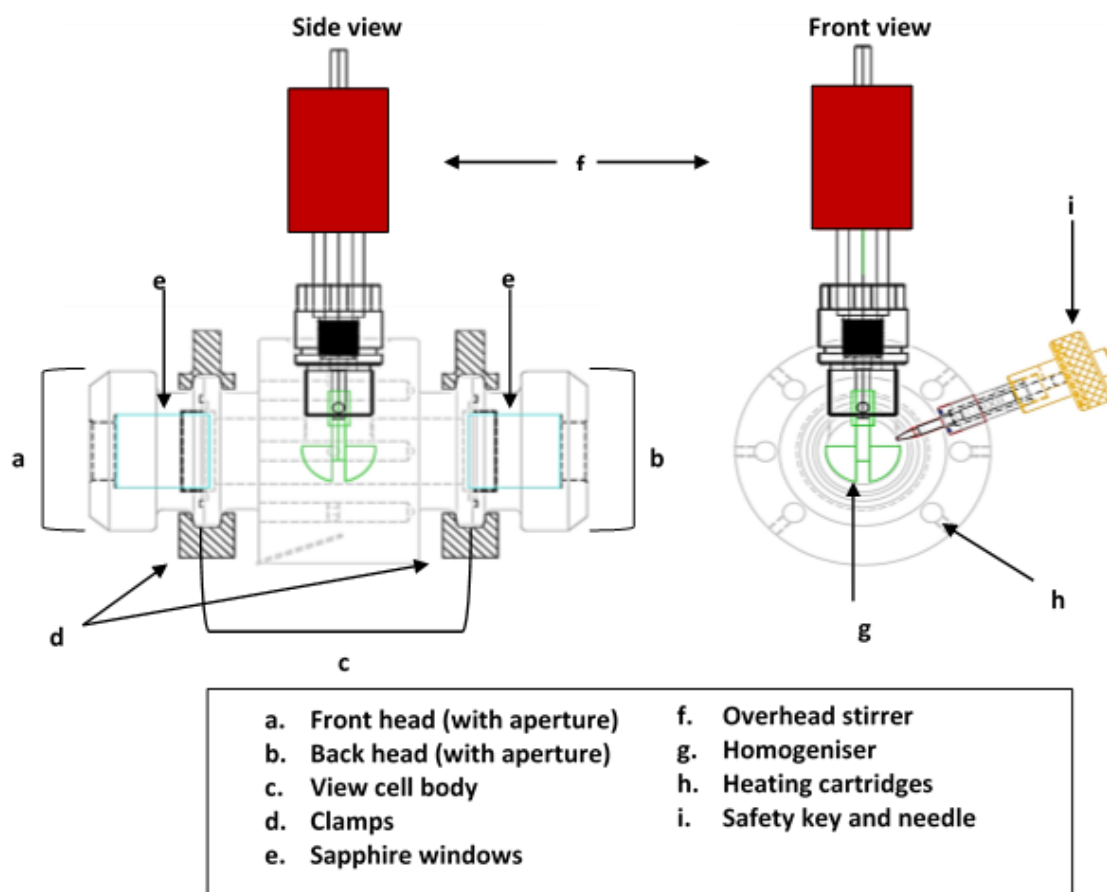


Figure 6 - Schematic diagram of high-pressure fixed volume view cell. The left-side diagram depicts the view cell body, the overhead stirrer, the front and back heads, with the two sapphire windows and their respective securing clamps. The right-side diagram shows the safety key, the heating cartridges, the homogeniser (stirrer blades) and the over head stirrer.

Both the front and back head were clamped to the main body and sealed with an EPDM O-ring. As previously mentioned with the Mk III autoclave, the clamps can only be undone with the key pinwheel that is specific to the clamp. The window was held in the metal head frame by an EPDM O-ring, which provides a seal. The O-rings determines the maximum operation conditions: -50 °C to 150 °C. To avoid sapphire to metal contact, which can compromise the window integrity, there is a Teflon spacer (Kalrez®) placed between the metal frame of the view cell head and the front of the window. Both the front and back head are identical.

The cell body was held in a purpose built frame and a Lexan™ blast shield was mounted in front of the front window as extra precaution in the case the window failed (Figure 7). The main body has four apertures into the vessel chamber, which were used for the CO₂ inlet and outlet, a safety valve/key and a K-type thermocouple for monitoring internal temperature.

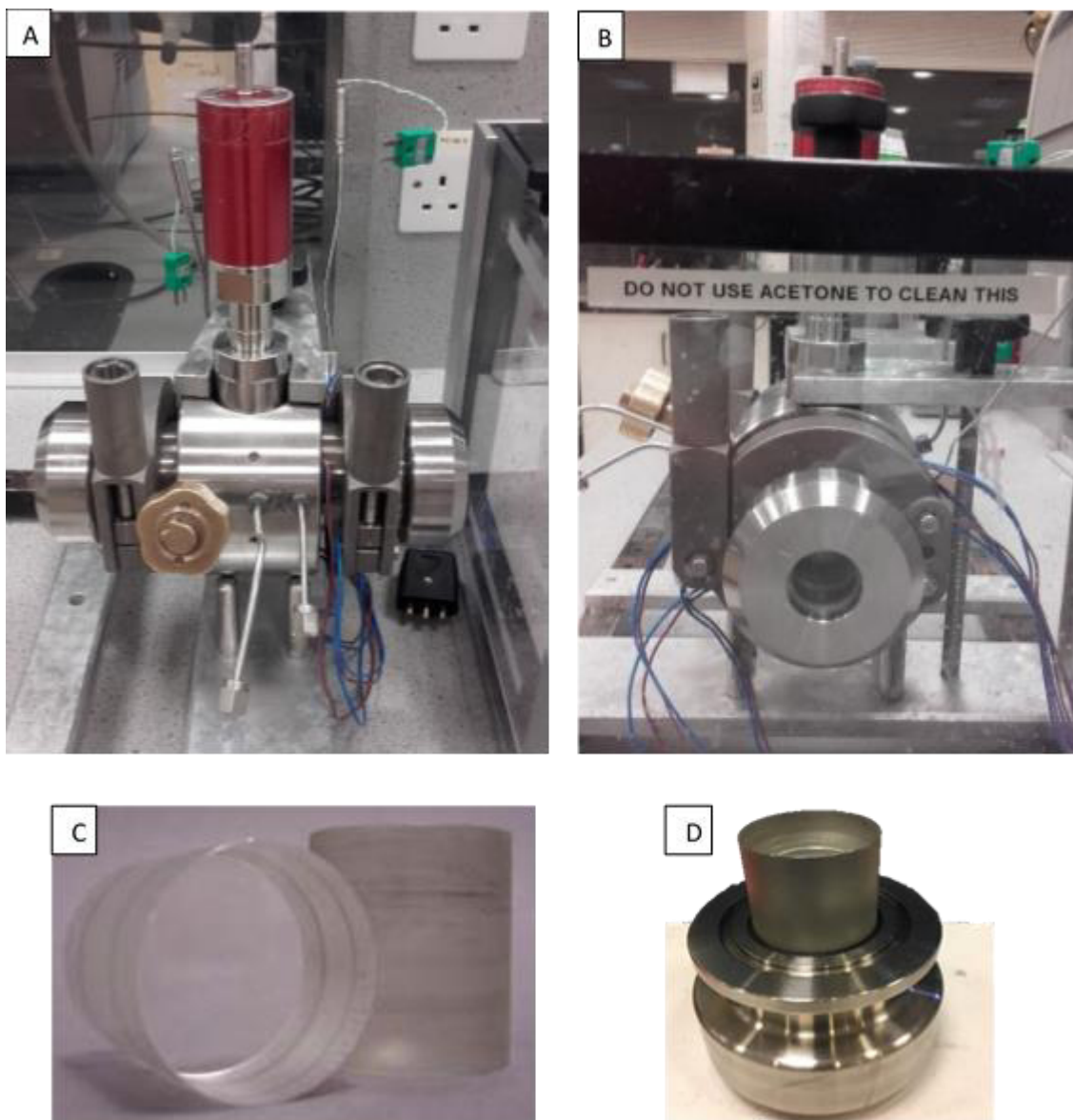


Figure 7 - Photographs of the high-pressure fixed volume view cell, which allows solubility studies at fixed reaction conditions. (A) view-cell side view, showing the internal and external thermocouples, clamps, safety key and heating cartridges (blue and red wires); (B) front view with safety Lexan™ screen; (C) sapphire windows; (D) Window assembly into head metal frame..

Heat is provided by six heating cartridges, which are inserted into cavities in the walls of the view-cell body. As the cell walls are very thick, there can be a large disparity between the temperature of the outer cell wall and the internal temperature. In order to avoid overheating, the temperature was controlled from a thermocouple in the cell wall near to the heating cartridges, and a second thermocouple was used to monitor the internal temperature. The internal pressure was measured by a piezoelectric transducer and

monitored using an in-house built digital pressure box. As for the Mk III autoclave, a trip-fuse box was used as an additional safety feature to avoid overheating.

2.3.7. SOP for fixed volume view cell

The following SOP describe the best working practice for all investigations using the fixed volume view cell and was rigorously followed to ensure safety. An outline for this procedure is given below.

1. The two windows were assembled by first placing a Kalrez[®] spacer into the stainless steel frame, then an EPDM O-ring was fitted around the sapphire window, before it was inserted into the aperture until it was positioned against the spacer.
2. The view cell body was checked to verify that the stirrer, heating cartridges and thermocouples were all connected. Both the temperature controllers and the pressure controller were checked to confirm they were operating normally, with the right pressure reading for ambient pressure and the adequate temperature reading according to the room temperature.
3. If a solid sample/reactant was being studied, it was placed inside the view cell body before the leak test. If necessary for visualisation, a sample could also be placed inside glass vial and fixed into a steel support (Figure 8). A light source was placed behind the back window and turned on.

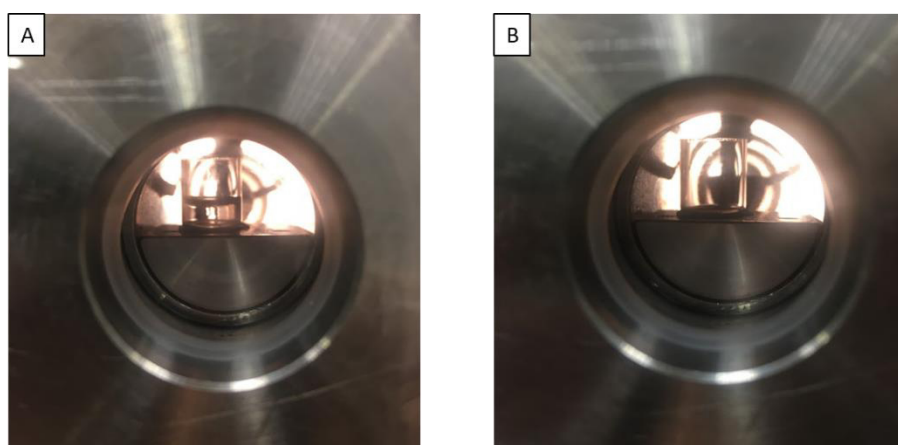


Figure 8 – Photographs of the fixed volume view cell with a glass vial and steel support, in (A) an initially insoluble liquid is present, while (B) shows the dissolution of the liquid in scCO₂, with the liquid now dissolved in the supercritical fluid.

4. The front and back head were clamped to the corresponding ends of the view cell, whilst ensuring that an EPDM-O-ring was situated between the sealing surfaces. The clamp was tightened with the safety key.
5. The inlet and outlet pipe were connected and the safety key was screwed into place to seal the view cell. The safety Lexan™ screen was placed in front of the front head.
6. A leak test was performed by adding CO₂ to the vessel up to *circa* 55 bar. Each pressure fitting and window was checked with Swagelok Snoop® and the pressure was monitored over a minimum of 2 hours. In the event of a leak the vessel was vented to atmospheric pressure prior to replacing the fitting or reassembling the window. If no leak was present, the cell was vented and the safety key removed.
7. The cell was subsequently purged with a flow of CO₂ at around 2 bar for 30 minutes in order to remove residual oxygen.
8. If liquid reactants were required, and no vial/steel stand was necessary, they were added by injection through the open safety valve keyhole. The injection was performed against a positive pressure of CO₂ to prevent the ingress of air (2 bar). After injection, the safety key was screwed into place, sealing the vessel.
9. The stirring was started at 300 rpm. The cell was pressurised to 55 bar and the desired temperature was set on the temperature controller. Both the internal and external temperatures were monitored separately, the internal temperature can often be several degrees below the reading at the cell wall (external thermocouple), and hence the set temperature must be adjusted accordingly.
10. When the temperature was stable, CO₂ was slowly added until the desired pressure was reached.
11. The study was visually monitored and photographs were taken accordingly. The pressure and temperature were also monitored throughout the experiment.
12. Upon completion of the experiment, the temperature control was set to 0°C and the heating cartridges disconnected from the temperature controller.
13. When the cell had cooled to ambient temperature, it was slowly vented through the outlet valve into a fume hood. Once at ambient pressure, the safety screen was removed and the cell was disassembled and cleaned with acetone.

2.3.7.1. Procedure for solubility studies in scCO₂

Solubility tests were carried out in a stainless steel view cell with two windows (as described in section 2.3.6), which permitted visual observation of the phase behaviour. An accurately weighed amount of CTA and monomer, simulating reaction conditions, were added to a small glass *vial* and placed inside of the view cell (Figure 8). The system was purged with CO₂ and gradually heated to 65 °C and pressurised to 276 bar. Solubility was visually evaluated after allowing the system to stabilise.

2.3.7.2. Procedure for nucleation onset studies in scCO₂

In a typical procedure, the static view cell was leak tested and degassed by purging with CO₂ at 2 bar for 30 minutes. MMA (0.1 mol), AIBN (0.08 mmol), PDMS-MA (5 wt % in relation to MMA) and the respective CTA (0.2 mmol), if used, were degassed by bubbling with argon for 30 minutes. The reactants were then added to the autoclave and the pressure and temperature adjusted as described in the SOP (Section 2.3.7.1.). The reaction was monitored, photographed and filmed throughout the nucleation phase, until complete blockage of the back light was observed.

2.3.8. High pressure variable volume view cell

The variable volume view cell can also be used to study the phase transition of materials in scCO₂ and was developed at the University of Nottingham. The main advantage of this setup in comparison to the previously described view cell is that it allows the possibility to control pressure independently of temperature, by varying the internal volume of the chamber. In this way, the phase behaviour in scCO₂ can be evaluated for a range of pressures at a set temperature, which is fundamental for cloud point analysis. The cloud point is the given pressure, at a specific temperature, when the solute precipitates out of the continuous phase, causing turbidity.

Different from the previous high-pressure equipment discussed in this chapter, the variable volume view cell is not connected to the CO₂ main line described in section 2.3.1. This is because the amount of CO₂ injected into the vessel must be known in order to perform cloud point studies. Originally, this was achieved by using a small high pressure cylinder, filled from the same line as the CO₂ supply. The amount of CO₂ inside the chamber could be calculated by weighing the cylinder before and after injection into the view cell. However, this

methodology was prone to over pressurisation of the cylinder and was updated to improve safety. In the new system, which was used throughout this thesis, CO₂ was delivered to the variable volume view cell *via* a 260D syringe pump (Teledyne ISCO, USA) connected to a Pickel pump fed by a CO₂ cylinder (Figure 9). The use of the syringe pump provided reproducible control over the amount of CO₂ supplied to the reaction chamber.

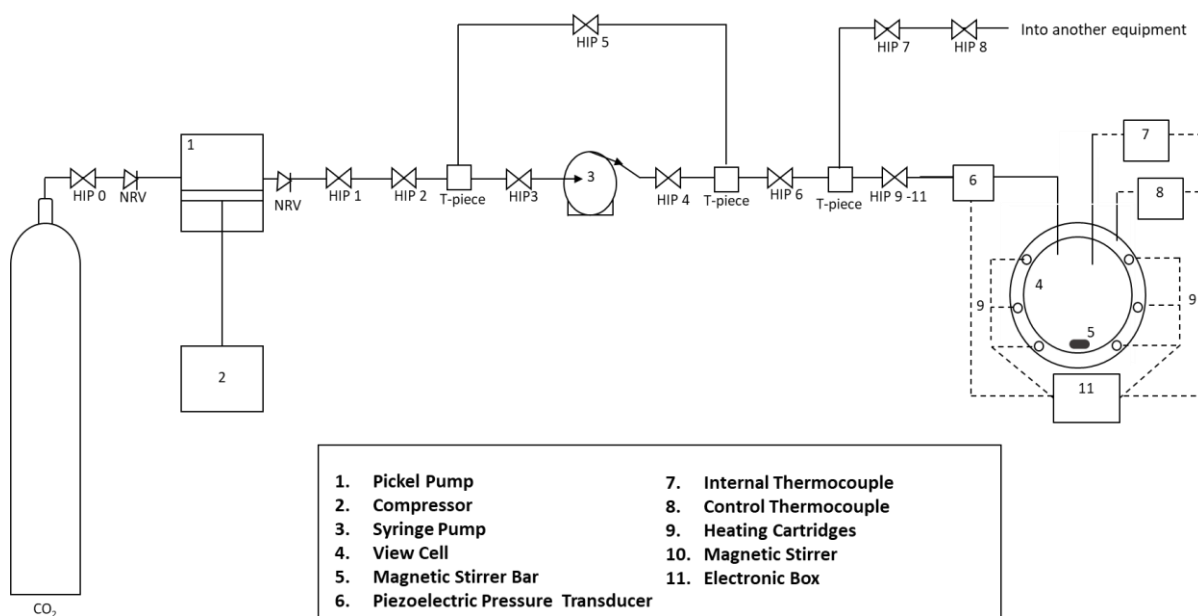


Figure 9 – Schematic diagram of high-pressure variable volume view cell rig setup. The scheme includes the Syringe Pump system, including all the pipework connecting it to the Pickel Pump, compressor and CO₂ cylinder. The pressure transducer (6), heating cartridges (9) and both thermocouples, internal (7) and control (external) (8), are all connected into the electronic box, where all the pressure and temperature readings are displayed and the heating is controlled. The Trip system is internal to the electronic box and therefore there is no Trip Box in this setup.

The apparatus has been fully detailed elsewhere.^{4,5} It is composed of three main components: the view cell body, a hydraulic intensifier unit and an integrated electronic box for monitoring and adjusting temperature and pressure within the cell (Figure 10).



Figure 10 – Photographs of the high-pressure variable volume view cell rig setup. (A) Main rig – with the intensifier, electronic box and view cell body; (B) Syringe Pump set up for the view cell feeding; (C) close up of the view cell body – showing the inlet, outlet, internal thermocouples, safety key, clamps, transducer, safety screen, back light and monitor for the intensifier pressure.

The variable volume view cell shares many features with the fixed volume view cell (described in section 2.3.6), it has two sapphire windows and a main stainless steel horizontal body, which is held in a purpose built frame with a safety Lexan™ screen placed in front and a light source placed at the rear. It also has a safety key/valve and uses the EPDM O-ring and clamp system to seal the head to the body. Furthermore, like the static view cell, heating is provided by cartridges inserted into the vessel walls. Heating of the vessel is controlled from a thermocouple in the cell wall near to the heating cartridges, while a second thermocouple monitors the internal chamber temperature. The maximum working temperature and pressure limits are the same as for the previous devices, 345 bar and -50°C to 150 °C.

Unlike the fixed volume view cell, both the outlet and the inlet use the same port in the variable volume view cell body and stirring is provided *via* a magnetically coupled stirrer positioned beneath the body of the view cell, which is used to rotate a magnetic stirrer bar inside the vessel. A trip-fuse control is present in the integrated electronic box, working as an additional safety feature, as for the Mk III autoclave. A detailed schematic of the variable volume view cell body is shown below (Figure 11).

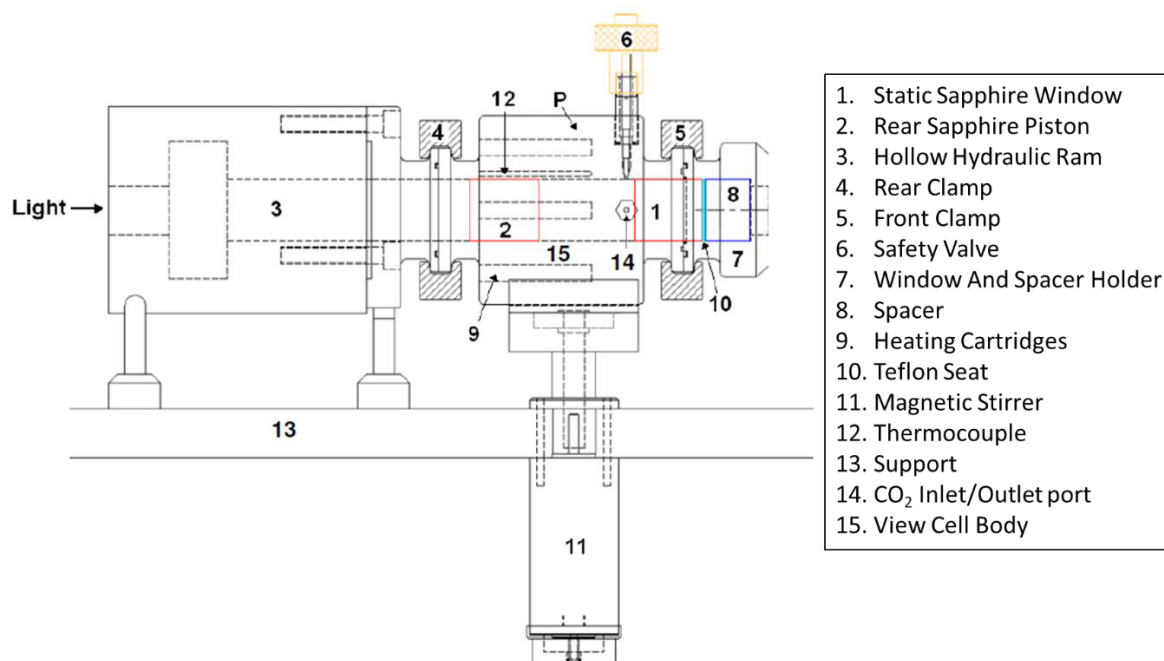


Figure 11 – Schematic diagram showing a lateral view of the high-pressure variable volume view cell, depicting the main body of the autoclave and additional features such as the magnetic stirrer, hollow hydraulic ram and light in the back of the system.

The variable volume view-cell has a static sapphire window at the front, which is assembled in the same way as the static view cell, with the addition of a metal spacer prior to the Teflon spacer (Figure 12). At the rear, a hollow hydraulic ram fitted with a transparent sapphire piston allows for the direct observation through the vessel, while the internal chamber volume can be changed as desired. Another clamp is used to connect the hollow hydraulic ram to the vessel body. The rear sapphire piston is fitted with a hydraulic type seal made of polytetrafluorethylene (PTFE) with a sprung stainless steel dented band facing the front of the vessel (Figure 13). The dented band expands under pressure and creates the seal. A polyether ether ketone (PEEK) backup ring is incorporated to prevent the hydraulic seal from creeping into the sapphire groove. Finally, two PTFE rings are placed around the sapphire piston to aid movement throughout the main cell body (Figure 13).

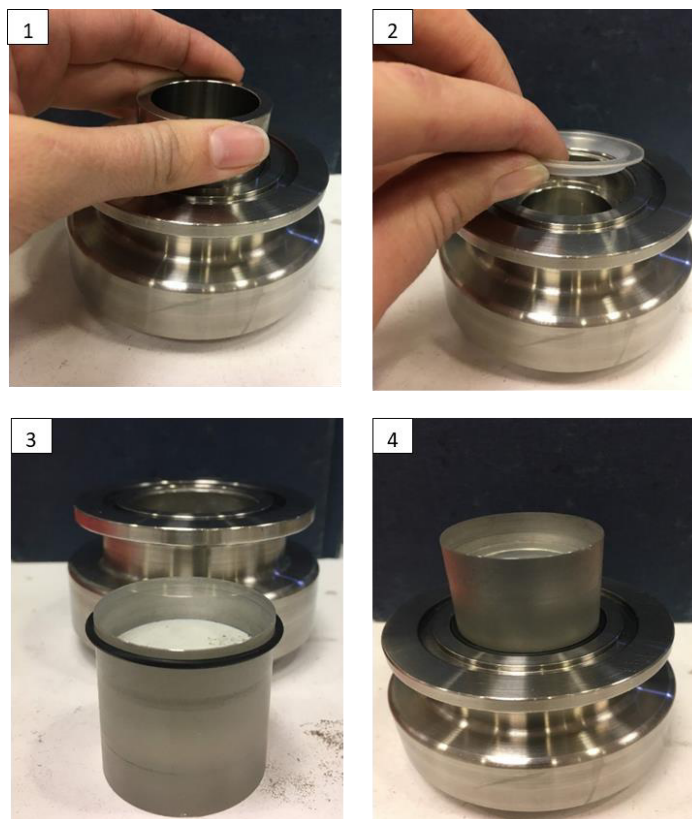


Figure 12 - Photographs of front window (static window) assembly. (1) First a metal spacer is inserted into the metal head frame; (2) then a Teflon spacer is placed above the spacer in order to protect the window; (3) an EPDM O-ring is placed around the sapphire window, in order to form a seal with the metal head frame; (4) and finally , the window is inserted gently into the head frame.

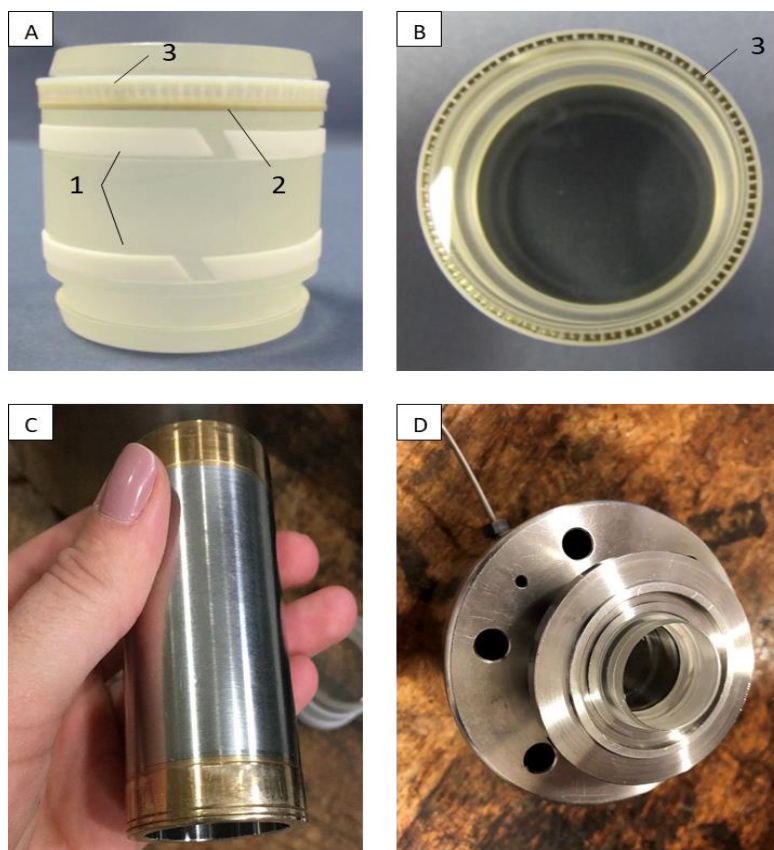


Figure 13 - Photographs of variable volume view cell back-window assembly. (A) Back window (sapphire piston) side view, showing the two PTFE rings (1), PEEK backup ring (2) and hydraulic PTFE seal(3); (B) Back window front view, showing the sprung stainless steel band of the hydraulic PTFE seal (3); (C) Hollow hydraulic ram; (D) Back window assembly, with hydraulic PTFE seal pointing the front of the view cell.

The rear sapphire piston can be moved by the hydraulic intensifier unit, to deliver a smooth flow of hydraulic fluid into and out of the hollow ram, which forces the sapphire piston to move within the view cell chamber. Moving the piston forward causes the volume to decrease and thus the pressure to increase. The chamber volume can be changed between 20 and 40 mL and the maximum pressure for the hydraulic system is 414 bar.

The cloud points were measured, using the variable volume view cell, as the point at which the LED lamp at the rear was completely obscured by precipitated polymer. A load of 20 g of CO₂ was used in all measurements, while the solute and any co-solvents, *e.g.*, monomer, were added in the desired concentrations as specified for the experiment. Each measurement was carried out by first achieving a stable temperature and then dissolving the solute by decreasing the volume of the cell by moving the piston forward, which in turn increase the

internal pressure. The more soluble a solute is the lower the pressure required to dissolve it. The pressure was then decreased slowly until precipitation occurred and the LED light could no longer be seen. The cloud point at each temperature was measured at least three times and an average was given as the observed cloud point. Figure 14 shows a schematic of the cloud point measurement procedure.

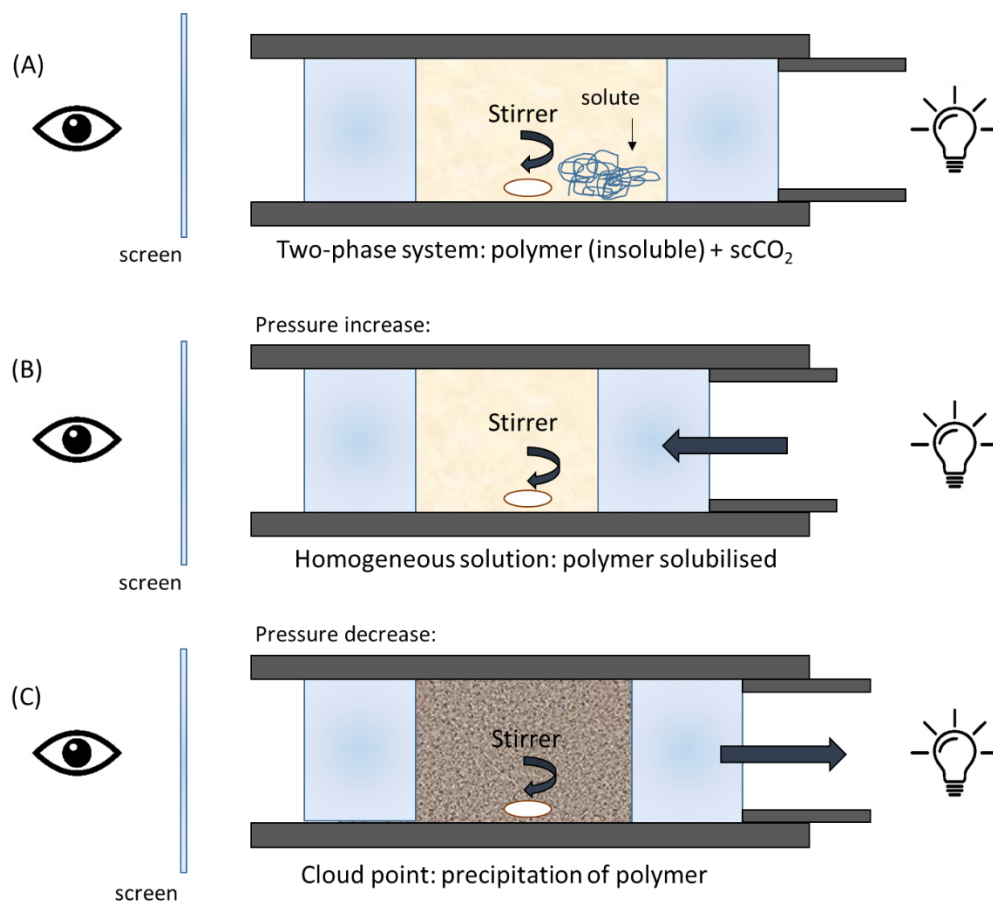


Figure 14 - Schematic depicting the procedure for the cloud point measurements. (A) The vessel, at a given temperature, contains a two-phase system, with the solute insoluble. (B) As the sapphire piston moves forward, the pressure is increased and the solute dissolves forming a homogeneous solution. (C) The piston is moved back, allowing pressure to drop until the cloud point pressure is reached and the LED light can no longer be seen.

2.3.9. SOP for variable volume view cell

The following SOP describes the best working practice for all investigations using the variable volume view cell and was rigorously followed to ensure safety. An outline for this procedure is given below.

1. The hollow hydraulic ram was placed into the back chamber and the back window was assembled, ensuring the hydraulic PTFE seal, PEEK backup ring and two PTFE bearing rings were attached to the sapphire piston.
2. The sapphire piston was inserted into the main chamber from the back, with the sprung stainless steel band pointing to the front, using a guide tool and wooden block.
3. The heating cartridges and thermocouple were inserted into the back of the main chamber; the main chamber was slid onto the hydraulic ram and clamped together. The clamp was tightened with the safety key. The initial position of the piston was set at the maximum volume.
4. The front head was assembled by placing the metal spacer into the metal head and then the same procedure as for fixed volume view cell SOP is followed (See section 2.3.7. - step 1).
5. The magnetic stirrer bar was placed into the main chamber and an EPDM O-ring was positioned between the sealing surfaces before the front head was clamped into place. The clamp was tightened with the safety key.
6. The inlet/outlet pipes were connected to the main CO₂ line and the safety key was screwed into place to seal the view cell. The safety Lexan™ screen was placed in front of the front head. The backlight, which is placed behind the hydraulic ram, was switched on.
7. The syringe pump was filled with CO₂ using a Pickel pump and set to the desired pressure on the syringe pump control panel.
8. Once ready to pressurise the view cell, the inlet tap was open, making sure the outlet tap was closed, and the syringe pump outlet was also opened. Once the desired pressure is reached, the pump stops automatically.
9. If a solid sample was analysed, it was added into the main chamber prior to the leak test. The stirrer and backlight were switched on.

10. The view cell was checked for leaks, similarly to the process described in the fixed volume view cell SOP (See section 2.3.7. - step 6).
11. In order to remove residual oxygen, the cell was then purged with a flow of CO₂ at around 2 bar for 30 minutes.
12. If the sample being analysed was liquid it was added by injection through the still open safety valve (keyhole). The injection was performed against a 2 bar flow of CO₂ to prevent the ingress of air.
13. The desired pressure was set on the syringe pump. The view cell has an operation volume of 20-40 mL. *Circa* 25 mL of scCO₂ at 75.8 bar were added to the view cell. The inlet tap was closed after the CO₂ addition.
14. The volume in the syringe pump was noted prior to and after filling of the view cell. The room temperature was also noted and the mass of CO₂ added was calculated.
15. The temperature was increased to desired temperature (maximum of 150 °C). After the temperature was stable, the pressure was increased by moving the piston using the controller box, making sure the ram speed was between 2 and 3.
16. At each temperature set point, the pressure was increased until the solute became soluble and only one phase was visible, making sure to not exceed the maximum pressure set by the trip system.
17. The pressure was then reduced slowly, while monitoring the phase behaviour (allowing time for stabilisation), until the point at which the backlight was completely obscure. This is the cloud point. The pressure and temperature were annotated.
18. Steps 16 and 17 were repeated at least three times for each set temperature. Accuracy of pressure transducer at ±0.5-1.0 bar and accuracy of K-type thermocouple at ±0.3 °C
19. Upon completion of the experiment, the temperature control was set to 0°C and the heating cartridges disconnected from the temperature controller.
20. When the cell had cooled to ambient temperature, it was slowly vented through the outlet valve into a fume hood. Once at ambient pressure, the safety screen was removed and the cell was disassembled and cleaned with acetone.

2.3.9.1. Procedure for cloud point study in variable volume view cell

Solubility tests of macro-CTAs and CTAs were carried out in the variable volume view cell. An accurately weighed amount of CTA/macro-CTA alone, typically 0.5 mmol, or in presence of

the monomer, *i.e.*, 33 mmol, which acts as co-solvent, were injected into the view cell. The system was filled with CO₂ using the syringe pump to allow *circa* 20 g of CO₂ to be injected. The exact mass was calculated using equation (1), where V_i is the volume in the syringe pump before filling the view cell and V_f is the volume in the syringe pump after filling the view cell. d is the density of CO₂ at the given room temperature and pressure set in the syringe pump, and MW is the molecular weight of CO₂ (44.01 g mol⁻¹). The density of CO₂ was obtained from the National Institute of Standards and Technology (NIST) webbook,⁶ considering an isobaric system with the specific pressure and temperature for the filling of the view cell. The isochoric properties were not used due to the variability of volume in the view cell. Therefore, if the piston is not positioned at the same condition for all experiments, the volume will be slightly different in each one. The SOP, described in section 2.3.9, was followed to observe the cloud point visually for each temperature. The process was repeated three times and an average was reported as the cloud point at that temperature.

$$CO_2 \text{ mass} = (V_i - V_f) \times d \times MW \quad (1)$$

2.3.10. High-pressure sampling autoclave

In order to allow sampling under pressure and therefore monitoring of the reaction kinetics, a novel sampling device was used. This device consists of a modified Mk III autoclave and a high pressure sampling cylinder and has been fully described in detail elsewhere and was developed by my colleague Kristorffer Kortsen, which will be part of his future thesis.⁷ The modified autoclave consisted of a 60 mL standard Mk III autoclave, already described in section 2.3.2, with the addition of an extraction port in the base of the vessel (2), which can be controlled by an HIP valve (1). A stand with aperture (6) was designed to hold the autoclave and allow access to the extraction port at the bottom. The extraction port allowed for attachment of a sampling unit consisting of a short connecting tube made up of Swagelok 1/8 inch tube and fittings, a HIP tap (3) and a high pressure sampling cylinder (4) (Figure 15). The sampling cylinder was equipped with a burst disk and tap (5) to prevent over pressuring and to allow safe operation. A full illustration of the sampling system is presented below, the modifications on the Mk III are labelled in red (Figure 15).

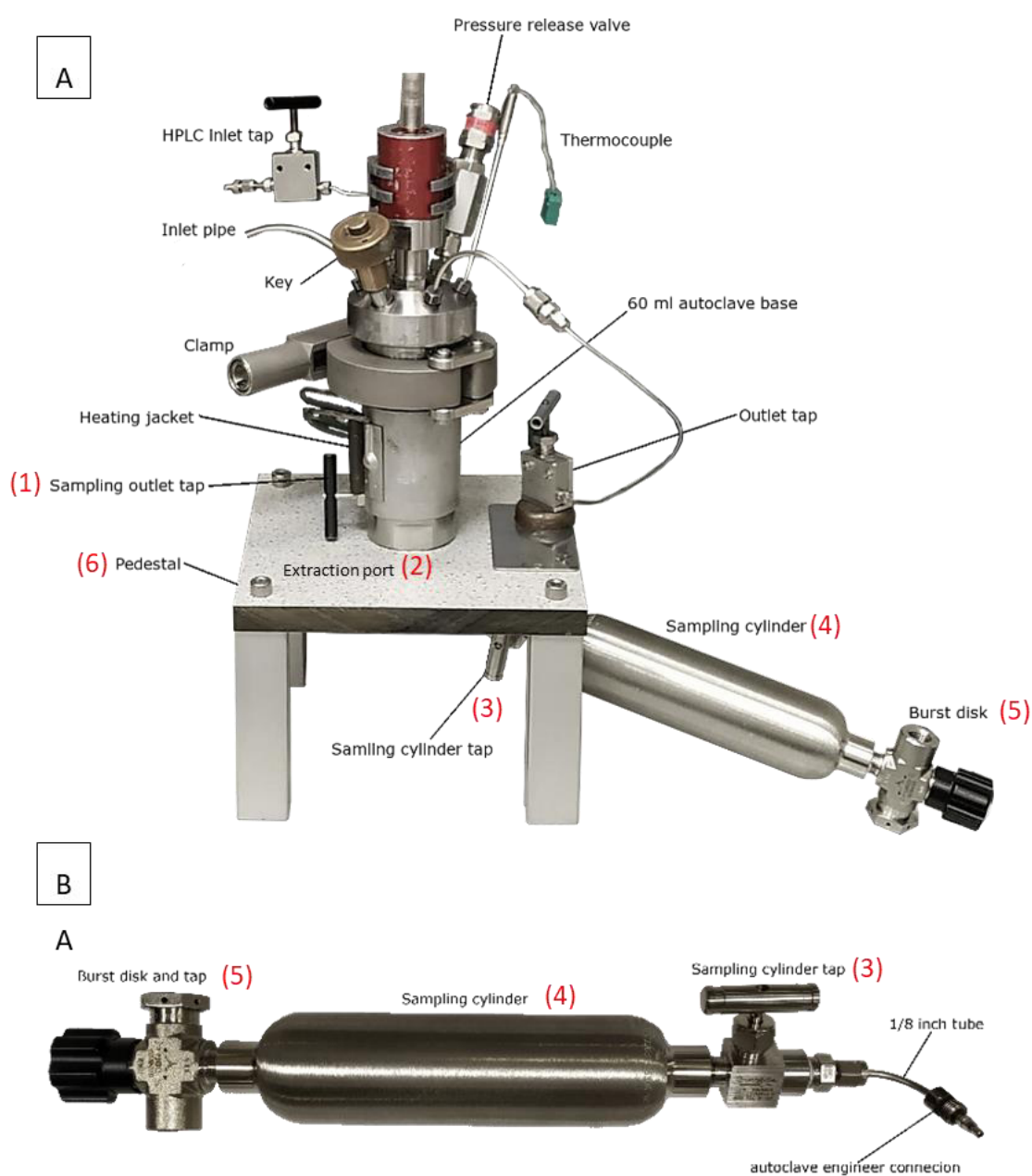


Figure 15 - Photographs of the sampling device. (A) Full sampling setup comprising the 60 mL Mk III autoclave, pedestal and sampling unit, the modifications on the original Mk III are labelled in red; (B) Sampling unit setup. Figure modified from Kortsen et al.⁷

Once the sampling cylinder (4) was attached to the bottom of the autoclave (2), it produced an effective pressure seal. When the sampling outlet tap (1) was opened, the pressure of the scCO_2 forced the reaction contents into the connecting pipe. Then the sampling outlet tap (1) was closed and the content of the pipe was safely sprayed into the sampling cylinder (4) by opening the sampling cylinder tap (3). Deuterated-chloroform (CDCl_3) was added to the

cylinder to collect the polymer and residual monomer. The choice of the solvent was based solely to facilitate the running NMR analysis immediately after collection to eliminate monomer losses. The sample was then dried and the CDCl_3 removed prior to analysis by SEC. The use of chlorinated solvents is only possible, because the internal surface of the stainless steel high pressure sampling cylinder was coated with PTFE, otherwise it could cause chloride pitting corrosion and lead to failure of the cylinder.

This novel sampling system allows both molecular weight and conversion to be efficiently monitored throughout the reaction. Previous sampling devices, only made use of a short piece of metal hollowed at one side, could not give accurate conversion measurements due to loss of the volatile monomer when unscrewing from the extraction port.

2.3.11. SOP for sampling autoclave

In order to perform a reaction in the sampling autoclave, the SOP for the standard high pressure Mk III sealed autoclave, described at section 2.3.2, was rigorously followed to ensure safety. To obtain samples, at any desired time, the following steps were followed:

1. The sampling cylinder was loaded with 5 mL CDCl_3 and the sampling unit was assembled by screwing the short connecting tube into the sampling cylinder.
2. The collection of samples causes a slight pressure drop in the autoclave, which could potentially affect solvation. To overcome this, pressure was topped up with an extra 14 bar prior to the extraction.
3. The sampling unit was attached to the extraction port (2) on the base of the autoclave, making sure that the sampling cylinder tap (3) was fully closed.
4. The sampling outlet tap (1) in the bottom of the autoclave base was then fully opened and the short connecting tube was filled with the reaction contents. This was guaranteed by leaving the tap open for 30 seconds. The tap was then closed. Pressure was monitored throughout that process. After taking the sample, if necessary, CO_2 was carefully added to the autoclave to return it to the original pressure.
5. The sampling cylinder tap (3) was opened, allowing the reaction content to spray from the short connecting tube into the cylinder (4) and dissolve in the solvent.
6. The sampling cylinder tap (3) was then closed and the sampling unit was carefully disconnected from the autoclave body.

7. The product, now dissolved in the NMR solvent, was collected by opening the sampling cylinder tap (3) over a vial, an aliquot of 0.6 mL was collected for NMR analysis and the sampling unit was disassembled.
8. The sample unit (sampling cylinder and the short connection tube) were cleaned with acetone and dried with compressed air. The sampling port at the base of the autoclave was cleaned with a cotton bud and acetone.
9. If further samples were required, the sampling pipe was re-attached and steps 1-8 repeated.

2.4. Characterisation techniques

2.4.1. Size exclusion chromatography

Molecular weight, usually measured as number-average molecular weight (M_n) or weight-average molecular weight (M_w), and dispersity (\mathcal{D}) are essential parameters for the characterisation of polymers. Size exclusion chromatography (SEC), a widely used technique for polymer characterisation, which allows both molecular weight and polydispersity to be determined, was used in this thesis to obtain information about the molecular weight distribution of polymers.^{8,9} SEC is a type of high performance liquid chromatography, which separates macromolecules according to their hydrodynamic volume in a selected solvent by passing them through a porous column packed with an inert stationary phase, usually a cross-linked polymer. Polymers adopt a coil conformation in solution, the size of which depends on the molar mass of the polymer and the interactions of the polymer with the solvent. Large coils are partially excluded from the stationary phase pores and elute quickly, while smaller coils take a longer pathway through the pores and are eluted later. Consequently, polymers elute from the column according to their molar mass. A general schematic of the SEC instrument setup is shown below (Figure 16).

Unfortunately, as the hydrodynamic volume also depends on the interaction of the polymer with the solvent, different materials may present distinct hydrodynamic volumes at the same molar mass. Thus, different polymers will not elute at the same rate. By calibrating the instrument against standards of a given polymer or by knowing the refractive index of the polymer being measured, accurate molar mass distributions can be calculated. However,

comparisons between chemically different polymers should be treated with caution as some differences can be significant.¹⁰

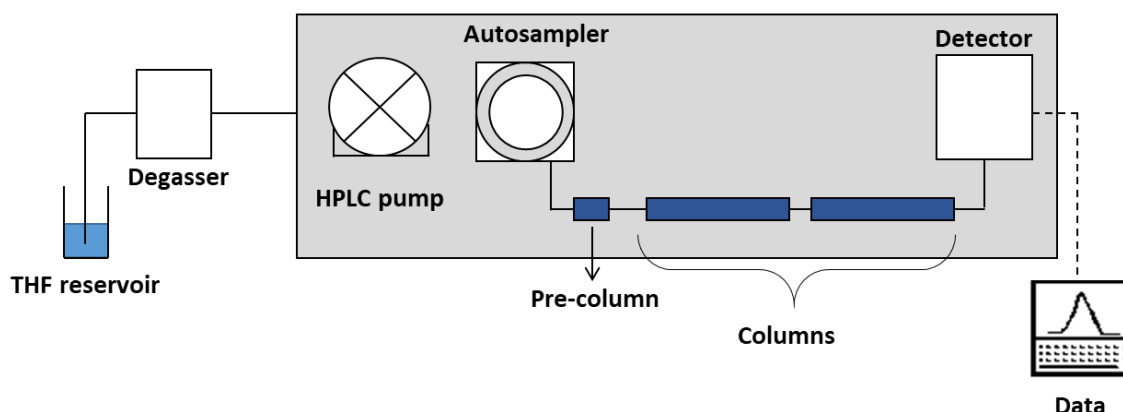


Figure 16 - Schematics of a THF SEC setup. The pump, automated sampler, columns and detectors are all housed in a single unit, with the solvent heated by an oven integrated into the system (not shown in the scheme).

Samples for SEC analysis were prepared at 2 mg mL^{-1} concentration and filtrated through a $0.45 \text{ }\mu\text{m}$ syringe filter from Sigma-Aldrich prior to injection. In this thesis, SEC samples were analysed using two different systems:

1. Using an SEC Agilent 1260 Infinity system equipped with a pre-column and two Agilent PL-gel mixed C columns in series, molecular weight range limits of $0.2\text{-}2000 \text{ kg mol}^{-1}$ for Polystyrene (PSt), with a triple detection comprising a Wyatt Optilab multi-angle light scattering (MALS) detector, an Agilent differential refractometer (RI), a Wyatt Optilab viscometer. The eluent was tetrahydrofuran (THF), kept at $40 \text{ }^\circ\text{C}$ and at a flow rate of 1 mL min^{-1} and an injection volume of $1 \text{ }\mu\text{L}$. Molar mass determination was carried out by Agilent® software and measured against PMMA standards. Three standard solutions were used (Agilent Calibration Kit), red, yellow and green, of different M_n mixings. Red: 2000, 252.2, 29.1 and 1.59 kg mol^{-1} ; Yellow: 969, 141.6, 13.3 and 0.92 kg mol^{-1} ; Green: 517, 69.4, 6.24, 0.66 kg mol^{-1} .

2. Using the same equipment as above but with a pre-column and two PL-gel mixed D columns ($7.5 \text{ mm} \times 50 \text{ mm}$), molecular weight range limits of $0.2\text{-}400 \text{ kg mol}^{-1}$ for Polystyrene (PSt). The eluent was THF, kept at $40 \text{ }^\circ\text{C}$ and at a flow rate of 1 mL min^{-1} and an injection volume of $1 \text{ }\mu\text{L}$. Molar mass determination was carried out by Agilent® software and measured against PMMA standards. Three standard solutions were used (Agilent Calibration Kit), red, yellow

and green, of different M_n mixings. Red: 2000, 252.2, 29.1 and 1.59 kg mol⁻¹; Yellow: 969, 141.6, 13.3 and 0.92 kg mol⁻¹; Green: 517, 69.4, 6.24, 0.66 kg mol⁻¹.

2.4.2. Nuclear magnetic resonance

Nuclear Magnetic Resonance (NMR) is a technique widely applied in the chemical, structural and electronic study of molecules. NMR makes use of the ability of nuclei possessing spins (¹H, ¹³C, etc.) to absorb and re-emit electromagnetic radiation when exposed to a constant applied magnetic fields. NMR allows a spectrum containing information about chemical structure of the analysed molecule to be generated.^{11, 12}

¹H NMR was used throughout this thesis to determine conversion of monomer to polymer and molecular weights for lower DP polymers. NMR was also used to confirm structure of materials synthesised and purity of purchased materials, for which ¹H and ¹³C NMR were used, and in some cases 2D analysis such as correlation spectroscopy (COSY) and heteronuclear single quantum coherence (HSQC) were also used. All samples were dissolved in deuterated chloroform (CDCl₃), unless stated differently, and analysed using a Bruker 400 Ultrashield, 400 MHz Spectrometer. Chemical shifts are reported in parts per million (ppm) relative to tetramethylsilane (TMS). All data were processed using MestRe-Nova[®] software.

2.4.3. Scanning electron microscopy

Scanning electron microscopy (SEM) is a technique for recording 2D images at high resolution and magnification. In SEM an electron gun, containing a tungsten filament, produces a beam of monochromatic electrons under high vacuum, which passes through a series of electromagnets (condensers) and apertures that focus the high-energy electron beam. The beam is then scanned by deflection coils across the sample to form an image and the final objective lens focus the beam onto the specimen. When the electrons interact with the sample, secondary electrons are ejected and hit a detector to produce an electrical signal and allow the construction of the final image by superposition of several scans.^{13, 14} Figure 17 shows the general layout of an SEM machine.

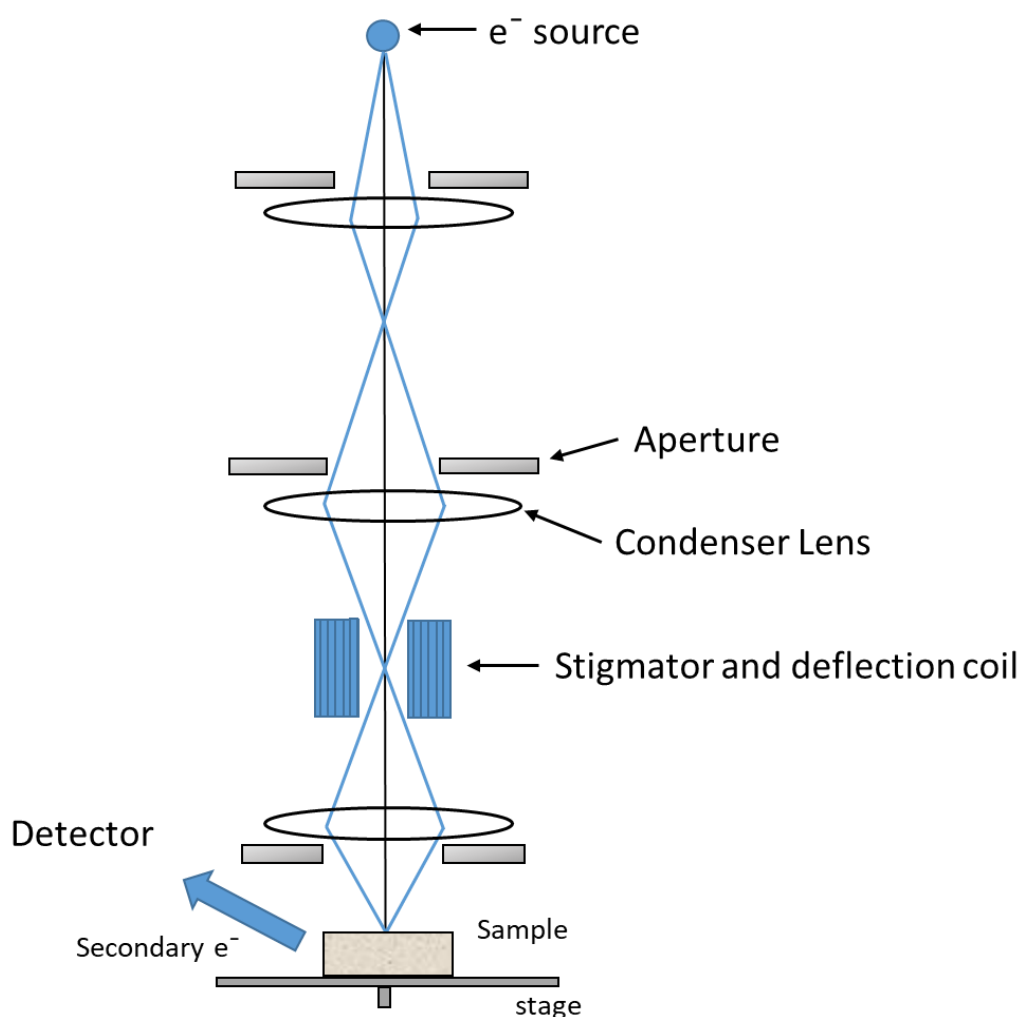


Figure 17 - Schematic of a basic SEM instrument setup. The electron beam is generated at the source and focussed by a series of apertures and condenser lenses. The beam is scanned by the stigmator and deflection coil to form an image. Upon interacting with the sample, secondary backscattered electrons interact with the detector to produce a signal and this signal is converted into the final image. Figure adapted from training material at Nanoscale and Microscale Research Centre (NMRC) at University of Nottingham.

All SEM images in this thesis were obtained using a JEOL 6060LV SEM at various magnifications and an accelerating voltage of 10 kV. Samples were mounted on aluminium stubs using adhesive carbon tabs and sputter-coated with platinum before analysis. Coating was done in a Polaron Emitech SC7640 sputter coater for 180 seconds at 12 mA and 2.2 kV. The mean particle diameter (D_n) was determined by measuring the diameter of at least 100 particles using ImageJ® software. The coefficient of variance (C_v) can give indication of particle size

distribution and was calculated by the ratio of the standard deviation (σ) by the mean particle diameter (Equation (2)).¹⁵

$$C_v = \sigma/D_n \times 100 \quad (2)$$

2.5. References

1. F. Furno, P. Licence, S. M. Howdle and M. Poliakoff, *Actual Chimique*, 2003, 62-66.
2. C. A. Kelly, Doctor of Philosophy, University of Nottingham, 2009.
3. H. M. Woods, N. Cecile, P. Licence, D. J. Irvine and S. M. Howdle, *Macromolecules*, 2005, **38**, 3271-3282.
4. P. Licence, M. P. Dellar, R. G. M. Wilson, P. A. Fields, D. Litchfield, H. M. Woods, M. Poliakoff and S. M. Howdle, *Rev. Sci. Instrum.*, 2004, **75**, 3233-3236.
5. H. Lee, E. Terry, M. Zong, N. Arrowsmith, S. Perrier, K. J. Thurecht and S. M. Howdle, *J Am Chem Soc*, 2008, **130**, 12242-12243.
6. N. I. o. S. a. T. NIST, Thermophysical properties of fluid systems, (<https://webbook.nist.gov/chemistry/fluid/> 2020).
7. K. Kortsen, A. A. C. Pacheco, J. C. Lentz, V. Taresco and S. M. Howdle, *J Supercrit Fluids*, 2021, **167**, 105047.
8. B. J. Hunt and M. I. James *Polymer Characterisation*, Blackie Academic & Professional, 1993.
9. S. Mori and H. G. Barth, *Size Exclusion Chromatography*, Springer, 1999.
10. A. Chaudhary, E. J. Beckman and A. J. J. Russell, *J Am Chem Soc*, 1995, **113**, 3728-3733.
11. R. N. Ibbett, *NMR Spectroscopy of Polymers*, Springer, 1993.
12. F. A. Bovey and P. A. Mirau, *NMR of Polymers*, Academic Press Inc. Ltd, 1996.
13. G. H. Michler, *Electron Microscopy of Polymers. Illustrated ed.*, Springer, 2008.
14. R. A. Pethrick, *Polymer Structure Characterization*, Royal Society of Chemistry, 2007.
15. H. M. Woods, C. Nouvel, P. Licence, D. J. Irvine and S. M. Howdle, *Macromolecules*, 2005, **38**, 3271-3282.

Contents

Chapter 3. Polydimethylsiloxane-based macro-CTAs for block copolymer synthesis with PMMA in scCO₂. ...97

3.1. Abstract	97
3.2. Introduction	98
3.2.1. Polymerisation-induced self-assembly	98
3.2.2. PISA in scCO ₂	105
3.2.2.1. RAFT polymerisation in scCO ₂ with fluorinated-based macro-CTAs	105
3.2.2.2. RAFT polymerisation in scCO ₂ with polydimethylsiloxane-based macro-CTAs	111
3.3. Aims	115
3.4. Experimental	116
3.4.1. Materials	116
3.4.2. Synthetic procedures	116
3.4.2.1. Synthesis of PDMS macro-CTAs	116
3.4.2.2. Standard dispersion polymerisation with macro-CTA in scCO ₂	117
3.4.2.3. Standard dispersion polymerisation in sampling autoclave	117
3.4.2.4. Standard solubility test in scCO ₂ in variable volume view cell	117
3.4.2.5. Hexane washes of polymer powders	118
3.4.3. Polymer characterisation	118
3.4.3.1. Size exclusion chromatography (SEC)	118
3.4.3.2. Proton nuclear magnetic resonance (1H NMR)	118
3.4.3.3. Fourier-transform infrared spectroscopy (FT-IR)	119
3.4.3.4. Ultraviolet-visible spectrophotometry (UV-vis)	119
3.4.3.5. Scanning electron microscopy (SEM)	119
3.5. Results and discussion	119
3.5.1. PDMS-DDMAT synthesis	119
3.5.2. Solubility of PDMS-DDMAT macro-CTAs in scCO ₂	126
3.5.3. PDMS-DDMAT application for polymerisation of MMA in scCO ₂	128
3.5.3.1. Control in the absence of the CTA chain-end	129
3.5.3.2. MMA polymerisation with PDMS ₁₂₈ -DDMAT	131
3.5.3.3. MMA polymerisation with PDMS ₆₅ -DDMAT	135
3.5.3.4. PDMS grafting efficiency onto the particles	139
3.5.3.5. MMA polymerisation with PDMS-DDMAT and DDMAT	143
3.6. Conclusions	147
3.7. References	148

Chapter 3. Polydimethylsiloxane-based macro-CTAs for block copolymer synthesis with PMMA in scCO₂.

3.1. Abstract

We explore the use of polydimethylsiloxane (PDMS)-based macromolecular chain transfer agents (macro-CTAs) for polymerisation induced self-assembly (PISA) in scCO₂. The methyl methacrylate (MMA) dispersion polymerisation in scCO₂ is selected as our model reaction. Although PISA mediated by reversible addition-fragmentation chain transfer (RAFT) has been previously performed in scCO₂ with fluorinated macro-CTAs, the use of PDMS-based macro-CTAs has only been briefly investigated in a previous thesis in the Howdle group. We report the synthesis of macro-CTAs *via* esterification of monocarbinol terminated PDMS (PDMS-OH) of different molecular weights with a CTA containing a carboxylic acid group, 2-(dodecylthiocarbonothioylthio)-2-methylpropionic acid (DDMAT). This CTA was selected according to promising results from the earlier mentioned thesis project in the Howdle group, in which PDMS-DDMAT was used for MMA polymerisation in scCO₂. That work was a step towards PISA polymerisation in scCO₂ with non-fluorinated macro-CTAs. In the present work, the effect of PDMS and PMMA molecular weight over particle morphology and RAFT control is investigated.

Although PDMS-DDMAT is able to stabilise PMMA particles, successful RAFT control is not obtained, and less than 50% PDMS-DDMAT is retained in the final product. The SEC studies also indicate the presence of unreacted macro-CTA. We hypothesise that the poor growth from the macro-CTA is a result of the poor RAFT control of PDMS-DDMAT at initial stages of the dispersion polymerisation. Individual spherical particles can be observed for polymerisations with high target DP of MMA. However, the particle size is above the expected for self-assembly, which suggests aggregation is taking place, and no morphology transition (sphere-to-worm-to-vesicle) was observed for the different DPs of MMA. A significant improvement on the PISA mechanism is observed on addition of DDMAT molecular CTA, with a final molecular weight closer to the theoretical one and with a narrower polydispersity. Finally, we corroborate our results and propose the best direction for future studies.

3.2. Introduction

3.2.1. Polymerisation-induced self-assembly

Implementation of reversible-deactivation radical polymerisation (RDRP) in dispersed systems was not trivial, mainly because of the inability of the chain transfer agent (CTA) to control the reaction at its *locus*.¹ Ferguson *et al.* overcame this issue through the synthesis of amphiphilic block copolymers.² The authors polymerised acrylic acid (AA) in aqueous solution to form a water-soluble polymer, and further used it in water by slowly feeding *n*-butyl acrylate (BA), a hydrophobic monomer. They obtained an amphiphilic block copolymer that could self-assemble into micelles that further swelled with BA and later formed particles. In this way, the CTA could mediate the two-step polymerisation in both the aqueous phase, as the molecular CTA, and in the organic phase, as a macro-CTA. This method required the slow addition of the solvophobic monomer in order to avoid droplet formation, which could cause the macro-CTA to partition between phases and thus not control the reaction.² However later, the polymerisation could be conducted in batch systems applying different macro-CTAs.^{3, 4}

This strategy based on the self-assembly of amphiphilic block copolymers has been termed polymerisation-induced self-assembly (PISA) (Figure 1).⁵ Depending on the solubility of the core-forming monomer in the continuous phase, PISA can be performed under either dispersion, if the monomer is soluble in the continuous phase, or emulsion, if the monomer is insoluble.

Without doubt, one main advantage of PISA is the facile production of various particle morphologies at high solid contents. However, a further advantage of PISA is the stabilisation of latex particles with only a few solvophilic living chains and in the absence of additional stabiliser/surfactant, eliminating the detrimental effects of surfactants on polymer latex and films.¹

A variety of morphologies can arise from the self-assembly occurring in PISA, similar to the morphologies obtained *via* solvent displacement.⁶ However, solvent displacement requires long equilibration times and is limited to very low solid contents, typically < 2 wt%.¹ PISA offers a faster and more straightforward way to achieve block copolymer nano-objects at high solid contents *via* dispersion polymerisation in a variety of solvents and in emulsion polymerisation in water.^{1, 7-10}

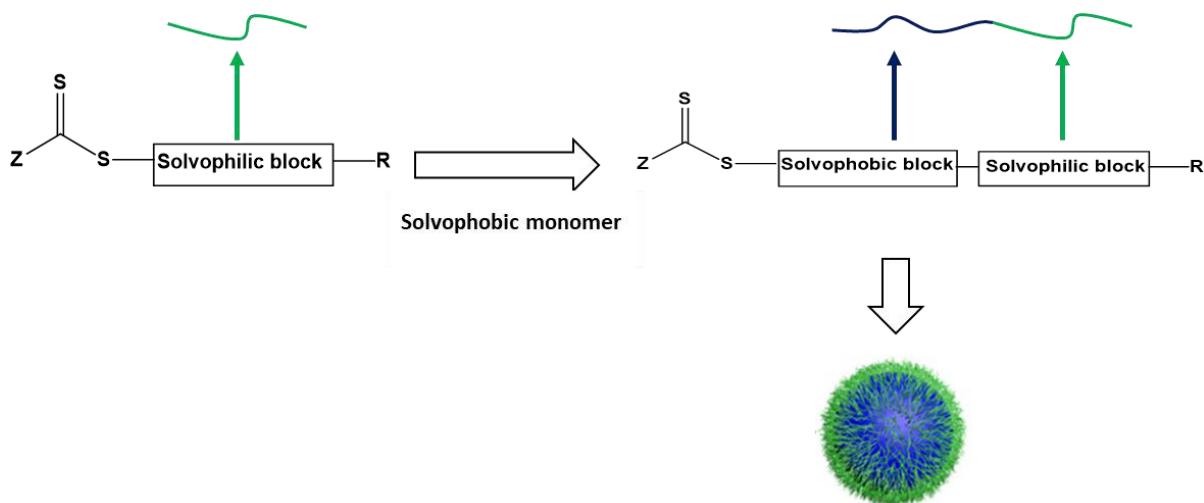


Figure 1 - Schematics of the PISA process via RAFT polymerisation. A solvophilic macro-CTA, produced in situ or in a previous step, chain extends with a solvophobic monomer to form amphiphilic block copolymer, which self-assembles into particles with the solvophilic block in the corona. Figure adapted from Chen et al.¹⁵

Obtaining such morphologies *via* PISA depends on various parameters, such as the packing parameter, the block architectures, the total solids content and the nature of the solvent being used (Figure 2).^{7, 11-13}

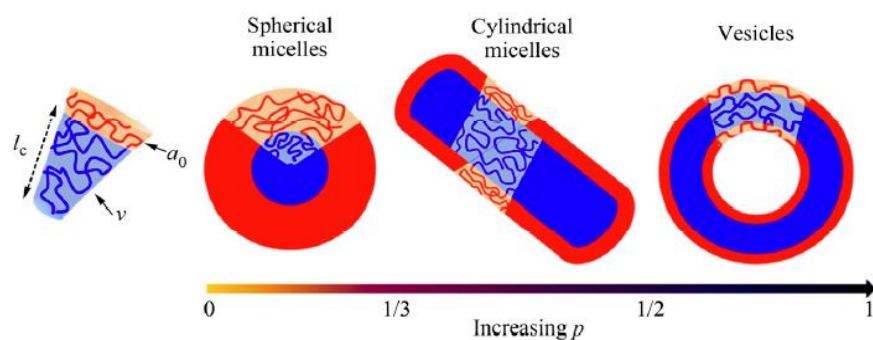


Figure 2 - Schematic to show nano-assemblies of amphiphilic diblock copolymers in a selected solvent with relation to packing parameter (p). The slice of the micelle shows the solvophobic segment volume (v), the contact area of the solvophilic group (a_0) and the length of the solvophobic group (l_c). Figure adapted from Chen et al.¹⁵

As defined in Chapter 1, the core radius and the stretching of chains in the core increase as the molecular weight of the core forming block increases, causing the transition from spheres to worms and to vesicles.⁶ In a more detailed study, it was observed that after worms are formed, as conversion increases, the linear worms become branched and “octopus-like”

structures form with radial polymer chains that resemble tentacles. ¹⁴ These structures then partially fuse to form “jellyfish-like” structures that finally reorganise into vesicles (Figure 3).¹⁴

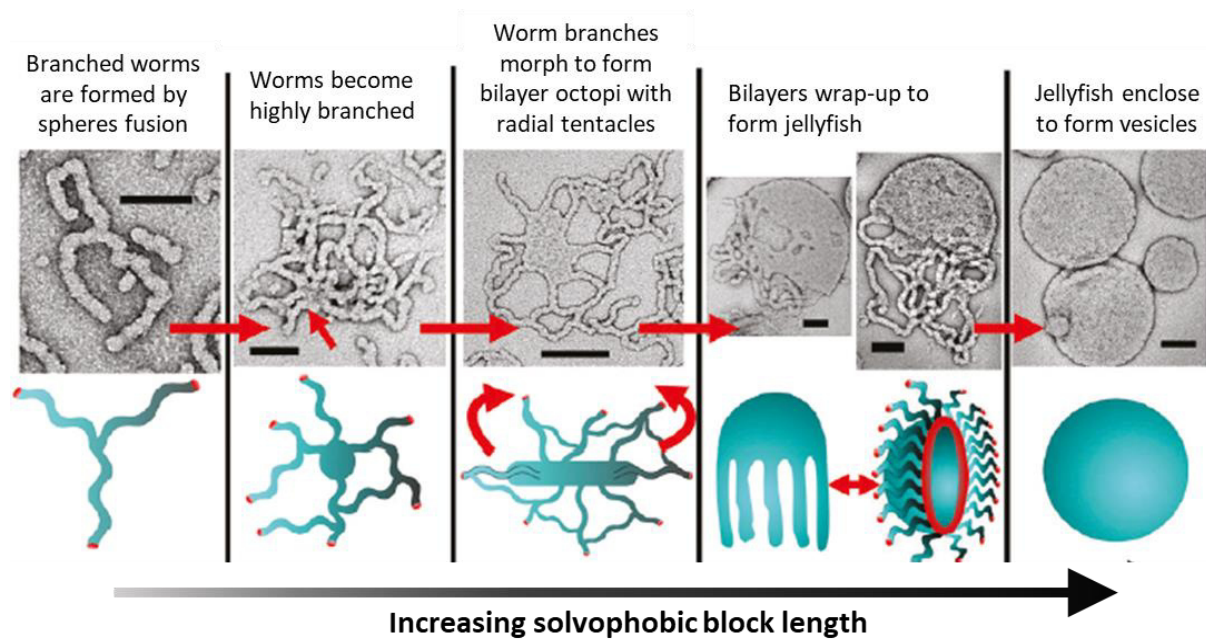


Figure 3 – Suggested mechanism for the worm-to-vesicle transformation during the polymerisation of 2-hydroxypropyl methacrylate (HPMA) from poly(glycerol mono methacrylate) (PGMA) macro-CTA, to achieve PGMA₄₇-b-PHPMA₂₀₀, by PISA via RAFT aqueous dispersion polymerisation. Figure adapted from Blanz et al.¹⁴

Some additional parameters influence the resulting morphologies obtained by PISA through RAFT dispersion polymerisation (Figure 4), such as: ¹

- The concentration of the solvophobic monomer, which affects the solvency of the continuous phase and the solids content. This is particularly important for PISA via dispersion polymerisation because the monomer is initially soluble in the continuous phase;
- The affinity of each block with the dispersing phase;
- The amount of residual monomer that swells the particles;
- The constant growth of the solvophobic block.

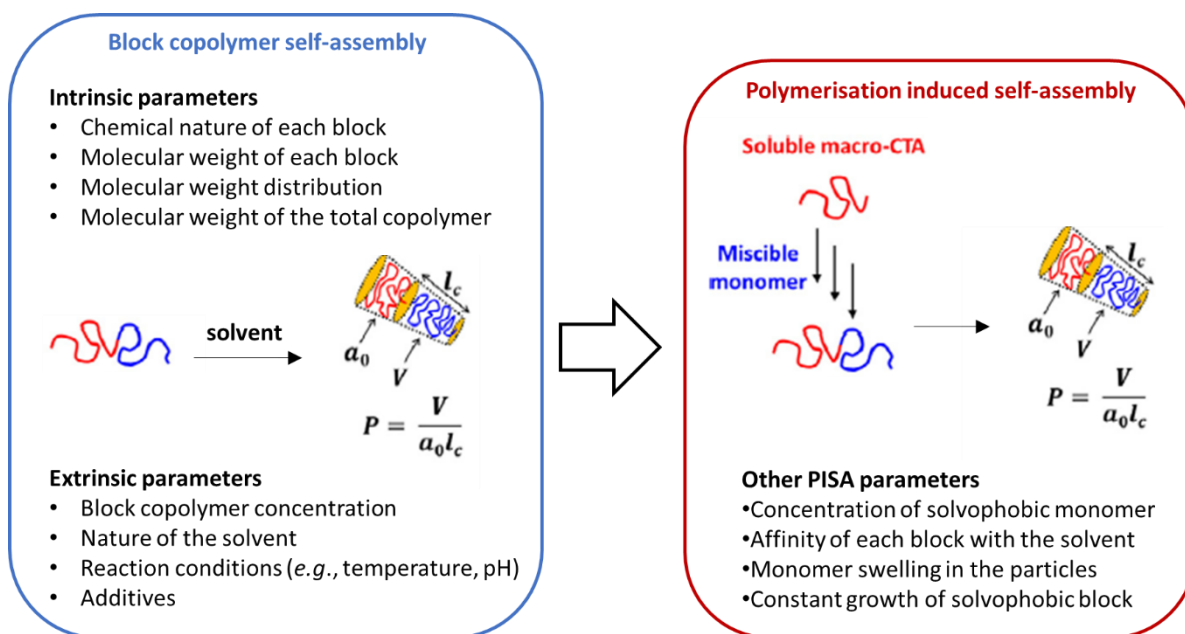


Figure 4 – The main parameters that define self-assembly of amphiphilic block copolymers (already prepared) and the extra parameters that define morphology for polymerisation-induced self-assembly. Figure adapted from Lansalot, Rieger and D’Agosto.³

The study of morphology transition by independently varying molecular weights of solvophilic/solvophobic blocks and solid content allows the construction of phase diagrams, which enable the reproducible targeting of a pure morphology of the studied block copolymer. A morphology can be targeted, if for a given solvophilic block, a specific degree of polymerization (DP) of the solvophobic block is achieved under the same reaction conditions as in the diagram, e.g., same solvent, temperature and solid content. Phase diagrams are usually represented as the plot of core-forming block DP versus total solids content.⁹ Although the construction of phase diagrams is a laborious and time demanding process, theoretical simulations are not always accurate, as kinetically trapped and thermodynamically controlled structures can be formed.¹

In the case of thermodynamically controlled structures, the morphology with the lowest free energy is favoured, whereas the kinetically controlled morphology is obtained when kinetic factors prevent the equilibrium morphology from forming. In this way, some syntheses will solely result in spherical morphology because the morphology is kinetically trapped.¹³ The nature of the monomers used also impacts morphology, with solvophilic blocks made up from

slightly less soluble monomers leading to formation of different morphologies at lower DP of the solvophobic block.¹⁵ At the same time, having a slightly more solvophilic core block was shown to improve mobility and thus favour morphology transitions.¹⁵

Although most studies achieved morphology transition by means of changing the DP of the solvophobic block, there was some investigation into the effect of the solvophilic block. For instance Lesage de la Haye *et al.* studied the effect of hydrophilic block topology over aqueous emulsion polymerisation of styrene.¹¹ Another study varied the molecular weight, composition and concentration of the hydrophilic macro-CTA, resulting in different morphologies, *i.e.*, spheres, fibres, and vesicles.¹⁶ The authors identified the molecular weight of both hydrophobic and hydrophilic blocks to be the main triggers for particle morphology change. Other experimental conditions such as temperature, initiator choice, monomer concentration and stirring rate also affect particle morphology. In particular, the evolution of spheres into worms has been attributed to the fusion of spherical micelles through inelastic collisions.¹⁵ Therefore, stirring rate and total solids concentration will have a direct effect upon morphology formation.

PISA in non-polar solvents has been less studied than in aqueous and alcoholic media. Fielding *et al.* reported for the first time that the same morphological control previously reported for PISA by RAFT dispersion in aqueous and alcoholic formulations could be achieved in non-polar solvents.¹⁷ The authors studied the synthesis of poly(lauryl methacrylate)-*b*-poly(benzyl methacrylate) (PLMA-*b*-PBzMA) in *n*-heptane (Figure 5A). Using a macro-CTA with DP ≥ 37 resulted in spherical particles of tunable size according to the targeted DP of PBzMA (Figure 5B), but when the macro-CTA DP was decreased to DP = 17, sphere-to-worm-to-vesicle morphology transition was observed (Figure 5C).

The authors reported that for PLMA₁₇-*b*-PBzMA the final diblock copolymer morphology was mainly dictated by the DP of the core-forming block, with only a weak correlation to concentration.¹⁷ In addition, it is interesting to notice that the worms had a high dispersity in terms of length but similar width to the spherical particles, consistently with the formation of worms by one-dimensional aggregation of spherical particles. The absence of a morphology transition at higher PLMA DPs was attributed to the effective steric stabilisation when the DP of the PLMA block is sufficiently high, which prevents one-dimensional fusion of spheres to form worms and after vesicles.¹⁷

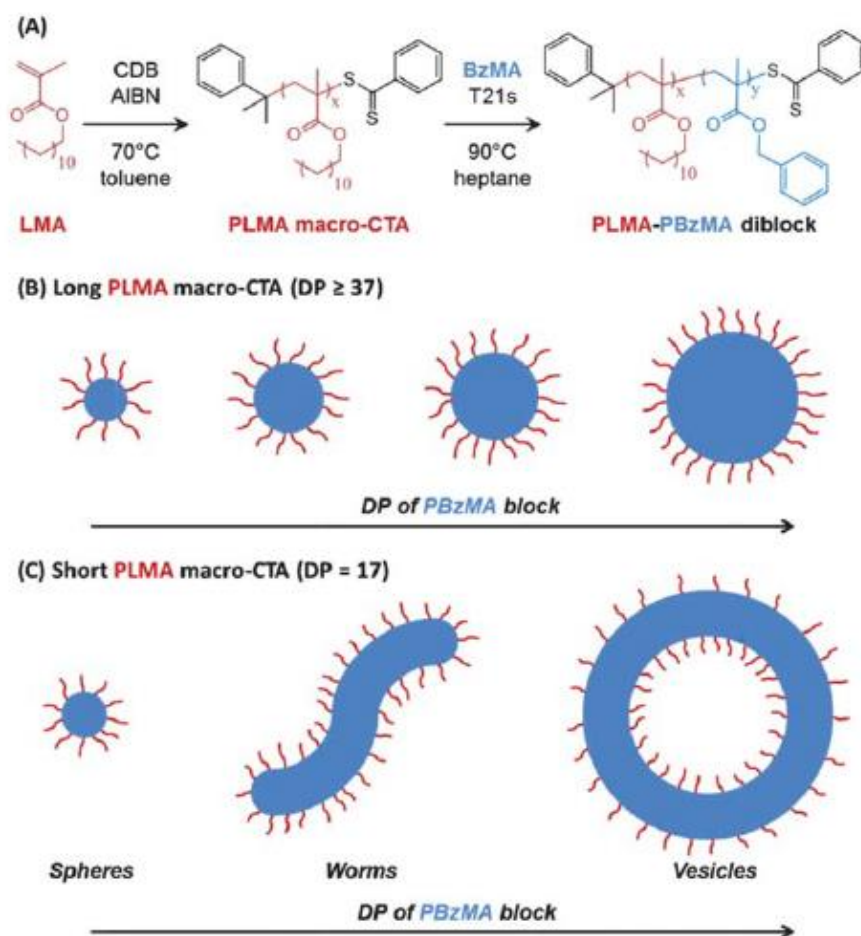


Figure 5 – Schematics showing (A) the PLMA-*b*-PBzMA synthesis, (B) a schematic of particle morphology change at different PBzMA target DP when using PLMA macro-CTA of DP ≥ 37 , (C) a schematic of morphology change at different PBzMA target DP when using PLMA macro-CTA of DP = 17. Figure adapted from Fielding *et al.*¹⁷

As mentioned in Chapter 1, Lopez-Oliva *et al.* studied PISA of PBzMA using polydimethylsiloxane (PDMS) as the stabilising block in *n*-heptane.⁷ The block copolymer was not prepared via a one-pot method, instead monohydroxyl terminated PDMS was purchased and coupled to the CTA. This method guaranteed the uniformity of the solvophilic block and was advantageous for the morphology transition study, making it possible to identify pure morphologies restricted to a narrow range of reaction conditions. For example, a pure worm morphology was restricted to a copolymer concentration $> 25\%$ w/v, with PBzMA DP = 80, which represents an extremely narrow region within the phase diagram (Figure 6).⁷ Overall control over molecular weight and molecular weight dispersity was good and the transition of sphere-to-worm-to-vesicle was confirmed by both transmission electron microscopy (TEM) and small-angle X-ray scattering (SAXS).⁷

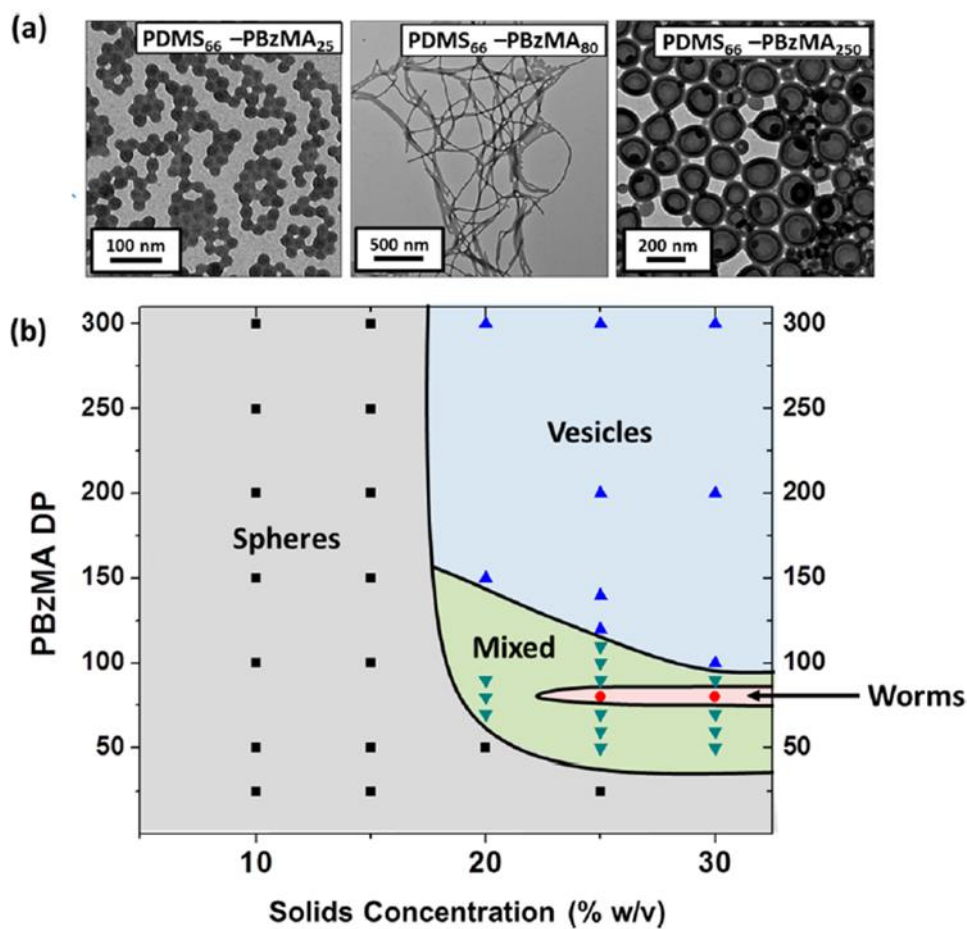


Figure 6 – (a) Representative TEM images for PDMS₆₆-PBzMA diblock copolymers at 25% w/v solids, from left to right: spheres, worms and vesicles. (b) Phase diagram constructed for PDMS₆₆-PBzMA diblock copolymers prepared via RAFT dispersion polymerization of BzMA in *n*-heptane at 70 °C using AIBN initiator. Figure adapted from Lopez-Oliva et al.⁷

A PDMS-based solvophilic macro-CTA, *i.e.*, PDMS₆₆ with 4-cyano-4-(2-phenylethanesulfanylthiocarbonyl)sulfanylpentanoic acid (PETTC) as CTA (PDMS₆₆-PETTC), was also used for the dispersion polymerisation of several methacrylic monomers in low viscosity silicone oil.¹⁸ Kinetically trapped spheres were obtained with all monomers, including methyl methacrylate (MMA). The only exception was the polymerisation with 2-(dimethylamino)ethyl methacrylate (DMAEMA), which presented a sphere-to-worm-to-vesicle transition.¹⁸

These successful results for PISA with PDMS as macro-CTA is of great interest because of the high solubility of PDMS in scCO₂, as will be explained in the next section.

3.2.2. PISA in scCO₂

There are only a few reports of PISA *via* RAFT polymerisation in scCO₂, from just a limited number of soluble polymers in scCO₂, the range being restricted to solvophilic block of amorphous fluoropolymers and silicones.¹⁹

3.2.2.1. RAFT polymerisation in scCO₂ with fluorinated-based macro-CTAs

The seminal work of McClain *et al.* confirmed that micelles can form when both a CO₂-philic and a CO₂-phobic block are present in a block copolymer.²⁰ The CO₂-phobic block segregates in the internal phase, while the CO₂-philic group extends into the CO₂ phase.²¹ The authors investigated a series of block copolymers composed of polystyrene (PSt), which is CO₂-phobic, and poly(1,1-dihydroperfluorooctyl acrylate) (PFOA), which is CO₂-philic.²⁰ The series of PSt-*b*-PFOA polymers was synthesised and then dissolved in scCO₂ for *in situ* small-angle neutron scattering (SANS). The block copolymers self-assembled into spherical core-shell structures of 15-20 nm in scCO₂ under 65 °C and 340 bar (Figure 7).

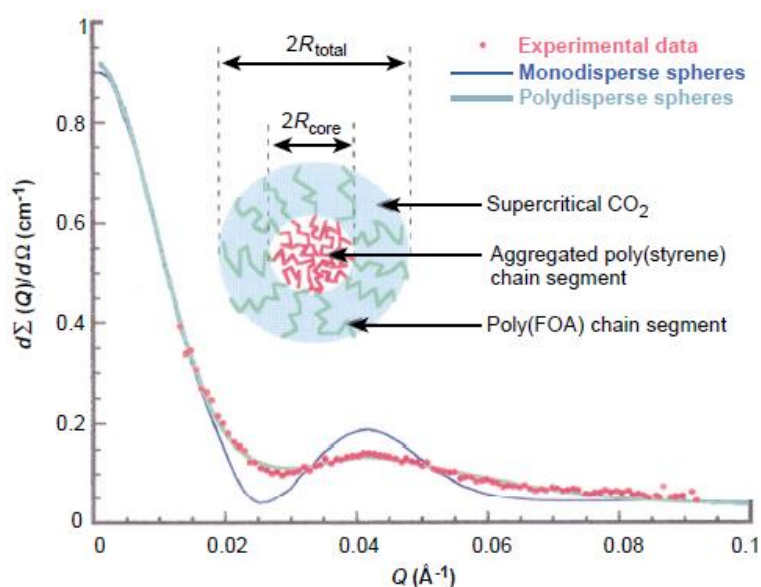


Figure 7 – *In situ* small-angle neutron scattering (SANS) of PSt-*b*-PFOA in scCO₂ under 65 °C and 340 bar – scCO₂ $d = 0.842 \text{ g cm}^{-3}$. Results fit well with a monodisperse spherical core-shell model. This confirms the self-assembly of amphiphilic block copolymers in scCO₂. Figure adapted from McClain *et al.*²⁰

The increase of PFOA molecular weight caused an increase in the total number of particles and reduced the swelling of the corona, while the increase of PSt molecular weight increased

the radius of the core and the number of block copolymer units per micelle. They also observed that an increase in scCO₂ density, by tuning temperature and pressure, resulted in smaller and more dispersed in size micelles (13.6 nm to 28.4 nm).²⁰ For example, a PSt₃₆-*b*-PFOA₉₈ had a micelle diameter of 17.8 nm at scCO₂ d= 0.842 g cm⁻³ and 13.6 nm when d= 0.934 g cm⁻³.

McClain *et al.* proved that amphiphilic block copolymers can self-assemble, but it was only in 2008 that Zong *et al.* reported the first use of a macro-CTA in RAFT dispersion polymerization in scCO₂.²² 2-cyanoprop-2-yl dithiobenzoate (CPDB) was used as CTA for the synthesis of Poly(1,1-dihydroperfluorooctyl methacrylate) (PFOMA) macro-CTA of 15 kg mol⁻¹ in bulk. The macro-CTA was then chain extended with MMA in scCO₂, giving self-stabilised PFOMA-*b*-PMMA particles. PMMA and PFOMA were selected because they should phase-separate, as they require a large enthalpy of mixing. All reactions were performed at 65 °C and 276 bar, with 2:1 macro-CTA:initiator ratio. As with McClain *et al.*, the obtained particles presented a core-shell structure with PFOMA in the corona and PMMA in the core, but were much larger, with 2-5 μm.²² The particles had a broad size distribution, which is not surprising for a RAFT polymerisation, because the inhibition caused by the CTA impacts upon the nucleation phase.²³

Transmission electron microscopy with energy dispersive X-ray analysis (EDX-TEM) analysis of a particle and a cross-sectioned particle (Figure 8) showed a fluorinated halo around the particles, with fluorine concentration up to three times higher at the corona than at the core.²² Within the core, the fluorine density becomes more uniform with no apparent phase separation between the PFOMA and PMMA. This was attributed to the enhanced miscibility of PFOMA and PMMA in scCO₂.²²

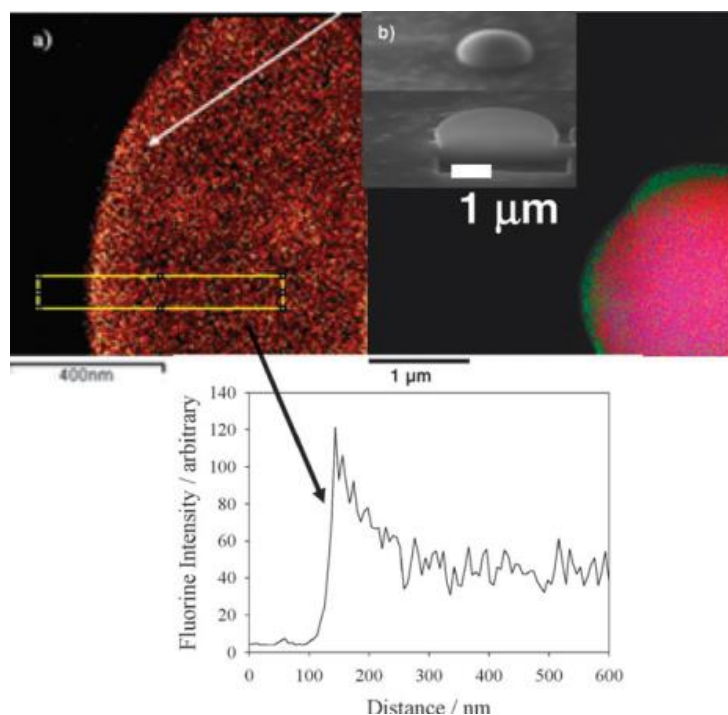


Figure 8 - EDX-TEM element maps showing (a) cross-sectional fluorine map across a section of a particle and the histogram for the area within the yellow box; (b) elemental distribution around an intact particle (red—carbon, pink—oxygen, and green—fluorine), showing a fluorine-rich halo. The inset shows the SEM image of a single particle before and after focussed ion beam slicing. Figure adapted from Zong et al.²²

The authors then investigated the polymerisation kinetics through a series of reactions stopped at different times.²² The kinetic plot followed a pseudo-first order rate of polymerisation (Figure 9A), and molecular weight increased linearly with conversion, while dispersity (\mathcal{D}) was narrow and decreased with conversion (Figure 9B). After 20 h of reaction, monomer conversion was almost complete and $\mathcal{D} = 1.22$ was obtained, while the number-average molecular weight (M_n) reached 76 kg mol^{-1} and was close to the theoretical M_n ($M_{n,\text{th}}$) of 74.9 kg mol^{-1} , indicating a well-controlled dispersion RAFT polymerisation.²² Surprisingly, a short inhibition period of 1 h was observed with the macro-CTA, while a inhibition period of 10 h was previously reported for MMA dispersion polymerisation in scCO_2 with molecular CPDB.²⁴

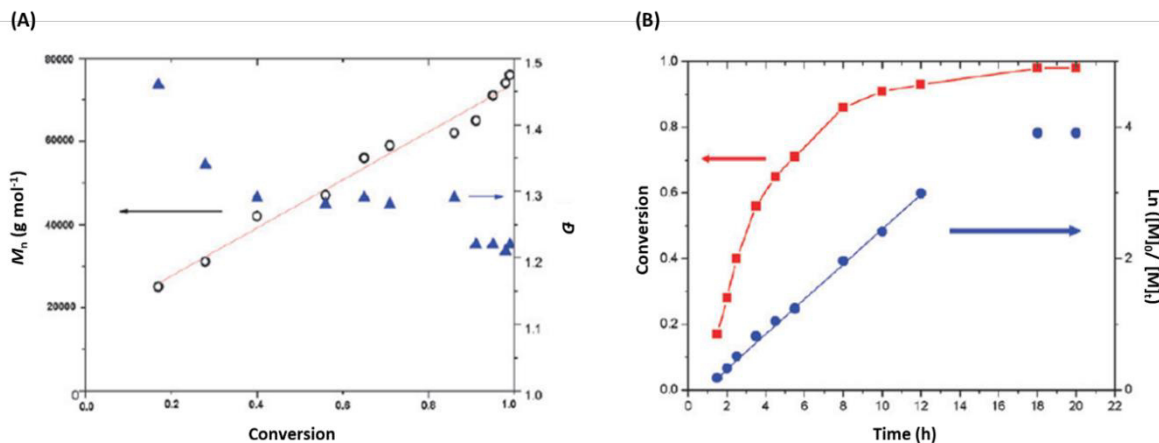


Figure 9 – MMA polymerisation kinetics with PFOMA macro-CTA 15 kg mol^{-1} . (A) Molecular weight evolution and dispersity against monomer conversion, showing the linear evolution and the expected narrowing of dispersity at higher conversions. (B) Conversion as a function of polymerisation time and pseudo first-order kinetic plot for polymerisation of MMA with PFOMA-CPAB 15 kg mol^{-1} . Figure adapted from Zong *et al.*²²

This work by Zong *et al.* can be seen in a first approximation as a PISA in scCO_2 .²² However, the large particles produced ($2\text{-}5 \mu\text{m}$) indicate aggregation, which may arise from the enhanced miscibility of PFOMA and PMMA in scCO_2 . Such miscibility would prevent successful self-assembly. It is also possible that self-assembly occurs and PISA is achieved, but the block copolymer particles aggregate because of the compatibility of both blocks. A more detailed *in situ* study would be necessary to identify which scenario is correct.

Following this work, Xu *et al.* explored the impact of solvophobic/solvophilic blocks molecular weight over PISA in scCO_2 .²⁵ The authors synthesised block copolymers by a two-step synthesis, first poly(dodecafluoroheptyl methacrylate) (PDFMA) was prepared in THF solution *via* RAFT with cumyldithiobenzoate (CDB) as CTA, and then PDFMA-CDB of different DPs (DP = 15, 32, 55) were chain extended with MMA in dispersion polymerisation in scCO_2 . SEC studies of the PDFMA-*b*-PMMA final product showed unimodal molecular weight distributions with $\bar{D} < 1.5$. As expected, the molecular weight of the block copolymers increased with increasing the targeted DP of PMMA and no unreacted macro-CTA was observed.²⁵ In addition, PDFMA-*b*-PMMA formed self-stabilised spherical particles with diameters ranging from 80 to 300 nm as consequence of varying PDFMA and PMMA blocks molecular weight.²⁵ When PMMA was below 300 DP, a solid block was obtained, as an effect

of plasticisation, which decreases glass transition temperature (T_g) in $scCO_2$.²⁵ Further increasing PMMA molecular weight beyond DP of 300 resulted in a mix of solid and free-flowing powders, with some spherical particles observed by scanning electronic microscopy (SEM). This still indicates insufficient stabilisation. Only, at PMMA DP > 500 a free-flowing powder composed of spherical particles was obtained (Figure 10).

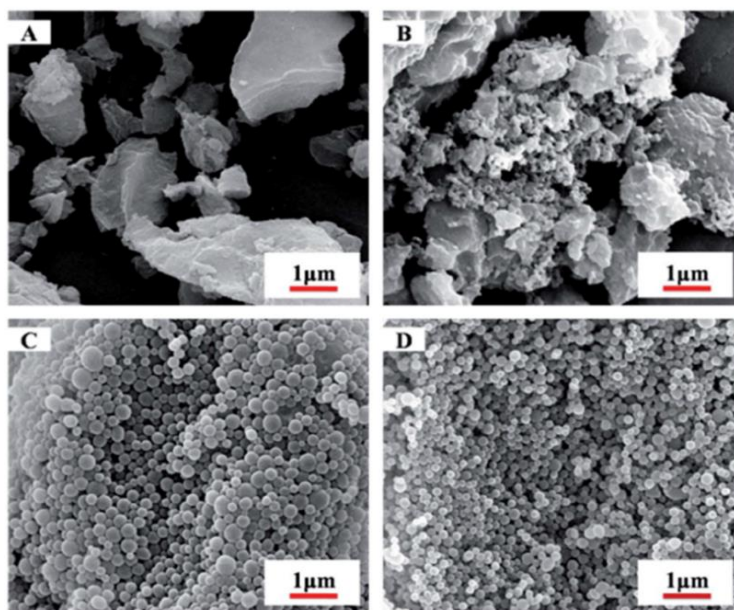


Figure 10 - SEM images of the $PDFMA_{15}\text{-}b\text{-}PMMA_x$ particles prepared by RAFT dispersion in $scCO_2$ using $PDFMA_{15}\text{-}CDB$ as a macro-CTA: (A) $PDFMA_{15}\text{-}b\text{-}PMMA_{98}$ – solid aggregates; (B) $PDFMA_{15}\text{-}b\text{-}PMMA_{351}$ – solid agglomerates and some spherical aggregates; (C) $PDFMA_{15}\text{-}b\text{-}PMMA_{533}$ – spherical particles; (D) $PDFMA_{15}\text{-}b\text{-}PMMA_{680}$ – smaller spherical particles. Figure adapted from Xu et al.²⁵

When increasing the DP of the PDFMA block from 15 to 55 for a constant PMMA DP of 500, the spherical particle size decreased from 259 nm to 81 nm.²⁵ This is because of the better stabilisation of polymer particles with longer stabilising blocks, similarly to what was observed in the synthesis of polymer particles in $scCO_2$ with stabilisers of different molecular weights.²⁶ These particle sizes (80-300 nm) are closer to that expected from block copolymers self-assembly, but still with some aggregation of the original block copolymer particles.

The authors also studied the effect of $scCO_2$ pressure upon particle morphology and observed a slight increase in particle size as pressure increased from 100 to 300 bar.²⁵ As pressure increases, the density of $scCO_2$ increases and the critical PMMA molecular weight where microphase separation is achieved moves to higher PMMA DPs. In the same way, the

solubility of PDFMA-*b*-PMMA copolymers increases with scCO₂ pressure, leading to well dispersed nanoparticles at 300 bar.

There are some factors that might lead to the presence of only a spherical morphology in scCO₂. Firstly, it is known that the T_g of polymers is decreased in scCO₂, which is exploited for polymer foaming.^{27, 28} This low T_g impacts the nucleation step, making it impossible to obtain well-defined PMMA particles when targeting low molecular weights and thus no morphology can be observed.²⁹ Furthermore, the immiscibility of both blocks is essential for phase separation to occur and induce morphology change, but scCO₂ is known to increase the miscibility between polymers, which likely contributes to the fact that only spheres can be observed. However, in general those obtained spheres were very big compared to the few tenth nanometre diameter expected from a pure self-assembly of block copolymers.^{24, 25} This indicates a strong aggregation is taking place.

More recently, Huo *et al.* also reported the synthesis of PDFMA-*b*-PMMA via PISA in scCO₂, but using DDMAT for the synthesis of the PDFMA macro-CTA in THF solution.³⁰ PDFMA-DDMAT macro-CTA with DP = 21 was chain extended with MMA in dispersion in scCO₂ at a 1500:4:1 ratio of MMA: macro-CTA: initiator, giving a block copolymer with $M_n = 38.1 \text{ kg mol}^{-1}$ which is close to $M_{n,th}$ of 37.2 kg mol^{-1} , and $\mathcal{D} = 1.24$,³⁰ SEM analysis showed the occurrence of spherical particles with a diameter of 425 nm obtained with a narrow size distribution of 1.13. If we consider C-C bond-length of 1.54 \AA and the molecular weight of 38.1 kg mol^{-1} , *i.e.*, DP= 380, the particle diameter should be of 117 nm if considering 2 x length of the core-forming block. Thus, the obtained big particle diameter (425 nm) evidences aggregation as for Xu *et al.*²⁵ Although this result shows good control over M_n and morphology with the DDMAT-based fluorinated macro-CTA, no SEC pictures or kinetic study were presented.

It is important to emphasise that particles obtained in these previous RAFT mediated PISA in scCO₂ were bigger than expected for a well controlled PISA,^{22, 25, 30} but within the PMMA particle size range previously reported in conventional dispersion radical polymerisation and RAFT polymerisation in scCO₂ (0.3 to 6 μm), which could be achieved with a range of different stabilisers.^{24, 31-40}

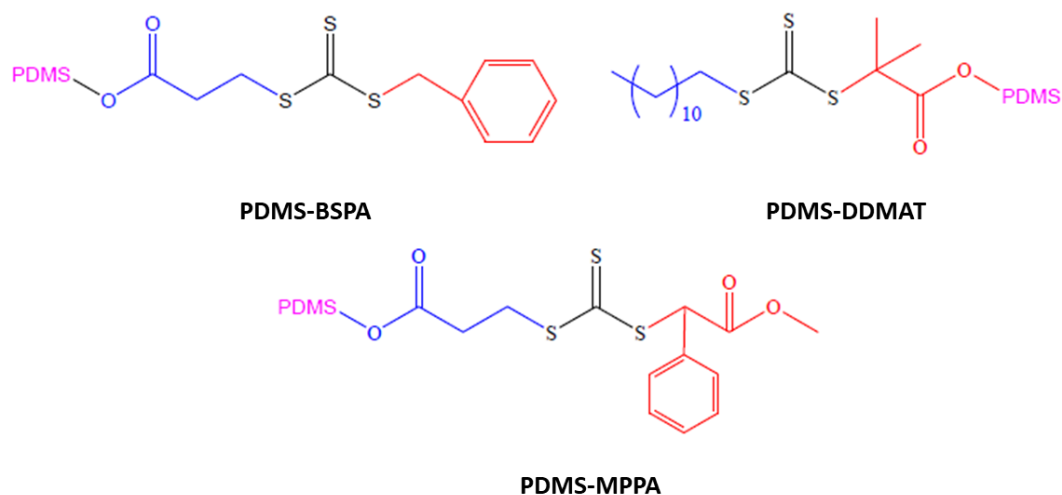


Figure 12 – Structure of macro-CTAs based on PDMS used by Zong in her thesis: PDMS-BSPA, PDMS-DDMAT and PDMS-MPPA. The R groups are presented in red and the Z groups in blue. PDMS-DDMAT has the CTA attached by the R group, while PDMS-BSPA and PDMS-MPPA have the CTA attached via the Z-group. Figure adapted from Zong’s doctoral thesis.⁴⁴

All three macro-CTAs were assessed for MMA dispersion polymerisation in scCO_2 at 2:1 CTA:initiator ratio, 276 bar, 65 °C with a target DP of 600 for the PMMA block. The reactions were tracked using a sampling port at the autoclave bottom.^{24,45} This system allows molecular weight to be tracked with precision, but the high volatility of MMA makes conversion calculation less precise due to monomer loss. Nevertheless, kinetic studies with the three macro-CTAs depicted a linear increase of M_n with conversion and pseudo first order kinetics (Figure 13).⁴⁴

Zong’s results showed that MMA polymerisation with PDMS-DDMAT was well controlled, with $M_n = 74.2 \text{ kg mol}^{-1}$ when the $M_{n,\text{th}}$ was 69.5 kg mol^{-1} and $\mathcal{D} = 1.38$.⁴⁴ Compared to the other two macro-CTAs, PDMS-DDMAT produced the best agreement between calculated and experimental molecular weights and the lowest dispersity.⁴⁴ This very good agreement between M_n and $M_{n,\text{th}}$ means that 100% of the macro-CTA is involved in the RAFT process, while in a conventional dispersion polymerisation only a small fraction of PDMS-MA, *i.e.*, a common stabiliser for PMMA polymerisation in scCO_2 , is known to be covalently bounded to PMMA particles in scCO_2 .^{36,37}

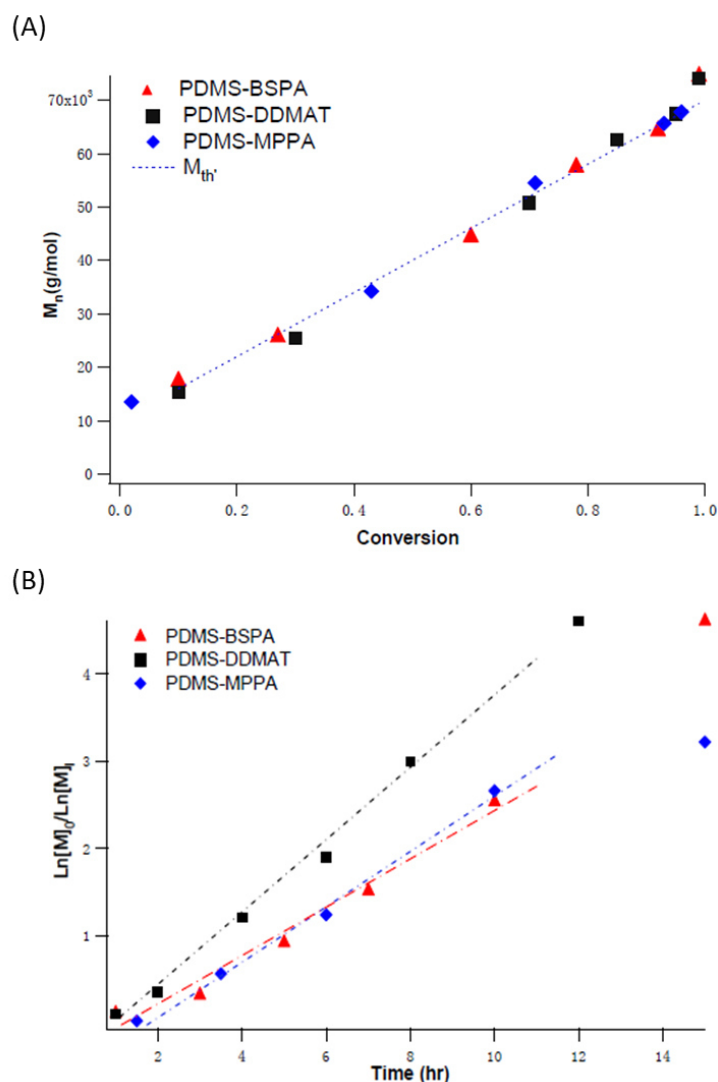


Figure 13 – Kinetic study of MMA dispersion polymerisation in $scCO_2$ with PDMS-BSPA, PDMS-DDMAT and PDMS-MPPA (65 °C, 276 bar). (A) Molecular weight evolution against conversion with all macro-CTAs (the dashed line represents the theoretical M_n based on the polymerisation of MMA in $scCO_2$). All three experiments presented a linear trend whatever the macro-CTA. (B) Kinetic plots of MMA conversion, showing pseudo first order kinetics. Figure adapted from Zong's doctoral thesis.⁴⁴

In addition, all polymerisations with the PDMS-based macro-CTAs gave discrete particles with a broad particle size distribution at a PMMA target DP = 600. The broad particle size distribution was attributed to an impact upon the nucleation when using a macro-CTA. The average diameter of the particles was 1-3 μm for the polymerisation mediated by PDMS-BSPA, 1-2 μm by PDMS-DDMAT and 2.7-5.5 μm by PDMS-MPPA.⁴⁴ This was similar to the particle size observed for MMA polymerisation with PFOMA-based macro-CTA (2-5 μm),²² but much bigger than what was reported with PDFMA-based CTAs (81 -425 nm).^{25, 30} Therefore,

if self-assembly of block copolymers is involved, the original formed particles must have aggregated.

A sample of the polymer particles synthesised with PDMS-MPPA was analysed by EDX-TEM (Figure 14). The silicon concentration at the surface of the particle was clearly higher, up to seven times higher than at the core (Figure 14D), indicating a core-shell structure.⁴⁴ At the core of the particle the silicon density becomes more uniform and no internal phase separation between PDMS and PMMA was observed.

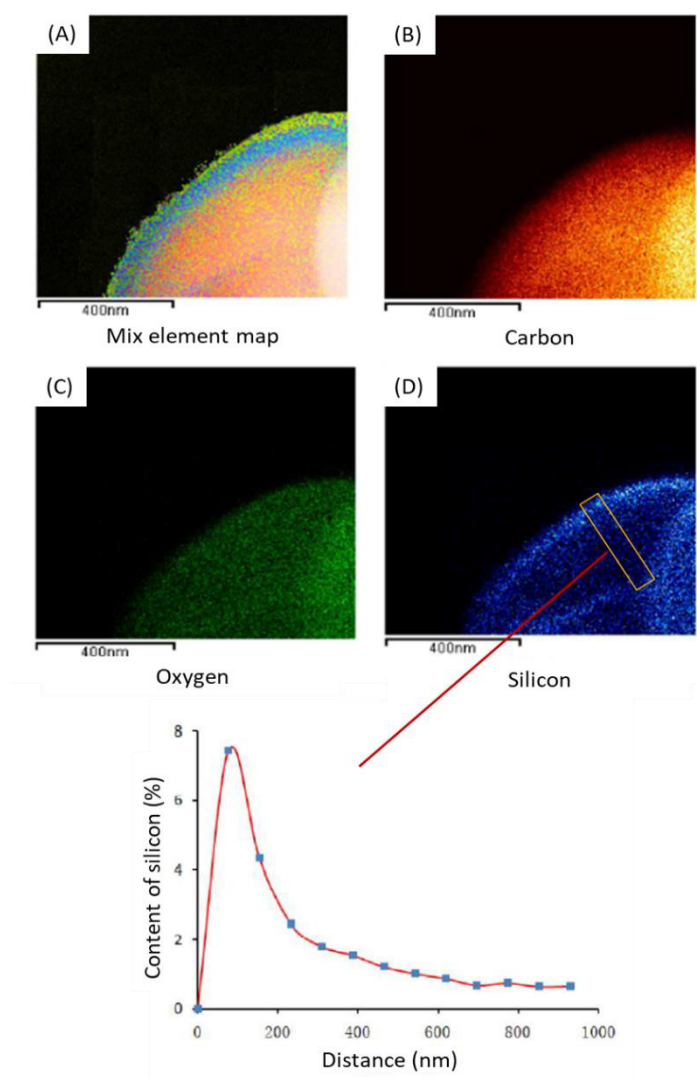


Figure 14 - EDX-TEM element map of a cross section PDMS-*b*-PMMA particle synthesised with PDMS-MPPA. A) Showing mixed elements distribution, B) carbon distribution; C) oxygen distribution and D) silicon distribution, the insert shows the histogram for the cross-sectional silicone map for the area within the yellow box. Figure adapted from Zong's doctoral thesis.⁴⁴

As for the PFOMA-*b*-PMMA particles,²² the absence of internal phase separation was attributed to the enhanced miscibility of PMMA and PDMS blocks in scCO₂, which resulted in a kinetically trapped morphology upon release of the scCO₂. However, it is important to emphasise that PDMS was less miscible with PMMA than PFOMA if we consider the element mapping of the cross-section of the particles (Figure 8 and Figure 14), PDMS was 7 times more likely to be found at the particle corona, while PFOMA was only 3 times more likely to be found at the corona. This makes PDMS-*b*-PMMA more likely to present some internal nanostructures by varying the volume fractions of the blocks, but also potentially to be a good candidate to fulfil the requirements of a proper PISA system.

Therefore, our aim is to set up a PISA system in scCO₂ with PDMS-based macro-CTAs and take a careful look at what should be fulfilled to consider it as a PISA, investigating its RAFT control, particle size, and the wt% of macro-CTA involved. This would allow us to understand the system in a way the literature has not addressed yet. In addition, PDMS-based macro-CTAs may potentially reduce costs for the synthesis of block copolymer particles in scCO₂ and can potentially lead to the first observation of morphology transitions by PISA *via* RAFT in scCO₂ dispersion. Thus in this chapter, I will explore the development of a PDMS-based PISA inspired polymerisation in scCO₂.

3.3. Aims

The aims of this Chapter are as follow:

- To reproduce the results presented by Zong in her thesis using PDMS-DDMAT as macro-CTA for MMA polymerisation.
- To obtain RAFT control over MMA dispersion polymerisation in scCO₂ with PDMS-DDMAT as macro-CTA.
- To obtain self-assemble of PDMS-*b*-PMMA particles in scCO₂.
- To study potential morphology transitions when targeting different DPs of PMMA.

This study is important to advance PISA polymerisation in scCO₂. Changing the fluorinated macro-CTAs for more affordable PDMS based macro-CTAs will make PISA in scCO₂ more viable in industrial scale. Besides that, PDMS is a better choice for medical applications, due to the toxicity of some fluorinated polymers.

3.4. Experimental

3.4.1. Materials

MMA was purchased from ProSciTech (99 %) and was filtered through aluminium oxide to remove the stabiliser prior to polymerisation. 2,2'-azobis(isobutyronitrile) (AIBN) was purchased from Sigma Aldrich UK (98%) and purified by recrystallization in methanol prior to use. All other chemicals were used as received. 2-(dodecylthiocarbonothioylthio)-2-methylpropionic acid (DDMAT) was purchased from Sigma-Aldrich UK. Methacrylate terminated polydimethylsiloxane (PDMS-MA) and monocabrinol terminated polydimethylsiloxane (PDMS-OH) were purchased from ABCR GmbH & Co and Fluorochem, respectively. Dicyclohexylcarbodiimide (DCC) was purchased from MP biomedical, 4-dimethylaminopyridine (DMAP) was purchased from Fluka. Hexane, methanol, dichloromethane (DCM), HPLC grade tetrahydrofuran (THF) and deuterated chloroform (CDCl₃) were all purchased from Fischer Scientific and used as received.

3.4.2. Synthetic procedures

3.4.2.1. Synthesis of PDMS macro-CTAs

The macro-CTAs were prepared *via* Steglich esterification of PDMS-OH, following a similar process to the one reported by Lopez-Oliva *et al.*⁷ In a typical procedure, the CTA (3.0 mmol) carrying a carboxylic acid group was placed in a previously dried 250 mL round-bottom flask and dissolved in DCM (100 mL). PDMS-OH (2.0 mmol), dicyclohexylcarbodiimide (DCC) (6.0 mmol) and 4-dimethylaminopyridine DMAP (0.30 mmol) were then added. The resulting solution was purged with argon for 30 min, sealed, and heated for 24 hours with continuous stirring. After quenching the reaction by exposure to air, the solution was filtered, concentrated under vacuum with the aid of a rotary evaporator, and passed through a silica gel column using DCM as eluent. The resulting clear liquid was washed three times with a 2:1 methanol/DCM mixture, and the organic layer was concentrated under vacuum to produce a clear yellow viscous oil. The synthesis of each macro-CTA was confirmed by ¹H NMR, UV-vis and FT-IR analysis.

¹H NMR (CDCl₃, 300 MHz, δ ppm): 4.25 (m, 2 H), 3.62 (t, 2 H), 3.41 (t, 2 H), 3.26 (t, 2 H), 1.70 (s, 6 H), 1.68 – 1.08 (m, 14 H), 0.88 (m, 6 H), 0.53 (m, 4 H), 0.06 (s, (O-Si(CH₂)-)).

3.4.2.2. Standard dispersion polymerisation with macro-CTA in scCO₂

A typical procedure used an in-house built high-pressure MKIII autoclave (20 mL),⁴⁶ which was degassed by purging with CO₂ at 2 bar for 30 minutes. In a typical polymerisation MMA (33 mmol), AIBN (0.028 mmol) and the macro-CTA (0.055 mmol) were degassed by bubbling with argon for 30 minutes in a vial. The reactants were then added to the autoclave through the keyhole against positive pressure of CO₂. The vessel was then sealed and pressurised to 50 bar, heated to 65 °C, and the pressure topped up to 276 bar. The reaction mixture was stirred at 300 rpm with an overhead magnet coupled stirrer. After 24 hours, the heating was turned off and the reactor was cooled to room temperature before being vented. All products were collected as dry free-flowing powders, unless stated differently. The samples were analysed *via* THF-SEC for M_n and \mathcal{D} , ¹H NMR for conversion and SEM for morphology.

3.4.2.3. Standard dispersion polymerisation in sampling autoclave

A typical procedure used an in-house built high-pressure sampling autoclave consisting of an 60 mL MKIII clamp sealed autoclave⁴⁶ with a cylinder sampling unit as described elsewhere,⁴⁷ which was degassed by purging with CO₂ at 2 bar for 30 minutes. MMA (0.1 mol), AIBN (0.08 mmol) and the macro-CTA (0.17 mmol) were degassed by bubbling with argon for 30 minutes. The reactants were then added to the autoclave through the keyhole against positive pressure of CO₂. The vessel was then sealed and pressurised to 50 bar, heated to 65 °C, and the pressure topped up to 276 bar. The reaction mixture was stirred at 300 rpm with an overhead magnet coupled stirrer. At sampling times, the sampling cylinder was loaded with 5 mL of deuterated chloroform and attached to the autoclave. A fraction of the reaction mixture was sampled into the small pipe space before the cylinder. The sampling caused a small pressure drop; therefore, pressure was topped up with an extra 14 bar prior to sample collection to avoid fluctuations below reaction conditions. The content of the pipe was then sprayed into the cylinder and collected into chloroform. The samples were analysed *via* THF-SEC for M_n and \mathcal{D} , ¹H NMR for conversion and SEM for morphology.

3.4.2.4. Standard solubility test in scCO₂ in variable volume view cell

Solubility test of macro-CTAs was carried out in a stainless-steel variable volume view cell, with a front sapphire window and a back mobile sapphire piston that can be moved by a hydraulic intensifier unit. An accurately weighed amount of macro-CTA (a typical quantity was 0.5 mmol, 5 wt% in relation to CO₂), was added into the chamber and the system was purged

with CO₂ for 30 minutes at room temperature. Then, 33 mmol (15 wt% in relation to CO₂) of MMA were added into the chamber through the keyhole and the system was filled with 20 g of CO₂ using a syringe pump and heated to the desired temperature. At each temperature set point, the pressure was increased until the solute became soluble and only one phase was visible. The pressure was then reduced slowly while monitoring the phase behaviour until the cloud point, *i.e.*, point at which the polymer precipitated and caused turbidity. The process was repeated three times and the final cloud point pressure was an average of these three values at a given temperature.

3.4.2.5. Hexane washes of polymer powders

The polymer powders obtained by dispersion polymerisation in scCO₂ was washed with hexane and homogenised in a vortex mixer prior to centrifuging at 3000 rpm for 5 minutes in order to decant the polymer powder and allow the hexane solution to be removed. The process was repeated three times and the polymer powder dried overnight at 25 °C under vacuum. The powder was analysed by ¹H NMR and THF-SEC. ¹H NMR resonance integrals of PDMS and PMMA repeating units was compared before and after washes. The percentage of PDMS retained after wash was calculated considering the integral of the PDMS resonance before washing to be 100%.

3.4.3. Polymer characterisation

3.4.3.1. Size exclusion chromatography (SEC)

The M_n and \bar{D} of polymers were obtained by SEC (PL-120, Polymer Labs) using a refractive index (RI) detector. The columns (30 cm PLgel Mixed-C, two in series) were eluted by THF and calibrated with PMMA standards. Calibration and analyses were performed at 40 °C with a flow rate of 1 mL min⁻¹. The device is equipped with multiple angle light scattering (MALS), refractive index (RI) and UV detectors.

3.4.3.2. Proton nuclear magnetic resonance (¹H NMR)

Product and reactant synthesis and monomer conversion was determined by ¹H NMR. The spectra were recorded in CDCl₃ using a Bruker DPX 400 MHz spectrometer, and referenced to CDCl₃ at 7.26 ppm.

3.4.3.3. Fourier-transform infrared spectroscopy (FT-IR)

IR spectra were recorded with an Attenuated Total Reflection Cary 630 FT-IR spectrophotometer (Agilent Technologies, Santa Clara, CA). 32 interferograms were recorded for each spectrum, with a resolution of 4 cm^{-1} , in the range $4000\text{--}650\text{ cm}^{-1}$. IR spectra were analysed by SpectraGryph1.2 software.

3.4.3.4. Ultraviolet–visible spectrophotometry (UV-vis)

Spectra were recorded with an Epoch 2 UV-vis multi microplate reader from Agilent. Samples were measured against DCM blanks in sealed cuvettes, and polymer functionalisation with the CTA was calculated using a calibration curve (absorbance versus concentration plot) constructed with the CTA in DCM.

3.4.3.5. Scanning electron microscopy (SEM)

Images of the particles were obtained using a JEOL 6060V SEM machine at various magnifications and an accelerating voltage of 10 kV. Samples were mounted on aluminium stubs using adhesive carbon tabs and sputter-coated with platinum before analysis. Mean particle diameter (D_n) was determined by measuring the diameter of 100 particles in ImageJ® and taking a mean of these data. The coefficient of variance (C_v) was calculated by the ratio of the standard deviation (σ) by the mean particle diameter as by Equation (2).

$$C_v = \sigma/D_n \times 100 \quad (2)$$

3.5. Results and discussion

3.5.1. PDMS -DDMAT synthesis

PDMS is a highly hydrophobic polymer with a low T_g that arises from the free rotation of its Si-O bonds, which also provide high solubility in $sc\text{CO}_2$.¹⁹ The standard method to prepare PDMS-containing block copolymers has been through sequential anionic polymerization where the non-PDMS block is polymerized first, followed by the PDMS block through the ring-opening polymerization of a cyclic siloxane.^{48, 49} However, this in tandem method is not compatible with a wide range of monomers. To overcome this issue and increase the library of PDMS block copolymers, end group functionalisation of PDMS for RDRP was investigated.⁴⁸

Stenzel and co-workers first introduced a PDMS macro-CTA for RAFT polymerisation in 2004.⁵⁰ Dihydroxy terminated PDMS was linked to an acid terminated CTA *via* esterification in the presence of DCC to produce a bi-functional PDMS macro-CTA and prepare triblock

copolymers. Pavlovic *et al.* used an almost identical approach for the synthesis of triblock copolymers based on PDMS.⁵¹ This time the carboxylic acid of the CTA was chlorinated prior to esterification with dihydroxy terminated PDMS in the presence of trimethylamine as base. A further strategy for the synthesis of CTAs is *via* brominating hydroxyl terminated PDMS prior to the linkage to a carboxylic acid containing xanthate in order to form diblock or triblock copolymers.^{52, 53}

Wadley *et al.* reported on the synthesis of PDMS-*b*-PSt *via* RAFT, using a macro-CTA formed by the DCC/DMAP catalysed esterification (Steglich esterification) of PDMS-OH with a CTA containing a carboxylic acid.⁴⁸ This same method was more recently used for the synthesis of PDMS-*b*-PBzMA.⁷ In this thesis, we used PDMS-OH of different molecular weights (≈ 5 and 10 kg mol^{-1}) to synthesise macro-CTAs *via* Steglich esterification with carboxylic acid terminated CTAs (Figure 15).

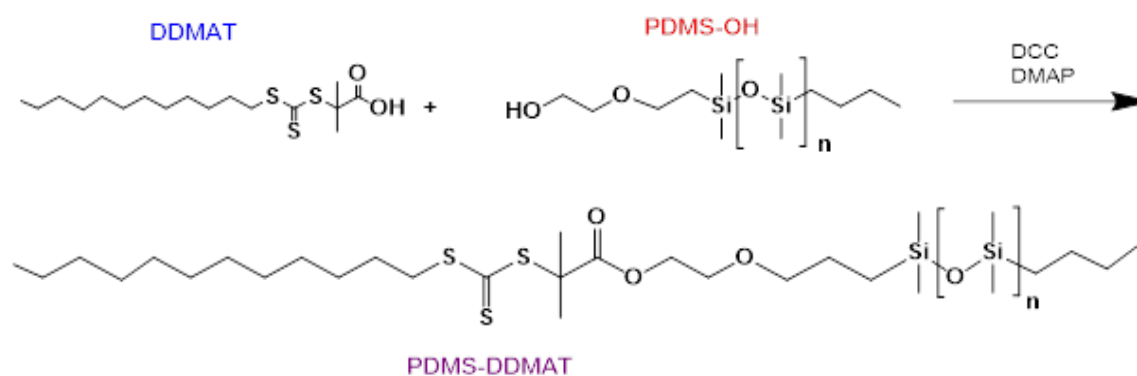


Figure 15 - Schematic of PDMS-DDMAT synthesis via Steglich esterification of PDMS-OH with DDMAT.

DDMAT (2-(dodecylthiocarbonothioylthio)-2-methylpropionic acid) was selected as the CTA to be coupled to PDMS-OH based on the previous results with PDMS₁₂₈-DDMAT for polymerisation of MMA in *scCO*₂.⁴⁴ This is however an unlikely choice for MMA polymerisation. DDMAT has a tertiary alkyl -R reinitiating group, which is known to not be applicable for methacrylates.⁵⁴ Besides that, the long thioalkyl -Z group is a very bulky stabilising group and normally a shorter -Z group or a better stabilizing group, such as a benzyl group, would be preferred.⁵⁵ However, the simple synthesis and purification of DDMAT (as it gives solid crystals) makes it a cheap commercially available CTA choice.

In addition to Zong's report with PDMS₁₂₈-DDMAT in *scCO*₂,⁴⁴ a series of block copolymers have been produced in *scCO*₂ using DDMAT as CTA for MMA polymerisation.^{56, 57} Therefore,

there was enough evidence for the use of this DDMAT in scCO₂, and it was selected for the present study.

Normally, commercial PDMS is characterised by its viscosity rather than the molecular weight. The molecular weight and DP of the PDMS-OH starting materials were thus calculated by ¹H NMR using Equation (3).

$$DP = \frac{a_x m_y n_y}{a_y m_x} \quad (3)$$

Where x denotes moieties from the backbone of PDMS and y, moieties from the monocarbinol termination. a_x is the integral of the ¹H NMR resonance for moiety x, *e.g.*, the repeating unit (-O-Si(CH₃)₂-) (6 - Figure 16). m_x is the number of protons from moiety x, *e.g.*, six protons for (-O-Si(CH₃)₂-) (6 - Figure 16). a_y is the integral of the ¹H NMR resonance for moiety y, *e.g.*, the methylene groups of the monocarbinol termination (1, 2 and 3 - Figure 16). n_y is the number of repeating units of moiety y, *e.g.*, one for the methylene groups of the OH functionalisation moiety, and m_y is the number of protons of moiety y, *e.g.*, two protons for the methylene groups (1, 2 and 3 - Figure 16).

PDMS-OH of two different molecular weights were used throughout this thesis and they had their average DP and molecular weight calculated to be as follows: (1) PDMS-OH (250 cSt), DP = 128 and M_n = 9.75 kg mol⁻¹; (2) PDMS-OH (120 cSt), DP = 65 and M_n = 4.99 kg mol⁻¹ (Table 1).

Table 1 – Monocarbinol terminated PDMS DP and molecular weights.

Expected M _n (kg mol ⁻¹)	PDMS Viscosity (cSt)	average DP ¹	M _n (kg mol ⁻¹) ²
10	250	128	9.75
5	120	65	4.99

¹ Average DP calculated from ¹H NMR spectra with equation (3), considering the resonances 1, 2 and 3 for moiety y and resonances 6, 10 and (5,7) for moiety x; ² Calculated using the DP obtained for each ¹H NMR spectrum.

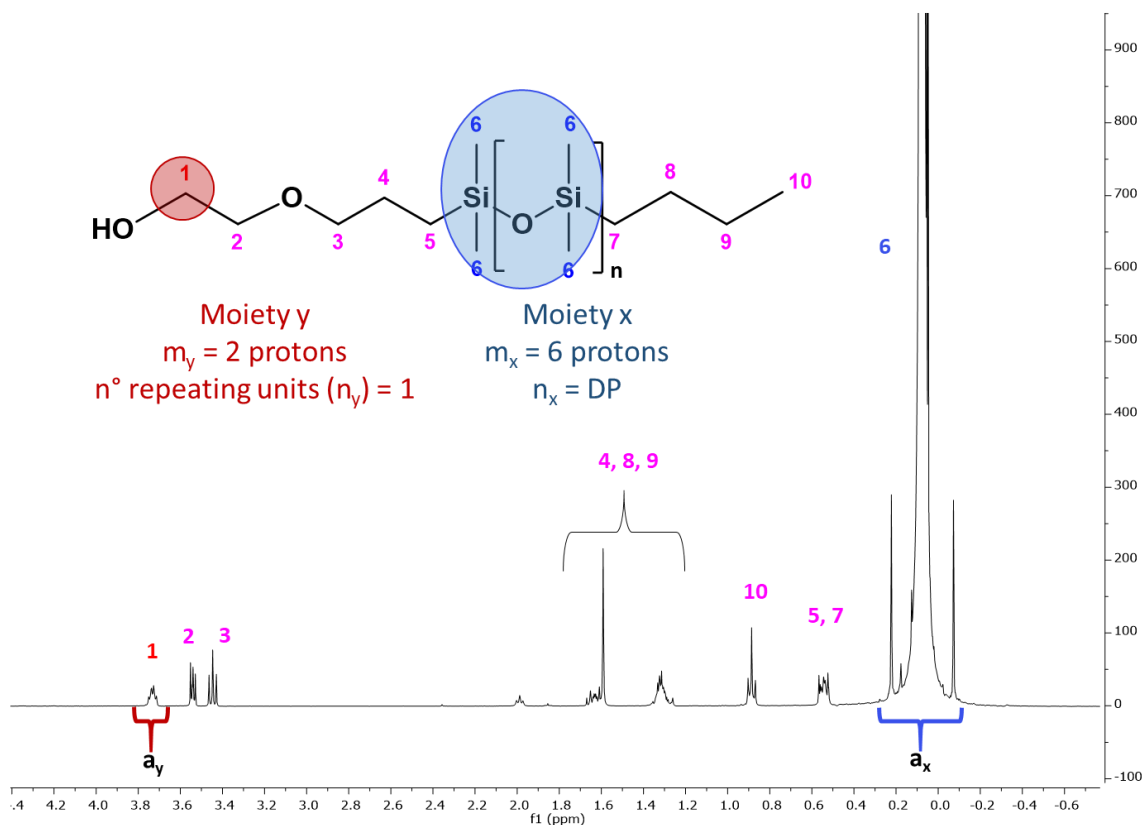


Figure 16 Example of DP calculation for PDMS-OH by ^1H NMR as described by Equation (3).

The purchased PDMS-OH units were then coupled to DDMAT by Steglich esterification to prepare macro-CTAs of well-defined molecular weights. Macro-CTA successful synthesis was confirmed by FT-IR (Figure 17). The IR spectra of the macro-CTAs showed the ester bond formation as observed by the appearance of the C=O stretching at 1740 cm^{-1} , which was not previously present in the spectrum for PDMS-OH. The typical absorption band at $1008 - 997\text{ cm}^{-1}$ for the stretching vibration of the Si–O bonds, the C–H methyl stretching at 2965 cm^{-1} and the silicon–methyl bond at 1260 cm^{-1} (bending) and at 790 cm^{-1} (CH_3 rocking and Si–C stretching in Si– CH_3) are assigned to the PDMS backbone.^{58, 59} In addition as expected, the C=O/Si– CH_3 intensity ratio, across the samples, increases with the decrease of PDMS molecular weight.

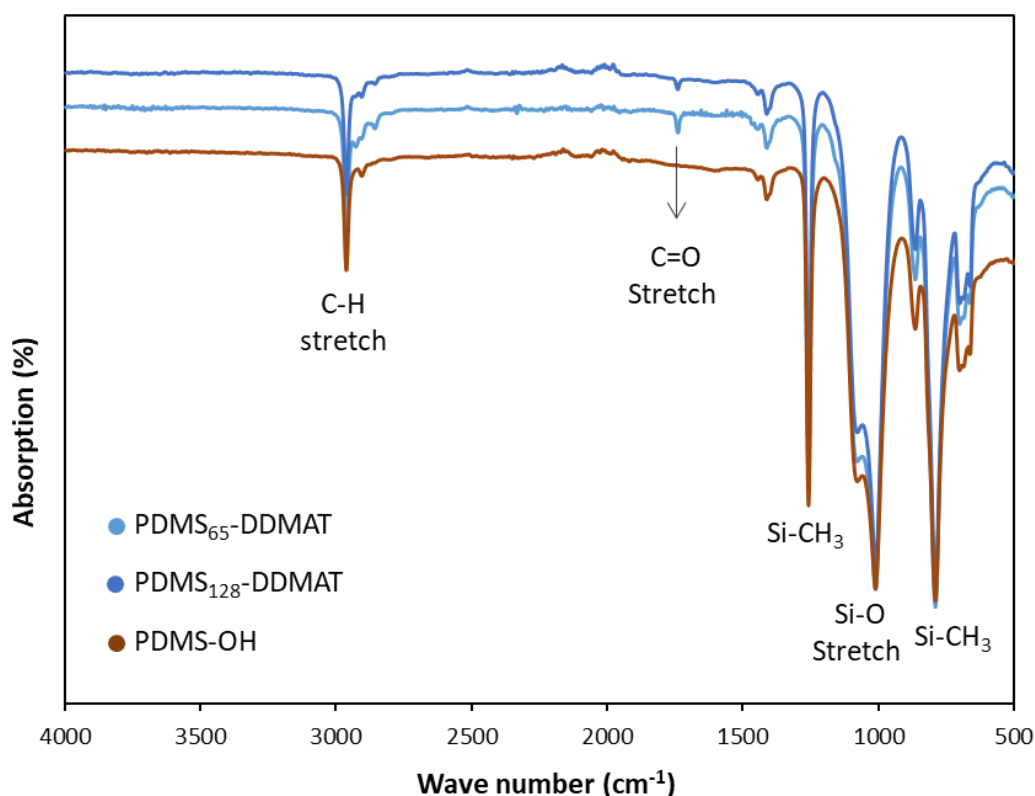


Figure 17 - FT-IR spectra of PDMS-OH (brown) and PDMS-DDMAT macro-CTAs (shades of blue). The carbonyl stretching ($C=O$, 1740 cm^{-1}) from the ester formed upon the PDMS and DDMAT coupling is seen for the macro-CTAs. The intensity of the $C=O$ stretching increases with the decrease of the PDMS DP.

The macro-CTA was also analysed by ^1H NMR (Figure 18). It was possible to assign the macro-CTA ^1H NMR spectrum by comparison to those of DDMAT and the PDMS-OH precursor. With the ester formation, the different chemical environment of proton g in PDMS-OH (Figure 18B) causes a shift to higher ppm and results in resonance q^* (Figure 18C). The functionalisation of PDMS-OH was quantitative, as the PDMS-OH resonances (g, h, i) are not present in the ^1H NMR of the macro-CTA (Figure 18C).

The degree of end group functionalisation with CTA was calculated by comparing the integral of the backbone dimethyl protons l and protons p, m and k with the protons associated to the ester bond formation, q^* , h' and i' in the 3-4 ppm region (Figure 18). The mean degree of esterification was calculated to be 96% for PDMS₁₂₈-DDMAT and 95% for PDMS₆₅-DDMAT (Table 2).

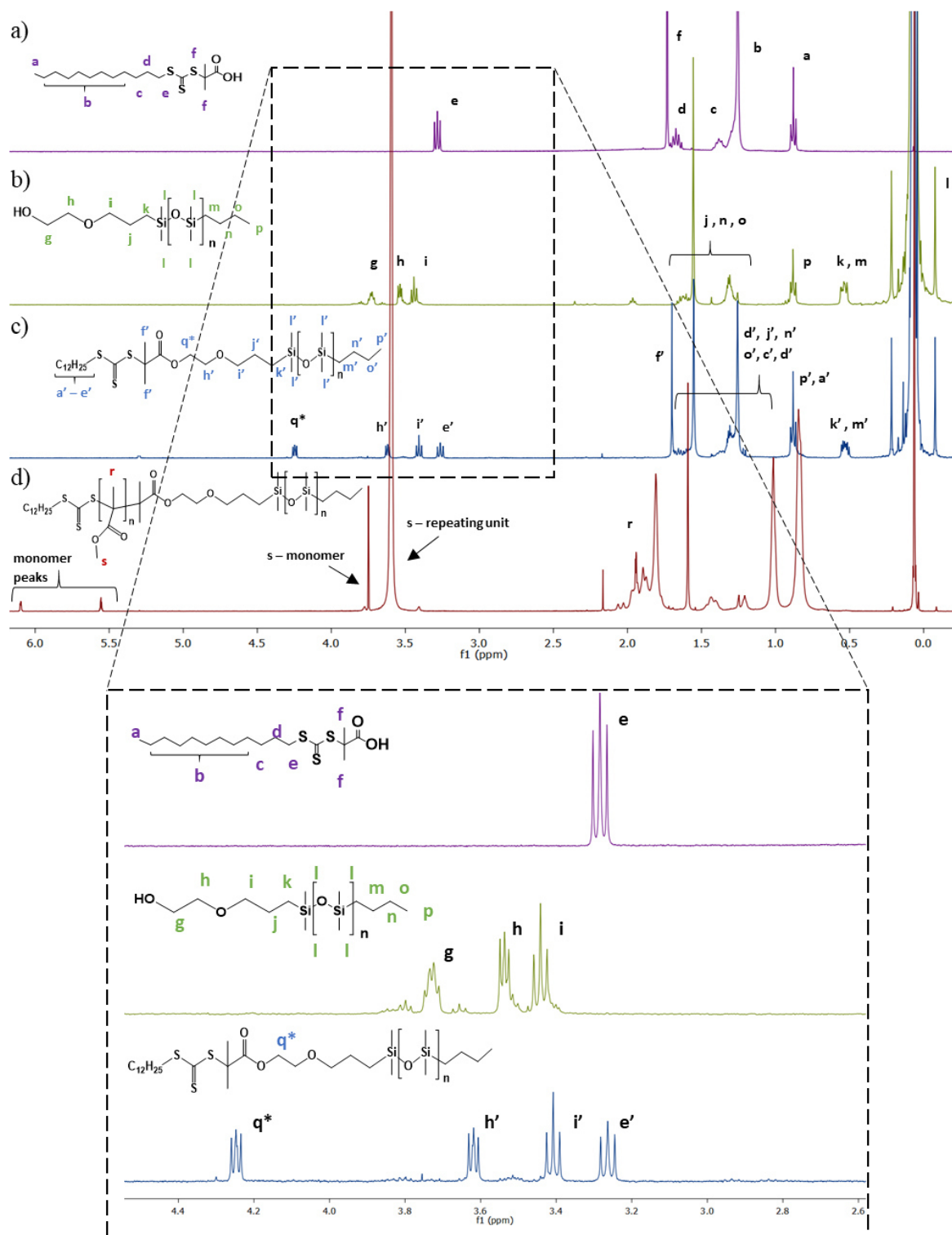


Figure 18 – ^1H NMR spectra in CDCl_3 of a) DDMAT b) PDMS₁₂₈-OH c) PDMS₁₂₈-DDMAT d) PDMS-b-PMMA, produced by chain extension of PDMS₁₂₈-DDMAT in scCO_2 with MMA at $60 \text{ kg}\cdot\text{mol}^{-1}$ PMMA target (AIBN (0.028 mmol), PDMS-DDMAT (0.055mmol) MMA (0.33mmol), at 65°C and 276 bar) and collected as a powder by venting the CO_2 after 24h reaction without any further purification.

The high degree of end group functionalisation with DDMAT was also confirmed by UV absorption spectroscopy. The molecular CTA resembles the macro-CTA end group, giving a similar UV absorption, which allows reliable end group analysis (Figure 19A).

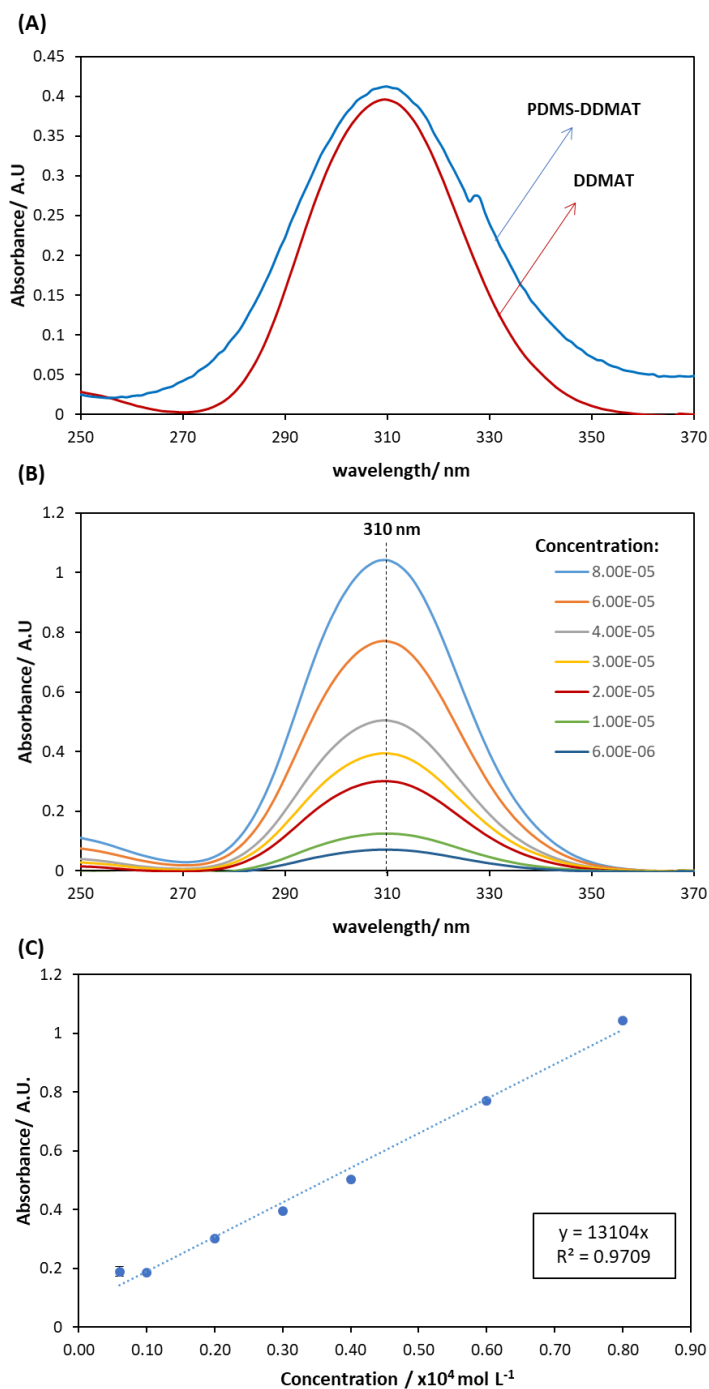


Figure 19 – UV-vis analysis of macro-CTA. Showing the absorption wavelengths of DDMAT versus PDMS-DDMAT (A), the absorbance for each sample at different DDMAT concentration, with a maximum absorbance at 310 nm (B) and the maximum absorbance versus conversion plot (C).

An absorbance versus concentration plot was constructed using DDMAT solutions of known concentrations in dichloromethane, ranging from 10^{-4} to 10^{-6} mol L⁻¹ (Figure 19B and C). A mean extinction coefficient (ϵ) of 13104 L mol⁻¹ cm⁻¹ was calculated for the absorption maximum at 310 nm. The UV absorbance at 310 nm for each macro-CTA was measured for solutions in DCM of known concentrations. Then, the end group functionalisation was calculated using the calibration curve of CTA absorbance versus concentration (Figure 19C) and the Beer–Lambert equation (4), where A is absorbance, c is the concentration of end groups, ϵ is the extinction coefficient and l is the path length of the UV cell, which is a fixed value for all samples measured.

$$A = \epsilon cl \quad (4)$$

It was possible to calculate the functionalisation degree of the macro-CTAs using equation (4) together with the absorbance recorded for the macro-CTAs in DCM at known concentrations. Functionalisation was found to be 97.2% for PDMS₁₂₈-DDMAT and 98.0% for PDMS₆₅-DDMAT. Within experimental error, these data are consistent with the esterification degrees calculated from ¹H NMR (Table 2).

Table 2 – Characterisation of PDMS-DDMAT macro-CTAs.

Sample	Expected M_n ¹	Esterification degree ² (%)	Exp. cte ³ .	Real cte ⁴ .	Functionalisation degree ⁵ (%)
PDMS ₁₂₈ -DDMAT	10.11	96.1	$2.08 \cdot 10^{-5}$	$2.14 \cdot 10^{-5}$	97.2
PDMS ₆₅ -DDMAT	5.36	95.4	$4.74 \cdot 10^{-5}$	$4.84 \cdot 10^{-5}$	98.0

¹ M_n given in kg mol⁻¹ and calculated based PDMS-OH DP obtained by ¹H NMR added of the CTA molecular weight (0.365 kg mol⁻¹). ² Calculated from ¹H NMR spectra; by comparing the integral of the PDMS backbone protons with the protons associated with the ester bond formation. ³ Experimental concentration obtained from equation (4) and UV absorption of macro-CTA solutions in DCM and given in mol L⁻¹. ⁴ Real concentration of macro-CTA solutions in DCM given in mol L⁻¹. ⁵ Functionalisation of macro-CTA given by UV absorption and calculated by the percent ratio of expected concentration by real concentration.

3.5.2. Solubility of PDMS-DDMAT macro-CTAs in scCO₂

The stabiliser is known to play a key role in dispersion polymerisation.⁶⁰ In a PISA system, the macro-CTA is expected to stabilise by the *in situ* formation of an amphiphilic block copolymer, while controlling the molecular weight and molecular weight dispersity.¹⁵ Therefore, the macro-CTA must be highly soluble in scCO₂, in order to produce a self-stabilised block copolymer particles.

Phase behaviour of the PDMS-DDMAT was investigated by cloud point measurements in a variable volume view cell (Figure 20). The cloud point is the pressure, at a specific temperature, when the solute precipitates out of the continuous phase, causing turbidity. For most solutes, it increases as the temperature increases, which is an effect of the density

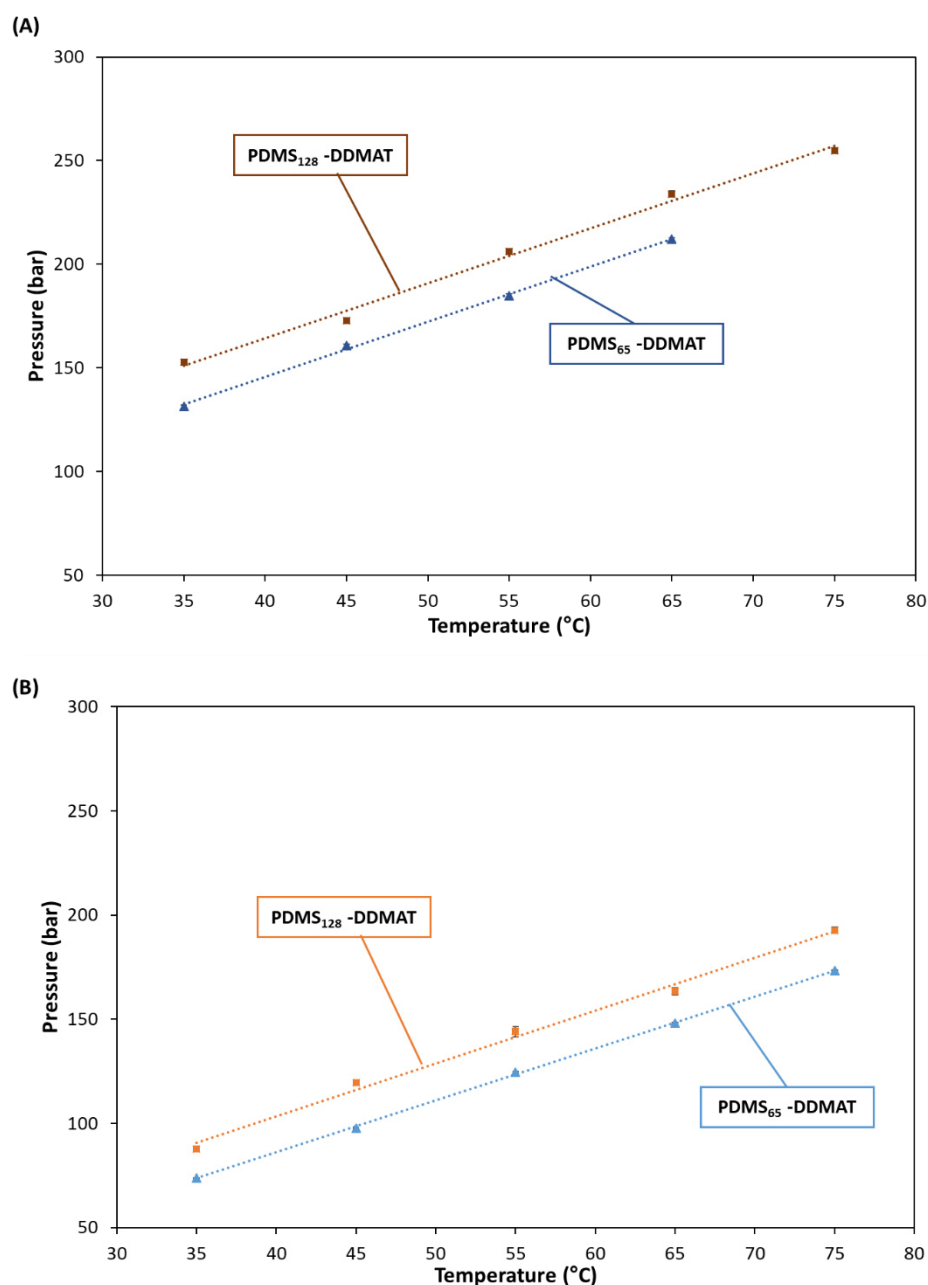


Figure 20 – Cloud point study of PDMS-DDMAT macro-CTAs of different molecular weights, measured (A) without MMA and (B) with MMA as co-solvent. More pressure was required to solubilise the macro-CTAs without the monomer (co-solvent). The cloud point increased with the PDMS molecular weight. decrease of CO₂.⁴³ The cloud points were measured with 5 wt% of the macro-CTA relative to scCO₂, in the presence and absence of MMA.

Indeed, the monomer can act as a co-solvent improving solubility of species, as can be noticed by the decrease in cloud point in the presence of MMA (Figure 20B) compared to its absence (Figure 20A). The measurements with MMA provided an identical chemical environment as would be found at the start of the polymerisation reactions, with MMA added to scCO₂ at the same ratio. Both PDMS-DDMAT macro-CTAs were soluble in scCO₂, with and without MMA, under autoclave standard polymerisation conditions of 65 °C and 276 bar (Table 3). It is important to notice that the cloud point increases with the increase in the PDMS molecular weight of the macro-CTA.

Table 3 – Cloud point study of PDMS-DDMAT.

Sample	Cloud point without MMA (bar) ¹	Cloud point with MMA (bar) ²
PDMS ₁₂₈ -DDMAT	234.0 (±1.4)	163.2 (±1.7)
PDMS ₆₅ -DDMAT	212.0 (±0.7)	148.0 (±0.5)

¹ Cloud point measured in variable volume view cell with 5 wt% macro-CTA in relation to CO₂. ² Cloud point measure in variable volume view cell with 5 wt% macro-CTA and 15 wt% MMA in relation to CO₂. All results given as an average of three measurements at 65°C, with standard deviation given in brackets. All results were converted from psi (equipment unit) to bar, 1 psi = 0.069 bar.

For comparison, PDMS-MA (250 cSt, ≈ 10 kg mol⁻¹), which is a common stabiliser for dispersion polymerisation in scCO₂,^{39, 40, 42} has a cloud point of 220.6 bar at 65 °C in the absence of MMA.⁴⁴ Under the same conditions, PDMS₁₂₈-DDMAT (10.11 kg mol⁻¹) has a cloud point of 234.0 bar. Therefore, PDMS₁₂₈-DDMAT is only slightly less soluble than the stabiliser PDMS-MA of similar molecular weight.

Knowing that these non-fluorinated macro-CTAs are soluble in scCO₂, they are likely to act as good stabilising blocks for PISA. Therefore, the macro-CTAs were then tested for the polymerisation of MMA, in the hope of achieving successful PISA in scCO₂ with PDMS-based macro-CTAs.

3.5.3. PDMS-DDMAT application for polymerisation of MMA in scCO₂

In this section, the synthesised PDMS-DDMAT macro-CTAs (Figure 21) were used in a PISA inspired polymerisation of MMA to form self-stabilised PDMS-*b*-PMMA particles, where the macro-CTA is expected to provide both stabilisation and RAFT control. A series of different molecular weights of the CO₂-phobic block (PMMA) were targeted, while keeping the same CO₂-philic block sizes of DP 128 and 65. When increasing PMMA molecular weight,

morphology change should occur, with precipitation of the PMMA block inducing firstly the formation of spherical particles.

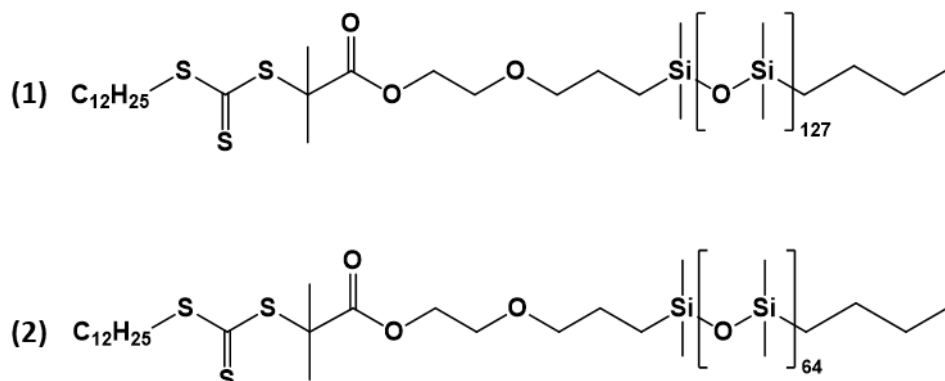


Figure 21 – Structures of PDMS-DDMAT macro-CTAs, (1) PDMS₁₂₈-DDMAT and (2) PDMS₆₅-DDMAT.

3.5.3.1. Control in the absence of the CTA chain-end

As seen in Section 3.5.1., PDMS-OH functionalisation with DDMAT was not 100%. Meaning that some PDMS-OH would be present. In order to investigate the effect upon stabilisation of the absence of the DDMAT at the end of PDMS, RAFT controlled dispersion polymerisations in scCO₂ of MMA with either no stabiliser, PDMS₁₂₈-OH (250 cSt, 10.11 kg mol⁻¹) or PDMS-MA (cSt 250, ≈ 10 kg mol⁻¹) as stabiliser (Table 4) at 5 wt % in relation to the monomer. This series of reactions used DDMAT as CTA and had a PMMA molecular weight target ($M_{n,tgt}$) of 60 kg mol⁻¹.

Table 4 – Comparison of PDMS-OH and PDMS-MA as stabilisers ($M_n \approx 10$ kg mol⁻¹) for MMA RAFT polymerisation in scCO₂ with DDMAT as CTA.

Expt.	Stabiliser ¹	Conv ² (%)	$M_{n,th}$ ³	M_n ⁴	\bar{D} ⁴	Appearance
A	PDMS-MA	98	57.6	65.0	1.33	Powder
B	PDMS-OH	46	24.1	18.7	1.28	Liquid
C	None	24	14.7	16.8	1.29	Liquid

¹ Both stabilisers had 250 cSt viscosity and a similar molecular weight (10 kg mol⁻¹) and were used at 5 wt% relative to MMA. ² Conversion calculated from ¹H NMR. ³ Theoretical M_n calculated relative to DDMAT and monomer concentration, and given in kg mol⁻¹. ⁴ \bar{D} and M_n (in kg mol⁻¹) obtained by THF-SEC with RI detector against PMMA standards. All reactions were performed at 2:1 CTA: AIBN ratio, 65 °C and 276 bar for 24 hours. See section 3.4.2.3. scCO₂ dispersion polymerisation reaction procedure.

A free-flowing powder was obtained at high conversion (98%) with PDMS-MA, with a final $M_n = 65.0 \text{ kg mol}^{-1}$ and particles with $D_n = 1.90 \mu\text{m}$ and $C_v = 21.07\%$ (experiment A - Table 4, Figure 22). On the other hand, results obtained with PDMS₁₂₈-OH were similar to those in the absence of any stabiliser (experiments B and C – Table 4, Figure 22), with a viscous liquid as final product.

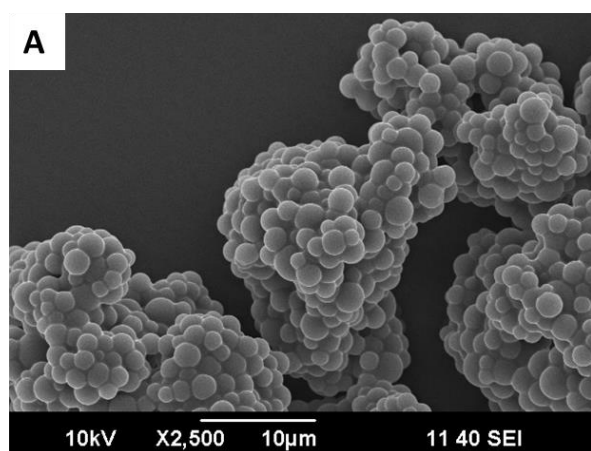
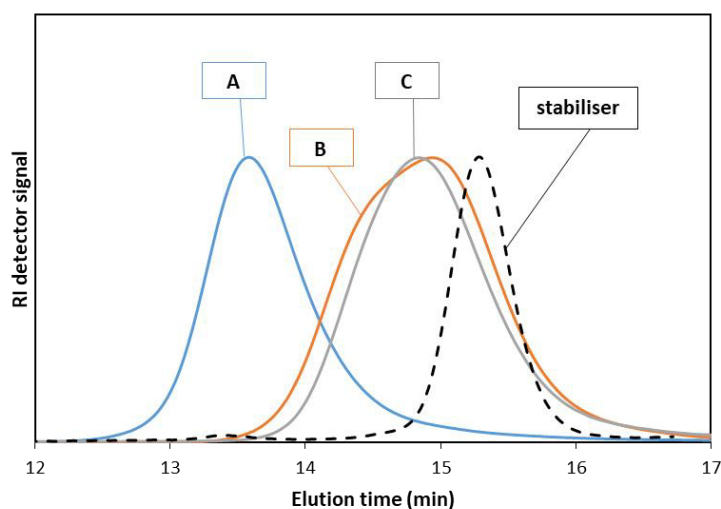


Figure 22 – THF-SEC data for MMA RAFT polymerisation with DDMAT as CTA and 5 wt% PDMS-MA as stabiliser (A), 5 wt% PDMS-OH as stabiliser (B) and without stabiliser (C). The THF-SEC trace for the stabiliser (PDMS-MA/PDMS-OH) is presented for comparison. SEM picture of spherical particles, $D_n = 1.90 \mu\text{m}$ and $C_v = 21.07\%$, produced in reaction A.

Without any stabiliser present, the polymer precipitates out of the continuous phase once it reaches the critical length, and polymer growth is then negatively impacted, giving low M_n and low conversion.²⁴ A suitable stabiliser must produce a stable dispersed phase during the reaction and lead to the formation of well-defined spherical particles. Neither of those

requirements were fulfilled with PDMS₁₂₈-OH, although it was confirmed to be soluble in scCO₂ under reaction conditions, with an average cloud point of 174.0 bar at 66 °C. This indicates that the monocarbinol termination does not provide a good anchoring group for stabilisation of PMMA particles.

Our results agreed with previous studies on anchoring group effectiveness for MMA polymerisation in scCO₂. A screening of perfluoropolyether (PFPE)-based stabilisers with acetate, methacrylate and alcohol anchoring groups showed that PFPE-alcohol was less effective than the other two stabilisers, as result of insufficient anchoring to the particles.³² In a similar way, DeSimone and co-workers reported that, differently from PDMS-MA, PDMS homopolymers, *i.e.*, without the methacrylic reactive group, were unsuccessful as stabilisers for PMMA, due to the absence of an anchoring group.³⁶ Therefore, we confirm that residual PDMS-OH cannot act as stabiliser, and stabilisation of the block copolymer in the next experiments must arise only from PDMS-DDMAT.

3.5.3.2. MMA polymerisation with PDMS₁₂₈-DDMAT

As discussed in the introduction (Section 3.2.2.2.), a previous thesis project in the Howdle research group investigated PDMS₁₂₈-DDMAT for MMA polymerisation in scCO₂.⁴⁴ In that work, they successfully obtained well-defined polymeric particles with well-controlled molecular weight ($M_n = 74.2 \text{ kg mol}^{-1}$, $M_{n,th} = 69.5 \text{ kg mol}^{-1}$) and low dispersity ($\mathcal{D} = 1.38$), with 2:1 macro-CTA:initiator ratio, at 276 bar and 65 °C.⁴⁴ It is important to notice that a 2:1 CTA:initiator ratio is used in scCO₂ because of the slower rate of decomposition of AIBN in scCO₂ compared to in benzene.⁶¹ This higher initiator ratio in scCO₂ than in conventional solvents is well established in the literature.^{24, 39, 56}

We thus first focused on this same macro-CTA and reaction conditions used by Zong,⁴⁴ while targeting a series of PMMA DPs in order to investigate the control over molecular weight and molecular weight distribution. The same CTA:initiator ratio of 2:1 and the same load of MMA was maintained for each reaction. A further aim was to identify possible particle morphology changes. According to reports of the PISA process in non-polar organic solvents, it may be expected to see a morphology transition from sphere-to-worm-to-vesicle as the DP of the solvophobic block increases, *i.e.*, PMMA in this case.^{7, 18}

Although high conversion and a free-flowing powder were obtained for all MMA polymerisations in the presence of PDMS₁₂₈-DDMAT, except for E1.5, results showed no optimal RAFT control over MMA polymerisation. In fact, molecular weights were far above the target and $\mathcal{D} > 1.8$ (Table 5). For example, when the block copolymer $M_{n,th} = 68.2 \text{ kg mol}^{-1}$, E1.3, a $M_n = 92.4 \text{ kg mol}^{-1}$ and $\mathcal{D} = 1.81$ was obtained. This is the same $M_{n,tgt}$ (70 kg mol^{-1}) as in the previous thesis project with PDMS₁₂₈-DDMAT, but they observed a more controlled reaction, with a $M_n = 74.2 \text{ kg mol}^{-1}$ and $\mathcal{D} = 1.38$.⁴⁴

Table 5 – MMA dispersion polymerisation in scCO₂ carried out in the presence of PDMS₁₂₈-DDMAT.

Expt.	PMMA $M_{n,th}$ ¹	block copolymer $M_{n,th}$ ²	PDMS wt% ³	Conv. ⁴ (%)	M_n ⁵	\mathcal{D} ⁵	Product	Morphology ⁶ (D_n / C_v)
E1.1	110.2	120.3	9.2	98	145.4	2.18	Powder	Spherical particles (0.82 μm / 22.5%)
E1.2	83.0	93.1	11.5	92	124.2	2.21	Powder	Spherical particles (1.05 μm / 12.6%)
E1.3	58.1	68.2	17.2	96	92.4	1.81	Powder	Particles and Agglomerates
E1.4	47.4	57.5	20.7	94	88.8	2.35	Powder	Agglomerates
E1.5	28.3	38.4	34.4	93	65.5	2.23	Lumps + solid	-

¹Theoretical M_n for MMA calculated relative to macro-CTA and monomer concentration and given in kg mol^{-1} .
²Theoretical M_n of the block copolymer = $M_{n,th}$ of PMMA + M_n of macro-CTA ($10.11 \text{ kg mol}^{-1}$), where $M_{n,th}$ of PMMA was calculated relative to macro-CTA and monomer concentration, given in kg mol^{-1} . The M_n of macro-CTA = M_n of PDMS-OH (9.75 kg mol^{-1}) + DDMAT molecular weight ($0.365 \text{ kg mol}^{-1}$).
³The weight percentage of PDMS in the reaction medium was calculated with respect to MMA.
⁴Conversion was calculated from ¹H NMR.
⁵ \mathcal{D} and M_n were obtained by THF-SEC with RI detector against PMMA standards.
⁶Overall morphology as determined by SEM, and where applicable D_n was calculated as an average of 100 particles measurements *via* Image J[®] and C_v was calculated by equation (2). E1.5 was not analysed by SEM as it was not a powder.

The THF-SEC traces for all reactions with PDMS₁₂₈-DDMAT showed broad unimodal distributions with a tail towards lower molecular weights (Figure 23). Although unfunctionalised PDMS is known to be iso-refractive to THF, its functionalisation allows a trace to be seen in the THF-SEC RI detector and thus it was plotted for comparison. The presence of unreacted residual PDMS₁₂₈-DDMAT was confirmed, as the RI traces overlap with the trace of the macro-CTA and the UV detector showed a signal at low molecular weight, which aligns with PDMS₁₂₈-DDMAT trace (Figure 23). All RI traces for E1.1-E1.5 can be seen plotted together in the appendix (Figure S1). Therefore, THF-SEC analysis shows that not all PDMS₁₂₈-DDMAT chains have grown equally and some of the macro-CTA was left unreacted.

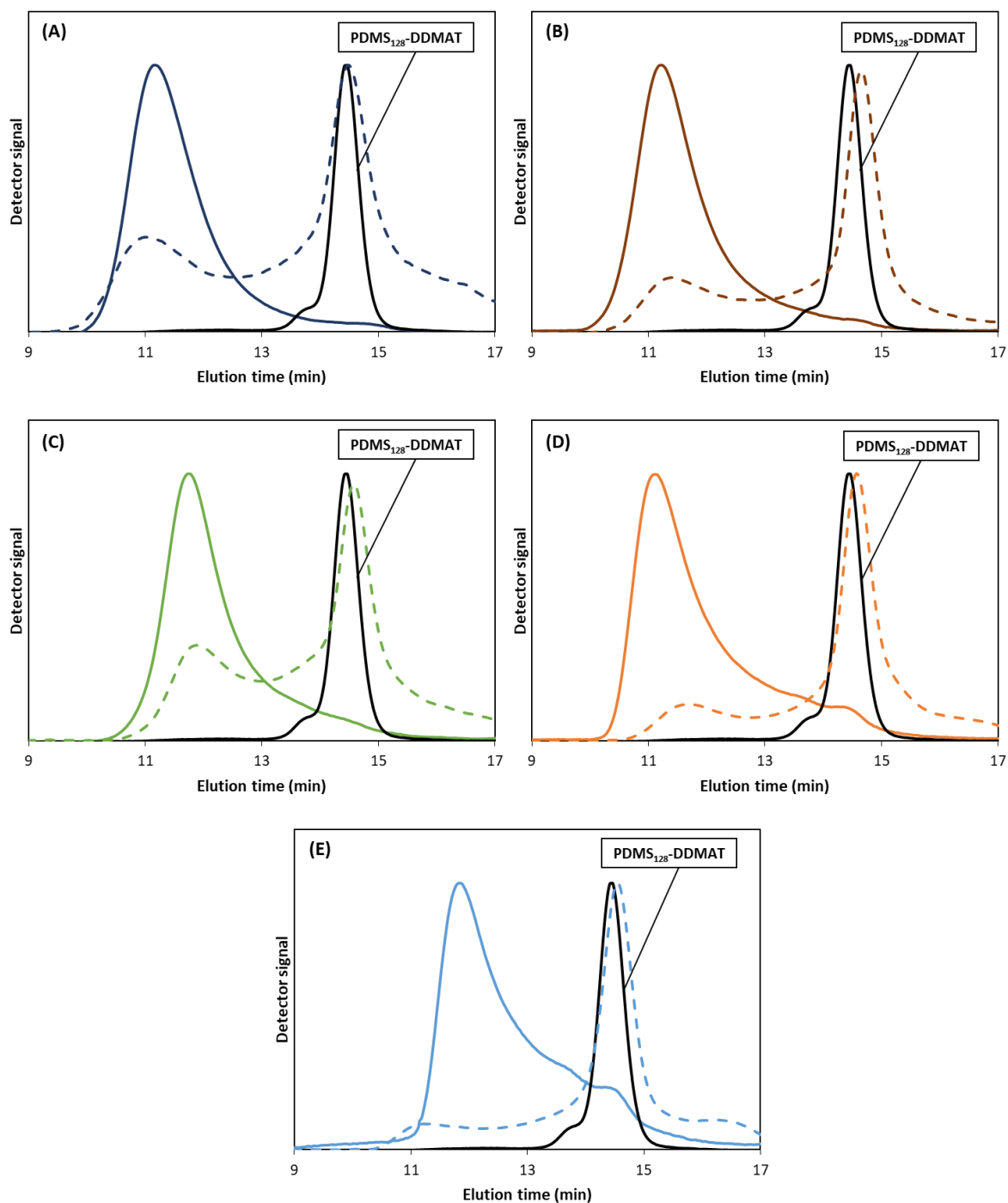


Figure 23 – THF-SEC study of MMA dispersion polymerisation in $scCO_2$ with $PDMS_{128}$ -DDMAT, showing normalised traces for the RI detector (solid line) and for the UV detector (dashed line) for experiments: (A) E1.1, (B) E1.2, (C) E1.3, (D) E1.4 and (E) E1.5. The shoulder presented for $PDMS_{128}$ -DDMAT is consistent with the starting material ($PDMS-OH$) and therefore was considered as an impurity.

In addition, the UV detector indicates the presence of CTA end-groups for the higher molecular weight traces, and thus it did not grow *via* conventional radical polymerisation. These results, and the fact that the macro-CTA purity is not 100%, explains why the high molecular weights were obtained compared to the $M_{n,th}$.

In agreement with Xu *et al.* study,²⁵ the two reactions targeting higher PMMA molecular weights, E1.1 and E1.2, produced well-defined spherical particles (Figure 24), although with particle diameters of 0.82 μm ($C_v = 22.5\%$) and 1.05 μm ($C_v = 12.6\%$), respectively. The expected approximate diameter for self-assembly, considering C-C bond-length of 1.54 \AA , are 345 nm for E1.1 and 277 nm for E1.2, considering 2 x the length of the block. We can rationalise the observed large particle size with the presence of unreacted PDMS₁₂₈-DDMAT in the THF-SEC analysis. Smaller particle size would be expected for a well-controlled PISA reaction where all macro-CTA chain extends with PMMA.

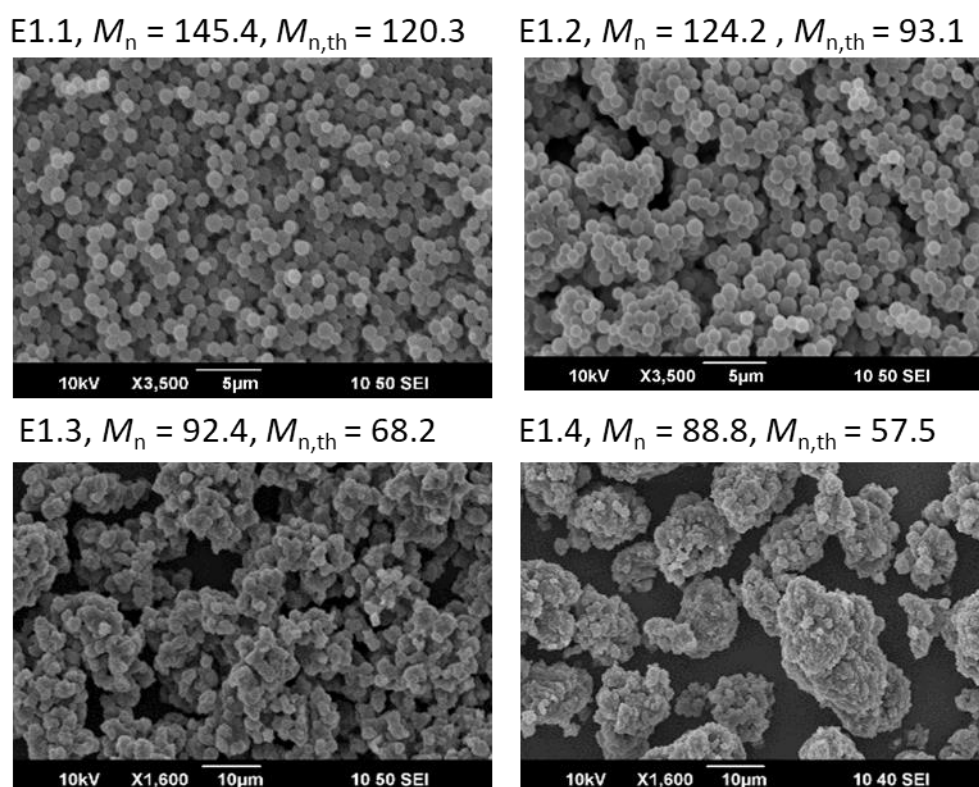


Figure 24 – SEM images of MMA polymerisation with PDMS₁₂₈-DDMAT, E1.1, E1.2, E1.3 and E1.4, with the respective M_n and $M_{n,th}$ for the block copolymer. The two products with higher PMMA molecular weights gave well-defined particles, E1.1 ($D_n = 0.82 \mu\text{m}$, $C_v = 22.5\%$) and E1.2 ($D_n = 1.05 \mu\text{m}$, $C_v = 12.6\%$), while E1.3 gave agglomerates and non-spherical individual particles (indicative diameter of 0.54 μm $C_v = 10.7\%$) and E1.4 showed agglomerates.

For E1.3, non-spherical individual particles with an indicative diameter of 0.54 μm ($C_v = 10.7\%$) were observed, which were aggregated into secondary structures (Figure 24). As the particles were not spherical, the diameter was estimated by fitting the apparent diameter into a spherical object for 100 particles in Image J[®]. The morphology observed for E1.3 was unexpected, since spherical particles with $D_n = 1\text{-}2 \mu\text{m}$ were obtained by Zong for a reaction under same conditions.⁴⁴ For E1.4 the SEM analysis showed large agglomerates, with individual non-spherical particles fused together. At $M_{n,\text{th}} = 38.4 \text{ kg mol}^{-1}$ (E1.5), solid lumps were obtained instead of a free-flowing powder, and therefore it was not analysed by SEM, but the physical aspect of the product already denoted different aggregation mode of particles.

These results for E1.3-E1.5 probably arise from the higher solubility of the block copolymer at a lower volume fraction of PMMA which enhances plasticisation/swelling and lowers the T_g in scCO_2 of the blocks comprising the block copolymer. In this way, the lower PMMA DP results in higher swelling of the particles, which become softer and more prone to fuse together. In fact, scCO_2 is known to cause plasticisation of polymers, which reduces T_g and the degree of crystallinity.⁶²⁻⁶⁴ For instance, the polymerisation of tert-butyl acrylate in scCO_2 results in a tacky foamed solid. The T_g of this polyacrylate is low, *i.e.*, 43 $^\circ\text{C}$, but higher than room temperature. However, the T_g is lowered in scCO_2 and with the depressurisation any well-defined morphology is lost.⁴⁴

In summary, our results are not in agreement with the good control reported by Zong in her thesis.⁴⁴ However, at that time Zong had not fully characterised the PDMS₁₂₈-DDMAT used, and there could have been significant presence of unreacted CTA in the reaction mixture, improving RAFT control. On the other hand, for the reactions presented here, we are confident in the absence of unreacted DDMAT, as we have analysed our macro-CTA by several techniques and have not observed the presence of unreacted CTA. Therefore, we can attribute the RAFT control, or the lack of it, solely to PDMS₁₂₈-DDMAT.

3.5.3.3. MMA polymerisation with PDMS₆₅-DDMAT

Following the experiments with the longer macro-CTA, PDMS₆₅-DDMAT was investigated for MMA dispersion polymerisation in scCO_2 . Again, different final block copolymer molecular weights were targeted (Table 6). The same CTA:initiator ratio of 2:1 was maintained for each reaction.

Table 6 – MMA dispersion polymerisation in scCO₂ carried out in the presence of PDMS₆₅-DDMAT.

Expt.	PMMA $M_{n,th}^1$	Block copolymer $M_{n,th}^2$	PDMS wt% ³	Conv. ⁴ (%)	M_n^5	\mathcal{D}^5	Morphology ⁶
E2.1	84.4	89.8	5.9	93	131.2	2.96	Non-spherical particles and agglomerates
E2.2	56.7	62.1	8.9	94	80.9	2.50	Non-spherical particles and agglomerates
E2.3	47.4	52.8	10.6	94	64.1	2.39	Porous agglomerates
E2.4	36.8	42.2	13.4	93	61.5	2.68	Porous agglomerates
E2.5	28.2	33.6	17.8	95	59.9	2.58	Fused porous agglomerates
E2.6	22.1	27.5	21.4	88	24.5	1.40	Amorphous agglomerates

¹Theoretical M_n for MMA calculated relative to macro-CTA and monomer concentration and given in kg mol⁻¹.

²Theoretical M_n of the block copolymer = $M_{n,th}$ of PMMA + M_n of macro-CTA (5.36 kg mol⁻¹), where $M_{n,th}$ of PMMA was calculated relative to macro-CTA and monomer concentration, given in kg mol⁻¹. The M_n of macro-CTA = M_n of PDMS-OH (4.99 kg mol⁻¹) + DDMAT molecular weight (0.365 kg mol⁻¹). ³The weight percentage of PDMS in the reaction medium was calculated with respect to MMA. ⁴Conversion was calculated from ¹H NMR. ⁵ \mathcal{D} and M_n were obtained by THF-SEC with RI detector against PMMA standards. ⁶Overall morphology as determined by SEM.

As for PDMS₁₂₈-DDMAT, the THF-SEC analysis showed unimodal peaks with long tails towards low molecular weights (Figure 25). The overlay of the RI traces for all the experiments can be found in the appendix (Figure S2). Unreacted macro-CTA is present, as can be observed by the overlap of the copolymer traces with the macro-CTA trace in both the RI and UV detectors. PDMS₆₅-DDMAT also did not provide ideal control over MMA polymerisation. High dispersities were observed, $\mathcal{D} > 2$ for all reactions, except from E2.6, which had $\mathcal{D} = 1.44$. However, this is more related to a shorter tail than to a better control. In addition, M_n was above the target for reactions E2.1 - E2.5. Molecular weight was closer to target for E2.3, $M_n = 64.1$ and $M_{n,th} = 52.8$ kg mol⁻¹. Strangely, reaction E2.3, E2.4 and E2.5 gave similar M_n , circa 60 kg mol⁻¹, although the theoretical molecular weights were different.

The SEM analysis for MMA polymerisations with PDMS₆₅-DDMAT showed no well-defined spherical particles for any of the reactions (Figure 26). As for PDMS₁₂₈-DDMAT, more defined particles could be observed only at higher PMMA molecular weights. Indeed, experiment E2.1 ($M_n = 131.2$ kg mol⁻¹) presented a mix of non-spherical particles and amorphous agglomerates, while E2.2 ($M_n = 80.9$ kg mol⁻¹) showed some agglomerates and non-spherical particles with rough edges. For E2.3 and E2.4, the lower content of PMMA relative to PDMS induced foaming, observed as porous structures in the particle agglomerates (Figure 26). This

was likely a result of increased plasticisation of the polymer by $scCO_2$, *i.e.*, increased solubility of CO_2 in the PMMA block, as the DP of the PMMA block decreased, which causes the polymer expansion and morphology loss and more intense agglomeration and fusion of particles. Despite the particle agglomeration and foaming, all reactions gave high conversion (> 88%) and free-flowing powders.

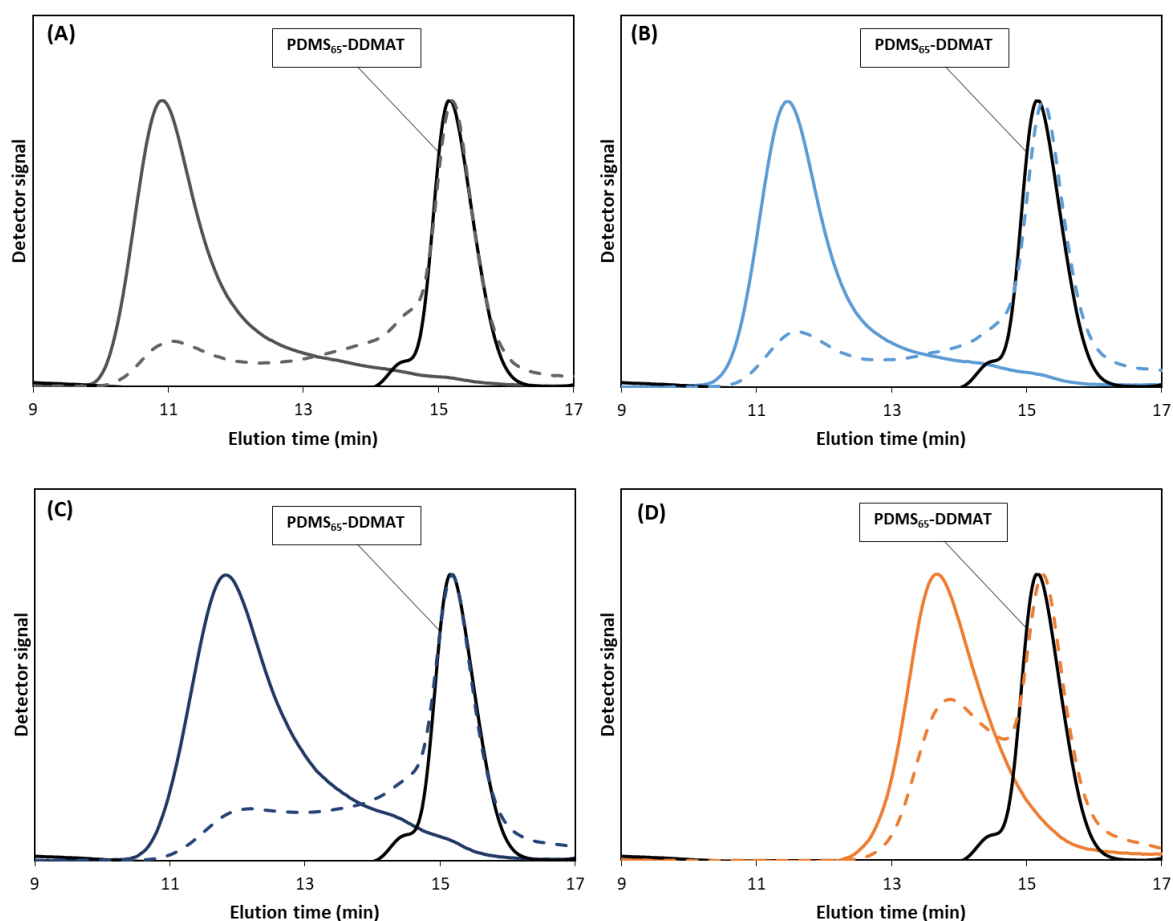
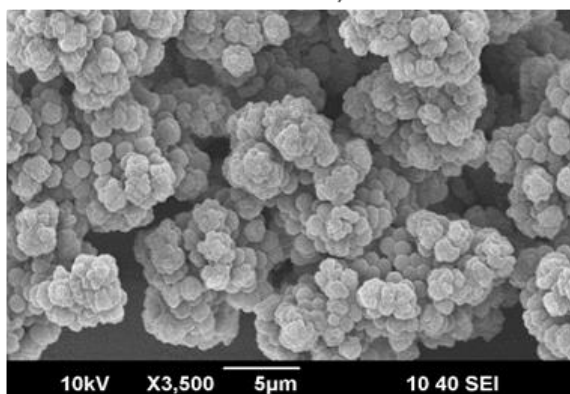


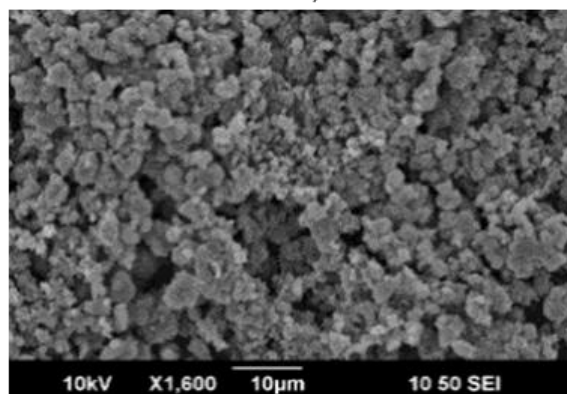
Figure 25 - THF-SEC study of MMA dispersion polymerisation in $scCO_2$ with $PDMS_{65}$ -DDMAT, showing normalised traces for the RI detector (solid line) and for UV detector (dashed line). for experiments: (A) E2.1, (B) E2.2, (C) E2.3 and (D) E2.6. The shoulder presented for $PDMS_{128}$ -DDMAT is consistent with

E2.6 had the lowest block copolymer molecular weight, *i.e.*, $M_{n,th} = 27.5 \text{ kg mol}^{-1}$, and resulted in a $M_n = 24.5 \text{ kg mol}^{-1}$ (Table 6). A lower molecular weight than the theoretical was achieved, which is unusual, but this must have resulted from a significant number of initiator-derived chains.⁶⁵ It also had the lowest conversion, 88%. The low molecular weight of the PMMA core further enhanced solubility of CO_2 in the PMMA block, causing plasticisation and resulting in large and fused agglomerates (Figure 26).

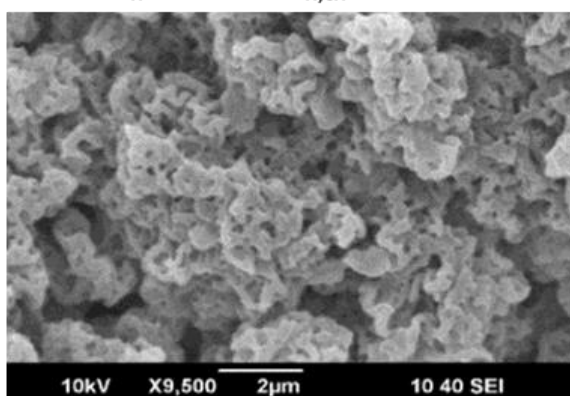
E2.1, $M_n = 131.2$, $M_{n,th} = 89.8$



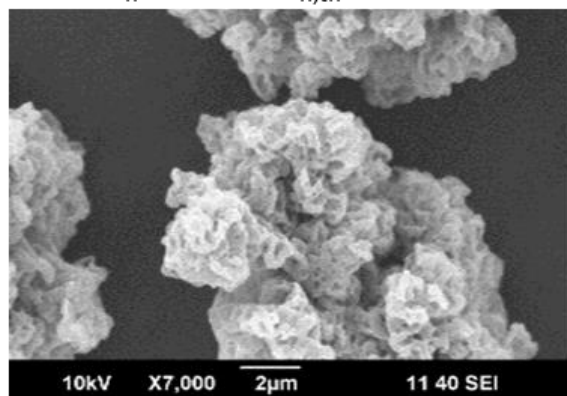
E2.2, $M_n = 80.9$, $M_{n,th} = 62.1$



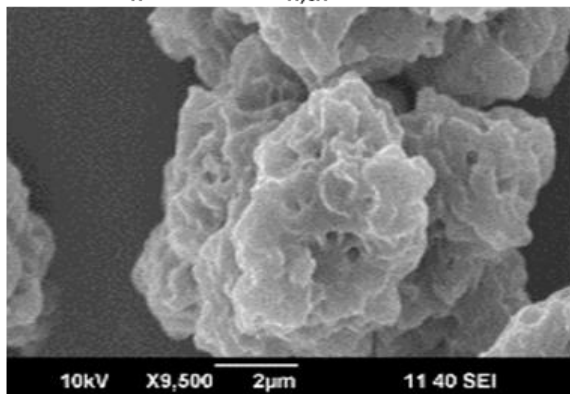
E2.3, $M_n = 64.1$, $M_{n,th} = 52.8$



E2.4, $M_n = 61.5$, $M_{n,th} = 42.2$



E2.5, $M_n = 5.9$, $M_{n,th} = 33.6$



E2.6, $M_n = 19.7$, $M_{n,th} = 27.5$

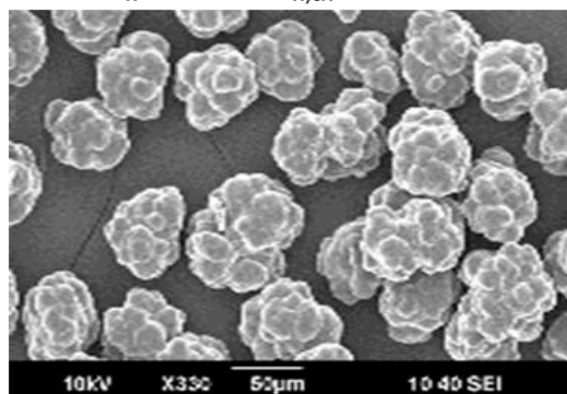


Figure 26 - SEM images of reactions E2.1 - E2.6 performed with PDMS₆₅-DDMAT. The products with higher molecular weights, E2.1 and E2.2 gave non-spherical individual particles and small agglomerates. E2.3 and E2.4 show occurrence of foaming, while the other two reactions, E2.5 and E2.6, show large fused agglomerates.

In summary, PDMS₆₅-DDMAT did not offer optimal RAFT control over MMA polymerisation in scCO₂ and no well-defined spherical particles could be observed. Further SEM pictures are presented in the Appendix (Figure S3-S8). However, it is interesting to notice that PDMS₆₅-DDMAT could stabilise the reaction in order to obtain high conversions and polymer powders, despite the lower molecular weight compared to PDMS₁₂₈-DDMAT.

We tested PDMS-MA with a shorter PDMS chain, PDMS-MA (120 cSt, $M_n \approx 5 \text{ kg mol}^{-1}$) for comparison. PDMS-MA (120 cSt) at 5 wt% was not capable of stabilising MMA polymerisation in scCO₂. The reaction achieved 42.9% monomer conversion and a low $M_n = 17.5 \text{ kg mol}^{-1}$. Therefore, it is remarkable that PDMS₆₅-DDMAT, which has PDMS $M_n = 4.99 \text{ kg mol}^{-1}$, stabilised MMA polymerisations in scCO₂ enough to obtain high conversions and polymer powders, as seen in E2.1-E2.6 (Table 6). In particular, E2.1 used 5.9 wt% PDMS₆₅-DDMAT with respect to MMA, and obtained conversion = 93% and non-spherical individual polymer particles could be observed (Figure 26).

The enhanced stabilisation power of PDMS₆₅-DDMAT compared to PDMS-MA (120 cSt) points to the formation of a more effective stabiliser by MMA chain extension from PDMS-DDMAT, *i.e.*, PDMS-*b*-PMMA. The stabilisation arising from the block copolymers should be superior to the stabilisation of PMMA particle *via* steric stabilisation through the single unit of methacrylate of PDMS-MA. However, it could also be simply due to better steric stabilisation from the DDMAT anchoring group compared to methacrylate. To identify which of these cases is true, we investigated the blocking efficiency of the polymerisations with PDMS-DDMAT in the next section.

3.5.3.4. PDMS grafting efficiency onto the particles

The incomplete consumption of the PDMS-based macro-CTAs in scCO₂ is puzzling, as this has not been observed previously with fluorinated macro-CTAs. According to previous studies in literature, MMA dispersion polymerisation in scCO₂ with PFOMA-CPAB²², PDFMA-CDB²⁵ and PDFMA-DDMAT³⁰ resulted in well-controlled molecular weight, low dispersity, and had no traces of unreacted macro-CTA. The presence of unreacted macro-CTA is also not mentioned by Zong when using PDMS-BSPA, PDMS-MPPA or PDMS-DDMAT.⁴⁴

Low blocking efficiency and residual unreacted macro-CTA have been previously observed in PISA reactions in conventional solvents. For example, although good control over morphology

was obtained, Fielding *et al.* observed a low molecular weight shoulder in SEC analysis, which was attributed to unreacted PLMA macro-CTA or prematurely terminated PLMA₁₇-PBzMA.¹⁷ In another work, a poly(ethylene oxide) based macro-CTA was used for alternating copolymerization of styrene and maleic anhydride in chloroform, however, monomer conversions were < 50% because one of the maleic anhydride was excluded from the growing copolymer micelle cores.⁶⁶

In order to investigate the grafting efficiency of PDMS-*b*-PMMA produced with PDMS-DDMAT, all polymer powders obtained were washed with hexane (See Section 3.4.2.5.). The PDMS macro-CTAs are soluble in hexane, while PMMA and the synthesised PDMS-*b*-PMMA are insoluble (Figure 27). Therefore, any unreacted PDMS-DDMAT was washed-off while the PDMS in the block copolymer remains in the powder (precipitate).

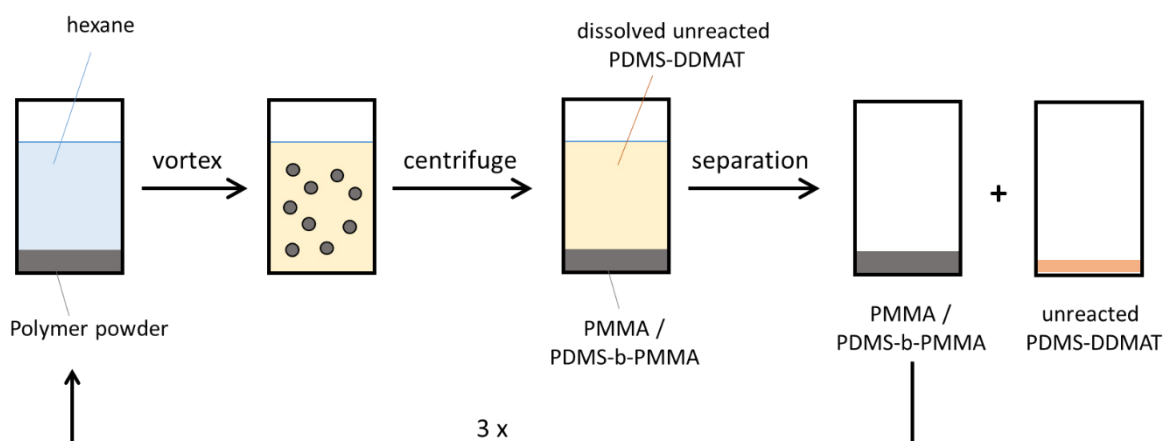


Figure 27 – Schematics showing the hexane washes procedure. Hexane was added to the polymer powder and the solution was homogenised with a vortex mixer. The suspension was centrifuged and the insoluble PMMA and PDMS-*b*-PMMA polymers precipitated, while the dissolved PDMS-DDMAT stayed in solution. The precipitated was submitted to the same process, totalising three washes, and was dried overnight at 25 °C under vacuum.

We have previously observed that part of the PDMS-DDMAT was left unreacted as evidenced by THF-SEC with both UV and RI detectors (Section 3.5.1.). However, at that point, we did not know the percentage of unreacted macro-CTA. The polymer powder before and after washes were analysed by THF-SEC and ¹H NMR and results were compared (Table 7 and Table 8). The percentage of PDMS chains attached to the block copolymer, *i.e.*, the macro-CTA block efficiency, was calculated by ¹H NMR integration of the resonance referent to PDMS repeating

unit (at ≈ 0.05 ppm) before and after the washing, relative to the integral of PMMA repeating unit (at ≈ 3.60 ppm) (Figure 28).

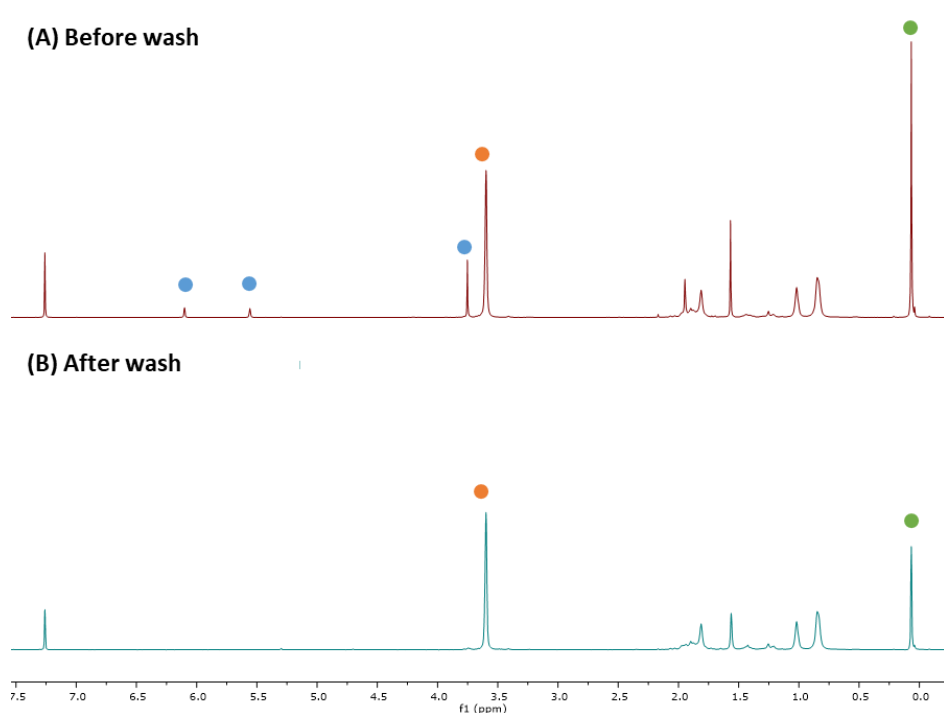


Figure 28 - Example of ^1H NMR of PDMS-*b*-PMMA powder before (A) and after (B) hexane wash (E2.6). The NMR resonances are labelled as follow: monomer (MMA) – blue, PMMA repeating unit – orange, PDMS repeating unit – green.

With PDMS₁₂₈-DDMAT, only up to 36.1% of the PDMS chains were retained on the final product (Table 7), while the shorter PDMS₆₅-DDMAT had a higher incorporation rate, up to 57.5% (Table 8). For PDMS₁₂₈-DDMAT, an increase in PDMS retention when lowering PMMA M_n was observed, with a plateau at approximately 34%. For PDMS₆₅-DDMAT (Table 8) PDMS retention increased with the increase in the initial load of PDMS (wt%) present in the reaction. E2.6 showed the highest PDMS retention, *i.e.*, 57.5%, amongst the series, while the block copolymer presented the lowest dispersity, $\mathcal{D} = 1.44$, and lower molecular weight, $M_n = 24.5$ kg mol⁻¹ (Table 6). In addition, E2.6 had the lowest MMA conversion, indicating slower kinetics.

Table 7 – Hexane washes of polymer powders obtained by dispersion polymerisation in scCO₂ with PDMS₁₂₈-DDMAT as macro-CTA.

Expt.	PDMS wt% ¹	Block copolymer $M_{n,th}$ ²	Conv. ³ (%)	M_n ⁴	\bar{D} ⁴	PDMS retained ⁵ (%)
E1.1	9.2	120.3	98	145.4	2.18	23.3
E1.2	11.5	83.1	92	124.2	2.12	28.9
E1.3	17.2	68.2	96	92.4	1.81	36.1
E1.4	20.7	57.5	94	88.8	2.35	33.3
E1.5	34.4	38.4	93	65.5	2.23	34.2

¹The weight percentage of PDMS in the reaction medium was calculated with respect to MMA. ²Block copolymer $M_{n,th} = PMMA M_{n,th} + M_n$ of macro-CTA (10.11 kg mol⁻¹), given in kg mol⁻¹. ³Conversion was calculated from ¹H NMR. ⁴Experimental M_n was obtained by THF-SEC of the block copolymer. ⁵The percentage of retained PDMS was obtained by comparing ¹H NMR resonance integrals for PDMS and PMMA repeating units before and after hexane wash, considering the integral before hexane wash to be 100%.

Table 8 – Hexane washes of polymer powders obtained by dispersion polymerisation in scCO₂ with PDMS₆₅-DDMAT as macro-CTA.

Expt.	PDMS wt% ¹	Block copolymer $M_{n,th}$ ²	Conv. ³ (%)	M_n ⁴	\bar{D} ⁴	PDMS retained ⁵ (%)
E2.1	5.9	89.8	93	131.2	2.96	27.5
E2.2	8.9	62.1	94	80.9	2.50	39.4
E2.3	10.6	52.8	94	64.1	2.39	45.7
E2.4	13.4	42.2	93	61.5	2.68	47.1
E2.5	17.8	33.6	95	60.3	2.50	52.8
E2.6	21.4	27.5	88	24.5	1.44	57.5

¹The weight percentage of PDMS in the reaction medium was calculated with respect to MMA. ²Block copolymer $M_{n,th} = PMMA M_{n,th} + M_n$ of macro-CTA (5.36 kg mol⁻¹), given in kg mol⁻¹. ³Conversion was calculated from ¹H NMR. ⁴Experimental M_n was obtained by THF-SEC of the block copolymer. ⁵The percentage of retained PDMS was obtained by comparing ¹H NMR resonance integrals for PDMS and PMMA repeating units before and after hexane wash, considering the integral before hexane wash to be 100%.

It is important to emphasise that in the experiments presented here, PDMS-DDMAT was expected not only to stabilise the particle, but also to control the growth of the PMMA chains. It is also expected to enable the formation of peculiar morphologies, like in the PISA systems described in the literature in conventional solvent. Therefore, each PDMS-DDMAT was expected to chain extend with MMA units and form a block copolymer. However, the hexane

washing results indicated a low blocking efficiency of PMMA for both macro-CTAs, with most of the macro-CTA not incorporated into the final polymer (Table 7 and Table 8). This ultimately resulted in the poor agreement between M_n and $M_{n,th}$ and quite broad molecular weight distributions.

Despite that, some control over molecular weight was achieved. Indeed, the THF-SEC UV detector and the hexane washes data, *i.e.*, 20% < PDMS retention < 60%, support that some MMA did chain extend from PDMS-DDMAT. For comparison one MMA dispersion polymerisation in scCO₂ was performed without any molecular or macromolecular CTA. 5 wt% PDMS-MA (10 kg mol⁻¹) was used as stabiliser and all other conditions kept the same. The polymerisation resulted in a $M_n = 470$ kg mol⁻¹ and $\bar{D} = 1.80$, while conversion was 98% and spherical individual PMMA particles were obtained with $D_n = 4.57$ μm. The molecular weights obtained with the macro-CTAs were lower than this and closer to the targeted molecular weight. Therefore, the macro-CTA is conferring control over molecular weight to a certain extent.

Furthermore, although the retention of PDMS-DDMAT was not as high as expected, it was greater than the incorporation of PDMS-MA (250 cSt) stabiliser into PMMA particles. As a macromonomer, PDMS-MA would be expected to copolymerise with MMA. However, previous studies by both DeSimone and Howdle groups demonstrated that only a small fraction of the stabiliser is incorporated into the polymer particles, *i.e.*, < 2 wt%.^{36, 37}

3.5.3.5. MMA polymerisation with PDMS-DDMAT and DDMAT

In the previous section, we observed that a significant part of the macro-CTA appears to not participate in the RAFT mechanism, but only provides stabilisation, thus we investigated what would be the effect of adding DDMAT as molecular CTA to the polymerisation. A series of RAFT dispersion polymerisations of MMA in scCO₂ using DDMAT as CTA at a DP target of 600 with either PDMS₁₂₈-DDMAT or PDMS-MA (250 cSt) as stabilisers at 1 and 5 wt%, were carried out in triplicate (Table 9). Both PDMS-based stabilisers have a similar molecular weight ≈ 10 kg mol⁻¹. The main aims were to investigate if a better control over molecular weight could be obtained with additional DDMAT and to compare the stabilisation obtained using PDMS-DDMAT with a classical stabiliser, PDMS-MA.

Table 9 – Stabilisation study for MMA RAFT dispersion polymerisation in scCO₂ with stabilisers of 10 kg mol⁻¹, PDMS₁₂₈-DDMAT and PDMS-MA 250 cSt.

PDMS ¹ (wt%)	Conv. ² (%)	$M_{n,th}$ ³	M_n ⁴	\mathcal{D} ⁴	D_n ⁵ (μm)	C_v ⁶ (%)
PDMS₁₂₈-DDMAT						
1	91.3 (±2.4)	55.0 (±1.8)	58.5 (±6.0)	1.74 (±0.11)	3.12 (±0.31)/ 1.34 (±0.07)	21.34 (±6.28)/ 21.62 (±2.90)
5	96.7 (±0.9)	58.2 (±0.8)	62.9 (±0.7)	1.34 (±0.02)	0.71 (±0.02)	18.18 (±3.32)
PDMS-MA (250cSt)						
1	94.3 (±2.4)	57.5 (±0.7)	73.6 (±2.5)	1.40 (±0.07)	10.69 (±0.11)/ 4.68 (±0.41)	20.61 (±5.18)/ 14.74 (±0.75)
5	97.8 (±0.2)	56.8 (±1.6)	63.3 (±3.2)	1.34 (±0.01)	1.94 (±0.12)	20.29 (±0.55)

¹ Weight percent load of PDMS-based stabiliser was calculated relative to monomer. ² Conversion was calculated from ¹H NMR. ³ Theoretical M_n calculated relative to DDMAT and monomer concentration and given in kg mol⁻¹, considering PDMS-DDMAT is not involved in the RAFT mechanism and only acts as a stabiliser for simplicity. ⁴ \mathcal{D} and M_n were obtained by THF-SEC with RI detector against PMMA standards. ⁵ Average particle size (D_n) was calculated as an average of 100 particles measurements *via* Image J®. ⁶ The coefficient of variance (C_v) was calculated by equation (2). All results given as an average of three measurements at 65 °C, with standard deviation given in brackets.

When using 1 wt% PDMS₁₂₈-DDMAT relative to MMA, a powder was obtained at 91.3% average monomer conversion. This already indicates a relatively good stabilisation. THF-SEC analysis showed a broad unimodal molecular weight distribution, with average $M_n = 58.5$ kg mol⁻¹ close to $M_{n,th} = 55$ kg mol⁻¹ and average $\mathcal{D} = 1.74$. Therefore, the molecular CTA appears to improve molecular weight control, although a broad dispersity is still in place. SEM images, however, showed two particle size populations with $D_n = 3.12$ μm and 1.34 μm (Figure 29A).

McAllister *et al.* have previously observed two populations of different particle sizes in a conventional radical polymerisation in scCO₂ when using 1 wt% PDMS-MA (≈ 10 kg mol⁻¹) as stabiliser.³⁹ This was attributed to insufficient stabilisation, which resulted in aggregation at the end of the particle growth stage. The agglomerated particles had a reduced total surface area, optimising stabilisation, and as result releasing some stabiliser molecules. Those allow for a second nucleation of particles to take place (Figure 30) Thus, PDMS₁₂₈-DDMAT at 1 wt% concentration appears to give a similar behaviour as described by McAllister *et al.* with PDMS-MA. To confirm this, we carried the polymerisation with 1 wt% of PDMS-MA (250 cSt), and particles of two different D_n , *i.e.*, 10.69 μm and 4.68 μm, were observed (Table 9, Figure 29C).

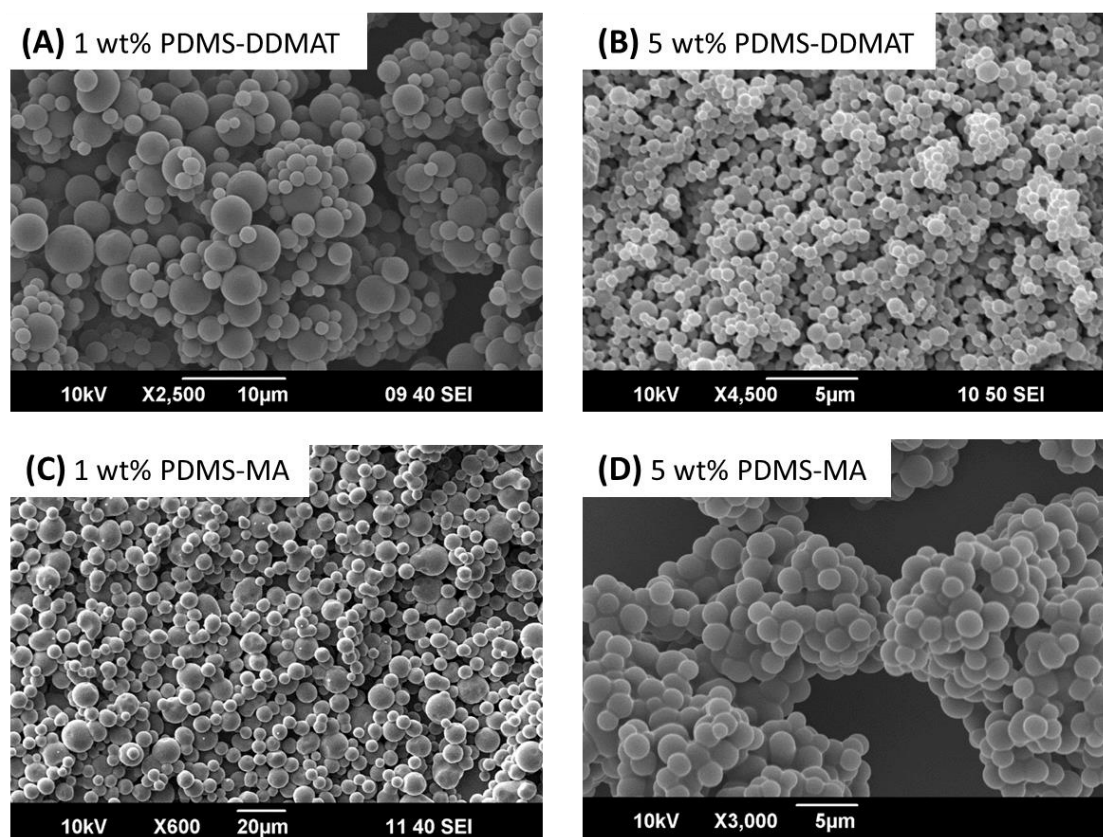


Figure 29 – SEM pictures of RAFT mediated MMA dispersion polymerisations in $scCO_2$ with DDMAT, targeting $DP = 600$ and using different stabilisers: $PDMS_{128}$ -DDMAT at 1 wt% (A) and 5 wt% (B) relative to the monomer; $PDMS$ -MA (250 cSt) at 1 wt% (C) and 5 wt% (D) relative to the monomer.

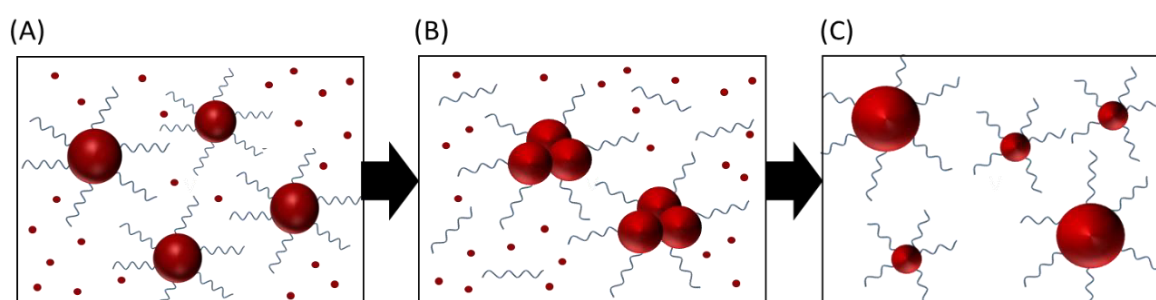


Figure 30 – Schematics of two nucleation events in dispersion polymerisation in $scCO_2$. (A) Stabilised polymer particles, which were formed by anchoring of stabiliser (blue) onto the polymer particles (red spheres). (B) If stabilisation is insufficient, the particles agglomerate and the surface area is reduced, allowing stabiliser to be released. (C) As polymerisation progresses the free stabiliser can stabilise growing polymer chains to form new particles, causing a second nucleation event.

Once the concentration of $PDMS$ -MA (250 cSt) was increased to 5 wt%, only one particle size distribution was observed (Figure 29D), 1.94 μm . In both cases, high conversions, *i.e.*, > 90%,

and good control over molecular weight and molecular weight distributions were observed (Table 9).

In the same way, when the loading of PDMS₁₂₈-DDMAT was increased from 1 to 5 wt%, only one particle size distribution was observed by SEM (Figure 29B), indicating sufficient stabilisation at the nucleation stage. The conversion was high, 97.8%, and molecular weight was close to target, $M_n = 63.3 \text{ kg mol}^{-1}$, while the dispersity was $\mathcal{D} = 1.34$, narrower than with 1 wt% of the same stabiliser (Table 9). This indicates a well controlled RAFT polymerisation is achieved when combining PDMS₁₂₈-DDMAT and DDMAT. In fact, the final molecular weight and dispersity are quite similar to results with PDMS-MA. This result suggests, the macro-CTA is not very reactive. If all the macro-CTA was growing PMMA chains, the final $M_{n,th}$ would be 45.7 kg mol^{-1} instead of 58.2 kg mol^{-1} .

It is interesting to notice that PMMA particle sizes obtained with PDMS-MA were much larger than the ones obtained with PDMS₁₂₈-DDMAT (Table 5, Figure 29C and 29D) at both concentrations of stabiliser. This suggests that, for a similar molecular weight, PDMS-DDMAT can stabilise a larger particle surface than PDMS-MA, resulting into smaller particles at the same stabiliser load. This is likely the result of a better anchor-soluble balance (ASB) for PDMS₁₂₈-DDMAT stabiliser, resulting from a more effective anchoring with the CTA anchor group.

In addition, as MMA is expected to chain extend from PDMS-DDMAT, the stabiliser would have a PMMA segment, which is known to provide a better anchoring group for PMMA particles than a single methacrylate unit.³² Woods *et al.* investigated PMMA polymerisation in *scCO*₂ with PFPE presenting four different anchoring groups: alcohol, acetate, a methacrylate unit and a PMMA block.³² The PFPE-*b*-PMMA stabiliser gave excellent PMMA yield, high molecular weight and fine morphology. However, the success of the PMMA anchoring group depended on molecular weight. For a PFPE of 1.75 kg mol^{-1} , increasing the PMMA block from 2 to 5 kg mol^{-1} led to aggregation and lower PMMA molecular weights resulted from the polymerisation.³² The authors attributed these results to a lower ASB of the stabiliser with longer PMMA chains.

Regardless of the stabilisation mechanism, PDMS₁₂₈-DDMAT demonstrated good stabilisation power for MMA dispersion polymerisation in *scCO*₂, comparable to results with PDMS-MMA

(250 cSt). More importantly, the use of molecular DDMAT together with PDMS₁₂₈-DDMAT improved RAFT control and morphology compared to the use of PDMS₁₂₈-DDMAT alone, suggesting that DDMAT is a good CTA for this polymerisation, while PDMS₁₂₈-DDMAT acts mainly as a stabiliser and not as a macro-CTA.

3.6. Conclusions

We presented the synthesis of two PDMS-based macro-CTAs, *i.e.*, PDMS₁₂₈-DDMAT and PDMS₆₅-DDMAT. The CTA was chosen based on previous studies in the Howdle group of silicone-based macro-CTAs for RAFT polymerisation of MMA in scCO₂. Our results demonstrated that both PDMS₁₂₈-DDMAT and PDMS₆₅-DDMAT can stabilise well the MMA dispersion polymerisation in scCO₂, resulting in a polymer powder at high conversion. However, control over molecular weight and dispersity was not obtained in the same way as in the previous work done by Zong with PDMS₁₂₈-DDMAT. Regardless of control, results with both PDMS₆₅-DDMAT and PDMS₁₂₈-DDMAT suggested a better stabilisation power than PDMS-MA of same molecular weight, which probably results from the chain extension of PDMS-DDMAT with MMA forming a more effective stabiliser. THF-SEC studies showed that part of the macro-CTA was left unreacted resulting in tailing of the molecular weight distributions, which increased the dispersity, while the obtained M_n was in most cases above the $M_{n,th}$. Nevertheless, the macro-CTA did exert control to some extent, as it had a better control over molecular weight compared to a conventional radical polymerisation and CTA chain-ends were present in the polymers, as observed by the THF-SEC UV-signal.

Further investigation into the grafting of PDMS macro-CTA to the polymer was carried out by means of a series of hexane washes. PDMS-DDMAT is soluble in hexane while PMMA and PDMS-*b*-PMMA are insoluble. The results confirmed that not all PDMS-DDMAT was involved in the reaction, with only up to 57% of the macro-CTA remaining attached to the copolymer after the washes. Therefore, a very significant part of the macro-CTA was not involved in the reaction or only acted as a steric stabiliser, absorbing onto the PMMA particles as unreacted macro-CTA or after PDMS chain extending a short PMMA chain.

Regarding morphology, at high PMMA molecular weights, E1.1 and E1.2, well-defined particles were obtained with PDMS₁₂₈-DDMAT, while less defined particles and agglomerates were obtained at lower $M_{n,th}$ of PMMA. When using PDMS₆₅-DDMAT as macro-CTA, no well-

defined spherical particles were obtained, and particle aggregation was more intense as the DP of the PMMA block decreased. This was likely an effect of swelling and T_g reduction in $scCO_2$ of the formed copolymers with higher PDMS volume fraction. The particle morphology could also be lost by potential collapse of structures at venting of the autoclave. Overall, all particles had a larger diameter than expected for PISA, suggesting agglomeration.

When combining DDMAT molecular CTA and PDMS-DDMAT for MMA dispersion polymerisation in $scCO_2$, improved RAFT control and morphology were observed compared to the use of PDMS₁₂₈-DDMAT alone, suggesting that DDMAT is a good CTA for this polymerisation. Results were similar to the RAFT dispersion polymerisation mediated by DDMAT with PDMS-MA as stabiliser, suggesting that PDMS₁₂₈-DDMAT acts mainly as a stabiliser and not as a macro-CTA. The choice of DDMAT for MMA polymerisation is however not trivial, as this CTA has a low chain transfer constant towards methacrylates. Therefore, the next chapter will focus on understanding the mechanism of RAFT dispersion polymerisation of MMA in $scCO_2$ with DDMAT and other molecular CTAs. This ultimately will help us to understand how to better pursue PISA mediated by RAFT in dispersion in $scCO_2$.

3.7. References

1. M. Lansalot, J. Rieger and F. D'Agosto, in *Macromolecular Self-Assembly*, eds. L. Billon and O. Borisov, John Wiley & Sons, New Jersey, United States of America, 2016, ch. 2, pp. 33-82.
2. C. J. Ferguson, R. J. Hughes, B. T. T. Pham, B. S. Hawkett, R. G. Gilbert, A. K. Serelis and C. H. Such, *Macromolecules*, 2002, **35**, 9243-9245.
3. J. Rieger, G. Osterwinter, C. Bui, F. Stoffelbach and B. Charleux, *Macromolecules*, 2009, **42**, 5518-5525.
4. J. Rieger, F. Stoffelbach, C. Bui, D. Alaimo, C. Jérôme and B. Charleux, *Macromolecules*, 2008, **41**, 4065-4068.
5. B. Charleux, G. Delaittre, J. Rieger and F. D'Agosto, *Macromolecules*, 2012, **45**, 6753-6765.
6. Y. Mai and A. Eisenberg, *Chem Soc Rev*, 2012, **41**, 5969-5985.
7. A. P. Lopez-Oliva, N. J. Warren, A. Rajkumar, O. O. Mykhaylyk, M. J. Derry, K. E. B. Doncom, M. J. Rymaruk and S. P. Armes, *Macromolecules*, 2015, **48**, 3547-3555.
8. P. B. Zetterlund, S. C. Thickett, S. Perrier, E. Bourgeat-Lami and M. Lansalot, *Chemical reviews*, 2015, **115**, 9745-9800.
9. M. J. Derry, L. A. Fielding and S. P. Armes, *Prog Polym Sci*, 2016, **52**, 1-18.
10. I. Chaduc, W. Zhang, J. Rieger, M. Lansalot, F. D'Agosto and B. Charleux, *Macromol Rapid Commun*, 2011, **32**, 1270-1276.
11. J. Lesage de la Haye, X. Zhang, I. Chaduc, F. Brunel, M. Lansalot and F. D'Agosto, *Angew Chem Int*, 2016, **55**, 3739-3743.
12. A. Blanzas, S. P. Armes and A. J. Ryan, *Macromolecular Rapid Communications*, 2009, **30**, 267-277.
13. S.-l. Chen, P.-f. Shi and W.-q. Zhang, *Chinese J Polym Sci*, 2017, **35**, 455-479.

14. A. Blanazs, J. Madsen, G. Battaglia, A. J. Ryan and S. P. Armes, *J Am Chem Soc*, 2011, **133**, 16581-16587.
15. F. D'Agosto, J. Rieger and M. Lansalot, *Angew Chem Int Ed*, 2020, **59**, 8368-8392.
16. W. Zhang, F. D'Agosto, O. Boyron, J. Rieger and B. Charleux, *Macromolecules*, 2012, **45**, 4075-4084.
17. L. A. Fielding, M. J. Derry, V. Ladmiral, J. Rosselgong, A. M. Rodrigues, L. P. D. Ratcliffe, S. Sugihara and S. P. Armes, *Chem Sci*, 2013, **4**, 2081.
18. M. J. Rymaruk, S. J. Hunter, C. T. O'Brien, S. L. Brown, C. N. Williams and S. P. Armes, *Macromolecules*, 2019, **52**, 2822-2832.
19. C. F. Kirby and M. A. McHugh, *Chemical reviews*, 1998, **99**, 565-602.
20. J. B. McClain, D. E. Betts, D. A. Canelas, E. T. Samulski, J. M. DeSimone, J. D. Londono, H. D. Cochran, G. D. Wignall, D. Chillura-Martino and R. Triolo, *Science*, 1996, **274**, 2049.
21. J. M. DeSimone and J. S. Keiper, *Curr Opin Solid State Mater Sci*, 2001, **5**, 331-341
22. M. Zong, K. J. Thurecht and S. M. Howdle, *Chem Commun*, 2008, **0**, 5942-5944.
23. P. J. Saikia, J. M. Lee, B. H. Lee and S. Choe, *J Polym Sci , Part A: Polym Chem*, 2007, **45**, 348-360.
24. A. M. Gregory, K. J. Thurecht and S. M. Howdle, *Macromolecules*, 2008, **41**, 1215-1222.
25. A. Xu, Q. Lu, Z. Huo, J. Ma, B. Geng, U. Azhar, L. Zhang and S. Zhang, *Rsc Adv*, 2017, **7**, 51612-51620.
26. W. P. Hems, T.-M. Yong, J. L. M. van Nunen, A. I. Cooper, A. B. Holmes and D. A. Griffin, *J Mater Chem*, 1999, **9**, 1403-1407.
27. C. Gualandi, L. J. White, L. Chen, R. A. Gross, K. M. Shakesheff, S. M. Howdle and M. Scandola, *Acta Biomater.* , 2010, **6**.
28. Y. L. Hsiao, E. E. Maury, J. M. Desimone, S. Mawson and K. P. Johnston, *Macromolecules* 1995, **28**.
29. Y. N. Pengcheng Yang, Thomas J. Neal, Elizabeth R. Jones, Bryony R. Parker and Steven P. Armes, *Chem Sci*, 2019, **10**.
30. Z Y Huo, P D Xia, U Azhar, J C Ma, X M Zhang, X Y Zhou, S. X. Z. and and A. H. Xu, *IOP Conf Ser: Mater Sci Eng*, 2019, **479**.
31. P. Christian, S. M. Howdle and D. J. Irvine, *Macromolecules*, 2000, **33**, 237-239.
32. H. M. Woods, C. Nouvel, P. Licence, D. J. Irvine and S. M. Howdle, *Macromolecules*, 2005, **38**, 3271-3282.
33. C. Lepilleur and E. J. Beckman, *Macromolecules*, 1997, **30**, 745-756.
34. J. M. DeSimone, E. E. Maury, Y. Z. Menceloglu, J. B. McClain, T. J. Romack and J. R. Combes, *Science*, 1994, **265**, 356-359.
35. Y.-L. Hsiao, E. E. Maury, J. M. DeSimone, S. M. Mawson and K. P. Johnston, *Macromolecules*, 1995, **28**, 8159-8166.
36. K. A. Shaffer, T. A. Jones, D. A. Canelas and J. M. DeSimone, *Macromolecules*, 1996, **29**, 2704-2706.
37. M. R. Giles, J. N. Hay, S. M. Howdle and R. J. Winder, *Polymer*, 2000, **41**, 6715-6721.
38. M. R. Giles, S. J. O'Connor, J. N. Hay, R. J. Winder and S. M. Howdle, *Macromolecules*, 2000, **33**, 1996-1999.
39. T. D. McAllister, L. D. Farrand and S. M. Howdle, *Macromol Chem Phys*, 2016, **217**, 2294-2301.
40. K. J. Thurecht, A. M. Gregory, W. Wang and S. M. Howdle, *Macromolecules*, 2007, **40**, 2965-2967.
41. E. Yilgor and I. Yilgor, *Prog. Polym. Sci.*, 2014, **39**, 1165-1195.
42. J. Jennings, G. He, S. M. Howdle and P. B. Zetterlund, *Chem Soc Rev*, 2016, **45**, 5055-5084.
43. Y. Xiong and E. Kiran, *Polymer* 1995, **36**, 4817-4826.
44. M. Zong, Doctor of Philosophy University of Nottingham, 2010.
45. K. J. Thurecht, A. Heise, M. deGeus, S. Villarroya, J. Zhou, M. F. Wyatt and S. M. Howdle, *Macromolecules*, 2006, **39**, 7967-7972.

46. F. Furno, P. Licence, S. M. Howdle and M. Poliakoff, *Actual Chimique*, 2003, 62-66.
47. K. Kortsen, A. A. C. Pacheco, J. C. Lentz, V. Taresco and S. M. Howdle, *J Supercrit Fluids*, 2021, **167**, 105047.
48. M. L. Wadley and K. A. Cavicchi, *Journal of Applied Polymer Science*, 2010, **115**, 635-640.
49. E. Pouget, J. Tonnar, P. Lucas, P. Lacroix-Desmazes, F. Ganachaud and B. Boutevin, *Chem. Rev.*, 2010, **110**, 1233-1277.
50. T. S. C. Pai, C. Barner-Kowollik, T. P. Davis and M. H. Stenzel, *Polymer*, 2004, **45**, 4383-4389.
51. D. Pavlović, J. G. Linhardt, J. F. Künzler and D. A. Shipp, *Journal of Polymer Science Part A: Polymer Chemistry*, 2008, **46**, 7033-7048.
52. C.-M. Guan, Z.-H. Luo and P.-P. Tang, *J Appl Polym Sci*, 2010, **116**, 3283-3290.
53. D. Pavlović, Q. Lou, J. G. Linhardt, J. F. Künzler and D. A. Shipp, *Journal of Polymer Science Part A: Polymer Chemistry*, 2017, **55**, 3387-3394.
54. G. Moad, E. Rizzardo and S. H. Thang, *Acc Chem Res*, 2008, **41**, 1133-1142.
55. D. J. Keddie, G. Moad, E. Rizzardo and S. H. Thang, *Macromolecules*, 2012, **45**, 5321-5342.
56. J. Jennings, M. Beija, A. P. Richez, S. D. Cooper, P. E. Mignot, K. J. Thurecht, K. S. Jack and S. M. Howdle, *J Am Chem Soc*, 2012, **134**, 4772-4781.
57. J. Jennings, M. Beija, J. T. Kennon, H. Willcock, R. K. O'Reilly, S. Rimmer and S. M. Howdle, *Macromolecules*, 2013, **46**, 6843-6851.
58. L. M. Johnson, L. Gao, C. W. Shields Iv, M. Smith, K. Efimenko, K. Cushing, J. Genzer and G. P. López, *Journal of Nanobiotechnology*, 2013, **11**, 22.
59. J. Pickering, D. van der Meer and G. Vancso, *J. Adhes. Sci. Technol.*, 2001, **15**, 1429-1441.
60. J. Herrera-Ordóñez, E. Saldívar-Guerra and E. Vivaldo-Lima, in *Handbook of Polymer Synthesis, Characterization, and Processing*, eds. E. Saldívar-Guerra and E. Vivaldo-Lima, John Wiley & Sons, New Jersey, United States of America, 2013, ch. Dispersed-Phase Polymerization Processes, pp. 295-315.
61. Z. Guan, J. R. Combs, Y. Z. Menceloglu and J. M. DeSimone, *Macromolecules*, 1993, **26**, 2663-2669.
62. A. I. Cooper, *J Mater Chem*, 2000, **10**, 207-234.
63. J. L. Kendall, D. A. Canelas, J. L. Young and J. M. DeSimone, *Chemical reviews*, 1999, **99**, 543-563.
64. C. Boyère, C. Jérôme and A. Debuigne, *Eur Polym J*, 2014, **61**, 45-63.
65. G. Moad, E. Rizzardo and S. H. Thang, *Aust J Chem*, 2005, **58**, 379-410.
66. W. Ji, J. Yan, E. Chen, Z. Li and D. Liang, *Macromolecules*, 2008, **41**, 4914-4919.

3.8. Appendix

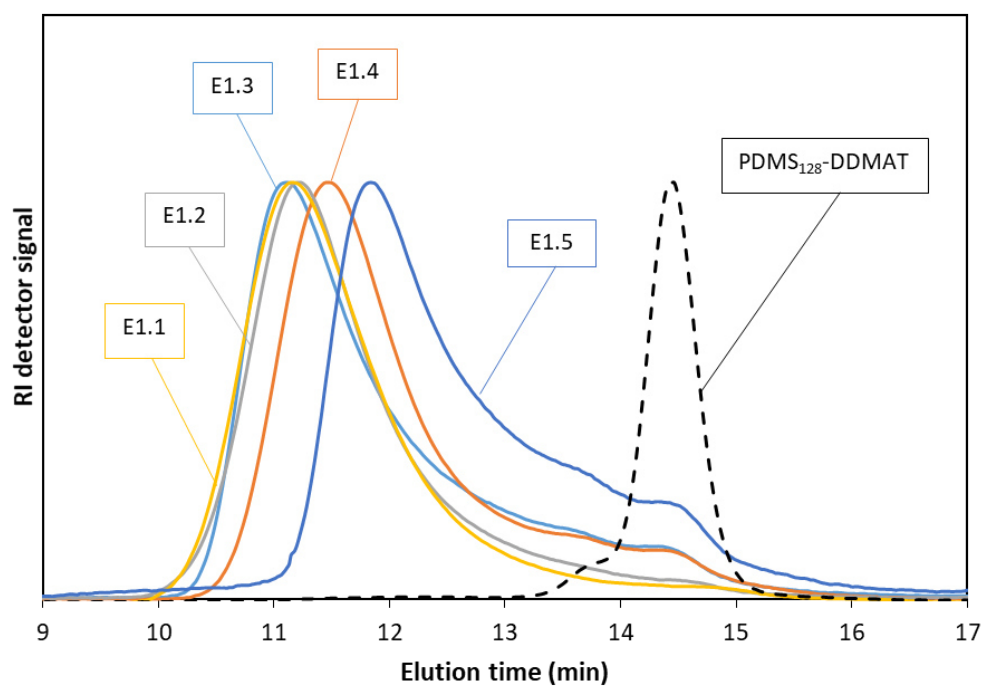


Figure S1 - THF-SEC study of MMA dispersion polymerisation in $scCO_2$ with PDMS₁₂₈-DDMAT, showing normalised traces for the RI detector for experiments E1.1 –E1.5. The trace for the unreacted macro-CTA is presented by a dashed line.

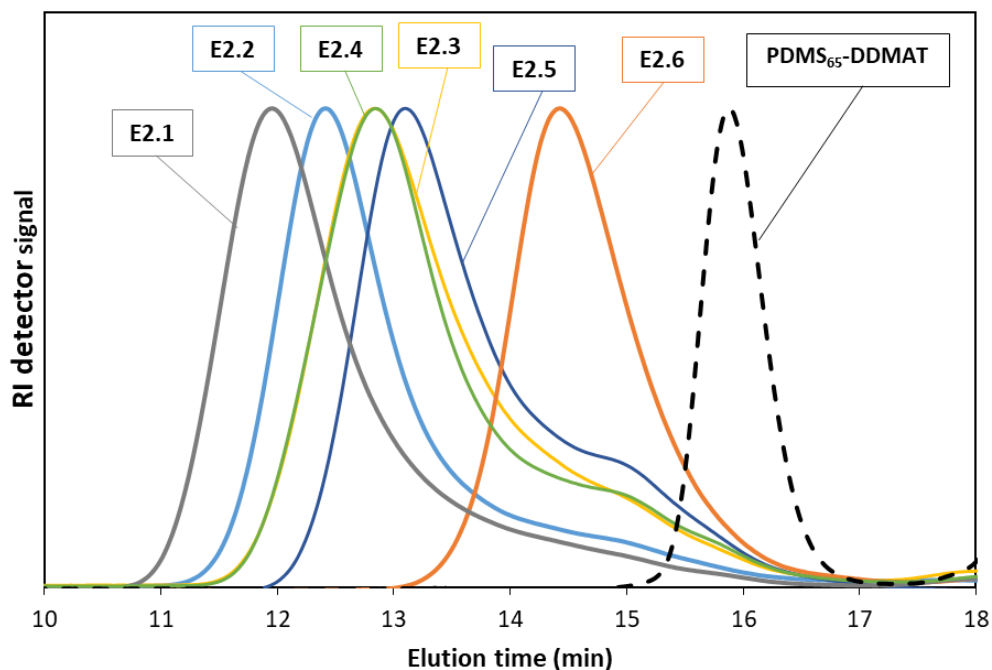


Figure S3 - THF-SEC study of MMA dispersion polymerisation in $scCO_2$ with PDMS₆₅-DDMAT, showing normalised traces for the RI detector for experiments E2.1 –E2.6. The trace for the unreacted macro-CTA is presented by a dashed line.

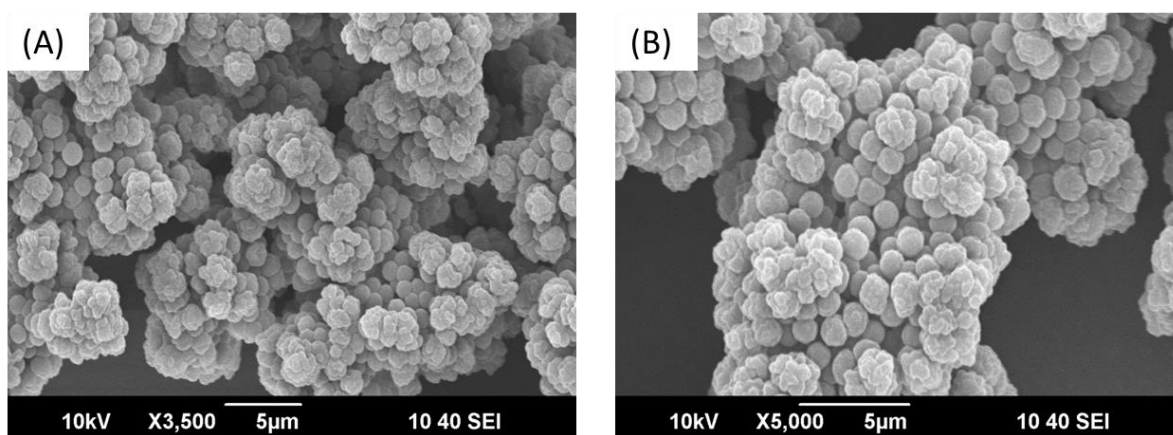


Figure S2 – SEM images of reaction E2.1 performed with PDMS₆₅-DDMAT at 3500 magnification (A) and 5000 magnification (B). The final product shows non-spherical individual particles and small amorphous agglomerates.

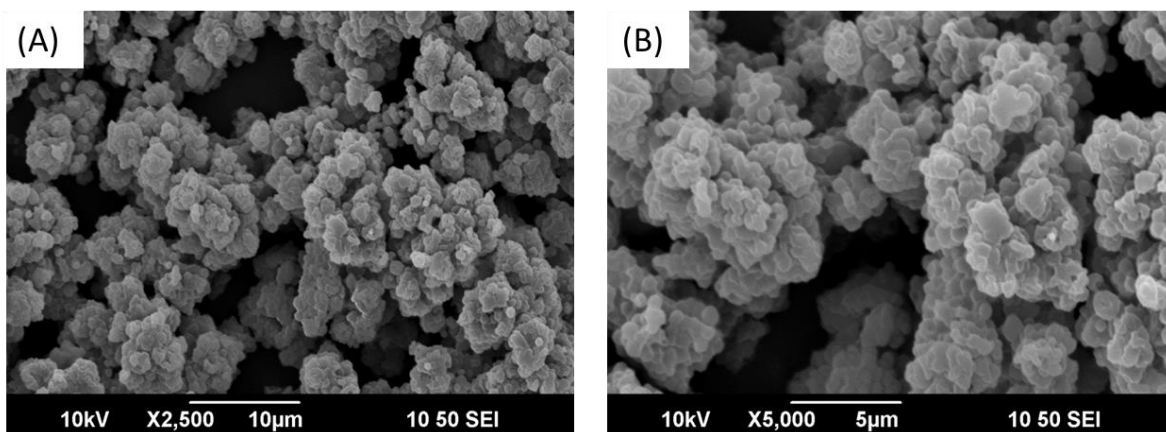


Figure S4 – SEM images of reaction E2.2 performed with PDMS₆₅-DDMAT at 2500 magnification (A) and 5000 magnification (B). The final product shows non-spherical individual particles organised into small agglomerates.

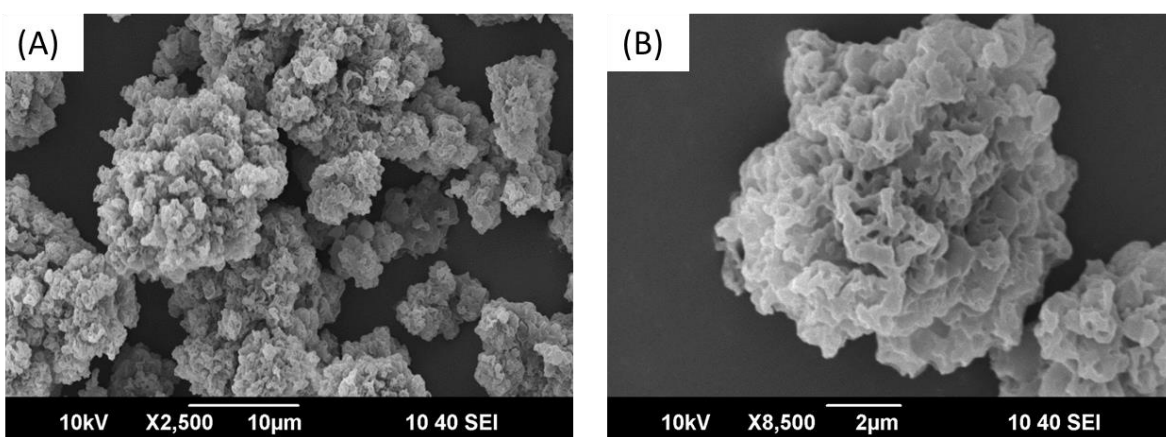


Figure S5 – SEM images of reaction E2.3 performed with PDMS₆₅-DDMAT at 2500 magnification (A) and 8500 magnification (B). The final product shows amorphous agglomerates with occurrence of foaming.

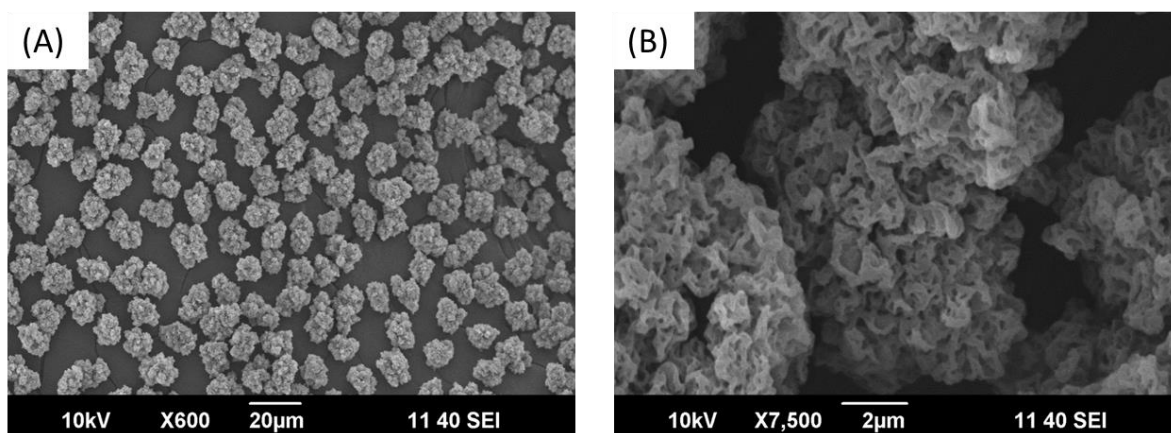


Figure S6 – SEM images of reaction E2.4 performed with PDMS₆₅-DDMAT at 20 magnification (A) and 7500 magnification (B). The final product shows amorphous agglomerates with occurrence of foaming.

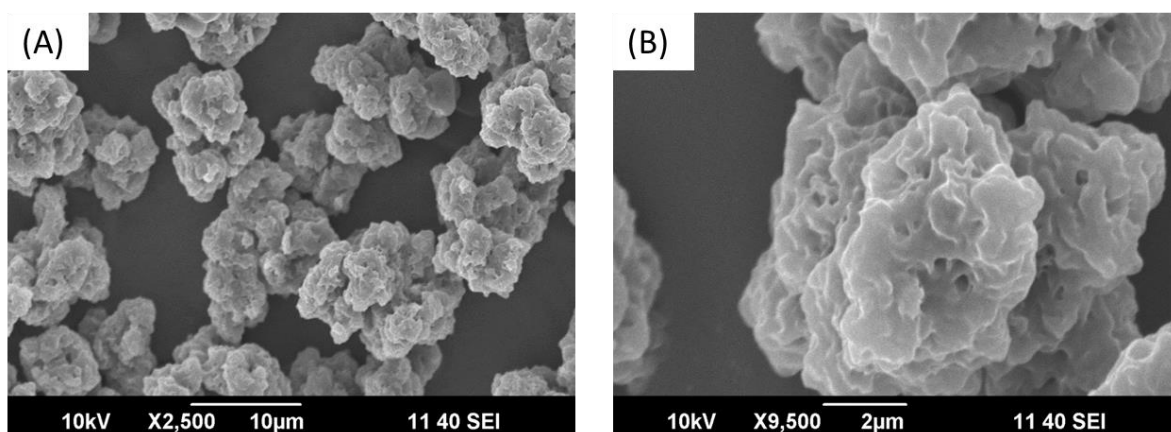


Figure S7 – SEM images of reaction E2.5 performed with PDMS₆₅-DDMAT at 2500 magnification (A) and 9500 magnification (B). The final product shows large fused agglomerates with some evidence of foaming.

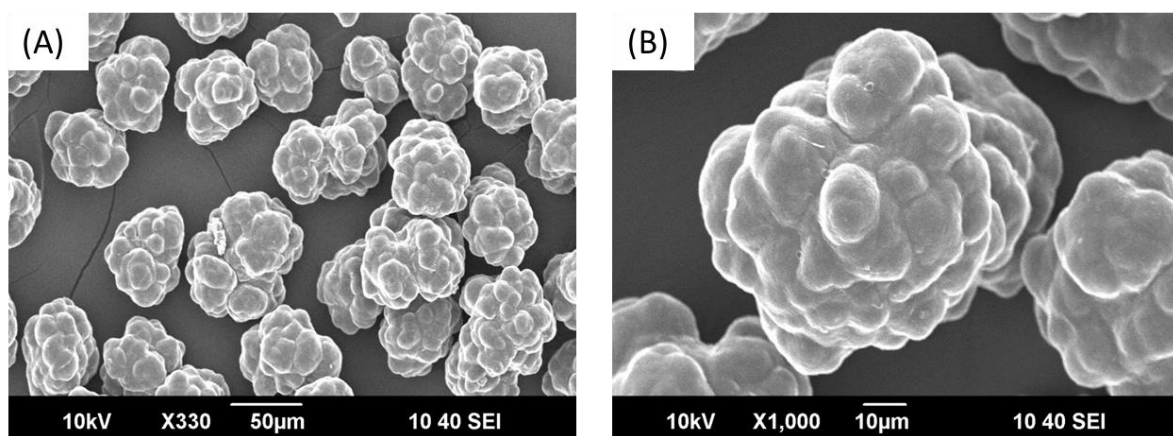


Figure S8 – SEM images of reaction E2.6 performed with PDMS₆₅-DDMAT at 330 magnification (A) and 1000 magnification (B). The final product shows large fused agglomerates.

Contents

Chapter 4. Influence of structure and solubility of chain transfer agents on the RAFT control of dispersion polymerisation in scCO₂	156 -
4.1. <i>Abstract</i>	156 -
4.2. <i>Introduction</i>	156 -
4.2.1. Dispersion polymerisation in scCO ₂	156 -
4.2.2. RAFT dispersion polymerisation	158 -
4.2.3. RAFT dispersion control in scCO ₂	162 -
4.2.4. RAFT control in scCO ₂ with DDMAT	164 -
4.3. <i>Aims</i>	166 -
4.4. <i>Experimental</i>	166 -
4.4.1. <i>Materials</i>	166 -
4.4.2. <i>Synthetic Procedures</i>	167 -
4.4.2.1. Standard RAFT solution polymerisation in toluene	167 -
4.4.2.2. Standard RAFT dispersion polymerisation in scCO ₂	167 -
4.4.2.3. Standard dispersion polymerisation in sampling autoclave	168 -
4.4.2.4. Standard dispersion polymerisation in scCO ₂ in static view cell	168 -
4.4.2.5. Standard two-stage polymerisation	168 -
4.4.2.6. Synthesis of 2-(propylthiocarbonothioylthio)-2-methylpropionic acid (PDMAT)	169 -
4.4.2.7. Synthesis of 4-cyano-4-thiothiopropylsulfanylpentanoic acid (CTPPA)	169 -
4.4.3. Standard solubility test in scCO ₂ in variable volume view cell	170 -
4.4.4. Computational modelling of CTA solvation	170 -
4.4.5. Polymer characterisation	171 -
4.5. <i>Results and discussion</i>	172 -
4.5.1. RAFT control of MMA polymerisation in scCO ₂ with DDMAT	172 -
4.5.1.1. Comparison of solution polymerisation in toluene and dispersion polymerisation in scCO ₂ with DDMAT	172 -
4.5.1.2. Kinetic study of MMA polymerisation in toluene and in scCO ₂ with DDMAT	175 -
4.5.1.3. Early stage of MMA dispersion polymerisation in scCO ₂ with DDMAT	181 -
4.5.1.4. Proposed mechanisms of RAFT control for scCO ₂ dispersion polymerisation with a bad choice of CTA	186 -
4.5.2. RAFT polymerisation of MMA in scCO ₂ with well-suited CTAs	188 -
4.5.2.1. Starting material assessment: CTA degradation	189 -
4.5.2.2. RAFT control of MMA polymerisation in scCO ₂ with CPAB	192 -
4.5.2.3. Two-stage RAFT dispersion polymerisation in scCO ₂ with CPAB	200 -

4.5.2.4. RAFT control of MMA polymerisation in scCO ₂ with CPDT	- 202 -
4.5.3. Solubility of CTAs	- 208 -
4.5.3.1. Computational solvation model for CTAs in scCO ₂	- 208 -
4.4.3.2. Cloud point studies of CTAs.....	- 213 -
4.5.4. CTAs comparison: control and phase behaviour	- 214 -
4.5.5. Solubility effect over CTAs control in scCO ₂ dispersion polymerisation.	- 219 -
4.5.6. Some further considerations (comparing to Gregory <i>et al.</i>).....	- 226 -
4.6. Conclusions.....	- 229 -
4.7. References	- 229 -
4.8. Appendix.....	- 233 -

Chapter 4. Influence of structure and solubility of chain transfer agents on the RAFT control of dispersion polymerisation in scCO₂

4.1. Abstract

Reversible addition-fragmentation chain transfer (RAFT) dispersion polymerisation of methyl methacrylate (MMA) is performed in supercritical carbon dioxide (scCO₂) using 2-(dodecylthiocarbonothioylthio)-2-methylpropionic acid (DDMAT) as chain transfer agent (CTA) which surprisingly shows good control over PMMA molecular weight. Kinetic studies of the polymerisation in scCO₂ also confirm these data. By contrast, only poor control of MMA polymerisation is obtained in toluene solution, as would be expected for this CTA, since DDMAT is known to be a good CTA towards acrylate rather than methacrylate RAFT polymerisation. To fully understand the peculiar behaviour of DDMAT and to extend our knowledge, we select a range of CTAs and use them to determine the parameters that must be considered for good control in dispersion polymerisation in scCO₂. A thorough investigation of the nucleation stage during the dispersion polymerisation reveals an unexpected “*in situ* two-stage” mechanism that explains well how the CTA works. Finally, using a novel computational solvation model, we identify a correlation between polymerisation control and the degree of solubility in scCO₂ of the CTAs. All of this ultimately give rise to a simple, elegant and counterintuitive guideline to select the best CTA for RAFT dispersion polymerisation in scCO₂.

4.2. Introduction

4.2.1. Dispersion polymerisation in scCO₂

scCO₂ is a benign, inert, nontoxic and non-flammable green solvent.^{1, 2} It has emerged as a potential replacement for common harmful, toxic and unsustainable organic solvents. The removal of the CO₂ after synthesis is not energy consuming and it can be recycled in an environmentally friendly way. Moreover, scCO₂ has an easily attainable critical point (31.1 °C, 73.8 bar), which requires low input of energy compared to other supercritical fluids. Above its critical point, CO₂ has unique physicochemical properties, such as liquid-like density and

gas-like diffusivity and viscosity,³ which can be further tuned to change solvation by adjusting pressure and/or temperature.

scCO₂ is essentially inert to reactions with radicals, which is ideal for use as a solvent in radical polymerisation.² Initially, research focused on precipitation polymerisation, due to the low solubility of most polymers in scCO₂.⁴ However, it was later recognised that the high solubility of most monomers, and the poor solubility of most polymers in scCO₂ makes it an ideal solvent for dispersion polymerisation.^{5, 6} This is because in a dispersion polymerisation all reactants, *i.e.* monomer, initiator, etc., must be soluble in the continuous phase at the reaction onset (Figure 1). After the polymerisation is initiated and a critical chain length (J_{crit}) is achieved, the growing polymer becomes insoluble and the small chains agglomerate and precipitate to form nuclei, which are then captured by stabiliser, leading to a colloidal dispersion.⁷ The fact that polymers are particularly insoluble in scCO₂ facilitates the nucleation stage. These nuclei are then enlarged by the inward diffusion and polymerisation of the remaining monomer,⁸ giving a latex with particle diameters spanning from 100 nm to 20 μm .⁹

In addition, dispersion polymerisation is reported to be aided by the low viscosity and high diffusivity of scCO₂, which can overcome known issues encountered in traditional heterogeneous polymerisations.^{1, 4} Nevertheless, the greatest advantage of conducting

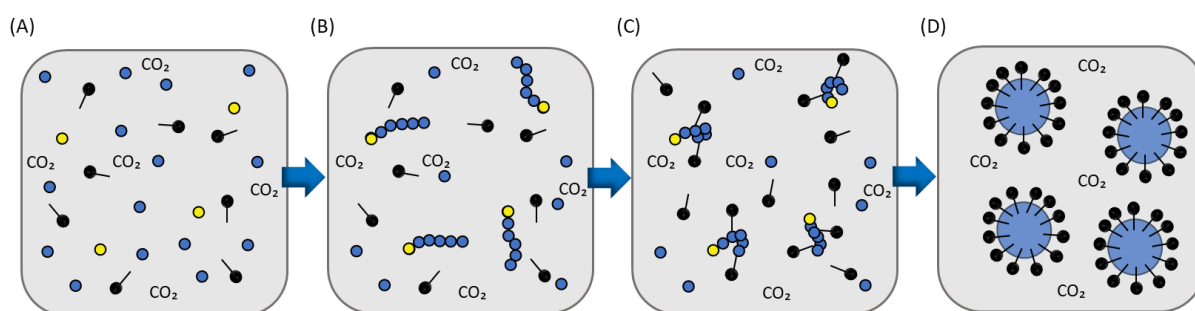


Figure 1 – Schematics of dispersion polymerisation: (A) The reaction begins with a homogeneous mixture of monomers (blue), initiator (yellow), stabiliser (black) and solvent. (B) Chains grow until the critical length (J_{crit}) is achieved. (C) As polymer chains precipitate, the stabiliser adsorbs to the polymer creating nuclei preventing agglomeration. This process takes place until a sufficient surface coverage of stabiliser is reached to prevent further aggregation, and stable nuclei are formed. (D) Further monomer and oligomers diffuse into the stabilised nuclei and the particles grow until reaction is completed.

dispersion polymerisations in $scCO_2$ is the facile and complete removal of solvent by simple depressurisation. Although most polymers are insoluble in $scCO_2$, it is known to plasticise polymers and as a result reduce the glass transition temperature (T_g), which can aid the removal of residual monomer, oligomers or other contaminants.⁴ Thus, the depressurisation step produces a dry, free-flowing polymer powder, composed by well-defined particles, that requires no further purification, *e.g.* drying, at the end of the synthesis.

Since the first reported successful radical dispersion polymerisations in $scCO_2$,¹⁰ many vinyl monomers have been polymerised in this reaction medium.^{9, 11-15} The unique properties of $scCO_2$ and the plasticisation of polymer particles can also have implications in the synthesis, in particular, of block copolymers with well-defined microstructures, as has been well exploited by the Howdle group and by others.¹⁶⁻²²

To summarise, heterogeneous dispersion polymerisation in $scCO_2$ allows access to unique well-defined materials of controlled polymer particle morphology and microstructure. It also provides a greener synthetic route than using toxic solvents or generating large amount of contaminated water and provides contaminant-free polymers which can find biomedical or pharmaceutical applications. Thus, there is now considerable scope for further research and industrial application of other monomers.

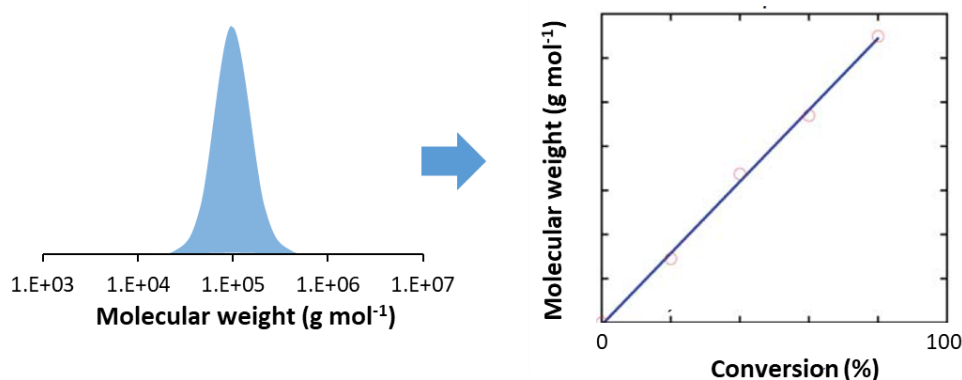
4.2.2. RAFT dispersion polymerisation

The advent of reversible-deactivation radical polymerisation (RDRP) has opened up the possibility to exert control over the number-average molecular weight (M_n) and dispersity (D), and to access well-defined and complex architectures *via* a free radical process. This is achieved via the implementation of a reversible termination or reversible transfer reaction inducing an equilibrium between active propagating species and their dormant form. Figure 2 shows the molecular weight distributions and molecular weight evolution (M_n vs Conversion) for RDRP and conventional radical polymerisation. It is important to notice that in a RDRP a linear increase in M_n *with* conversion is expected, while for the conventional radical process, M_n increases rapidly with conversion and reaches a plateau.

There is an extensive and growing research interest in RDRP in $scCO_2$.¹⁷ However, in this project we focus on reversible addition-fragmentation chain transfer (RAFT),⁶ which is a well-established, robust and versatile RDRP technique based on a reversible and degenerative

chain transfer.²³ The reaction conditions for RAFT polymerisation are very similar to conventional radical polymerisation, with the addition of a chain transfer agent (CTA; Z-C(=S)-SR) that can be a dithioester, a trithiocarbonate, a dithiocarbonate (xanthate) or a dithiocarbamate.^{24, 25} In addition, RAFT synthesised polymers are free from undesirable metal

(A) Reversible-Deactivation Radical Polymerisation



(B) Conventional Radical Polymerisation

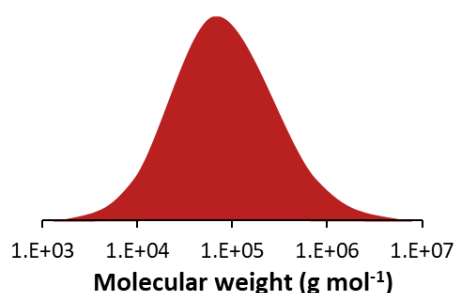


Figure 2 – Representation of the final molecular weight distribution and of the molecular weight vs conversion in a RDRP (A) and molecular weight distribution in a conventional radical polymerisation (B).

catalysts that can be present in other RDRP techniques, *e.g.* atom transfer radical polymerisation.²⁶

Transposition of RDRP from homogeneous to dispersed systems is not straightforward. Radical polymerization in heterogeneous systems is more complex than homogeneous systems due to various mechanistic aspects, *e.g.*, entry/exit events into particles and compartmentalisation, as well as aspects related to colloidal stability. As an example, the early attempts to implement RDRP based on reversible termination, using nitroxide mediated polymerisation for styrene in dispersion in decane²⁷ or alcohols²⁸ showed long polymerisation

times, low conversion, broad particle size distribution and poor control, with broad molecular weight distribution and M_n away from target. This occurs because in RDRP a large number of chains remain inactive and grow slowly at the same time.

In a conventional radical polymerisation, chains of high molecular weight form at an early stage, *i.e.*, already for very low conversions, which leads to a rapid nucleation. In fact, in a conventional dispersion polymerisation J_{crit} of an individual chain is reached in $\ll 1$ s.²⁹ Once the nuclei are formed, any further polymer formed precipitates into the nuclei and grows the particle. By contrast, when using RAFT, the slow formation of many low molecular weight chains all growing at the same rate, as molecular weight increases linearly with conversion, delays the nucleation. Therefore, J_{crit} will be achieved at much higher conversion for RAFT and, consequently, it affects both the nucleation and stability of the resulting particles and the further control of their polymerisation once the particles have been formed.^{30, 31}

The effect of nucleation in a dispersed system can be more easily noticed on the particle size distribution. A short nucleation stage is required for all particles to form simultaneously and grow to the same size. As the RDRP elongates the nucleation, the particle size distribution is broadened.³²⁻³⁴ However, if the J_{crit} is very low, relatively low dispersities in particle size can be obtained.^{35, 36} This will be intrinsic to each monomer/solvent system, but J_{crit} can be also decreased by reducing the initial monomer concentration and thus decreasing the solubilising power of the continuous phase.

This effect of long nucleation in RDRP was rationalised by Winnik and Song.³⁷ They studied the dispersion polymerisation of styrene *via* RAFT and iodine transfer polymerisation (ITP), another RDRP technique based on reversible chain transfer, conducted in ethanol or mixtures of ethanol and water. To achieve successful control of the polymerisation and a narrow particle size distribution, the authors developed a two-stage approach in order to take advantage of the efficient nucleation in a conventional radical dispersion polymerisation.

In other words, first, it is necessary to have a conventional dispersion polymerisation to achieve J_{crit} fast and form nuclei, and only after nucleation is the CTA added and thus can start controlling the polymerisation of further monomer. This approach will unavoidably form a bimodal distribution with a lower M_n population grown via RDRP and a higher M_n population grown in a conventional way. The authors observed two peaks at 4.5 hours, 6% conversion: a large and broad peak $M_n \approx 16\ 000$ g mol⁻¹ and $\mathcal{D} = 2.4$ corresponding to the polymer formed

in the first stage; and a smaller, narrower peak $M_n \approx 800 \text{ g mol}^{-1}$ and $\mathcal{D} = 1.15$, corresponding to the oligomers formed in the presence of the CTA (Figure 3).³⁵

However, as J_{crit} is achieved at very low monomer conversions, below 6% monomer conversion in this case, the number of high molecular weight polymer chains is negligible at

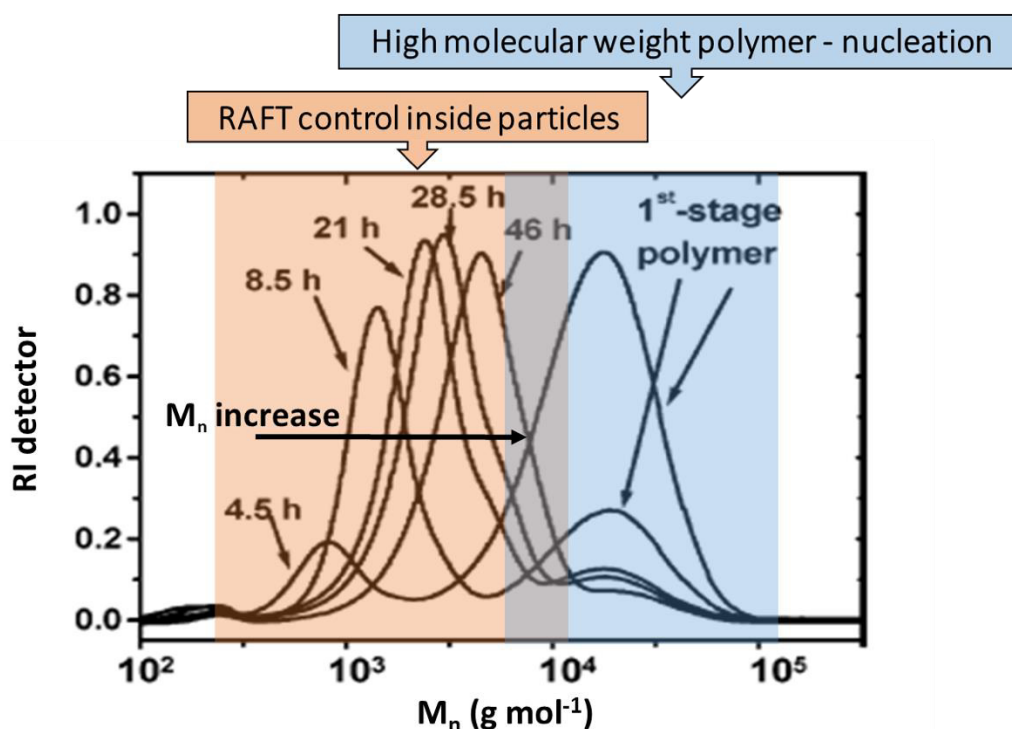


Figure 3 – SEC chromatograms of polystyrene from the latex particles prepared by Winnik and Song using their two-stage approach for RAFT-mediated dispersion polymerization in ethanol-water (95/5, w/w) at different reaction times (St : CTA : initiator – 200 : 2 : 1 mole ratio).³⁷ All traces presented are from after the addition of the CTA. The first traces, 4.5 h and 8.5 h, show the high molecular weight distribution of the polymer generated in the first-stage, highlighted in blue. As the reaction progresses, the second molecular weight distribution, under RAFT control, is shifted towards higher molecular weight values and becomes the dominant population, highlighted in orange. Figure adapted from Winnik and Song.³⁵

reaction completion. As can be noticed in Figure 3, the prominent distribution (blue) from the first stage of the reaction observed at 4.5 hours becomes less significant with time. At 8.5 h: $M_n = 1.3 \text{ kg mol}^{-1}$, $\mathcal{D} = 1.19$; At 21 h: $M_n = 2.2 \text{ kg mol}^{-1}$, $\mathcal{D} = 1.38$; At 28.5 h: $M_n = 2.7 \text{ kg mol}^{-1}$, $\mathcal{D} = 1.47$; and at the end of the reaction, 46 h, $2.0 \text{ }\mu\text{m}$ isometric particles were obtained, coefficient of variance < 3%, with a final $M_n = 4.0 \text{ kg mol}^{-1}$ and $\mathcal{D} = 1.49$.

This study opened the way for RDRP in dispersion with the simple adaptation of the two-stage dispersion polymerisation approach.

4.2.3. RAFT dispersion control in scCO₂

scCO₂ has low viscosity, almost one order of magnitude lower than a typical solvent, and high diffusivity, up to two orders of magnitude higher than for small molecules in typical solvents.⁶ These characteristics, allied to the low solubility of most polymers and the plasticisation effect of scCO₂, make it an interesting medium for dispersion RAFT polymerisation.

In a dispersion polymerisation, the *locus* of reaction is mostly associated to the particles after nucleation. Therefore, after J_{crit} is reached, the RAFT moieties are expected to be located inside the particles, *i.e.* CTA end-group in the insoluble polymeric species, thus the higher mobility of species in scCO₂ and the plasticisation of the polymer are expected to facilitate the access of monomer and oligomers to the growing chain ends. In addition, the low solubility of polymers in scCO₂ is expected to decrease the J_{crit} with respect to conventional solvents, and thus accelerate nucleation and improve control over molecular weight, particle size and molecular weight distributions.

In 2007, dispersion RAFT polymerisation of methyl methacrylate (MMA) in scCO₂ was reported using a dithiobenzoate CTA,³² and this was the main monomer studied in this thesis. Reasonable control was observed; $\bar{D} \approx 1.5$ with good agreement between theoretical and

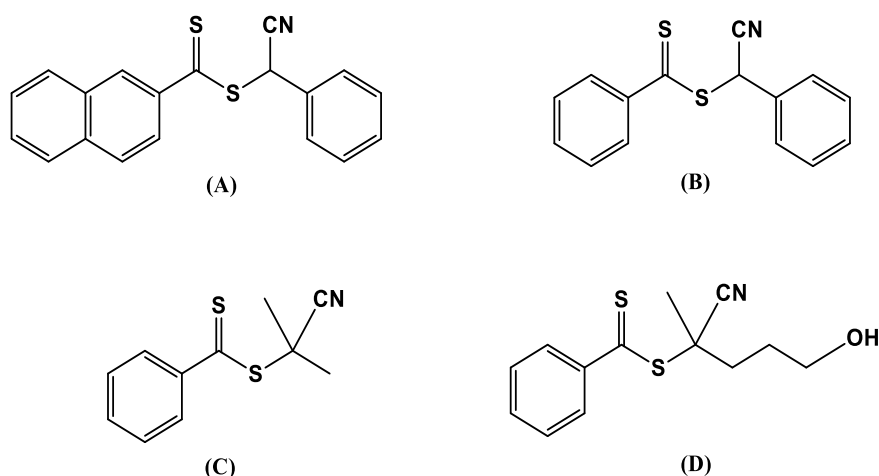


Figure 4 – CTAs tested in previous literature by Gregory et al.³³ (A) α -cyanobenzyl dithionaphthalate, (B) α -cyanobenzyl benzodithioate, (C) 2-cyano-2-propyl benzodithioate (CPDB), (D) 4-cyano-1-hydroxypentyl benzodithioate (CPOB).

experimental M_n , and the product was obtained at high conversion as a free-flowing powder, with 1–2 μm spherical particles. Subsequently, a more detailed study on the effects of three dithiobenzoate and a dithionaphthalate as CTAs for MMA polymerisation in scCO_2 was reported (Figure 4).³³ All polymerisations gave fine, free-flowing powder at high conversion (> 90%), with $\sim 1.4 \mu\text{m}$ spherical particles (Figure 5).

Very prolonged induction periods (5–13 h) were observed for the four CTAs (Figure 4);³³ much longer than in bulk/solution.³⁸ A long induction period can be partially attributed to the addition-fragmentation pre-equilibrium (See Section 1.3.3.) of those CTAs. Nevertheless, all four CTAs resulted in a linear evolution of M_n with conversion, leading to M_n close to target

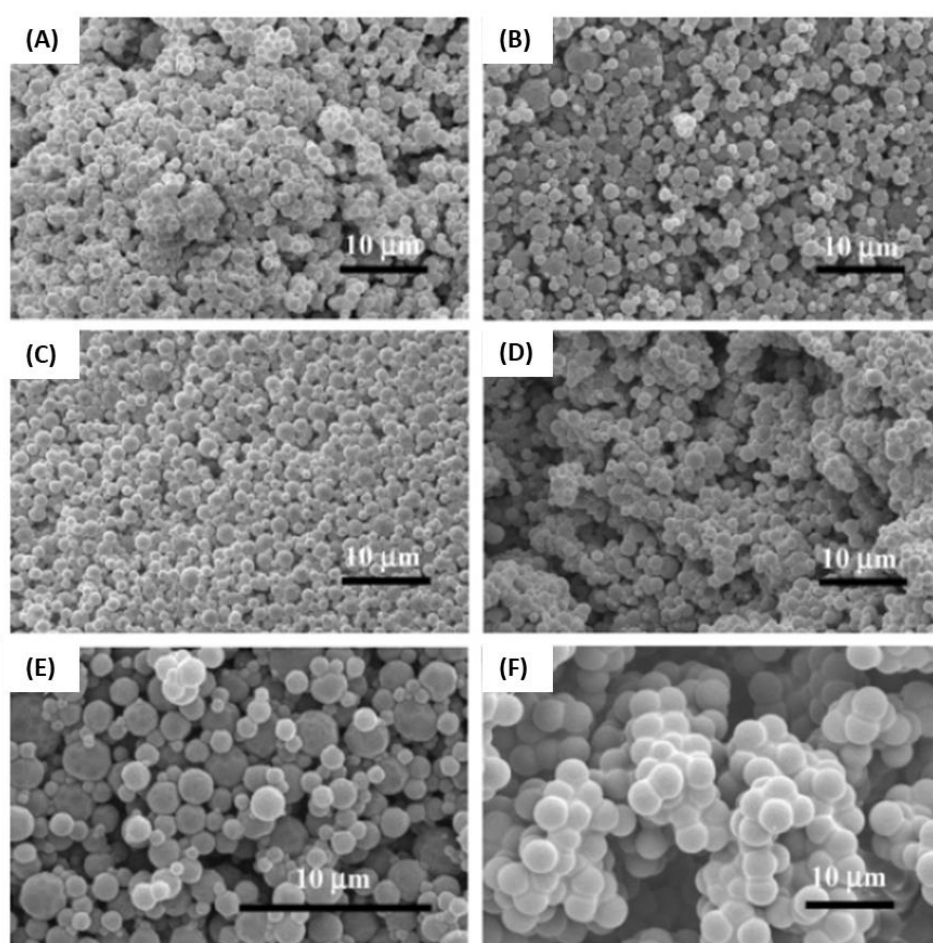


Figure 5 - SEM images showing discrete PMMA particles synthesised by Gregory et al.³³ (A) using CTA A-Figure 4, $d = 1.29 \mu\text{m}$, coefficient of variance (C_v) = 31.0%. (B) using CTA B-Figure 4, $D_n = 1.43 \mu\text{m}$, $C_v = 43.8\%$. (C) using CTA C-Figure 4, $D_n = 1.40 \mu\text{m}$, $C_v = 43.0\%$. (D) using CTA D-Figure 4, $D_n = 1.39 \mu\text{m}$, $C_v = 29.8\%$. (E) shows the higher magnification image of PMMA sample formed with CTA B-Figure 4, and (F) shows the product when no CTA was added, $D_n = 3.91 \mu\text{m}$, $C_v = 6.73\%$. Figure adapted from Gregory et al.³³

and low D (~ 1.20),³³ in accordance with a successful transposition of RAFT polymerisation from solution polymerisation in conventional solvents to $scCO_2$ dispersion polymerisation.

This excellent control across all the CTAs tested by Gregory *et al.* can be ascribed to the selection of CTAs carrying R reinitiating groups leading to strongly stabilised expelled radicals after fragmentation which are well known to be suited for RAFT polymerisation of methacrylates.³⁸⁻⁴⁰ In addition, the authors explained that good control over dispersion polymerisation in a single step could be attributed to the high mobility of species in the polymer particles that were highly plasticised by the $scCO_2$, thus providing a much reduced viscosity in the particles.³³

An additional contributing factor to the control in the reaction is thought to be the reduction of J_{crit} , due to the low solvation power of $scCO_2$ for PMMA when compared to other conventional solvents.³³ They speculated that the lower the J_{crit} , the smaller would be the CTA effect in delaying nucleation, thus, leading to better control. It is interesting to notice that particle size was smaller and particle size distribution was higher for RDRP controlled reactions (Figure 5 A-E) than for the conventional radical polymerisation (Figure 5 F). Therefore, the RDRP delayed nucleation enough to impact over the particle size distribution, although not as significantly as in conventional solvents.

Neither of the authors' hypotheses, the high mobility of species or the lower J_{crit} , has been proven so far. Nevertheless, it is clear that a two-stage polymerisation is not required in $scCO_2$ to obtain good control and well-defined morphology.

4.2.4. RAFT control in $scCO_2$ with DDMAT

Trithiocarbonates are also known to be good CTAs for the polymerisation of "more-activated monomers" (MAMs), such as MMA.⁴¹ However, as mentioned above, the choice of the R group is critical in the case of methacrylates, with the most effective CTA carrying R reinitiating group leading to strongly stabilised radicals such as a tertiary cyanoalkyl or cumyl.⁴² Indeed, DDMAT (2-(dodecylthiocarbonothioylthio)-2-methylpropionic acid), which has a tertiary alkyl -R reinitiating group, is known to be a good CTA for acrylates, but not applicable for methacrylates,⁴³ as it is well documented for RAFT solution polymerisation.⁴²

Therefore, it was very surprising that initial CTA screening for the preparation of block copolymers, from unpublished works in the Howdle research group, had shown that both

DDMAT and the dithiobenzoate 2-cyano-2-propyl benzodithioate (CPDB, Figure 4) could give similar control, *i.e.*, low \bar{D} and good agreement between theoretical and experimental M_n , over MMA polymerisation. This similar result was obtained despite the different chain transfer constants (C_{tr}) of the CTAs. This initial outcome, led to the successful synthesis of block copolymers based on PMMA, poly(benzyl methacrylate) (PBzMA), poly(4-vinyl pyridine) (P4VP), poly (dimethylaminoethyl methacrylate) (PDMAEMA), polystyrene (PSt) and N,N-dimethylacrylamide (PDMA). As a result, the group has developed a wide range of block copolymer particles with internal nanostructures. These block copolymer particles were obtained starting from PMMA particles synthesised via DDMAT-mediated RAFT dispersion polymerisation in $scCO_2$ (Figure 6).^{16, 44}

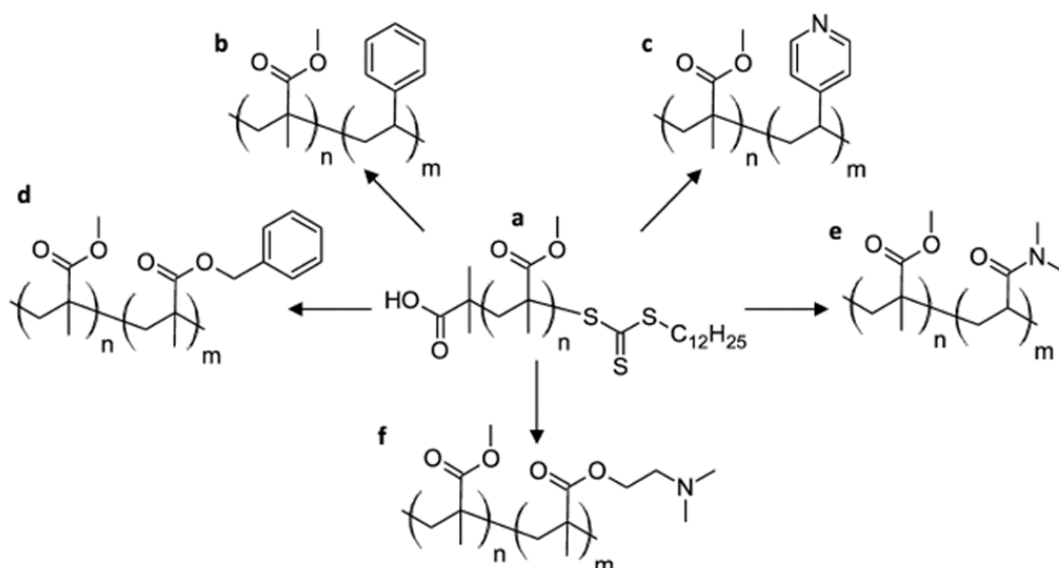


Figure 6 - Chemical structures of the block copolymers synthesised via RAFT dispersion polymerisation in $scCO_2$ by Jennings *et al.* All blocks were extended from (a) PMMA macro-CTA synthesised with DDMAT, (b) PMMA-*b*-PSt, (c) PMMA-*b*-P4VP, (d) PMMA-*b*-PBzMA, (e) PMMA-*b*-PDMA, (f) PMMA-*b*-PDMAEMA. Figure modified from Jennings *et al.*¹⁶

But this was very puzzling, as DDMAT is not a good choice of CTA for this reaction. So, how could it control the reaction so well? At the time, the PMMA chain extension was performed without studying in detail the possible mechanism of control. The group further built upon these data to develop fine control of the internal morphology that arises from phase separation for a series of PMMA-based block copolymer microparticles and these were studied *via in situ* small-angle X-ray scattering (SAXS).⁴⁵

In addition in the previous chapter, *i.e.*, Chapter 3, we have seen that the addition of DDMAT to MMA polymerisation mediated by a scCO_2 -soluble macro-CTA improved control over molecular weight and molecular weight distribution.

So why does the DDMAT work well in scCO_2 ? This chapter will focus on our attempts to better understand the RAFT polymerisation of MMA in scCO_2 dispersion polymerisation, and more broadly to better understand the reaction process and parameters that should be considered for the selection of the best CTAs for successful RAFT or more generally speaking RDRP dispersion polymerisation in scCO_2 .

4.3. Aims

The aims of this Chapter are as follow:

- To understand how DDMAT can control the RAFT dispersion polymerisation of MMA in scCO_2 despite its low C_{tr} towards methacrylates.
- To propose a mechanism of RAFT polymerisation in scCO_2 .
- To test other CTAs for polymerisation of MMA in scCO_2 , and understand what are the requirements for a CTA to control well this RAFT polymerisation.

This is important to fill the gap in the understanding of RAFT polymerisations in scCO_2 and thus allow future investigations in the field to make assertive choices of CTAs. A better RAFT control in scCO_2 will allow the synthesis of complex polymer architectures, such as multiblock, graft and star block copolymers, in a nontoxic solvent and greener approach. Therefore, advancing research into advanced materials for applications ranging from electronics and catalysis, to medical and pharmaceutical.

4.4. Experimental

4.4.1. Materials

MMA was purchased from ProSciTech (99 %) and was filtered through aluminium oxide to remove the stabiliser prior to polymerisation. 2,2'-azobis(isobutyronitrile) (AIBN) was purchased from Sigma Aldrich (98%) and purified by recrystallisation in methanol prior to use.

All other chemicals were used as received. All CTAs were purchased from Sigma-Aldrich, with exception of PDMAT and CTPPA. The synthesis of PDMAT is reported in the next section, while CTPPA was synthesised according to previous work.⁴⁶ Methacrylate terminated polydimethylsiloxane (PDMS-MA) 10 kg mol⁻¹ was purchased from ABCR GmbH & Co. Heptane, toluene, tetrahydrofuran (HPLC grade), deuterated chloroform (CDCl₃) and methanol were all purchased from Fischer Scientific.

4.4.2. Synthetic Procedures

4.4.2.1. Standard RAFT solution polymerisation in toluene

A typical procedure in which PMMA with a molecular weight of 60 kg mol⁻¹ was targeted, used AIBN (0.017 mmol), CTA (0.083 mmol), MMA (49.9 mmol) and 5 mL of toluene. All reactants were transferred to a 25 mL Schlenk tube with a magnetic stirrer, which was then sealed and degassed by at least three freeze-pump-thaw cycles. The tube was then heated to 65 °C in an oil bath and agitated by magnetic stirring. Samples were taken periodically with a syringe for analysis. After 24 hours, the vessel was cooled and the polymer was precipitated from solution in a ~10-fold volume of methanol, filtered and dried *in vacuo*. The product was then analysed by THF-SEC and proton NMR.

4.4.2.2. Standard RAFT dispersion polymerisation in scCO₂

A typical procedure used an in-house built high-pressure Mk III autoclave (20 mL),⁴⁷ which was degassed by purging with CO₂ at 2 bar for 30 minutes. MMA (33 mmol), AIBN (0.028 mmol), PDMS-MA (5 wt % with respect to MMA) and the CTA (0.055 mmol) were degassed by bubbling with argon for 30 minutes. The reactants were then added to the autoclave through the keyhole against positive pressure of CO₂. The vessel was then sealed and pressurised to 50 bar, heated to 65 °C, and the pressure topped up to 276 bar (4000 psi). The reaction mixture was stirred at 300 rpm with overhead magnet coupled stirrer. After 24 hours, heating was turned off and the reactor was cooled below supercritical conditions before being vented. All products were collected as dry free-flowing powders, unless stated differently, and taken for analysis by THF-SEC and proton NMR

4.4.2.3. Standard dispersion polymerisation in sampling autoclave

A typical procedure used an in-house built high-pressure sampling autoclave consisting of an 60 mL Mk III clamp sealed autoclave⁴⁷ with a cylinder sampling unit as described elsewhere,⁴⁸ which was degassed by purging with CO₂ at 2 bar for 30 minutes. MMA (0.1 mol), AIBN (0.08 mmol), PDMS-MA (5 wt % with respect to MMA) and the CTA (0.17 mmol) were degassed by bubbling with argon for 30 minutes. The reactants were then added to the autoclave through the keyhole against positive pressure of CO₂. The vessel was then sealed and pressurised to 50 bar, heated to 65 °C, and the pressure topped up to 276 bar. The reaction mixture was stirred at 300 rpm with overhead magnet coupled stirrer. At sampling times, the sampling cylinder was loaded with 5 mL of deuterated chloroform and attached to the autoclave. A fraction of the reaction mixture was sampled into the small pipe space before the cylinder. The sampling caused a small pressure drop; therefore, pressure was topped up with an extra 14 bar prior to sample collection to avoid fluctuations below reaction conditions. The content of the pipe was then sprayed into the cylinder and collected into chloroform. The samples were analysed *via* THF-SEC and proton NMR.

4.4.2.4. Standard dispersion polymerisation in scCO₂ in static view cell

A typical procedure used an in-house built high-pressure static view cell, which was degassed by purging with CO₂ at 2 bar for 30 minutes. MMA (0.1 mol), AIBN (0.08 mmol), PDMS-MA (5 wt % with respect to MMA) and the CTA (0.2 mmol), if used, were degassed by bubbling with argon for 30 minutes. The reactants were then added to the autoclave through the keyhole against positive pressure of CO₂. The vessel was then sealed and pressurised to 50 bar, heated to 65 °C, and the pressure topped up to 276 bar. The reaction mixture was stirred at 300 rpm with overhead magnet coupled stirrer. The reaction was monitored and recorded throughout the nucleation phase until complete blockage of back light.

4.4.2.5. Standard two-stage polymerisation

A typical procedure used an in-house built high-pressure autoclave coupled to a HPLC pump. The autoclave was loaded with two thirds of the total MMA (0.1 mol), of AIBN ($2.8 \cdot 10^{-5}$ mol), and PDMS-MA (5 wt% in relation to the total monomer). The pressure and temperature were raised to 276 bar and 65 °C and the reaction proceeded for 45 minutes prior to injecting a degassed solution of CPAB in MMA (0.51 mol L⁻¹) via HPLC pump. The pump operated at 0.2

mL min⁻¹ and injection was performed for 5:30 min, giving a total of 5.6 10⁻⁵ mol CPAB injected. This ensured a load of CPAB equivalent to previous reactions performed with this CTA, and with CTA/AIBN ratio 2:1. The full procedure for injection via HPLC can be found at Section 2.3.5. After the injection, the reaction was allowed to proceed for 24 hours. Heating was then turned off and the reactor was cooled below supercritical conditions before being vented. All products were collected as dry free-flowing powders, unless stated differently, and taken for analysis by THF-SEC and proton NMR

4.4.2.6. Synthesis of 2-(propylthiocarbonothioylthio)-2-methylpropionic acid (PDMAT)

The shorter Z-group CTA equivalent to DDMAT, PDMAT, was synthesised according to Lai *et al.*⁴³ A solution of 40 mmol propanethiol (3.06 g; 0.040 mol) in 24 mL acetone and 1 mol% of Aliquat 336, as phase transfer agent, was cooled at 10 °C. A solution of 50 wt% NaOH (3.5 mL) was added dropwise, followed after 15 minutes by the addition of carbon disulfide (3.05 g; 40 mmol) dissolved in 5 mL acetone. Then 4.8 mL of chloroform were added, followed by the dropwise addition of 16 mL 50 wt% NaOH solution. The reaction was stirred at 0 °C for 2 hours and then left stirring at room temperature overnight. The following day, the medium was acidified to pH < 2 with HCl, and then extracted with diethyl ether. The ether solution was dried over magnesium sulfate before removal of the solvent under vacuum. The yellow oily medium obtained was purified by chromatographic column eluting with 10% (v/v) ethyl acetate/hexane. The final product was a yellow oil. The ¹H NMR spectrum is presented in the appendix – Figure S1.

¹H NMR (400 MHz, CDCl₃), δ (ppm): 3.27 (t, J = 7.4 Hz, 2H), 1.72 (m, 8H), 0.99 (t, J = 7.4 Hz, 3H). ¹³C NMR (100 MHz, CDCl₃), δ (ppm): 221.2, 178.3, 56.4, 39.2, 25.3, 25.0, 13.9.

4.4.2.7. Synthesis of 4-cyano-4-thiothiopropylsulfanylpentanoic acid (CTPPA)

The synthesis of CTPPA was achieved by following a procedure previously reported.⁴⁶ Carbon disulfide (4.16 mL; 0.065 mol) was added at 0 °C drop by drop to sodium propanethiolate (5.59 g; 54 mmol) dispersed in THF (75 mL). The mixture was stirred for one hour at room temperature and then filtered. After evaporation of the solvent under vacuum, an orange solid was obtained. This latter was dissolved in deionized water and the solution was cooled at 0 °C. Potassium ferricyanide (20.68 g; 62 mmol) dissolved in deionized water (60 mL) was added dropwise to the solution under stirring. The mixture was left under stirring during one

hour at room temperature. Diethyl ether was then added to the mixture to extract the organic phase. Aqueous phase was washed several times with this same solvent (30 mL). The organic phases were grouped and dried on anhydrous MgSO_4 and the ether was evaporated, giving an orange oil (bis(propylsulfanylthiocarbonyl) disulfide).

Bis(propylsulfanylthiocarbonyl) disulfide (6.80 g; 22 mmol) was dissolved in 130 mL of ethyl acetate. Then, 1.1 equivalents of 4,4'-azobis(4-cyanopentanoic acid) (7.85 g; 25 mmol) were introduced. The reaction medium was placed under reflux overnight at 98 °C. The following day, the solvent was evaporated under vacuum. A column purification was performed with diethyl ether/heptane (1:2 v/v ratio) as eluent and then with pure ethyl acetate. After solvent evaporation, a very viscous orange oil was obtained. The ^1H NMR spectrum is presented in the appendix – Figure S2.

^1H NMR (CDCl_3 , 300 MHz, δ ppm): 3.3 (t, 2H, $\text{CH}_2\text{-S}$); 2.3-2.8 (m, 4H, $-\text{CH}_2\text{-CH}_2\text{-COOH}$); 1.8 (s, 3H, $\text{CH}_3\text{-C}(\text{CN})$); 1.7 (m, 2H, $\text{CH}_2\text{-CH}_3$); 1.0 (t, 3H, CH_3).

4.4.3. Standard solubility test in scCO_2 in variable volume view cell

Solubility test of CTAs was carried out in a stainless-steel variable volume view cell, with a front sapphire window and a back mobile sapphire piston that can be moved by a hydraulic intensifier unit. An accurately weighed amount of CTA (a typical quantity was 0.5 mmol), was added as a solid into the chamber and the system was purged with CO_2 for 30 minutes at room temperature. Then, 33 mmol of MMA were added into the chamber through the keyhole and the system was filled with 20 g of CO_2 using a syringe pump and heated to the desired temperature. At each temperature set point, the pressure was increased until the solute became soluble and only one phase was visible. The pressure was then reduced slowly while monitoring the phase behaviour until the cloud point (point at which the backlight is completely obscured). The process was repeated three times and an average of the cloud point pressure was taken as the cloud point at that temperature.

4.4.4. Computational modelling of CTA solvation

To emulate the important quadrupolar moment of CO_2 in the supercritical state, the EPM2 model was used,⁴⁹ which is purely based on point charges. Hence, in our solvation model it is specifically fitted to the potential of supercritical CO_2 . The CTA molecules were described by

the CHARMM general force field (CGenFF). The size of the cubic box was set as 10 nm initially. MD simulations were performed using the GROMACS package (v2019)⁵⁰ with NPT ensemble at 338.15 K and 276 bar coupled by the Berendsen model. This resulted in a supercritical fluid with a density of 0.657 g cm⁻³. The time step was 1 fs. The cut-off length for intermolecular potential calculations was 1.2 nm. Ewald summation was adopted to compute the long-range electrostatic interactions. The system was simulated for 100 ns for the production dynamics. For toluene, the potential was obtained from <http://virtualchemistry.org/>. MD simulations were performed with NPT ensemble at 338.15 K and 14.5 psi (room pressure) coupled by the Berendsen model. The density of the solvent was thus 0.845 g cm⁻³. The other details of the simulation protocol were as for the CTA simulation.

4.4.5. Polymer characterisation

The M_n and D of polymers were obtained by size exclusion chromatography (SEC) (PL-120, Polymer Labs) using a refractive index (RI) detector. The columns (30 cm PLgel Mixed-C, two in series) were eluted by THF and calibrated with PMMA standards. Calibration and analysis were performed at 40 °C with a flow rate of 1 mL min⁻¹. A UV-vis detector connected to the SEC instrument was used to detect active molecules (free CTAs or macromolecules-bearing CTAs) were performed by using a UV-vis detector. Monomer conversion was determined by proton nuclear magnetic resonance (¹H NMR). The spectra were recorded in CDCl₃ using a Bruker DPX 400 MHz spectrometer, and referenced to CDCl₃ at 7.26 ppm. Scanning electron microscopy (SEM) images were obtained using a JEOL 6060V SEM machine at various magnifications and an accelerating voltage of 10 kV. Samples were mounted on aluminium stubs using adhesive carbon tabs and sputter-coated with platinum before analysis. Mean particle diameter (D_n) was determined by measuring the diameter of 100 particles in ImageJ[®] and taking a mean of these data. The coefficient of variance (C_v) was calculated by the ratio of the standard deviation (σ) by the mean particle diameter (Equation (1)).

$$C_v = \sigma/D_n \times 100 \quad (1)$$

4.5. Results and discussion

4.5.1. RAFT control of MMA polymerisation in scCO₂ with DDMAT

As presented in the introduction, DDMAT is not an ideal choice of CTA for the controlled polymerisation of MMA. However, it has been successfully used as CTA for the preparation of PMMA macro-CTAs in scCO₂, which were then used to synthesise block copolymers. The mechanism for such unusual result was not studied and therefore the question remained: Why does DDMAT control well the polymerisation of MMA in scCO₂?

In this section, we investigate the polymerisation of MMA in scCO₂ mediated by DDMAT. The results are compared to the solution polymerisation of MMA in toluene. We then further investigate the kinetics and the early stages of the reaction, with the aim of better understanding how DDMAT can control the polymerisation of MMA in scCO₂.

4.5.1.1. Comparison of solution polymerisation in toluene and dispersion polymerisation in scCO₂ with DDMAT.

DDMAT (CTA 1, Figure 7) was used as CTA for the polymerisation of MMA both in toluene solution and in dispersion in scCO₂ to assess the control given by this unconventional choice of CTA for a methacrylate polymerisation.

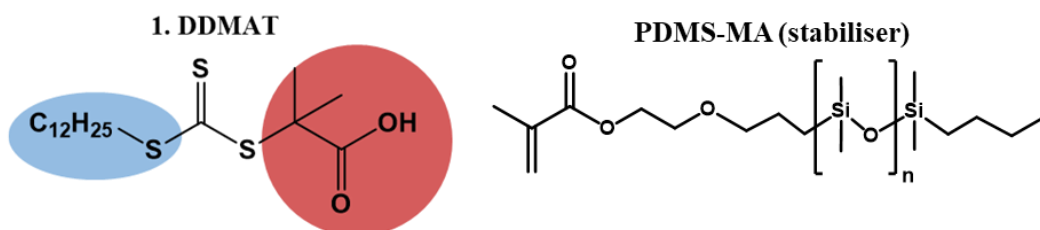


Figure 7 - Chain transfer agent (CTA) structure 1: DDMAT (2-(Dodecylthiocarbonothioylthio)-2-methylpropionic acid), with the R group in red and the Z group in blue; and the stabiliser PDMS-MA (methacrylate terminated polydimethylsiloxane, $M_n=10 \text{ kg mol}^{-1}$).

The RAFT solution polymerisation in toluene was performed using AIBN as initiator with a CTA/AIBN ratio of 5:1 (E1.1, Table 1). The results confirm the inability of DDMAT to finely control MMA polymerisation, leading to PMMA chains with a large molecular weight dispersity ($\mathcal{D} = 1.60$) and a final M_n that does not match the expected theoretical value ($M_n = 82.3 \text{ kg mol}^{-1}$ vs. $M_{n,\text{th}} = 40.1 \text{ kg mol}^{-1}$).

This is not surprising giving the known poor control of DDMAT towards methacrylates. Rizzardo *et al.* undertook a study with different CTAs mediating the polymerisation of MMA and found that Z moieties with an electron-withdrawing group (*e.g.* benzyl ring) enhance addition to the C=S bond, due to the increased electrophilic character of the thiocarboxylic sulfur; while electron-donating groups (*e.g.* thiododecyl group, as in DDMAT) impair addition to the C=S bond.⁵¹

For dispersion polymerisations in scCO₂, the temperature and pressure were selected to ensure solubility of the PDMS-MA, which acts as a stabiliser in the process.⁵² The CTA/AIBN ratio used in scCO₂ (2:1) was lower than in toluene (5:1). The use of higher concentrations of initiator was established previously,^{9, 16, 33} because the rate of decomposition of AIBN in scCO₂ is 2.5 times slower than in the equivalent reactions in benzene.⁵³ The higher initiator concentration at the start of the reaction ensures a reasonable radical generation for the initiation of polymer chains.

For clarity, the role of PDMS-MA (Figure 7) is to stabilise the nuclei formed during the initial stages of the reaction. The rate of consumption of the stabiliser is not fully known, but there is good evidence that it is consumed mainly during the initial stages of the reaction, as the concentration of stabiliser influences the final PMMA particle size.^{9, 11} Furthermore, as a macromonomer, we expect that some PDMS-MA will co-polymerise with MMA, but it has been previously reported that only up to 3.5% of the stabiliser is covalently bonded to the final product when copolymerising MMA with ethyl methacrylate and <1% for MMA homopolymer.^{54, 55} The remaining PDMS-MA apparently acts as a stabiliser by anchoring through physical association of the methacrylate terminal group to the PMMA particle surface.

Table 1 - RAFT polymerisation of MMA in toluene and in scCO₂ dispersion polymerisation with DDMAT.

Expt.	Synthesis	Conv ¹ (%)	$M_{n,th}$ ²	M_n ³	\mathcal{D} ³
E1.1	Solution-toluene	66	40.1	82.3	1.60
E1.2	Dispersion-scCO ₂	99	59.4	51.1	1.20
E1.3	Dispersion-scCO ₂	97	57.6	61.5	1.27
E1.4	Dispersion-scCO ₂	98	58.2	62.1	1.18

¹ Conversion calculated from ¹H NMR. ² Theoretical M_n calculated relative to CTA and monomer concentration and given in kg mol⁻¹. ³ \mathcal{D} and M_n (in kg mol⁻¹) obtained by THF-SEC with RI detector against PMMA standards. Molar ratio DDMAT/AIBN 2:1, 65 °C, 276 bar, 300 rpm stirring rate, 5 wt%(based on MMA) of PDMS-MA as stabiliser).

DDMAT led to good control of MMA polymerisation in scCO₂ (E1.2), with $\mathcal{D} = 1.20$ and M_n (51.1 kg mol⁻¹) close to $M_{n,th}$ (59.4 kg mol⁻¹). Two repeats (E1.3 and E1.4) confirmed the reproducibility of the reaction, with good control obtained. This was in agreement with previous unpublished work developed by Howdle research group, but as mentioned in the introduction, it is an unusual outcome for this choice of CTA. Additionally, all reactions proceeded to near completion (> 95%) and a free-flowing powder composed of well-defined spherical particles of average 2.08 μm were obtained for all dispersion reactions in scCO₂ (Table 2, Figure 8).

Table 2 – Particle size analysis of PMMA particles synthesised *via* scCO₂ dispersion polymerisation.

Expt.	D _n ¹ (μm)	C _v ² (%)
E1.2	2.10	16.9
E1.3	2.22	18.4
E1.4	2.09	21.4

¹ Average particle size (D_n) is calculated as an average of 100 particles measurements *via* Image J®. ² The coefficient of variance (C_v) by equation (1);

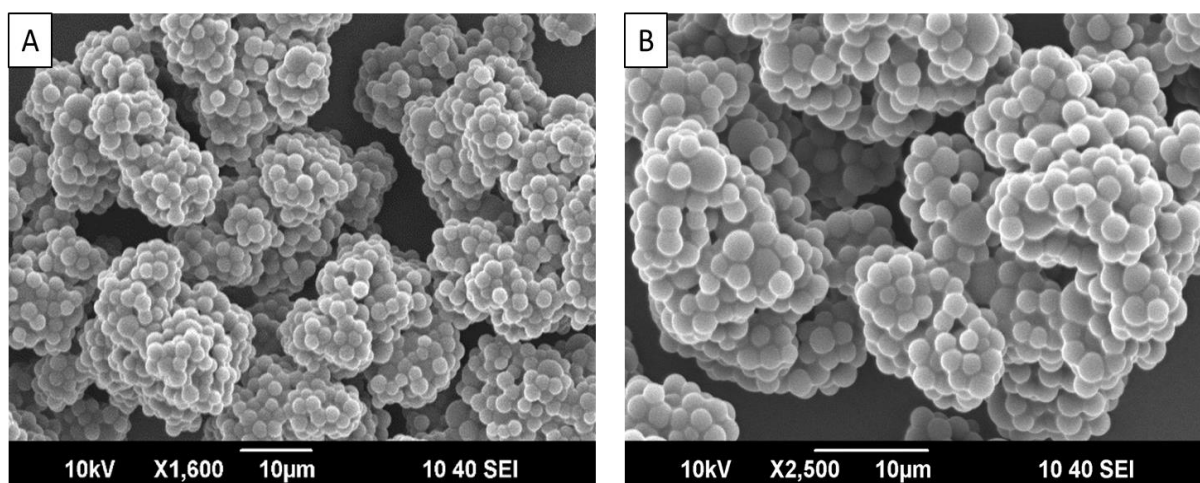


Figure 8 - SEM images of E1.4 obtained using a JEOL 6060LV SEM at accelerating voltage of 10 kV and at A) 1600x magnification and B) 2500x magnification.

These results confirm the good control provided by DDMAT for the polymerisation of MMA in scCO₂ and are consistent with the previous results reported for block copolymers particle syntheses from similar PMMA particles.^{16, 44} Such unexpected results further hint that the control observed in scCO₂ must arise from the mechanisms at play and the physico-chemistry associated with dispersion polymerisation. To investigate this, we then followed the kinetics of the reaction both in toluene and in scCO₂.

4.5.1.2. Kinetic study of MMA polymerisation in toluene and in scCO₂ with DDMAT

The kinetics of a successful RAFT controlled polymerisation, as for other RDRPs, should depict a linear evolution of molecular weight with increase in conversion as shown in the introduction (See section 4.2.2.). Therefore, the MMA dispersion polymerisation in scCO₂ mediated by DDMAT should present this characteristic kinetics if the reaction is occurring *via*

the RAFT mechanism. To verify this, we must track the polymerisation over time. We also followed the kinetics of the RAFT mediated MMA polymerisation in toluene for comparison.

The tracking of ongoing polymerisation reactions in traditional solvents can be easily achieved through a variety of methods.⁵⁶ For this thesis, the solution polymerisation in toluene was tracked by sampling a known volume from the reactor with a degassed syringe at regular intervals. The samples were quenched by crash cooling. The resulting kinetics for DDMAT mediated polymerisation of MMA in toluene showed, as expected, that this CTA does not provide optimum control of the reaction. While the conversion did increase over time (Figure 9A), the THF-SEC analyses (Figure 9B) show that the final dispersity is high ($D > 1.6$) and the final molecular weight is achieved rapidly, while the plot of M_n versus conversion does not feature the characteristic linear trend of a RDRP (Figure 9C).

Monitoring a reaction in $scCO_2$ is more challenging, as the system must remain sealed under elevated pressures. Indirect monitoring techniques such as FTIR⁵⁷, turbidimetry^{52, 58-60} and Raman spectroscopy⁶¹ were previously used to gain information on reaction kinetics. However, they required probes or windows to be added to the autoclave setup, which are substantial modifications, which are expensive and complex to implement.

Therefore, in order to further investigate the physico-chemistry of the dispersion polymerisation in $scCO_2$, we made use of a recently developed sampling system⁴⁸ (See section 2.3.10) to try to combine kinetic information with the already obtained colloidal features of the system. This device consist of an Mk III clamp sealed autoclave⁴⁷ with a high pressure cylinder sampling unit which is inserted into the extraction port in the bottom of the device. Deuterated chloroform ($CDCl_3$) was added into the cylinder to collect the reaction mixture, minimizing any losses of residual monomer. In this way, both molecular weight and conversion could be efficiently monitored.⁴⁸ Previous sampling devices used to this end did not allow accurate conversion measurements due to loss of the volatile monomer.^{33, 62}

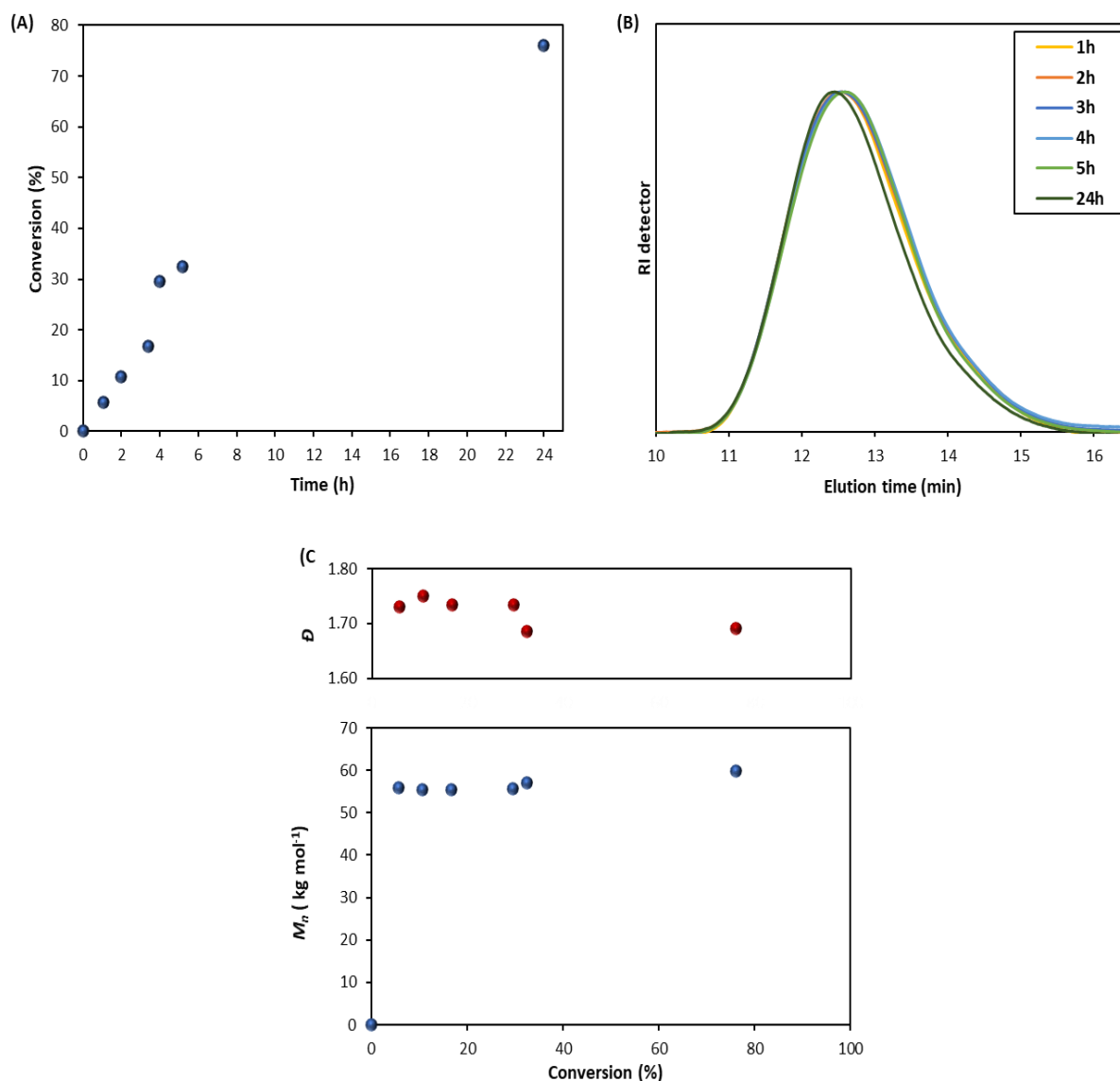


Figure 9 - Solution polymerisation of MMA in toluene using DDMAT as CTA, (A) Evolution of MMA conversion versus time, (B) Normalised SEC traces showing the molecular weight distributions of the samples withdrawn, (C) Evolution of \bar{D} (red) and M_n (blue) versus conversion. (Molar ratio DDMAT/AIBN 5:1, 65 °C, 300 rpm stirring rate, 1:1 volume ratio of toluene to MMA).

A disadvantage inherent to any high-pressure sampling autoclave design is the variation in pressure. Every time a sample is collected, part of the scCO₂ is extracted and the loss of CO₂ causes a pressure drop of up to 14 bar. As pressure is closely linked to solvation properties of supercritical fluids, fluctuations in pressure could affect species solubility and thus the dispersion polymerisation. In order to minimise the impact of pressure fluctuations, CO₂ was slowly added to the autoclave to increase 14 bar in pressure immediately before sampling collection. By this mean, pressure will drop upon collection back to the original pressure and

thus solubility variation is minimised. Additionally, to avoid any possible samples contamination, the content from the sampling port was purged into a small sampling pipe, and the connection at the bottom of the autoclave was cleaned with acetone prior to connecting the high pressure cylinder.

Kortsen *et al.* previously performed a kinetic study via a sequential batch approach to confirm the reliability of the sampling system under conventional radical polymerisation conditions, which used 1 wt% AIBN relative to MMA.⁴⁸ This laborious approach consists on setting several identical reactions that are then quenched by crash cooling at specific reaction time intervals.

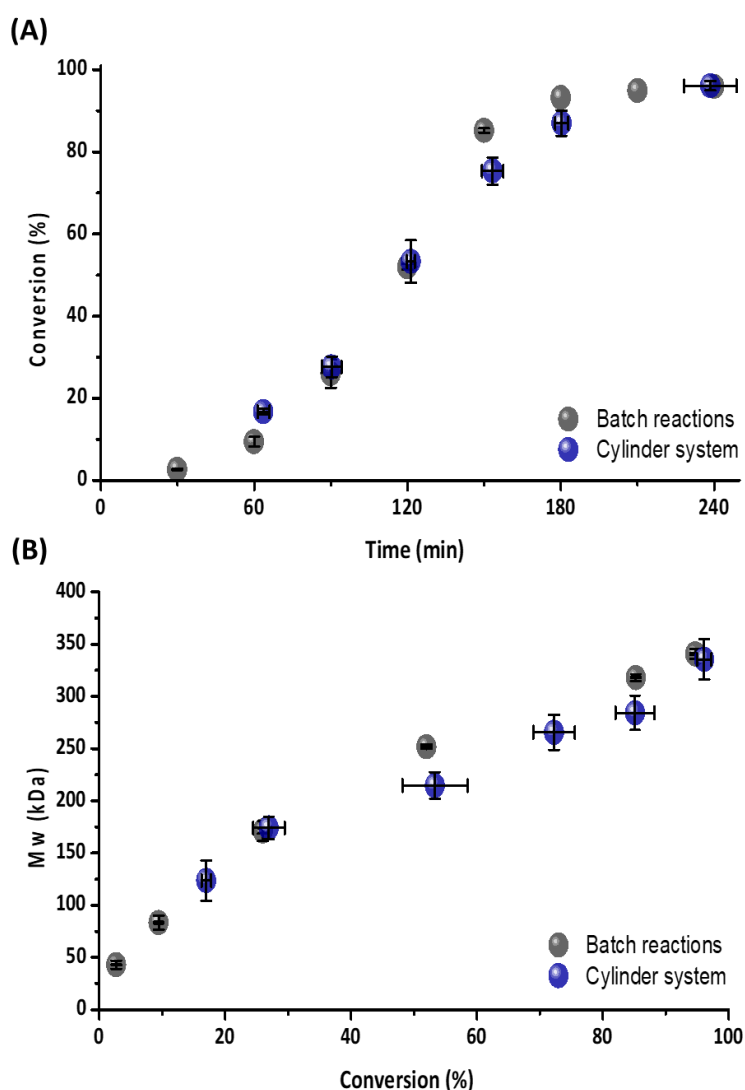


Figure 10 – (A) Conversion of MMA as a function of reaction time and (B) M_w as a function of conversion from samples obtained using the cylinder system (blue) compared to sequential batch reactions quenched by crash cooling (grey). Reaction conditions: 10 mL of MMA, 0.468 g of PDMS-MA, 93.6 mg of AIBN, 220 bar and 65 °C. Figure reproduced from Kortsen *et al.*⁴⁸

The comparison between kinetics results from the batch approach with results from the sampling system proved that samples obtained using the cylinder system are representative of the ongoing polymerisation, as can be seen by the conversion of MMA as a function of reaction time and M_w as a function of conversion (Figure 10).⁴⁸

The application of this sequential batch approach is unviable here considering the longer duration of the RAFT controlled reactions and the timeframe to which this project is restricted. Nonetheless, a batch reaction was set under the same conditions as for the sampling autoclave and quenched after 4 hours of reaction. The resulting product was a viscous opaque liquid since conversion was only 11% as per ¹H NMR. The THF-SEC results were analysed and plotted against the equivalent sample obtained at 4 hours using the sampling autoclave. Both samples shown reasonably similar M_n and conversion (Table 3).

Table 3 – Comparison between MMA dispersion polymerisation in scCO₂ using the sampling autoclave with the batch approach crash cooled at 4 hours of reaction.

Type of sampling	Conv ¹ (%)	$M_{n,th}$ ²	M_n ³	\mathcal{D} ³
Batch approach	11.0	6.9	9.9	1.45
Sampling	13.0	11.0	13.8	1.62

¹ Conversion calculated from ¹H NMR. ² Theoretical M_n calculated relative to CTA and monomer concentration and given in kg mol⁻¹. ³ \mathcal{D} and M_n (in kg mol⁻¹) obtained by THF-SEC with RI detector against PMMA standards. Molar ratio DDMAT/AIBN 2:1, 65 °C, 276 bar, 300 rpm stirring rate, 5 wt%(based on MMA) of PDMS-MA as stabiliser).

The kinetic study of MMA polymerisation with DDMAT was then performed in triplicate using the high-pressure sampling system (Table 4). The study showed increase of the conversion with time (Figure 11A and 11B) and a linear evolution of M_n with monomer conversion while maintaining low dispersity (Figure 11C), as expected for RDRP. However, a deviation from the theoretical trend line, *i.e.*, solid black line, is seen in the early stage of reaction, *i.e.*, 0-40% conversion (Figure 11C). This could be related to the low control of the reaction with DDMAT when the dispersed system behaves as a solution polymerisation, *i.e.*, at low conversions, similar to what was observed in toluene solution polymerisation (Figure 9). The linear trend after 40% conversion ($*M_n$) is close to the theoretical trend line (black solid line) and it should be noted that dispersity was also consistently low ($\mathcal{D} \approx 1.30$) after 40% conversion ($*\mathcal{D}$) until the reaction completion (Figure 11C).

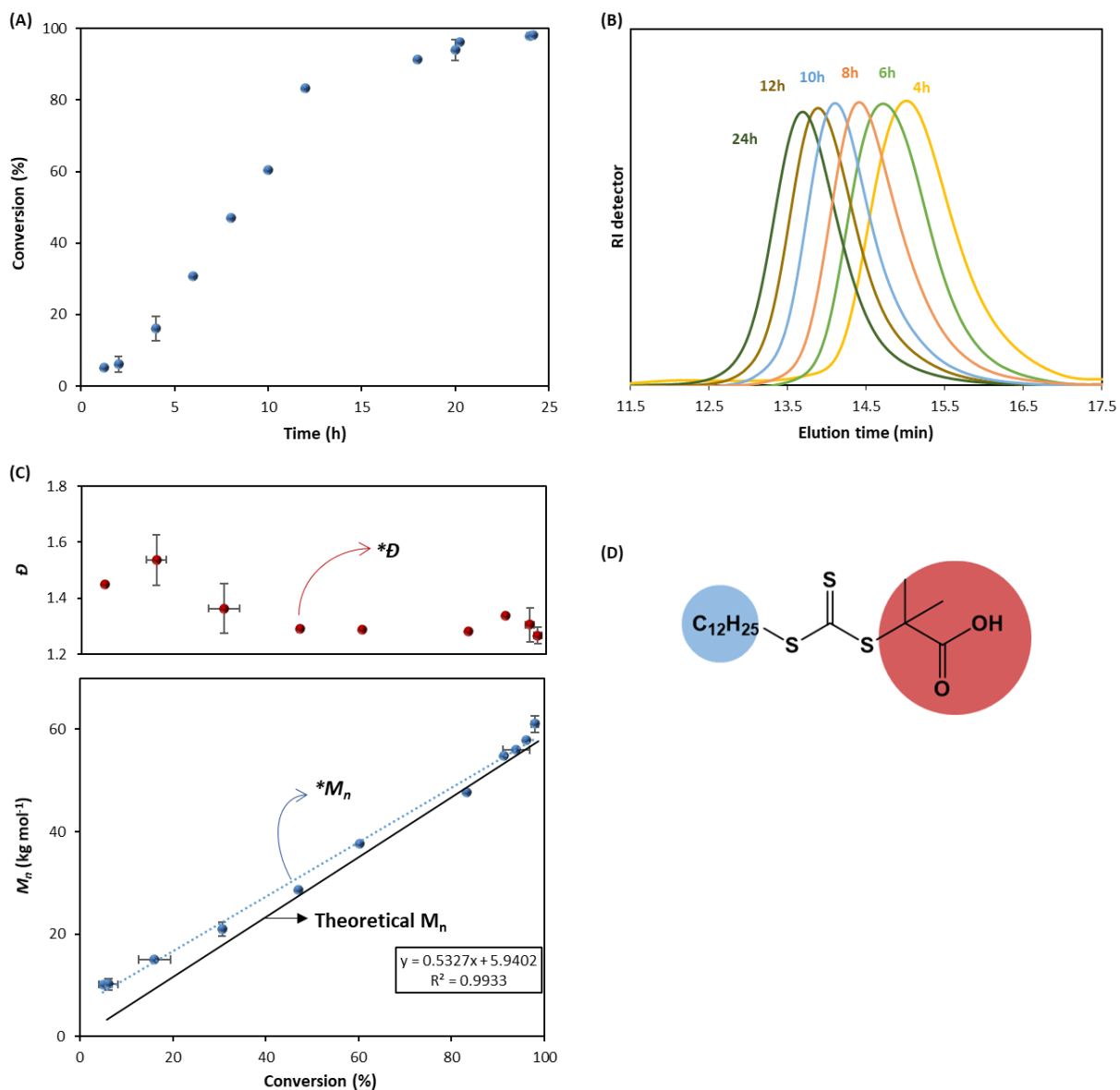


Figure 11 - Dispersion polymerisation of MMA in $sc\text{CO}_2$ using DDMAT as CTA. (A) Evolution of MMA conversion versus time, (B) Normalised SEC traces showing the molecular weight distributions of the samples withdrawn, (C) Evolution of \bar{D} (red) and M_n (blue) versus conversion; solid trend line is the theoretical M_n and dashed trend line is the linear fitting of experimental data, (D) DDMAT structure, with the R group in red and Z group in blue. (Molar ratio DDMAT/AIBN 2:1, 65 °C, 276 bar, 300 rpm stirring rate, 5 wt%(based on MMA) of PDMS-MA as stabiliser). A deviation from expected RDRP behaviour is observed until approximately 40% conversion ($*M_n$ and $*\bar{D}$).

Furthermore, the reaction with DDMAT showed a shorter induction time compared to what was reported by Gregory *et al.*³³ Indeed, they reported induction of up to 13 hours with dithioester CTAs, with no conversion observed before that point. It is important to reiterate

that their data were obtained from much less reliable and older style kinetic measurements. The methodology consisted of sequential batch reactions quenched by crash cooling the reactor at set times, where samples at low conversion were collected by dissolution in THF and precipitated in cold hexane. The further precipitation of product could exclude low molecular weight chains and artificially delay the observation of polymerisation onset. Therefore, their induction period was likely shorter than reported.

Table 4 – Summary of results from MMA dispersion polymerisation kinetics in scCO₂ with DDMAT as CTA. Reaction monitored with the high-pressure sampling system.

Time (h)	Conversion ¹ (%)	M_n ²	\bar{D} ²
2	6.1 (±0.4)	10.2 (±0.1)	1.35 (±0.01)
4	16.0 (±2.1)	15.0 (±1.1)	1.54 (±0.05)
6	30.6 (±3.4)	20.9 (±0.2)	1.36 (±0.05)
8	46.9 (±0.4)	28.6 (±1.4)	1.29 (±0.01)
10	60.3	37.6	1.29
18	91.4	54.8	1.34
20	93.9 (±2.9)	56.0 (±0.4)	1.36 (±0.03)
20.3	96.1	57.9	1.30
24	98.1 (±0.8)	61.0 (±1.6)	1.28 (±0.01)

Results given as average from repeats, standard deviation given in brackets.¹ Conversion calculated from ¹H NMR. ² \bar{D} and M_n (in kg mol⁻¹) obtained by THF-SEC with RI detector against PMMA standards. (Molar ratio DDMAT/AIBN 2:1, 65 °C, 276 bar, 300 rpm stirring rate, 5 wt%(based on MMA) of PDMS-MA as stabiliser).

Therefore, our results with the sampling autoclave confirm the livingness of MMA dispersion polymerisation in scCO₂ with DDMAT and shows the presence of an early stage deviation of the molecular weight evolution compared to the expected trend.

4.5.1.3. Early stage of MMA dispersion polymerisation in scCO₂ with DDMAT

Although the kinetic results do confirm the very good control obtained with DDMAT, they do not rationalise the surprising RAFT control in scCO₂ with this CTA of low C_{tr} towards MMA. In an effort to better understand the process of RAFT dispersion polymerisation in scCO₂, we visually followed the dispersion polymerisation of MMA in a static double window view cell to study the early reaction stages (See Sections 2.3.6 and 2.3.7.). Once the J_{crit} is achieved, the growing polymer becomes insoluble and nucleation starts. The forming particles will cause

the once homogeneous system to become turbid. Thus, the onset of nucleation can be followed by the appearance of turbidity.

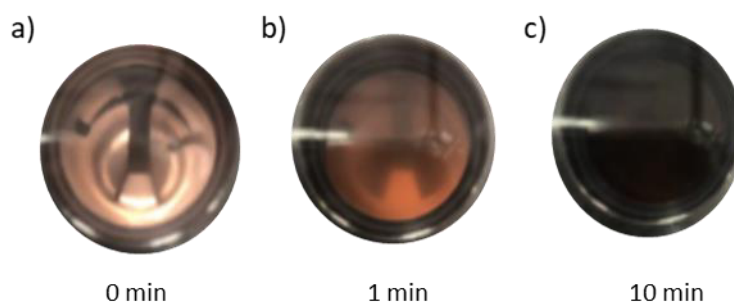


Figure 12 - View cell photographs showing the phase behaviour of the conventional radical dispersion polymerisation of MMA in $scCO_2$. a) Prior to reaction onset the reactants are all soluble in $scCO_2$ and one can see through the view-cell; b) After 1 minute of reaction, turbidity is noticeable; c) At 10 minutes, the passage of light is completely blocked. Reaction set at 276 bar, 65 °C, MMA (0.1 mol), AIBN (0.08 mmol) and PDMS-MA (10 kg mol^{-1} , at 5 wt% relative to MMA).

In the absence of DDMAT, with all other conditions remaining the same, a turbid system was observed within the first minute, in agreement with literature observation.⁵⁹ Complete obscurity, *i.e.* no observable light passing through the view cell, was observed within 10 minutes from the start of the reaction (Figure 12). In fact, Ballauff and Fehrenbacher have previously monitored the early stages ($\leq 300 \text{ s}$) of MMA conventional radical dispersion polymerisation in $scCO_2$ *via* turbidimetry,^{58,59} and observed that nucleation started before 0.1 wt% MMA was converted into polymer. Furthermore, a previous kinetic study of conventional MMA radical polymerisation in $scCO_2$, at 1 wt% AIBN relative to MMA, has shown conversions of 2.6% at 30 minutes from reaction onset.⁴⁸ At that time nucleation has already occurred.

When DDMAT-mediated RAFT dispersion polymerisation was studied, turbidity was first observed 10 minutes after the start of reaction and complete obscurity occurred only after 75 minutes, at which point the conversion was found to be below 4% (Figure 13A). Therefore, nucleation is very clearly delayed by addition of DDMAT. Without DDMAT the timings were 1 minute for start of turbidity and 10 min for total obscurity.

In a well-controlled RAFT polymerisation, the slow growth of the polymer chains leads to J_{crit} being achieved later than in conventional radical polymerisation, resulting in a delayed nucleation. In addition, inhibition and retardation are typically seen in RAFT polymerisation,

in particular with dithiobenzoates. All three, kinetics, inhibition and retardation have to be taken into account as factors able to delay the nucleation in a RAFT controlled dispersion polymerisation.

It is important though to reiterate that nucleation is related to the M_n of the polymer chains and not to monomer conversion. Once the J_{crit} is reached, the polymer will precipitate from solution and start nucleating, regardless of the monomer conversion. The J_{crit} will, however, be influenced by the solvency of the system, with MMA acting as a co-solvent. Therefore, at lower conversions, less MMA has been consumed and more co-solvent is present.

We then repeated the MMA polymerisation targeting 60 kg mol^{-1} using DDMAT as CTA in the sampling autoclave in order to obtain aliquots on the timeframe observed for the nucleation process. Interestingly, THF-SEC analysis of the aliquots taken immediately after turbidity onset, *i.e.*, 10 minutes, showed a dominant PMMA population with high dispersity, $M_n > 400 \text{ kg mol}^{-1}$; $\mathcal{D} = 1.5$ (population **1**), and a second population of much smaller intensity, $M_n \approx 10 \text{ kg mol}^{-1}$, $\mathcal{D} = 1.34$ (population **2**) (Figure 13B). As the reaction progressed, further aliquots revealed that population **2** became the dominant species from 75 minutes into the reaction, 3.8% monomer conversion, as clearly shown by the SEC weight-fraction (%) increase over time (Figure 13C). Population **2** was already >95% of the total weight fraction at the final sampling point of 120 minutes, when monomer conversion was only at 5.7% (Figure 13C).

In addition, population **2** was also found to present a UV signal at 300 nm, characteristic of C=S bond on the trithiocarbonate chain end (Figure 14), strongly indicating that population **2** corresponds to living chains, with the CTA end-group. Indeed, as the reaction progressed population **2** grew steadily to higher molecular weight, $M_n = 62.2 \text{ kg.mol}^{-1}$; $\mathcal{D} = 1.22$, 98.9% conversion after 24 hours. Additionally, we found that population **1** does not show a UV signal, which likely indicates that the corresponding chains are not carrying the trithiocarbonate chain end (Figure 14).

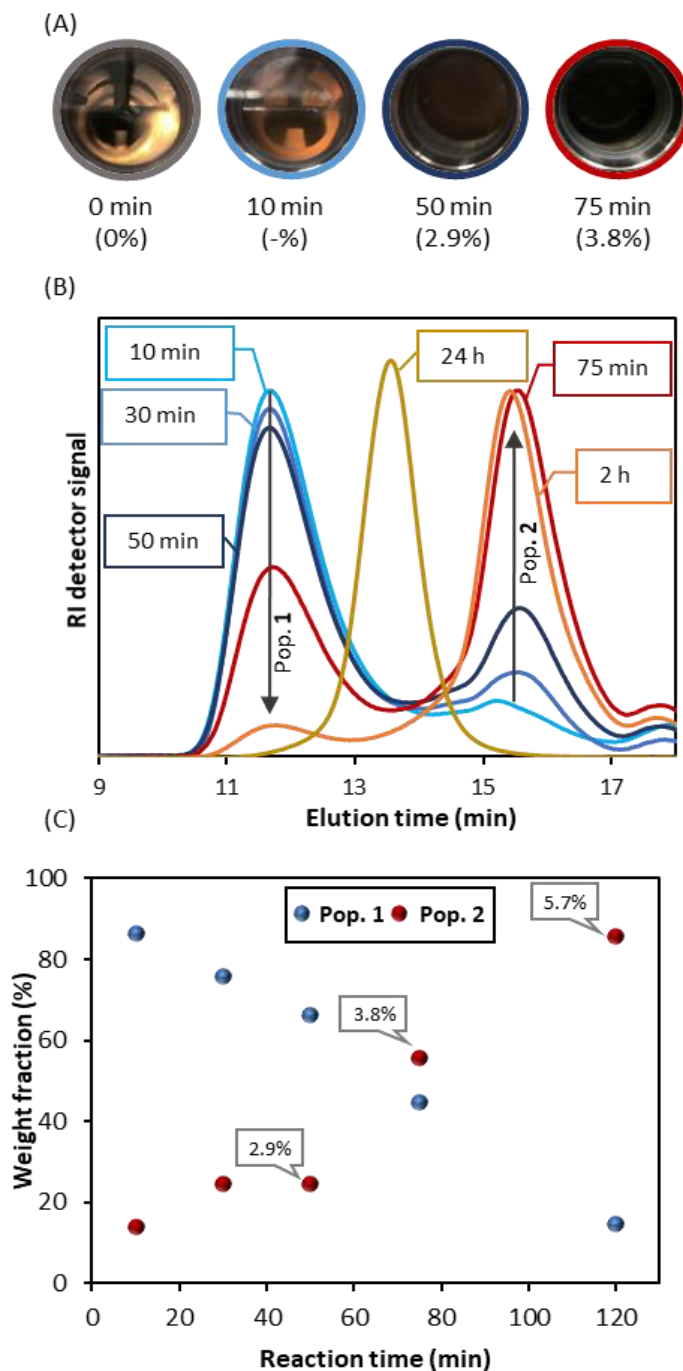


Figure 13 - Early stage studies of RAFT dispersion polymerisation of MMA in $scCO_2$ with DDMAT. (A) Photographs of view cell study at different reaction times show the evolution of turbidity in the dispersion polymerisation; conversion is presented in brackets, the sample at 10 minutes gave undetectable conversion by 1H NMR. (B) THF-SEC study of aliquots from reaction on sampling device. Inside the boxes, the reaction time is given to depict the normalised SEC traces. (C) Weight fraction % of population 1 against population 2 as a function of time. Two distinct M_n populations are observed, population 1 (FRP) and population 2 (RAFT controlled), conversion at time points given in the boxes. (Molar ratio DDMAT/AIBN 2:1, 65 °C, 276 bar, 300 rpm stirring rate, 5 wt%(based on MMA) of PDMS-MA as stabiliser).

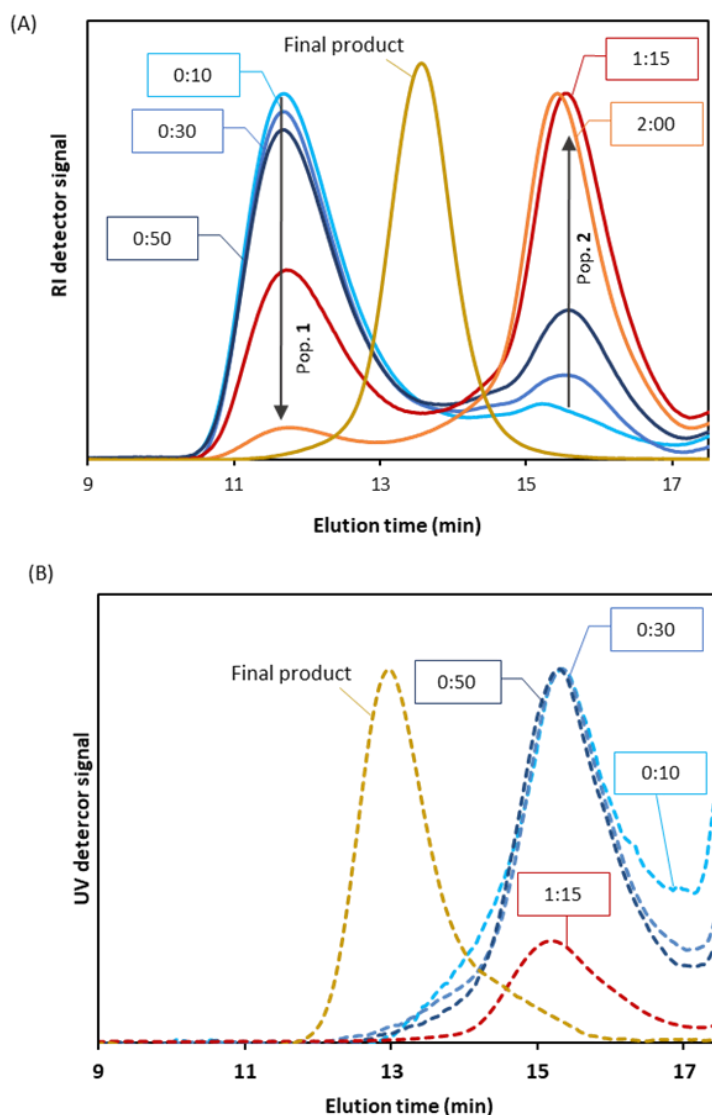


Figure 14 - Early stage study of RAFT dispersion polymerisation of MMA in $scCO_2$ with DDMAT, showing the THF-SEC study of aliquots from the reaction sampling device against the RI detector (A) and the UV detector (B). It is noticeable that population 1 does not present a UV signal, while population 2 shows UV absorption at 300 nm. Inside the boxes, the reaction time is given to depict the normalised SEC traces. Results in (A) are normalised while the UV response is not normalised. (Molar ratio DDMAT/AIBN 2:1, 65 °C, 276 bar, 300 rpm stirring rate, 5 wt%(based on MMA) of PDMS-MA as stabiliser).

As mentioned in the introduction (See section 4.2.2), in 2006 Winnik and Song demonstrated that RAFT control in dispersion polymerisation in conventional solvent could only be achieved by delayed addition of the CTA.³⁷ This creates a two-stage dispersion polymerisation, in which a small population of high molecular weight polymer forms in the first stage *via* a conventional radical process. This yields enough high molecular weight chains to induce nucleation, *i.e.*

seeds. Then, after injection of the CTA, lower molecular weight living chains are formed inside the particles, and as the reaction progresses this second population becomes the dominant species.³⁷ Winnik and Song obtained a final M_n that matched the theoretical value, with low dispersity. The weight fraction of the original high molecular weight population was too low to be detectable by THF-SEC, although it would still be present. Their results for a two-stage polymerisation aligns with our observations in RAFT dispersion polymerisation in $scCO_2$ (Figure 13 and Figure 14). But, our system is a one-step reaction, with all reactants added together at reaction start. Therefore, some mechanism occurring in $scCO_2$ must create similar conditions to a two-stage polymerisation.

4.5.1.4. Proposed mechanisms of RAFT control for $scCO_2$ dispersion polymerisation with a bad choice of CTA

DDMAT is not supposed to be a good control agent for MMA polymerisation, as demonstrated in toluene (E1.1, Table 1). Thus, it seems reasonable to assume that RAFT control of the polymerisation of MMA in $scCO_2$ will not be very efficient in the early stages of the process. At this point the system is still homogeneous and the continuous phase is the reaction *locus*.⁵⁸ As a result, some chains will certainly escape the expected RAFT equilibrium, and grow by conventional radical polymerisation to yield a high molecular weight population, which will nucleate very efficiently into PMMA particles and form a polymer-rich phase. This was confirmed in the previous section (See Section 4.5.1.3.) by the presence of two distinct polymer populations at the early stage of the reaction. What then happens is that DDMAT, AIBN and MMA begin to diffuse into those seed particles (Figure 15), which then become the main *locus* of the reaction where controlled polymerisation begins to take place.^{58, 59, 63, 64} This

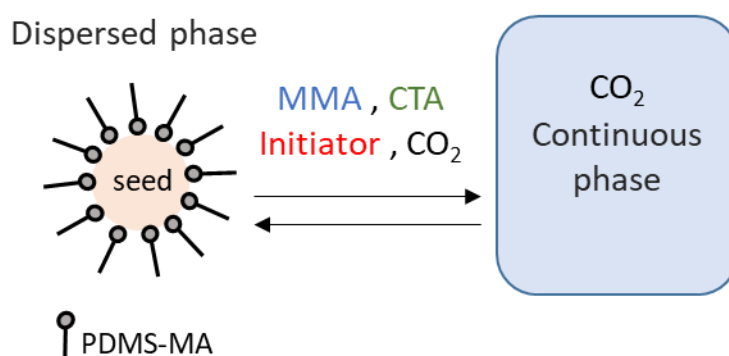


Figure 15 - Schematics of partition of species between the continuous phase and dispersed phase (particles seeds) in a dispersion polymerisation in $scCO_2$.

mechanism would also explain the poorer control observed at the beginning of the reaction in the plot of M_n versus conversion (Figure 11C).

Although there is general agreement in defining the particles as the main reaction *locus*, it remains difficult to assess the concentration of each species in the different phases of the polymerisation and define the exact *loci* of the polymerisation in scCO₂. The initiator (AIBN) is known to have high solubility in scCO₂ as observed by DeSimone *et al.*⁵³ Other studies also indicate that AIBN can equipartition between both phases, or it can have a partition coefficient (K_j) = 2,⁶⁵ or K_j = 0.5,⁶⁶ where K_j is the ratio of the concentration in the dispersed polymer-rich phase by the concentration in the continuous phase as given in Equation (3).

$$K_j = [j]_{(dispersed\ phase)} / [j]_{(continuous\ phase)} \quad (3)$$

The solvent (CO₂) and low molecular weight species, such as MMA, are known to diffuse into the PMMA particles very effectively under scCO₂ conditions. This has been demonstrated by the observation of efficient chain extension and formation of block copolymer particles.^{16-18, 45} Additionally, the swelling and sorption of PMMA films with MMA has been studied extensively in scCO₂.⁶⁷⁻⁶⁹ As PMMA particles have a higher surface area than films, they are even more likely to swell, with a K_j estimated at 0.4 for MMA and 0.25 for CO₂.⁷⁰ No information on the partition of CTAs in scCO₂ systems is currently available in the literature. However, the results we present here do show that controlled polymerisation starts when nucleation starts. In addition, the good agreement between expected and theoretical M_n values tells us that all the DDMAT is involved in the control, so its diffusion into the particles, either as free CTA molecule or as oligomers, must be near quantitative.

As DDMAT is a poor choice of CTA for the polymerisation of MMA a question remains, how can this CTA control the polymerisation even if it diffuses quantitatively into the reaction *locus*?

Good polymerisation control with a poorly selected CTA has been very recently demonstrated in RAFT emulsion polymerisation.⁷¹ Perrier and co-workers coupled the carboxylic R-group of DDMAT with a hydrophilic poly(ethylene oxide) (PEO) to make an amphiphilic macromolecular CTA (macro-CTA). Despite its low C_{tr} , the macro-CTA showed good control over the emulsion polymerisation of MMA, butyl methacrylate (BMA) and hexyl methacrylate (HMA). However, when the reaction was performed under solution or miniemulsion

conditions, high \bar{D} were obtained. The authors attributed this behaviour to the in-built monomer-feeding mechanism of emulsion polymerisation, which is not in place in miniemulsion or solution polymerisation.

In emulsion polymerisation, the monomer has only a very limited solubility in the continuous aqueous phase and thus forms droplets, which effectively serve as a constant supply of monomer feeding the growing particles. As a result, the monomer concentration can be kept constant low throughout the particle growth stage. This low monomer concentration in relation to the CTA concentration ($[M]/[CTA]$) at the reaction *locus* leads to addition of fewer monomer units per activation/deactivation cycle, which in turn overcomes the low C_{tr} and gives low \bar{D} and controlled molecular weight.

In our system, as MMA is expected to mainly be consumed inside the particles, the monomer is continuously supplied to maintain an overall constant concentration of MMA within the particles with respect to PMMA and CO₂, establishing a limiting feed, until there is no more MMA in the continuous phase. This results in a low MMA/DDMAT molar ratio in the dispersed phase, which can overcome the low chain transfer constant of DDMAT, in a similar fashion as described by Perrier and co-workers.⁷¹ In this way we can rationalise the surprisingly good control we observed with DDMAT.

Therefore, our results show that an *a priori* poor CTA in solution polymerisation can be used to achieve very good control in a single stage dispersion in scCO₂ by effectively creating an *in situ* two-stage process. The poor efficiency of the CTA can be counterbalanced once the particles are formed as a result of the local modification of the $[M]/[CTA]$ molar ratio.

4.5.2. RAFT polymerisation of MMA in scCO₂ with well-suited CTAs

To broaden our understanding and corroborate our data we next looked at a range of other molecules previously established to be good CTAs for MMA. Once we identified the importance of having an *in situ* two-stage mechanism for the control of the reaction, we postulated the question: would a well-suited CTA be unable to provide such mechanism and thus fail to control the reaction?

Rizzardo *et al.* observed that cyanoalkyls are efficient R reinitiating groups,^{51,38} which are known to be effective leaving groups for MAMs.^{42, 72} With that in mind, we selected 4-cyano-4-(phenylcarbonothioylthio) pentanoic acid (CPAB) (CTA 2, Figure 16), which has been

reported to be well suited to control the polymerisation of MMA.⁷³ Another control agent that we also looked at in detail was 2-cyano-2-propyl(dodecyltrithiocarbonate) (CPDT) (CTA 3, Figure 16).⁴⁸ CPDT is amongst the most active CTAs and thus it is particularly good for controlling polymerisation of MAMs, such as MMA.²³

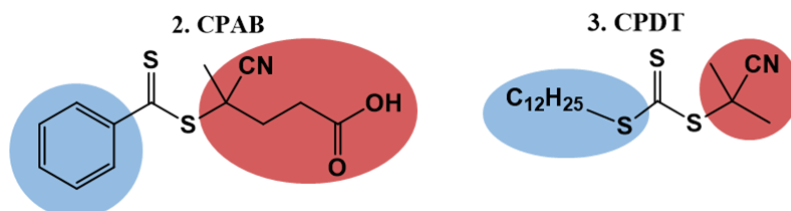


Figure 16 - Chain transfer agent (CTA) structures with the R group in red and the Z group in blue: structure 2. CPAB (4-Cyano-4-(phenylcarbonothioylthio)pentanoic acid); structure 3. CPDT (2-Cyano-2-propyl dodecyl trithiocarbonate).

4.5.2.1. Starting material assessment: CTA degradation

CTAs containing both a cyano and a carboxylic acid functional group can undergo degradation of the cyano group into amide, even when stored at recommended conditions. Water acts as a nucleophile and attacks the protonated cyano group, this mechanism leads to formation of the amide moiety (Figure 17). The amide formation can be monitored by ¹H NMR and ¹³C NMR as described by Fuchs *et al.*⁷⁴ The conversion of the cyano group in the R- reinitiating fragment

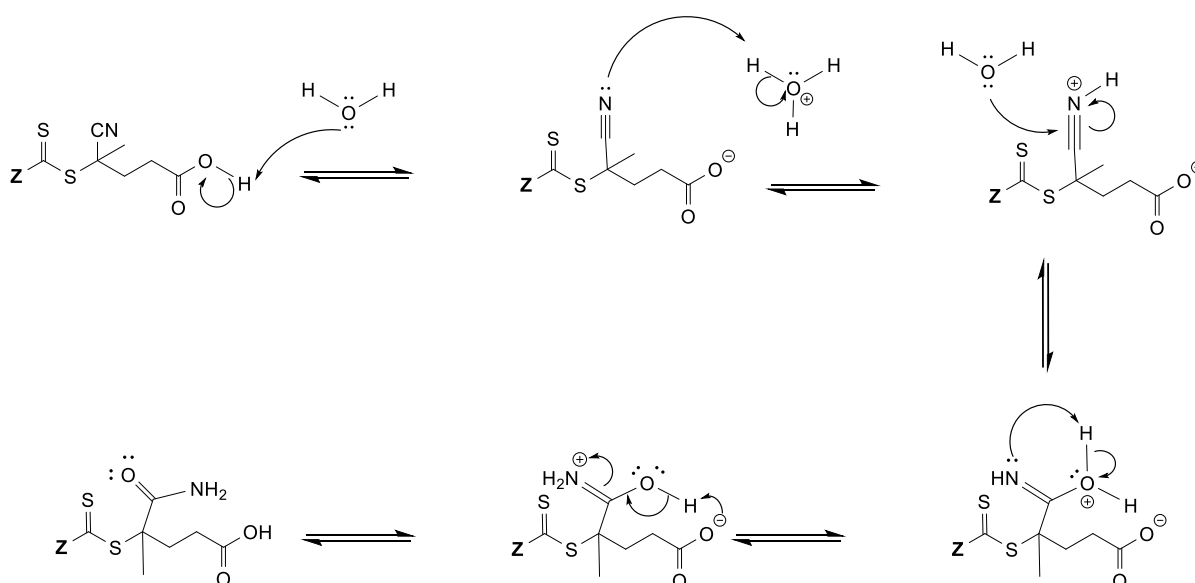


Figure 17 - Proposed acid-catalysed cyano-hydrolysis mechanism of CTAs containing a cyano and a carboxylic acid group.

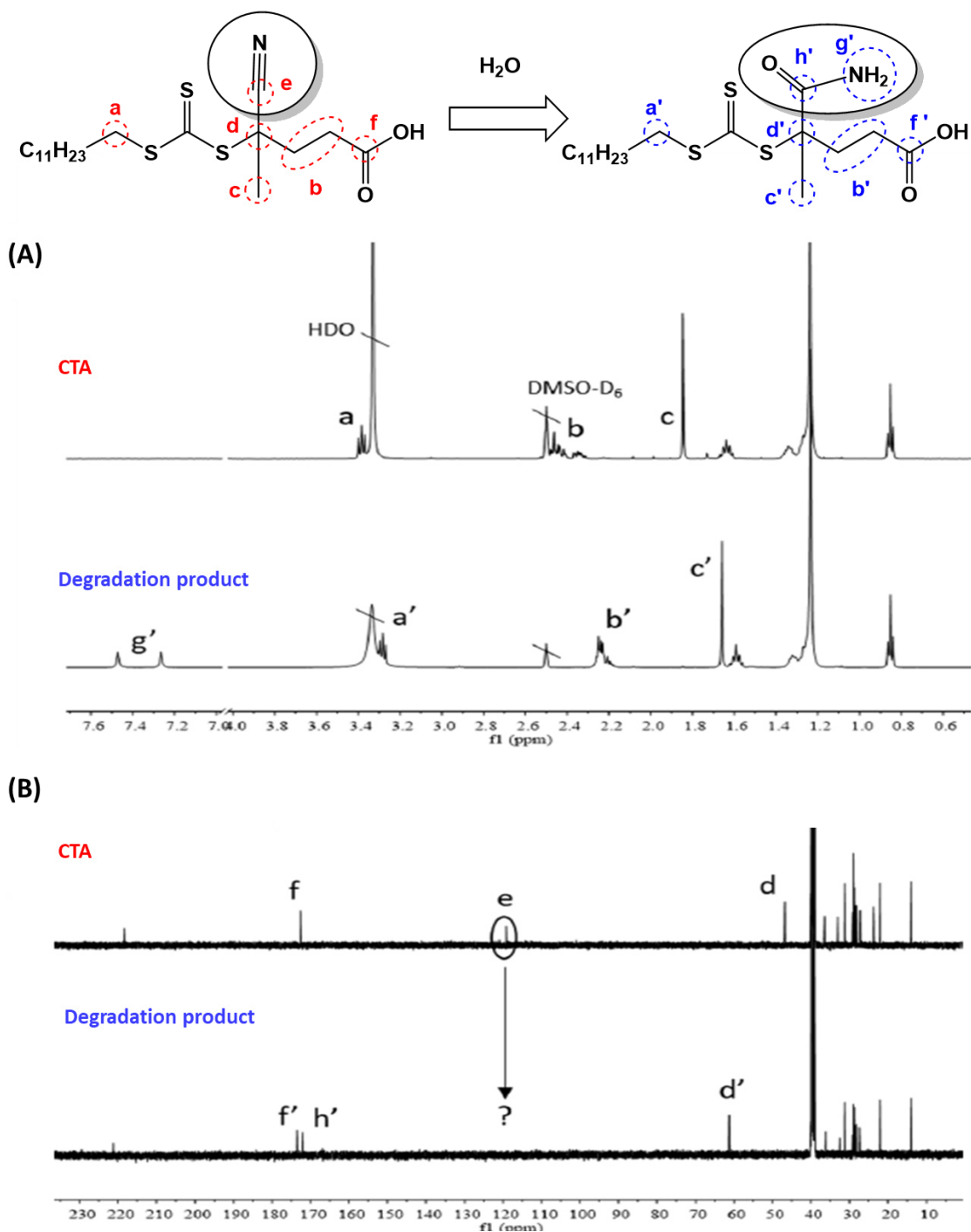
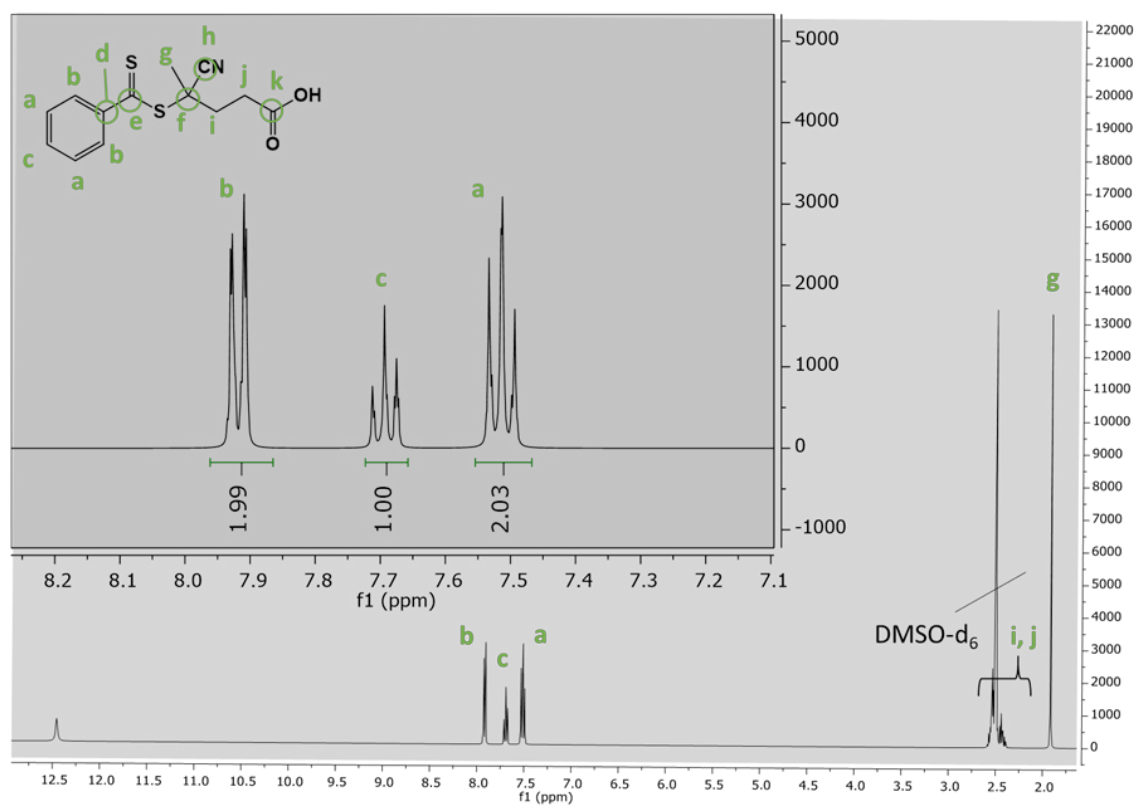


Figure 18 - CPAD degradation monitoring by (A)¹H NMR and (B)¹³C NMR in DMSO-D₆. Figure modified from Fuchs *et al.*⁷⁴

of the CTA is detrimental to RAFT control, such as increased molecular weight dispersity and loss of end-group fidelity.⁷⁴

In accordance with Fuchs *et al.*, the degradation of 4-Cyano-4-[(dodecylsulfanylthiocarbonyl)sulfanyl]pentanoic acid (CPAD) would show a significant shift of the methyl protons (c) and the methylene protons (a and b) on ¹H NMR in deuterated

(A)



(B)

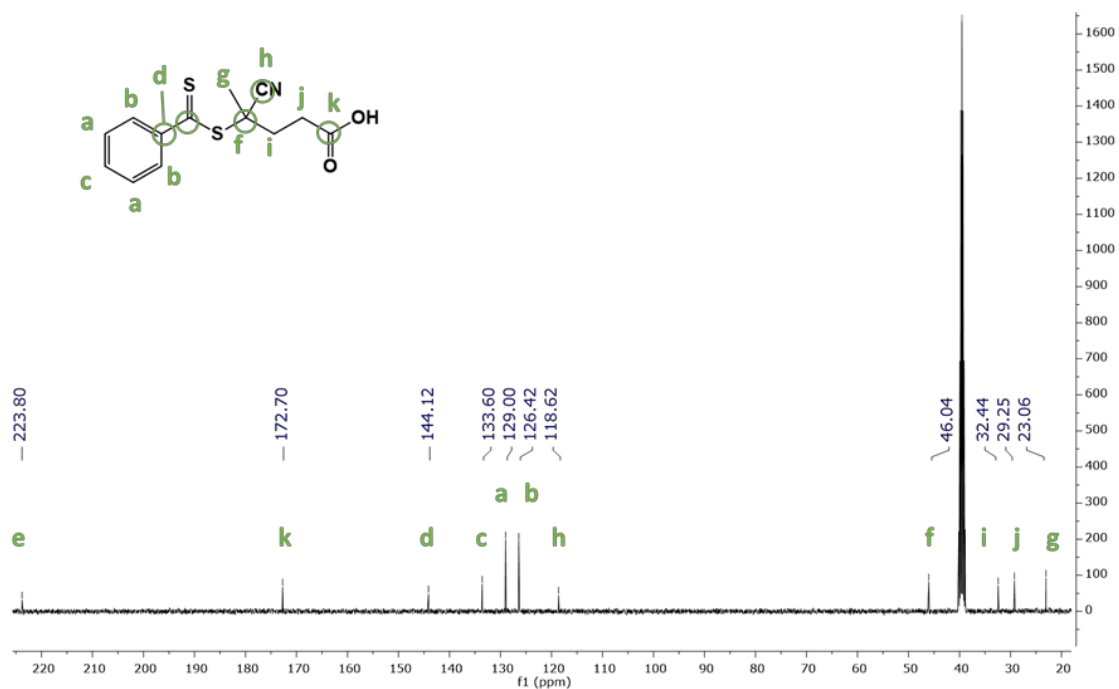


Figure 19 - CPAB purity investigation by (A) ^1H NMR spectrum of CPAB in DMSO- D_6 (400 MHz). δ ^1H (ppm): 7.96 – 7.86 (2 H, m), 7.72 – 7.66 (1 H, m), 7.55 – 7.47 (2 H, m), 2.60 – 2.38 (4 H, m), 1.92 (3 H, s); (B) ^{13}C NMR spectrum of CPAB in DMSO- D_6 (400 MHz). δ ^{13}C (ppm): 223.80, 172.70, 144.12, 133.60, 129.00, 126.42, 118.62, 46.04, 32.44, 29.25, 23.06.

dimethyl sulfoxide (DMSO- D_6), as depicted in Figure 18A.⁷⁴ The formation of amide can be also observed by ^{13}C NMR by the appearance of a second carbonyl peak at 172 ppm (**h'**), along with the disappearance of the cyano carbon at 119.1 ppm (**e**) and shift of the quaternary carbon from 46.7 to 61.2 ppm (**d'**)(Figure 18B).⁷⁴

In the same way, the formation of amide degradation product can be monitored for CPAB by NMR spectroscopy. In the case of amide formation, the 1H NMR would show additional peaks at 7.5 ppm overlapping with the phenyl protons (≈ 7.3 ppm), which refer to the protons attached to the nitrogen of the amide moiety. In the ^{13}C NMR, in the same way as for CPAD, the carbon of the cyano group (**h** -Figure 19) at 119 ppm would shift to ≈ 170 ppm with formation of the amide. The quaternary carbon (**f** - Figure 19) also would show a shift from ≈ 45 ppm to ≈ 60 ppm with degradation. None of these indicators of degradation were observed by the analysis of CPAB in our hands (Figure 19A and B).

4.5.2.2. RAFT control of MMA polymerisation in $scCO_2$ with CPAB

In order to examine further the impact of the $scCO_2$ dispersion polymerisation mechanism upon the RAFT control, the CTAs were also tested in toluene solution polymerisation. CPAB has proven good control in toluene, as observed by the low dispersity and molecular weight on target (E2.1 Table 5).

Furthermore, the kinetic study of the solution polymerisation showed a linear evolution of M_n with conversion and dispersity lower than 1.3 throughout the reaction (Table 6 and Figure 20A and 20B).

By contrast, in $scCO_2$ control was poor with the average M_n obtained 50% higher than the target, average $M_n = 83.4 \text{ kg mol}^{-1}$ vs. average $M_{n,th} = 58.2 \text{ kg mol}^{-1}$, and a high dispersity, $\mathcal{D} = 1.48$ on average (E2.2-E2.7, Table 5). Although the reaction itself did appear to perform well, with high conversion ($> 95\%$), and formed a free-flowing powder composed by well-defined particles (Figure 21, Table 7), there was no optimum RAFT control.

Table 5 - RAFT polymerisation of MMA in toluene solution polymerisation and in scCO₂ dispersion polymerisation with CPAB (2).

Expt.	Solvent	Conv ¹ (%)	$M_{n,th}$ ²	M_n ³	\bar{D} ³
E2.1	toluene	81	48.6	49.7	1.21
E2.2	scCO ₂	99	59.7	76.1	1.41
E2.3	scCO ₂	93	56.7	81.9	1.39
E2.4	scCO ₂	99	58.9	73.8	1.48
E2.5	scCO ₂	95	56.5	84	1.51
E2.6	scCO ₂	98	58.7	86.4	1.53
E2.7	scCO ₂	98	58.7	98.5	1.59
Avg. (E2.2-E2.7)	scCO ₂	97	58.2	83.4	1.48

¹ Conversion calculated from ¹H NMR. ² Theoretical M_n calculated relative to CTA and monomer concentration and given in kg mol⁻¹. ³ \bar{D} and M_n (in kg mol⁻¹) obtained by THF-SEC with RI detector against PMMA standards. (E2.1: Molar ratio CPAB/AIBN 5:1, 65 °C, 300 rpm stirring rate, 1:1 volume ratio of toluene to MMA). (E2.2-E2.7: Molar ratio CPAB/AIBN 2:1, 65 °C, 276 bar, 300 rpm stirring rate, 5 wt%(based on MMA)).

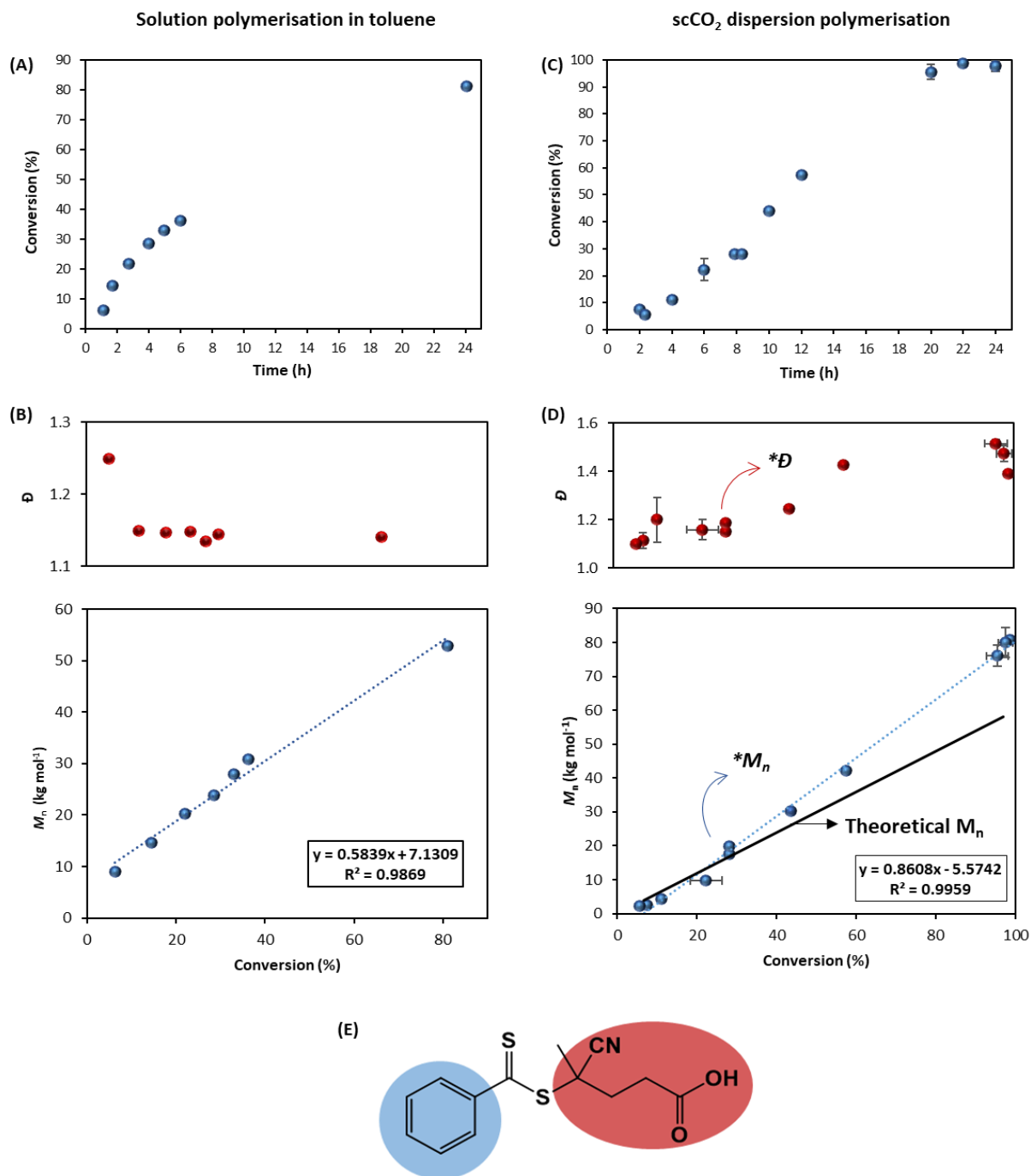


Figure 20 - Polymerisation of MMA using CPAB as CTA: evolution of MMA conversion versus time (A) and evolution of M_n (blue) and \bar{D} (red) versus conversion (B) for the solution polymerisation in toluene; evolution of MMA conversion versus time (C) and evolution of M_n (blue) and \bar{D} (red) versus conversion (D) for the scCO₂ dispersion polymerisation. Structure of CPAB, with R group in red and Z group in blue (E).

Table 6 – Summary of results from kinetics of MMA toluene solution polymerisation with CPAB as CTA

Time (h)	Conversion ¹ (%)	M_n ²	\bar{D} ²
1.2	6.2	8.9	1.25
1.8	14.5	14.6	1.15
2.8	21.9	20.2	1.15
4.0	28.6	23.8	1.15
5.0	32.9	27.9	1.13
6.0	36.3	30.9	1.14
24.0	81.0	52.9	1.14

¹ Conversion calculated from ¹H NMR. ² \bar{D} and M_n (in kg mol⁻¹) obtained by THF-SEC with RI detector against PMMA standards. (Molar ratio CPAB/AIBN 5:1, 65 °C, 300 rpm stirring rate, 1:1 volume ratio of toluene to MMA).

Table 7 – Particle size analysis of PMMA particles synthesised *via* scCO₂ dispersion polymerisation with CPAB (2) as CTA.

Expt.	D_n ¹ (μm)	C_v ² (%)
E2.3	2.38	15.8
E2.4	2.94	17.0
E2.6	2.83	16.3
E2.7	2.43	15.0

¹ Average particle size (D_n) is calculated as an average of 100 particles measurements *via* Image J[®]. ² the coefficient of variance (C_v) is calculated by the ratio of the standard deviation (σ) by the mean particle diameter as by equation (1).

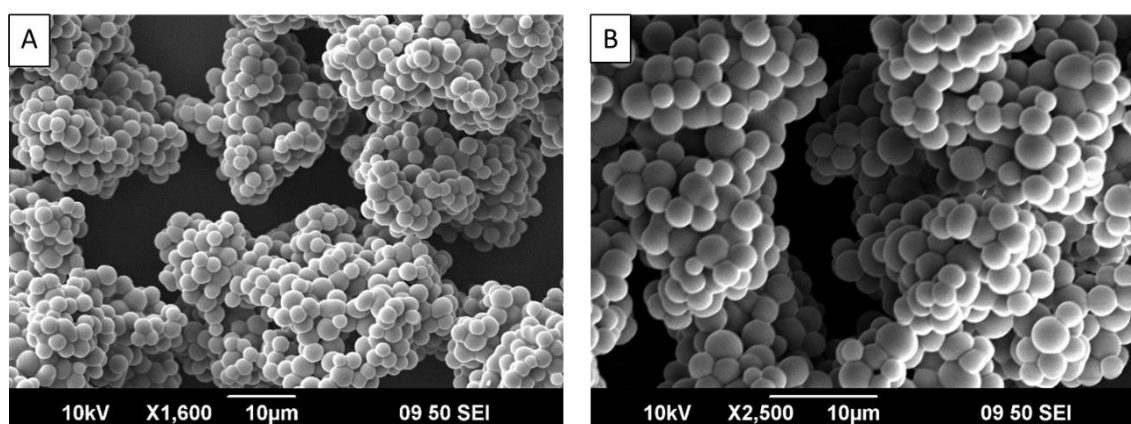


Figure 21 - SEM images of E2.7 obtained using a JEOL 6060LV SEM at accelerating voltage of 10 kV and at A) 1600x magnification and B) 2500x magnification.

The sampling of the reaction showed consistent growth of M_n with time (Table 8, Figure 20C). Looking in detail into the kinetics, after 30% conversion the plot of molecular weight against conversion (Figure 20D) shows a deviation ($*M_n$) from the theoretical trend, *i.e.*, black line, towards higher molecular weights, clearly showing sub-optimal control.

Table 8 – Summary of results from kinetics of MMA dispersion polymerisation in scCO₂ with CPAB as CTA. Reaction monitored with the high-pressure sampling system.

Time (h)	Conversion ¹ (%)	M_n ²	\mathcal{D} ²
2	7.4 (±0.9)	2.4 (±0.2)	1.1 (±0.03)
2.3	5.7	2.3	1.1
4	11.0 (±0.8)	4.2 (±0.5)	1.2 (±0.1)
6	22.3 (±3.9)	9.8 (±0.9)	1.2 (±0.04)
7.8	28.1	17.6	1.2
8.3	28.2	19.9	1.2
10	43.8	30.1	1.2
12	57.4	42.1	1.4
20	95.5 (±2.8)	76.0 (±3.2)	1.5
22	98.6	80.8	1.4 (±0.0)
24	97.6 (±1.9)	79.9 (±4.4)	1.5 (±0.0)

Results given as average from repeats, standard deviation given in brackets.¹ Conversion calculated from ¹H NMR. ² \mathcal{D} and M_n (in kg mol⁻¹) obtained by THF-SEC with RI detector against PMMA standards. (Molar ratio CPAB/AIBN 2:1, 65 °C, 276 bar, 300 rpm stirring rate, 5 wt%(based on MMA) PDMS-MA as stabiliser).

It is also very interesting that the reaction with CPAB shows initially very good dispersity (Figure 20D), especially when compared with the reaction controlled by DDMAT, which was presented earlier (Figure 11B, Table 4). However, after 30% conversion ($*\mathcal{D}$), the dispersity drifts upwards (Figure 20D). Since CPAB has a very high chain transfer constant towards MMA we should expect better control in the early stages of the process, in the same way as is observed in toluene solution (E2.1). However, one would expect to see the same good control throughout the reaction.

To investigate this unexpected result, the early stage of the scCO₂ dispersion polymerisation with CPAB was analysed in the view cell (Figure 22A).

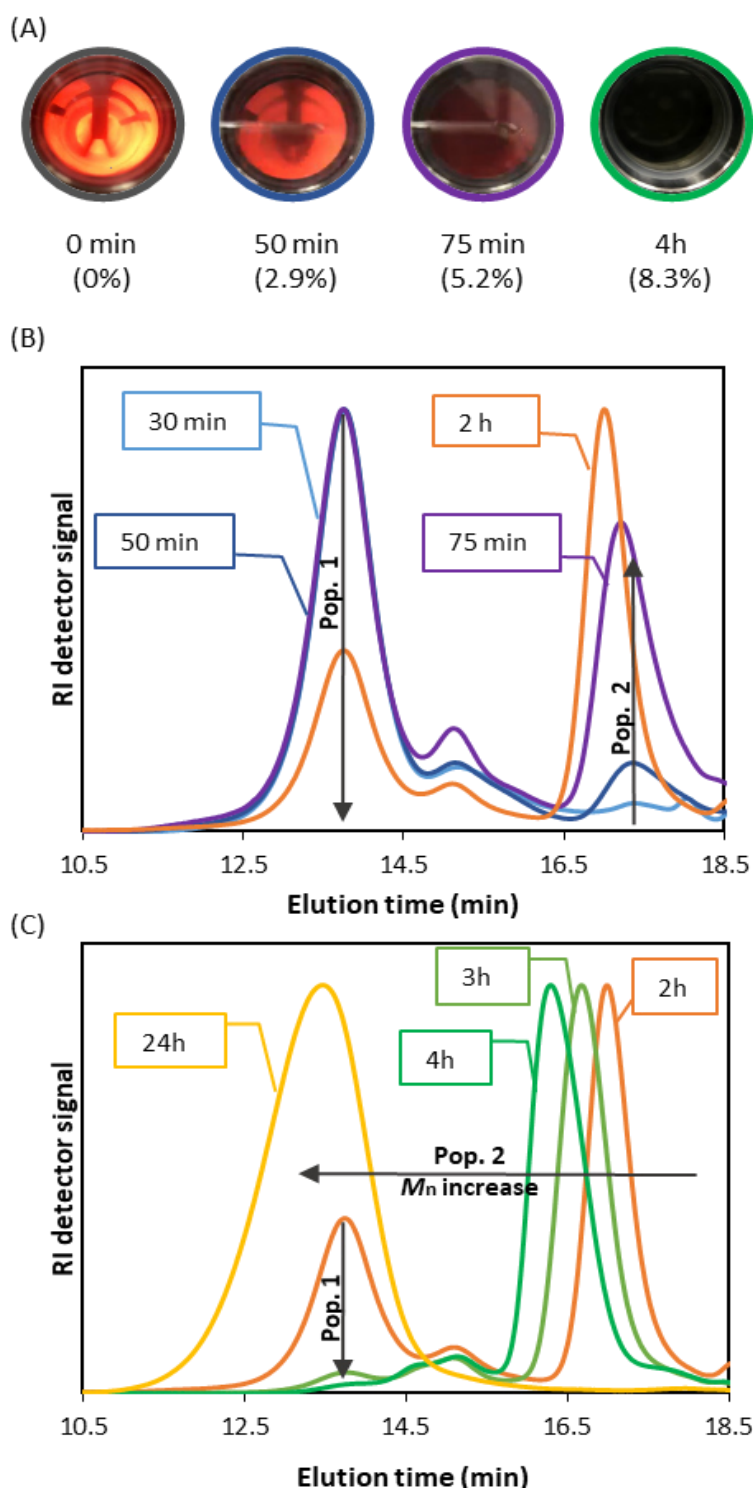


Figure 22 - THF-SEC study at reaction early stage (nucleation) of MMA dispersion polymerisation in $scCO_2$ with CPAB. A) Photographs of view cell study at different reaction times. Aliquots from (B) 30 minutes to 2 hours and (C) 2 to 4 hours and final product at 24 hours. Two distinct populations are observed, population 1 (FRP) and population 2 (RAFT controlled). Inside the boxes, the reaction time is given to depict the SEC traces.

This time the onset of turbidity was observed after a much longer period of 43 minutes (conversion at 50 minutes = 2.9%), which indicate that CPAB, a better CTA for methacrylates, is controlling the polymerisation and delaying nucleation. As a consequence, the *in situ* two-stage mechanism that we saw with DDMAT might not be happening effectively with CPAB. However, the THF-SEC analyses of the early stage for the CPAB controlled reaction (Figure 22B and 22C) show a similar behaviour to that of DDMAT. A bimodal molecular weight distribution was observed, with two distinct polymer populations. Again, the high molecular weight population (population 1) presented no UV signal (Figure 23) and this population became less dominant over time. In addition, population 1 had lower M_n with CPAB, $\approx 70 \text{ kg mol}^{-1}$, compared to the reaction with DDMAT, $M_n > 400 \text{ kg mol}^{-1}$, and closer to the targeted M_n ($M_{n,tgt}$) = 60 kg mol^{-1} .

As mentioned earlier, it is important to remember that inhibition and retardation are other factors that can delay nucleation in RAFT controlled polymerisation. In particular, inhibition and retardation are known to be frequently observed with dithiobenzoates such as CPAB.⁵⁴
⁵⁵ This might explain the delayed nucleation, but does not explain the observed kinetic behaviour, with M_n closer to $M_{n,th}$ before 30% monomer conversion (Figure 20D).

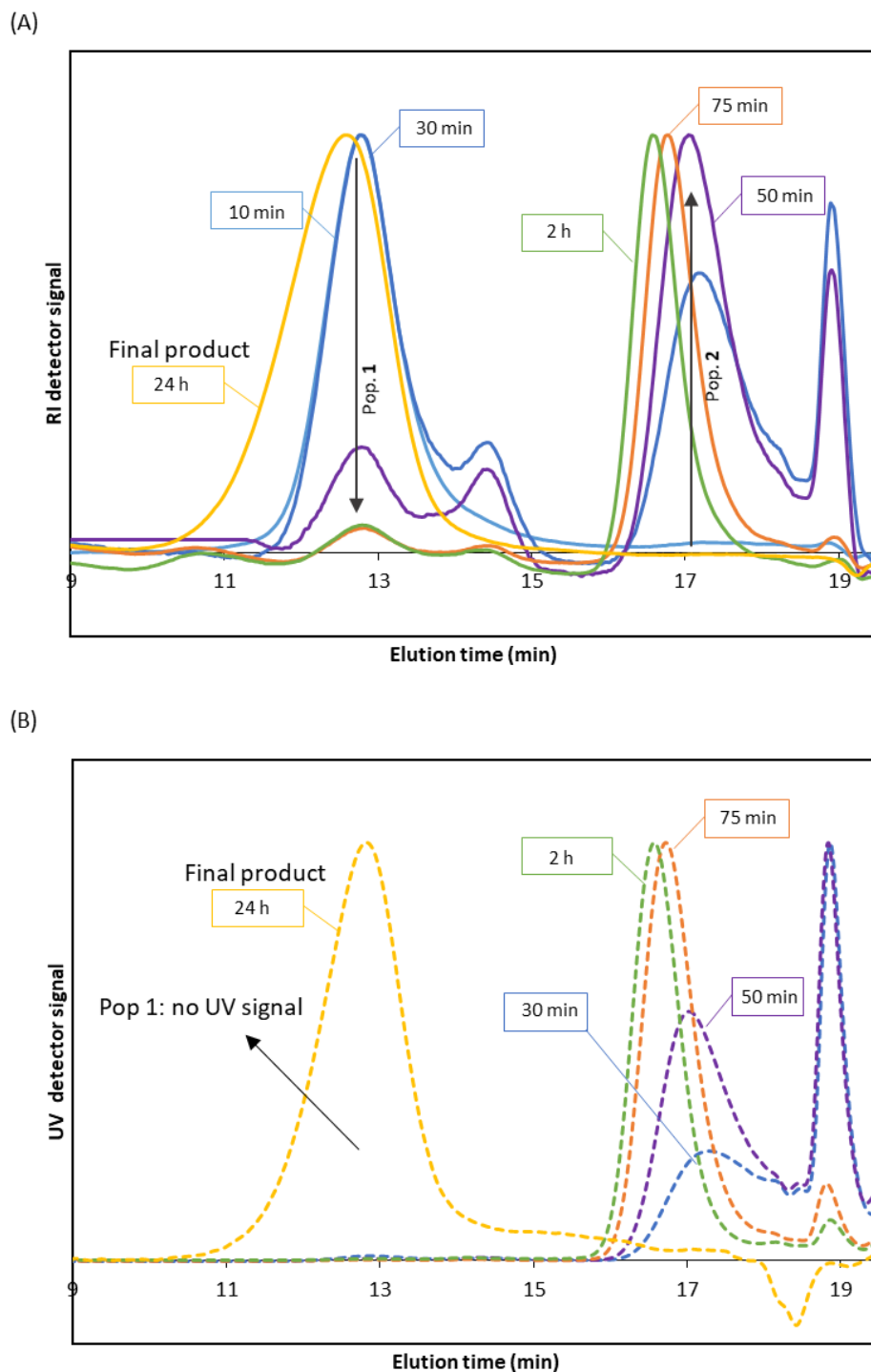


Figure 23 - Early stage study of a RAFT dispersion polymerisation of MMA in $scCO_2$ with CPAB, showing the THF-SEC study of aliquots from reaction on sampling device against the RI detector (A) and the UV detector (B). It is noticeable that population 1 does not present a UV signal, while population 2 shows UV absorption at 300 nm. Results in (A) are normalised while the UV response is not normalised. Inside the boxes, the reaction time is given to depict the SEC traces.

4.5.2.3. Two-stage RAFT dispersion polymerisation in scCO₂ with CPAB

As mentioned above, the *in situ* two-stage mechanism observed in the polymerisation with DDMAT appears to be advantageous for reaction control. Although the same mechanism was seen to take place with CPAB, nucleation is significantly delayed with this CTA. The lower control offered by DDMAT allows the polymerisation to occur via conventional radical polymerisation at the start of the polymerisation and achieve J_{crit} quickly. With the particles formed, DDMAT partitioning between the two phases dictates the *locus* of the reaction, with the reaction main *locus* being the dispersed phase.

The better control offered by CPAB could thus delay occurrence of the two-stage polymerisation, with J_{crit} only achieved later into the reaction, *i.e.*, at a higher conversion. The SEC analysis of the reaction with CPAB showed that indeed the reaction gave a much lower molecular weight for population **1** (70 kg mol⁻¹ with CPAB (Figure 22) vs. 400 kg mol⁻¹ with DDMAT (Figure 11)). It is reasonable to expect that this lower molecular weight population **1** might not nucleate as efficiently and thus affect control. Furthermore, it took one hour longer with CPAB to reach the same proportion of population **2** in relation to population **1**. The occurrence of the reaction as a single stage polymerisation with CPAB could thus cause loss of control and be responsible for the lower control observed with this CTA.

In order to investigate if the CPAB control over MMA in scCO₂ could be improved by a faster nucleation stage, a two-stage polymerisation was induced with use of an adapted reaction setup.

A duplicate of the two-stage polymerisation was performed by starting the reaction via conventional radical polymerisation (Table 9) prior to injecting CPAB, dissolved in MMA, *via* HPLC pump, ensuring a CTA/AIBN ratio of 2:1. The full procedure for injection via HPLC can be found in Section 2.3.5. After CPAB injection, the reaction was allowed to proceed for 24 hours. The product was recovered as a free-flowing light pink powder at high conversion (95%) and the SEM analysis showed one population of individual spherical particles (Figure 24), with diameter and coefficient of variance consistent with previous single-step reactions. This result indicates the injection of monomer and CTA did not disturb the nucleation, as particles were formed and there is no sign of a second nucleation stage happening. In addition, smaller particles were produced with the two-stage method, with diameter below

2 μm and C_v was circa 20% (Table 9), which is in line with what is usually seen for dispersions in scCO_2 , but slightly higher than for the single stage reactions (average $C_v = 16\%$, Table 7).

Table 9 - Two-stage RAFT scCO_2 dispersion polymerisation of MMA with CPAB (2).

Expt.	Conv ¹ (%)	$M_{n,\text{th}}$ ²	M_n ³	\mathcal{D} ³	D_n ⁴ (μm)	C_v ⁵ (%)
E2.8	95	61.2	113.4	1.35	1.80	20.5
E2.9	95	61.4	146.1	1.34	1.93	19.7

¹ Conversion calculated from ^1H NMR. ² Theoretical M_n calculated relative to CTA and monomer concentration and given in kg mol^{-1} . ³ \mathcal{D} and M_n (in kg mol^{-1}) obtained by THF-SEC with RI detector against PMMA standards. ⁴ Average particle size (D_n) is calculated as an average of 100 particles measurements *via* Image J[®]. ⁵ the coefficient of variance (C_v) is calculated by equation (1).

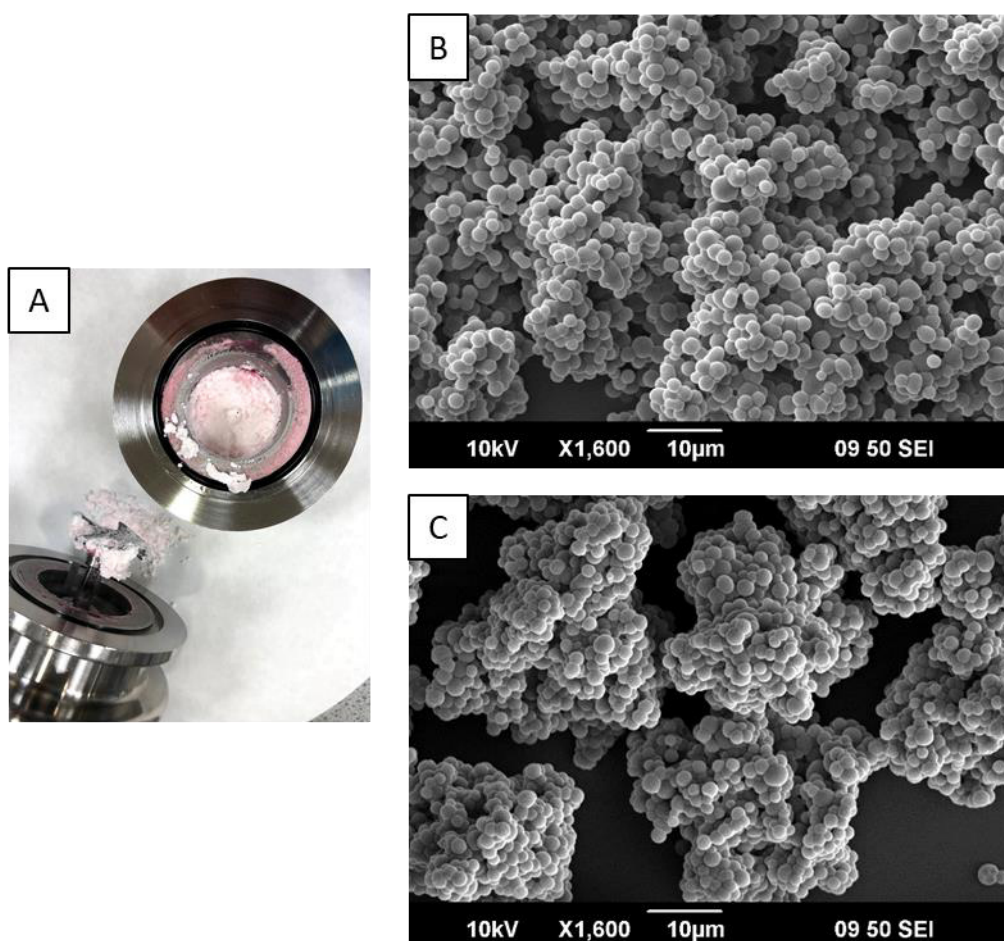


Figure 24 - Picture of final product obtained as a light pink powder for E2.8 (A); and SEM picture of E2.8 (B) and of E2.9 (C), both obtained using a JEOL 6060LV SEM at accelerating voltage of 10 kV and at 1600x magnification.

The implementation of the induced two-stage polymerisation improved the dispersity (E2.8 - $\bar{D} = 1.34$, E2.9- $\bar{D} = 1.35$), but \bar{D} was still higher than that observed with DDMAT as CTA (E1.2-E1.4, average $\bar{D} = 1.22$, Table 1). In addition, it did not improve molecular weight control (E2.8, $M_{n,th} = 61.2 \text{ kg mol}^{-1}$, $M_n = 113.4 \text{ kg mol}^{-1}$) compared to the single step reaction (E2.2-E2.7, average $M_{n,th} = 58.2 \text{ kg mol}^{-1}$, average $M_n = 83.4 \text{ kg mol}^{-1}$, Table 5). In fact, the final M_n is further away from the target in the two-stage polymerisation. Both reactions gave molecular weights about twice those of the target (Table 9). This was not expected, as one would think that the overall RAFT control should improve in a two-stage strategy in accordance to Winnik and Song.³⁷ Therefore, another phenomenon must be responsible for the loss of polymerisation control in this reaction.

4.5.2.4. RAFT control of MMA polymerisation in scCO₂ with CPDT

We then tested 2-cyano-2-propyl(dodecyltrithiocarbonate) (CPDT) (structure 3, Figure 16) as CTA for the polymerisation of MMA.⁴⁸ CPDT is amongst the most active CTAs and is particularly good for controlling polymerisation of MAMs such as MMA;²³ and presents a cyanoalkyl R group, which gives an effective re-initiating group for MMA.^{42, 72} Therefore, this CTA is well-suited for methacrylate polymerisation in homogeneous medium, as evidenced by the low dispersity, $\bar{D} = 1.18$ and good agreement of M_n (43.6 kg mol^{-1}) with the theoretical molecular weight (41.3 kg mol^{-1}) obtained for the toluene solution polymerisation of MMA (E3.1, Table 10).

Table 10 - RAFT polymerisation of MMA in toluene and in scCO₂ dispersion polymerisation with CPDT (3).

Expt.	Solvent	Conv ¹ (%)	$M_{n,th}$ ²	M_n ³	\bar{D} ³
E3.1	toluene	65	41.3	43.6	1.18
E3.2	scCO ₂	98	58.6	60.0	1.20
E3.3	scCO ₂	99	58.7	60.5	1.22
E3.4	scCO ₂	98	58.7	57.3	1.20

¹ Conversion calculated from ¹H NMR. ² Theoretical M_n calculated relative to CTA and monomer concentration and given in kg mol^{-1} . ³ \bar{D} and M_n (in kg mol^{-1}) obtained by THF-SEC with RI detector against PMMA standards. E3.2-E3.4 are replicates. (E3.1: Molar ratio CPDT/AIBN 5:1, 65 °C, 300 rpm stirring rate, 1:1 volume ratio of toluene to MMA) (E3.2-E3.4: Molar ratio CPDT/AIBN 2:1, 65 °C, 276 bar, 300 rpm stirring rate, 5 wt%(based on MMA) PDMS-MA as stabiliser)

The kinetic plot of MMA solution polymerisation with CPDT further confirms the RAFT control (Table 11, Figure 25A and 25B). The molecular weight increased linearly with conversion and the dispersity decreased throughout the reaction until a final value of 1.26. This dispersity is

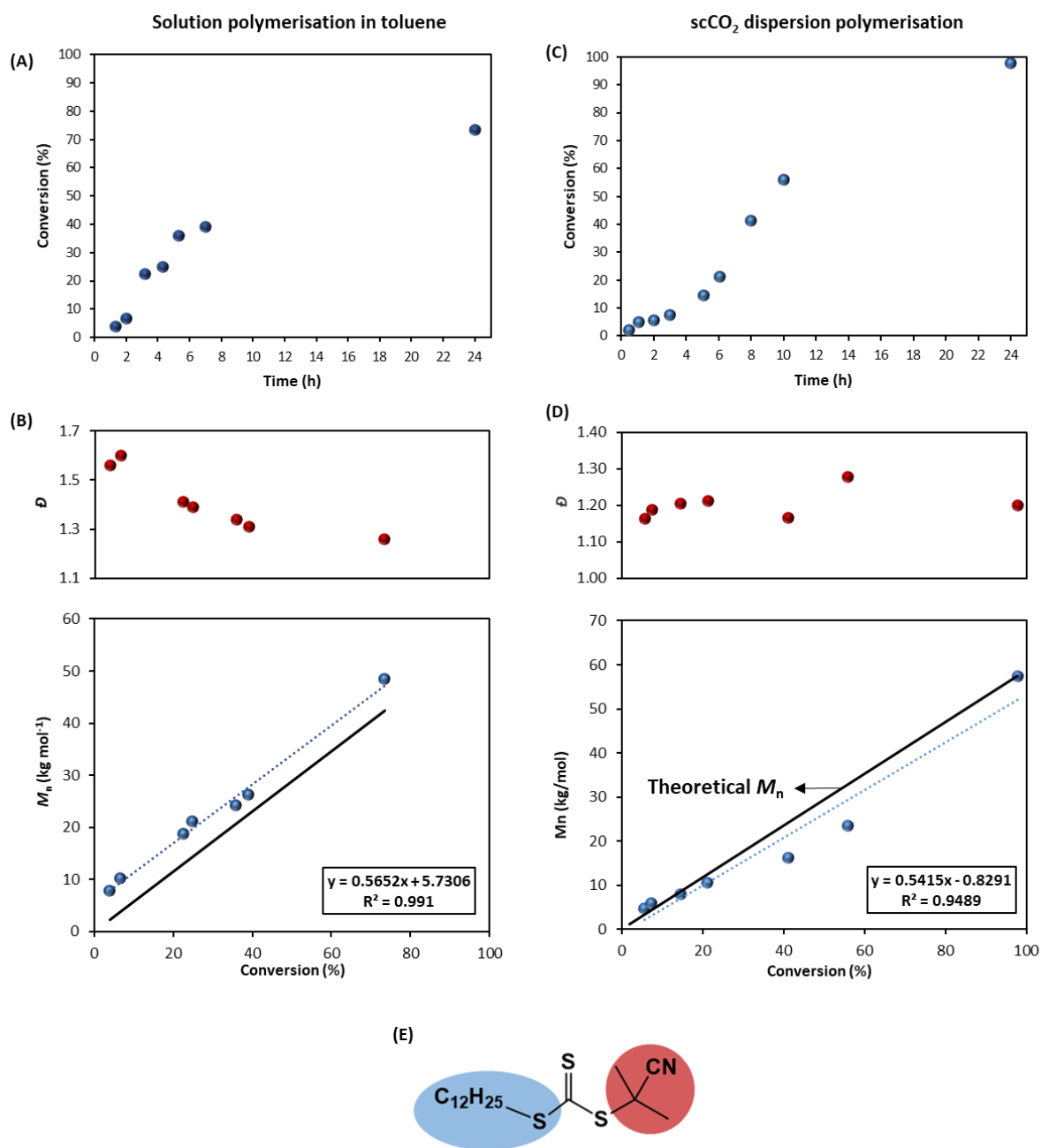


Figure 25 - Polymerisation of MMA using CPDT as CTA: evolution of MMA conversion versus time (A) and evolution of M_n (blue) and \bar{D} (red) versus conversion (B) for the solution polymerisation in toluene; evolution of MMA conversion versus time (C) and evolution of M_n (blue) and \bar{D} (red) versus conversion (D) for the scCO₂ dispersion polymerisation. Structure of CPDT, with R group in red and Z group in blue (E).

not as low as observed for the reaction with CPAB (E2.1) or that presented in E3.1, however $\mathcal{D} < 1.30$.

In contrast to CPAB, we found that CPDT exerts good control of MMA dispersion polymerisation in $scCO_2$, with low dispersity $\mathcal{D} = 1.21$ and molecular weight on target, average $M_n = 59.3 \text{ kg mol}^{-1}$ vs. average $M_{n,th} = 58.7 \text{ kg mol}^{-1}$ (E3.2-E3.4, Table 9).

Table 11 – Summary of results from kinetics of MMA solution polymerisation in toluene with CPDT as CTA.

Time (h)	Conversion ¹ (%)	$M_{n,th}$ ²	M_n ³	\mathcal{D} ³
1.3	3.8	2.2	7.8	1.56
2.0	6.5	3.8	10.2	1.60
3.2	22.5	12.9	18.7	1.41
4.3	24.8	14.3	21.1	1.39
5.3	35.9	20.7	24.2	1.34
7.0	39.0	22.5	26.2	1.31
24.0	73.5	42.3	48.4	1.26

¹ Conversion calculated from ¹H NMR. ² Theoretical M_n calculated relative to CTA and monomer concentration and given in kg mol^{-1} . ³ \mathcal{D} and M_n (in kg mol^{-1}) obtained by THF-SEC with RI detector against PMMA standards. (Molar ratio CPDT/AIBN 5:1, 65 °C, 300 rpm stirring rate, 1:1 volume ratio of toluene to MMA)

In the kinetic study of $scCO_2$ dispersion polymerisation, the linear evolution of M_n as a function of conversion shows good agreement with pseudo-living behaviour, as the linear trend of the experimental data is closely aligned with the theoretical molecular weight increase (Table 13, Figure 25C and 25D).⁴⁸ Control was further confirmed by the low dispersity observed throughout the reaction, $\mathcal{D} \leq 1.30$. In addition, the conversion was high for all reactions in $scCO_2$ with a free-flowing powder obtained with an average diameter of 2.49 μm and average C_v of 19.2% (Table 12, Figure 26).

Investigation on the early stage of MMA polymerisation with CPDT shows that turbidity, and hence nucleation, begins just 19 minutes into the reaction (Figure 27A). One may keep in mind that, as a trithiocarbonate, CPDT would likely suffer lower impact from inhibition and retardation than CPAB. Therefore, it is not surprising that nucleation in the presence of CPDT would start quicker than for CPAB. THF-SEC analysis showed a bimodal molecular weight distribution (Figure 27B), in a similar way to the previous studies with DDMAT and CPAB. The UV detector in the THF-SEC indicated that population **2** has the CTA end-group attached

(Figure 27C), population **2** which became the dominant species within the first 50 minutes of reaction, while population **1** has no UV signal.

Table 12 – Particle size analysis of PMMA particles synthesised *via* scCO₂ dispersion polymerisation with CPDT (3) as CTA.

Expt.	D _n ¹ (μm)	C _v ² (%)
E3.2	2.87	13.6
E3.3	2.26	20.5
E3.4	2.34	23.5

¹ Average particle size (D_n) is calculated as an average of 100 particles measurements *via* Image J®. ² the coefficient of variance (C_v) is calculated by the ratio of the standard deviation (σ) by the mean particle diameter as by equation (1).

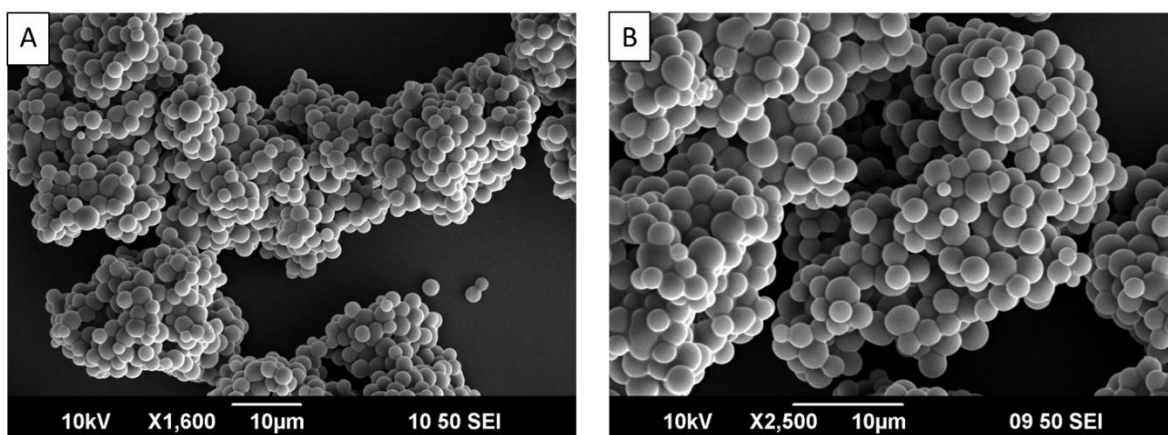


Figure 26 - SEM images of E3.3 obtained using a JEOL 6060LV SEM at accelerating voltage of 10 kV and at A) 1600x magnification and B) 2500x magnification.

Table 13 – Summary of results from kinetics of MMA dispersion polymerisation in scCO₂ with CPDT as CTA. Reaction monitored with the high-pressure sampling system.

Time (h)	Conversion ¹ (%)	$M_{n,th}$ ²	M_n ³	\mathcal{D} ³
1	4.8	1.2	4.4	1.19
2	5.7	2.8	4.8	1.16
3	7.4	3.	5.9	1.19
5	14.5	4.4	8	1.21
6	21.3	8.5	10.5	1.21
8	41.2	12.5	16.2	1.16
10	56.0	24.2	23.5	1.28
24	97.8	32.9	57.3	1.20

¹ Conversion calculated from ¹H NMR. ² \mathcal{D} and M_n (in kg mol⁻¹) obtained by THF-SEC with RI detector against PMMA standards. (Molar ratio CPDT/AIBN 2:1, 65 °C, 276 bar, 300 rpm stirring rate, 5 wt%(based on MMA) PDMS-MA as stabiliser)

To summarise, for the reactions with all three CTAs, we have confirmed that DDMAT, a poor choice of CTA, controls well MMA polymerisation in scCO₂. However, CPAB, which should be a good choice of CTA, gives poor control over M_n and dispersity, while CPDT, another good choice of CTA, gives good control. In addition to this, the Howdle group has previously reported good control of scCO₂ dispersion of MMA with other well-suited CTAs for the control of MMA polymerisation.^{32, 33}

Clearly, there must be other factors at play that are important in determining the final control we observe in these RAFT dispersion polymerisations. Independent of the CTA, the mechanism of reaction appears to follow a two-stage mechanism. This highlights the importance of establishing a high molecular weight species capable to rapidly nucleating particles at the start of the reaction. If this is a general trend, the partitioning of the CTA once the particles are formed must be crucial to control the polymerisation that is taking place now essentially in the dispersed phase, *i.e.*, inside the particles. Therefore, the solubility of the CTA in scCO₂ and the subsequent effects on partitioning into the particles may be the cause of the unexpected behaviour we observed with these CTAs. Previous computational simulations assumed that mobility of CTAs was effectively the same as the monomer or that the CTA was completely and instantaneously transported into the dispersed phase.^{66, 75-77}

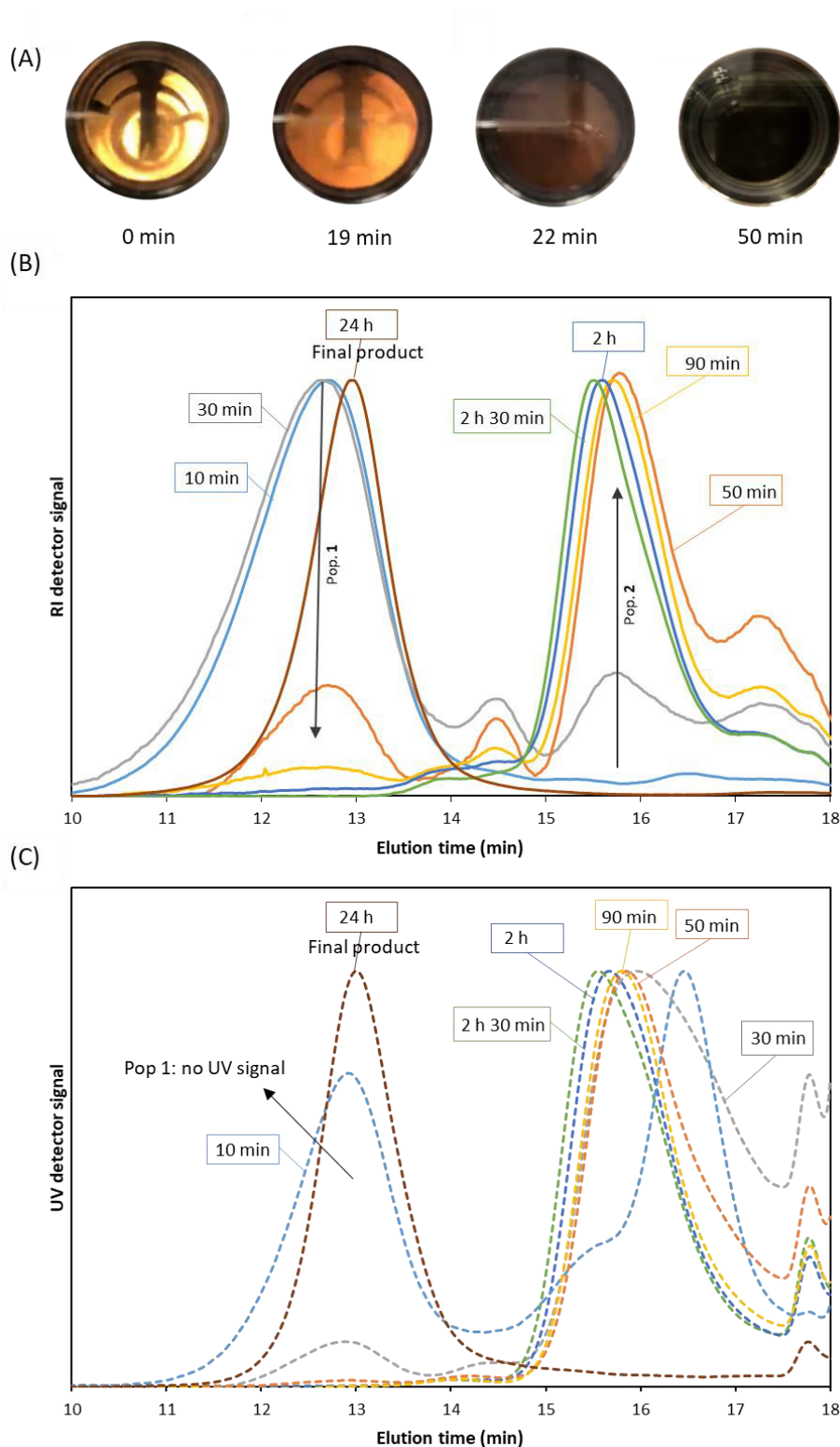


Figure 27 - Early stage study of a RAFT dispersion polymerisation of MMA in $scCO_2$ with CPDT, showing view cell pictures (A), and THF-SEC study of aliquots from reaction on sampling device against the RI detector (B) and the UV detector (C). It is noticeable that population 1 does not present UV signal (apart from sample at 10 and 30 min), while population 2 shows UV absorption at 300 nm. Results in (B) are normalised while the UV response (C) is not normalised.

In the following section, we try to identify the solvent factors that might tune the behaviour of these CTAs. Computational solvation models were used to probe the affinities of the different CTAs towards toluene and scCO₂ and we use the data to explain the disparity in behaviour of the different CTAs on the control of MMA polymerisation.

4.5.3. Solubility of CTAs

Since the solubility of CTAs could potentially influence reaction control, we investigated the impact of the CTAs structure on their solubility in scCO₂ by collaboration with Professor Jonathan Hirst and co-workers at the University of Nottingham, in order to develop a computational solvation model, and by means of cloud point studies in a variable volume view cell.

4.5.3.1. Computational solvation model for CTAs in scCO₂

Even though there are several models that attempt to explain the solvation mechanism of scCO₂ (acid-base Lewis, π - π interactions),^{78, 79} it is generally accepted that quadrupole-polar interactions play a significant role. To probe how the solvent influences the control of the polymerisation, pair distribution or radial distribution functions (RDF) were computed from molecular dynamics simulations. An RDF represents the relative probability of an interacting atom being found at a distance r from another reference atom. The RDFs of pairs of atoms that are strongly interacting through space will display two key features: (i) a maximum greater than unity, and (ii) peaks shifted to shorter distances, *i.e.* to the left, since the atoms are closer (Figure 28).

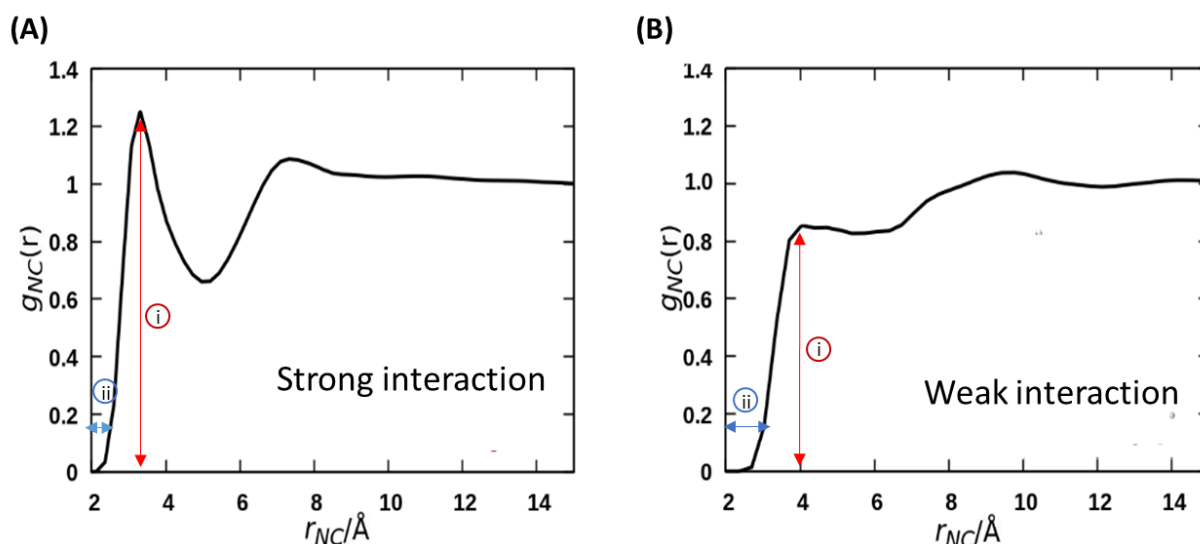


Figure 28 - RDFs of pairs of atoms showing a strong interaction (A) and a weak interaction (B). Strong interactions between two atoms have: (i) a higher peak in the Y axis, with a maximum greater than unity; and (ii) a peak closer to the origin, i.e., shifted to the left, indicating a shorter distance between the atoms.

The area under the first peak corresponds to the number of atoms directly interacting with the reference atom. For our purposes, the reference atoms were chosen to be C, O, N and S and the interacting atoms are the carbon atoms for both scCO_2 and toluene. In our scCO_2 polymerisation experiments with DDMAT, CPAB and CPDT we see positive, negative and no impact over the control of MMA polymerisation, respectively. Can the calculations pick out features that show such behaviour?

A recurring feature for all interactions involving scCO_2 is its affinity for unsaturated polar bonds, as is the case for the C=O and N \equiv C bonds that are present in the CTAs (DDMAT, CPAB, CPDT). All CTAs structures studied here also have an unsaturated C=S bond, which does have affinity with scCO_2 . This feature was not included on the solvation model of the CTAs, as it is a common feature. CO_2 interacts more effectively with C=O and N \equiv C bonds than toluene (Figure 29). For example, the C=O interactions with scCO_2 are more intense (Figure 29a) compared to the interactions with toluene (Figure 29B), as indicated by the peak shifted to shorter distances and the greater maximum at 1.2.

scCO_2 is well known to interact strongly with small apolar molecules and with polar unsaturated bonds.^{78,79} In particular, the N \equiv C group has a very strong affinity with an intense peak only seen for the scCO_2 distributions (Figure 29e and 29g) at around 2.5 Å, a value that

is consistent with strong non-covalent interactions.⁸⁰ N≡C has much weaker interaction with toluene (Figure 29f and 29h) as is evident from the less intense first maximum in the RDF at a longer distance.

On the other hand, it is known that scCO₂ solvation capacity diminishes rapidly for high molecular weight apolar groups and we would expect that the thiododecyl Z group in DDMAT and CPDT would lower the solubility in scCO₂. By contrast, toluene has a high affinity for heavy hydrocarbons and does not form polar interactions. The full RDF for the three CTAs in toluene and in scCO₂ can be found in the appendix (Figures S3 –S8).

The nature of the solvation mechanism of scCO₂ is elusive and still a topic of debate. In order to propose a model based on the interactions we have seen from the molecular dynamics simulations we will consider the N≡C moiety to have a strong interaction as indicated by the intense peak in the RDFs (Figure 29e and 29g) and the C=O moiety to have a moderate interaction (Figure 29a and 29c). Our aim is to provide a quick predictive tool to look at the behaviour of the CTAs in the scCO₂ controlled dispersion polymerisations.

In light of this, we can rationalise the observation that CPAB controls the reaction poorly in scCO₂ but performs well in toluene. CPAB possesses two unsaturated groups (C=O and N≡C) besides the C=S (Figure 30). This gives a high affinity for scCO₂ that will move the partitioning of the CTA towards the continuous phase. This would move the radical fragment away from the primary reaction *locus*, *i.e.*, the growing PMMA particles. In toluene, since these two unsaturated groups do not show high affinity to solvent molecules, the radical fragment is allowed to fully act on the reaction *locus*, promoting polymer growth effectively. In fact, the only group toluene displays affinity for are phenyl rings.

By contrast, DDMAT possesses only one unsaturated group (C=O) besides C=S for which scCO₂ has only a moderate affinity (Figure 30). DDMAT also has the thiododecyl Z group, which is not favoured by scCO₂ but will provide good affinity to the environment in the polymeric particles. In combination, these factors tend to push DDMAT to partition towards the dispersed phase. Therefore, the sole carbonyl group is not sufficient to cause the reaction to be delayed in scCO₂. In toluene DDMAT interacts heavily with the solvent through its long dodecyl chain, so in addition to the low chain transfer constant towards MMA, the DDMAT molecule becomes shielded by solvent molecules.

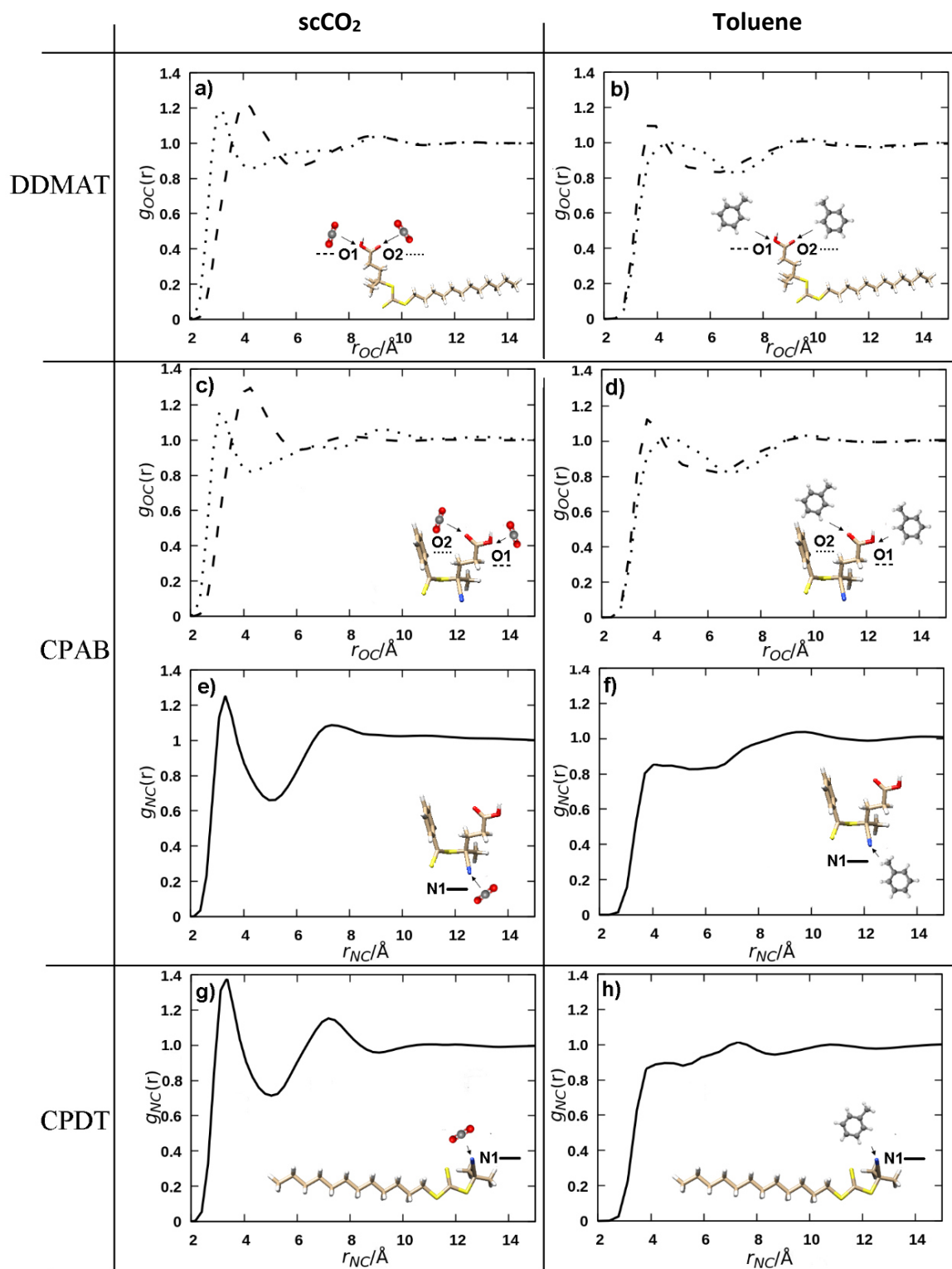


Figure 29 - Radial distribution functions showing the functional groups interactions with the solvent, $g_{ij}(r)$ ($i = O1$ - - -, $O2$ or $N1$ ___ and $j =$ carbon atoms of either CO_2 or toluene) vs. interatomic distances for a) Oxygen atoms of DDMAT in scCO₂, b) Oxygen atoms of DDMAT in toluene, c) Oxygen atoms of CPAB in scCO₂, d) Oxygen atoms of CPAB in toluene, e) Nitrogen atom of CPAB in scCO₂, f) Nitrogen atom of CPAB in toluene, g) Nitrogen atom of CPDT in scCO₂, h) Nitrogen atom of CPDT in toluene.

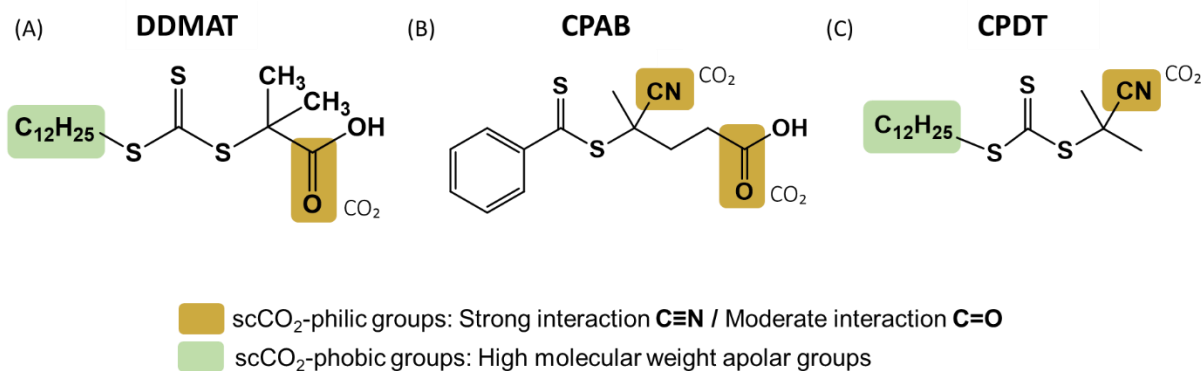


Figure 30 - Schematic showing the different interactions of CTAs functional groups with scCO_2 . (A) DDMAT: one scCO_2 -philic and one scCO_2 -phobic group (B) CPAB: two scCO_2 -philic groups and (C) CPDT: one scCO_2 -philic group and one scCO_2 -phobic group

For CPDT, there is one $\text{N}\equiv\text{C}$ moiety with a strong affinity for scCO_2 and this tends to have good solubility in the scCO_2 phase, but this is counterbalanced by the dodecyl group which would again present better affinity within the polymer particles (Figure 30). In toluene, the dodecyl group balances out the presence of the $\text{N}\equiv\text{C}$ group and thus solvation does not disrupt the good reaction control expected for its reactive radical group, in addition to its high chain-transfer constant towards MMA.

We emphasise that our solvation model focusses upon understanding the solubility of the CTAs at the beginning of the reaction. The RAFT reaction mechanism will unavoidably lead to the formation of an insoluble macro-CTA because of the addition of the monomer units as the reaction progresses.⁵ As a result, at a certain critical molecular weight the macro-CTA will become insoluble in the CO_2 -rich phase and will then be restricted to the dispersed phase. Nevertheless, the solubility model of the low molecular weight CTAs provides a powerful comparison between the solubility of the CTAs and the macro-CTAs that they then become, whilst maintaining the simplicity of the model. In addition, the kinetic study shows that the early stage of the reaction could well be of great importance in defining the overall RAFT control, as both DDMAT and CPAB have very different reaction profiles below 30% conversion.

Furthermore, we earlier demonstrated that an *in situ* two-stage polymerisation mechanism is in place in the RAFT dispersion in scCO_2 , which provides a heterogeneous system to which the unreacted CTA and CTA-oligomers can partition whilst still below the critical molecular weight. If the CTA and CTA-oligomers have a lower solubility in scCO_2 , they will enter the

particles earlier, increasing the CTA concentration at the reaction *locus*. Hence, the study of the low molecular weight CTA solubility and behaviour is still very relevant to our system.

4.5.3.2. Cloud point studies of CTAs

In order to further access the solubility of the CTAs used in this thesis, cloud point studies were performed in a variable volume view cell. This analysis was done visually and followed the procedure described in Section 4.4.3. and in Section 2.3.9., where the full equipment setup and operation procedure are described. The cloud point is the given pressure at a certain temperature when the solute precipitates out of the continuous phase, thus causing turbidity. At pressures above the cloud point the solute is soluble, and the lower the scCO₂ pressure required to solubilise a given solute, the higher its solubility.

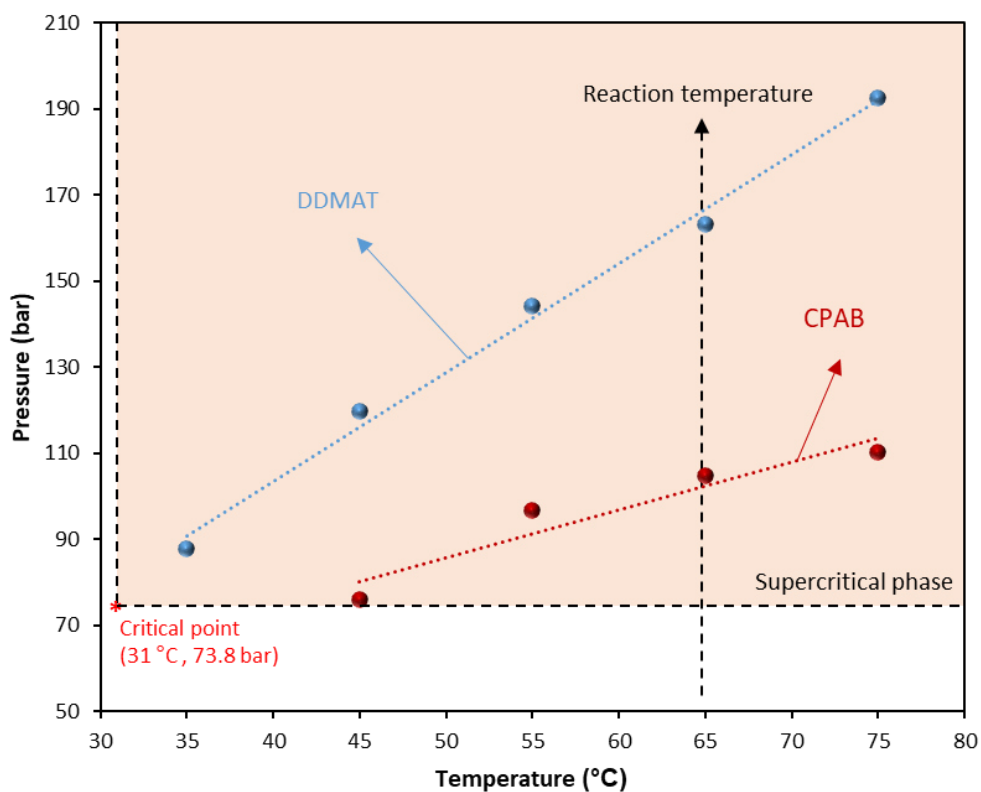


Figure 31 - Cloud point study of CTAs in variable volume view cell for DDMAT (blue) vs CPAB (red). The cloud point indicates the minimal pressure needed for solubilising the solute at a given temperature; as the cloud point for CPAB is lower than for DDMAT at all pressures, CPAB is more soluble in scCO₂ than DDMAT. The supercritical phase is demarcated by a red shade and the critical point is presented in the graph. (Cloud point study performed with 20 g of CO₂, 33 mmol of MMA and $6.30 \cdot 10^{-5}$ mol of CTA).

Analyses were performed as triplicates in an identical chemical environment as for the reactions, meaning that MMA was added to scCO₂ at the same ratio. Due to restrictions in time, only DDMAT and CPAB were analysed by this method (Figure 31).

In agreement with the computational model predictions, CPAB showed a much higher solubility in scCO₂ than DDMAT. Meaning that a lower pressure was required to dissolve the CTA at a given temperature. In fact, at 35 °C, CPAB was already soluble below supercritical conditions (73.8 bar), therefore, no cloud-point data could be collected at that temperature. At the standard reaction temperature, *i.e.* 65 °C, CPAB cloud point was 110.3 bar while DDMAT cloud point was 192.6 bar, which is a substantial difference in solubility. Keeping in mind that reactions were performed at 276 bar, both CTAs were soluble at reaction start and the system was homogeneous.

4.5.4. CTAs comparison: control and phase behaviour

In light of the computational solvation modelling results from the previous section (See Section 4.5.3.1.), we can better understand the distinct results observed for dispersion polymerisation in scCO₂ for each of the tested CTAs.

The polymeric microparticles have previously been defined as the main *locus* for conventional radical polymerisation of MMA in scCO₂.^{52, 60} It is known that at the very beginning of the reaction, the *locus* is in the continuous phase; this was demonstrated by turbidimetry analysis.^{58, 59} Mueller *et al.* modelled in detail MMA conventional radical polymerisation in scCO₂ and evaluated the influence of the rates of interphase radical transport, *i.e.* diffusion of growing chains, and of termination rates to define the reaction *locus*.^{63, 64} They identified that after the initial stage of reaction, the particles are the main *locus* of the reaction, with any new radicals generated in the continuous phase rapidly migrating irreversibly into the dispersed phase prior to termination. However, their simulations also showed that if termination in the continuous phase occurred at a similar rate or faster than the diffusion of growing chains into particles, then a bimodal molecular weight distribution would be obtained. In this case, low molecular weight chains would be formed in the continuous phase and higher molecular weight chains would be formed inside the particles, *i.e.*, the dispersed phase.⁶³

Very few studies have tried to model RAFT dispersion polymerisation in scCO₂.^{66, 75, 77, 81} In those studies, the particles were assumed to be the main *locus* of the reaction as for

conventional radical polymerisation. López-Domínguez *et al.* used Predici® software to study the RAFT polymerisation of styrene with AIBN initiator and *S*-thiobenzoyl thioglycolic acid (TBTGA) as the CTA in scCO₂.⁶⁶ They considered both the continuous and the dispersed phases in their simulations. When the CTA was present, the simulations reported that large dormant polymer chains were produced in the continuous phase at a significant level, while lower molecular weight chains were formed in the dispersed phase, where they assumed the CTA would mainly partition.⁶⁶ In those simulations, all chains were considered to be solely initiated *via* RAFT. However, our data show that this is not the case in reality. We do observe bimodal molecular weight distributions, with SEC-UV data showing that the higher molecular weight population, *i.e.*, population **1**, does not show a UV signal, which indicates that this has grown in an uncontrolled manner *via* conventional radical polymerisation and not *via* RAFT.

As previously mentioned, DDMAT shows surprising control with MMA. As discussed in Section 4.5.1.4., a high concentration of CTA in the particles and the slow feed of MMA into particles as the reaction progresses would provide conditions for the unexpected good control, in similar way to what was previously observed by Perrier and co-workers.⁷¹ For DDMAT, the presence of only one C=O of moderate interaction with CO₂, and the existence of the thiododecyl Z group of good affinity with the polymeric phase, means that its solubility in scCO₂ is considerably lower than CPAB. Therefore, it is not unreasonable that it would diffuse more promptly into the particles and that the MMA/CTA ratio would be decreased. This scenario would favour transfer reactions over propagation, and this would counterbalance the known low chain transfer constant of DDMAT. Thus, the performance of DDMAT as a control agent will strongly be improved, and the MMA polymerisation will resume in a controlled way, generating living growing chains.

By contrast, if the CTA is too soluble in CO₂, as for example CPAB, it will be less partitioned into the particles and the higher concentration of MMA/CTA in the particles will result in loss of control. Even if the CTA has a high chain transfer constant (C_{tr}), the high MMA/CTA ratio inside the particles will result in an artificially high theoretical M_n . In this way the solubility of the CTA will severely influence the level of control obtained (Figure 32).

In addition, the monomer conversion *versus* time plot provides important mechanistic insight. More specifically, the semi-logarithmic plot clearly evidences the presence of different regimes and it has been previously used to show the onset of nucleation.^{82, 83} Furthermore, as

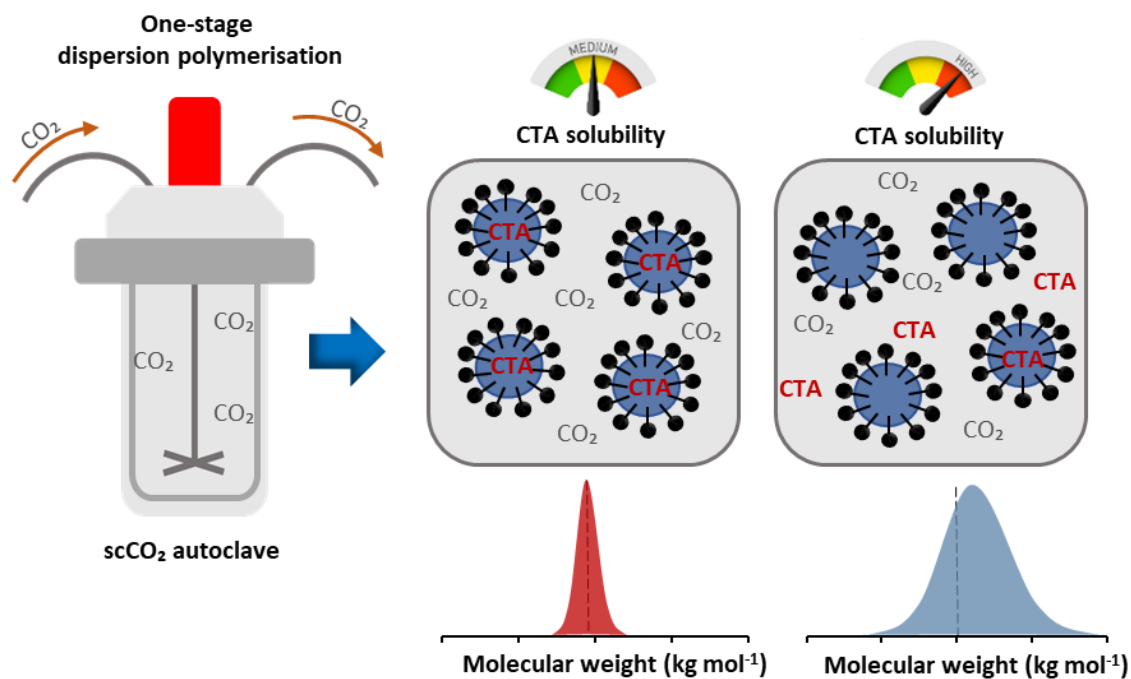


Figure 32 - Schematic of dispersion polymerisation in $scCO_2$ with CTAs offering different control as consequence of the partition between the reaction locus (i.e. particles) and the continuous phase, according to their solubility in $scCO_2$.

the polymer nuclei will swell with monomer, the high local concentration presented in the particles can cause a significant increase of the reaction rate.

Two regimes can be observed when using CPAB (Figure 33A). The nucleation onset is at 48 minutes, as determined by the X axis intercept of the first regime (red), and this is in good agreement with the time at which turbidity was observed by naked eye in the view cell, i.e. 43 minutes. The second regime (black) represents a 6.33-fold increase in the polymerisation rate. Interestingly, the timing of the inflexion between the two regimes, i.e. 10 h - Figure 33A, coincides with the deviation of M_n from $M_{n,th}$ trend line (Figure 20D), observed after 30% conversion. At 10 h the average conversion was 44 % and $M_n = 30.10 \text{ kg mol}^{-1}$. Before this point, the molecular weights were all closer to the expected values presented by the $M_{n,th}$ trend line. In addition, the final product obtained by the reaction with CPAB had a higher molecular weight than the targeted M_n ; this usually indicates incomplete usage of the CTA.²⁴ Therefore, it is in agreement with our hypothesis that the observed poor control of MMA polymerisation in $scCO_2$ with CPAB results from poor partitioning of the CTA and CTA-oligomers into the polymer particles at the early stage of reaction. This would result in a

smaller number of active dithiobenzoate moieties present inside each particle after nucleation and thus in a higher M_n .

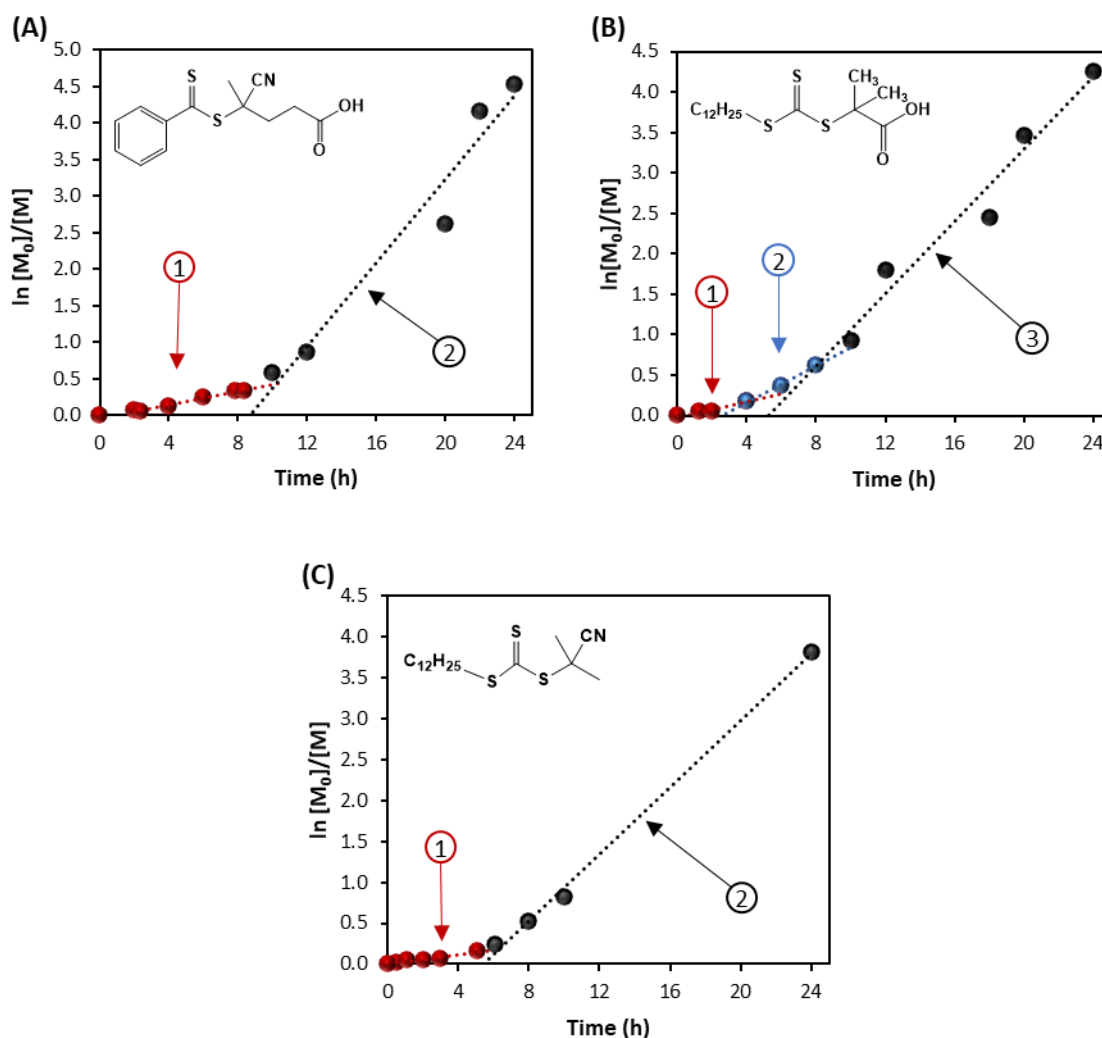


Figure 33 - Pseudo-first-order kinetic plot of monomer conversion as a function of reaction time for the dispersion polymerisation of MMA in $scCO_2$ with (B) DDMAT, highlighting three distinct regimes (red, blue, black); while (A) CPAB and (C) CPDT show two distinct regimes (red, black).

The mechanism for the reaction with DDMAT appears to be more complex. There are three distinct regimes (Figure 33B). The nucleation onset, *i.e.* first regime – red, appears at 27 minutes, while in the view cell turbidity was observed as early as 15 minutes. The second (blue) regime is from 4 to 8 hours, where the rate of polymerisation increases by 2.3-fold compared to first regime. Then there is a third (black) regime which shows a further 1.65-fold rate increase (Figure 33B). The presence of three regimes might not be so surprising, since

the dispersion polymerisation of MMA in scCO₂ can be considered to have three regimes in terms of monomer conversion.⁷⁷ At the first stage, polymerisation can only occur in the continuous phase, then in phase two, both in continuous and dispersed phases, and finally, polymerisation occurs only in the dispersed phase. As we expect all DDMAT to migrate rapidly into the particles, the second regime would have some contribution of conventional radical polymerisation taking place in the continuous phase simultaneously with the RAFT polymerisation occurring in the dispersed phase, while the final regime would be RAFT controlled and only take place inside the particles.

For CPDT, we see two regimes, similar to CPAB, with nucleation onset calculated at 18 minutes (Figure 33C), which is close to turbidity onset, 19 min, as observed in the view cell (Figure 27A). With this CTA, the second regime starts at 6 hours and represents a 7.25-fold increase in the rate of polymerisation. However, different from the reaction in presence of CPAB, the final molecular weight was in agreement with the theoretical value.

Furthermore, unlike CPAB, the kinetic study did not show a deviation of M_n from $M_{n,th}$ trend line (Figure 25D).⁴⁸ Therefore, the increase in the polymerisation rate is not likely caused by a low concentration of CTA present into the dispersed phase. In addition, the solubility of CPDT is in between DDMAT and CPAB. The lower solubility compared to CPAB appears to be enough to allow a good partitioning of the CTA into the particles and therefore good control is obtained. The absence of a third inflexion as seen for DDMAT might indicate that CPDT solubility is high enough to prevent a step where polymerisation only can take place inside the particles and therefore some polymerisation might still occur in the continuous phase.

4.5.5. Solubility effect over CTAs control in scCO₂ dispersion polymerisation.

To test the ability of our model, we selected four further CTAs to probe the importance of partitioning and CTA solubility on RAFT control in scCO₂ (Figure 34).

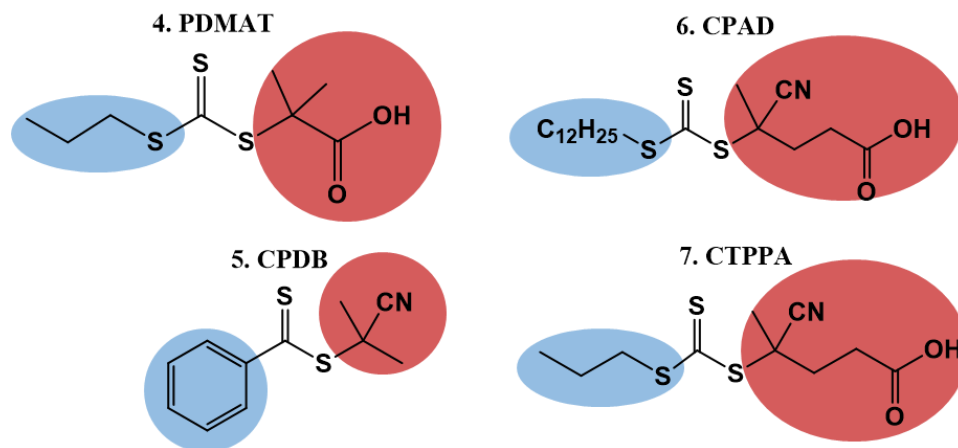


Figure 34 - Chain transfer agent (CTA) library with the R group in red and the Z group in blue: 4. PDMAT (2-(Propylthiocarbonothioylthio)-2-methylpropionic acid); 5. CPDB (2-Cyano-2-propyl benzodithioate); 6. CPAD (4-Cyano-4-[(dodecylsulfanylthiocarbonyl)sulfanyl]pentanoic acid); 7. CTPPA (4-cyano-4-thiothiopropylsulfanylpentanoic acid).

PDMAT, a trithiocarbonate identical to DDMAT but with a shorter Z stabilising group (thiopropyl) (Structure 4, Figure 34), was synthesised according to Lai *et al.* (See Section 4.4.2.6).⁴³ PDMAT is likely to be more soluble in scCO₂ than DDMAT. Studies on *n*-alkanes solubility in scCO₂ showed that solubility decreases as chain length increases.⁸⁴ The chain length of the alkyl tail in acrylate monomers was shown to impact the solubility in the same way.⁸⁵ In both cases, the loss of solubility comes from the reduction of polarity of the molecule with increasing alkyl chain length leading to a mismatch in the energy of solvation. Cloud point analysis (See Section 4.4.3.) confirmed that PDMAT has a higher solubility than DDMAT in scCO₂ (Figure 35). In other words, a lower pressure of scCO₂ was required to fully dissolve PDMAT compared to DDMAT at a given temperature. It is interesting to notice that the difference in solubility of the CTAs is more pronounced at higher temperatures and the reaction temperature is 65 °C.

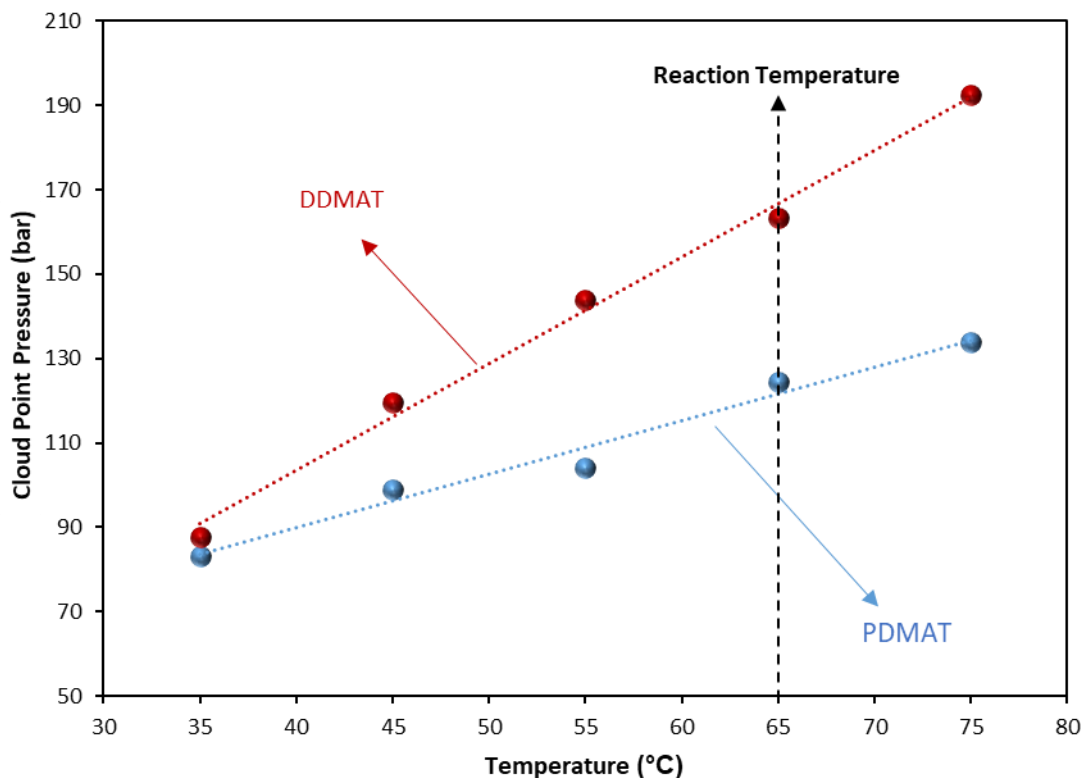


Figure 35 - Cloud point study of CTAs in variable volume view cell for DDMAT (red) vs PDMAT (blue). The cloud point indicates the minimal pressure needed for solubilising the solute at a given temperature; as the cloud point for PDMAT is lower than for DDMAT at all pressures, PDMAT is more soluble in $scCO_2$ than DDMAT. (Cloud point study performed with 20 g of CO_2 , 33 mmol of MMA and $6.30 \cdot 10^{-5}$ mol of CTA). Note that, at reaction temperature, both PDMAT and DDMAT required less pressure than the reaction pressure (276 bar).

We then used PDMAT for polymerisation of MMA both in $scCO_2$ and in toluene and assessed the corresponding control against the use of DDMAT (Table 14). The THF-SEC traces for these reactions demonstrate poor control in toluene, $M_n = 108.3 \text{ kg mol}^{-1}$; $M_{n,th} = 49.2 \text{ kg mol}^{-1}$; $\mathcal{D} = 1.49$, just like with DDMAT (Figure 36). This is not surprising as PDMAT has the same R reinitiating group as DDMAT. However, in $scCO_2$, PDMAT showed less control than DDMAT with M_n more than twice that predicted, $M_n = 101.2 \text{ kg mol}^{-1}$ and $M_{n,th} = 60.6 \text{ kg mol}^{-1}$, and a higher dispersity ($\mathcal{D} = 1.50$). Therefore, the increase in solubility of the CTA conferred by the shorter alkyl group does indeed negatively influence reaction control, in accordance with our hypothesis.

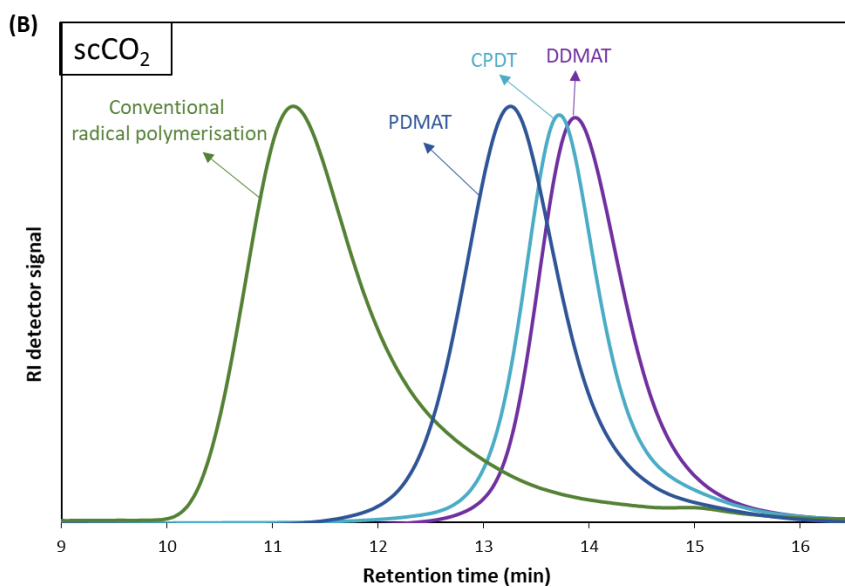
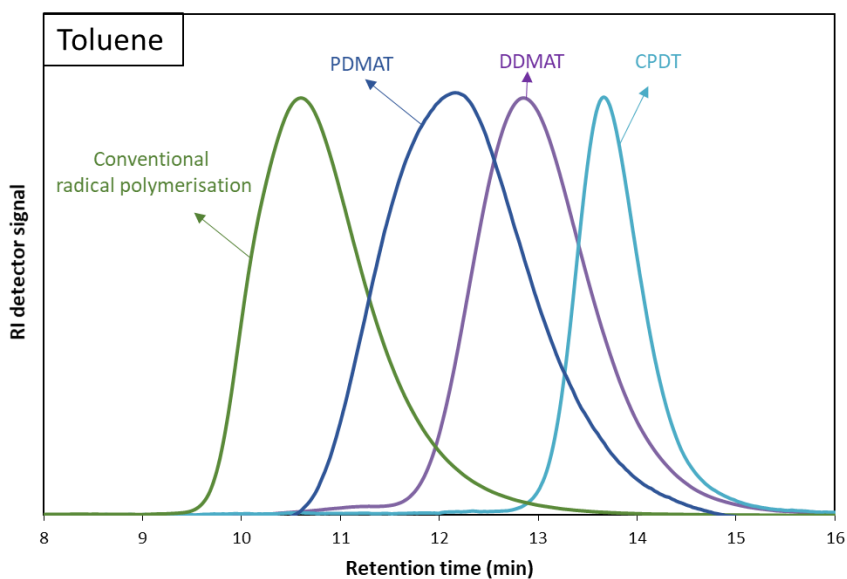


Figure 36 - THF-SEC traces of the final PMMA samples obtained by toluene solution polymerisation (A) and $scCO_2$ dispersion (B) with PDMAT and DDMAT. PMMA synthesized by conventional radical polymerisation and by well-controlled RAFT polymerisation with CPDT are shown for comparison.

Table 14 - Results of MMA polymerisation with PDMAT and DDMAT in (A) toluene solution (B) scCO₂ dispersion.

Expt.	CTA	Conv ¹ (%)	$M_{n,th}$ ²	M_n ³	\mathcal{D} ³
(A) Toluene Solution Polymerisation					
E1.1	DDMAT	66	40.1	82.3	1.60
E4.1	PDMAT	76	49.2	108.3	1.49
(B) scCO ₂ Dispersion Polymerisation					
E1.2	DDMAT	99	59.4	51.1	1.20
E4.2	PDMAT	98	60.6	101.2	1.50

¹ Conversion calculated from ¹H NMR. ² M_n theoretical calculated relative to CTA and monomer concentration and given in kg mol⁻¹. ³ \mathcal{D} and M_n obtained by THF-SEC with RI detector against PMMA standards, M_n given in kg mol⁻¹.

We then tested a further set of CTAs (Structures 5-7, Figure 34) for dispersed RAFT polymerisation in scCO₂ and toluene solution polymerisation (Table 15). The solvation analysis of these CTAs and their respective RDFs can be found in the appendix (Figures S9 –S14).

As CPAD and CTPPA present both a cyano group and an acid group, they can undergo degradation into amide in the same way as CPAB. Therefore, these CTAs were carefully inspected for degradation by ¹H NMR and ¹³C NMR in DMSO-D₆ as described by Fuchs *et al.*⁷⁴ No sign of degradation was observed and both CPAD and CTPPA could be used without further purifications. The NMR data is presented in the appendix (Figures S15 and S16).

In all cases, a loss of control in scCO₂ is systematically observed when a carboxylic acid is present in the CTA. For example, the pair CPAB/CPDB gives similar good control in toluene but the equivalent CTA with a carboxylic acid (CPAB) shows significantly poorer control in the scCO₂ dispersion (E2.2-2.7, Table 5 and E5.2, Table 15). The reaction with CPAB gave on average $M_n = 83.4$ kg mol⁻¹ against $M_{n,th} = 58.2$ kg mol⁻¹ and $\mathcal{D} = 1.48$; while the reaction with CPDB gave $M_n = 58.4$ kg mol⁻¹ against $M_{n,th} = 54.4$ kg mol⁻¹ and $\mathcal{D} = 1.28$. Since the addition of the acid group adds a C=O unsaturated group on the overall CTA structure, this makes the CTA more soluble in the continuous scCO₂ medium and hence less likely to partition into the growing polymer particles, negatively impacting control. The same trend can be observed for the CTA pair CPAD/CPDT (E6.2, Table 15 and E3.2-E3.4, Table 10). The reaction with CPAD gave $M_n = 84.1$ kg mol⁻¹ against $M_{n,th} = 59.4$ kg mol⁻¹ and $\mathcal{D} = 1.59$; while the reaction with CPDT gave on average $M_n = 59.3$ kg mol⁻¹ against $M_{n,th} = 58.7$ kg mol⁻¹ and $\mathcal{D} = 1.21$.

Table 15 - RAFT polymerisation of MMA with further CTAs by toluene solution polymerisation and dispersion polymerisation in scCO₂.

Expt.	CTA	Solvent	Conv ¹ (%)	$M_{n,th}$ ²	M_n ³	\mathcal{D} ³
E5.1	5-CPDB	toluene	92	50.5	55.1	1.17
E5.2	5-CPDB	scCO ₂	96	54.4	58.4	1.28
E6.1	6-CPAD	toluene	50	30.0	24.9	1.30
E6.2	6-CPAD	scCO ₂	99	59.4	84.1	1.59
E7.1	7-CTPPA	toluene	65	39.5	53.1	1.29
E7.2	7-CTPPA	scCO ₂	97	58.0	114.1	1.42

¹ Conversion calculated from ¹H NMR. ² Theoretical M_n calculated relative to CTA and monomer concentration and given in kg mol⁻¹. ³ \mathcal{D} and M_n (in kg mol⁻¹) obtained by THF-SEC with RI detector against PMMA standards. See experimental section for reaction conditions used for scCO₂ dispersion polymerisation. (Molar ratio CTA/AIBN 5:1, 65 °C, 300 rpm stirring rate, 1:1 volume ratio of toluene to MMA) (scCO₂: Molar ratio CTA/AIBN 2:1, 65 °C, 276 bar, 300 rpm stirring rate, 5 wt%(based on MMA) of PDMS-MA as stabiliser).

The pair CTPPA/CPAD shows again the effect that the alkyl moiety in the Z group can have over reaction control (E6.2 and E7.2, Table 15). CTPPA has the shorter alkyl chain, 3 carbons, which makes it more soluble in scCO₂ and thus leads to poorer control in scCO₂, with M_n = 114.1 kg mol⁻¹ against $M_{n,th}$ = 58.0 kg mol⁻¹ and \mathcal{D} = 1.42. On the other hand, CPAD, which has the longer Z group, 12 carbons, gave a lower deviation from the targeted M_n , M_n = 84.1 kg mol⁻¹ against $M_{n,th}$ = 59.4 kg mol⁻¹, although dispersity was still broad \mathcal{D} = 1.59. This result reinforces our earlier findings with DDMAT and PDMAT, where control was impaired by higher solubility in scCO₂.

Regardless of the control attained, all reactions with this new set of CTAs (Structures 4-7, Figure 34) in scCO₂ gave high conversions (>95%) and a free-flowing powder as product. The SEM analysis showed similar particle sizes around 2 μm for all samples (Figure 37, Table 16).

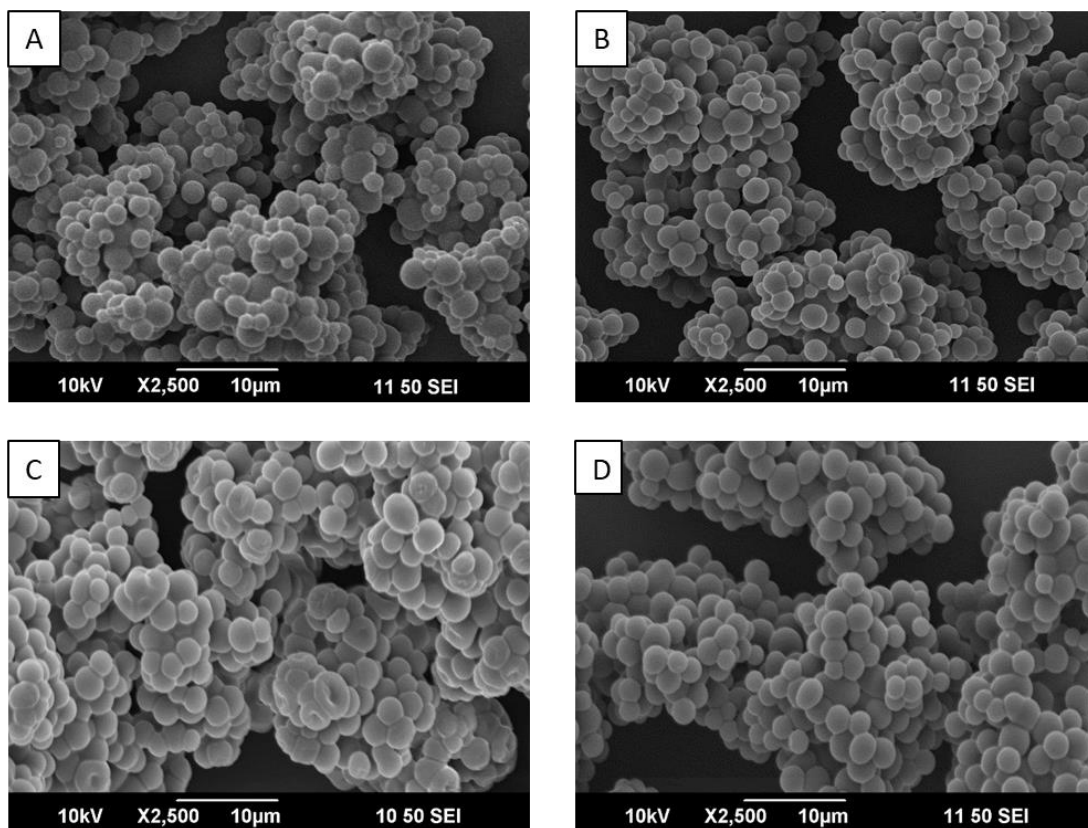


Figure 37 - SEM images of (A) E4.2 – PDMAT, (B) 5.2 – CPDB, (C) 6.2 – CPAD and (D) 7.2 – CTPPA; obtained using a JEOL 6060LV SEM at accelerating voltage of 10 kV and at 2500X magnification.

Table 16 - Particle size analysis of PMMA particles synthesised *via* scCO₂ dispersion polymerisation with PDMAT (4), CPDB (5), CPAD (6) and CTPPA (7) as CTA.

Expt.	CTA	D _n ¹ (µm)	C _v ² (%)
E4.2	4-PDMAT	2.15	28.9
E5.2	5-CPDB	1.90	16.5
E6.2	6-CPAD	2.59	15.9
E7.2	7-CTPPA	2.32	22.0

¹ Average particle size (D_n) is calculated as an average of 100 particles measurements *via* Image J®. ² The coefficient of variance (C_v) is calculated by equation (1).

All of these data show us that for dispersion polymerisation in scCO₂ the solubility of the CTA must not be so high that the ability to diffuse into the dispersed phase and control the polymerisation is impaired. On the other hand, as for all dispersion polymerisation mechanisms, there must be an initial homogeneous system at reaction onset, so the CTA must

have some solubility in scCO₂. In fact, our data suggest that solubility must follow a Goldilocks' principle: "not too little, not too much, but just right".

To corroborate our findings, the selection of CTAs for dispersion polymerisation in scCO₂ must consider the balance of CO₂-philic and CO₂-phobic features in the molecule, in order to control its phase behaviour (Table 17, Figure 38). The best CTAs for the dispersion polymerisation of MMA in scCO₂ had one CO₂-philic group, either N≡C or C=O, and one polymer-philic group (thiododecyl Z group). When two or more CO₂-philic groups were present, e.g. CPAB and CPAD, with both C=O and N≡C, control was compromised.

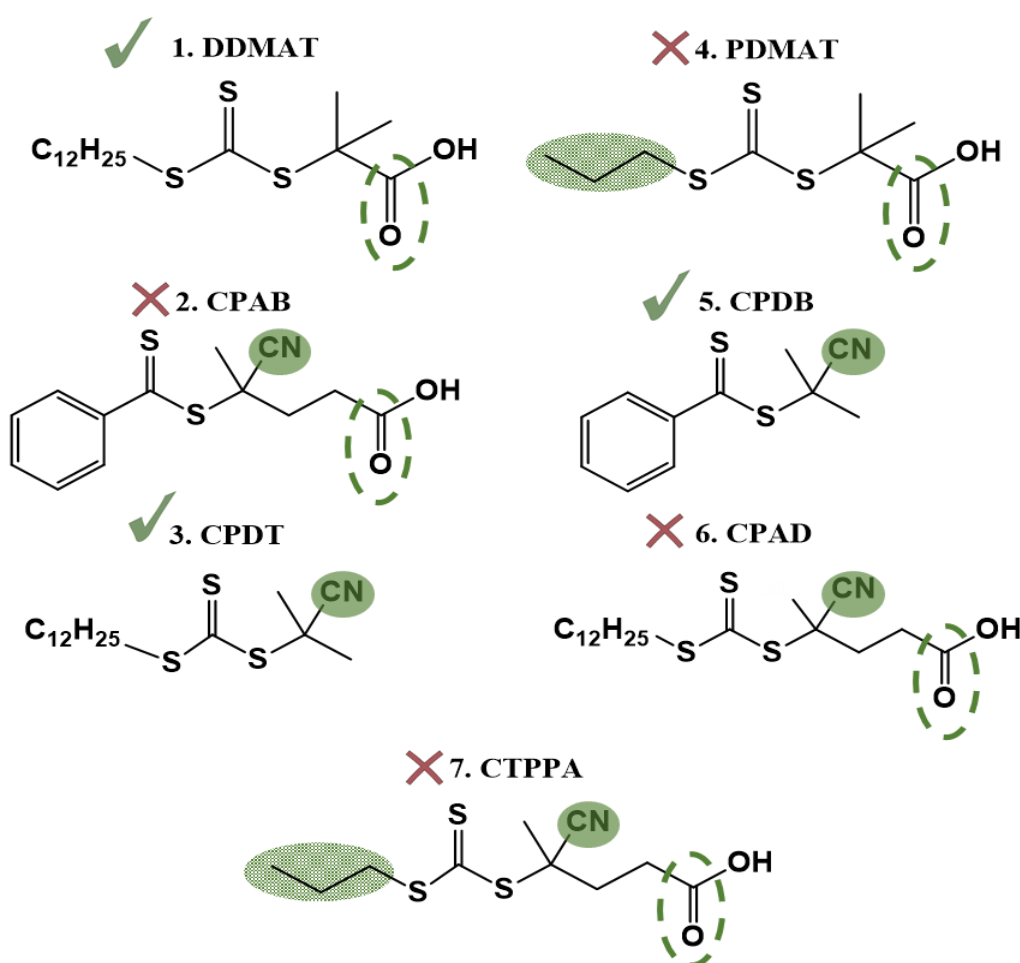


Figure 38 - Representation of CTAs groups that enhance solubility in scCO₂. Block green fill: N≡C, alternating fill: C₃H₆ and dashed circle: C=O. C₃H₆ does not provide a specific interaction with CO₂ molecules, however the lower molecular weight makes it more soluble compared to the other Z groups here presented. CTAs that have more than one solubility enhancing group provided poor control in scCO₂ (cross mark), while CTAs with only one group provided good control (tick mark).

Table 17 - Correlation of the number of CO₂-philic and polymer-philic groups of a CTA with polymerisation control for MMA dispersion polymerisation in scCO₂.

CTA	CO ₂ -philic groups	Polymer-philic groups	Solubility in scCO ₂	Control
DDMAT	1	1	Average	Good
CPAB	2	0	High	Poor
CPDT	1	1	Average	Good
PDMAT	1	0	High	Poor
CPDB	1	0	Average	Good
CPAD	2	1	High	Poor
CTPPA	2	0	High	Poor

CPDT and DDMAT both showed optimal solubility for controlling the MMA dispersion polymerisation, and we consider these two as the best choice of CTA for this reaction in scCO₂, despite the DDMAT poor performance in homogeneous conditions in toluene.

4.5.6. Some further considerations (comparing to Gregory *et al.*)

At first, CPAB poor control in scCO₂ was unexpected, since Gregory *et al.* obtained optimal control with similar dithioesters (Figure 39).³³ In an attempt to reproduce the same good results they obtained, we tried to change some of the reaction conditions with CPAB as CTA. Experiment B2 used same reaction conditions as Gregory *et al.* (Table 18).

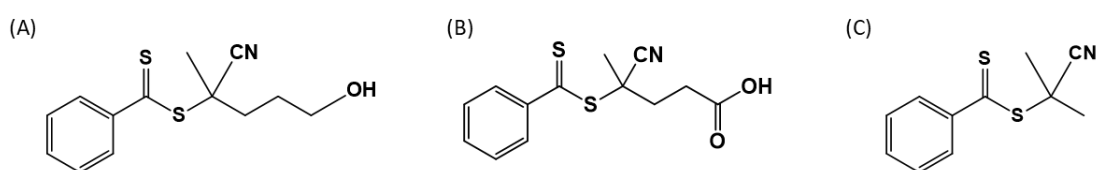


Figure 39 - Structures of CTAs used in this section: (A) CPOB, CTA used by Gregory *et al.*,²⁵ (B) CPAB, CTA 2; (C) CPDB, CTA 5.

Interestingly, targeting a lower M_n of 25 kg mol⁻¹ with CPAB did not improve control compared to reactions targeting 60 kg mol⁻¹ (respectively exp. B2 and B - Table 18). RAFT polymerisation is known to have less control at higher degree of polymerisation, as result of reduction of the number of chains and increase of the time each chain is active, which increases the probability of termination. However, in this case the reaction seems to be more uncontrolled when

targeting the lower M_n , with $\mathcal{D} = 1.75$ and M_n almost 4-fold higher than desired, compared to when 60 kg mol^{-1} was targeted, $M_n = 83.4 \text{ kg mol}^{-1}$ and $\mathcal{D} = 1.48$ (Table 18).

However, when AIBN content was increased from 2:1 to 1:1 CTA/AIBN molar ratio (exp. B3 - Table 18), surprisingly, the control improved. Dispersity was 1.27 and M_n was closer to the target than in experiment B, although still twice above the theoretical value, $M_n = 43.6 \text{ kg mol}^{-1}$ and $M_{n,\text{th}} = 24.0 \text{ kg mol}^{-1}$ (Table 18). With the higher AIBN content, one would expect the opposite as result of increased number of dead chains and, therefore, control is expected to be lower. However, the higher AIBN content improves the initial nucleation stage and thus could improve control *via* a more robust *in situ* two-stage polymerisation. Nevertheless, these results are far from the control observed by Gregory with CPOB (Figure 39A). Here it is important to emphasise that the CTA used by Gregory *et al.*³³, CPOB (CTA A – Figure 39), carries an OH end-group, while CPAB has a carboxylic acid as end-group.

Table 18 – Comparing results from Gregory *et al.*³³ for RAFT polymerisation of MMA with CTAs in scCO_2 dispersion polymerisation.

Expt.	CTA	AIBN/CTA	Conv ¹ (%)	$M_{n,\text{th}}$ ²	M_n ³	\mathcal{D} ³	D_n ⁴ (μm)	C_v ⁵ (%)
A*	CPOB	1:1	99	24.75	26.00	1.19	1.39	19.8
B**	2-CPAB	2:1	97	58.2	83.4	1.48	2.65	16.0
B2	2-CPAB	2:1	97	24.43	77.90	1.75	1.66	24.4
B3	2-CPAB	1:1	97	23.99	43.60	1.27	1.75	22.8
C*	5-CPDB	1:1	96	23.75	23.60	1.14	1.40	43.0
C1**	5-CPDB	2:1	96	54.4	58.4	1.28	1.90	16.5
C2	5-CPDB	1:1	98	25.2	29.6	1.14	1.69	27.3

¹ Conversion calculated from $^1\text{H NMR}$. ² Theoretical M_n calculated relative to CTA and monomer concentration and given in kg mol^{-1} . ³ \mathcal{D} and M_n (in kg mol^{-1}) obtained by THF-SEC with RI detector against PMMA standards. See experimental section for reaction conditions used for scCO_2 dispersion polymerisation. ⁴ Average particle size (D_n) is calculated as an average of 100 particles measurements via Image J[®]. ⁵ the coefficient of variance (C_v) is calculated by equation (1). * Results extracted from Gregory *et al.*³³; ** Results from previous sections, B = average of E2.2-E2.7 in Table 5, and C1 = E5.2 in Table 15.

In fact, according to our solvation model, the carboxylic group will increase solubility due to the unsaturated functional group while the alcohol group will not provide any beneficial interaction with CO₂ resulting in a lower solubility of CPOB than CPAB in scCO₂ (RDF for CPOB is presented in Figure 40). Therefore, CPOB will partition more into the dispersed phase of the heterogeneous system and this will improve control compared to CPAB.

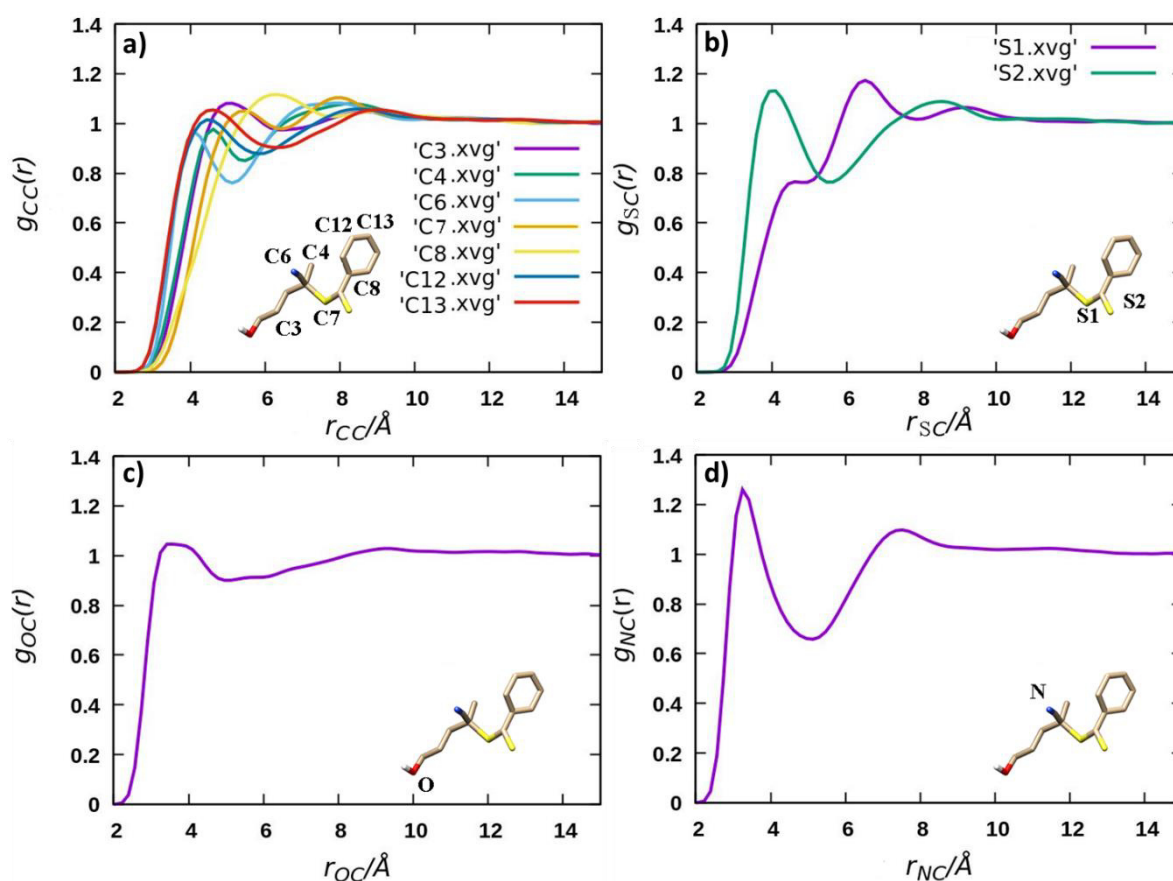


Figure 40 - Radial distribution functions showing the functional groups of CPOB interactions with the solvent, $g_{ij}(r)$ ($i = O1 \text{ ---}, O2 \text{ or } N1 \text{ ---}$ and $j =$ carbon atoms of CO₂ vs. interatomic distances for a) Carbon atoms in scCO₂, b) Sulfur atoms in scCO₂, c) Oxygen atom in scCO₂, d) Nitrogen atom in scCO₂.

CPDB (5) was another efficient CTA presented in Gregory's work (Figure 39B).³³ In our hands too, CPDB performed well (C1 - Table 18) under however different conditions ($M_{n \text{ targeted}} = 60 \text{ kg mol}^{-1}$). To compare these results (C - Table 18) with ours, a further reaction (C2 – Table 18) was performed at the same reaction conditions they used ($M_{n \text{ targeted}} = 25 \text{ kg mol}^{-1}$). This time reducing the targeted M_n improved dispersity (from 1.28 for C1 to 1.14 for C2) while in both reactions a similar control over M_n was observed (Table 18). Thus, CPDB gave good RAFT control. These results further prove that the control observed by the different CTAs presented

by Gregory *et al.* is in agreement with our model and confirmed our hypothesis of CTA solubility influencing control of the dispersion polymerisation in scCO₂.

4.6. Conclusions

Our study confirmed the surprising control of DDMAT over the polymerisation of MMA in scCO₂, despite the known poor control of this trithiocarbonate CTA over methacrylate polymerisation in conventional solvents. With the use of a recently developed sampling instrument, we have been able to accurately follow the kinetic evolution and uncover new insights into the early stage of RAFT dispersion polymerisation in scCO₂. The good control of DDMAT was then attributed to the local modification of the monomer/CTA molar ratio inside the particles that are created under an *in situ* two-stage process.

In order to broaden the palette of experimental observations and to corroborate our understanding, six more CTAs were studied for their ability to control MMA dispersion polymerisation in scCO₂. We also present a novel computational solvation model based on molecular simulations to understand the effect of various moieties upon the solubility of the CTAs in scCO₂. We have utilised this to identify correlations between polymerisation control and solubility of the CTA in scCO₂. Our data also align with previous observations of two-stage dispersion polymerisation in conventional solvents.

We thus present a simple approach to identify the best CTA for RAFT dispersion polymerisation based upon solubility in scCO₂ and the likely partitioning between the scCO₂ continuous phase and the growing PMMA microparticles environment. Our approach can explain the distinct RAFT control observed with the different CTAs we tested and with CTAs presented in previous publications. We believe that these principles and the guideline that came from them, offer a valuable addition for the field of polymerisation in scCO₂ and that it can be extended more broadly to controlled dispersion polymerisations of other monomers in scCO₂ and in other solvents.

4.7. References

1. H. M. Woods, C. Nouvel, P. Licence, D. J. Irvine and S. M. Howdle, *Macromolecules*, 2005, **38**, 3271-3282.
2. E. J. Beckman, *J Supercrit Fluids*, 2004, **28**, 121-191.

3. A. Clifford, *Fundamentals of Supercritical Fluids*, Oxford Science Publications, 1999.
4. J. L. Kendall, D. A. Canelas, J. L. Young and J. M. DeSimone, *Chemical reviews*, 1999, **99**, 543-563.
5. P. B. Zetterlund, Y. Kagawa and R. K. O'Reilly, *Chem. Rev.*, 2008, **108**.
6. P. B. Zetterlund, F. Aldabbagh and M. Okubo, *J Polym Sci A Polym Chem*, 2009, **47**, 3711-3728.
7. L. H. Sperling, *Introduction to Physical Polymer Science*, Wiley Interscience, Bethlehem, Pennsylvania, 2001.
8. S. Shen, E. D. Sudol and M. S. El-Aasser, *J Polym Sci A Polym Chem*, 1994, **32**, 1087-1100.
9. T. D. McAllister, L. D. Farrand and S. M. Howdle, *Macromol Chem Phys*, 2016, **217**, 2294-2301.
10. J. M. DeSimone, E. E. Maury, Y. Z. Menceloglu, J. B. McClain, T. J. Romack and J. R. Combes, *Science*, 1994, **265**, 356-359.
11. P. Christian, M. R. Giles, R. M. T. Griffiths, D. J. Irvine, R. C. Major and S. M. Howdle, *Macromolecules*, 2000, **33**, 9222-9227.
12. M. R. Giles, J. N. Hay and S. M. Howdle, *Macromol Rapid Commun*, 2000, **21**, 1019-1023.
13. A. I. Cooper, *J Mater Chem*, 2000, **10**, 207-234.
14. H. Shiho and J. M. DeSimone, *J Polym Sci A Polym Chem*, 1999, **37**, 2429-2437.
15. H. Shiho and J. M. DeSimone, *J Polym Sci A Polym Chem*, 2000, **38**, 3783-3790.
16. J. Jennings, M. Beija, A. P. Richez, S. D. Cooper, P. E. Mignot, K. J. Thurecht, K. S. Jack and S. M. Howdle, *J Am Chem Soc*, 2012, **134**, 4772-4781.
17. J. Jennings, G. He, S. M. Howdle and P. B. Zetterlund, *Chem Soc Rev*, 2016, **45**, 5055-5084.
18. T. M. Bennett, G. He, R. R. Larder, M. G. Fischer, G. A. Rance, M. W. Fay, A. K. Pearce, C. D. J. Parmenter, U. Steiner and S. M. Howdle, *Nano Lett*, 2018, **18**, 7560-7569.
19. A. J. Haddleton, T. M. Bennett, X. Chen, R. L. Atkinson, V. Taresco and S. M. Howdle, *Polym Chem*, 2020, **11**, 5029-5039.
20. A. Xu, Q. Lu, Z. Huo, J. Ma, B. Geng, U. Azhar, L. Zhang and S. Zhang, *Rsc Adv*, 2017, **7**, 51612-51620.
21. Z Y Huo, P D Xia, U Azhar, J C Ma, X M Zhang, X Y Zhou, S. X. Z. and A. H. Xu, *IOP Conf. Ser.: Mater. Sci. Eng.*, 2019, **479**.
22. Z. Ma and P. Lacroix-Desmazes, *Polymer*, 2004, **45**, 6789-6797.
23. S. Perrier, *Macromolecules*, 2017, **50**, 7433-7447.
24. G. Moad, E. Rizzardo and S. H. Thang, *The Strem Chemiker*, 2011, **25**, 1-10.
25. D. J. Keddie, G. Moad, E. Rizzardo and S. H. Thang, *Macromolecules*, 2012, **45**, 5321-5342.
26. J.-S. Wang, D. Greszta and K. Matyjaszewski, *Polym Mater Sci Eng*, 1995 **73**, 416-417.
27. M. Hölderle, M. Baumert and R. Mülhaupt, *Macromolecules*, 1997, **30**, 3420-3422.
28. L. I. Gabaston, R. A. Jackson and S. P. Armes, *Macromolecules*, 1998, **31**, 2883-2888.
29. P. B. Zetterlund, Y. Kagawa and M. Okubo, *Chemical reviews*, 2008, **108**, 3747-3794.
30. P. J. Saikia, J. M. Lee, B. H. Lee and S. Choe, *J Polym Sci A Polym Chem*, 2007, **45**, 348-360.
31. P. B. Zetterlund, S. C. Thickett, S. Perrier, E. Bourgeat-Lami and M. Lansalot, *Chemical reviews*, 2015, **115**, 9745-9800.
32. K. J. Thurecht, A. M. Gregory, W. Wang and S. M. Howdle, *Macromolecules*, 2007, **40**, 2965-2967.
33. A. M. Gregory, K. J. Thurecht and S. M. Howdle, *Macromolecules*, 2008, **41**, 1215-1222.
34. R. McHale, F. Aldabbagh, P. B. Zetterlund, H. Minami and M. Okubo, *Macromolecules*, 2006, **39**, 6853-6860.
35. J.-S. Song and M. A. Winnik, *Macromolecules*, 2006, **39**, 8318-8325.
36. A. J. Paine, W. Luymes and J. McNulty, *Macromolecules*, 1990, **23**, 3104-3109.
37. J.-S. Song and M. A. Winnik, *Macromolecules*, 2006, **39**, 8318-8325.
38. Y. K. Chong, J. Kristina, T. P. T. Le, G. Moad, A. Postma, E. Rizzardo and S. H. Thang, *Macromolecules*, 2003, **36**, 2256-2272.
39. C. Li and B. C. Benicewicz, *J. Polym. Sci. A Polym. Chem.*, 2005, **43**, 1535-1543.

40. J. Chiefari, R. T. A. Mayadunne, C. L. Moad, G. Moad, E. Rizzardo, A. Postma and S. H. Thang, *Macromolecules*, 2003, **36**, 2273-2283.
41. G. Moad, E. Rizzardo and S. H. Thang, *Aust J Chem*, 2005, **58**, 379-410.
42. G. Moad, E. Rizzardo and S. H. Thang, *Acc Chem Res*, 2008, **41**.
43. J. T. Lai, D. Filla and R. Shea, *Macromolecules*, 2002, **35**, 6754-6756.
44. J. Jennings, M. Beija, J. T. Kennon, H. Willcock, R. K. O'Reilly, S. Rimmer and S. M. Howdle, *Macromolecules*, 2013, **46**, 6843-6851.
45. M. Alauhdin, T. M. Bennett, G. He, S. P. Bassett, G. Portale, W. Bras, D. Hermida-Merino and S. M. Howdle, *Polym Chem*, 2019, **10**, 860-871.
46. T. Boursier, I. Chaduc, J. Rieger, F. D'Agosto, M. Lansalot and B. Charleux, *Polym Chem*, 2011, **2**, 355-362.
47. F. Furno, P. Licence, S. M. Howdle and M. Poliakoff, *Actual Chimique*, 2003, 62-66.
48. K. Kortsen, A. A. C. Pacheco, J. C. Lentz, V. Taresco and S. M. Howdle, *J Supercrit Fluids*, 2021, **167**, 105047.
49. J. G. Harris and K. H. Yung, *J Phys Chem*, 1995, **99**, 12021-12024.
50. M. J. Abraham, T. Murtola, R. Schulz, S. Páll, J. C. Smith, B. Hess and E. Lindahl, *SoftwareX*, 2015, **1-2**, 19-25.
51. E. Rizzardo, M. Chen, B. Chong, G. Moad, M. Skidmore and S. H. Thang, *Macromol Symp*, 2007, **248**, 104-116.
52. M. L. O'Neill, M. Z. Yates, P. J. Johnston, S. C. D. and S. P. Wilkinson, *Macromolecules*, 1998, **31**, 2838-2847.
53. Z. Guan, J. R. Combs, Y. Z. Menceloglu and J. M. DeSimone, *Macromolecules*, 1993, **26**, 2663-2669.
54. M. R. Giles, J. N. Hay, S. M. Howdle and R. J. Winder, *Polymer*, 2000, **41**, 6715-6721.
55. K. A. Shaffer, T. A. Jones, D. A. Canelas and J. M. DeSimone, *Macromolecules*, 1996, **29**, 2704-2706.
56. J. J. Haven and T. Junkers, *European J Org Chem*, 2017, 6474-6482.
57. J.-N. Ollagnier, T. Tassaing, S. Harrisson and M. Destarac, *React Chem Eng*, 2016, **1**, 372-378.
58. U. Fehrenbacher and M. Matthias Ballauff, *Macromolecules*, 2002, **35**, 3653-3661.
59. U. Fehrenbacher, O. Muth, T. Hirth and M. Ballauff, *Macromol Chem Phys*, 2000, **201**, 1532-1539.
60. M. L. O'Neill, M. Z. Yates, K. P. Johnston, C. D. Smith and S. P. Wilkinson, *Macromolecules*, 1998, **31**, 2848-2856.
61. B. Grignard, B. Gilbert, C. Malherbe, C. Jérôme and C. Detrembleur, *ChemPhysChem*, 2012, **13**, 2666-2670.
62. K. J. Thurecht, S. Villarroya, J. Zhou, S. M. Howdle, A. Heise, M. Degeus and M. F. Wyatt, *Macromolecules*, 2006, **39**, 7967-7972.
63. P. A. Mueller, G. Storti and M. Morbidelli, *Chem Eng Sci*, 2005, **60**, 1911-1925.
64. P. A. Mueller, G. Storti and M. Morbidelli, *Chem Eng Sci*, 2005, **60**, 377-397.
65. J. J. Shim and K. P. Johnston, *AIChE J.*, 1989, **3**, 1097-1106.
66. P. López-Domínguez, G. Jaramillo-Soto and E. Vivaldo-Lima, *Macromol React Eng*, 2018, **12**, 1800011.
67. A. Rajendran, B. Bonavoglia, N. Forrer, G. Storti, M. Mazzotti and M. Morbidelli, *Ind Eng Chem Res*, 2005, **44**, 2549-2560.
68. B. Bonavoglia, G. Storti, M. Morbidelli, A. Rajendran and M. Mazzotti, *J Polym Sci B Polym Phys*, 2006, **44**, 1531-1546.
69. U. Fehrenbacher, T. Jakob, T. Berger, W. Knoll and M. Ballauff, *Fluid Phase Equilib.*, 2002, **200**, 147-160.
70. A. Quintero-Ortega, G. Jaramillo-Soto, P. R. García-Morán, M. L. Castellanos-Cárdenas, G. Luna-Bárceñas and E. M. R. E. Vivaldo-Lima, *Macromol React Eng*, 2008, **2**, 304-230.

71. R. A. E. Richardson, T. R. Guimarães, M. Khan, G. Moad, P. B. Zetterlund and S. Perrier, *Macromolecules*, 2020, **53**, 7672–7683.
72. G. Moad, E. Rizzardo and S. H. Thang, *Aust J Chem*, 2005, **58**, 379-410.
73. G. Moad, E. Rizzardo and S. H. Thang, *Aust J Chem*, 2012, **65**, 985-1076.
74. A. V. Fuchs and K. J. Thurecht, *ACS Macro Lett.*, 2017, **6**, 287-291.
75. G. Jaramillo-Soto, M. L. Castellanos-Cárdenas, P. R. García-Morán, E. Vivaldo-Lima, G. Luna-Bárcenas and A. Penlidis, *Macromol Theory Simul*, 2008, **17**, 280-289.
76. G. Jaramillo-Soto, P. R. Garcia-Moran, F. J. Enriquez-Medrano, H. Maldonado-Textle, M. E. Albores-Velasco, R. Guerrero-Santos and E. Vivaldo-Lima, *Polymer*, 2009, **50**, 5024-5030.
77. P. López-Domínguez, J. E. Rivera-Peláez, G. Jaramillo-Soto, J. F. Barragán-Aroche and E. Vivaldo-Lima, *React Chem Eng*, 2020, **5**, 547-560.
78. F. J. Gutiérrez Ortiz and A. Kruse, *React Chem Eng*, 2020, **5**, 424-451.
79. F. Ingrosso and M. F. Ruiz-López, *ChemPhysChem*, 2017, **18**, 2560-2572.
80. G. Cavallo, P. Metrangolo, R. Milani, T. Pilati, A. Priimagi, G. Resnati and G. Terraneo, *Chem. Rev.*, 2016, **116**, 2478-2601.
81. G. Jaramillo-Soto, P. R. Garcia-Moran and E. Vivaldo-Lima, *Macromol Symp*, 2010, **289**, 149-154.
82. A. Blanazs, J. Madsen, G. Battaglia, A. J. Ryan and S. P. Armes, *J Am Chem Soc*, 2011, **133**, 16581-16587.
83. L. A. Fielding, M. J. Derry, V. Ladmiral, J. Rosselgong, A. M. Rodrigues, L. P. D. Ratcliffe, S. Sugihara and S. P. Armes, *Chem Sci*, 2013, **4**, 2081.
84. Q. Shi, L. Jing and Q. W., *J CO2 Util*, 2015, **9**, 29-38.
85. C. F. Kirby and M. A. McHugh, *Chem rev*, 1998, **99**, 565-602.

4.8. Appendix

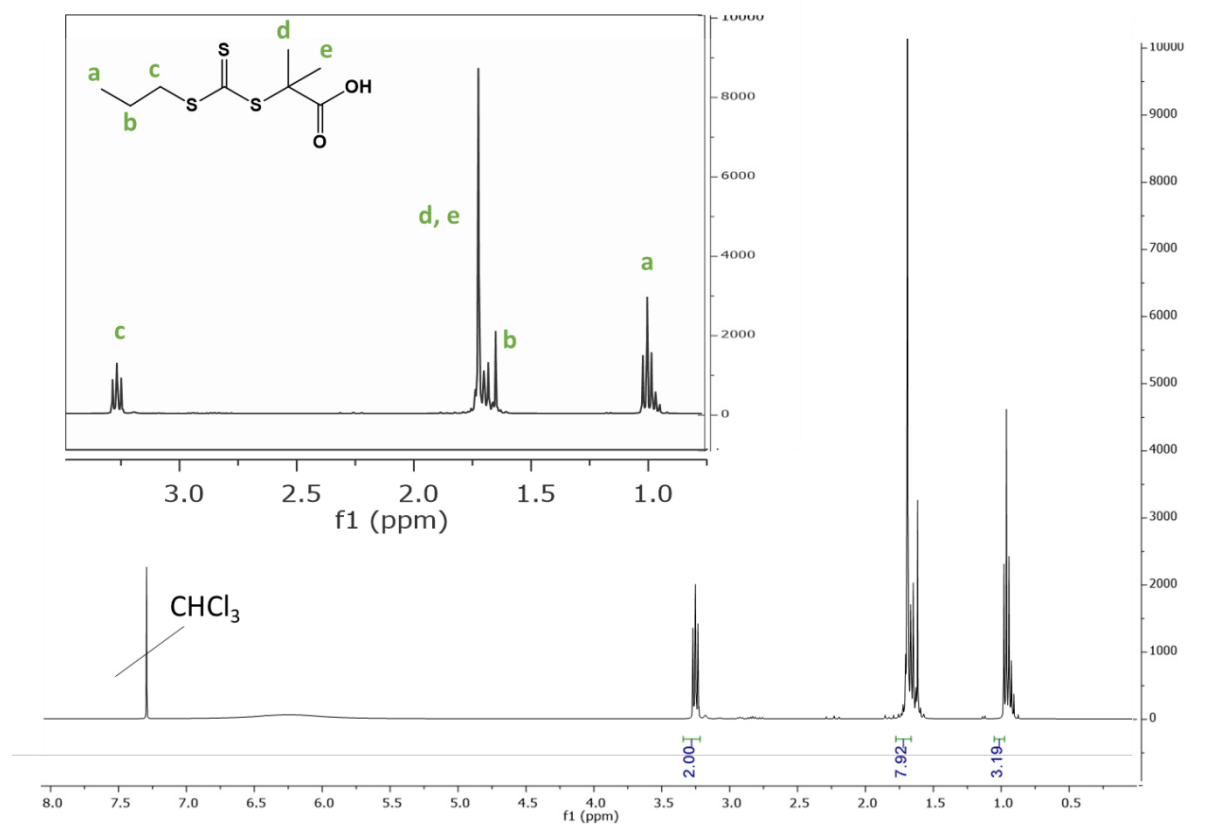


Figure S1 ^1H NMR of PDMAT (400 MHz, CDCl_3), δ (ppm): 3.27 (t, $J = 7.4$ Hz, 2H), 1.72 (m, 8H), 0.99 (t, $J = 7.4$ Hz, 3H).

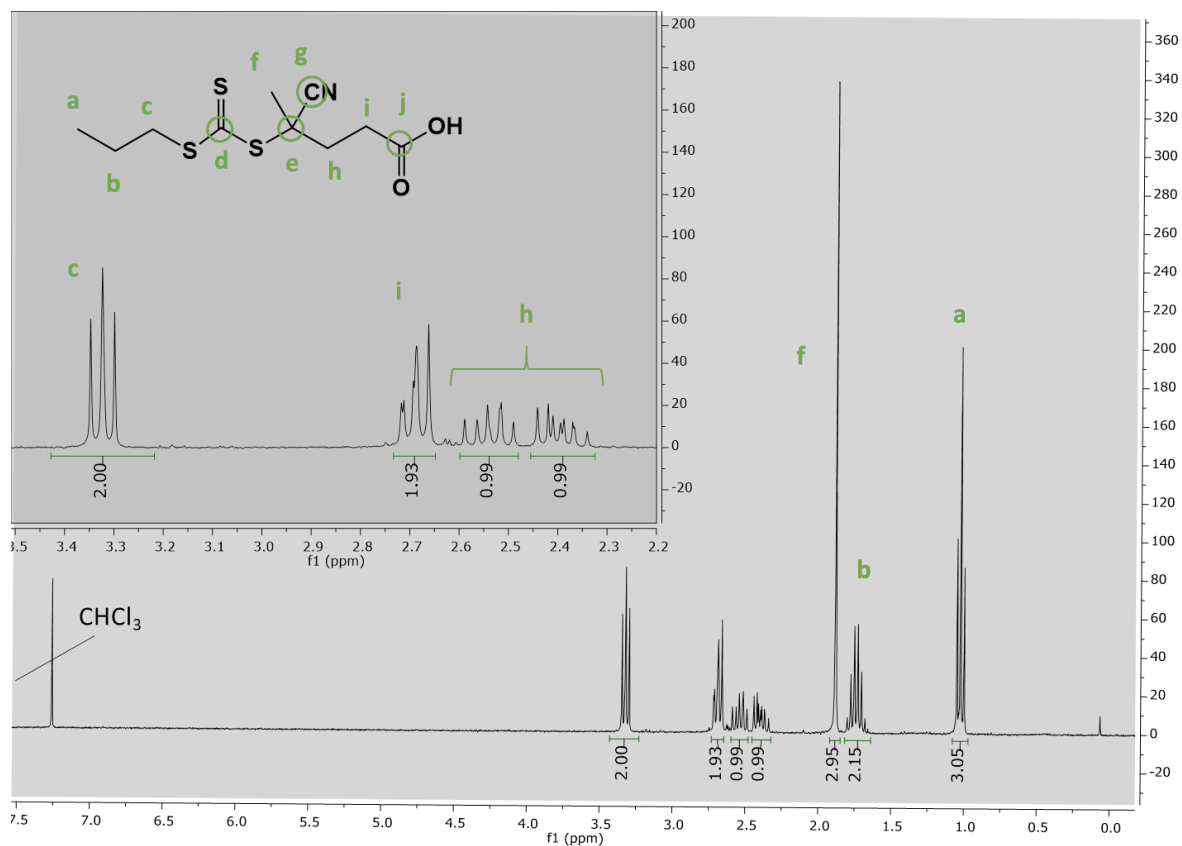


Figure S2 ^1H NMR of CTPA (400 MHz, CDCl_3), δ (ppm): 3.27 (t, $J = 7.4$ Hz, 2H), 1.72 (m, 8H), 0.99 (t, $J = 7.4$ Hz, 3H).

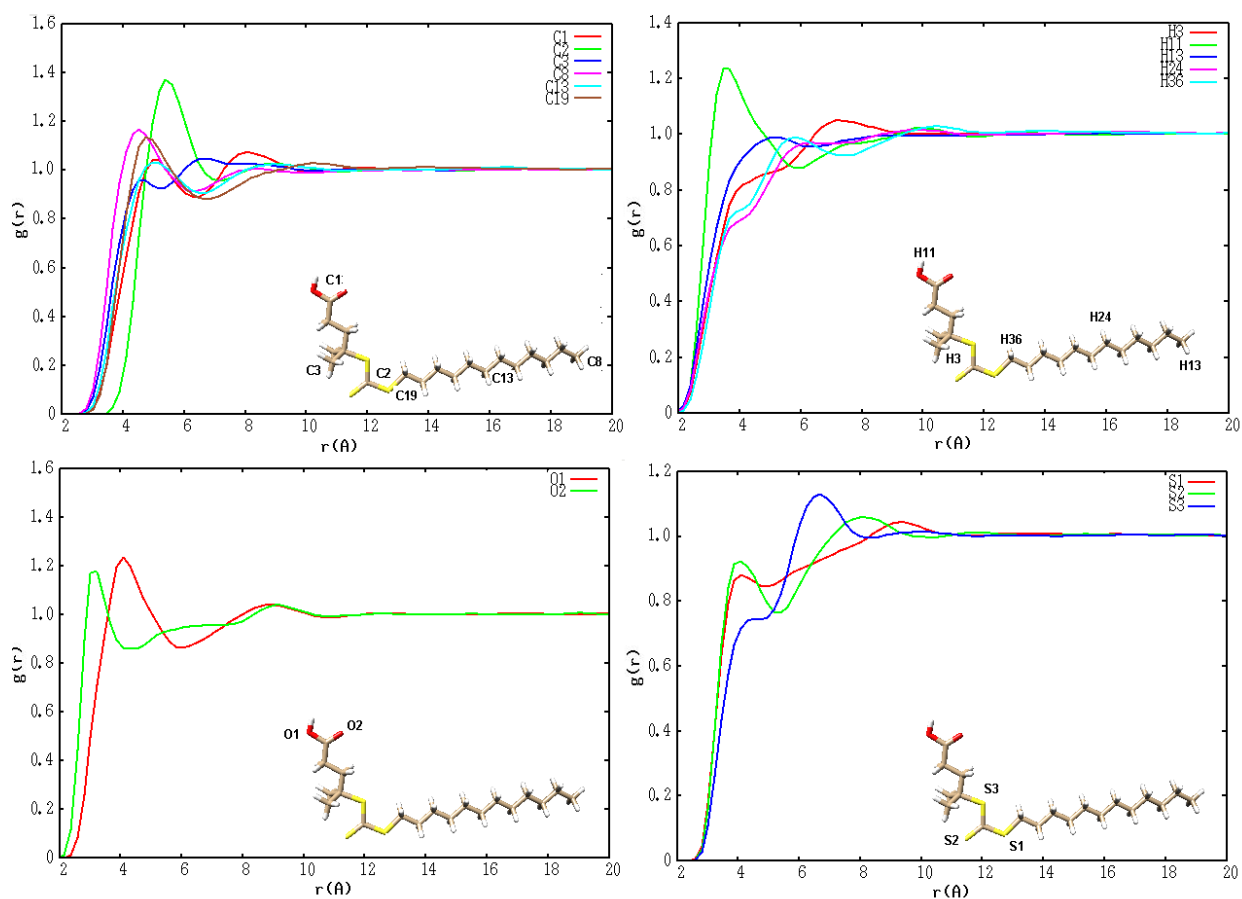


Figure S3 - Radial distribution functions $g(r)$, for the carbon atoms of *s*CCO₂ and the carbon, hydrogen, oxygen and sulfur atoms of DDMAT

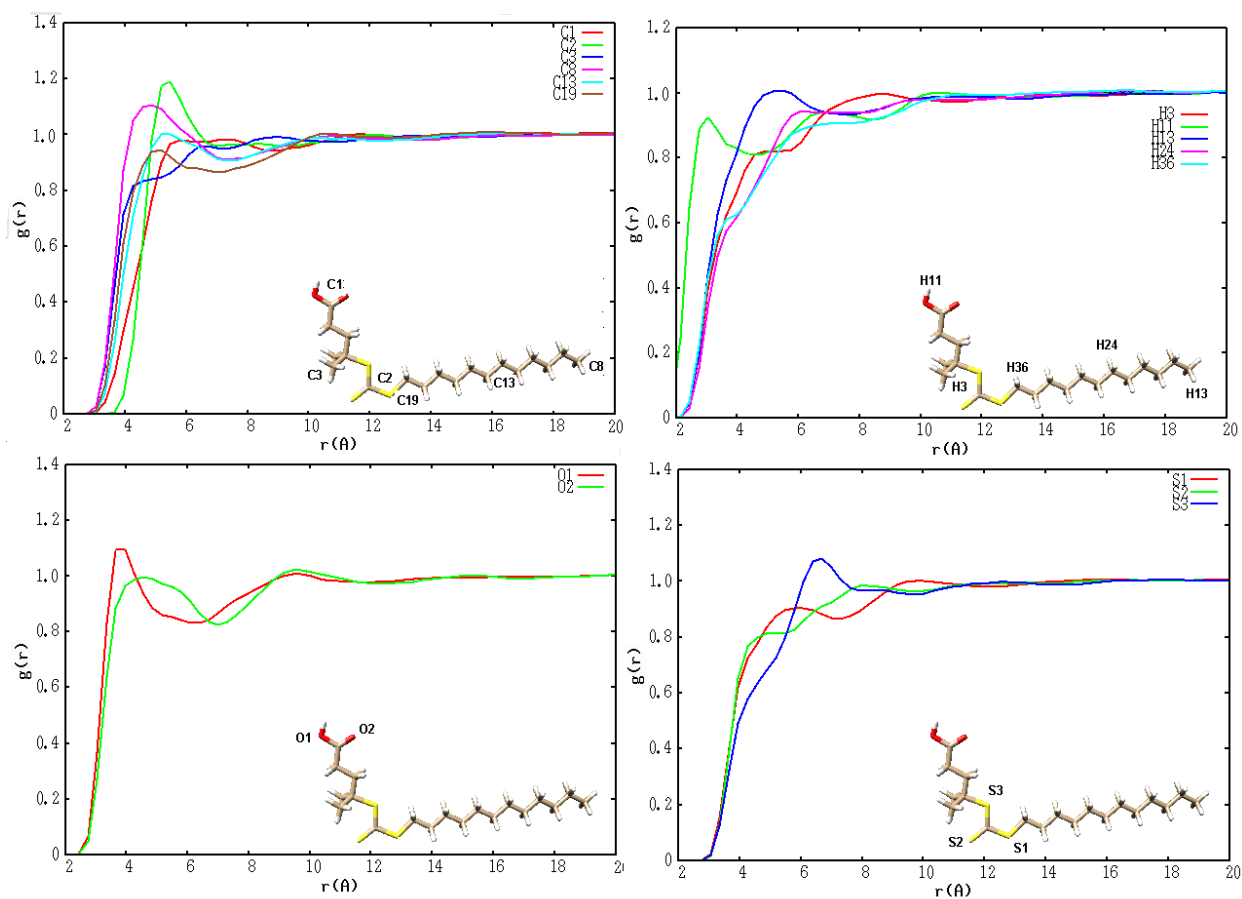


Figure S4 - Radial distribution functions $g(r)$, for the carbon atoms of toluene and the carbon, hydrogen, oxygen and sulfur atoms of DDMAT.

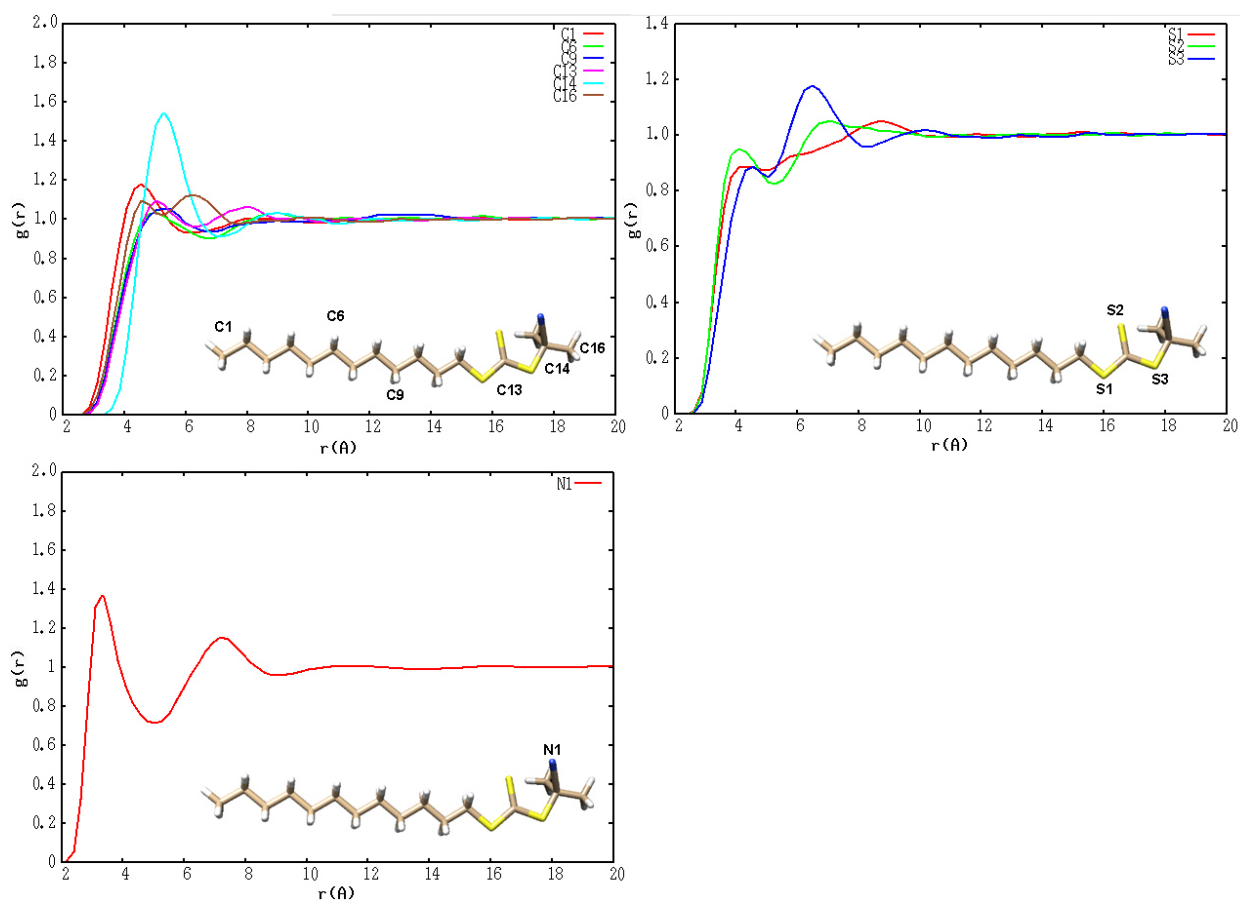


Figure S5 - Radial distribution functions $g(r)$, for the carbon atoms of $scCO_2$ and the carbon, sulfur and nitrogen atoms of CPDT.

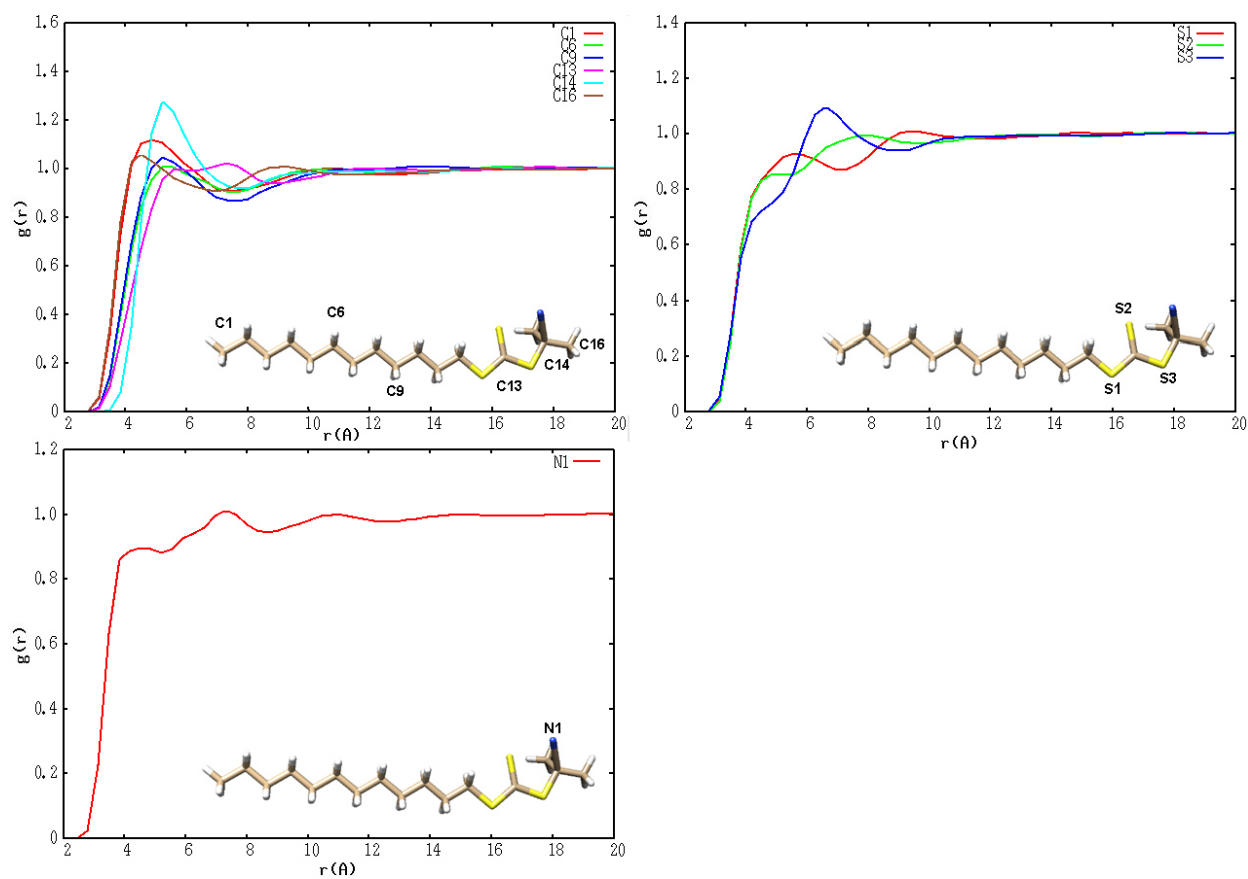


Figure S6 - Radial distribution functions $g(r)$, for the carbon atoms of toluene and the carbon, sulfur and nitrogen atoms of CPDT.

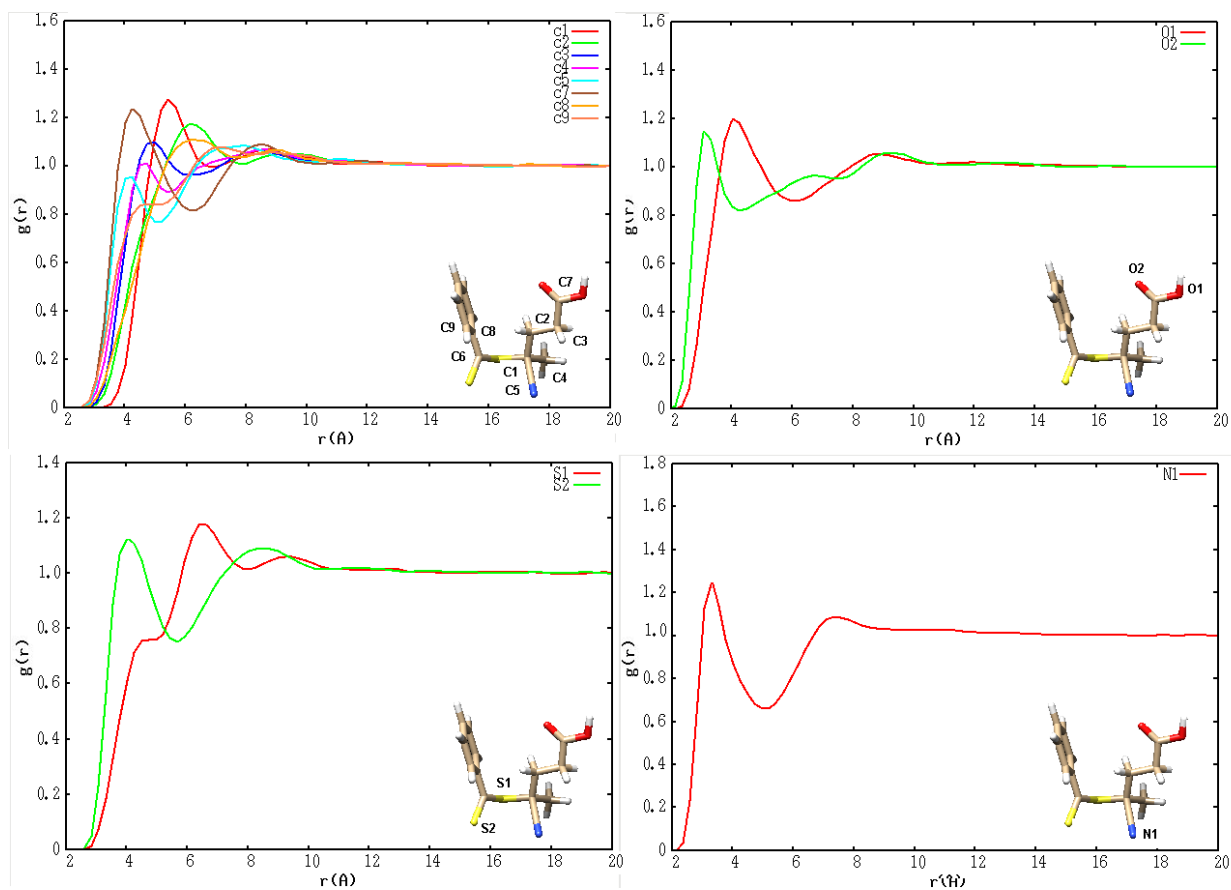


Figure S7 - Radial distribution functions $g(r)$, for the carbon atoms of $scCO_2$ and the carbon, oxygen, sulfur and nitrogen atoms of CPAB.

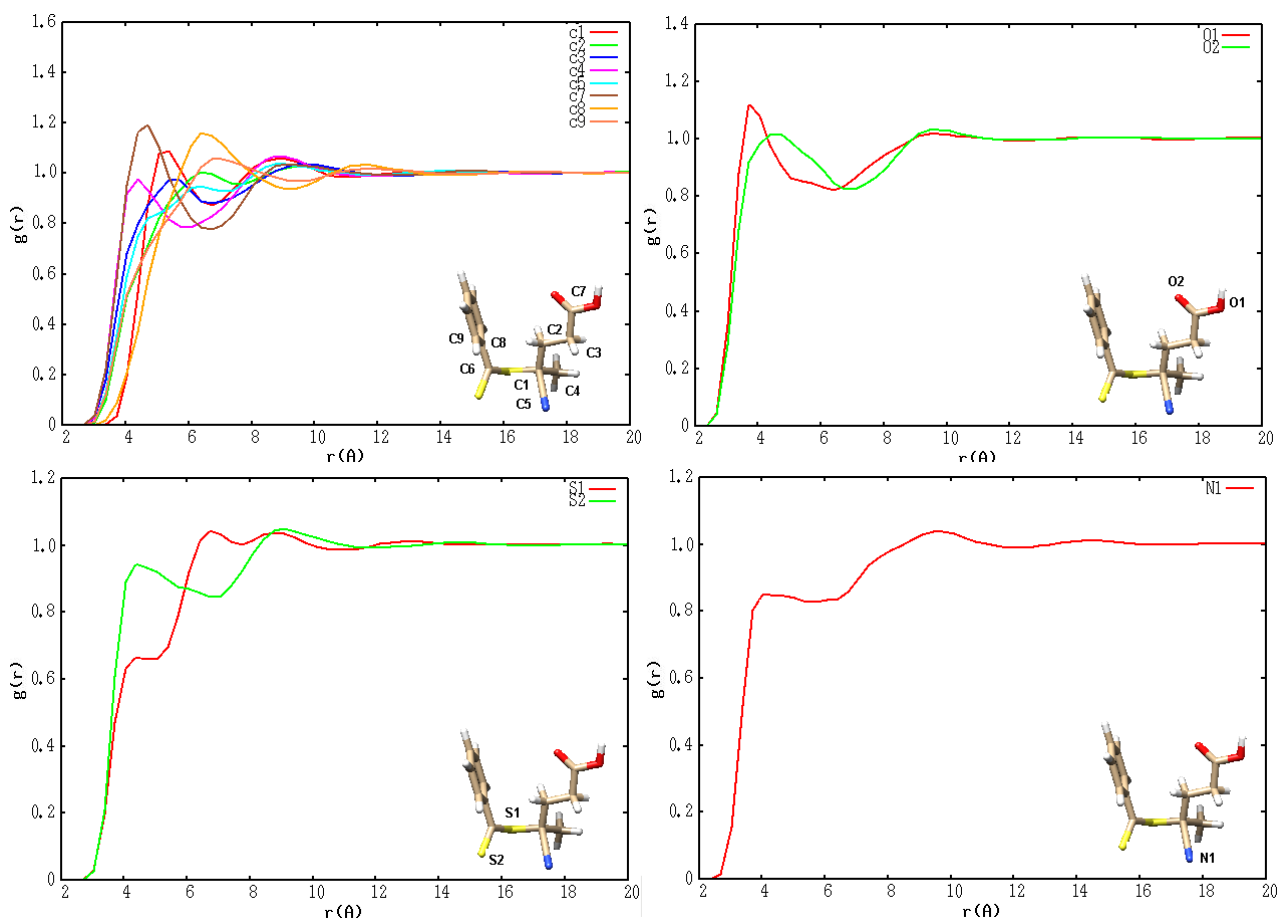


Figure S8 - Radial distribution functions $g(r)$, for the carbon atoms of toluene and the carbon, oxygen, sulfur and nitrogen atoms of CPAB.

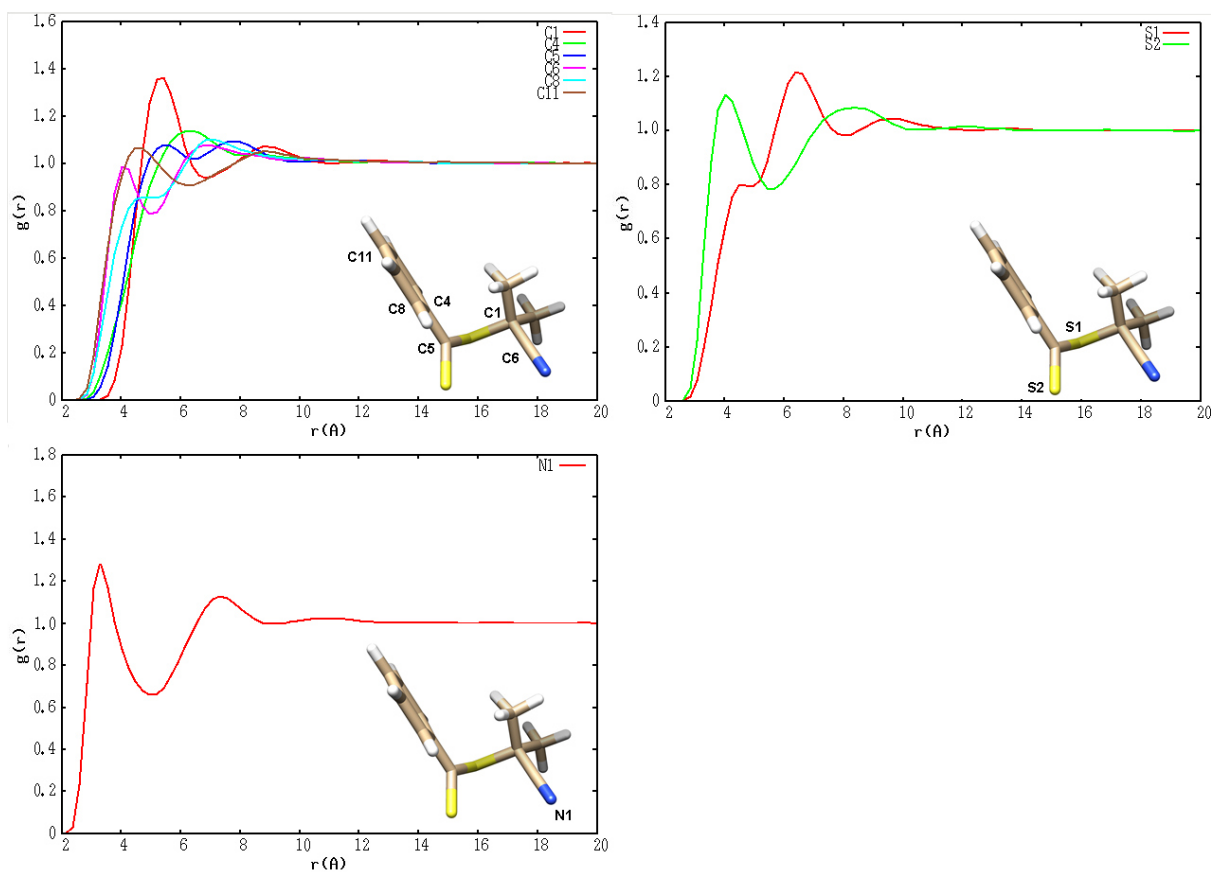


Figure S9 - Radial distribution functions $g(r)$, for the carbon atoms of $scCO_2$ and the carbon, sulfur, and nitrogen atoms of CPDB.

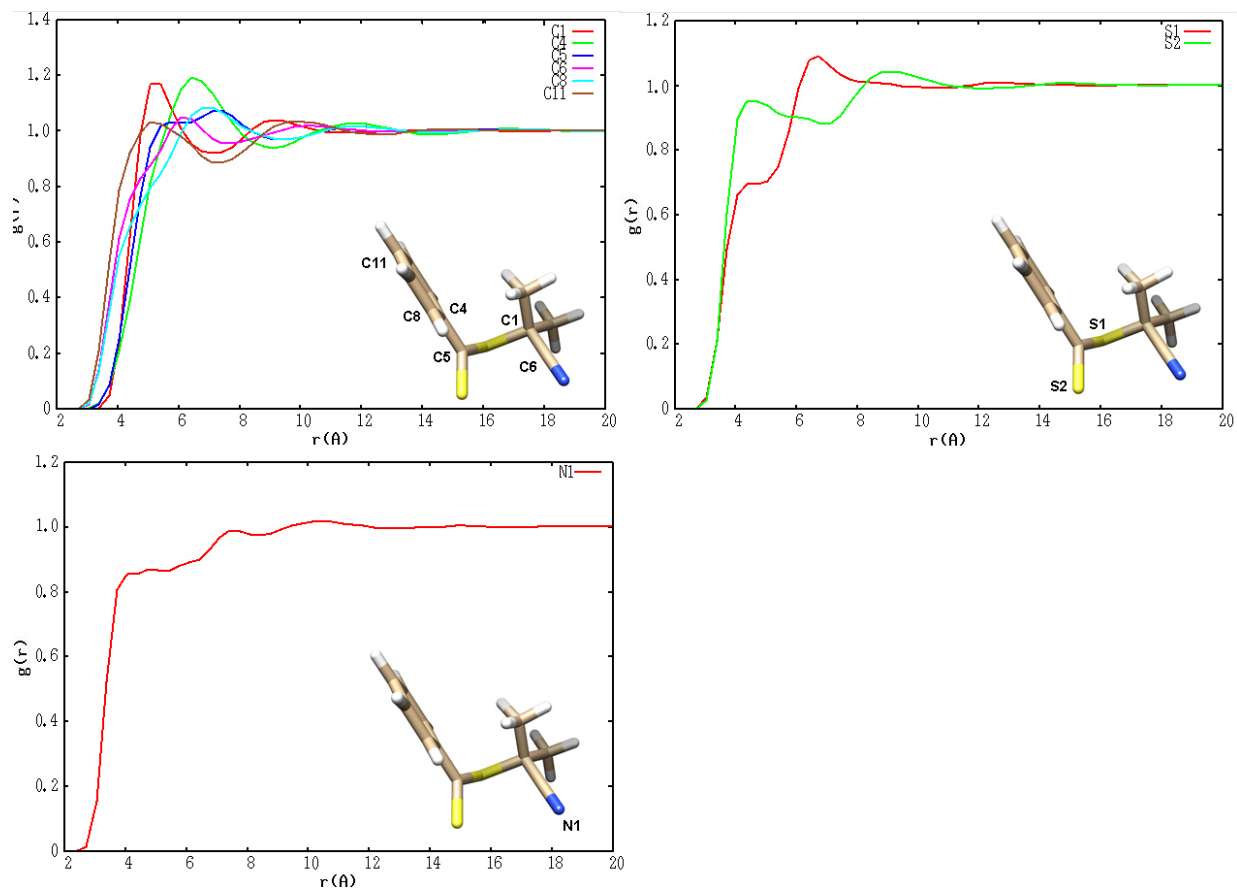


Figure S10 - Radial distribution functions $g(r)$, for the carbon atoms of toluene and the carbon, sulfur, and nitrogen atoms of CPDB.

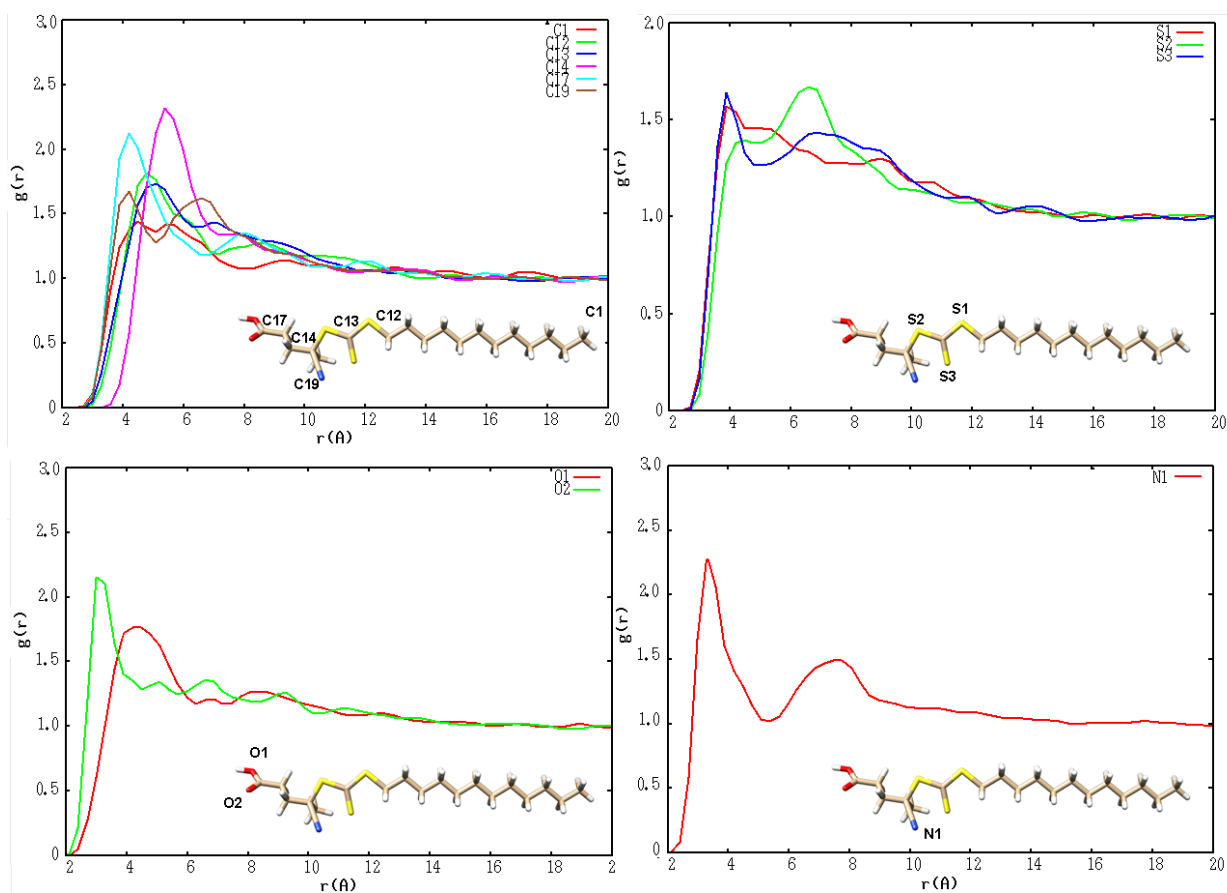


Figure S11 - Radial distribution functions $g(r)$, for the carbon atoms of $scCO_2$ and the carbon, sulfur, oxygen and nitrogen atoms of CPAD.

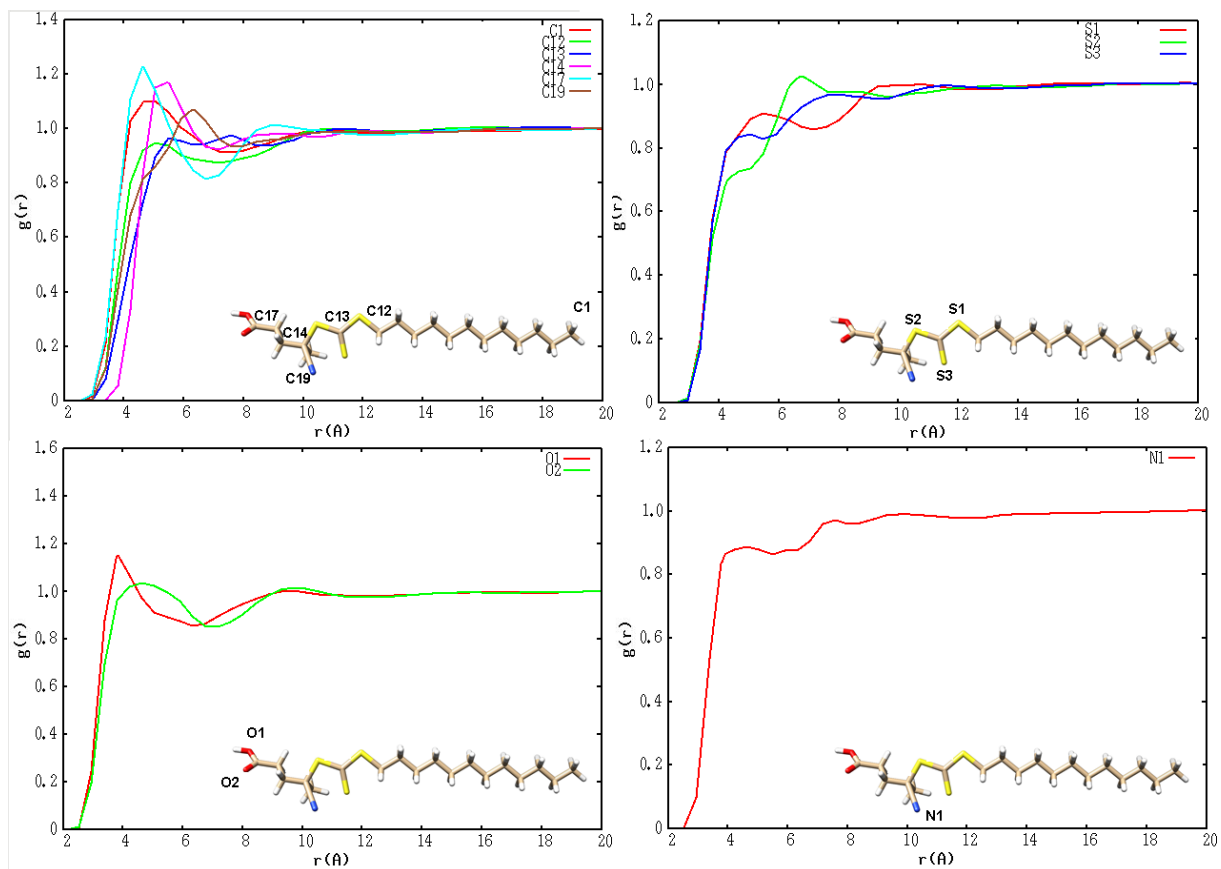


Figure S12 - Radial distribution functions $g(r)$, for the carbon atoms of toluene and the carbon, sulfur, oxygen and nitrogen atoms of CPAD.

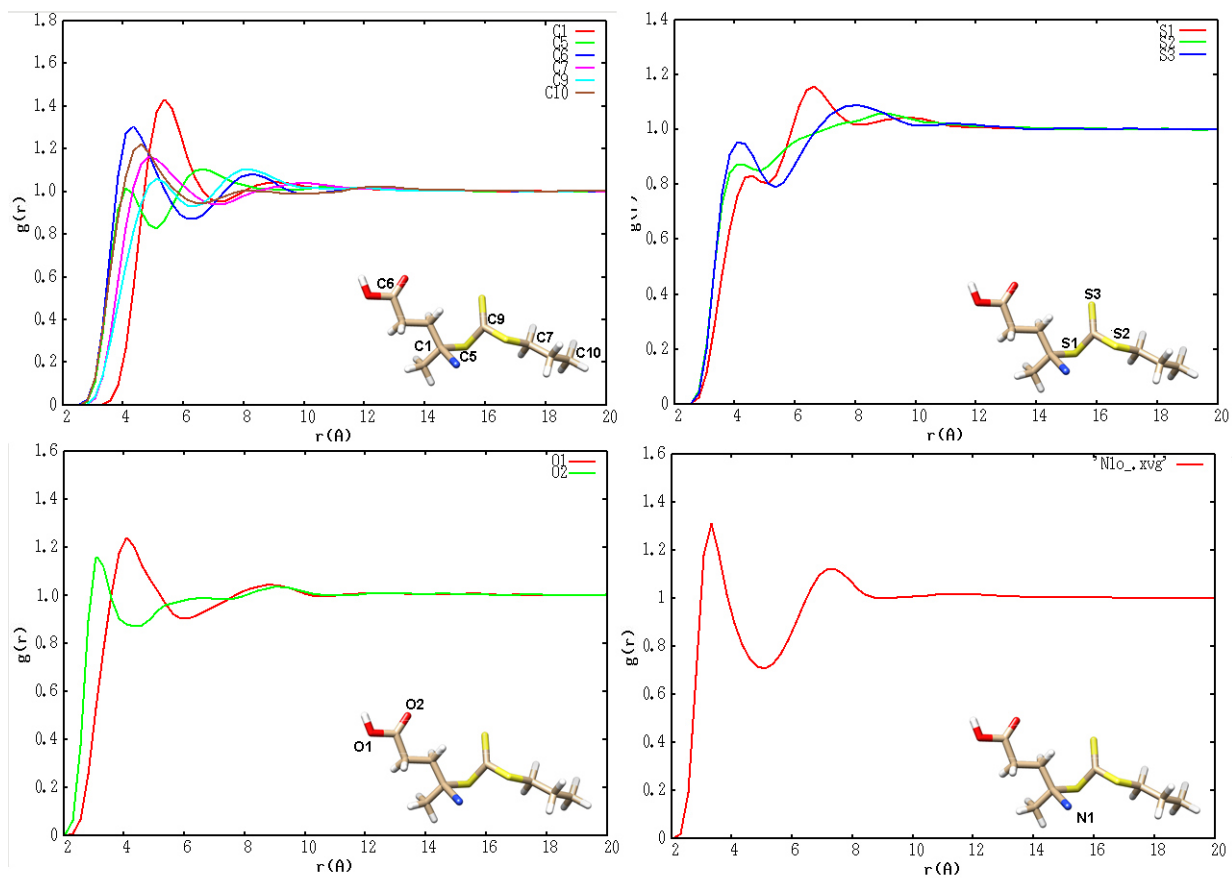


Figure S13 - Radial distribution functions $g(r)$, for the carbon atoms of $s\text{CCO}_2$ and the carbon, sulfur, oxygen and nitrogen atoms of CTPA.

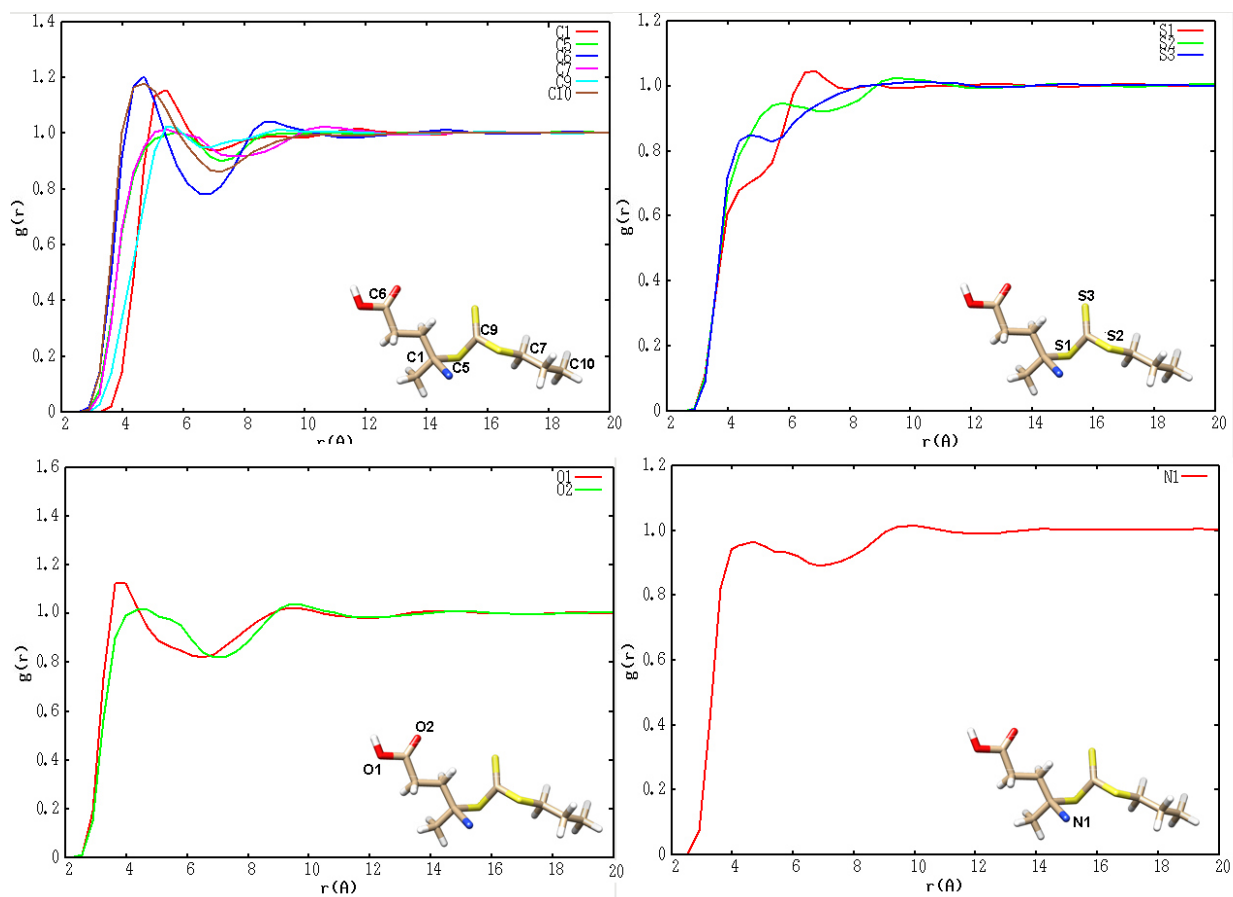
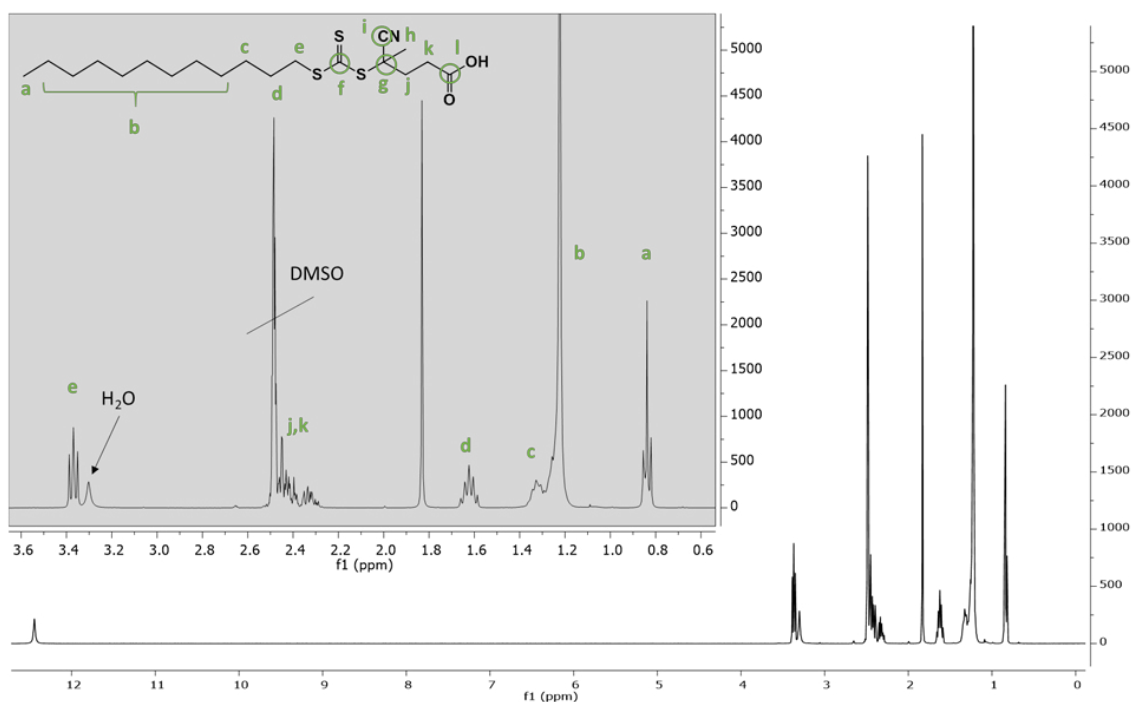


Figure S14 - Radial distribution functions $g(r)$, for the carbon atoms of toluene and the carbon, sulfur, oxygen and nitrogen atoms of CTPPA.

(A)



(B)

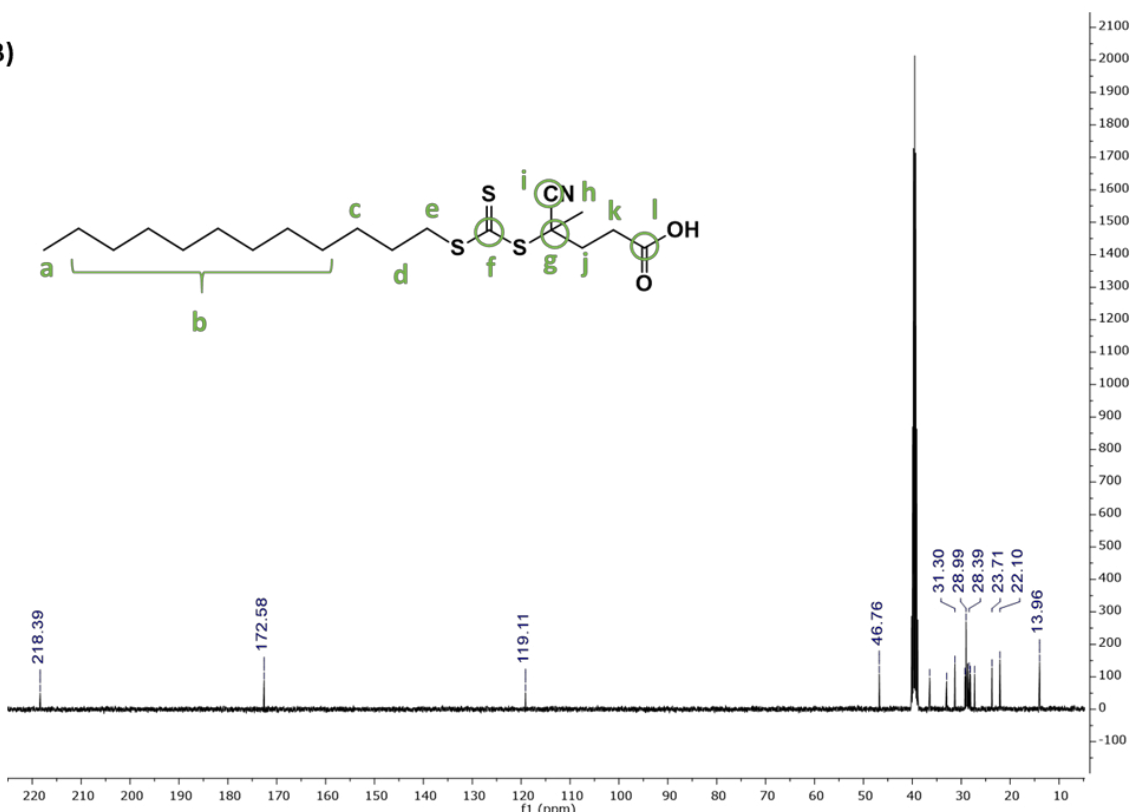


Figure S15 - CPAD degradation investigation by (A) ^1H NMR spectrum of CPAD in DMSO-D_6 . (400 MHz). δ ^1H (ppm): 3.39 (2 H, t, J 7.3), 2.48 – 2.39 (3 H, m), 2.39 – 2.30 (1 H, m), 1.85 (3 H, s), 1.64 (2 H, m), 1.34 (2 H, m), 1.24 (18 H, s), 0.91 – 0.80 (3 H, m). (B) ^{13}C NMR spectrum of CPAD in DMSO-D_6 . (400 MHz). δ ^{13}C (ppm): 218.39, 172.58, 119.11, 46.76, 36.43, 32.98, 31.30, 29.24, 28.99, 28.90, 28.79, 28.70, 28.39, 28.13, 27.26, 23.71, 22.10, 13.96.

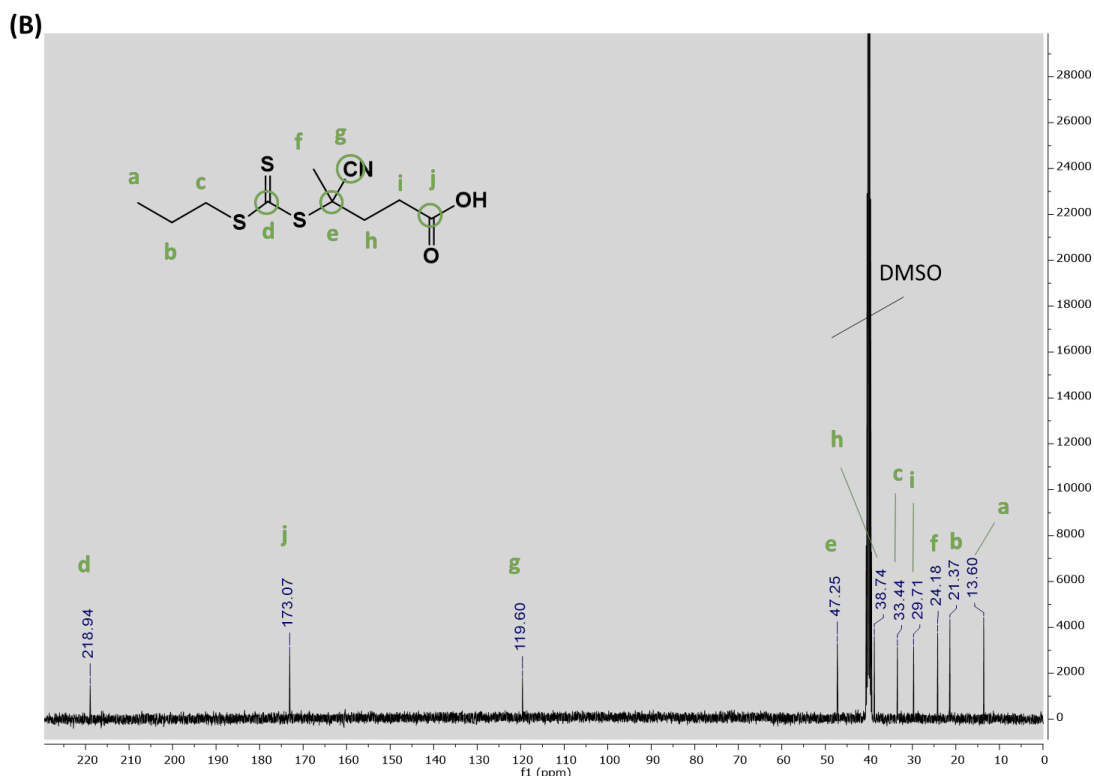
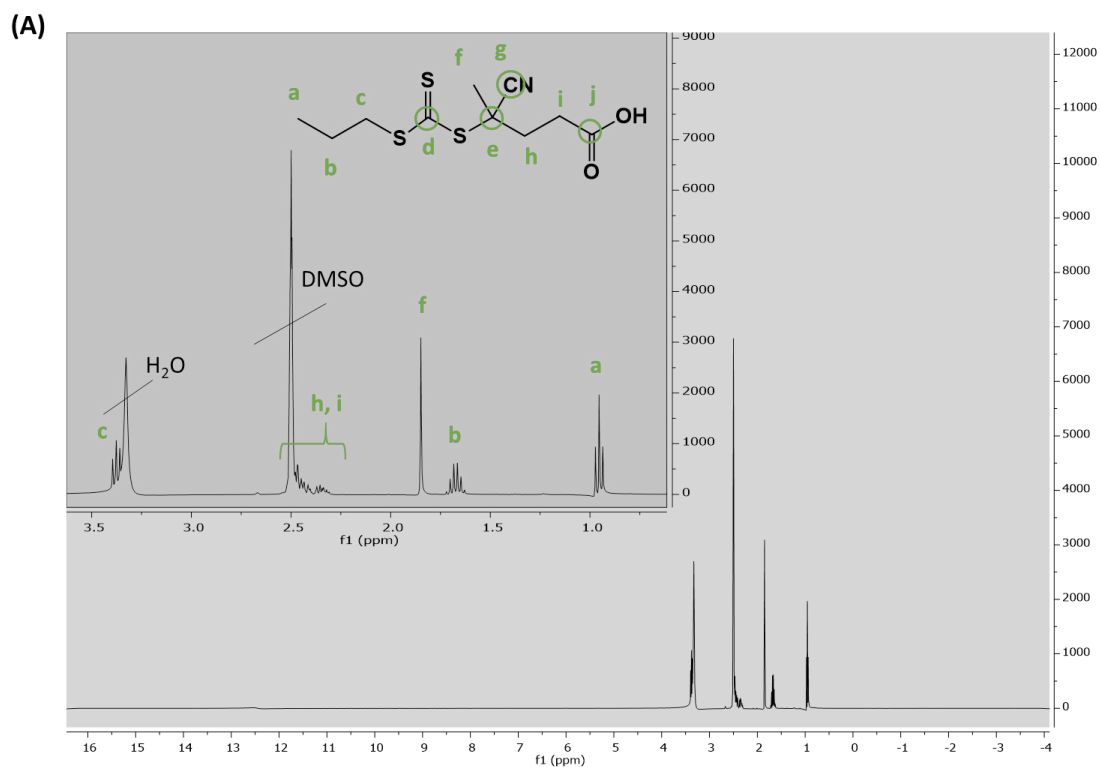


Figure S 16 - CTTPA degradation investigation by (A) ^1H NMR spectrum of CTTPA in DMSO-D₆. (400 MHz) δ ^1H (ppm): 3.42 – 3.33 (2 H, m), 1.85 (3 H, s), 1.67 (2 H, q, J 7.3), 0.95 (3 H, t, J 7.3). (B) ^{13}C NMR spectrum of CTTPA in DMSO-D₆. (400 MHz). δ ^{13}C (ppm): 218.94, 173.07, 119.60, 47.25, 38.74, 33.44, 29.71, 24.18, 21.37, 13.60.

Contents

Chapter 5. MMA polymerisation in scCO₂ with polydimethylsiloxane-based macro-CTAs of high chain transfer constant towards methacrylates	249
5.1. Abstract	249
5.2. Introduction	250
5.3. Aims	253
5.4. Experimental	253
5.4.1. Materials	253
5.4.2. Synthetic procedures	254
5.4.2.1. Synthesis of 4-cyano-4-thiothiopropylsulfanylpentanoic acid (CTPPA)	254
5.4.2.2. Synthesis of PDMS macro-CTAs	254
5.4.2.3. Standard dispersion polymerisation with macro-CTA in scCO ₂	255
5.4.2.4. Standard dispersion polymerisation in sampling autoclave	255
5.4.2.5. Standard solubility test in scCO ₂ in variable volume view cell	256
5.4.2.6. Hexane washes of polymer powders	256
5.4.2.7. Peak deconvolution	257
5.4.3. Polymer characterisation	257
5.4.3.1. Size exclusion chromatography (SEC)	257
5.4.3.2. Proton nuclear magnetic resonance (¹ H NMR)	257
5.4.3.3. Fourier-transform infrared spectroscopy (FT-IR)	257
5.4.3.4. Ultraviolet–visible spectrophotometry (UV-vis)	258
5.4.3.5. Scanning electron microscopy (SEM)	258
5.5. Results and discussion	258
5.5.1. Synthesis	258
5.5.2. Solubility of the PDMS-based macro-CTAs in scCO ₂	263
5.5.3. Polymerisation of MMA with CTPPA- and CPAB-based PDMS macro-CTAs	265
5.5.4. Kinetics of MMA polymerisation with PDMS-CTPPA	270
5.5.4.1. Kinetics of MMA polymerisation with PDMS ₆₅ -CTPPA	270
5.5.4.2. Kinetics of MMA polymerisation with PDMS ₁₂₈ -CTPPA	281
5.5.5. PDMS grafting efficiency onto the particles	292
5.6. Conclusions	295
5.7. References	297
5.8. Appendix	298

Chapter 5. MMA polymerisation in scCO_2 with polydimethylsiloxane-based macro-CTAs of high chain transfer constant towards methacrylates

5.1. Abstract

In this Chapter, reversible addition-fragmentation chain transfer (RAFT) dispersion polymerisation of methyl methacrylate (MMA) is performed in supercritical carbon dioxide (scCO_2) using polydimethylsiloxane (PDMS)-based macromolecular chain transfer agents (macro-CTAs). We previously studied, in Chapter 3, the coupling of monocarbinol terminated PDMS (PDMS-OH) of different molecular weights to 2-(dodecylthiocarbonothioylthio)-2-methylpropionic acid (DDMAT), and the use of the synthesised PDMS-DDMAT for MMA polymerisation in scCO_2 . Based on the outcomes from Chapter 3 and on the findings about RAFT mechanism and behaviour of CTA in scCO_2 , reported in Chapter 4, PDMS-based macro-CTAs with higher chain transfer constant (C_{tr}) towards MMA may offer advantages for achieving polymerisation self-assembly (PISA) in scCO_2 .

We report here the synthesis of macro-CTAs *via* esterification of PDMS-OH of different molecular weights with two CTAs containing a carboxylic acid group, which have high C_{tr} towards methacrylates: 4-cyano-4-(phenylcarbonothioylthio)pentanoic acid (CPAB) and (4-cyano-4-thiothiopropylsulfanyl)pentanoic acid (CTPPA).

These synthesised macro-CTAs are used for the first time for MMA polymerisation in scCO_2 . The assessment of the reaction kinetics and SEM studies of the reactions show an overall improvement of MMA polymerisation and RAFT control in scCO_2 compared with results using PDMS-DDMAT. Although the expected particle diameter and morphology transition are not observed, the macro-CTA is consumed and block copolymer particles are formed as expected in a PISA mechanism. This is a step forward towards PISA polymerisation *via* RAFT in scCO_2 . In addition, the use of macro-CTAs free of fluorine opens more possibilities for polymerisation in scCO_2 and the results presented here help to propose the best direction for future studies on PISA in scCO_2 with PDMS-based macro-CTAs.

5.2. Introduction

From what we learned in Chapter 4, 2-(dodecylthiocarbonothioylthio)-2-methylpropionic acid (DDMAT) was demonstrated to provide good control over the methyl methacrylate (MMA) dispersion polymerisation in $scCO_2$ (See section 4.5.1.). However, the macro-CTA based on polydimethylsiloxane (PDMS) coupling to DDMAT did not provide good RAFT control and blocking efficiency (Chapter 3).

In Chapter 4, we observed that the low C_{tr} of DDMAT towards MMA resulted in nucleation of PMMA homopolymer by precipitation before the reversible chain transfer reaction could take place. This was observed in SEC as the formation of high molecular weight polymer at the start of reaction (See section 4.5.1.). In this way the MMA dispersion polymerisation in $scCO_2$ with DDMAT behaved as the two-stage mechanism postulated by Winnik and Song.¹ After nucleation, the relatively poor solubility of DDMAT in $scCO_2$ made it prone to diffuse into the polymer-rich phase and control the reaction in the main reaction locus, *i.e.*, the particles. In this way DDMAT could provide a good RAFT control over MMA polymerisation despite the low C_{tr} .

So, why in Chapter 3 did we observe that the PDMS-DDMAT macro-CTA did not control the dispersion polymerisation of MMA? Firstly, the coupling of DDMAT with PDMS causes the loss of $-COOH$ group, which affects the CTA phase behaviour. In Chapter 4, we presented a novel computational solvation model, which indicated a correlation between polymerisation control and the degree of solubility in $scCO_2$ of the CTAs. The higher solubility of some CTAs resulted in exclusion from the polymer particles and negatively impacted RAFT control. Secondly, these two systems are not the same. In Chapter 4, RAFT dispersion polymerisation in $scCO_2$ with DDMAT was studied, while Chapter 3 explored the use of PDMS-DDMAT for a PISA inspired dispersion polymerisation in $scCO_2$.

In PISA, a solvophobic block grows from a solvophilic block, which is PDMS-DDMAT in our case. Therefore, the macro-CTA must be chain extended in a controlled way *via* RAFT in solution conditions until the PMMA block is long enough for the block copolymer to self-assemble (Figure 1A). As PISA *via* RAFT requires the addition of a radical initiator, the particle formation process may suffer from competition between the desired self-assembly

nucleation and unwanted homogeneous nucleation.² Homogeneous nucleation may result from too low a transfer efficiency to the CTA, too high a concentration of initiator or too low a CTA concentration in the continuous phase. While homogeneous nucleation may be beneficial when we only want to control the growth of the polymer chains inside particles as was the case when DDMAT was employed in scCO₂, only nucleation by self-assembly of block copolymers is targeted in PISA.

Therefore, it would not be surprising for PDMS-DDMAT to allow homogeneous nucleation at the beginning of the reaction in a similar way to the two-stage polymerisation of Winnik and Song.¹ As a result, conventional radical polymerised PMMA would nucleate, while PDMS-DDMAT sterically stabilises the particles, just as PDMS-MA would in a conventional dispersion polymerization in scCO₂ (Figure 1A). In fact, we found in Chapter 3 that about half of the PDMS-DDMAT was left unreacted and did not graft onto the particles. Another possibility is the self-assembly causing nucleation, in this case, PDMS-DDMAT chain extends MMA in solution to form oligomers until the block copolymer self-assembles into stable particles/micelles (Figure 1B). There is also a third possibility, in which PDMS-DDMAT chain extends MMA in solution to form oligomers that adsorb onto already formed PMMA particles (Figure 1C).

Hence, substituting DDMAT by other CTAs more suitable for MMA polymerisation may improve blocking efficiency and favour the PISA mechanism compared to results obtained with PDMS-DDMAT. Indeed, in Chapter 4, the RAFT control for MMA polymerisation in scCO₂ was improved in the initial stages of the reaction when using 4-cyano-4-(phenylcarbonothioylthio)pentanoic acid (CPAB) and (2-cyano-2-propyl(dodecyltrithiocarbonate) (CPDT), which are CTAs with higher C_{tr} towards methacrylates. For a PISA system, the macro-CTA will chain extend in solution (homogeneous system) until it self-assembles to form *nuclei*. Therefore, better control over the initial stages of the MMA dispersion polymerisation is a prerequisite for a successful RAFT-mediated PISA in dispersion in scCO₂ while it is not the case for a successful RAFT dispersion polymerization in scCO₂.

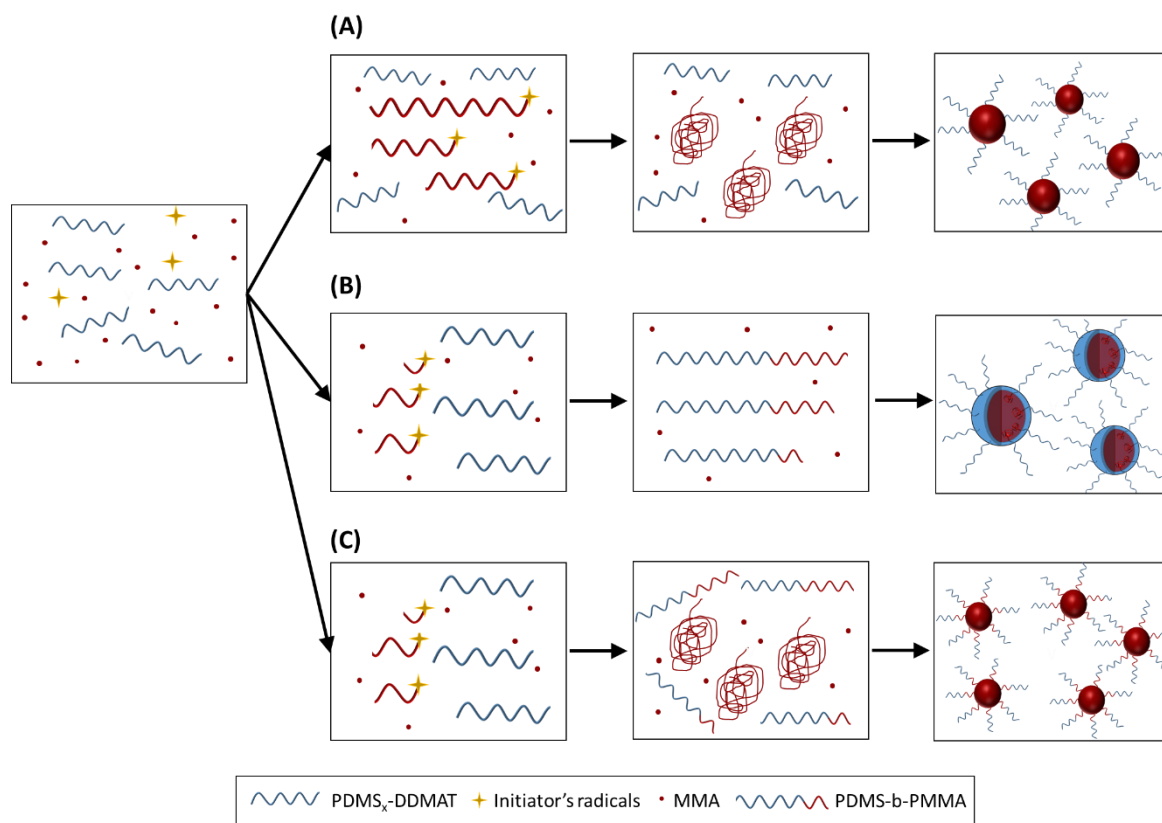


Figure 1 – Schematics of different reaction pathways for MMA dispersion polymerisation in $scCO_2$ with PDMS-DDMAT. PMMA homopolymers grow via conventional radical polymerisation and nucleate, with PDMS-DDMAT acting only as stabiliser (A). PMMA chains are initiated and chain extended from PDMS-DDMAT to form PDMS-b-PMMA, which self-assembles into particles (B). PDMS-DDMAT chain extends to form short PDMS-b-PMMA oligomers that absorb onto already formed PMMA particles, stabilising them (C).

In this chapter, we explore other PDMS-based macro-CTAs by using two CTAs with better C_{tr} towards methacrylate polymerisation. We selected two CTAs that were previously presented in Chapter 4, CPAB and (4-cyano-4-thiothiopropylsulfanyl)pentanoic acid (CTPPA) for coupling with PDMS. Both CPAB and CTPPA presented good control over MMA polymerisation in solution (Section 4.5.2.2. and 4.5.5.) and have a carboxylic acid moiety that allows coupling with PDMS-OH by Steglich esterification. Here the macro-CTAs are synthesised, characterised and tested for MMA polymerisation in $scCO_2$ *via* PISA inspired method.

5.3. Aims

The aims of this Chapter are as follow:

- To improve PDMS retention in the final polymer (PDMS-b-PMMA) by making a macro-CTA through the coupling of PDMS with CTAs of higher C_{tr} towards MMA. With MMA being used as a model monomer, because of the greater number of study of its polymerisation by dispersion in $scCO_2$ compared to other monomers.
- To obtain better control of PISA polymerisation in $scCO_2$ as assessed by the proximity of M_n to $M_{n,th}$ and dispersity (\mathcal{D}) of the final polymer.
- To obtain well-defined spherical particles and particles of higher morphologies (*i.e.* worms or vesicles).

This is important because this different morphologies will bring new mechanical properties, and will allow the synthesis of a series of materials through a greener path without the need of toxic solvents or water waste treatment. These particles may for example find applications as impact modifiers and in drug delivery for agrochemical or pharmaceutical applications. Furthermore there is the possibility of obtaining new internal nanostructures and different unique morphologies due to the high diffusivity of $scCO_2$.

5.4. Experimental

5.4.1. Materials

MMA was purchased from ProSciTech (99 %) and was filtered through aluminium oxide to remove the stabiliser prior to polymerisation. 2,2'-azobis(isobutyronitrile) (AIBN) was purchased from Sigma Aldrich UK (98%) and purified by recrystallization in methanol prior to use. All other chemicals were used as received. 4-cyano-4-(phenylcarbonothioylthio)pentanoic acid (CPAB) was purchased from Sigma-Aldrich UK and CTPPA was synthesised according to previous work detailed in the next section.³ Carbon disulfide, 4,4'-azobis(4-cyanopentanoic acid), propane thiolate and potassium ferricyanide were purchased from Sigma-Aldrich UK. Methacrylate terminated polydimethylsiloxane (PDMS-MA) and monocarbinol terminated polydimethylsiloxane (PDMS-OH) were purchased from ABCR GmbH & Co and Fluorochem, respectively. Dicyclohexylcarbodiimide (DCC) was purchased from MP biomedical, 4-dimethylaminopyridine (DMAP) was purchased from Fluka. Anhydrous magnesium sulphate, dichloromethane (DCM), hexane, heptane, ethyl acetate,

diethyl ether, methanol, dichloromethane (DCM), toluene, tetrahydrofuran (THF, HPLC grade) and deuterated chloroform (CDCl_3) were all purchased from Fischer Scientific and used as received.

5.4.2. Synthetic procedures

5.4.2.1. Synthesis of 4-cyano-4-thiothiopropylsulfanylpentanoic acid (CTPPA)

The synthesis of CTPPA was achieved by following a procedure previously reported.³ Briefly, carbon disulfide (4.16 mL; 0.065 mol) was added drop by drop to sodium propanethiolate (5.59 g; 54 mmol) dispersed in THF (75 mL), at 0 °C. The final mixture was stirred for one hour at room temperature and then filtered. After evaporation of the solvent under vacuum, an orange solid was obtained. The latter was dissolved in deionized water and the solution was cooled at 0 °C. Potassium ferricyanide (20.68 g; 62 mmol) dissolved in deionized water (60 mL) was added dropwise to the solution under stirring. The mixture was stirred for an extra hour at room temperature. Diethyl ether was then added to the mixture to extract the organic phase. The aqueous phase was washed several times with the same organic solvent (30 mL). The organic phases were grouped and dried on anhydrous MgSO_4 and the ether was evaporated, giving an orange oil (bis(propylsulfanylthiocarbonyl) disulfide).

Subsequently, bis(propylsulfanylthiocarbonyl) disulfide (6.80 g; 22 mmol) was dissolved in 130 mL of ethyl acetate. To this, 1.1 equivalents of 4,4'-azobis(4-cyanopentanoic acid) (7.85 g; 25 mmol) were added. The reaction medium was placed under reflux overnight at 98 °C. The following day, the solvent was evaporated under vacuum. A column purification was performed with diethyl ether/heptane (1:2 v/v ratio) as eluent and then with pure ethyl acetate. After solvent evaporation, a very viscous orange oil was obtained. The ^1H NMR spectrum is reported in the appendix – Figure S1.

^1H NMR (CDCl_3 , 300 MHz, δ ppm): 3.3 (t, 2H, $\text{CH}_2\text{-S}$); 2.3-2.8 (m, 4H, $-\text{CH}_2\text{-CH}_2\text{-COOH}$); 1.8 (s, 3H, $\text{CH}_3\text{-C(CN)}$); 1.7 (m, 2H, $\text{CH}_2\text{-CH}_3$); 1.0 (t, 3H, CH_3).

5.4.2.2. Synthesis of PDMS macro-CTAs

The macro-CTAs were prepared *via* Steglich esterification of PDMS-OH, following a similar process to the one reported by Lopez-Oliva *et al.*⁴ In a typical procedure, the CTA (3.0 mmol) carrying a carboxylic acid group was placed in a previously dried 250 mL round-bottom flask and dissolved in DCM (100 mL). PDMS-OH (2.0 mmol), dicyclohexylcarbodiimide (DCC) (6.0

mmol) and 4-dimethylaminopyridine DMAP (0.30 mmol) were then added. The resulting solution was purged with argon for 30 min, sealed, and heated for 24 hours with continuous stirring. After quenching the reaction by exposure to air, the solution was filtered, concentrated under vacuum with the aid of a rotary evaporator, and passed through a silica gel column using DCM as eluent. The resulting clear liquid was washed three times with a 2:1 methanol/DCM mixture, and the organic layer was concentrated under vacuum to produce a clear yellow viscous oil. The synthesis of each macro-CTA was confirmed by ^1H NMR, UV-vis and FT-IR analysis.

PDMS-CTPPA: ^1H NMR (CDCl_3 , 300 MHz, δ ppm): 4.25 (m, 2 H), 3.63 (m, 2 H), 3.43 (t, 2 H), 3.32 (t, 2 H), 2.70 -2.33 (m, 4H), 1.87 (s, 3 H), 1.79 – 1.15 (m, 8 H), 1.02 (m, 3 H), 0.88 (m, 3 H), 0.53 (m, 4 H), 0.06 (s, (O-Si(CH₂)-)).

PDMS-CPAB: ^1H NMR (CDCl_3 , 300 MHz, δ ppm): 7.90 (d, 2 H), 7.54 (m, 2 H), 7.40 (t, 1 H), 4.26 (m, 2 H), 3.64 (m, 2 H), 3.43 (t, 2 H), 2.77 – 2.41 (m, 4 H), 1.92 (m, 3 H), 1.78 -1.17 (m, 6 H), 0.89 (t, 3 H), 0.53 (m, 4 H), 0.06 (s, (O-Si(CH₂)-)).

5.4.2.3. Standard dispersion polymerisation with macro-CTA in scCO_2

A typical procedure used an in-house built high-pressure MKIII autoclave (20 mL),⁵ which was degassed by purging with CO_2 at 2 bar for 30 minutes. In a typical polymerisation MMA (33 mmol), AIBN (0.028 mmol) and the macro-CTA (0.055 mmol) were degassed by bubbling with argon for 30 minutes in a vial. The reactants were then added to the autoclave through the keyhole against positive pressure of CO_2 . The vessel was then sealed and pressurised to 50 bar, heated to 65 °C, and the pressure topped up to 276 bar. The reaction mixture was stirred at 300 rpm with an overhead magnet coupled stirrer. After 24 hours, the heating was turned off and the reactor was cooled to room temperature before being vented. All products were collected as dry free-flowing powders, unless stated differently. The samples were analysed *via* THF-SEC, ^1H NMR and SEM.

5.4.2.4. Standard dispersion polymerisation in sampling autoclave

A typical procedure used an in-house built high-pressure sampling autoclave consisting of an 60 mL MKIII clamp sealed autoclave⁵ with a cylinder sampling unit as described elsewhere,⁶ which was degassed by purging with CO_2 at 2 bar for 30 minutes. MMA (0.1 mol), AIBN (0.08

mmol) and the macro-CTA (0.17 mmol) were degassed by bubbling with argon for 30 minutes. The reactants were then added to the autoclave through the keyhole against positive pressure of CO₂. The vessel was then sealed and pressurised to 50 bar, heated to 65 °C, and the pressure topped up to 276 bar. The reaction mixture was stirred at 300 rpm with an overhead magnet coupled stirrer. At sampling times, the sampling cylinder was loaded with 5 mL of deuterated chloroform and attached to the autoclave. A fraction of the reaction mixture was sampled into the small pipe space before the cylinder. The sampling caused a small pressure drop; therefore, pressure was topped up with an extra 14 bar prior to sample collection to avoid fluctuations below reaction conditions. The content of the pipe was then sprayed into the cylinder and collected into chloroform. The samples were analysed *via* THF-SEC and ¹H NMR.

5.4.2.5. Standard solubility test in scCO₂ in variable volume view cell

The solubility test of macro-CTAs was carried out in a stainless-steel variable volume view cell, with a front sapphire window and a back mobile sapphire piston that can be moved by a hydraulic intensifier unit. An accurately weighed amount of macro-CTA (a typical quantity was 0.5 mmol, 5 wt% in relation to CO₂), was added into the chamber and the system was purged with CO₂ for 30 minutes at room temperature. Then, 33 mmol (15 wt% in relation to CO₂) of MMA were added into the chamber through the keyhole and the system was filled with 20 g of CO₂ using a syringe pump and heated to the desired temperature. At each temperature set point, the pressure was increased until the solute became soluble and only one phase was visible. The pressure was then reduced slowly while monitoring the phase behaviour until the cloud point, *i.e.*, the point at which the polymer precipitated and caused turbidity. The process was repeated three times and the final cloud point pressure was an average of these 3 values at a given temperature.

5.4.2.6. Hexane washes of polymer powders

The polymer powder obtained by dispersion polymerisation in scCO₂ was washed with hexane and homogenised in a vortex mixer prior to centrifuging at 3000 rpm for 5 minutes in order to decant the polymer powder and allow the hexane solution to be removed. The process was repeated three times and the polymer powder dried overnight at 25 °C under vacuum. The powder was analysed by ¹H NMR and THF-SEC. ¹H NMR resonance integrals of PDMS and PMMA repeating units were compared before and after washes. The percentage of PDMS

retained after wash was calculated considering the integral of the PDMS resonance before washing to be 100%.

5.4.2.7. Peak deconvolution

Peak deconvolution was performed using OriginPro8[®] with the Peak Analyser feature. The THF-SEC traces were plotted as log of molecular weight versus $dwt/d[\log(MW)]$ in OriginPro8[®] and a Gaussian fitting was performed for fitting 2-3 curves to the polymer trace until the data converged and the least squares function was minimized. The software requires the input of peak maximum position (x_c), which was evaluated visually and assigned to the maxima of the peaks and “shoulders”. To verify if results were not affected by x_c estimation, x_c was estimated by Particle Swarm Optimization (PSO) algorithm written in Python, then a Levenberg-Marquardt algorithm was used to obtain a Gaussian fitting for fitting 2-3 curves to the polymer trace. This analysis proved the robustness of the deconvolution method in OriginPro8[®].

5.4.3. Polymer characterisation

5.4.3.1. Size exclusion chromatography (SEC)

The M_n and \mathcal{D} of polymers were obtained by SEC (PL-120, Polymer Labs) using a refractive index (RI) detector. The columns (30 cm PLgel Mixed-C, two in series) were eluted by THF and calibrated with PMMA standards. Calibration and analyses were performed at 40 °C with a flow rate of 1 mL min⁻¹. The device was equipped with multiple angle light scattering (MALS), refractive index (RI) and UV detectors.

5.4.3.2. Proton nuclear magnetic resonance (1H NMR)

The synthesis of products and reactants and the monomer conversion were determined by ¹H NMR. The spectra were recorded in CDCl₃ using a Bruker DPX 400 MHz spectrometer, and referenced to CHCl₃ at 7.26 ppm.

5.4.3.3. Fourier-transform infrared spectroscopy (FT-IR)

IR spectra were recorded with an Attenuated Total Reflection Cary 630 FT-IR spectrophotometer (Agilent Technologies, Santa Clara, CA). 32 interferograms were recorded for each spectrum, with a resolution of 4 cm⁻¹, in the range 4000–650 cm⁻¹. IR spectra were analysed by SpectraGryph1.2 software.

5.4.3.4. Ultraviolet–visible spectrophotometry (UV-vis)

Spectra were recorded with an Epoch 2 UV-vis multi microplate reader from Agilent. Samples were measured against DCM blanks in sealed cuvettes, and polymer functionalisation with the CTA was calculated using a calibration curve (absorbance *versus* concentration plot) constructed with the CTA in DCM.

5.4.3.5. Scanning electron microscopy (SEM)

Images of the particles were obtained using a JEOL 6060V SEM machine at various magnifications and an accelerating voltage of 10 kV. Samples were mounted on aluminium stubs using adhesive carbon tabs and sputter-coated with platinum before analysis. Mean particle diameter (D_n) was determined by measuring the diameter of 100 particles in ImageJ® and taking a mean of these data. The coefficient of variance (C_v) was calculated by the ratio of the standard deviation (σ) by the mean particle diameter as by Equation (1).

$$C_v = \sigma/D_n \times 100 \quad (1)$$

5.5. Results and discussion

5.5.1. Synthesis

As for the synthesis of PDMS-DDMAT in Chapter 3, CPAB and CTPPA were coupled *via* Steglich esterification to PDMS-OH of different molecular weights, PDMS₁₂₈-OH (9.75 kg mol⁻¹) and PDMS₆₅-OH (4.99 kg mol⁻¹), to form the macro-CTAs (Figure 2). These are the same PDMS-OH used in Chapter 3 and their characterisation can be found in section 3.5.1. The successful synthesis of PDMS₆₅-CTPPA and PDMS₆₅-CPAB was confirmed by ¹H NMR (Figure 3 and Figure 4) and by FT-IR (Figure S2).

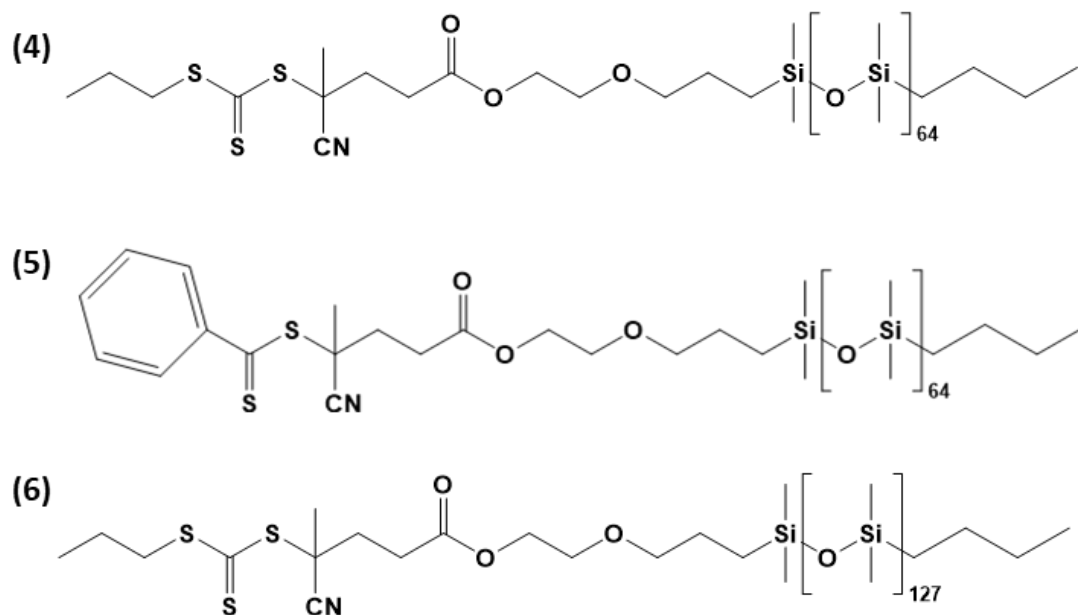


Figure 2 – Structures of macro-CTAs with different CTAs: (4) PDMS₆₅-CTPPA, (5) PDMS₆₅-CPAB and (6) PDMS₁₂₈-CTPPA.

It was possible to assign the macro-CTA ¹H NMR spectrum by comparison to the CTAs and the PDMS-OH spectrum as done for PDMS-DDMAT (Chapter 3.4.1.). The degree of end group functionalisation with CTA was calculated by comparing the integral of the backbone dimethyl protons l and protons p, m and k with the protons associated to the ester bond formation, q*, h' and i' in the 3-4 ppm region (Figure 3 and Figure 4). The mean degree of esterification was calculated to be 97.1% for PDMS₆₅-CTPPA (4), 88.2% for PDSM₆₅-CPAB (5) and 89.2% for PDSM₁₂₈-CTPPA (6) (Table 1).

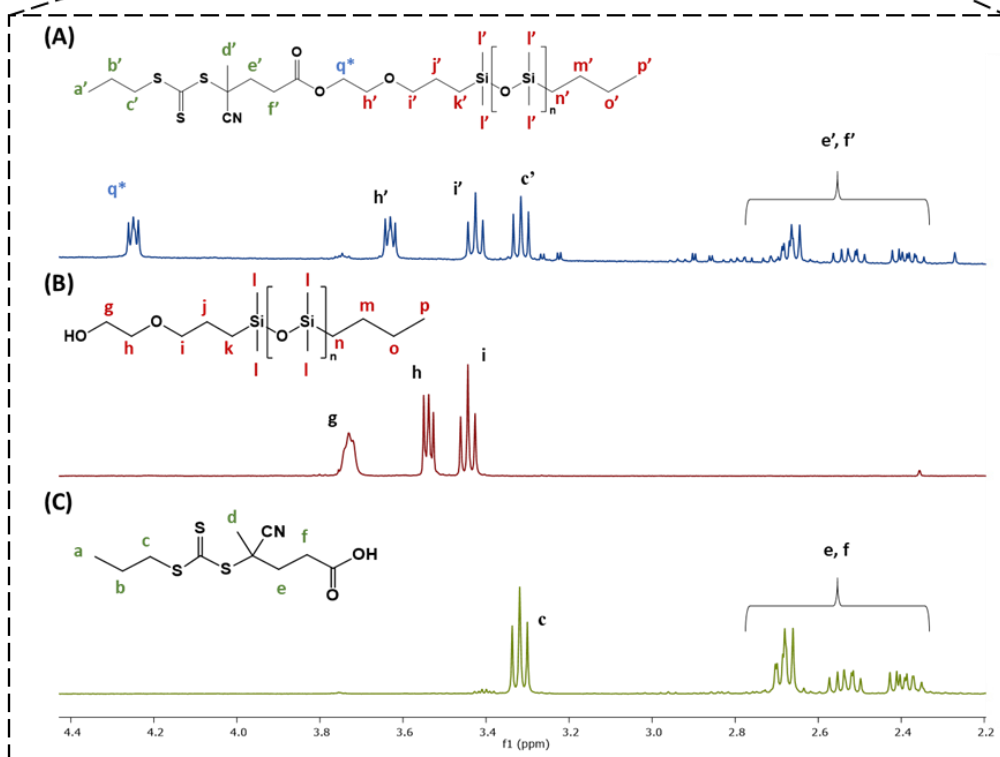
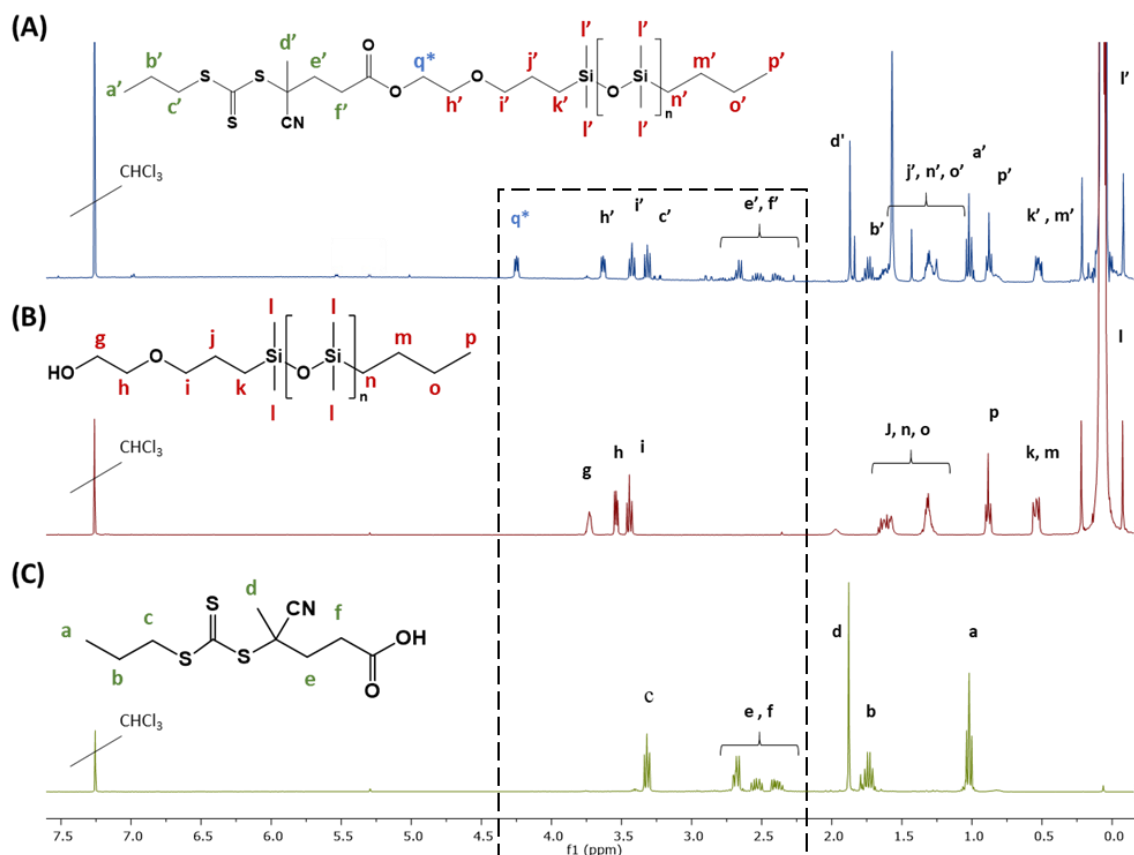


Figure 3 - ^1H NMR spectra in CDCl_3 of A) $\text{PDMS}_{65}\text{-CTPPA}$, B) $\text{PDMS}_{65}\text{-OH}$ and C) CTPPA.

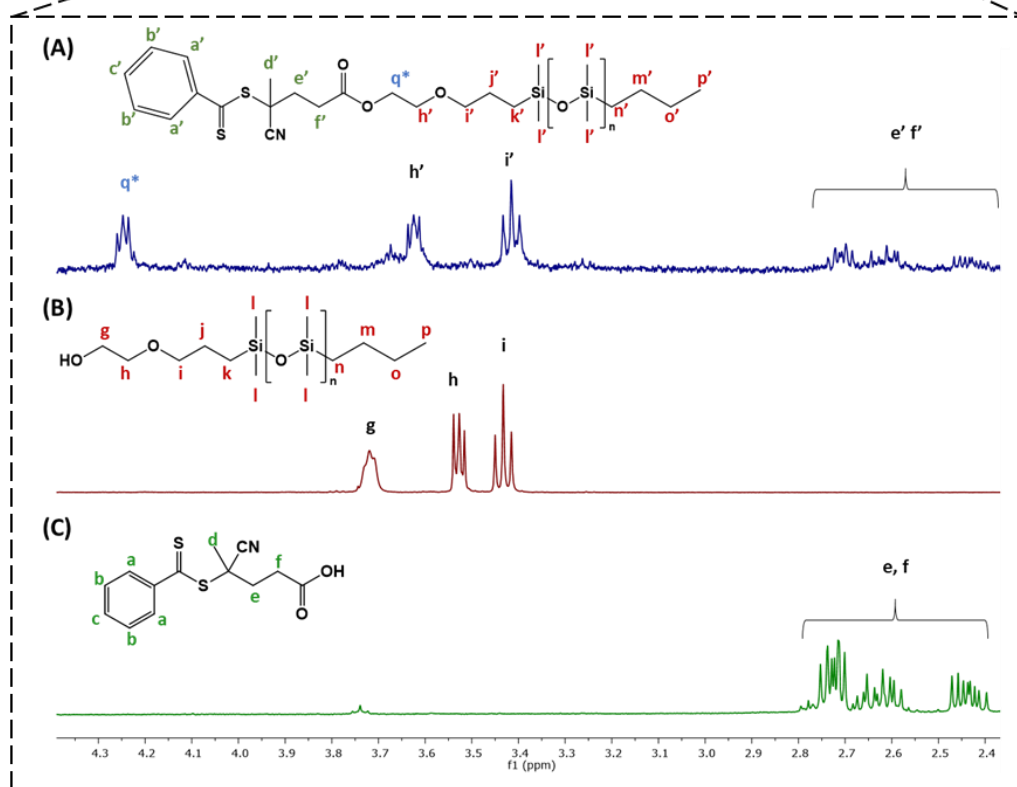
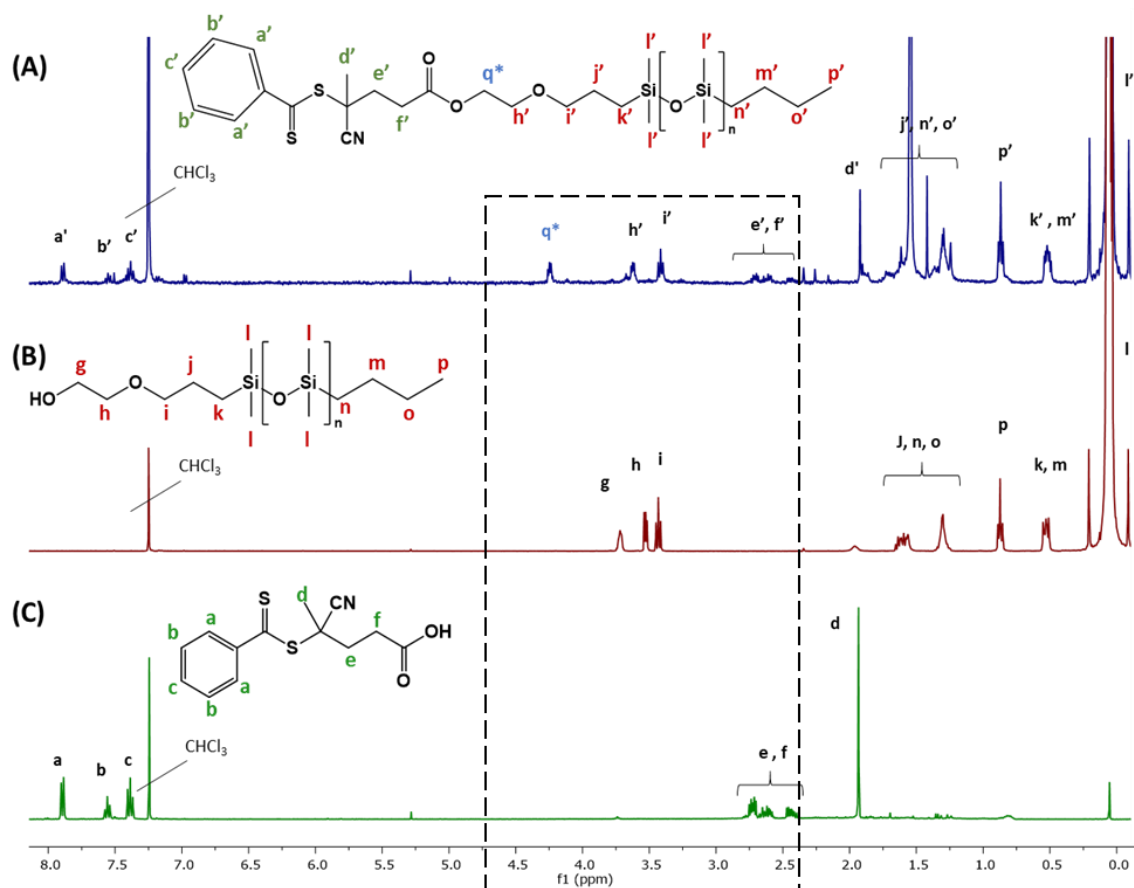


Figure 4 - ^1H NMR spectra in CDCl_3 of A) PDMS₆₅-CPAB, B) PDMS₆₅-OH and C) CPAB.

PDMS₁₂₈-CTPPA and PDMS₆₅-CTPPA also had their functionalisation assessed by UV-vis spectrophotometry. As for DDMAT, the free CTA resembles the macro-CTA end group, giving a similar UV absorption, which allows reliable end group analysis. A calibration curve was prepared with eight CTPPA solutions in DCM at different known concentrations (Figure 5), and the extinction coefficient (ϵ) was calculated at maximum absorbance, *i.e.* 275 nm and $\epsilon = 8489.8 \text{ L mol}^{-1} \text{ cm}^{-1}$.

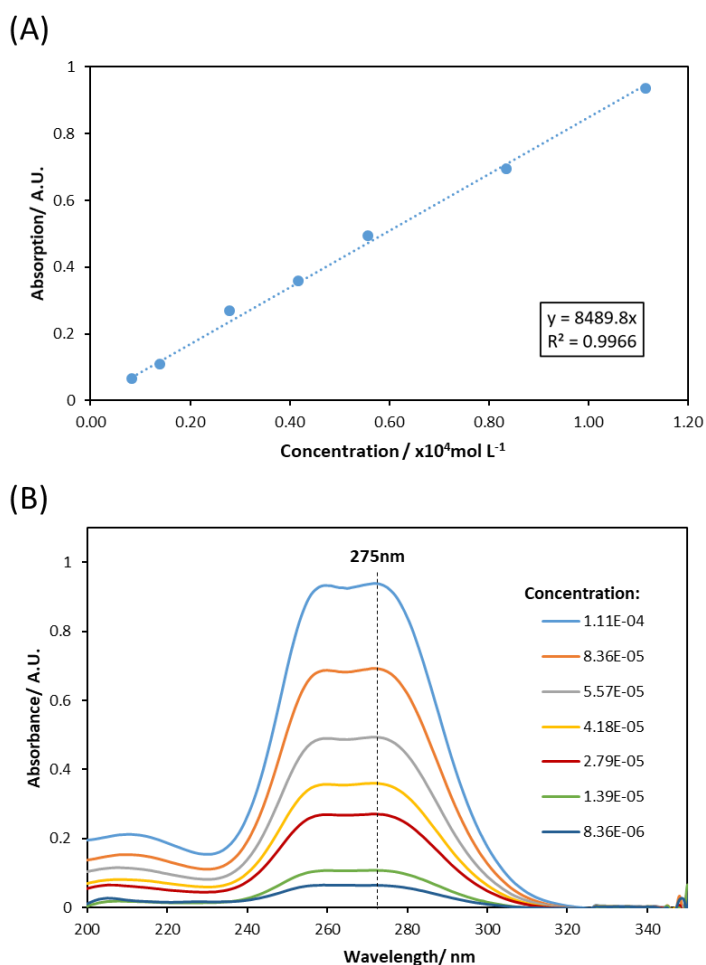


Figure 5 - UV absorption calibration for CTPPA, showing the absorbance versus conversion plot (A) and the wavelength for each sample at different concentrations, with a maximum absorbance at 275 nm (B).

The end group functionalisation was calculated using the Beer-Lambert Equation (2) and the absorbance recorded for the macro-CTAs in DCM at known concentrations. A is absorbance, c is the concentration of end groups, ϵ is the extinction coefficient and l is the path length of the UV cell, which is a fixed value for all samples measured.

$$A = \epsilon cl \quad (2)$$

Functionalisation was calculated to be 90.4% for PDMS₁₂₈-CTPPA and 97.6% for PDMS₆₅-CTPPA (Table 1). These results are close to the functionalisation calculated by ¹H NMR, considering possible experimental error.

Table 1 – Functionalisation of PDMS macro-CTAs PDSM₆₅-CTPPA (4), PDMS₆₅-CPAB (5) and PDMS₁₂₈-CTPPA (6).

Macro-CTA	Expected M_n ¹	Esterification degree ² (%)	Exp. [CTA] ³	Real [CTA] ⁴	Functionalisation degree ⁵ (%)
(4) PDMS ₆₅ -CTPPA	5.26	97.1	2.69 10 ⁻⁵	2.76 10 ⁻⁵	97.6
(5) PDMS ₆₅ -CPAB	5.27	88.2	-	-	-
(6) PDMS ₁₂₈ -CTPPA	10.01	89.2	2.20 10 ⁻⁵	2.44 10 ⁻⁵	90.4

¹ M_n given in kg mol⁻¹ and calculated based on the molar mass of PDMS-OH DP obtained by ¹H NMR and added to the CTA molar mass. ² Calculated from ¹H NMR spectra; by comparing the integral of the PDMS backbone protons with the protons associated with the ester bond formation. ³ Experimental concentration obtained from equation (4) and UV absorption of macro-CTA solutions in DCM and given in mol L⁻¹. ⁴ Real concentration of macro-CTA solutions in DCM given in mol L⁻¹. ⁵ Functionalisation of macro-CTA given by UV absorption and calculated by the percent ratio of expected concentration to the real concentration.

5.5.2. Solubility of the PDMS-based macro-CTAs in scCO₂

In a PISA system, the macro-CTA is expected to induce the *in situ* formation of an amphiphilic block copolymer, while controlling the molecular weight and molecular weight dispersity.⁷ Therefore, the macro-CTA must be highly soluble in scCO₂, in order to produce self-stabilised block copolymer particles. The phase behaviour of the two PDMS-CTPPAs and PDMS₆₅-CPAB was investigated by cloud point measurements in a variable volume view cell. The cloud point is the pressure, at a specific temperature, when the solute precipitates out of the continuous phase, causing turbidity. The cloud points were measured with 5 wt% macro-CTA relative to scCO₂, in the presence or absence of 15 wt% of MMA, which acts as a co-solvent in the dispersion polymerisation (Figure 6).

Table 2 – PDMS-CTPPA and PDMS-CPAB cloud point study

Sample	Cloud point without MMA (bar) ¹	Cloud point with MMA (bar) ²
(4) PDMS ₁₂₈ -CTPPA	225.5 (±0.6)	177.0 (±0.6)
(5) PDMS ₆₅ -CPAB	208.0 (±3.0)	-
(6) PDMS ₆₅ -CTPPA	193.2 (±3.2)	135.8 (±0.3)

¹ Cloud point measured in variable volume view cell with 5 wt% macro-CTA in relation to CO₂. ² Cloud point measure in variable volume view cell with 5 wt% macro-CTA and 15 wt% MMA in relation to CO₂. All results given as an average of three measurements at 65 °C, with standard deviation given in brackets. All results were converted from psi (equipment unit) to bar, 1 psi = 0.069 bar.

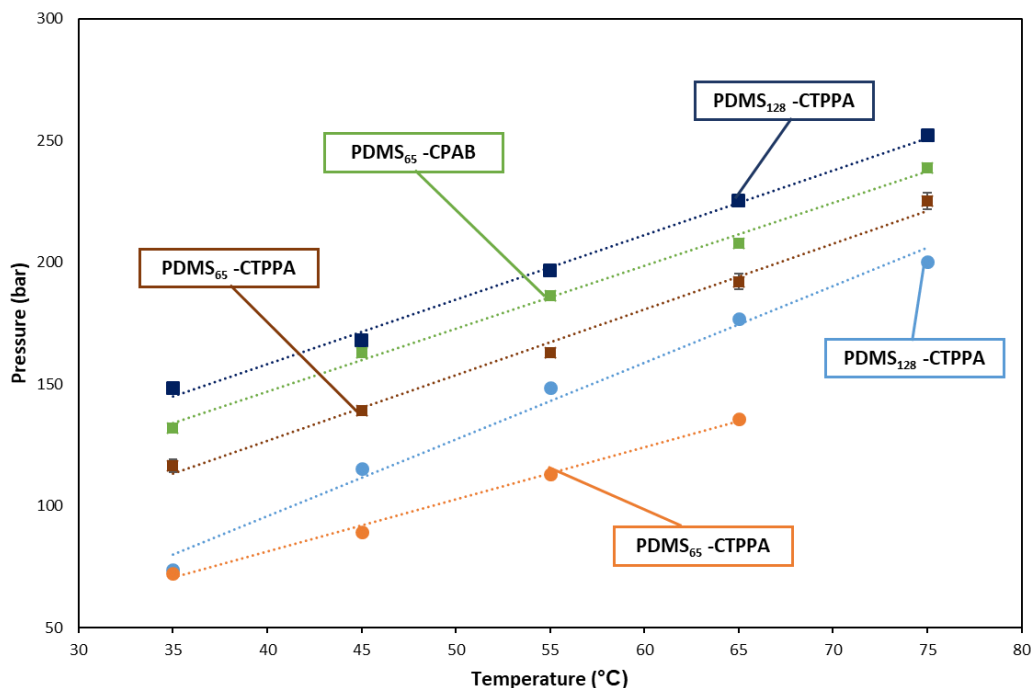


Figure 6 - Cloud point study of PDMS₆₅-CTPPA, PDMS₁₂₈-CTPPA and PDMS₆₅-CPAB measured with MMA (circular markers) and without MMA (square markers). More pressure was required to solubilise the macro-CTAs without the monomer, which acts as a co-solvent. The cloud point increased with the PDMS molecular weight increase.

All three macro-CTAs were soluble in scCO₂ under autoclave standard polymerisation conditions of 65 °C and 276 bar, in the presence or absence of MMA. PDMS₆₅-CPAB was tested only in the absence of MMA due to time and materials restrictions (Table 2). Cloud points increase with the increase in the PDMS molecular weight. In addition, it is possible to observe that PDMS₆₅-CPAB is less soluble than PDMS₆₅-CTPPA, clearly demonstrating the influence of the CTA functional end group.

For comparison, PDMS-MA stabiliser (250 cSt, $\approx 10 \text{ kg mol}^{-1}$) has a cloud point of 220.6 bar at 65 °C in the absence of MMA, while PDMS₁₂₈-CTPPA, which has a similar molecular weight, had a cloud point of 225.5 bar. Therefore, PDMS₁₂₈-CTPPA and PDMS-MA (250 cSt) are rather similarly soluble in scCO₂. In addition, the cloud-point for PDMS-DDMAT was measured in Chapter 3, and at 65 °C, PDMS₁₂₈-DDMAT had a cloud-point of 234.0 bar in absence of MMA and 163.2 bar in presence of MMA and PDMS₆₅-DDMAT had a cloud-point of 212.0 bar without MMA and 148.0 bar with MMA. Therefore, PDMS-CTPPA and PDMS-CPAB of comparable molecular weight are slightly more soluble than PDMS-DDMAT.

Since the macro-CTAs have been synthesised, characterised and confirmed to solubilise under reaction conditions, they were then evaluated in the dispersion polymerisation of MMA in scCO₂. This will be discussed in next section.

5.5.3. Polymerisation of MMA with CTPPA- and CPAB-based PDMS macro-CTAs

Dispersion polymerisations of MMA in scCO₂ with a targeted DP of 600 were first performed in scCO₂ with PDMS₆₅-CTPPA and PDMS₆₅-CPAB, E4.1 and E5.1, respectively, to assess the RAFT control on the formation of PDMS-*b*-PMMA block copolymers offered by these two different macro-CTAs. With both macro-CTAs, monomer conversion was >90% (Table 3) and a free-flowing powder was obtained, demonstrating a good stabilisation efficiency. A further experiment (E4.2) used PDMS₆₅-CTPPA and targeted a PMMA DP of 300.

Table 3 – Results for MMA dispersion polymerisation in scCO₂ performed with PDMS₆₅-CTPPA (4) and PDMS₆₅-CPAB (5) after 24 h polymerisation.

Expt.	Macro-CTA	PDMS wt% ¹	Conv ² (%)	PMMA $M_{n,th}$ ³	Block copolymer $M_{n,th}$ ⁴	THF-SEC full peak	
						M_n ⁵	\bar{D} ⁵
E4.1	(4) PDMS ₆₅ -CTPPA	8.8	93.8	56.4	64.5	112.0	3.61
E4.2	(4) PDMS ₆₅ -CTPPA	17.4	92.7	28.0	36.1	32.4	1.63
E5.1	(5) PDMS ₆₅ -CPAB	8.8	93.3	55.7	63.8	109.3	3.25

¹ The weight percentage of PDMS in the reaction medium was calculated with respect to MMA. ² Conversion calculated from ¹H NMR. ³ Theoretical M_n for PMMA calculated relative to macro-CTA and monomer concentration and given in kg mol⁻¹. ⁴ Theoretical M_n of the block copolymer = PMMA $M_{n,th}$ + M_n of macro-CTA (8.1 kg mol⁻¹ for both macro-CTAs) as calculated in THF-SEC, where PMMA $M_{n,th}$ was calculated relative to macro-CTA and monomer concentration, given in kg mol⁻¹. ⁵ \bar{D} and M_n (in kg mol⁻¹) for the full peak, including both populations, were obtained from THF-SEC traces with RI detector against PMMA standards. See section 5.4.2.3 for reaction conditions used for dispersion polymerisation in scCO₂ (24 h).

Surprisingly, THF-SEC traces for the three polymerisations showed bimodal molecular weight distributions (solid traces -Figure 7). This could indicate poor blocking efficiency and formation of PMMA homopolymers. However, in the THF-SEC trace (dashed traces -Figure 7), the UV detection showed that the two populations absorb at 300-275 nm, showing that the corresponding chains are carrying a C(=S) moiety originating from the CTA. In addition, according to the RI trace, the macro-CTA appears to be largely consumed, although not quantitatively, as the UV detector shows a shoulder at low molecular weight (peak B-Figure 7). Perhaps the two polymer populations are a result of macro-CTA chain extension in two different environments: inside formed particles and in scCO₂ continuous phase. E4.1 also

shows an extra UV signal at low molecular weight (peak C - Figure 7), the nature of this signal was not identified and was considered simply as an impurity.

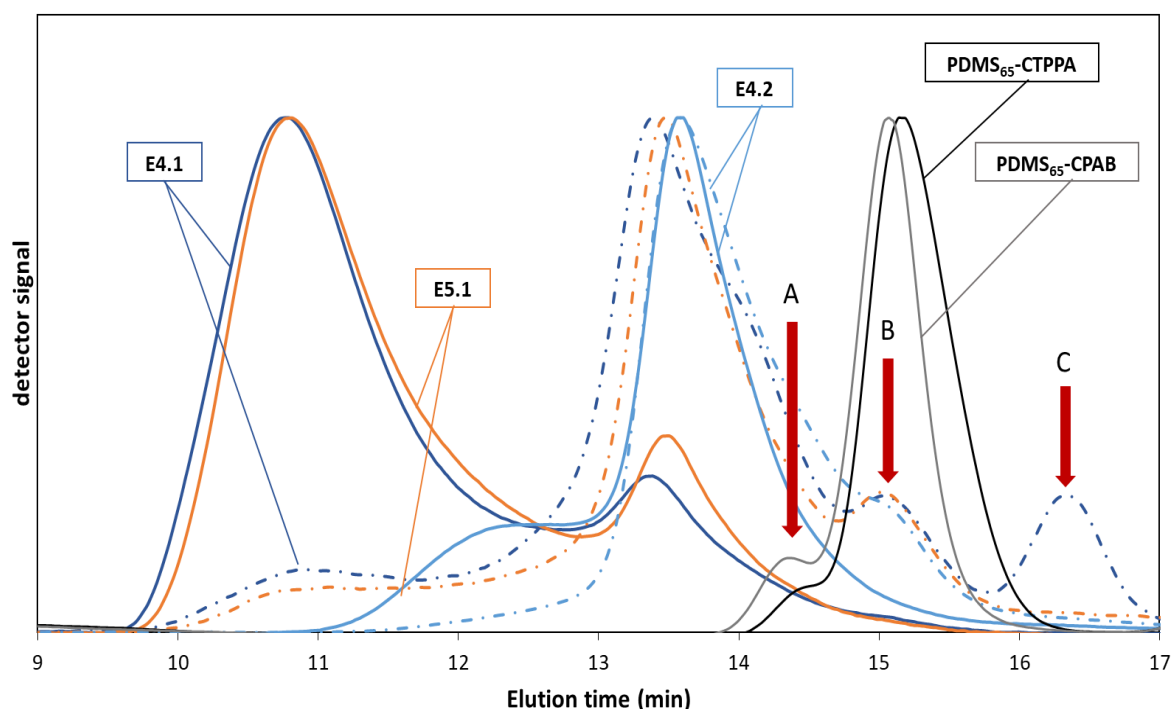


Figure 7 - THF-SEC study of MMA dispersion polymerisation in $scCO_2$ with PDMS₆₅-CTPPA, targeting DP of 600 (E4.1) and 300 (E4.2), and with PDMS₆₅-CPAB targeting a DP of 600 (E5.1), showing the traces for the RI detector (solid line) and the UV detector (dashed line). Peak A refers to a high molecular weight shoulder present in the macro-CTAs traces. Peak B indicates the presence of unreacted macro-CTA. Peak C refers to a low molecular weight population of unknown origin observed for E4.1

It is also interesting to notice that both starting macro-CTAs presented a shoulder of higher molecular weight around 14.3 minutes of elution time in the RI detector (peak A - Figure 7). However, no UV signal was observed for the shoulder. PDMS-OH also presented the same SEC trace with a shoulder at 14.3 minutes (Figure 8). This data suggests that the starting material, *i.e.*, PDMS-OH, had a higher molar mass population of PDMS impurity that does not carry an OH termination, since it did not present a UV signal after the esterification with the CTA. It should thus not be involved in the RAFT process implemented and remain in $scCO_2$ phase as spectator.

In order to better analyse the THF-SEC data, we performed a peak deconvolution for E4.1, E4.2 and E5.1 (Table 4). SEC traces were plotted as log of molecular weight *versus* $dwt/d[\log(MW)]$ in OriginPro8® with the Peak Analyser feature. A Gaussian fitting was

performed for fitting two or three curves until the data converged and the least squares function was minimised. The software requires the input of peak maximum position (x_c), which was evaluated visually and assigned to the peaks and “shoulders” maxima. The best fitting was always obtained with two polymer populations (Figure 9). M_n and \mathcal{D} were calculated from the two distributions generated by peak deconvolution (Table 4).

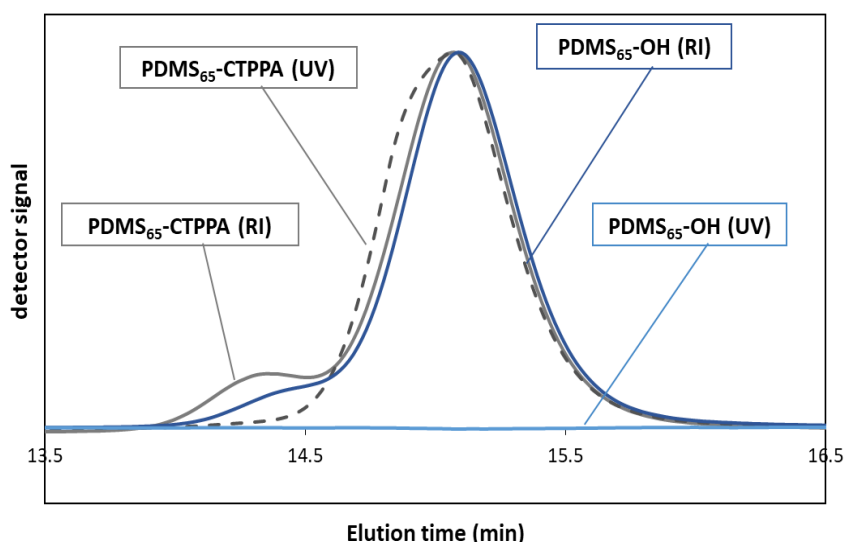


Figure 8 - THF-SEC study of PDMS₆₅-OH and PDMS₆₅-CTPPA macro-CTA, showing the traces for the RI detector (solid line) and the UV detector (dashed line). PDMS-OH does not present UV signal and the shoulder at 14.3 min for PDMS₆₅-CTPPA also does not present a UV trace.

Table 4 – Results for peak deconvolution of E4.1, E4.2 and E5.1

Expt.	Macro-CTA	PDMS wt% ¹	Peak A (blue)			Peak B (red)		
			M_n^2	\mathcal{D}^2	A% ²	M_n^2	\mathcal{D}^2	A% ²
E4.1	(4) PDMS ₆₅ -CTPPA	8.8	51.0	1.37	26.8	297.3	1.86	73.2
E4.2	(4) PDMS ₆₅ -CTPPA	17.4	29.0	1.38	88.8	124.3	1.15	11.2
E5.1	(5) PDMS ₆₅ -CPAB	8.8	35.4	1.64	28.6	283.4	1.76	71.4

¹The weight percentage of PDMS in the reaction medium was calculated with respect to MMA. ² \mathcal{D} and M_n (in kg mol⁻¹) and area percentage of the peak (A%) obtained by peak deconvolution in OriginPro8® of THF-SEC traces with RI detector against PMMA standards. See section 5.4.2.7 for the deconvolution method. See section 5.4.2.3 for reaction conditions used for dispersion polymerisation in scCO₂ (24 h).

To verify if the method was robust and was not affected by the initial assumption of x_c , peaks were also analysed by a numerical procedure, developed in Python, where the Particle Swarm Optimization (PSO) algorithm was used to select the best initial x_c estimates.^{8, 9} Then a Gaussian fitting was performed using the Levenberg-Marquardt algorithm, in order to fit two

or three peaks within the experimental data. Results obtained by OriginPro8[®] and from Python were virtually identical, and thus the robustness of OriginPro8[®] method was confirmed. Therefore, all following calculations were performed only in OriginPro8[®].

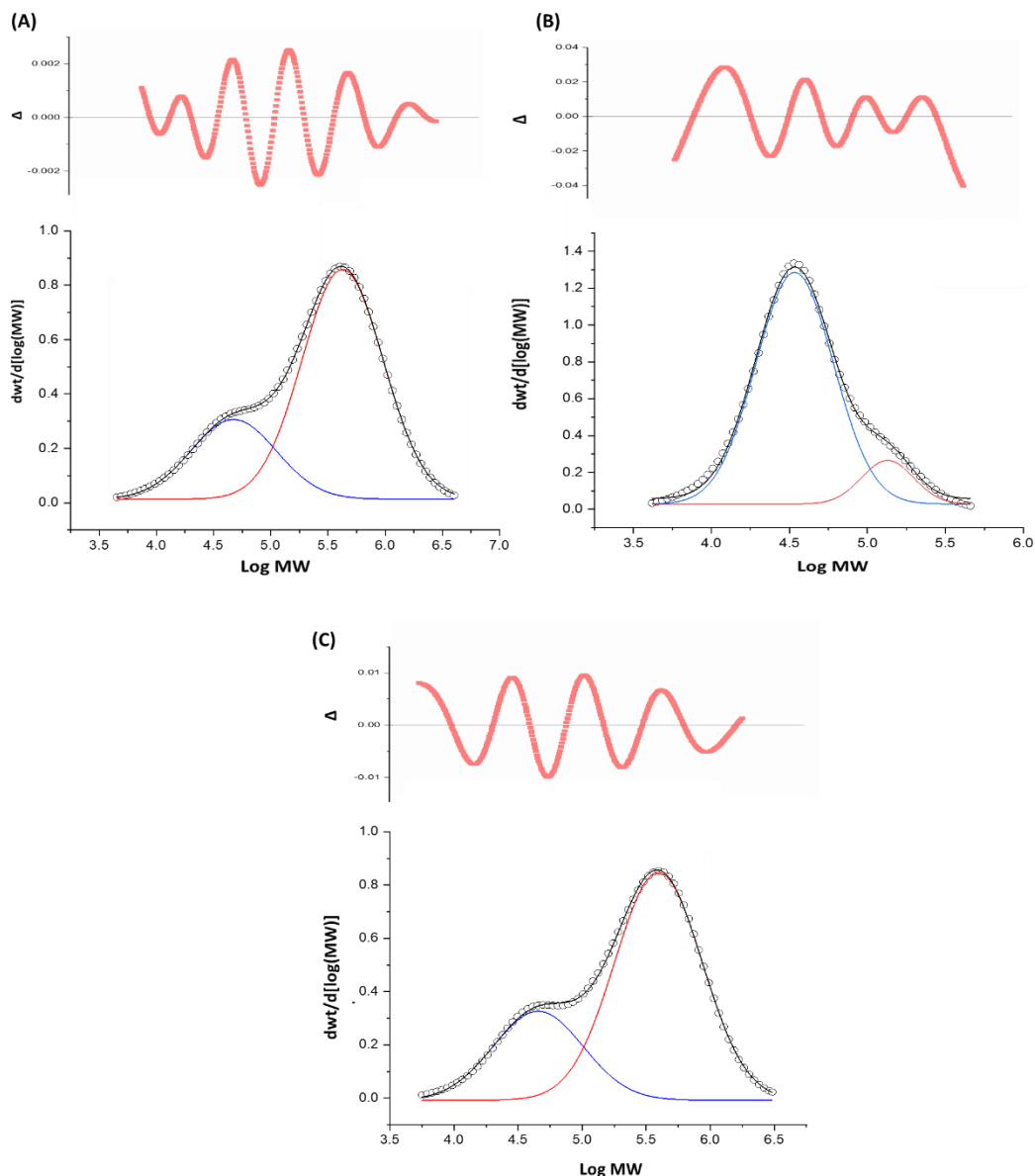


Figure 9 – Peak deconvolution in OriginPro8[®] of the product from (A) E4.1, (B) E4.2, (C) 5.1. The cumulative fit of both peaks is presented in black; the experimental data points are presented by circles (o); Peak A is presented in blue; and peak B is presented in red. The residual between the fit and the data (Δ) is presented over the trace.

The trace observed in THF-SEC for E4.2, $M_{n,th} = 28.0 \text{ kg mol}^{-1}$, shows a higher contribution of Peak A (88.8%) compared to Peak B (11.2%) (Table 4, Figure 9B). On the other hand, when targeting a high $M_{n,th}$, the higher molecular weight peak (Peak B) corresponds to 73.2% of the

molecular weight distribution for E4.1, and 71.4% for E5.1 (Table 4, Figure 9A and C). It is also interesting to notice that peak A (blue) had roughly the same molecular weight for all reactions, circa 4.5 logMW in Figure 9. This may indicate a critical molecular weight, above which control over the block copolymer growth is lost.

At the PMMA $M_{n,th} \approx 60 \text{ kg mol}^{-1}$, both E4.1 and E5.1 gave similar results, with overlapping THF-SEC traces (Figure 7) and similar M_n and \mathcal{D} (Table 3 and Table 4). No particular improvement in RAFT control was observed by changing CTPPA for CPAB in the macro-CTA, thus we decided to further study only PDMS-CTPPA due to time and materials constraints.

Regarding particle morphology, E4.1 and E5.1 presented individual spherical particles, with $D_n = 1.30 \mu\text{m}$, $C_v = 23.6\%$ and $D_n = 0.74 \mu\text{m}$, $C_v = 21\%$, respectively (Figure 10A and 10B). E4.2 resulted in a flaky yellow compacted powder and the SEM analysis showed large agglomerates, which upon closer inspection were also composed of small individual non-spherical particles (Figure 10C).

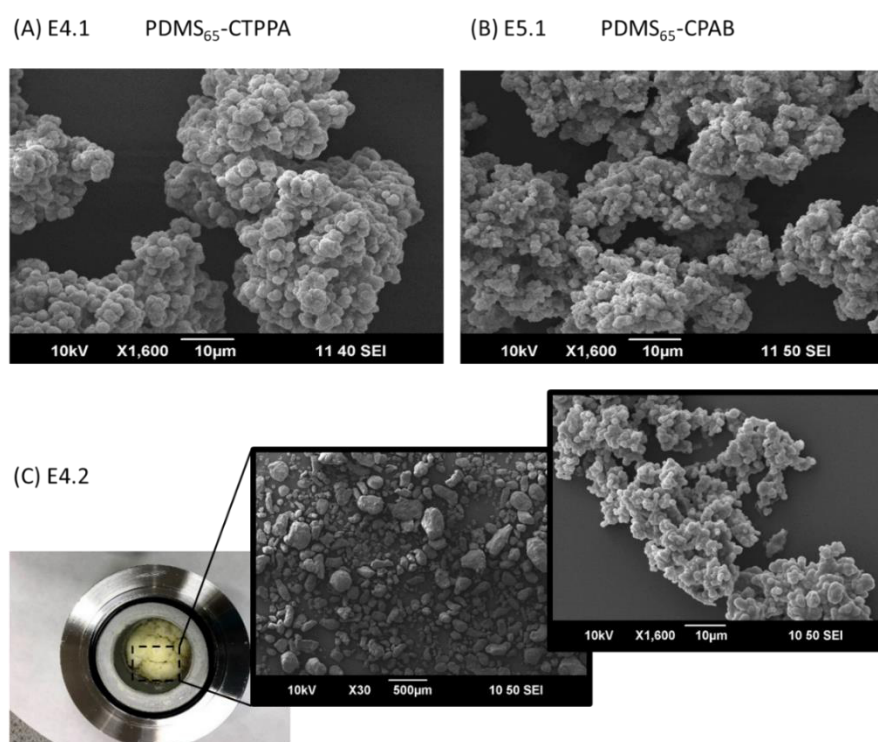


Figure 10 – SEM pictures of product from MMA dispersion polymerisation in $sc\text{CO}_2$ with target DP = 600 using different macro-CTAs: E4.1 - PDMS₆₅-CTPPA (A), E5.1 - PDMS₆₅-CPAB (B). Photo of reaction product and SEM pictures from MMA dispersion polymerisation in $sc\text{CO}_2$ with target DP = 300 using PDMS₆₅-CTPPA, E4.2 (C).

This more intense aggregation at lower DP of the PMMA block for E4.2 was likely a result of glass transition temperature (T_g) decrease in scCO₂. Indeed, scCO₂ is known to cause plasticisation and swelling of polymers, which reduces T_g and degree of crystallinity.^{10, 11} In addition the polymer particles can lose their morphology during CO₂ venting after the polymerisation, because the CO₂ inside the particles will be expelled out, this a phenomenon is commonly exploited for polymer foaming in scCO₂.^{12, 13}

In order to investigate the hypothesis of a critical molecular weight and to understand when each molecular weight population is formed during the polymerisation, we present in the next section a series of kinetic studies.

5.5.4. Kinetics of MMA polymerisation with PDMS-CTPPA

In light of the more encouraging results from E4.1 and E4.2, in this section we assess if PDMS-CTPPA can effectively provide RAFT control over MMA polymerisation. The kinetics was tracked using a recently developed sampling high-pressure autoclave (See section 2.3.10).⁶ The kinetics of a successful RAFT controlled polymerisation, as for other RDRPs, should depict a linear evolution of molecular weight with increase in conversion as shown in the Introduction and in Chapter 4. To better assess control over molecular weight and molecular weight dispersity, a set of three reactions targeting different final PMMA DPs were performed with each macro-CTA.

5.5.4.1. Kinetics of MMA polymerisation with PDMS₆₅-CTPPA

In this section, we discuss the results from kinetic studies of MMA polymerisation mediated by PDMS₆₅-CTPPA. Three different PMMA DPs were targeted, *i.e.*, 1200 (E4.3), 600 (E4.4) and 300 (E4.5) (Table 5). A macro-CTA:initiator ratio of 2:1 and the same MMA amount was maintained for each reaction.

The PDMS₆₅-CTPPA starting material presented a RI trace in THF-SEC with $M_n = 8.1 \text{ kg mol}^{-1}$ and $\mathcal{D} = 1.09$, which was used as Y intercept for $M_{n,th}$ trend line in the kinetic study. This value is far from the M_n calculated by ¹H NMR for PDMS₆₅-CTPPA, *i.e.*, 5.26 kg mol^{-1} , which was calculated by the sum of CTPPA molecular weight (265 kg mol^{-1}) to the M_n calculated by ¹H NMR for PDMS₆₅-OH (4.99 kg mol^{-1}). This can be attributed to the different nature of the PMMA standards used for THF-SEC calibration and the polymer being analysed, PDMS.

Table 5 – Results for MMA dispersion polymerisation in scCO₂ with different wt% of PDMS₆₅-CTPPA after 24 h polymerisation.

Expt.	PDMS wt% ¹	Conv ² (%)	Block copolymer $M_{n,th}$ ³	Peak B		Peak A	
				M_n ⁴	\mathcal{D} ⁴	M_n ⁴	\mathcal{D} ⁴
E4.3	4.4	95.3	122.4	208.3	1.47	70.5	1.49
E4.4	8.8	90.7	62.5	172.9	1.30	54.0	1.41
E4.5	17.5	90.6	35.4	148.1	1.22	27.9	1.16

¹ The weight percentage of PDMS in the reaction medium was calculated with respect to MMA. ² Conversion calculated from ¹H NMR. ³ Theoretical M_n of the block copolymer = PMMA $M_{n,th}$ + M_n of macro-CTA (8.1 kg mol⁻¹) as calculated in THF-SEC, where PMMA $M_{n,th}$ was calculated relative to macro-CTA and monomer concentration, given in kg mol⁻¹. ⁴ \mathcal{D} and M_n (in kg mol⁻¹) obtained by peak deconvolution in OriginPro8® of THF-SEC traces with RI detector against PMMA standards. See section 5.4.2.4. for reaction conditions used for scCO₂ dispersion polymerisation (24 h).

We will first discuss DP 1200, the full kinetic data are in Table S1 in the Appendix. The first aliquot for E4.3, at 30 minutes, showed a high M_n population (Pop1, Figure 11A), which had no signal in the THF-SEC UV detector (Figure 11B). Pop 1 was not seen for the aliquots from 1 hour onwards, indicating the number of high M_n chains became negligible. These indicates the occurrence of nucleation *via* PMMA homopolymer in a similar way as described by Winnik and Song¹ and as demonstrated in Chapter 4 for MMA polymerisation in scCO₂ with molecular CTAs. However, the precipitating PMMA must be stabilised in order to induce nucleation, and PDMS-MA stabiliser is absent. Therefore, stabilisation must come from a different source. For instance, PDMS₆₅-CTPPA may be simultaneously chain extending and forming surface-active PDMS-*b*-PMMA, which aggregate to the forming PMMA homopolymer and provide stabilisation. Another possibility is PDMS₆₅-CTPPA acting as stabiliser alone by physical adsorption via the CTA anchoring group.

A population referent to the unreacted macro-CTA was also observed with the RI detector for aliquots collected at 30 minutes and 1 hour (Figure 11A). But all following aliquots presented only one polymer population (Pop 2) tailing towards lower molecular weights, denoting the presence of shorter PMMA-*b*-PDMS chains and/or unreacted macro-CTA. As expected, the M_n of Pop 2 grew as the reaction progressed, as evidenced by its shift to the left (Figure 11A). However, a high molecular weight population was noticed for the two last aliquots. The peak deconvolution for 24 h aliquot (Figure S3) showed a $M_n = 70.5$ kg mol⁻¹ and $\mathcal{D} = 1.49$ for the

lower molecular weight population, while the other peak had $M_n = 208.3 \text{ kg mol}^{-1}$ and $\mathcal{D} = 1.47$ (Table 5).

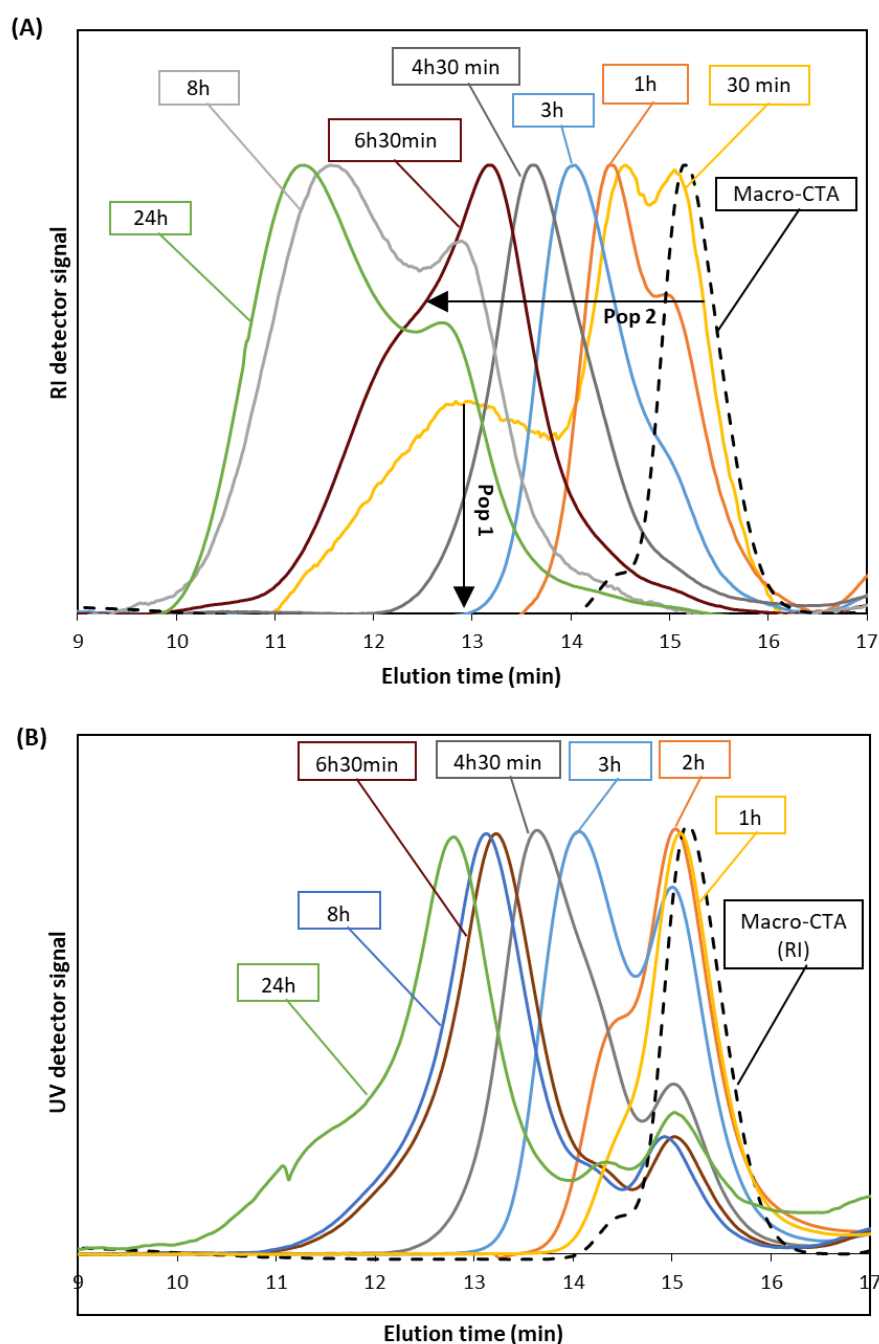


Figure 11 – Normalised THF-SEC study of MMA dispersion polymerisation in $sc\text{CO}_2$ with $\text{PDMS}_{65}\text{-CTPPA}$ and $\text{PMMA DP} = 1200$ (E4.3) showing aliquots from reaction with the sampling device against the RI detector (A) and the UV detector (B). Two distinct populations are observed, population 1 and population 2. Inside the boxes, the reaction time is given to depict the SEC traces.

Poor control at such high targeted DP ($\text{DP} = 1200$) is not unexpected, as RAFT is usually more successful when targeting M_n in the range $1\text{-}100 \text{ kg mol}^{-1}$.¹⁴ However, two distinct populations

were not expected. A controlled reaction was achieved up until 15% conversion (*i.e.*, 4.5 h) for E4.3, when $M_{n,th} = 26.4 \text{ kg mol}^{-1}$ and $M_n = 26.9 \text{ kg mol}^{-1}$ and $\mathcal{D} = 1.30$. This indicates control over the molecular weight distribution. After that point the experimental M_n started to deviate from $M_{n,th}$ (Figure 12) and a bimodal molecular weight distribution was noticed in the THF-SEC. Peak deconvolution of the two last samples (8h and 24h) showed the same molecular weight (70.5 kg mol^{-1}) for the low molecular weight population, while the high molecular weight population increased with conversion (TableS1- Appendix). Therefore, RAFT control was achieved at the initial stage of reaction, but was lost later into the polymerisation and the molecular weight of Pop 2 appears to reach a plateau after 8 h of reaction.

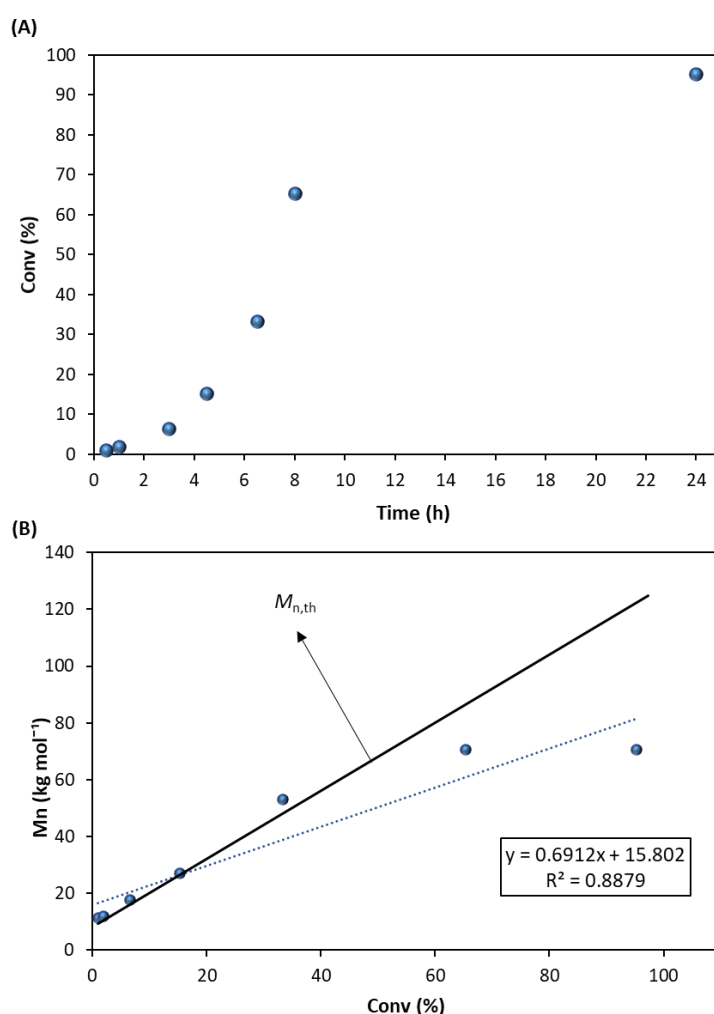


Figure 12 – Kinetic study of MMA dispersion polymerisation in $sc\text{CO}_2$ with $\text{PDMS}_{65}\text{-CTPPA}$ and $M_{n,th} = 122.4 \text{ kg mol}^{-1}$ (E4.3) showing (A) the plot of conversion with time and (B) the evolution of M_n of Pop 2 versus conversion. The final two M_n were calculated by peak deconvolution. The solid trend line is the $M_{n,th}$ and dashed trend line is the linear fitting of experimental data.

In addition, the evolution of conversion with time appears to show a sigmoidal profile, in agreement with dispersion polymerisation, however more data points between 10 and 24 h reaction time would be required to confirm this (Figure 12A).

When targeting 60 kg mol^{-1} , E4.4, a similar behaviour as for E4.3 was observed in the SEC-THF (Figure 13). All data from the collected aliquots of E4.4 can be found in the Appendix (Table S2). A high molecular weight population, *i.e.*, Pop 1, was observed in the initial aliquots and then decreased in intensity with reaction time. The higher molecular weight population (Pop 1) was only negligible after 8h of reaction, at which point the THF-SEC trace shows a unimodal peak. At 8h of reaction, conversion was 32.9% and $M_{n,th} = 27.8 \text{ kg mol}^{-1}$, while $M_n = 21.4 \text{ kg mol}^{-1}$ and $\mathcal{D} = 1.24$ (Table S2).

The second polymer population, *i.e.*, Pop 2, had a lower molecular weight and became the dominant species with reaction time (Figure 13A). Pop 2 presented a UV signal, indicating that the chains preserved the CTA end-group, and it grew in molecular weight with conversion (Figure 13B). This behaviour is quite similar to what was presented in Chapter 4 for the molecular CTAs, which suggests PMMA nucleation is happening *via* conventional radical polymerisation. In addition, the molecular weight of Pop 2 increased with time and the macro-CTA was consumed with the conversion increase, although it was not totally consumed as seen in the UV detector signal (Figure 13B). Furthermore, the UV trace for aliquots at 8 h and 24 h of reaction do not align with the RI trace. Although this difference was noticed, at the moment we cannot explain this observation.

The THF-SEC data for E4.4 is in accordance with block copolymer synthesis, with continuous growth of a population containing CTA end-groups with conversion increase. Therefore, it is surprising that the final aliquot showed a bimodal distribution of molecular weights. Peak deconvolution of the 24 h aliquot (90.7% conversion) showed two polymer populations, one with $M_n = 172.9 \text{ kg mol}^{-1}$ and $\mathcal{D} = 1.30$ and another with $M_n = 54.0 \text{ kg mol}^{-1}$ and $\mathcal{D} = 1.41$ (Figure S4), as calculated by peak deconvolution. This last polymer population is close to $M_{n,th} = 62.5 \text{ kg mol}^{-1}$ for the block copolymer.

The lower PMMA $M_{n,th}$ of E4.4 appears to improve reaction control, but the bimodal molecular weight distribution was still observed at higher conversions. As this high molecular weight population has a UV signal, it is unlikely to be termination by combination. In addition,

the reaction kinetics for E4.4 appears to be slower. At 8 h, only 32% conversion was achieved, while for E4.3, 65.4% was observed for the same reaction time. Although a linear trend for M_n versus monomer conversion was observed for E4.4 (Figure 14), it was below the theoretical trend line.

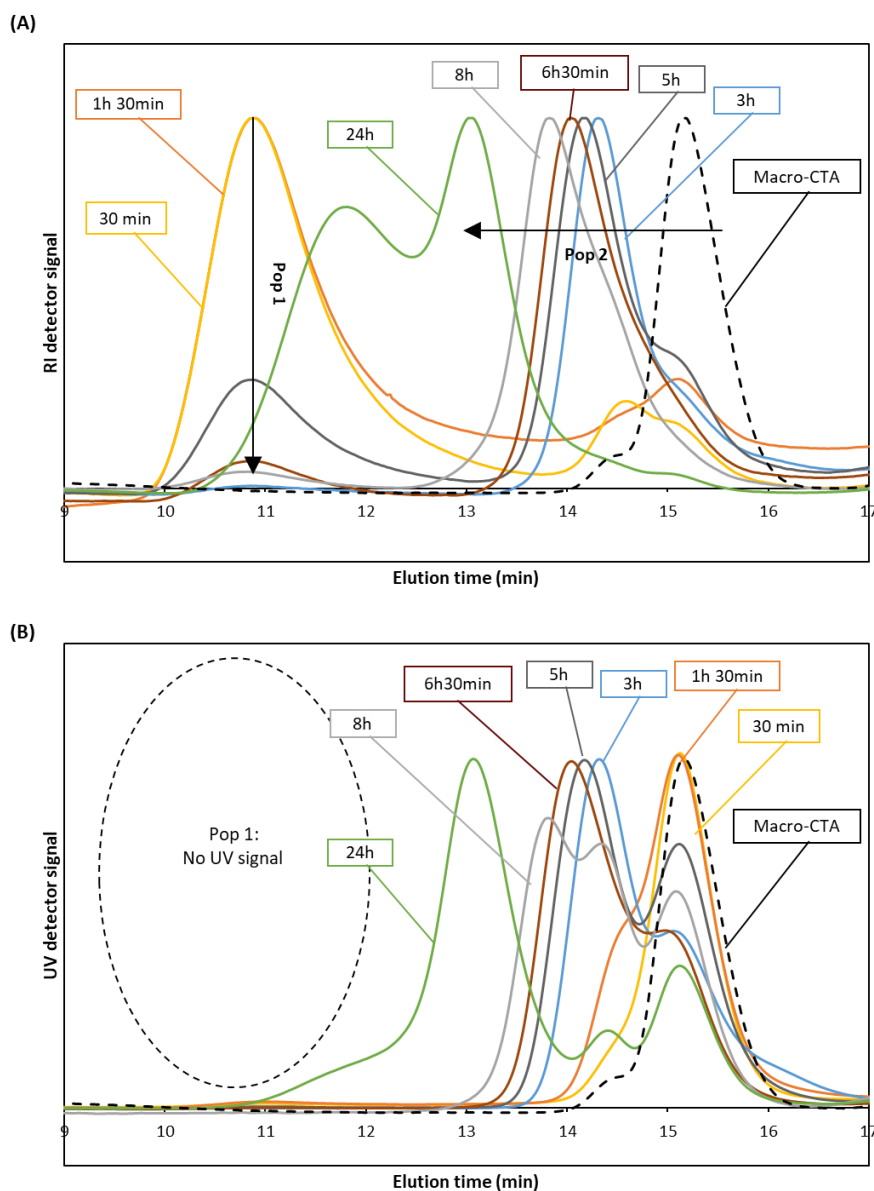


Figure 13 – Normalised THF-SEC study of MMA dispersion polymerisation in $scCO_2$ with $PDMS_{65}$ -CTPPA and PMMA DP = 600 (E4.4). Showing aliquots from reaction on sampling device against the RI detector (A) and the UV detector (B). Two distinct populations are observed, population 1 and population 2. Inside the boxes, the reaction time is given to depict the SEC traces.

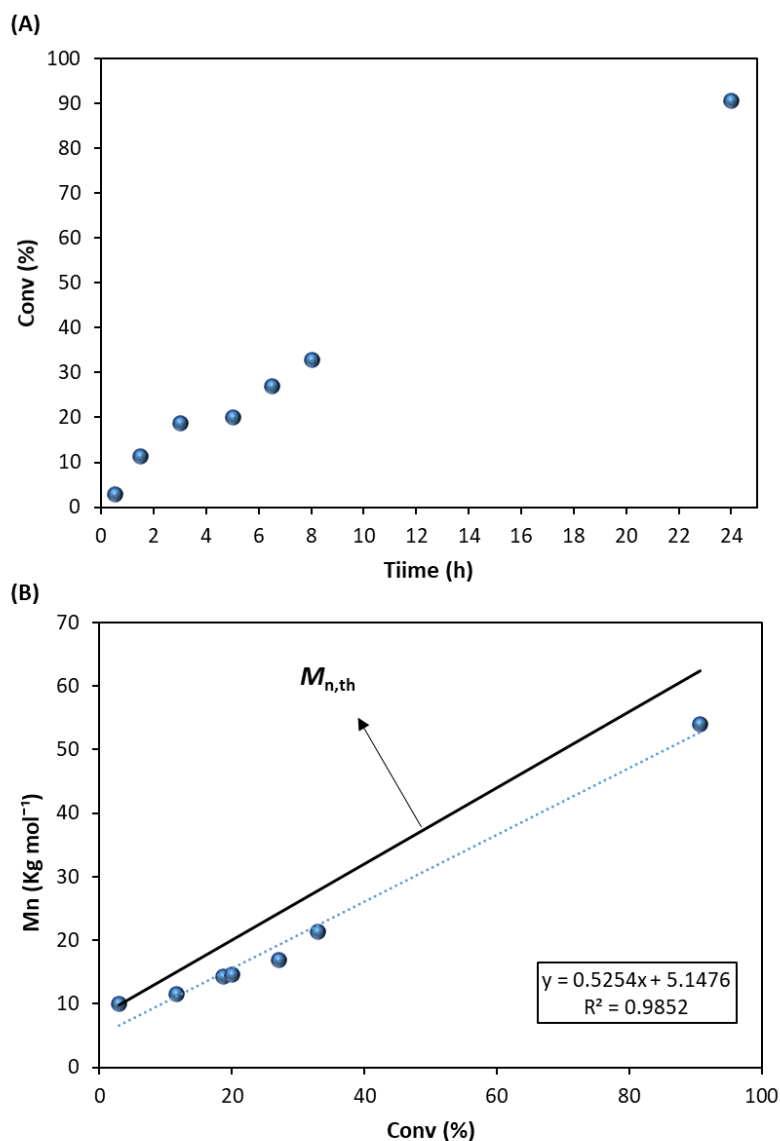


Figure 14 - Kinetic study of MMA dispersion polymerisation in $scCO_2$ with PDMS₆₅-CTPPA and $M_{n,th} = 62.5 \text{ kg mol}^{-1}$ (E4.4) showing (A) the plot of conversion with time and (B) the evolution of M_n of Pop 2 versus conversion; the solid trend line is the $M_{n,th}$ and dashed trend line is the linear fitting of experimental data.

At the lowest molecular weight target with PDMS₆₅-CTPPA, *i.e.*, 30 kg mol^{-1} for E4.5, only a unimodal molecular weight distribution was observed for all aliquots up to 8h of reaction, 30.7% monomer conversion (Figure 15). However, as for the previous reactions, the last aliquot, at 24 h of reaction and 90.6% conversion, presented a high molecular weight population, which has some UV signal. This last sample is strange and perhaps is the result of a long period of heating without conversion variation. In addition, different from E4.3 and

E4.4, no high molecular weight population at the start of the reaction was observed, which indicates that no nucleation occurred *via* conventional radical polymerisation.

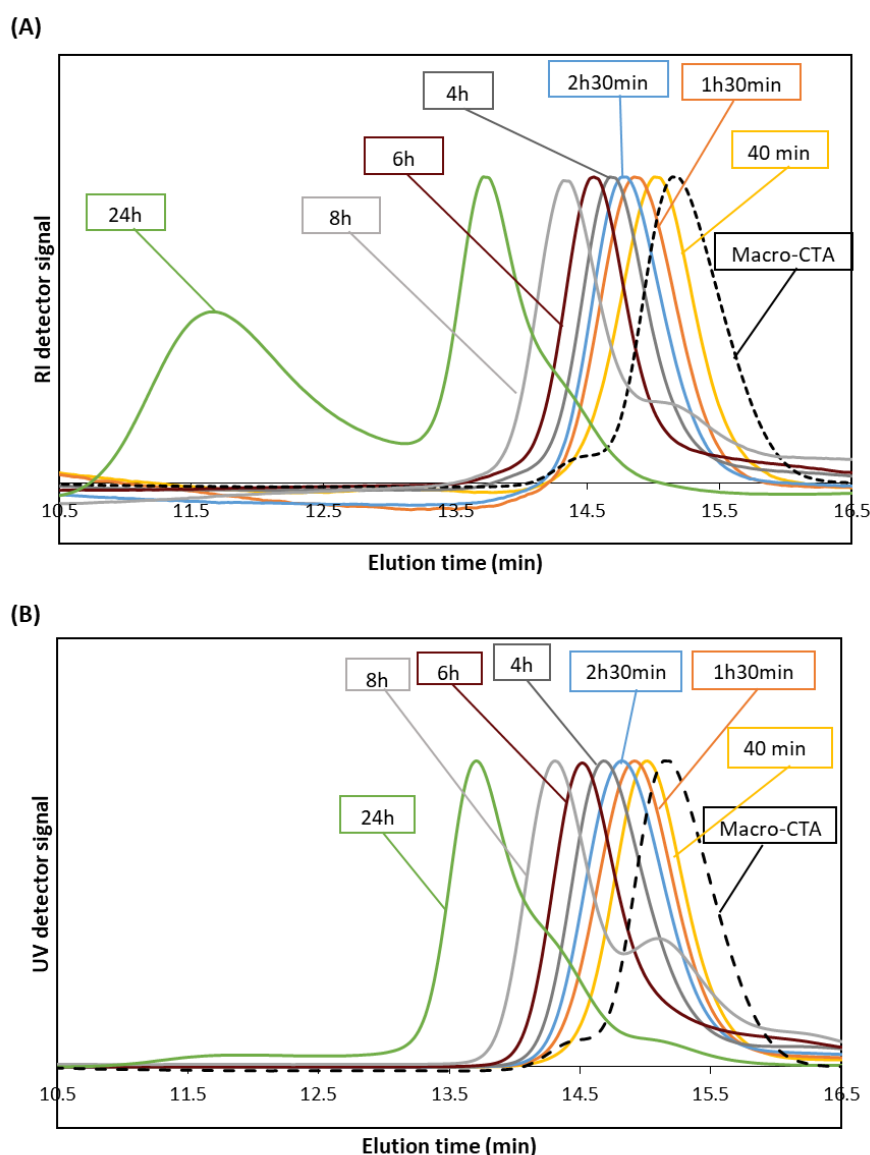


Figure 15 – Normalised THF SEC study of MMA dispersion polymerisation in $scCO_2$ with PDMS₆₅-CTPPA and PMMA DP = 300 (E4.5). Showing aliquots from reaction on sampling device against the RI detector (A) and the UV detector (B). Inside the boxes, the reaction time is given to depict the SEC traces.

Peak deconvolution was once more used to calculate molecular weight and dispersity for the final aliquot, although the peaks were not superimposed (Figure S5). The two peaks had $M_n = 148.1 \text{ kg mol}^{-1}$, $\mathcal{D} = 1.22$ and $M_n = 27.9 \text{ kg mol}^{-1}$, $\mathcal{D} = 1.16$, while the $M_{n,th} = 35.4 \text{ kg mol}^{-1}$. Considering only the low molecular weight population, this was the closest M_n to $M_{n,th}$ obtained with PDMS₆₅-CTPPA. A linear trend was presented for the plot of M_n against

conversion, but it did not align with the theoretical trend line (Figure 16). All data from the collected aliquots of E4.5 can be found in the Appendix (Table S3).

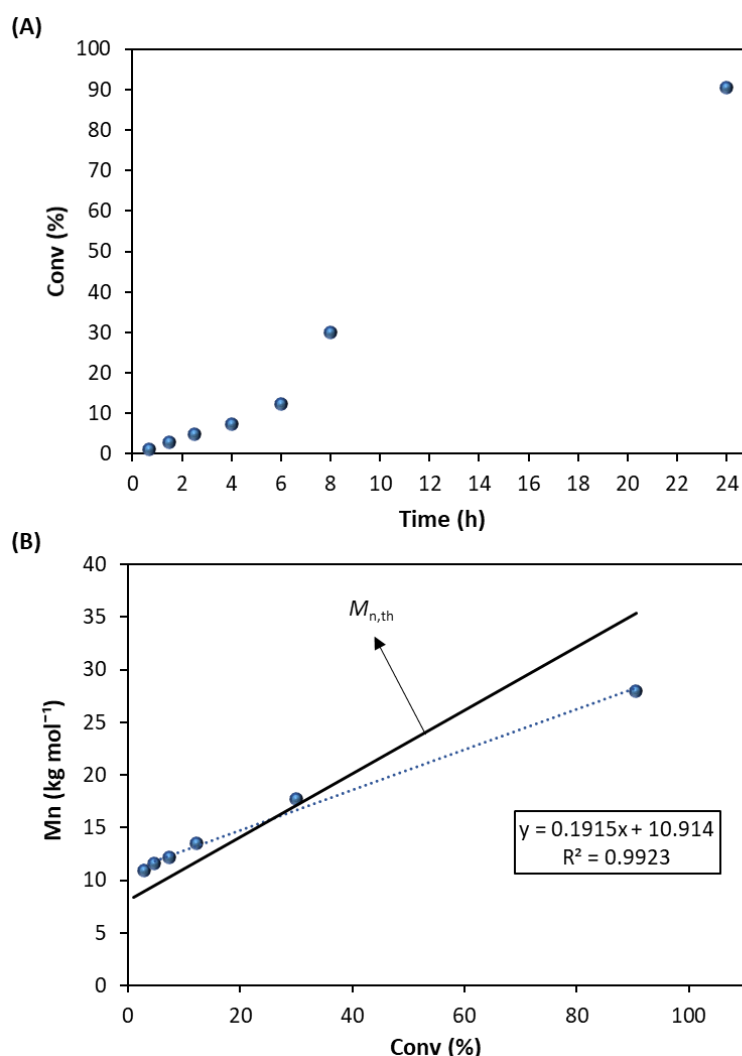


Figure 16 - Kinetic study of MMA dispersion polymerisation in $scCO_2$ with PDMS₆₅-CTPPA and $M_{n,th} = 35.4 \text{ kg mol}^{-1}$ (E4.5) showing (A) the plot of conversion with time and (B) the evolution of M_n of Pop 2 versus conversion; the solid trend line is the $M_{n,th}$ and dashed trend line is the linear fitting of

After 24 h of reaction, all kinetic reactions with PDMS₆₅-CTPPA presented bimodal molecular weight distributions at the end of reaction (Figure 17), as for the 24 h sample of E4.1 and E4.2 in previous section (Figure 7). It is interesting to notice that the high molecular weight population that appears at high conversions is accompanied by a UV signal, which indicates it is not resulting from termination by combination.

However, we so far do not understand how it is formed. Another interesting observation is that such bimodality is only observed when molecular weight for Pop 2 is higher than 27 kg

mol⁻¹. E4.3 had a unimodal peak at 4.5 h, when $M_n = 26.9$ kg mol⁻¹. E4.4, had a unimodal peak until 8 h, when $M_n = 21.4$ kg mol⁻¹. E4.5 only presented a bimodal peak in the final aliquot (24 h), when $M_n = 27.9$ kg mol⁻¹ according to peak deconvolution. Therefore, this can represent a critical molecular weight, perhaps corresponding to the switch from solution to dispersed media. In this way, above the critical molecular weight, the PDMS-*b*-PMMA chains self-assemble and the system passes from homogeneous to heterogeneous. And after the formation of a dispersed phase, the PDMS-*b*-PMMA chains fails to control MMA polymerisation for some physicochemical reason. A reaction targeting a lower PMMA M_n would be important in order to confirm this. Unfortunately, this was not done in the present work due to time constrains resulting from the COVID-19 pandemic.

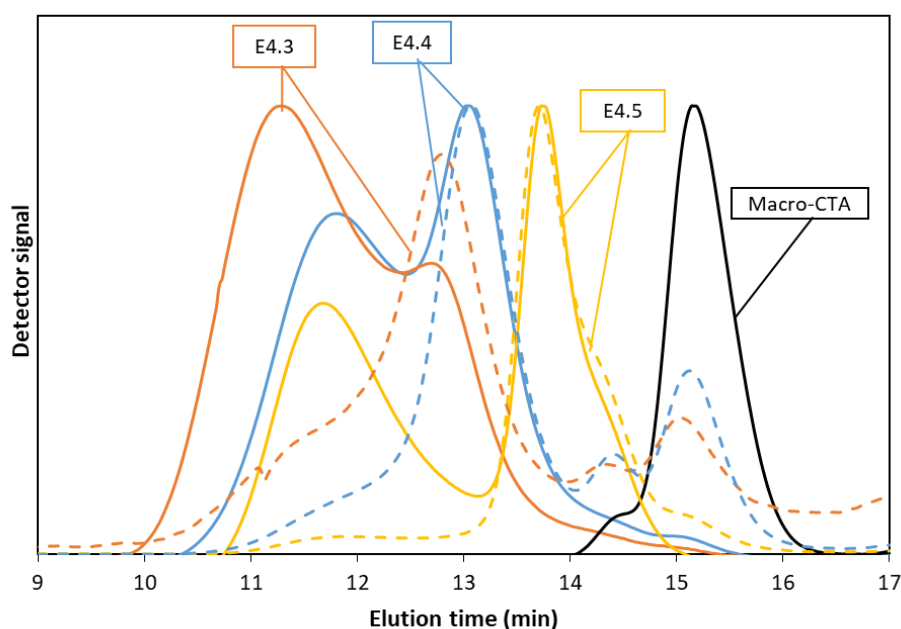
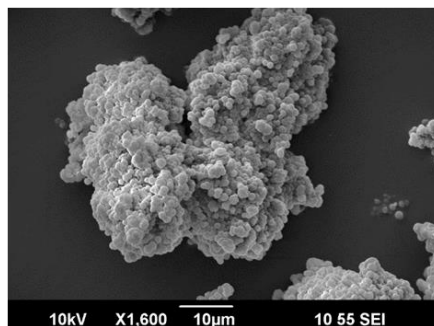
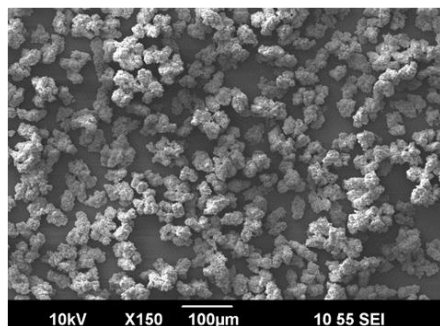


Figure 17 – Normalised THF-SEC traces for the final product of MMA dispersion polymerisation in *scCO*₂ with PDMS₆₅-CTPPA. PMMA target DP was 1200 for E4.3, 600 for E4.4 and 300 for E4.5. The dashed traces are the UV detector signal and the solid traces are the RI detector signal. The macro-CTA trace is presented in black. All polymerisations were carried out for 24 h under 65 °C and 276 bar with 2:1 macro-CTA:initiator ratio.

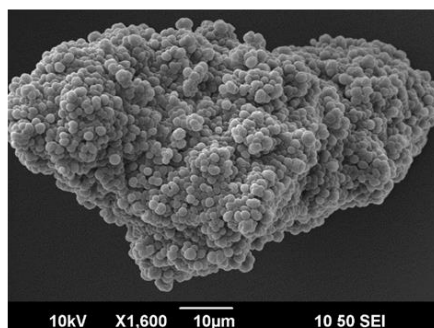
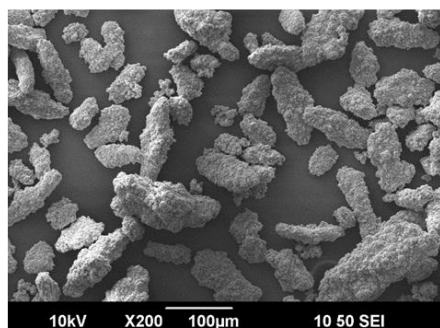
Regarding the particle morphology, all three polymer powders were analysed by SEM and the particle diameters were measured. At the lowest targeted DP of 30 kg mol⁻¹, E4.5, the product was a flaky yellow powder, while E4.3 and E4.4 gave free-flowing powders. All polymerisations gave individual particles that aggregated into secondary structures (Figure 18). Particles produced in E4.3 had $D_n = 0.95$ μm and $C_v = 19.3\%$, while E4.4 produced bigger

particles, with $D_n = 1.38 \mu\text{m}$ and $C_v = 23.5\%$. For E4.5, particles were smaller and less uniform, with $D_n = 0.77 \mu\text{m}$ and $C_v = 36.2\%$. Particles were larger than expected for block copolymer self-assembly.

(A) E4.3



(B) E4.4



(C) E4.5

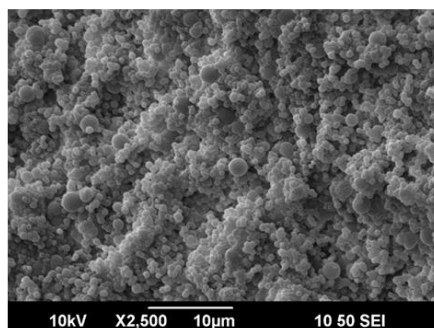
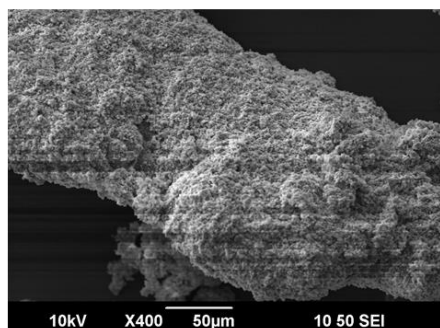


Figure 18 – SEM pictures of the final polymer products for MMA polymerisation with PDMS₆₅-CTPPA. (A) E4.3, PMMA DP =1200, (B) E4.4, PMMA DP = 600 and (C) E4.5, PMMA DP = 300.

In fact, the expected maximum diameter, if considering fully extended chains, can be calculated considering the PMMA DP and the length of a C-C bond (1.54 \AA), using Equation (4). The length of one PMMA segment gives the radius, thus the expected diameter ($D_{n,th}$) is twice this value.

$$D_{n,th} = 2 \times ((DP - 1) \times 1.54 \text{ \AA}) \quad (4)$$

In this way, considering the targeted DP, the expected diameter for E4.3, E4.4 and E4.5 are calculated to be 369 nm, 185 nm and 92 nm, respectively. It is not possible to know if self-assembly into particles of these smaller diameters occurred during the reaction in scCO₂ before venting the reactor, but the particles observed for the dry powder are much bigger than the expected ones for a PISA mechanism. The secondary structures can result from the presence of block copolymers with short PMMA blocks that are still soluble in scCO₂, and unreacted PDMS₆₅-CTPPA. These soluble polymers will coat the particles once the CO₂ is removed, making the particles “stick” together into aggregates.

The particles morphology of E4.4 was similar to what we observed for E4.1 (Figure 10) and both polymerisations had similar $M_{n,th}$. In addition, both reactions had similar molecular weights, E4.1 had a final block copolymer M_n of 51.0 kg mol⁻¹ and E4.4 had a final block copolymer M_n of 54.01 kg mol⁻¹.

In conclusion, PDMS₆₅-CTPPA was able to stabilise MMA polymerisation in scCO₂, providing high conversion. However, control over molecular weight and kinetics were not trivial, with a bimodal population formed at high conversions. The recovered polymer powders were composed by individual particles aggregated into larger agglomerates. However, the particles were bigger than expected for self-assembly and no morphology transition was evidenced by targeting different DP for the PMMA block.

5.5.4.2. Kinetics of MMA polymerisation with PDMS₁₂₈-CTPPA

We additionally studied the kinetics for MMA polymerisation with PDMS₁₂₈-CTPPA at three different targeted DP of the PMMA block, *i.e.*, DP = 1801 (E6.1), 920 (E6.2) and 476 (E6.3) (Table 6). A macroCTA:initiator ratio of 2:1 and the same MMA amount was maintained for each reaction. The kinetics of the three reactions were tracked by aliquots withdrawn with the high-pressure sample autoclave.

Table 6 – Results for MMA dispersion polymerisation in scCO₂ with PDMS₁₂₈-CTPPA after 24 h polymerisation.

Expt.	PDMS wt% ¹	Conv ² (%)	PMMA $M_{n,th}$ ³	<i>Block copolymer</i> $M_{n,th}$ ⁴	M_n ⁵	\mathcal{D} ⁵
E6.1	5.7	97.1	175.4	192.4	227.6	1.48
E6.2	11.1	98.6	90.8	107.9	155.7	1.32
E6.3	21.6	96.9	46.1	63.3	96.6	1.25

¹ The weight percentage of PDMS in the reaction medium calculated with respect to MMA. ² Conversion calculated from ¹H NMR. ³ Theoretical M_n for PMMA calculated relative to macro-CTA and monomer concentration, given in kg mol⁻¹. ⁴ Theoretical M_n of the block copolymer = PMMA $M_{n,th}$ + M_n of macro-CTA (17.1 kg mol⁻¹) as calculated by THF-SEC, given in kg mol⁻¹. ⁵ \mathcal{D} and M_n (in kg mol⁻¹) obtained by peak deconvolution in OriginPro8® of THF-SEC traces with RI detector against PMMA standards. See section 5.4.2.4. for reaction conditions used for scCO₂ dispersion polymerisation (24 h).

Once more, the molecular weight given by THF-SEC for the PDMS macro-CTA, 17.1 kg mol⁻¹, was quite different from the one calculated for PDMS₁₂₈-CTPPA by ¹H NMR, *i.e.*, 10.01 kg mol⁻¹. As for the shorter macro-CTA, M_n was calculated by the sum of CTPPA molecular weight (265 kg mol⁻¹) to the M_n calculated by ¹H NMR for PDMS₆₅-OH (9.75 kg mol⁻¹). This difference can be attributed to the different nature of the PMMA standards used for THF-SEC calibration and the polymer being analysed (PDMS).

E6.1 had a PMMA block $M_{n,th} = 175.4 \text{ kg mol}^{-1}$. As for the reactions with PDMS₆₅-CTPPA, a portion of the macro-CTA was left unreacted and tailing was present in THF-SEC traces for all aliquots.

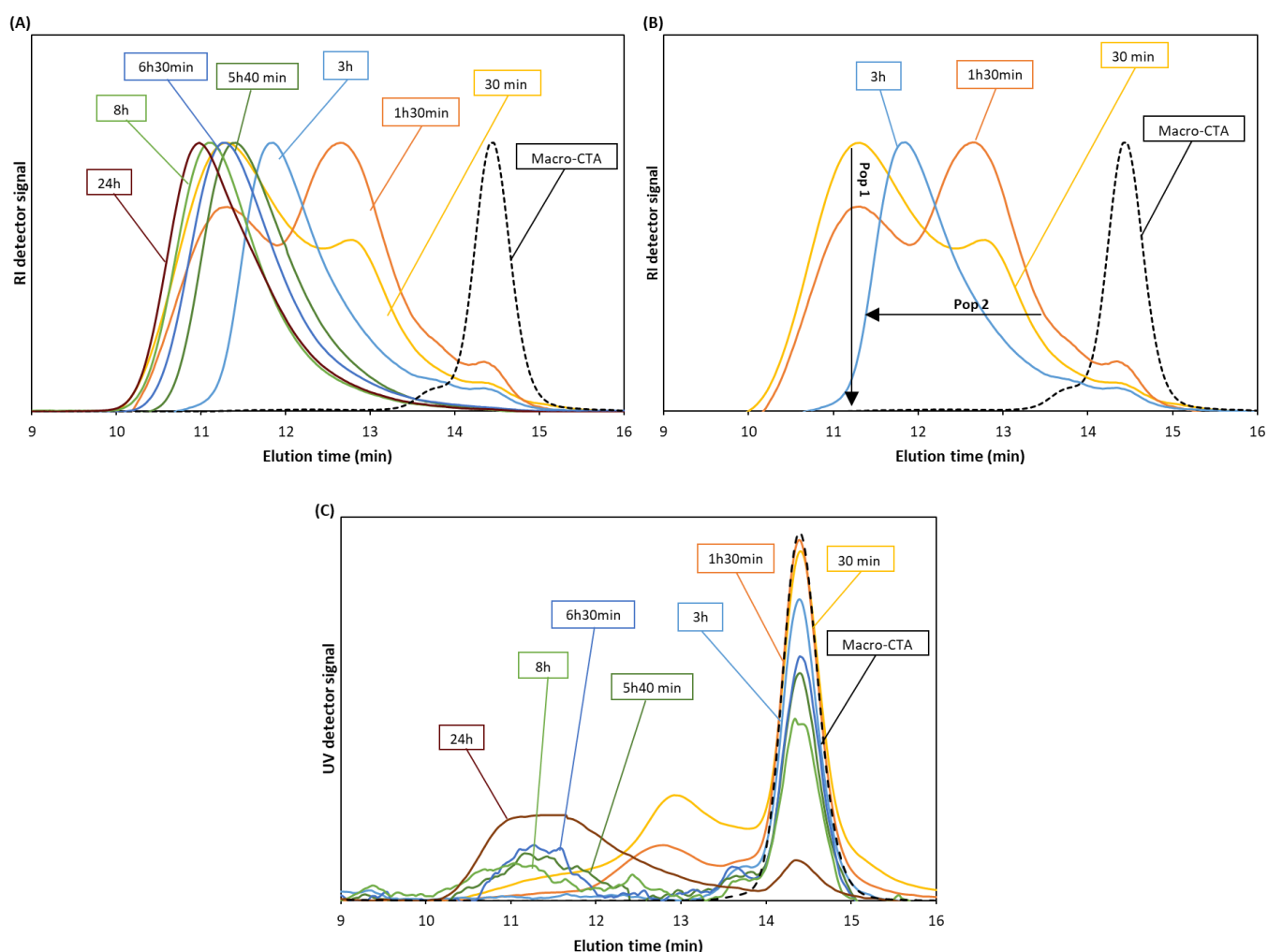


Figure 19 - Normalised THF-SEC study of MMA dispersion polymerisation in $scCO_2$ with PDMS₁₂₈-CTPPA and PMMA DP = 1801 (E6.1). Showing aliquots from reaction on sampling device against the RI detector (A) and the UV detector (B). A closer view at the start of the reaction defining Pop 1 and Pop 2 is presented in (C). Inside the boxes, the reaction time is given to depict the SEC traces.

The first samples, 30 and 90 minutes, show a high molecular weight population, Pop 1. After 3 hours of reaction, Pop 1 became negligible and the low molecular weight population bearing CTA end-groups, Pop 2, became the dominant species (Figure 19).

This indicates, as for E4.3 and E4.4 with the shorter PDMS-CTPPA, a nucleation *via* PMMA homopolymerisation as described by Winnik and Song.¹ Therefore, stabilisation must be provided by PDMS₁₂₈-CTPPA or by surface-active PDMS-*b*-PMMA, which is formed

simultaneously by PDMS₁₂₈-CTPPA chain extension. In addition, the UV detector presents signals for the polymer traces and the presence of unreacted PDMS₁₂₈-CTPPA.

Differently from E4.1-E4.5, only one unimodal molecular weight distribution was observed at the end of E6.1 polymerisation. The plot of conversion versus time shows a faster reaction compared to the shorter PDMS based macro-CTA, with over 90% conversion at 8h of reaction (Figure 20).

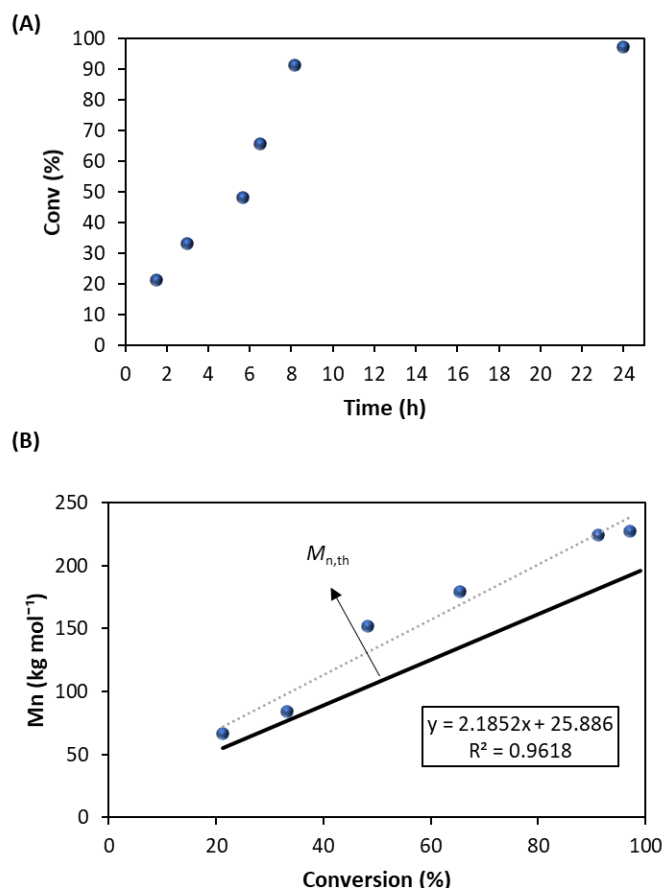


Figure 20 - Kinetic study of MMA dispersion polymerisation in *scCO*₂ with PDMS₁₂₈-CTPPA and $M_{n,th} = 192.4 \text{ kg mol}^{-1}$ (E6.1) showing (A) the plot of conversion with time and (B) the evolution of M_n of Pop 2 versus conversion; the solid trend line is the $M_{n,th}$ and dashed trend line is the linear fitting of experimental data.

The dispersity was higher than 1.30 throughout E6.1 polymerisation (Table S4), and at the end of the reaction, *i.e.*, 24 h, M_n was $227.6 \text{ kg mol}^{-1}$ while $M_{n,th} = 192.4 \text{ kg mol}^{-1}$ and $\mathcal{D} = 1.48$, which already gives a clue about the RAFT control of the reaction (Table 6). In addition, the plot of M_n against monomer conversion does not show good agreement with a linear trend

(Figure 20), staying always above the theoretical trend line. Thus confirming that indeed RAFT control was compromised at this high molecular weight target.

When targeting a PMMA block of 92.1 kg mol^{-1} , E6.2, a high molecular weight population without UV signal was observed only for the first aliquot, *i.e.*, 30 minutes, while tailing or a low molecular weight shoulder was present in all aliquots (Figure 21).

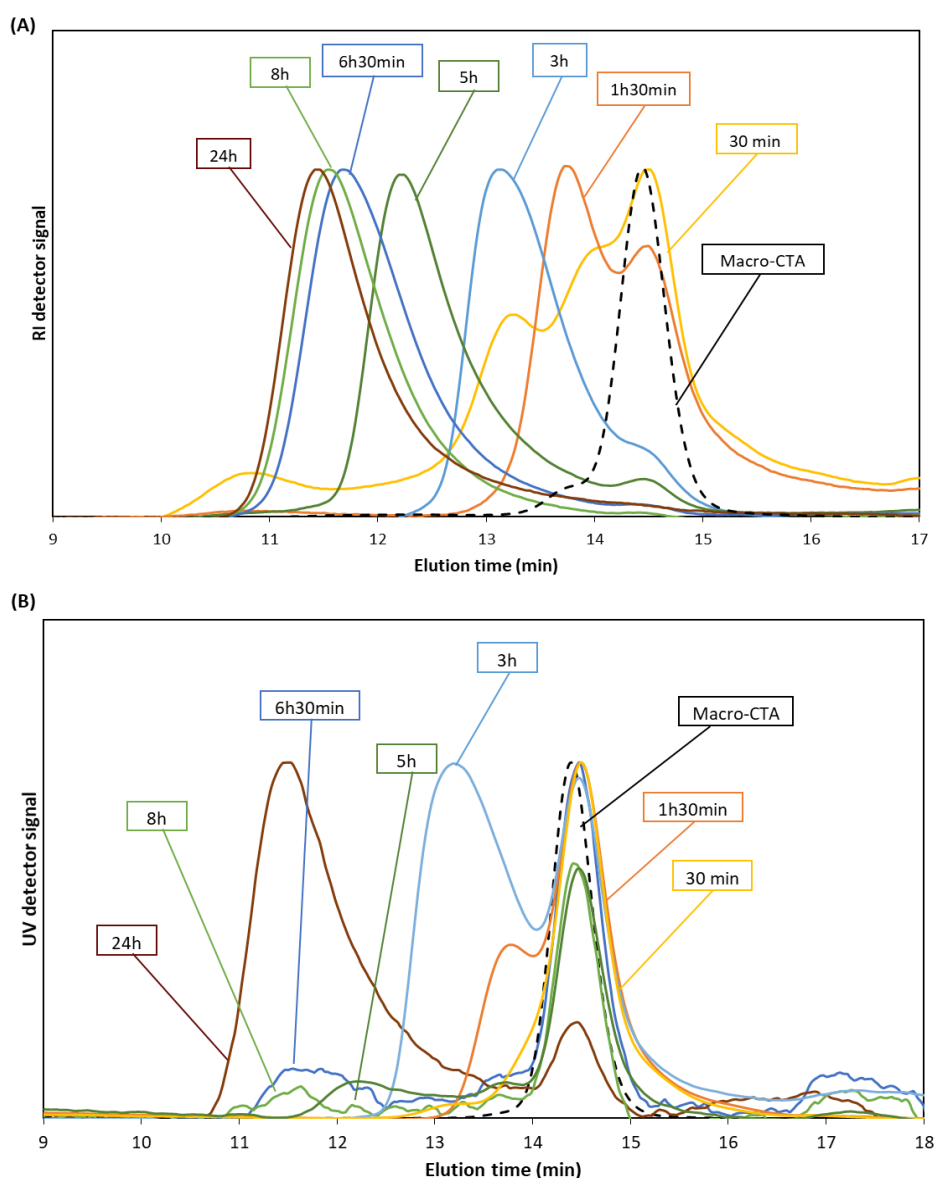


Figure 21 – Normalised THF-SEC study of MMA dispersion polymerisation in $sc\text{CO}_2$ with $\text{PDMS}_{128}\text{-CTPPA}$ and $\text{PMMA DP} = 920$ (E6.2). Showing aliquots from reaction on sampling device against the RI detector (A) and the UV detector (B). Inside the boxes, the reaction time is given to depict the SEC traces.

This indicates that initiation was slow and that the macro-CTA was mostly consumed early in the reaction, although it was not completely consumed. The UV signal from THF-SEC traces

showed a signal for unreacted macro-CTA and for the block copolymer, indicating that CTA end-groups were present in these polymers. Therefore, the effective $M_{n,th}$ would be higher, considering not all the macro-CTA was engaged in the reaction.

Molecular weight distribution was broad throughout E6.2 reaction, and narrowed to $\mathcal{D} = 1.32$ at the reaction end (Table S5). Nevertheless, the kinetic study showed a linear increase of M_n with conversion, which indicates a controlled radical polymerisation is taking place and not a conventional radical polymerisation, although it is above the theoretical trend line (Figure 22).

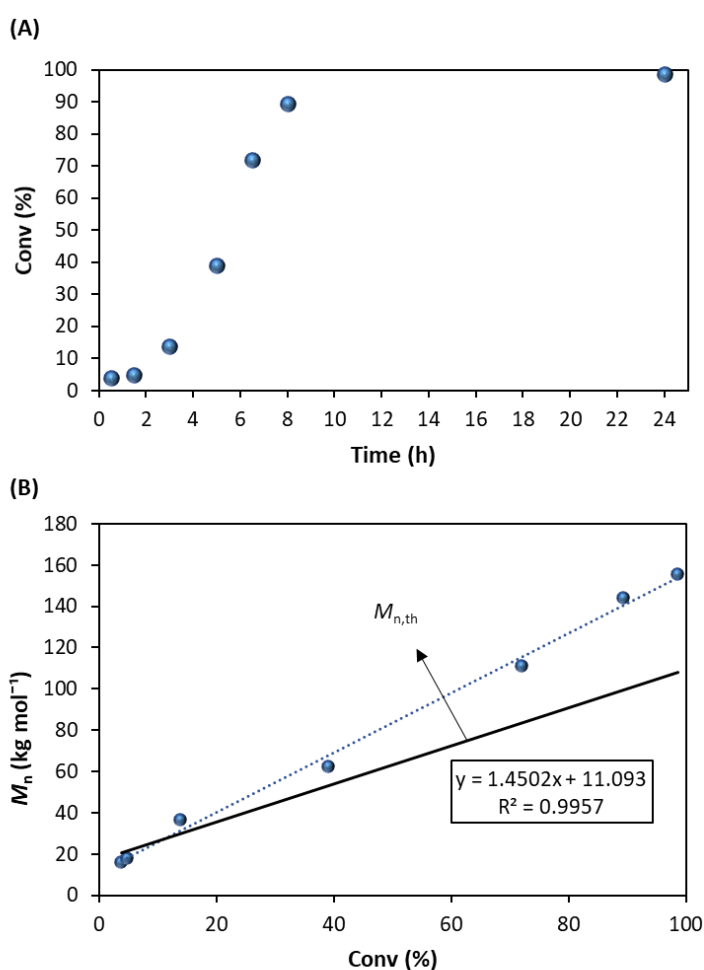


Figure 22 - Kinetic study of MMA dispersion polymerisation in $sc\text{CO}_2$ with $\text{PDMS}_{128}\text{-CTPPA}$ and $M_{n,th} = 107.9$ (E6.2) showing (A) the plot of conversion with time and (B) the evolution of M_n of Pop 2 versus conversion; the solid trend line is the $M_{n,th}$ and dashed trend line is the linear fitting of experimental data.

In addition, E6.2 had 39% monomer conversion up to 5 h of reaction, and after that conversion rapidly increased to 72% at 6h 30 minutes. At 24 h, E6.2 had a final conversion of

98.6% and $M_n = 155.7 \text{ kg mol}^{-1}$, which is above $M_{n,\text{th}}$ of $100.9 \text{ kg mol}^{-1}$. This result was further away from $M_{n,\text{th}}$ than for E6.1, although E6.2 targeted a lower PMMA DP.

The block copolymer $M_{n,\text{th}}$ for E6.3 was 63.3 kg mol^{-1} , and at this lower $M_{n,\text{th}}$, a lower dispersity was achieved, $\mathcal{D} = 1.25$. However, the final molecular weight still exceeded the theoretical one by 30 kg mol^{-1} (Table 6). The disagreement between M_n and $M_{n,\text{th}}$ was more accentuated from 8 h of reaction onward (Table S6). Again, as for E6.2, two polymer populations of different molecular weights were observed at the start of the reaction and became negligible after 3 hours into the reaction (Figure 23).

The higher M_n population, Pop 1, observed for aliquots at 30 minutes and 90 minutes had no UV signal (Figure 23B). Thus, this polymer population most likely grew *via* conventional radical polymerisation, leading to nucleation. This high molecular weight population of uncontrolled PMMA was accompanied by already chain extended PDMS₁₂₈-DDMAT, which likely provides enough block copolymer to stabilize nuclei and allow nucleation to take place. The block copolymer population, Pop 2, presented UV signal and chain extended with reaction progression, as denoted by the shift to the left of the THF-SEC traces from the aliquots (Figure 23). However, unreacted macro-CTA is still present as indicated by the UV detector, as is the case with all reactions using this macro-CTA (PDMS₁₂₈-CTPPA).

Despite these results, a linear trend could be observed for E6.3 plot of M_n versus monomer conversion, although it did not line up with the theoretical trend line (Figure 24). This is in accordance with a RAFT controlled reaction where not all the macro-CTA is engaged in the reaction, which is the case, as evident by the presence of unreacted macro-CTA in the THF-SEC study (Figure 23). In this way, the targeted molecular weight would be artificially higher. It is also interesting to notice that the obtained M_n were below the expected value up until 4 h of reaction, 18.0% conversion, but after that the M_n is above $M_{n,\text{th}}$.

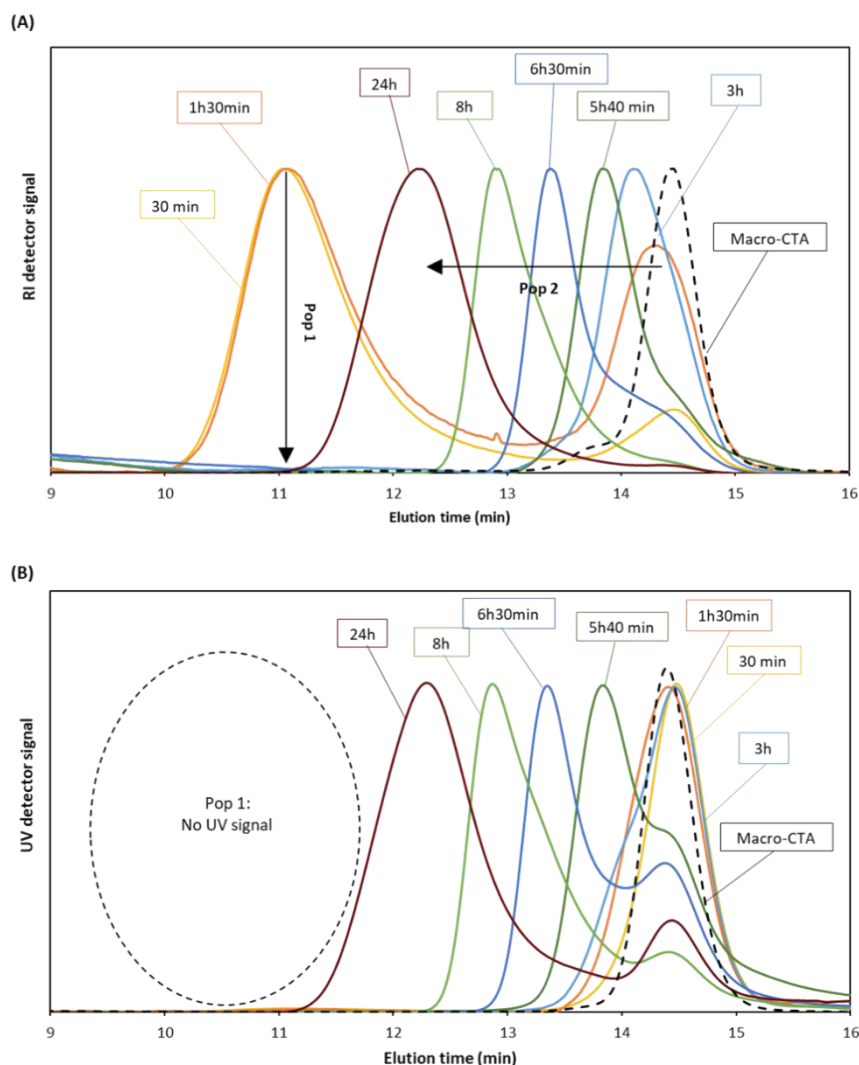


Figure 23 – Normalised TH- SEC study of MMA dispersion polymerisation in $scCO_2$ with $PDMS_{128}$ -CTPPA and $PMMA DP = 476$ (E6.3). Showing aliquots from reaction on sampling device against the RI detector (A) and the UV detector (B). Inside the boxes, the reaction time is given to depict the SEC traces.

Interestingly, with $PDMS_{128}$ -DDMAT, unimodal molecular weight distributions were observed at the end of all three reaction (Figure 25). Differently from polymerisations with $PDMS_{65}$ -CTPPA, a critical molecular weight does not seem to be involved for this longer macro-CTA. Perhaps the longer PDMS chain is providing a better stabilisation, as is the case for $PDMS$ -MA. McAllister *et al.* previously observed that $PDMS$ -MA with 5 kg mol^{-1} was less effective than $PDMS$ -MA with 10 kg mol^{-1} to stabilise conventional radical polymerisation of MMA in $scCO_2$.¹⁵ Another possibility, is that the molecular weight required for self-assembly, and thus creation of a dispersed system, was not reached. Further studies on the phase behaviour of this reaction would be required to define if that is the case.

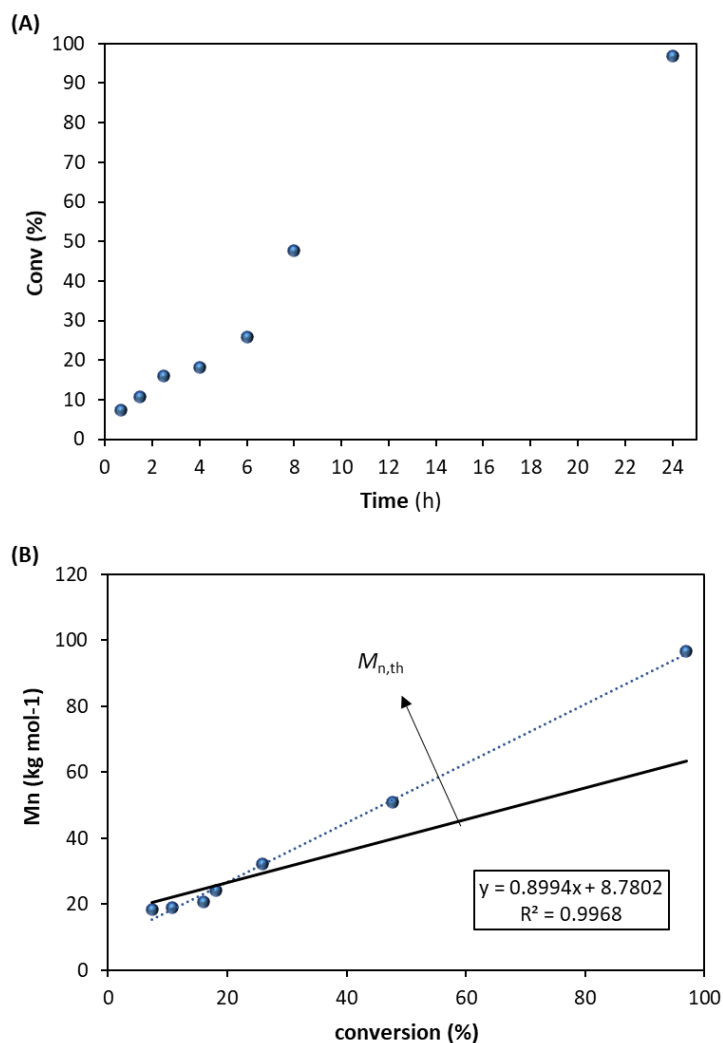


Figure 24 - Kinetic study of MMA dispersion polymerisation in $scCO_2$ with PDMS₆₅-CTPPA and $M_{n,th} = 63.3 \text{ kg mol}^{-1}$ (E6.3) showing (A) the plot of conversion with time and (B) the evolution of M_n of Pop 2 versus conversion.; the solid trend line is the $M_{n,th}$ and dashed trend line is the linear fitting of experimental data.

The UV detector traces and a tail towards low molecular weight in the RI detector indicated incomplete incorporation of the macro-CTA in all three reactions, which likely caused M_n to be above the theoretical value (Table 6). Nevertheless, it is important to emphasise that THF-SEC data was obtained against PMMA standards, which does not represent a perfect match with the block copolymers under analysis.

Therefore, the inconsistency between M_n and $M_{n,th}$ could be simply result from the poor description of PDMS-*b*-PMMA against a PMMA calibration. Thus, it is perhaps more

interesting to observe that the molecular weights increased steadily with conversion and the final polymer carried CTA chain-ends.

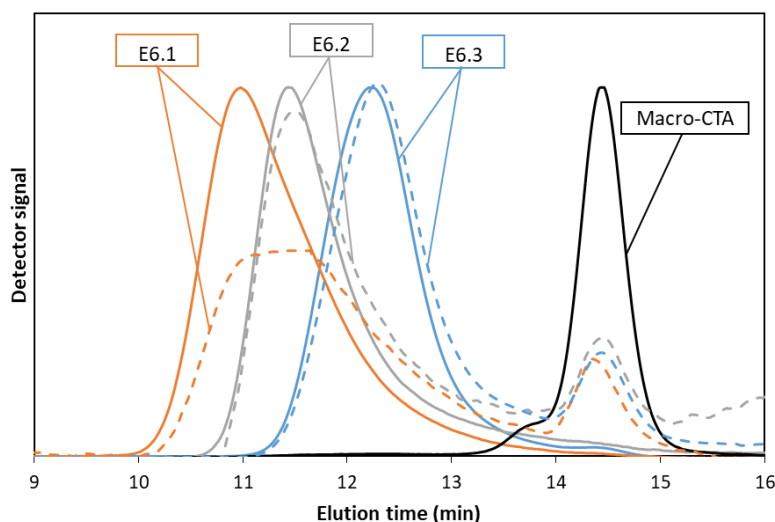


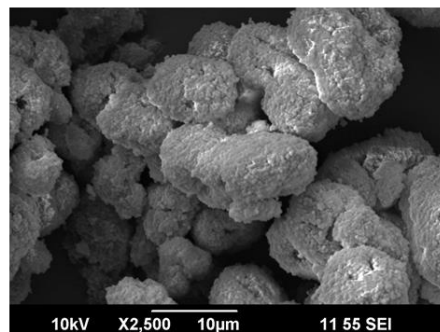
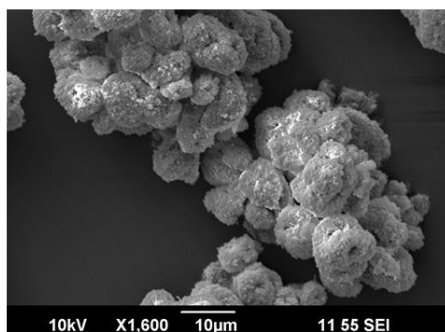
Figure 25 – Normalised THF-SEC traces for the final products of MMA dispersion polymerisation in $scCO_2$ performed with different PDMS₁₂₈-CTPPA concentration. PMMA target DP was 1801 for E6.1, 920 for E6.2 and 476 for E6.3. The dashed traces are the UV detector signal and the solid traces are the IR detector signal. The macro-CTA trace is presented in black. All polymerisations carried out for 24 h under 65 °C and 276 bar with CTA:initiator ratio of 2:1.

Regarding the particle morphology, the polymer powders obtained for the three polymerisations with PDMS₁₂₈-CTPPA were analysed by SEM. E6.1 showed large rounded secondary structures of around 9.9 μm in length, formed by individual particles that fused together (Figure 26). A more intense fusion of particles is observed for E6.2, where the secondary structures are larger than for E6.1, with approximately 35.9 μm in length. For E6.3, large solid amorphous lumps formed by fused polymer, with only few individual particles observed. This agrees with our hypothesis of morphology loss at higher block copolymer solubility. At lower DP of PMMA block, the block copolymers are more soluble and have lower T_g in $scCO_2$, causing a more intense swelling and thus the morphology is less well defined.

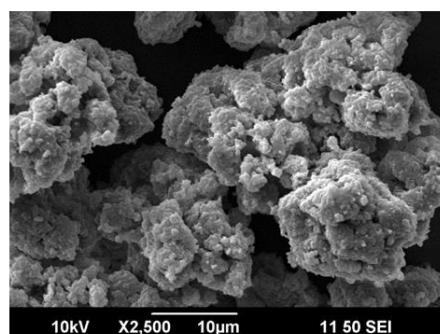
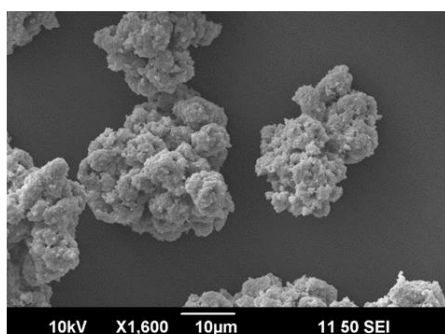
Again, the obtained aggregates are not the expected morphology for block copolymer self-assembly. In fact, calculating the expected particle diameter with base in the length of the C-C bonds of the targeted PMMA DP, E6.1, E6.2 and E6.3 have $D_{n,th}$ of 554 nm, 283 nm and 146 nm, respectively. Although it was not possible to measure the individual particles composing

the large agglomerates, the overall diameter is clearly larger than the calculated diameter for a PISA mechanism.

(A) E6.1



(B) E6.2



(C) E6.3

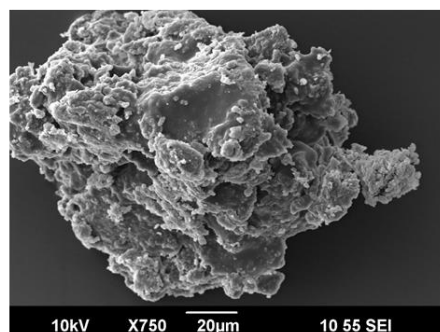
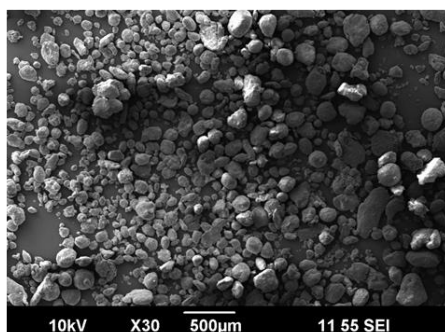


Figure 26 - SEM pictures of polymer products for MMA polymerisation with PDMS₁₂₈-CTPPA. (A) E6.1 $M_{n,th} = 192.4 \text{ kg mol}^{-1}$, (B) E6.2 $M_{n,th} = 107.9 \text{ kg mol}^{-1}$ and (C) E6.3 $M_{n,th} = 63.3 \text{ kg mol}^{-1}$.

The results for MMA polymerisation with both PDMS-CTPPA (Figure 17- Table 5 and Figure 25- Table 6) confirmed the formation of block copolymers, demonstrated by: (1) the chain extension was constant as conversion increased, as seen in the kinetic studies; (2) the presence of CTA end-groups denoted by the UV signal for the synthesised polymer; and (3) the consumption of the macro-CTA, although it is slower than expected and not complete. Therefore, in the next section we investigate how much of the macro-CTA is covalently bound to the PMMA polymer particles.

5.5.5. PDMS grafting efficiency onto the particles

As for MMA polymerisations with PDMS-DDMAT (Chapter 3), the reactions with PDMS-CTPPA show the presence of unreacted macro-CTA. To determine how much of the macro-CTA was actually grafted to the block copolymers, we performed hexane washes of the polymer powders produced with PDMS-CTPPA (See section 5.4.2.6. for the methodology).

Only 30 to 60% of the PDMS-based macro-CTA was grafted to the polymer particles synthesised with PDMS-CTPPA (Table 7 and Table 8). This number is surprisingly low, as we expected every PDMS-CTPPA chain would be chain extended simultaneously, but it is higher than the values observed with PDMS-DDMAT (Chapter 3 – results recalled in Table 7 and Table 8). The highest PDMS retention using PDMS₁₂₈-DDMAT was 36.1% for E1.3, with PMMA targeted DP of 600.

Table 7 – Hexane washes of polymer powders obtained by dispersion polymerisation in scCO₂ with PDMS₁₂₈-CTPPA and with PDMS₁₂₈-DDMAT as macro-CTA.

Expt.	CTA end group	PDMS wt% ¹	Block copolymer $M_{n,th}$ ²	Conv. ³ (%)	Block copolymer M_n ⁴	\bar{D} ⁴	PDMS retained ⁵ (%)
E6.1	CTPPA	5.7	192.4	97	227.6	1.48	31.2
E6.2	CTPPA	11.1	107.9	99	155.7	1.32	61.1
E6.3	CTPPA	21.6	63.3	97	96.6	1.25	41.4
E1.1	DDMAT	9.24	122.5	98	145.4	2.18	23.3
E1.2	DDMAT	11.5	100.3	92	124.2	2.12	28.9
E1.3	DDMAT	17.2	70.6	96	92.4	1.81	36.1
E1.4	DDMAT	20.7	60.5	94	88.8	2.35	33.3
E1.5	DDMAT	34.4	40.5	93	65.5	2.23	34.2

¹The weight percentage of PDMS in the reaction medium was calculated with respect to MMA. ² M_n theoretical was calculated relative to CTA and monomer concentration and given in kg mol⁻¹. ³ Conversion was calculated from ¹H NMR. ⁴ Experimental M_n and \bar{D} were obtained by THF-SEC of the block copolymer. ⁵ The percentage of retained PDMS was obtained by comparing ¹H NMR resonance integrals for PDMS and PMMA repeating units before and after hexane wash, considering the integral before hexane wash to be 100%.

Comparing PDMS retention with PDMS₁₂₈-CTPPA and PDMS₁₂₈-DDMAT (Table 7), we observed an improvement in blocking efficiency for PDMS₁₂₈-CTPPA compared to PDMS₁₂₈-DDMAT of similar M_n . For example, E6.2, $M_n = 155.7$ kg mol⁻¹, had over 61% PDMS grafted, while E1.1, $M_n = 145.4$ kg mol⁻¹, only had 23% of the PDMS covalently bonded to the block copolymer particles. On the other hand, a similar PDMS retention was observed for both

macro-CTAs at $M_n \approx 90 \text{ kg mol}^{-1}$. E6.3, $M_n = 96.6 \text{ kg mol}^{-1}$, had 40.4% of the PDMS grafted, while E1.3, $M_n = 96.6 \text{ kg mol}^{-1}$, had 36.1% of the PDMS grafted (Table 7). Interestingly, the higher retention with PDMS₁₂₈-CTPPA was obtained for E6.2, which presented 61% of the macro-CTA retained in the block copolymer, while E6.3, which had the lowest M_n with PDMS₁₂₈-CTPPA, had only 40.4% of the PDMS grafted to the polymer (Table 7).

For the shorter macro-CTA, *i.e.*, PDMS₆₅-CTPPA, the highest PDMS retention (56%) was obtained for E4.5, which had the lowest $M_n = 27.9 \text{ kg mol}^{-1}$ of the reactions with PDMS₆₅-CTPPA (Table 8). It is interesting to observe that block copolymers of similar molecular weight had a similar PDMS retention, showing a good reproducibility. Both E4.1 and E4.4 targeted a $M_n \approx 50 \text{ kg mol}^{-1}$ and had approximately 35% of the macro-CTA grafted. The same can be seen for E4.2 and E4.5, which had $M_n \approx 30 \text{ kg mol}^{-1}$ and around 54% of the PDMS grafted.

Table 8 – Hexane washes of polymer powders obtained by dispersion polymerisation in sCO_2 with PDMS₆₅-CTPPA and with PDMS₆₅-DDMAT as macro-CTA.

Expt.	CTA end group	PDMS wt% ¹	Block copolymer $M_{n,th}$ ²	Conv. ³ (%)	Block copolymer M_n ⁴	\mathcal{D} ⁴	PDMS retained ⁵ (%)
E4.1	CTPPA	8.8	64.5	94	51.0*	1.37*	33.3
E4.2	CTPPA	17.4	36.1	93	29.0*	1.38*	52.4
E4.3	CTPPA	4.4	122.4	95	70.5*	1.49*	50.0
E4.4	CTPPA	8.8	62.5	91	54.0*	1.41*	37.0
E4.5	CTPPA	17.5	35.4	91	27.9*	1.16*	56.2
E2.1	DDMAT	5.9	96.1	93	131.2	2.96	27.4
E2.2	DDMAT	8.9	65.7	94	80.9	2.50	39.4
E2.3	DDMAT	10.6	55.8	94	64.1	2.39	45.7
E2.4	DDMAT	13.4	45.0	93	61.5	2.68	47.1
E2.5	DDMAT	17.8	35.1	95	60.3	2.50	52.8
E2.6	DDMAT	21.4	30.5	88	24.5	1.44	57.5

¹The weight percentage of PDMS in the reaction medium was calculated with respect to MMA. ² M_n theoretical was calculated relative to CTA and monomer concentration and given in kg mol^{-1} . ³ Conversion was calculated from ¹H NMR. ⁴ Experimental M_n and \mathcal{D} were obtained by THF-SEC of the block copolymer. ⁵ The percentage of retained PDMS was obtained by comparing ¹H NMR resonance integrals for PDMS and PMMA repeating units before and after hexane wash, considering the integral before hexane wash to be 100%. * M_n and \mathcal{D} obtained by peak deconvolution for the lower molecular weight peak (peak A in the peak deconvolution).

Figure 27 shows the percent of PDMS macro-CTA grafted to the copolymers against the theoretical M_n . Overall, a similar PDMS retention was observed for both PDMS₆₅-CTPPA and PDMS₆₅-DDMAT (Table 8) at the same targeted MMA molecular weights, a trend in increase of PDMS retention as lowering the copolymer M_n can be observed (Figure 27). In addition, better agreement between M_n and $M_{n,th}$ was observed with PDMS₆₅-CTPPA (Table 8). With the longer PDMS macro-CTAs, *i.e.*, PDMS₁₂₈-CTPPA and PDMS₁₂₈-DDMAT, a trend was not observed, although all reactions got less than 45% PDMS retention, except E.6.2 that had 61.1% of PDMS macro-CTA retained in the polymer after hexane washes.

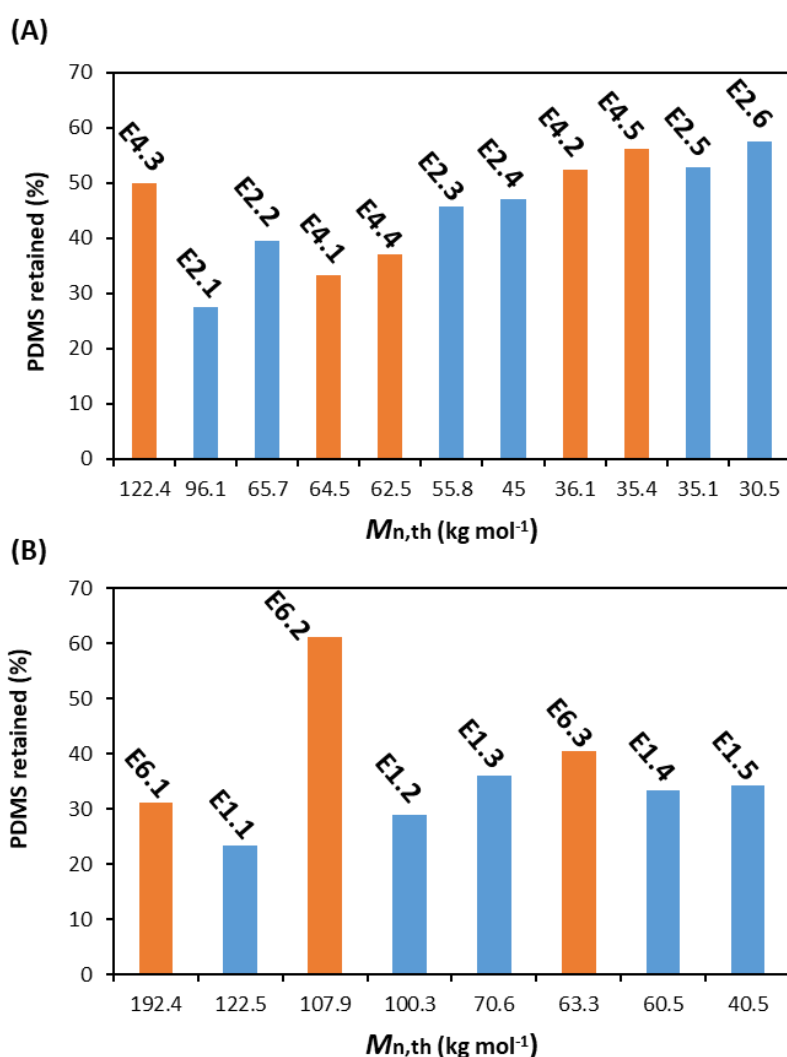


Figure 27 – Plot of PDMS retained (%) versus $M_{n,th}$ of MMA polymerisations with (A) PDMS₆₅-based macro-CTA, PDMS₆₅-CTPPA (orange) and PDMS₆₅-DDMAT (blue); with (B) PDMS₁₂₈-based macro-CTA, PDMS₁₂₈-CTPPA (orange) and PDMS₁₂₈-DDMAT (blue).

Although the retention of both PDMS-CTPPA and PDMS-DDMAT macro-CTA was not as high as expected, it was greater than the incorporation of PDMS-MA (250 cSt) stabiliser into PMMA particles. This reactive stabiliser would be expected to copolymerise with MMA, but previous studies showed that only a small fraction of the stabiliser is incorporated into the polymer particles, *i.e.*, < 2 wt%.^{16, 17}

It is also important to notice that the hexane washes give an estimative of PDMS macro-CTA grafting to the copolymers, however it is prone to fails, as short PDMS-*b*-PMMA chains can potentially be solubilised into hexane together with unreacted macro-CTA. This would give a lower percent of PDMS grafting to the copolymer that in reality, suggesting a lower blocking efficiency that actually obtained.

5.6. Conclusions

This work represents a step forward on the understanding of RAFT polymerisation in $scCO_2$. By coupling PDMS-OH to CTAs of high C_{tr} towards MMA polymerisation, the initial stage of polymerisation, *i.e.*, solution polymerisation conditions, could be improved and thus, the efficiency of block copolymer formation was improved. As both CPAB and CTPPA had similar preliminary results over MMA polymerisation in $scCO_2$, only CTPPA was taken forward for further studies.

Even though this CTA has a high C_{tr} , homopolymerisation still occurred at the early polymerisation stage, as observed by THF-SEC. This indicates the occurrence of an *in situ* two-stage polymerisation, similar to what we observed in chapter 4 and as proposed by Winnik and Song in their seminal work.¹ The RAFT pre-equilibrium and short inhibition allows the homopolymerisation to take place, creating a nucleation stage similar to the two-stage polymerisation observed in RAFT polymerisation in $scCO_2$ in Chapter 4. The simultaneous growth of PDMS-*b*-PMMA chains with short PMMA blocks can result in enough stabiliser to allow nucleation of PMMA particles, and some PDMS-CTPPA may act as stabiliser by physical adsorption to the particles.

With PDMS₆₅-CTPPA, bimodal molecular weight distributions were observed at high monomer conversion. Peak deconvolution allowed the characterisation of two distinct polymer populations that composed the THF-SEC traces for MMA polymerisation with

PDMS₆₅-CTPPA. RAFT control with PDMS₆₅-CTPPA was obtained at low and medium monomer conversion, before the bimodal molecular weight distribution was observed by THF-SEC.

The presence of CTA end-groups in both polymer populations allows us to discard the occurrence of termination by combination. Instead, both populations may arise from polymerisation in different environments, *i.e.*, in the continuous and in the dispersed phase, when molecular weight is above a critical molecular weight. According to the kinetic data, such critical molecular weight appears to be 27 kg mol⁻¹, above which PDMS-*b*-PMMA chains self-assemble and the system passes from homogeneous to heterogeneous.

With PDMS₁₂₈-CTPPA, such bimodal molecular weight distribution was not observed, instead unimodal traces tailing towards low molecular weights were observed. The UV detector confirmed the presence of CTA end-groups, but part of the macro-CTA was left unreacted. It is possible that the molecular weight required for self-assembly, and thus creation of a dispersed system, was not reached.

Overall, better control over molecular weight was obtained with PDMS-CTPPA compared to PDMS-DDMAT. The THF-SEC data confirmed the consumption of the macro-CTA (although a bit slow and not complete) and the constant chain extension with conversion, signalling the successful synthesis of block copolymers. However, hexane washes were performed to evaluate PDMS grafting to the polymer, and only up to 60% of the macro-CTA was retained by covalent bonds into the block copolymer at the end of the reaction. Better evaluation of the blocking efficiency is necessary in order to confirm that information, as some short PDMS-*b*-PMMA can also be solubilised in hexane.

Unfortunately, no sphere-to-worm-to-vesicle morphology transition was observed with PDMS-CTPPA. Individual spherical particles could be obtained with PDMS₆₅-CTPPA, although those were bigger than the expected diameter for block copolymer self-assembly. When decreasing the PMMA targeted DP, agglomeration increased, and secondary structures composed by clusters of particles were observed. With PDMS₁₂₈-CTPPA, particles were less defined and more fused together to form the secondary structure clusters. The particles were more fused together for lower targeted PMMA DPs. The occurrence of kinetically trapped spheres at high PMMA DP is in agreement with previous study of PISA *via* RAFT in scCO₂.¹⁸

Moreover, the high-pressure sampling autoclave system used in our study allows the tracking of molecular weight and conversion, but it does not allow the tracking of particles morphology because the polymer is dissolved in solvent as it is vented into the sampling cylinder. In addition, the removal of scCO₂ *via* depressurisation can cause the collapse of soluble chains and of present particles morphologies. Therefore, it would be interesting to track the reaction *via in situ* SAXS or SANS in order to observe the particles in the dispersed system.¹⁹

In conclusion, the synthesis of block copolymers *via* RAFT in scCO₂ with PDMS-CTPPA is possible and produces block copolymers but does not allow so far to take advantage of the multiple well-defined morphologies that a PISA process can provide in conventional organic solvents or in aqueous dispersion. The present work helps to elucidate PDMS macro-CTA behaviour in scCO₂ and can be applied for future projects designing, which is something our lab will pursue in future studies.

5.7. References

1. J.-S. Song and M. A. Winnik, *Macromolecules*, 2006, **39**, 8318-8325.
2. M. Lansalot, J. Rieger and F. D'Agosto, in *Macromolecular Self-Assembly*, eds. L. Billon and O. Borisov, John Wiley & Sons, New Jersey, United States of America, 2016, ch. 2, pp. 33-82.
3. T. Boursier, I. Chaduc, J. Rieger, F. D'Agosto, M. Lansalot and B. Charleux, *Polym Chem*, 2011, **2**, 355-362.
4. A. P. Lopez-Oliva, N. J. Warren, A. Rajkumar, O. O. Mykhaylyk, M. J. Derry, K. E. B. Doncom, M. J. Rymaruk and S. P. Armes, *Macromolecules*, 2015, **48**, 3547-3555.
5. F. Furno, P. Licence, S. M. Howdle and M. Poliakoff, *Actual Chimique*, 2003, 62-66.
6. K. Kortsen, A. A. C. Pacheco, J. C. Lentz, V. Taresco and S. M. Howdle, *J Supercrit Fluids*, 2021, **167**, 105047.
7. F. D'Agosto, J. Rieger and M. Lansalot, *Angew Chem Int Ed*, 2020, **59**, 8368-8392.
8. D. Wang, D. Tan and L. Liu, *Soft Computing*, 2018, **22**, 387-408.
9. R. Poli, J. Kennedy and T. Blackwell, *Swarm Intelligence*, 2007, **1**, 33-57.
10. J. L. Kendall, D. A. Canelas, J. L. Young and J. M. DeSimone, *Chemical reviews*, 1999, **99**, 543-563.
11. C. Boyère, C. Jérôme and A. Debuigne, *Eur Polym J*, 2014, **61**, 45-63.
12. C. Gualandi, L. J. White, L. Chen, R. A. Gross, K. M. Shakesheff, S. M. Howdle and M. Scandola, *Acta Biomater.*, 2010, **6**.
13. Y. L. Hsiao, E. E. Maury, J. M. Desimone, S. Mawson and K. P. Johnston, *Macromolecules* 1995, **28**.
14. S. Perrier, *Macromolecules*, 2017, **50**, 7433-7447.
15. T. D. McAllister, L. D. Farrand and S. M. Howdle, *Macromol Chem Phys*, 2016, **217**, 2294-2301.
16. M. R. Giles, J. N. Hay, S. M. Howdle and R. J. Winder, *Polymer*, 2000, **41**, 6715-6721.
17. K. A. Shaffer, T. A. Jones, D. A. Canelas and J. M. DeSimone, *Macromolecules*, 1996, **29**, 2704-2706.
18. A. Xu, Q. Lu, Z. Huo, J. Ma, B. Geng, U. Azhar, L. Zhang and S. Zhang, *Rsc Adv*, 2017, **7**, 51612-51620.
19. M. Alauhdin, T. M. Bennett, G. He, S. P. Bassett, G. Portale, W. Bras, D. Hermida-Merino and S. M. Howdle, *Polym Chem*, 2019, **10**, 860-871.

5.8. Appendix

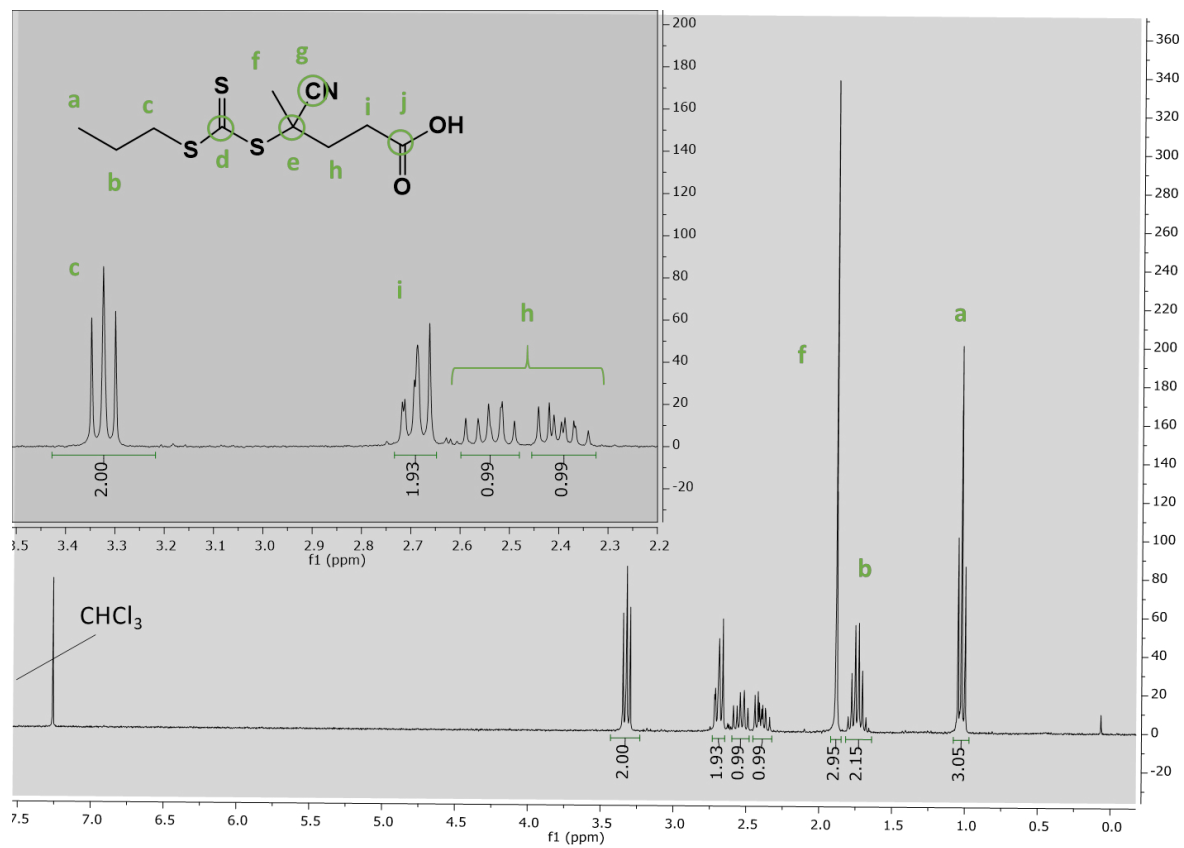


Figure S1 - ¹H NMR of CTPPA (400 MHz, CDCl₃), δ (ppm): 3.27 (t, J = 7.4 Hz, 2H), 1.72 (m, 8H), 0.99 (t, J = 7.4 Hz, 3H).

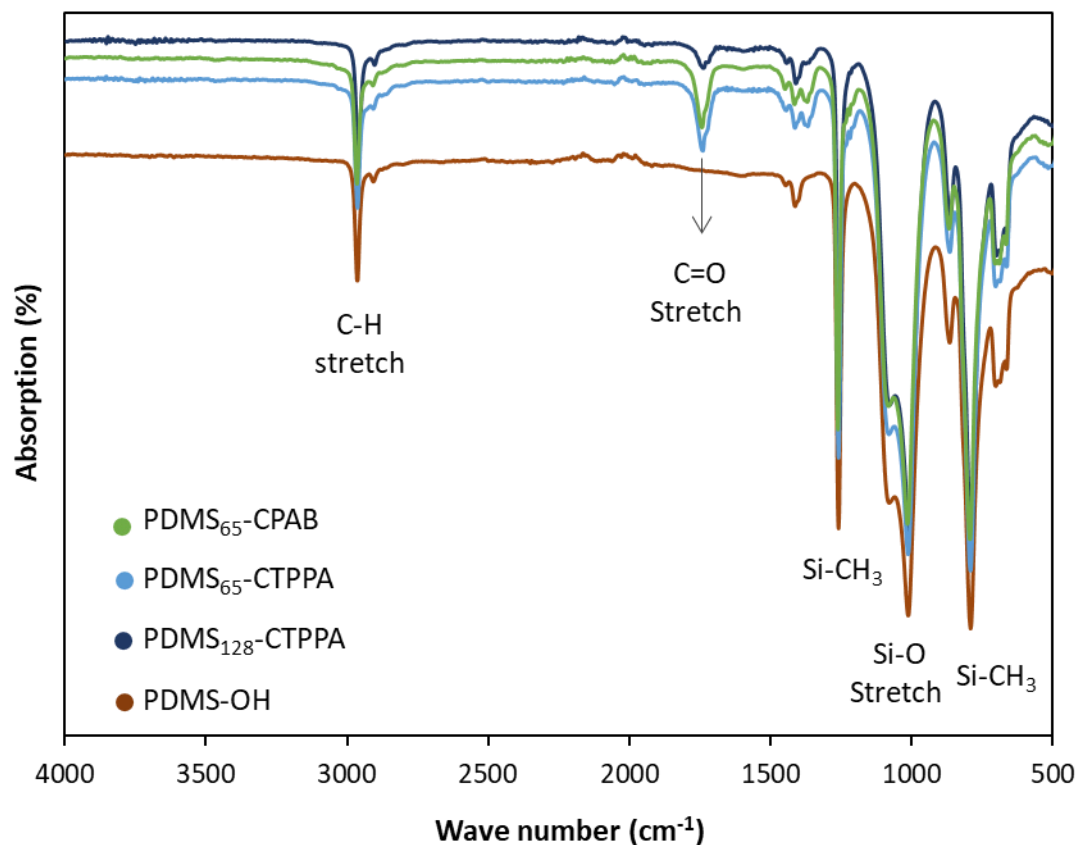


Figure S2 - FT-IR spectra of PDMS-OH (brown), PDMS₁₂₈-CTPPA (dark blue), PDMS₆₅-CTPPA (light blue) and PDMS₆₅-CPAB (green) macro-CTAs. The carbonyl stretching ($\text{C}=\text{O}$, 1740 cm^{-1}) from the ester formed upon the PDMS and CTA coupling is seen for the macro-CTAs. The intensity of the $\text{C}=\text{O}$ stretching increases with the decrease of the PDMS DP.

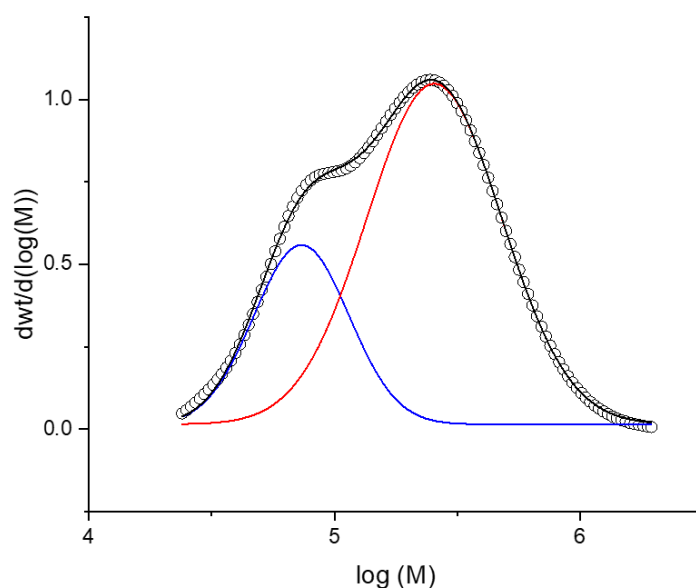


Figure S3 - Peak deconvolution in OriginPro8® of the final product from E4.3 (24 h reaction). The cumulative fit of both peaks is presented in black; the experimental data points are presented by circles (o); Peak A is presented in blue; and peak B is presented in red. Peak B: $M_n = 208.3 \text{ kg mol}^{-1}$ and $\bar{D} = 1.47$. Peak A: $M_n = 70.5 \text{ kg mol}^{-1}$ and $\bar{D} = 1.49$. See section 5.4.2.7 for the deconvolution method.

Table S1 – Summary of results from MMA dispersion polymerisation kinetics in sCO_2 with PDMS₆₅-CTPPA as macro-CTA with a targeted PMMA DP = 1200 (E4.3). Reaction monitored with the high-pressure sampling system.

Time (h)	Conversion ¹ (%)	$M_{n,\text{th}}^2$	Pop 2 M_n^3	\bar{D}^3
0.5	1.0	9.30	11.3	1.20
1	2.0	10.50	12.0	1.21
3	6.5	15.95	17.7	1.23
4.5	15.2	26.39	26.9	1.30
6.5	33.3	48.08	53.0	1.63
8	65.4	86.54	102.1*/70.5**	1.96*/1.47**
24	95.3	122.45	136.2*/70.5**	1.80*/1.49**

¹ Conversion calculated from ¹H NMR. ² Theoretical M_n of the block copolymer = PMMA $M_{n,\text{th}}$ + M_n of macro-CTA (8.1 kg mol^{-1}) as calculated in THF-SEC, where PMMA $M_{n,\text{th}}$ was calculated relative to macro-CTA and monomer concentration, given in kg mol^{-1} . ³ \bar{D} and M_n (in kg mol^{-1}) obtained by THF-SEC with RI detector against PMMA standards. * Considering both molecular weight populations together. ** considering only the low molecular weight population obtained by peak deconvolution. (Molar ratio macro-CTA:AIBN of 2:1, 65 °C, 276 bar, 300 rpm stirring rate, 4.4 wt% of macro-CTA).

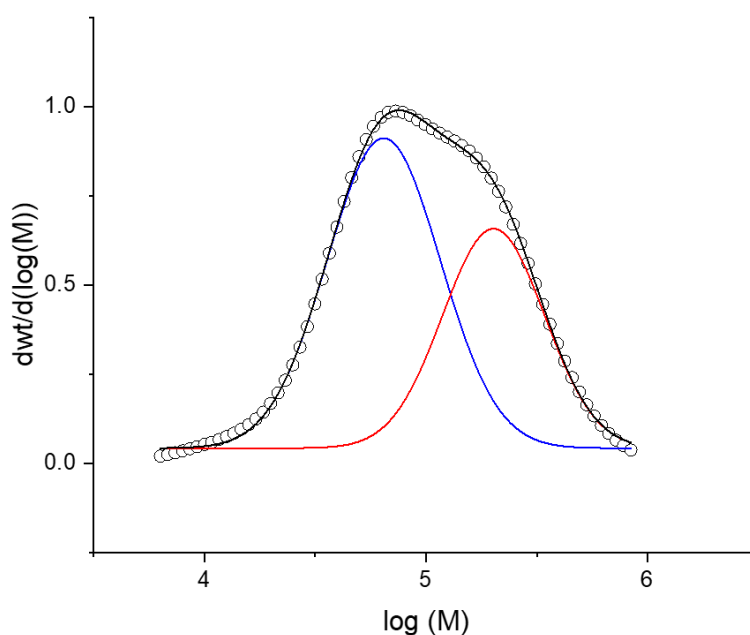


Figure S4 - Peak deconvolution in OriginPro8® of the final product from E4.4 (24h reaction). The cumulative fit of both peaks is presented in black; the experimental data points are presented by circles (o); Peak A is presented in blue; and peak B is presented in red. Peak B: $M_n = 172.9 \text{ kg mol}^{-1}$ and $\mathcal{D} = 1.30$. Peak A: $M_n = 54.1 \text{ kg mol}^{-1}$ and $\mathcal{D} = 1.41$. See section 5.4.2.7 for the deconvolution method.

Table S2 – Summary of results from MMA dispersion polymerisation kinetics in scCO_2 with PDMS₆₅-CTPPA as macro-CTA with a targeted PMMA DP = 600 (E4.4). Reaction monitored with the high-pressure sampling system.

Time (h)	Conversion ¹ (%)	$M_{n,\text{th}}^2$	Pop 2 M_n^3	\mathcal{D}^3
0.5	2.9	9.85	10.0	1.28
1.5	11.5	15.00	11.6	1.15
3	18.7	19.31	14.4	1.18
5	20.0	20.09	14.6	1.27
6.5	27.0	24.29	17.0	1.22
8	32.9	27.82	21.4	1.24
24	90.7	62.46	75.7*	1.73*

¹ Conversion calculated from ¹H NMR. ² Theoretical M_n of the block copolymer = PMMA $M_{n,\text{th}}$ + M_n of macro-CTA (8.1 kg mol^{-1}) as calculated in THF-SEC, where PMMA $M_{n,\text{th}}$ was calculated relative to macro-CTA and monomer concentration, given in kg mol^{-1} . ³ \mathcal{D} and M_n (in kg mol^{-1}) obtained by THF-SEC with RI detector against PMMA standards. * Considering both molecular weight populations together. (Molar ratio macro-CTA:AIBN of 2:1, 65 °C, 276 bar, 300 rpm stirring rate, 8.8 wt% of macro-CTA).

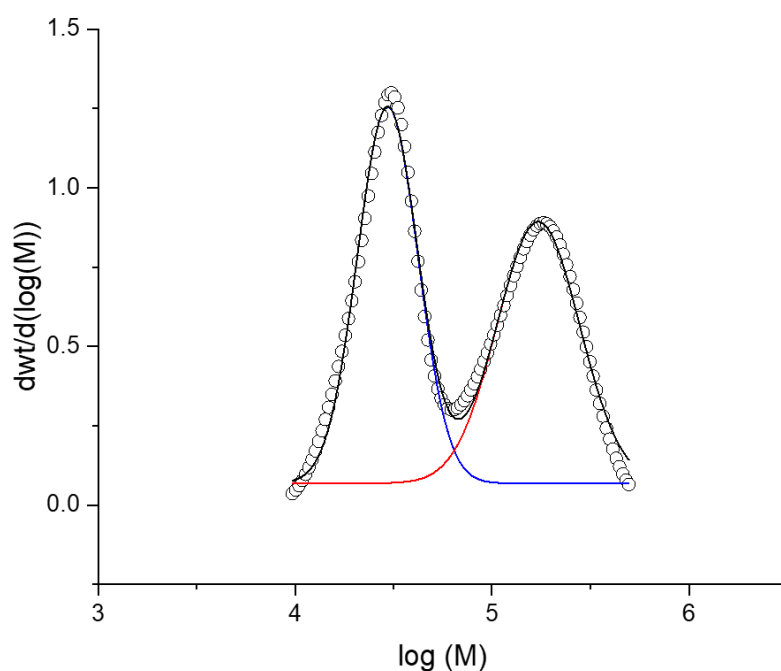


Figure S5 - Peak deconvolution in OriginPro8® of the final product from E4.5 (24h reaction). The cumulative fit of both peaks is presented in black; the experimental data points are presented by circles (o); Peak A is presented in blue; and peak B is presented in red. Peak B: $M_n = 148.1 \text{ kg mol}^{-1}$ and $\mathcal{D} = 1.22$. Peak A: $M_n = 27.9 \text{ kg mol}^{-1}$ and $\mathcal{D} = 1.16$. See section 5.4.2.7 for the deconvolution method.

Table S3 – Summary of results from MMA dispersion polymerisation kinetics in scCO_2 with PDMS₆₅-CTPPA as macro-CTA with a targeted PMMA DP = 300 (E4.5). Reaction monitored with the high-pressure sampling system.

Time (h)	Conversion ¹ (%)	$M_{n,\text{th}}^2$	M_n^3	\mathcal{D}^3
0.7	1.0	8.40	9.6	1.07
1.5	2.9	8.98	10.9	1.06
2.5	4.8	9.53	11.6	1.06
4	7.4	10.33	12.2	1.09
6	12.3	11.80	13.5	1.10
8	30.1	17.15	17.7	1.03
24	90.6	35.36	26.4*	1.1*

¹ Conversion calculated from ¹H NMR. ² Theoretical M_n of the block copolymer = PMMA $M_{n,\text{th}}$ + M_n of macro-CTA (8.1 kg mol^{-1}) as calculated in THF-SEC, where PMMA $M_{n,\text{th}}$ was calculated relative to macro-CTA and monomer concentration, given in kg mol^{-1} . ³ \mathcal{D} and M_n (in kg mol^{-1}) obtained by THF-SEC with RI detector against PMMA standards. * Considering only the low molecular weight populations. (Molar ratio macro-CTA:AIBN of 2:1, 65 °C, 276 bar, 300 rpm stirring rate, 17.5 wt% of macro-CTA).

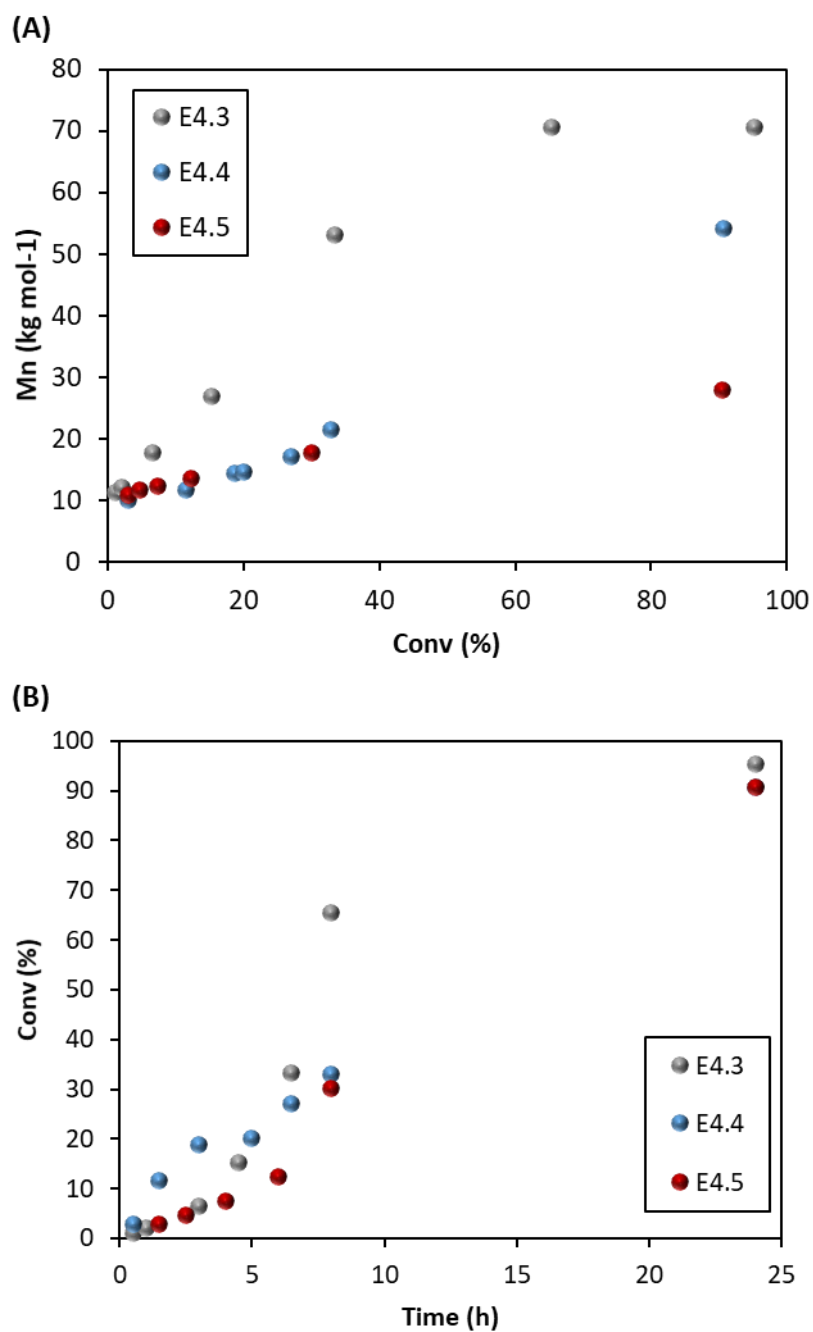


Figure S6 - Kinetic study of MMA dispersion polymerisation in $sc\text{CO}_2$ with $\text{PDMS}_{65}\text{-CTPPA}$ for reactions E4.3 (grey), E4.4 (blue) and E4.5 (red). (A) shows the plot of conversion with time and (B) shows the evolution of M_n versus conversion.

Table S4 - Summary of results from MMA dispersion polymerisation kinetics in scCO₂ with PDMS₁₂₈-CTPPA as macro-CTA with a targeted PMMA DP = 1801 (E6.1). Reaction monitored with the high-pressure sampling system.

Time (h)	Conversion ¹ (%)	$M_{n,th}$ ²	M_n ³	\mathcal{D}^3
0.7	-	-	51.3	1.34
1.5	21.3	48.40	66.5	1.22
2.5	33.2	70.05	84.3	1.59
4	48.2	97.03	152.2	1.42
6	65.5	128.32	179.5	1.43
8	91.2	174.65	224.2	1.41
24	97.1	185.35	227.6	1.48

¹ Conversion calculated from ¹H NMR. ² Theoretical M_n of the block copolymer = PMMA $M_{n,th}$ + M_n of macro-CTA (10.01 kg mol⁻¹), where PMMA $M_{n,th}$ was calculated relative to macro-CTA and monomer concentration, given in kg mol⁻¹. The M_n of macro-CTA = M_n of PDMS-OH (9.75 kg mol⁻¹) + CTPPA molecular weight (0.265 kg mol⁻¹). ³ \mathcal{D} and M_n (in kg mol⁻¹) obtained by THF-SEC with RI detector against PMMA standards. (Molar ratio macro-CTA:AIBN of 2:1, 65 °C, 276 bar, 300 rpm stirring rate, 5.7 wt% of macro-CTA).

Table S5 - Summary of results from MMA dispersion polymerisation kinetics in scCO₂ with PDMS₁₂₈-CTPPA as macro-CTA with a targeted PMMA DP = 920 (E6.2). Reaction monitored with the high-pressure sampling system.

Time (h)	Conversion ¹ (%)	$M_{n,th}$ ²	M_n ³	\mathcal{D} ³
0.5	3.8	13.6	16.2	1.74
1.5	4.8	14.4	18.0	1.32
3	13.8	22.7	36.4	1.24
5	39.0	45.9	62.3	1.53
6.5	72.0	76.4	111.1	1.46
8	89.3	92.3	143.9	1.33
24	98.6	100.9	155.7	1.32

¹ Conversion calculated from ¹H NMR. ² Theoretical M_n of the block copolymer = PMMA $M_{n,th}$ + M_n of macro-CTA (10.01 kg mol⁻¹), where PMMA $M_{n,th}$ was calculated relative to macro-CTA and monomer concentration, given in kg mol⁻¹. The M_n of macro-CTA = M_n of PDMS-OH (9.75 kg mol⁻¹) + CTPPA molecular weight (0.265 kg mol⁻¹). ³ \mathcal{D} and M_n (in kg mol⁻¹) obtained by THF-SEC with RI detector against PMMA standards. (Molar ratio macro-CTA:AIBN of 2:1, 65 °C, 276 bar, 300 rpm stirring rate, 11.1 wt% of macro-CTA).

Table S6 - Summary of results from MMA dispersion polymerisation kinetics in scCO₂ with PDMS₁₂₈-CTPPA as macro-CTA with a targeted PMMA DP = 476 (E6.3). Reaction monitored with the high-pressure sampling system.

Time (h)	Conversion ¹ (%)	$M_{n,th}$ ²	M_n ³	\mathcal{D} ³
0.7	7.4	13.5	18.3	1.11
1.5	10.7	15.1	18.9	1.11
2.5	16.0	17.6	20.8	1.09
4	18.0	18.6	24.0	1.11
6	25.9	22.4	32.2	1.15
8	47.6	32.7	50.9	1.13
24	96.9	56.2	96.6	1.25

¹Conversion calculated from ¹H NMR. ²Theoretical M_n of the block copolymer = PMMA $M_{n,th}$ + M_n of macro-CTA (10.01 kg mol⁻¹), where PMMA $M_{n,th}$ was calculated relative to macro-CTA and monomer concentration, given in kg mol⁻¹. The M_n of macro-CTA = M_n of PDMS-OH (9.75 kg mol⁻¹) + CTPPA molecular weight (0.265 kg mol⁻¹). ³ \mathcal{D} and M_n (in kg mol⁻¹) obtained by THF-SEC with RI detector against PMMA standards. (Molar ratio macro-CTA:AIBN of 2:1, 65 °C, 276 bar, 300 rpm stirring rate, 21.6 wt% of macro-CTA).

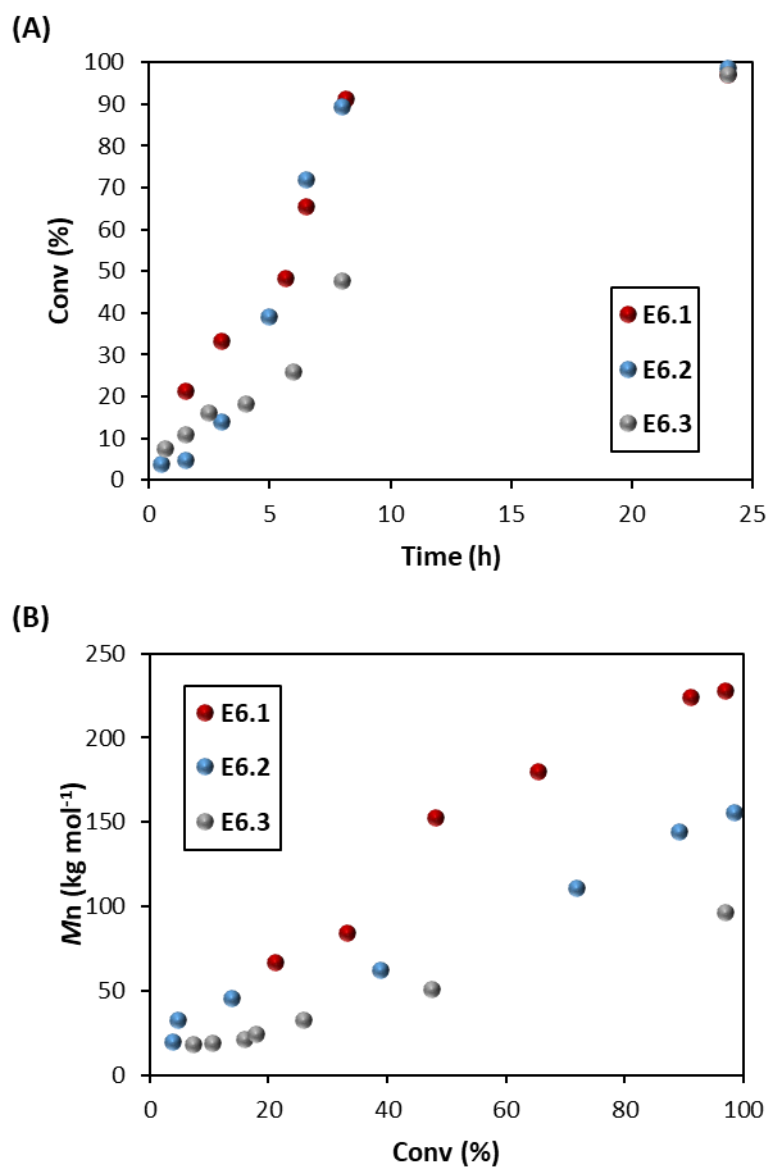


Figure S7 - Kinetic study of MMA dispersion polymerisation in sCO_2 with PDMS_{128} -CTPPA for reactions E6.1 (red), E6.2 (blue) and E6.3 (grey). (A) shows the plot of conversion with time and (B) shows the evolution of M_n versus conversion.

Contents

Chapter 6 :Conclusions.....	308
6.1. Conclusions	308
6.2. Future Work	310

Chapter 6: Conclusions

6.1. Conclusions

At the Abstract of this thesis, we set that our aim was to make a positive use of captured carbon dioxide (CO₂) as an alternative green solvent for polymer synthesis through the investigation of reversible addition-fragmentation chain transfer (RAFT) polymerisation in scCO₂ with molecular chain transfer agents (CTAs) and with macromolecular CTAs (macro-CTAs) soluble in scCO₂.

These objectives were addressed in three experimental chapters, using methyl methacrylate (MMA) as a model monomer. Experiments regarding the polymerisation with macro-CTAs was presented in chapter 3 and 5, while the polymerisation with CTAs was discussed in chapter 4.

In chapter 3, the first of the 3 experimental chapters presented in this thesis, the synthesis of macro-CTAs *via* esterification of monocarbinol terminated PDMS (PDMS-OH) of different molecular weights with a CTA containing a carboxylic acid group, 2-(dodecylthiocarbonothioylthio)-2-methylpropionic acid (DDMAT) were reported. This CTA was selected according to promising results from a previous thesis project in the Howdle group, in which PDMS-DDMAT was used for MMA dispersion polymerisation in scCO₂.

The synthesised PDMS-DDMAT were thoroughly characterised and their solubility in scCO₂ was determined using a variable volume view cell. These macro-CTAs were then used for polymerisation-induced self-assembly (PISA) inspired dispersion polymerisation of MMA. Although PDMS-DDMAT macro-CTAs were able to stabilise PMMA particles, successful RAFT control was not attained, and part of the macro-CTA remained unreacted. Hexane washes of the products demonstrated that about 70% PDMS-DDMAT was not retained in the final product. In addition, Scanning Electron Microscopy (SEM) studies showed that well-defined large spherical particles were observed only at high degree of polymerisation (DP) of PMMA, while amorphous materials were obtained at lower DPs and no sphere-to-worm-to-vesicle morphology transition was observed. The use of molecular DDMAT together with PDMS-DDMAT improved RAFT control and morphology, suggesting DDMAT is a good CTA for this polymerisation.

In Chapter 4, RAFT dispersion polymerisation of MMA was performed in scCO₂ using DDMAT as molecular CTA. Despite the known low chain-transfer constant (C_{tr}) towards methacrylates in conventional solvents, DDMAT showed good control over PMMA molecular weight in scCO₂. In order to fully understand the peculiar behaviour of DDMAT, a thorough investigation of the nucleation stage during the dispersion polymerisation revealed an unexpected “*in situ* two-stage” mechanism that explains well how this CTA works.

To extend our knowledge, a range of CTAs were used for MMA dispersion polymerisation in scCO₂. Finally, using a novel computational solvation model, a correlation between polymerisation control and the degree of solubility in scCO₂ of the CTAs was found. All of this ultimately gave rise to a guideline to select the best molecular CTA for RAFT dispersion polymerisation in scCO₂.

In Chapter 5, the final experimental chapter presented in this thesis, we reported the synthesis of macro-CTAs *via* esterification of PDMS-OH of different molecular weights with 4-cyano-4-(phenylcarbonothioylthio)pentanoic acid (CPAB) and (4-cyano-4-thiothiopropylsulfanyl)pentanoic acid) (CTPPA), two CTAs that have high C_{tr} towards methacrylates and contain a carboxylic acid group. In a PISA system, the macro-CTA will chain extend in solution (homogeneous system) until it self-assembles to form *nuclei*. Therefore, a better control over the initial stages of the MMA dispersion polymerisation is a prerequisite for a successful RAFT-mediated PISA in dispersion in scCO₂ while it is not the case for a successful RAFT dispersion polymerisation in scCO₂. With bases on the findings presented in the two previous experimental chapters, CTAs with high C_{tr} towards methacrylates resulted into a better RAFT control at the initial stage of MMA dispersion polymerisation in scCO₂. Therefore, coupling PMDS with CPAB and CTPPA could result in a better macro-CTA for MMA dispersion polymerisation.

The assessment of the reaction kinetics and SEM studies of the MMA polymerisations with PDMS-CTPPA showed an overall improvement of MMA polymerisation and RAFT control in scCO₂ compared with results using PDMS-DDMAT. A bimodal molecular weight distribution was observed at high conversions when using the shorter PDMS₆₅-CTPPA. The presence of CTA end-groups in both polymer populations discard the occurrence of termination by combination. Instead, both populations may arise from polymerisation in different environments, *i.e.*, in the continuous and in the dispersed phase. This seems to agree with the observation of an apparent critical molecular weight of 27 kg mol⁻¹, below which, a sole molecular weight population was observed and it was in good agreement to the theoretical molecular weight. With PDMS₁₂₈-CTPPA, such bimodal molecular weight distribution was not observed.

Although the expected particle diameter and morphology transition were not observed and there is room for improvement on molecular weight and dispersity, the macro-CTA was consumed, MMA chain extended continuously, and block-copolymers particles were formed as expected in a PISA mechanism. This work helps to elucidate PDMS macro-CTAs behaviour in scCO₂ and is a step forward towards PISA polymerisation *via* RAFT in scCO₂ with macro-CTAs free of fluorine. The findings here presented can be applied for future projects designing, which is something our lab will pursue in future studies.

6.2. Future Work

As future work, it would be interesting to track the PISA reactions with the PDMS based macro-CTAs described in this thesis *via in situ* SAX or SANS in order to observe any possible morphology transitions that may occur as PMMA chain extends from the PDMS macro-CTA. The removal of $scCO_2$ *via* depressurisation can cause the collapse of morphologies in the colloidal dispersion and thus compromise the observation of any morphology transitions. This effect is expected to be more accentuated for block copolymers with a high PDMS content, which reduces the copolymer T_g and increases its solubility. Equipment for *in situ* SAX and SANS in $scCO_2$ exist in the Howdle group (at a different site) and in other research groups, and could be used through collaborations.

Another important advance would be the study the reaction kinetics of the MMA polymerisation with PDMS-DDMAT to understand the RAFT mechanism and consumption of the macro-CTA. Unfortunately, the pandemic and restrictions placed in the research laboratory hours and equipment made impossible to follow the reaction kinetics for this polymerisations.

In addition, it would be interesting to have computational solubility studies of the PDMS based macro-CTAs presented in Chapter 3 and Chapter 5, although it is clear that attaching a highly soluble PDMS chain to the CTA will increase its solubility and we presented their cloud points.

Regarding Chapter 3, it would be also interesting to expand the number of comparative experiments using PDMS-MA versus PDMS-DDMAT with other wt% of stabiliser. This would help us to understand how the higher load of PDMS-DDMAT can be affecting morphology and trace a parallel with PDMS-MA. In addition, it would good to compare both PDMS based polymers as stabilisers (PDMS-MA and PDMS-DDMAT) in the absence of molecular CTA (DDMAT), to better assess if PDMS-DDMAT exerts any RAFT control or only helps stabilising the PMMA polymer particles. Unfortunately, it was not possible to execute all this experiments due to time constrains, which were exacerbated after the beginning of 2020's pandemic.

The work presented in Chapter 4 has been successfully published (DOI: 10.1039/d0sc05281g) and we are confident that it will inspire new original work and further investigations on the influence of solubility of CTAs in heterogeneous polymerisation systems, not limited to $scCO_2$ systems.

It would be interesting to expand the scope of the screening presented in Chapter 4 with further CTAs to better evaluate the influence of different Z and R groups on the solubility in $scCO_2$. Of particular interest, the synthesis of further CTAs analogous to DDMAT and PDMAT with thioalkyl Z group of different chain length could provide information on the maximum CTA solubility, which still does not affect control in $scCO_2$. It would also be interesting to investigate the RAFT $scCO_2$ dispersion

polymerisation of further monomers in order to unlock kinetic information and investigate reaction mechanisms. This would also test the universality of our CTA selection guideline.

For the polymerisation of MMA with PDMS-CTPPA and PDMS-CPAB (Chapter 5) it would be interesting to further investigate the causes for the bimodal SEC distribution observed in the dispersion polymerisation of MMA in $scCO_2$ mediated by PDMS₆₅-CTPPA. Results suggested a critical PMMA molecular weight around 27 kg mol^{-1} . Above that, RAFT control was lost and a high molecular weight population was formed. In order to confirm this hypothesis, MMA polymerisation at molecular weight target lower than 27 kg mol^{-1} must be studied. Therefore, it would be interesting to test PDMS₆₅-CTPPA for polymerisation of MMA with targeted MMA DP of 100 and 200, in order to confirm if the hypothesis is correct. It would also be interesting to test the solubility of PDMS₆₅-*b*-PMMA with different MMA DPs in $scCO_2$. In addition, it would be ideal to gather more data points between 8 and 24 h of reaction in the kinetic studies.

PDMS₁₂₈-CTPPA experiments did not show a bimodal distribution and therefore, it is possible that the critical molecular weight required for self-assembly, and thus creation of a dispersed system, was not reached. To further confirm the absence of a critical molecular weight for PDMS₁₂₈-CTPPA, it is important to evaluate the solubility of PDMS₁₂₈-*b*-PMMA and evaluate the control of this polymerisation at lower PMMA targeted DP.

In Chapters 3 and 5, hexane washes were performed to evaluate PDMS grafting to the final polymer, and only up to 60% of the macro-CTA was retained after the washes. Regarding the results from Chapter 5, better evaluation of the blocking efficiency is necessary in order to confirm this information, as some short PDMS-*b*-PMMA can also be solubilised in hexane. Therefore, it would be fundamental to further assess the liquid phase resulting from the hexane washes in order to confirm if PDMS-*b*-PMMA is present. Blocking efficiency of MMA polymerisation with PDMS-CTPPA could also be investigated by others through the chain extension of the produced copolymers.

A further parameter that can influence morphology in PISA is the total solids content. In this thesis, all reactions aimed at the same solid contents, *i.e.*, $\approx 16 \text{ \% w/v}$, due to the characteristics of the high pressure autoclave. Ongoing studies at the Howdle group are investigating what is the maximum safe solid contents that can be achieved in this high pressure system. Future works could thus investigate the impact of solid contents over self-assembly morphology.

It is important to notice that the scope of this work was limited due to COVID-19 restrictions and the challenges that came from it. For example, it would have been of interest for this work to have further investigated via MALDI-TOF mass spectrometry the samples obtained with the sampling cylinder

device at the early reaction stages. This could offer information on the termination of the polymer chains and better distinguish the presence of chains initiated *via* conventional radical polymerisation and *via* RAFT polymerisation. However, the instrument was not accessible for a long time and once re-opened, the access was only arranged as a service with a limited schedule. This work could also be expanded to the investigation of the CTAs solubility impact in the dispersion polymerisation of MMA in other solvents; however, the understanding of scCO₂ dispersion polymerisation was prioritised given the shortened timescale of this work.

Finally, considering all the data presented in this thesis, we believe two lines of study could be explored for obtaining successful PISA polymerisations in scCO₂ with PDMS based macro-CTAs, they are:

- Use of a non-soluble radical initiator. A choice of a different initiator to AIBN, which has low solubility in scCO₂ must guarantee that the locus of the reaction will be restricted to the particles formed at the start of the reaction. This would overcome the problems observed in chapter 5, with bimodal molecular weight distributions.
- Use of macro-CTAs with PDMS Z-group instead of R-group. This change would likely improve PDMS retention in the final polymer. In addition, the less soluble R-group would reduce issues with CTA entering particles (frustrated enter) and make the migration of R-groups between phases less frequent.